ALFRED-WEGENER-INSTITUT
HELMHOLTZ-ZENTRUM FÜR POLAR- UND MEERESFORSCHUNG

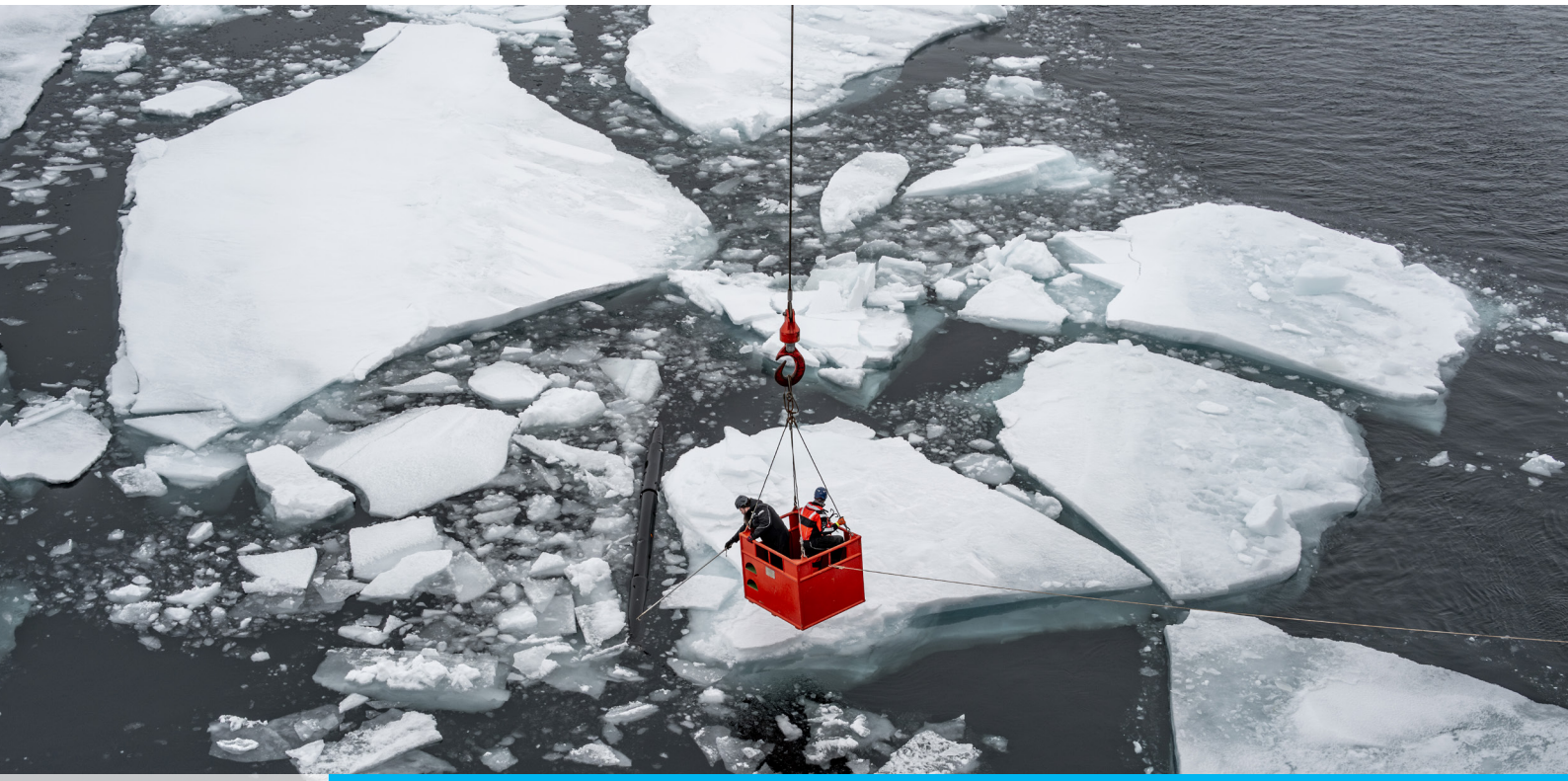

794
2025

Berichte
zur Polar- und Meeresforschung
Reports on Polar and Marine Research

The Expedition PS144 of the Research Vessel POLARSTERN to the Arctic Ocean in 2024

Edited by

Benjamin Rabe and Walter Geibert
with contributions of the participants

HELMHOLTZ

Die Berichte zur Polar- und Meeresforschung werden vom Alfred-Wegener-Institut, Helmholtz-Zentrum für Polar- und Meeresforschung (AWI) in Bremerhaven, Deutschland, in Fortsetzung der vormaligen Berichte zur Polarforschung herausgegeben. Sie erscheinen in unregelmäßiger Abfolge.

Die Berichte zur Polar- und Meeresforschung enthalten Darstellungen und Ergebnisse der vom AWI selbst oder mit seiner Unterstützung durchgeführten Forschungsarbeiten in den Polargebieten und in den Meeren.

Die Publikationen umfassen Expeditionsberichte der vom AWI betriebenen Schiffe, Flugzeuge und Stationen, Forschungsergebnisse (inkl. Dissertationen) des Instituts und des Archivs für deutsche Polarforschung, sowie Abstracts und Proceedings von nationalen und internationalen Tagungen und Workshops des AWI.

Die Beiträge geben nicht notwendigerweise die Auffassung des AWI wider.

Herausgeber
Dr. Horst Bornemann

Redaktionelle Bearbeitung und Layout
Susan Amir Sawadkuhi

Alfred-Wegener-Institut
Helmholtz-Zentrum für Polar- und Meeresforschung
Am Handelshafen 12
27570 Bremerhaven
Germany

www.awi.de
www.awi.de/reports

The Reports on Polar and Marine Research are issued by the Alfred Wegener Institute, Helmholtz Centre for Polar and Marine Research (AWI) in Bremerhaven, Germany, succeeding the former Reports on Polar Research. They are published at irregular intervals.

The Reports on Polar and Marine Research contain presentations and results of research activities in polar regions and in the seas either carried out by the AWI or with its support.

Publications comprise expedition reports of the ships, aircrafts, and stations operated by the AWI, research results (incl. dissertations) of the Institute and the Archiv für deutsche Polarforschung, as well as abstracts and proceedings of national and international conferences and workshops of the AWI.

The papers contained in the Reports do not necessarily reflect the opinion of the AWI.

Editor
Dr. Horst Bornemann

Editorial editing and layout
Susan Amir Sawadkuhi

Alfred-Wegener-Institut
Helmholtz-Zentrum für Polar- und Meeresforschung
Am Handelshafen 12
27570 Bremerhaven
Germany

www.awi.de
www.awi.de/en/reports

Titel: Auf der Jagd nach "Nessie": Eine Rohrverankerung auf der Flucht
(Foto: Christian Rohleder, AWI)

Cover: Hunting for "Nessie": A tube mooring on the run
(Photo: Christian Rohleder, AWI)

The Expedition PS144 of the Research Vessel POLARSTERN to the Arctic Ocean in 2024

Edited by

Benjamin Rabe and Walter Geibert
with contributions of the participants

Please cite or link this publication using the identifiers

https://epic.awi.de/id/eprint/60077
https://doi.org/10.57738/BzPM_0794_2025

ISSN 1866-3192

PS144 / ArcWatch-2 (TransArc)

09 August 2024 – 13 October 2024

Tromsø – Bremerhaven

Chief scientist
Benjamin Rabe

Co-chief scientist
Walter Geibert

Coordinator
Ingo Schewe

Contents

1. ÜBERBLICK UND EXPEDITIONSVERLAUF

Benjamin Rabe, Walter Geibert DE.AWI

Das Ziel der Expedition war die großskalige, quasi-synoptische Aufnahme des eurasischen und zentralen Nordpolarmeeres und des Barentsseekontinentalhangs im Nansenbecken. Dies beinhaltet Änderungen über die ganze Tiefe des Ozeans, des Meereises und der unteren Atmosphäre. Änderungen im Jahresgang des Meereises bei sich gleichzeitig verändernden ozeanischen Strömungen in die Arktis und Mustern atmosphärischen Drucks werfen den Bedarf auf, die großskalige Variabilität über die gesamte eurasische Arktis umfassend zu verstehen. Vorangehende Expeditionen mit diesem Ziel waren unter anderem ArcWatch-1 (2023), TransArc II (2015), TransArc (2011) und SPACE (2007) während des internationalen Polarjahres (International Polar Year IPY) sowie Beobachtungen durch andere Schiffe während des Synoptic Arctic Survey (SAS) und anderen Expeditionen während des IPY. Die bekannten und zu erwartenden Änderungen sind die Folge großskaliger Umweltprozesse und reflektieren die Beiträge unterschiedlicher Quellen und der Bedingungen am Rand der Arktis. Die Beobachtungen sind Teil eines mehr als 30 Jahre langen Datensatzes, der die Variabilität im dreidimensionalen Raum und in der Zeit widerspiegelt. Unsere Expedition ist die erste Wiederaufnahme in dieser Breite an beobachteten Variablen und mit dieser umfangreichen Abdeckung seit 2015 (TransArc II). Dies beinhaltete eine wiederholte Messung mehrerer Stationen / Schnitte durch reguläre und spurenmetallreine Beprobung. Die Untersuchung kleinskaliger, lokaler Umweltprozesse waren auch Teil dieser Expedition und das Vermächtnis vorhergehender Expeditionen, wie das Multidisciplinary Observatory for the Study of Arctic Climate (MOSAiC). Zitate von Fahrtberichten und wissenschaftlicher Literatur sind hier nicht aufgeführt und finden sich in den fachspezifischen Kapiteln 2 – 7.

ArcWatch-2/TransArc ist ein Beitrag zu den internationalen Programmen GEOTRACES, Arctic ROOS/EuroGOOS und dem internationalen arktischen Bojenprogramm (International Arctic Buoy Programme; IABP). Es ist Teil der langfristigen Beobachtungen (Long-Term Observations; LTO) ArcWatch / Arctic Ocean und der Helmholtz programmgebundenen Forschung POF 4 „Changing Earth – Sustaining our Future“, insbesondere der Topics 1, 2 und 6. Die Expedition ist ein Vermächtnis des Helmholtz „strategic investment“ Frontiers in Arctic Marine Monitoring (FRAM) und ist ein Beitrag zur Infrastruktur Marine Umweltrobotik und -Sensorik für nachhaltige Erforschung (MUSE).

ArcWatch-2 startete am 9. August 2024 in Tromsø, von wo *Polarstern* nach Longyearbyen (Svalbard, Norwegen) fuhr (Abb. 1.1 und 2.2). Verschiedene „underway“-Messungen wurden bereits in der Barentssee und während der gesamten Expedition durchgeführt. In Longyearbyen wurden zwei Wissenschaftler ausgetauscht und das schiffseigene EK80 Echolot kalibriert. Danach fuhren wir zu einer Teststation nördlich des Archipels bei 83°N, wo wir das pelagische Schleppnetz am Kontinentalhang testeten. Nachdem wir in das das Packeis gefahren waren, führten wir eine Test-Eisstation mit parallelem hydrographischem Betrieb um 85°N, 42°E durch, wo wir die Backbordseite als Zugang zum Eis über eine Gangway nutzten und die Steuerbordseite zum Ausbringen von wasserprofilierenden und beprobenden Instrumenten. Das Schiff wurde oft mit Eisankern und Leinen fixiert, um stabil zu bleiben, insbesondere bei starkem Wind. Unglücklicherweise erlaubte das Wetter zu diesem Zeitpunkt noch keine helikopterbasierten

Messungen. Aufgrund der allgemeinen Eissituation (verhältnismäßig geringe Eiskonzentration im östlichen und zentralen Nordpolarmeer) wurde entschieden, den Hauptteil des Programms am östlichen Schnitt zu beginnen („Section III“, Abb. 1.1). Während des ostwärtigen Transits hielten wir für Stationsarbeiten um 60°E, die gegen Ende der Expedition wiederholt werden sollten, womit wir auch spurenmetallreine Inkubationsexperimente begannen. Auf dem Weg weiter östlich, Richtung „Section III“ (Abb. 1.1.) fingen wir an, Einmalsysteme (XCTD) zur Beobachtung der Wassersäule einzusetzen, und hielten für eine hydrographische Station in einer Tiefe des Gakkelrückens an, die Signale hydrothermaler Aktivität in der Wassersäule zeigte. Da ein Crew-Mitglied krank wurde, mussten wir an dieser Stelle für eine medizinische Evakuierung Richtung Svalbard zurückkehren. Die Länge der Evakuierung konnte durch den Einsatz von Langstreckenhelikoptern („Super Puma“; Abb. 1.3) des „Sysselmesteren“ von Longyearbyen verkürzt werden, welche entschieden, mehr als 400 nmi zur *Polarstern* zu fliegen. Daher waren wir in der Lage, ungefähr eine Woche später wieder zu unserem Arbeitsgebiet zurückzukehren. Wir setzten dann unsere hydrographischen Arbeiten fort und begannen den Schnitt „Section III“, welcher die Nansen- und Amundsenbecken in das Makarovbecken querte. Dies beinhaltete die Beprobung und Prozessstudien an verschiedenen Eisstationen, die parallel zum extensiven Wassersäulenprogramm auf der Steuerbordseite des Schiffs verliefen Das Wassersäulenprogramm umfasste die reguläre CTD, die spurenmetallreine CTD (Abb. 1.4) und den Einsatz verschiedener Netze für biologische Proben. Transitzeiten waren in dieser Region relativ kurz, aufgrund der allgemein losen Eisbedeckung. Am Ende von Section III konnte auch der Einsatz der Helikopter beginnen, wenn auch immer noch mit Einschränkungen durch die weiterhin bestehenden, schlechten Wetterbedingungen. „Section III“ beinhaltete auch die Bergungen zweier Verankerungen im östlichen Amundsenbecken, welche in 2023 ausgebracht worden waren, und die Wiederauslegung einer reduzierten Version einer der Verankerungen. Auch wenn die Bergung im Eis eine große Herausforderung darstellte, gelang dies bei beiden Verankerungen. Ein Kuriosum erlebten wir, als wir einen großen Eisrücken entlang unseres Weges passierten. Die Größe entsprach der eines Eisberges, der Eiskörper stellte sich jedoch am Ende als zusammengeschobenes Schelfeis heraus (Abb. 1.5). Die offenen Schmelztümpel an der Meereisoberfläche änderten sich während unserer Fahrt entlang des Schnittes, indem sie überfroren und mit Schnee bedeckt wurden (siehe Flächenphotos der Drohnen in Appendix A.5). Da der Schnitt „Section III“ als Priorität angesehen wurde, führten wir auch die Verlängerung durch, welche in der Fahrtplanung als Option aufgeführt war. Diese Entscheidung sollte zu einem besseren quantitativen Bild des momentanen Zustands der Transpolardrift nahe ihrer Quelle führen. Nachdem der Schnitt beendet war, fuhren wir zu einem Wiederbesuch einer Station um 180°E, die im Sommer 2015 von sowohl *Polarstern* als auch USCG *Healy* beprobt worden war („GEOTRACES crossover station“). Neben Arbeiten in der Wassersäule führten wir hier auch eine lange Eisstation durch (Abb. 1.6). Wir fuhren dann zum Schnitt „Section II“, der im Makarovbasin anfing und mit extensiven Stationsarbeiten entlang 125°E über den Lomonosovrücken und zum Nordpol führte. Am Nordpol führten wir eine extensive Station mit Hydrographie- und Eisarbeiten durch. Hier entstand auch ein Photo des Wissenschaftspersonals an Bord (Abb. 1.7). Wir fuhren dann entlang des Schnitts in Richtung Gakkelrücken, wo unser Fokus auf einer weiteren, extensiven Eis- und Wassersäulenstation über einer topographischen Vertiefung lag, welche auch in 2015 besucht worden war. Weiter südwärts entlang 60°E wurden wir durch den recht späten Reisezeitpunkt bereits mit ungünstigen Eisbedingungen konfrontiert, die uns zwangen, an einigen Stationen mehrere nautische Meilen westwärts vom geplanten Schnitt abzuweichen. Nach dem Ende des Schnitts um 85°E, inklusive eines Wiederbesuchs von PS144_9, knapp nördlich der russischen Wirtschaftszone, fuhren wir zu unserem finalen Schnitt. Entlang des Weges führten wir Helikopterflüge und Schleppnetzarbeiten durch. Die Fahrt durch das Eis gen Westen blieb eine Herausforderung, was uns zwang, eine südwestliche Route zu ungefähr 30°E einzuschlagen, die Länge unseres finalen Schnittes. Die durch die medizinische Evakuation verlorene Zeit verringerte unsere ursprünglich geplante Stationszeit

entlang des Schnitts „Section I“ erheblich. Allgemein ermöglichte nur das gute Vorankommen entlang „Section III“ und gen Nordpol genug Zeit, trotz der medizinischen Evakuierung alle geplanten Arbeiten entlang „Section III“ und „Section II“, und einige wenige Stationen entlang „Section I“, durchzuführen. Nach dem Beenden unserer Stationsarbeiten fuhren begannen wir mit dem Rückweg nach Bremerhaven (Abb. 1.2), wobei wir „underway“-Messungen entlang des Weges bis in die Nordsee durchführten. Wir kamen am morgen des 13. Oktober 2024 im Hafen an.

Neben der helikopterbasierten Eiserkundung, welche die Navigation des Schiffs durch das Eis unterstützte, war die Verfügbarkeit satellitenbasierten Karten und erweiterter Datenverarbeitung von sehr hohem Nutzen. Dadurch waren satellitengestützte Eisradarbeobachtungen und zeitliche Driftkorrektur der Bilder täglich verfügbar. Tests mit unterschiedlichen Drohnen zur Eisbeobachtung zeigten ermutigende Ergebnisse für künftige Entwicklung eines automatisierten Eiserkundungssystems. Zudem ist die Rückverfolgung der Drift einzelner Eisschollen in unserem Forschungsgebiet nicht nur wichtig für die wissenschaftliche Analyse, sondern war auch nützlich zur Abschätzung der zu erwartenden Eistypen entlang unserer geplanten Route.

Unsere Stationen und Schnitte wiederholten nicht nur vorangegangene, hydrographische Beobachtungen der Hydrographie, von Spurenmetallen, Nährstoffen, Schadstoffen und mehrerer biologisch wichtiger Substanzen in Wasserproben, sondern auch Netzfischerei, teilweise zum ersten Mal in der zentralen Arktis (pelagisches Schleppnetz). Die Nutzung unterschiedlicher Geräte und Beobachtungsmethoden stellte auf dieser multidisziplinären Expedition eine Herausforderung dar, und nur die effiziente und konstruktive Kooperation aller Mitglieder der Wissenschaft und Crew machte dieses Unterfangen möglich. Die unterschiedlichen Eisinformationen wurden vollständig zur Planung der hydrographischen Schnitte, Eisstationen und Schleppaktivitäten herangezogen, und der Einsatz könnte sogar erweitert werden, indem zusätzliche Satellitenprodukte gekauft werden, um die zeitliche Verfügbarkeit von Eisinformationen zu verbessern. Eine zusätzliche Hilfe bezüglich der Eisstationssicherheit war die „First Navy“ Infrarotkamera, ein System, dass hochfrequente Thermalbilder der gesamten Umgebung (mit einer kleinen Lücke achtern, blockiert durch den Krähennestmast): Eisbären können durch dieses Kamerasystem sogar unter schlechten Sichtbedingungen, wie Dunkelheit oder Schneestürmen, erkannt werden (Abb. 1.8).

Zusätzlich zu *in situ*-Beobachtungen haben wir mehrere Fernerkundungsbeobachtungen durchgeführt, per Helikopter (z.B. Eisdicke), Radar (z.B. Wolken) und Radiometer (Oberflächenstrahlung). Extensives Ausbringen von eisbasierten, autonom messenden Systemen (driftende „Bojen“) und eine Verankerung erweiterten weiterhin unsere Sensormessungen in Raum und Zeit. Die geborgenen Verankerungen schlossen auch autonom arbeitende Wasser- und Sinkstoffbeprobung mit ein.

Unsere Beobachtungen erlauben einen Vergleich zu vorangegangenen Beobachtungen, um Veränderungen zu erfassen und eine verbesserte Referenz („baseline“) zu etablieren. Die Beobachtungsaufnahme ging quer über die tiefen eurasischen und Makarov-Becken, sowie die Gakkel- und Lomonosowrücken, praktisch quer zur Eis- und Ozeanzirkulation, die sich nahe der Oberfläche als Transpolardrift von den sibirischen Schelfgebieten bis zur Framstraße manifestiert. Die verschiedenen Substanzen, die in der Wassersäule durch die CTD/Rosettenprofile, sowie im Schnee und im Meereis beprobt wurden, erlauben Rückschlüsse auf die Details der Ozean- und Meereiszirkulation, sowie den Transport verschiedener Substanzen, z.B. Schadstoffe, Sediment oder Nährstoffe.

„Underway“-Beobachtungen durch CTD, Wasserprobennahmen und verschiedene akustische Geräte tragen weiterhin zu unseren Studien bei, und ermöglichten im Falle des Fischecholots, sogar die operationelle Planung der Netzeinsätze. Diese Beobachtungen wurden großenteils

bis in die Nordsee fortgesetzt und helfen uns, die Ergebnisse aus der Arktis im den Kontext niedererer Breiten zu interpretieren.

Änderungen sowohl im Meereis als auch in der Schichtung des oberen Ozeans werden von Atlantifizierung beeinflusst, wobei die Bedingungen im eurasischen Nordpolarmeer sich denen im Nordatlantik annähern, zusammen mit Änderungen im zeitlichen Ablauf von Meereisbildung und -schmelze. Dies wiederum zeigt Wechselwirkungen mit der Zirkulation des flüssigen Ozeans und des Meereises, in engem Zusammenhang mit der Verteilung verschiedener Substanzen, z.B. Makronährstoffe, Spurenstoffe („trace elements“) und deren Isotope, und einigen Tracern, unter anderem Fluorchlorkohlenwasserstoffe (FCWK), Mikronährstoffe, natürlich vorkommende und anthropogene Radioisotope as Zeitmarker, und potentielle Schadstoffe, wie Blei und Quecksilber. Einige davon sind passive Tracer, während andere mit der biogeochemischen Umgebung und dem Ökosystem interagieren, weshalb sie besonders zur Detektion entsprechender Änderungen geeignet sind. Die Quellen dieser Substanzen reichen von lokalem Niederschlag und Aerosolen bis hin zu Kontinentalabfluss und Austausch mit Ozeanen niederer Breiten. Eine Aufnahme der Meereisdicke und -verteilung verfolgt den fortschreitenden Rückgang der arktischen Meereisbedeckung. Zusätzlich werden die Beobachtungen der lokalen Oberflächenstrahlungsemission und spezifischen Phänomenen, wie Schmelztümpel, helfen, Satellitenmessungen in und um das Meereis zu verbessern. Eine umfangreiche Aufnahme des Ökosystems beinhaltete auch die Genetik kleiner Tiere, die Verteilung von planktonischen und sympagischen Arten bis hin zu den Habitaten und dem Verhalten größerer Organismen, wie dem Polardorsch. Ein wichtiger Aspekt ist hier der Vergleich mit ähnlichen Beobachtungsdaten in anderen Teilen der Arktis, z.B. der Beringsee. Zusätzlich zur Verbesserung unseres Verständnisses des kontemporären Ökosystems helfen die Messungen auch der Interpretation paläozenographischer Daten. Zusammen mit atmosphärischen Beobachtungen von Wolken, Niederschlag, Windgeschwindigkeit, einfallender Solarstrahlung und Aerosolen liefert Arc-Watch 2 eine umfangreiche Aufnahme des Atmosphäre-Meereis-Ozeansystems im zentralen Nordpolarmeer und eines Teiles des Kontinentalhangs der westlichen Barentssee.

Das Datenmanagement (“data management”) der einzelnen Gruppen an Bord sowie des übergreifenden Tasks „buoys“ (Bojen) wird in den jeweiligen Kapiteln beschrieben. In Publikationen von gruppenübergreifender Forschung und Daten kann auch die „Grant Number“ **AWI_PS144_00** genannt werden.

SUMMARY AND ITINERARY

The aim of this expedition was the large-scale, quasi-synoptic assessment of changes in the eurasian / central Arctic Ocean and on the Barents Sea continental slope. This includes changes throughout the full-depth ocean, the sea ice and the lower atmosphere. Changes in the seasonal cycle of sea ice amid varying atmospheric pressure patterns and ocean inflows have been prompting the need to thoroughly understand large-scale variability across the Eurasian Arctic. Prior expeditions that have followed the same aim include ArcWatch-1 (2023), TransArc II (2015), TransArc (2011) and SPACE/DAMOCLES (2007) during the International Polar Year (IPY); and observations by other ships during the Synoptic Arctic Survey (SAS) and other IPY expeditions. The known and expected changes mirror the impact of large-scale environmental processes, and the contributions from different sources and conditions

at the Arctic boundaries. The observations form part of a more than 30 years long data set that manifest variability in three-dimensional space and in time. Our expedition represents the first reassessment with a comprehensive breadth of observed variables and with a wide spatial coverage since 2015 (TransArc II), which includes revisiting several stations / sections with extensive regular and "trace-metal clean" sampling. Smaller-scale, local environmental processes were also a focus of this expedition and follow in the legacy of prior expeditions, such as the Multidisciplinary Observatory for the Study of Arctic Climate (MOSAiC). References to the cruise reports and the scientific literature are not given here; instead, the reader is referred to the Chapters 2 – 7 for each discipline.

ArcWatch-2/TransArc is a contribution to the international programmes GEOTRACES, Arctic ROOS/EuroGOOS and the International Arctic Buoy Programme (IABP). It is part of the Long-Term Observations (LTO) ArcWatch / Arctic Ocean and the Helmholtz programme oriented research POF 4 "Changing Earth – Sustaining our Future"; in particular, Topics 1, 2 and 6. The expedition forms a legacy to the Helmholtz strategic investment Frontiers in Arctic Marine Monitoring (FRAM) and forms a contribution to the infrastructure Marine Umweltrobotik und -Sensorik für nachhaltige Erforschung (MUSE; marine environmental robotics and sensors for sustainable exploration).

ArcWatch-2 set off in Tromsø on 9 August 2024, with *Polarstern* sailing to Longyearbyen (Svalbard, Norway; Fig. 1.1 and 1.2). Various underway measurements were carried out already in the Barents Sea and throughout the expedition. In Longyearbyen, we exchanged 2 scientists and carried out a calibration of the ship's EK80 echosounder. We then moved toward a test hydrographic station northeast of the archipelago around 83°N, carrying out a test with the pelagic trawl fishnet on the continental slope. After entering the consolidated sea ice, a test ice station with parallel hydrographic work followed around 85°N, 42°E, where we used the portside to access the ice via a gangway and the starboard side to deploy water profiling and sampling gear. The ship was often fixed with ice anchors and lines to be stable, in particular, in the presence of strong winds. Unfortunately, the weather did not allow helicopter surveys, yet at this point. Due to the overall ice situation (relatively low ice concentration in the Eastern and Central Arctic Ocean), it was decided to start the main programme with the easternmost transect (Section III, Fig. 1.1). On the intersect of the transit there with 60°E, we stopped for a station that would be re-assessed later in the season on the way back, also beginning trace-metal clean experimental incubation work. On the further way east toward Section III (Fig. 1.1) we started to carry out water column observations by expendable systems (XCTD) and stopped for one hydrographic station in a deep part of the Gakkel Ridge which showed signals of hydrothermal activity in the water column. Due to a crew member falling sick we had to return to Svalbard for a medical evacuation. The duration of the evacuation could be shortened because a long-distance helicopter ("Super Puma"; Fig. 1.3) of the "Sysselmesteren" of Longyearbyen took the decision to travel more than 400 nmi towards *Polarstern*. We were thus able to return to our working area only about one week later. We continued our hydrographic work and commenced with Section III, crossing the Nansen and Amundsen Basins into the Makarov Basin. This included sampling and process studies at different ice stations, that ran in parallel to extensive water column work, on the starboard side of the ship, including regular CTD, clean CTD (Fig. 1.4) and different nets for biological samples. Transit times in this region were fairly short due to overall loose ice cover. Finally, helicopter work commenced, albeit limited by the still prevailing bad weather conditions. Section III also included recovery of two seafloor-mounted moorings in the eastern Amundsen Basin, deployed in 2023, and re-deployment of a reduced version of one of the moorings. Although recovery in the ice was a great challenge, we managed to retrieve both moorings. As a curiosity we passed a large ice ridge along our way, on the surface the size of an iceberg, that turned out to be rafted shelf ice (Fig. 1.5). The open melt ponds on the sea ice changed as we progressed along the section to refrozen and snow-covered (see aereal drone photographs in Appendix A.5). As Section III was considered

a priority, its extension, which had been included as an option in the cruise proposal, became part of the actual cruise track. This decision was taken to get a better quantitative picture of the current state of the transpolar drift near its source. After ending Section III, we proceeded to a revisit of a station around 180°E, covered by both *Polarstern* and USCG *Healy* in summer 2015 ("GEOTRACES crossover station"). Next to water column work we also carried out a long ice station at this location (Fig. 1.6). We then proceeded to Section II, starting in the Makarov Basin along 125°E, crossing the Lomonosov Ridge, and onto the North Pole with extensive station work. At the North Pole we carried out another extensive station with hydrography and ice work, including a photo of the shipboard scientific party (Fig. 1.7). We then moved along the section towards the Gakkel Ridge, where we focused another extensive ice and water column station on a topographic depression, previously visited in 2015. Continuing south along about 60°E, we faced adverse ice conditions, forcing us to deviate several nmi westwards of the intended section for a few stations. Ending around 85°E, with a re-visit of PS144_9, just north of the Russian Exclusive Economic Zone, we proceeded towards our final section, carrying out helicopter flights and trawls along the way. Progress through the ice remained challenging on our way west, forcing us to take a route southwestward towards about 30°E, the longitude of the final section. The time lost due to the MedEvac forced us to significantly cut the station work along Section I. Overall, only the good progress made during Section III and toward the North Pole provided us with sufficient time, despite the MedEvac, to carry out all planned work in Sections III and II, and a few stations along Section I. After finishing our station work then commenced with our return home to Bremerhaven (Fig. 1.2), carrying out underway observations along the way into the North Sea, and arrived in port on the morning of 13 October, 2024.

Apart from helicopter-based route surveys assisting navigation of the ship through the ice, we greatly benefited from the satellite maps and advanced processing available, providing sub-km resolution remote ice radar observations and temporal drift correction of the images available approximately at daily frequency. Tests with different drones for ice observations showed promising results for future development of an *in situ*, uncrewed ice reconnaissance system. In addition, the backtracking of ice floes in our research area is not only important for scientific analysis but was also useful to estimate what type of ice to expect along the route.

Our stations and sections not only repeated prior observations of hydrography, trace metals, nutrients, contaminants and several biologically relevant substances in water samples but also net fishing, some carried out for the first time in the central Arctic (pelagic trawl). The use of different devices and observing methods represented a challenge on this multidisciplinary expedition, and only the efficient and constructive cooperation of all science and crew made this endeavour possible. The different types of available ice information were fully utilized to plan hydrographic sections, ice stations and trawls, and could even be expanded by purchasing additional satellite products to aid timely availability of ice information. An additional aid to ice station safety was the "First Navy" infrared camera, a system that provide a high-frequency thermal image of the full surroundings (with a small gap aft, blocked by the crow's nest superstructure): Polar bears can be detected with this camera, even in low-light or snow-storm conditions (Fig. 1.8).

In addition to *in situ* observations, we carried out several remote sensing observations, by helicopter (e.g. ice thickness), by radar (e.g. clouds) and radiometers (e.g. surface radiation).

Extensive deployments of autonomous ice-tethered systems (drifting "buoys") and a seafloor-mounted mooring further extend our sensor observations in space and time. The recovered moorings also included autonomous water and sediment sampling.

Our observations allow a comparison to prior observations to detect changes and establish an improved baseline. The survey crossed the deep Eurasian basins and part of the Makarov

Basin, as well as the Gakkel and Lomonosov ridges, thus effectively crossing the ice and ocean circulation, that near the surface is manifested as the Transpolar Drift from the Siberian shelves to the Fram Strait. The various substances sampled in the water column by CTD/ rosette casts and in the snow and sea ice allow to infer details of ocean and sea ice circulation, as well as the transport of various substances, such as pollutants, sediment or nutrients.

Underway observations by CTD, water samplers and various acoustic devices further aid our studies, and, in the case of the fish echosounder, even facilitated operational planning of net trawls. These observations largely continued from the Arctic into the North Sea and help us put the Arctic results in context with lower latitudes.

Changes in both upper ocean stratification and sea ice are subject to Atlantification, whereby conditions in the Eurasian Arctic Ocean approach those of the North Atlantic, along with changes in the timing of sea-ice formation and melt. This, in turn, feeds back with liquid ocean and sea-ice circulation, closely related to the distribution of various substances, such as macronutrients, trace elements and their isotopes, and a set of tracers, including Cluorofluorocarbons (CFC), micronutrients, naturally occurring and anthropogenic radioisotopes as time markers, and potential pollutants, such as lead and mercury. Several of these are passive tracers, whereas others interact with the biogeochemical environment and the ecosystem, making them powerful tracers of related changes. The sources of these substances range from local precipitation and aerosols to continental runoff and exchanges with lower-latitude oceans. An assessment of sea-ice thickness and distribution follow up on the ongoing decrease of the Arctic sea-ice cover. As an additional benefit, the observations of local surface emissivity and specific features, such as melt ponds, will help improve satellite remote sensing of the sea ice environment. A comprehensive assessment of the ecosystem also included the genetics of small animals, the distribution of planktonic and sympagic species up to the habitats and behaviour of larger organisms, such as polar cod. An important aspect here is the comparison to similar observational data in other parts of the Arctic, such as the Bering Sea. In addition to improving our understanding of the contemporary ecosystem the measurements also help the interpretation of palaeoceanographic records. Together with atmospheric observations of clouds, precipitation, wind speed, incoming solar radiation and aerosols ArcWatch 2 delivers a comprehensive assessment of the atmosphere-sea ice-ocean system in the central Arctic Ocean and, to a limited extent, the western Barents Sea slope.

Details of the data management for each on-board group and the overarching task “buoys” are given in the corresponding chapters. For cross-group research and data publications, the Grant Number **AWI_PS144_00** may also be used.

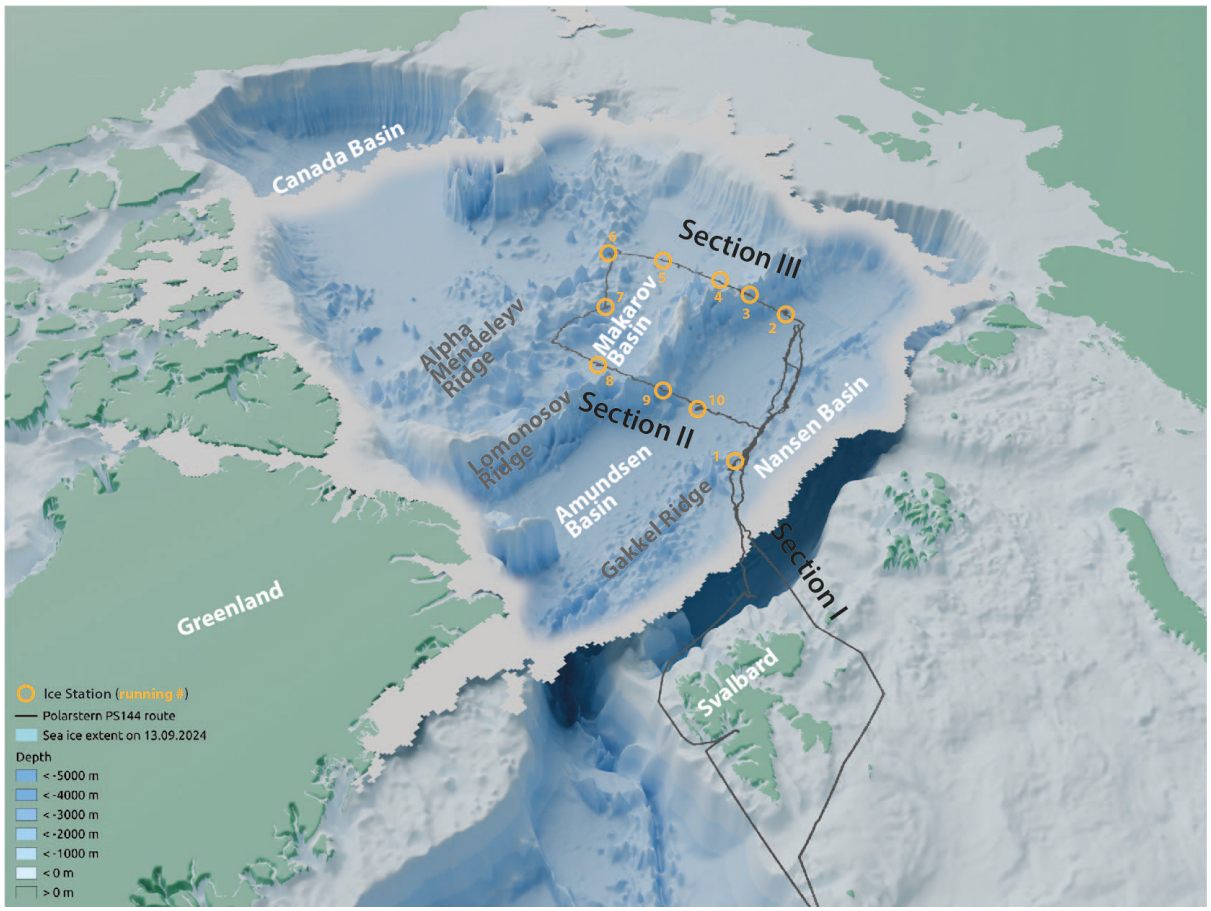

Abb. 1.1: Fahrtroute und Stationen sowie hydrographische Schnitte I – III der Expedition PS144 (ArcWatch-2/TransArc). Die Reise begann am 9. August 2024 in Tromsø und endete am 13. Oktober 2024 in Bremerhaven. Die Karte zeigt die Fahrtroute über einer dreidimensionalen Topographie (IBCAO V. 4.2; Jakobsson et al., 2020), eingebettet in die Eisausdehnung am 13. September, 2024. Auch gezeigt sind die die Positionen der Eisstationen, fortlaufend numeriert. Das entsprechende Event-Label findet sich in Appendix A.4. Der Nordpol liegt nahe der Eisstation 8 in der Karte, und die "Crossover" GEOTRACES-Station ist an der Position von Eisstation 7. Schnitt I besteht aus drei Stationen am Kontinentalhang und einer auf dem Schelf östlich von Svalbard.
3-D-Karte mit Legende von Jonathan Bahlmann.

Fig. 1.1: Cruise track and stations as well as hydrographic sections I – III of the expedition PS144 (ArcWatch-2/TransArc) around the main working area. The expedition started on 9 August 2024 in Tromsø and ended on 13 October 2024 in Bremerhaven. The map shows the cruise track with three-dimensional topography (IBCAO V. 4.2; Jakobsson et al., 2020), embedded in the ice extent on 13 Sep, 2024. Also shown are the location of the ice station, labelled by a running number. The corresponding event label can be found in Appendix A.4. The north pole is close to ice station 8 in the map, and the crossover GEOTRACES station is at the location of ice station 7. Section I consists of three stations on the continental slope and one on the shelf east of Svalbard.
3-D map and legend by Jonathan Bahlmann

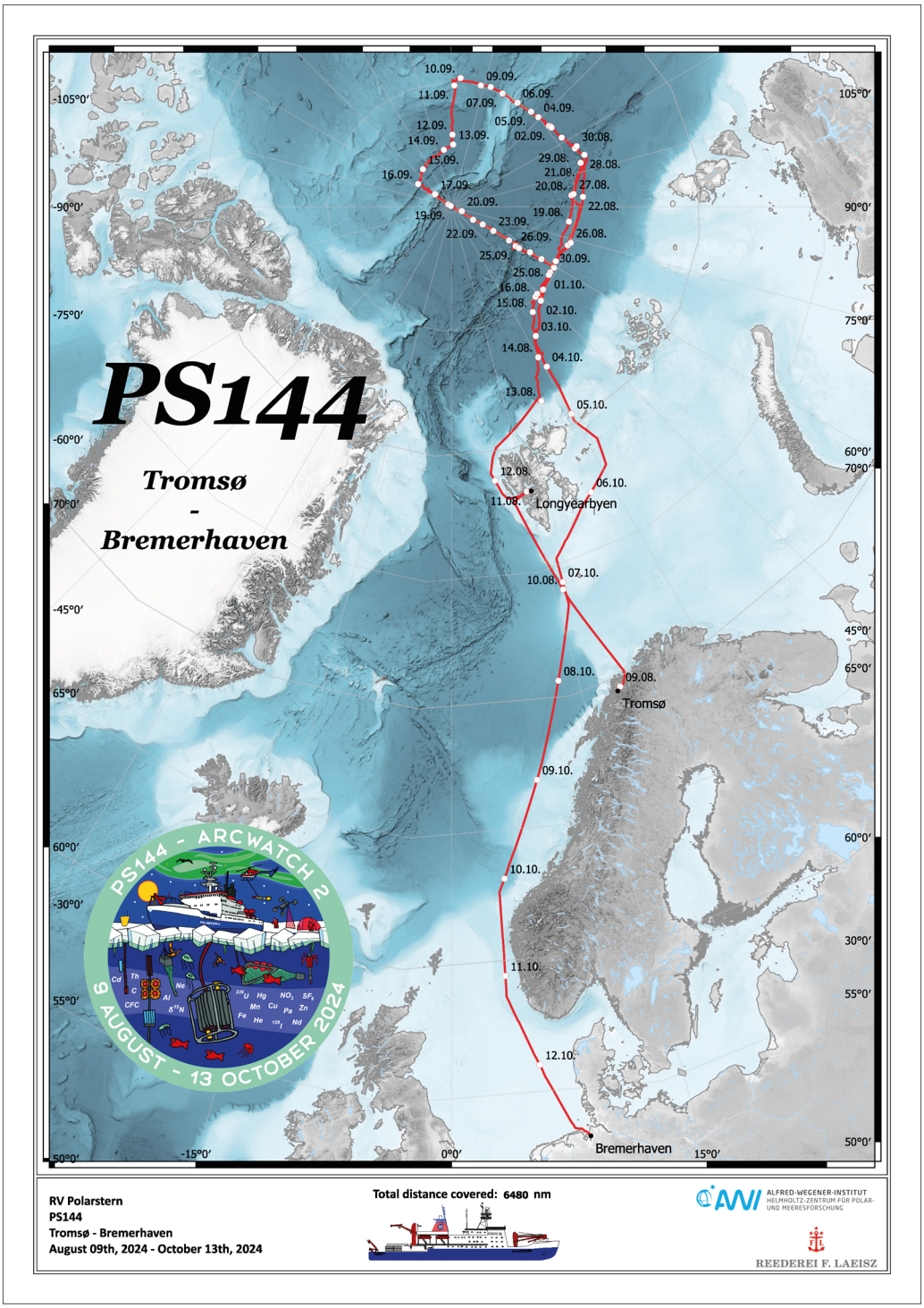

Abb. 1.2: Die Karte zeigt die gesamte Fahrtroute zwischen Abfahrts- und Ankunftshafen, mit Datum (Monat, Tag) entlang der Route. Siehe https://doi.pangaea.de/10.1594/PANGAEA.974029 für eine Darstellung des Master tracks in Verbindung mit der Stationsliste für PS144. Karte: Andreas Winter

Fig. 1.2: The map shows the full cruise track between ports of departure and arrival, with dates (month, day) along the track. See https://doi.pangaea.de/10.1594/PANGAEA.974029 to display the master track in conjunction with the station list for PS144. Map: Andreas Winter

Abb. 1.3: Der Helikopter vom Typ “Super Puma” landet am 24. August 2024 auf Polarstern während der medizinischen Evakuation. Foto: Christian Rohleder

Fig. 1.3: The “Super Puma” helicopter landing on the Polarstern during the medical evacuation on 24 August 2024. Photo: Christian Rohleder

Abb. 1.4: Foto beider auf PS144 genutzten CTD/Rosetten-Systeme. Das “reguläre” System (links) und das spurenmetallreine System mit “Badehauben” zum Schutz vor Kontamination (rechts). Foto: Walter Geibert

Fig. 1.4: Photo of both CTD/rosettes used during PS144. The regular system (left) and the trace-metal clean system with “shower caps” to protect from contamination (right). Photo: Walter Geibert.

Abb. 1.5: Dronenfoto des großen Eisrückens, der am Ende als übereinander geschobenes Schelfeis identifiziert wurde, um 85°N, 130°E am 3. September 2024. Polarstern ist im Hintergrund als Größenvergleich zu sehen (Event PS144_ICE_RIDGE_MAVIC).
Foto: Niklas Neckel

Fig. 1.5: Drone photo of the large ice ridge that turned out to be rafted shelf ice around 85°N, 130°E on 3 September 2024 with Polarstern in the background (Event PS144_ICE_RIDGE_MAVIC).
Photo: Niklas Neckel

Abb. 1.6: Dronenfoto der Eisstation an der Position der “Crossover”-Station um 180°E (PS144_85-1). Polarstern ist am Eis mit Festmacherleinen und Eisankern festgemacht. Foto: Niklas Neckel

Fig. 1.6: Drone photo of ice station at the crossover station around 180°E (PS144_85-1). Polarstern is fixed to the ice floe by lines and ice anchors. Photo: Niklas Neckel

Abb. 1.7: Gruppenfoto am Ende der Eisstation nahe Nordpol, 19. September 2024 (PS144_109-1). Foto: Klaus Guba

Fig. 1.7: Group photograph near the end of the ice station close to the North Pole, 19 September 2024 (PS_144_109-1). Photo: Klaus Guba

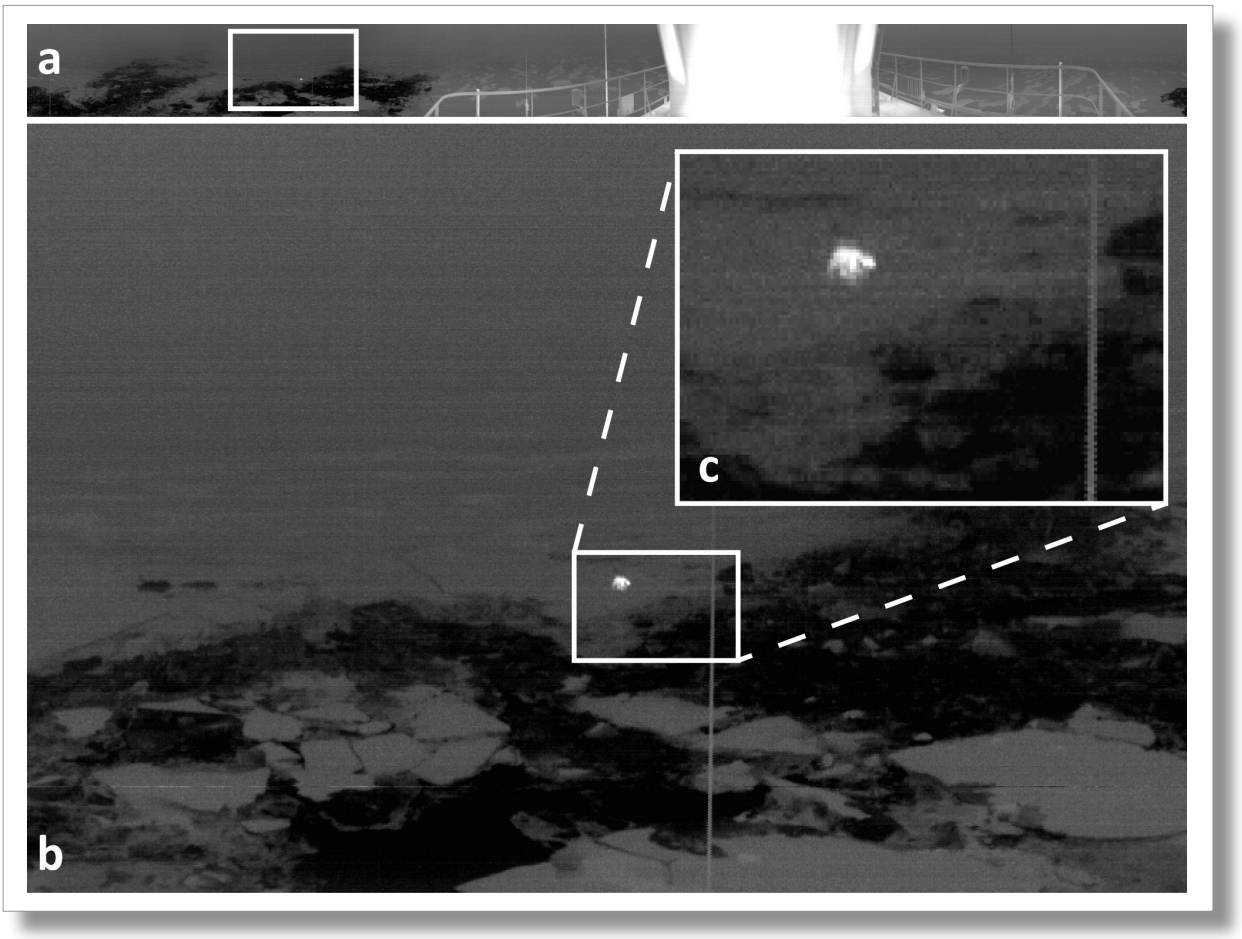

Abb. 1.8: "First Navy" thermales Infrarotbild, wobei warme Signale in weiss und kalte in schwarz dargestellt sind. Gezeigt sind die Übersicht (a), eine Vergrößerung der weißen Box (b) und eine Vergrößerung des Eisbären (c). Die Kamera war im Krähennest der Polarstern installiert. Bild: First Navy Kamera, kompiliert von Mario Hoppmann

Fig. 1.8: "First Navy" thermal infrared image, with warm signals in white and cold in black. Shown are the full view (a), zoom into the white box in a (b) and zoomed onto a polar bear (c). The camera was mounted in the crow's nest of Polarstern. Image: First Navy Camera, compiled by Mario Hoppmann

References

Jakobsson M, Mayer LA, Bringensparr C et al. (2020) The International Bathymetric Chart of the Arctic Ocean Version 4.0. Sci Data 7, 176. https://doi.org/10.1038/s41597-020-0520-9

WEATHER CONDITIONS DURING PS144

Patrick Suter, Christian Rohleder DE.DWD

Transit Tromsø (Norway) – Longyearbyen (Svalbard)

Polarstern departed from Tromsø on the afternoon of 9 August, with. On the transit to Svalbard, *Polarstern* travelled between a low-pressure area east of Iceland and a high-pressure area over the Kara Sea in a fresh to strong easterly current. After initially cloudy and partly wet conditions, the sun began to shine more and more from 10 August. The waves reached 1 to 1.5 m. The easterly to southeasterly wind strengthened to 7 to 8 Bft just west of the southern tip of Svalbard with jet effects on the night to 11 August, then fluctuated between 4 and 7 Bft during the day along the coast and in the Isfjord off Longyearbyen. Without docking in Longyearbyen, there was an exchange of people and first test measurements from the afternoon of 11 August. With a foehn-like southeasterly wind, this was accompanied by mostly sunny and exceptionally warm conditions of up to 20°C.

Transit Longyearbyen (Svalbard) – Section III

On the night to 12 August, *Polarstern* left the Isfjord and travelled northwards in the eastern part of the Fram Strait. In the meantime, a low-pressure trough had moved from the Lofoten Islands into the Fram Strait. In the morning hours, this caused a sharp transition from sunshine to overcast stratus clouds and fog. Subsequently, nimbostratus clouds also brought rain and drizzle, while the wind and temperatures decreased significantly.

By the morning of 14 August, *Polarstern* travelled north of Svalbard to the northeast with first research works and had reached loose sea ice last evening. An increasingly strong southwesterly current developed between a low in the northeast of Greenland and a high over the Barents Sea. The air was quite humid and repeatedly prone to fog. Travelling further eastwards along approximately 85°N, the work now took place in dense sea ice throughout. By 15 August, the aforementioned high had moved into the Kara Sea. On its northwestern edge, the westerly wind weakened. At the same time, a secondary low had developed north of Svalbard by 16 August. The weak secondary low subsequently moved eastwards just south of the ship, accompanied by weak winds and a lot of moisture. As a result, fog and occasional light drizzle were recorded for over 40 hours without interruption until the night to 17 August.

On 17 August, a ridge joined the high-pressure zone over the Kara Sea to the north. With mostly moderate winds from northeast and slightly drier and cooler air near the ground, the stratus clouds lifted slightly and broke up at times. At the same time, a warm front from a strong low over the Fram Strait approached into the night. With negative temperatures on the ground, the warm front lead to freezing rain and some ice accumulation on the ship until the morning. Behind the warm front and with intermediate high-pressure influence, the low clouds temporarily dissipated on 18 August, but returned in the afternoon as partly very low stratus and fog.

By 19 August, a secondary low had formed north of Svalbard. This subsequently moved eastwards with a lot of moisture to the north of the sailing area. The southeasterly wind increased to 5 to 6 Bft and turned over west to southwest during the day. The high-pressure

zone over the Kara and Laptev Sea then took over again until 21 August. *Polarstern* slowly moved eastwards on its northern flank under weakening westerly winds. With ongoing warm air advection and saturated air in the lower layers, low clouds and fog continued to be loyal companions.

On the evening of 21 August, research operations had to be interrupted due to a medical emergency on board. The ship turned around north of Severnaya Zemlya and shortly before reaching Section III, heading back to Svalbard. On the return transit along about 85°N to the west, the ship moved between the high-pressure zone over the Laptev Sea and a low-pressure zone between the North Pole and north of Svalbard, within a strong southwesterly current. Starting from the low-pressure zone, a low approached from the west until 23 August. While south-westerly winds of 6 to 7 Bft and nimbostratus clouds prevailed in the warm front, the winds temporarily eased as the centre of the low approached. In the afternoon, colder and increasingly drier air flowed in behind a cold front with renewed strong northerly winds. By 24 August, a high had established itself to the northeast of Svalbard. To the north of this, the current turned to west with a decrease and the low cloudiness changed to lifted altocumulus with very good visibility. Due to favourable flight conditions, the expedition member was evacuated by CHC Helicopter Service AS on the evening of 24 August. During this SAR operation, the rescue helicopter covered around 450 nautical miles each way from Longyearbyen and was refuelled on board.

Polarstern then headed east again. Initially, the ship moved along the western edge of the eastward-moving high. The cloud cover continued to decrease, but from midday on 25 August stratus formed, which in the afternoon, in the form of a wall of fog, led to an abrupt end to the ship's own helicopter operations. A strong low-pressure complex then approached from Svalbard. Between the pressure systems, the southeasterly current increased to 6 to 7 Bft by 26 August, with gale-force gusts of around 8 Bft at times. As the wind increased, the cloud cover temporarily lifted again during the day ahead of a warm front. By the evening, the warm front and strong warm air advection were followed by low-lying nimbostratus clouds. This initially brought snow and, in the night to 27 August, prolonged freezing rain. Until 29 August, the ship remained in front of the slowly northeastward-moving low-pressure zone under the influence of a strong and humid south to southwesterly current. Overcast and low-lying cloud conditions as well as repeated fog and light drizzle were a permanent feature. Meanwhile, *Polarstern* had reached the starting point of Section III north of the Laptev Sea near 84°13‘N 109°40’E on 28 August.

Section III (from 84°13´N 109°40´E to 85°46´N 179°30´E)

Section III ran between 84° and 85°N, whereby this was processed station by station with a slow eastward shift. On 29 August, the low-pressure zone moved north of *Polarstern* to the east. The strong southwesterly current turned to northwest behind the low. This improved the weather conditions with the inflow of colder and slightly unstable air until 30 August. In the afternoon, a new small low was already approaching from northwest. With warm air advection, this once again caused deep stratus and partly freezing fog, but a weakening westerly wind. The intermittent light precipitation was a mixture of snow drizzle and supercooled drizzle.

Already on 1 September, the ship moved onto the downstream area of the next low-pressure zone in the west. The current from southwest to west reached 6 Bft and a warm front with partly freezing drizzle took over. The low moved northeastwards and with its cold front, the current turned north with 6 to 7 Bft until 2 September. The precipitation turned into partly moderate snowfall. Temperatures dropped from around 0°C into the negative range, where they would remain until the beginning of October. As a result, the air was dried out from above, but fields of mist remained close to the ground, while the sun was shining through.

Another low, moving eastwards to the north of Svalbard, touched the research area during the night to 3 September and in the morning. This was accompanied by decreasing westerly winds, a frontal system and more moisture. On 4 September, northwesterly winds of 5 to 7 Bft and somewhat friendlier conditions with a few snow showers prevailed behind the low. The low-pressure activity did not come to an end in the following days. On 5 and 6 September, the research took place between two lows. With moderate southerly winds at times, a transition to low-lying nimbostratus took place, from which snow fell repeatedly. On 7 September, the lows shifted to the northeast. Once again, the current turned to northerly directions with 5 to 6 Bft, and somewhat drier and slightly unstable air with good visibility flowed in behind the low-pressure zone.

After this, a high moved from the southwest across the research area to the northeast. Cold and drier air caused the clouds to dissipate in the course of 8 September. On 9 September, in addition to sunshine, there was an increase in the formation of shallow mist and fog patches with rime frost. At the same time, a stationary low persisted north of the Bering Strait. Starting from this, a surface trough approached by the evening, bringing increasing moisture with weak to moderate southeasterly winds and warm air advection. This led to a lot of cloud cover, occasional light snow and a few episodes of fog. On 11 September, Section III was completed in the area of the dateline at 180°E.

Transit to Section II

From 11 September, the transit first led northwards along 180°E to a station near 87°30'N. From 14 September, the ship continued northeastwards. A high-pressure ridge approached from 12 September, starting from a strong high north of Svalbard. This led to a significant improvement in the weather. With easterly winds of 4 to 5 Bft and the influx of very cold air, the fog lifted abruptly in the afternoon and the sun shone alongside medium-level cloud fields. At temperatures of around -12°C, the few open water areas increasingly saw the formation of lake smoke and very shallow patches of fog. After the fog patches spread further at first and gained vertical thickness, they dissipated again on 13 September with northerly winds. As a result, despite denser stratocumulus and altocumulus fields, it was friendly and partly sunny. These medium-level cloud fields also dissipated. This meant that the low standing sun undisputedly took over the sceptre on 14 September.

In the meantime, the high had moved into the Kara and Laptev Sea and by 15 September, *Polarstern* found itself between two lows. One was located near the North Pole and the second north of Canada. Moderate to fresh southwesterly winds again brought in humid air and thus dense cloud cover. This repeatedly resulted in light snow, which in some cases led to whiteout conditions.

Section II (from 88°20´N 125°W across the North Pole to 85°15´N 60°E)

By 16 September, the first station of Section II was reached, near 88°20'N 125°W. In the meantime, the first low moved away towards the Laptev Sea. The second slowly weakened, but remained stationary north of the Queen Elizabeth Islands and continued to shovel moisture into the research area in phases. At the same time, a high-pressure zone formed near the North Pole. With decreasing winds, only a little snow and occasionally lifted cloud bases, the weather improved somewhat at times. In addition to further station work along 125°W, *Polarstern* reached the North Pole on the evening of 18 September. During the ice station at the North Pole on 19 September, high-pressure weather prevailed temporarily, with repeated patches of fog spreading during the course of the day after the clouds had cleared and the air had cooled.

In the course of 20 September, a low over the Beaufort Sea with winds from northwest to west 4 to 5 Bft brought a weakly active warm front and thus increasingly dense cloud cover and some snow to the North Pole. Meanwhile, *Polarstern* had moved away from the North Pole to do further station work along around 60°E. From 21 September, high-pressure weather prevailed again. Starting from a high over the Fram Strait, a ridge reached until north of Greenland, but slowly moved eastwards towards the North Pole. As the ridge axis moved through, the wind slowly shifted from north/northwest to west/southwest. With very cold air and temperatures as low as -15°C, this resulted in quite sunny weather in addition to occasional shallow patches of fog and a few altocumulus fields. Just in time for the astronomical start of autumn, the polar day ended in the afternoon of 22 September with the first sunset.

On 23 September, the high-pressure zone had shifted slightly towards the Kara Sea and a weak low slowly moved across the research area from the North Pole. After westerly winds of 4 to 5 Bft initially blew on its southern flank, the temporarily variable winds shifted to northeast as the low passed through by 24 September. The low also brought moderately humid air and often very cloudy conditions. With repeatedly light snow, there were at times moderate to poor visibility as well as poor contrast and horizon.

By 25 September, a high had established at the North Pole. The low moved westwards and thus lost influence. The current turned east to southeast and temporarily freshened up a little with 5 to 6 Bft. On 26 September, a high-pressure ridge moved westwards from the high over *Polarstern*. This led to a wind shift to northeast to east. With the high pressure at the North Pole and the slight approach of a storm over the Barents Sea, the wind increased to mostly 6 Bft from 27 September. During these days, the weather was variable. Bad conditions with repeatedly with low stratus, light snow, rare patches of fog and better phases with lifted clouds and good visibility as well as better contrasts and horizon alternated.

By 29 September, the centre of the high had shifted slightly towards Greenland and a ridge formed north of *Polarstern* in the direction of the Laptev Sea. At the same time, the storm over the Barents Sea weakened somewhat. This led to a decrease in the pressure gradient, resulting in weaker winds from northeast to east and calm conditions. As the cloud cover decreased at the same time, the air near the ground cooled considerably. This caused fog to form on the ground, which subsequently remained quite persistent and formed a few centimetres of rime frost on the ship. The lowest temperature of the expedition was measured on 29 September at -16.9°C. On the night to 1 October, Section II ended with the station near 85°15‘N 59°30’E. Until then, the calm, but repeatedly foggy weather persisted with the high-pressure ridge north of *Polarstern*.

Transit to Section I

The transit to Section I ran to the southwest. Meanwhile, on 1 October, the above-mentioned ridge moved southwards over the sailing area and the current turned to northerly directions with 4 to 5 Bft. With the simultaneously drier air, the fog lifted in the afternoon and, apart from a few high clouds, it was mostly sunny. In the night to 2 October, a small-scale low with more moisture followed from the north. During the course of the day, this moved just east of the ship to the south and temporarily caused a freshening northwesterly current. In addition to en-route measurements, another station work was done near 83°50’N 33°E on 3 October. This was followed by another small low north of Greenland by 3 October, which touched the research area to the southwest. With this repeated succession of several lows and at times frontal-like systems, dense low clouds and occasional snow with poor visibility, contrast and horizon often prevailed from 2 October onwards. There was also a brief episode of fog, on 3 October. Meanwhile, *Polarstern* had reached the sea ice edge northeast of Svalbard on 4 October. This was the starting point for Section I with a first station near 82°42‘N 30°50’E.

Section I (from 82°42´N 30°50´E to 81°51°N 30°55´E)

Embedded in the northerly current, another low moved from the north to just south of the ship by 4 October. On its rear side, the current from the northeast to east reached 5 to 6 Bft. As the ship travelled south in open water, the weather improved slightly in the afternoon and the dense low stratus lifted to stratocumulus. On the evening of 5 October, the station work was completed with a CTD just west of the island of Kvitøya (Svalbard). The return transit in the northern Barents Sea then began.

Transit to Bremerhaven

A low moved southwest from Franz Josef Land and accompanied *Polarstern* in the Barents Sea with a frontal-like system and northerly winds of 4 to 5 Bft. By 7 October, another small low had formed south of Svalbard. As a result, *Polarstern* travelled just behind of it in the northern part of the Norwegian Sea. The current turned east to southeast, fluctuating between 3 and 6 Bft. The weather was changeable with variable cumulus clouds and intermittent snow/small hail showers. In addition, on 7 October, air temperatures above the freezing level were recorded for the first time since 1 September. On 8 October, the low moved away to the west. At the same time, a surface trough remained on the Norwegian coast. The return transit was also very calm at first in terms of waves, with heights of 1 to 1.5 m. By 10 October, a storm had formed from the surface trough near the Lofoten Islands. By then, *Polarstern* was already moving far to the south within northerly winds of 4 to 6 Bft and again changeable showery weather. In the course of 10 October, an increasing swell from northwest of 2.5 to 3 m arrived. With partly clear skies, polar lights adorned the night sky over the Norwegian Sea several times.

On 11 October, a secondary low moved from the Shetland Islands to southern Norway. However, the strongest wind field of the surface trough was south of the sailing area. The northwesterly to westerly wind fluctuated between 4 and 6 Bft with numerous showers. In the North Sea on 12 October, *Polarstern* was moving on the downstream area of a gale near the Hebrides. The stormy current from southwest to south blew with 7 to 8 Bft. The sea with swell from the northwest to west reached up to 3.5 m. The gale moved southeastwards across the North Sea and steered an active cold front across the German Bight during the night to 13 October. In connection with this, 9 Bft and gusts of up to 50 KT (10 Bft) were temporarily measured. The rear side of the low also gave the expedition participants a stormy reception in Bremerhaven. *Polarstern* docked in Bremerhaven in the morning of 13 October, bringing the PS144 expedition to an end after 66 days at sea and in the ice.

2. MARINE GEOCHEMISTRY – MGC

Stephan Krisch[1,2], Alexandra Bettinelli[3], Frederik Gäng[4], Walter Geibert[3], Aude Pin[1], Andreia C. M. Rodrigues[5], Yaqing Ruan[1], Ingrid Stimac[3], Marcel Scheiwiller[6], Christian Völkner[3]
not on board: Eric Achterberg[1], Alex Baker[7], Thomas Browning[1], Tim M. Conway[8], Lars-Eric Heimbürger-Boavida[5], Katharina Pahnke[4], Laura Whitmore[9], Núria Casacuberta Arola[6], Mengli Chen[10], Xianfeng Wang[11]

[1]DE.GEOMAR
[2]DE.TUBS
[3]DE.AWI
[4]DE.UOL
[5]FR.MIO
[6]CH.ETH
[7]UK.UEA
[8]US.USF
[9]US.UAlaskaFairbanks
[10]SI.NUS
[11]SI.NTU

Grant-No. AWI_PS144_01

Objectives

Introduction

While the importance of trace elements for biota and as tracers in the ocean has long been recognized, the ability to measure the most contamination-prone of them only developed in the last decades. In the following decades, a large assessment of the global distribution of trace elements and their isotopes (TEIs) evolved, internationally organized and co-ordinated in the GEOTRACES programme (www.geotraces.org). This programme aims at producing section studies and process studies of the world's oceans that cover the most important water masses and processes, with pre-defined sampling, intercalibration and data reporting requirements. As an exception, the Arctic Ocean is now covered for the second time by the GEOTRACES programme, also building on previous cruises in the International Polar Year, recognizing its particularly sensitive nature to warmer temperatures. The marine geochemistry team covers very diverse tracers with vastly differing sampling requirements, which is why they are described in sections by the individual sub-teams below. The work is closely connected to other working groups, in particular BTM, MBC and PO. The AWI trace-metal clean CTD is a relatively new addition to the pool of sampling devices at AWI, and it is run here in a collaborative effort by scientists from GEOMAR and AWI, joined by other national and international expert groups that are presented below.

Tab. 2.1: GEOTRACES parameters sampled during PS144

GEOTRACES parameter	Name	Institute
Bio-essential TM	Yaqing Ruan Stephan Krisch Eric Achterberg	DE.GEOMAR
Particulate TM	Stephan Krisch Yaqing Ruan Eric Achterberg	DE.GEOMAR

GEOTRACES parameter	Name	Institute
Fe isotopes	Stephan Krisch Tim M. Conway	DE.TUBS
Pb, Pb isotopes	Yaqing Ruan Mengli Chen Xianfeng Wang	DE.GEOMAR SI.NUS SI.NTU
Hg, MeHg	Andreia C. M. Rodrigues Lars-Eric Heimbürger-Boavida	FR.MIO
REE, Nd isotopes	Frederik Gäng Katharina Pahnke	DE.UOL
^{14}C, ^{39}Ar, ^{129}I, ^{236}U	Marcel Scheiwiller Núria Casacuberta Arola	CH.ETH
$^{230,232,234}Th$, ^{231}Pa, $^{226,228}Ra$ isotopes	Walter Geibert	DE.AWI
Ba	Walter Geibert	DE.AWI
$DI^{13}C$	Walter Geibert	DE.AWI
NO_3 and Si isotopes	Raja Ganeshram, Margot Debyser	UK.UEdinburgh
Ga	Laura Whitmore	US.UAlaskaFairbanks
Aerosols	Alex Baker	UK.UEA

Tab. 2.2: Ancillary parameters sampled during PS144.

Parameter	Name	Institute
Macronutrients (NO_3, NO_2, PO_4, $Si(OH)_4$)	Sinhué Torres-Valdes André Mutzberg	DE.AWI DE.GEOMAR
DIC/TA	Martha Gledhill	DE.GEOMAR
Bioassays	Aude Pin Stephan Krisch Thomas Browning	DE.GEOMAR
DOC (for MBC group)	Rainer Amon	US.TAMU
$\delta^{18}O$ (for MBC group)	Dorothea Andersen	DE.CAU
Salinity (for PO group)	Sandra Tippenhauer, Céline Heuzé	DE.AWI

Aerosol trace metals and major ions

Atmospheric deposition is an important source of nutrients to the open ocean (Hamilton et al., 2022). Advection of air masses across the shelf break has the potential to connect the continental interior to nutrient demand in remote ocean regions. Although Arctic Ocean productivity does not usually depend on aerosol deposition, recently it has been suggested that Siberian forest fires and long-range transport of smoke increased offshore productivity in the Eurasian Basin in summer (Ardyna et al., 2022). Aerosols advected from lower latitudes may also carry a significant load of (natural or anthropogenic) pollutants to the Arctic (Law and Stohl, 2007). High concentrations of aerosol pollutants including lead, copper and cadmium are typically observed in winter and spring (‘Arctic haze’) (De Vera et al., 2021; Gong and Barrie, 2005), however, local sources and long-distant transport of pollutants may also be present in summer (Conca et al., 2019). During PS144, we have obtained 10 samples during the ships voyage across the study region. Due to snowing, aerosol sampling focussed on the

Eurasian Basin where snow events where much less prominent. With these samples, we wish to assess atmospheric contributions to the marine pool of bio-essential (i.e. Fe, Mn, Co, Ni, Cu, Zn, Cd) and pollutant (i.e. Cd, Pb, As) aerosol trace metals and major ions (i.e. Na^+, Cl^-, SO_4^{2-}, NO_3^-, PO_4^{3-}). After analyses at the UEA, it is our aim to investigate the source regions of aerosols and its impact on primary production in the Eastern Arctic Ocean. Through dissolution experiments, we will determine the fraction of aerosol trace metals and macronutrients that are potentially available to phytoplankton in late summer.

Nutrient addition bioassay experiments

The Arctic Ocean has seen an increase in primary production of ~57% between 1998 and 2018 (Lewis et al., 2020), which is most likely supporting higher trophic levels and enhanced carbon export. Although this being the case, little is known about the factors that controls phytoplankton growth in the Arctic. From trace metal data of PS94 and calculation of nutrient deficiencies relative to typical phytoplankton requirements (Rijkenberg et al., 2018), it has been suggested that primary production in the Nansen Basin is limited by the availability of dissolved iron (Fe), conditions, which in future - due to “Atlantification” of large parts of the Eastern Arctic Ocean - might become increasingly prominent. While there is evidence for light and fixed nitrogen (N) being the primary factors controlling phytoplankton growth in the western parts of the Arctic Ocean (Mills et al., 2018; Ortega-Retuerta et al., 2012), with evidence of phytoplankton co-limitation by light, fixed N and the micronutrient Fe in late summer (Taylor et al., 2013), experimental evidence on the nature of surface phytoplankton nutrient limitation is missing for the Eastern and Central Arctic Ocean. In the scope of PS144, we aimed to provide experimental evidence on the nature of phytoplankton nutrient limitation through the conduction of bioassay (nutrient addition) experiments, testing for Fe, N or Fe/N (co-)limitation of phytoplankton growth along the cruise track. Major aim of the experimental work on-board and in the home-based laboratory is to quantify the response of phytoplankton growth (measured as Chlorophyll-a) to additions of potentially limiting nutrients, and establish relationships to prevailing water masses in the Eastern and Central Arctic Ocean. To monitor the initial conditions and to investigate into potential responses to future change, our work included the sampling for the micronutrients iron (Fe), manganese (Mn), cobalt (Co), nickel (Ni), copper (Cu), zinc (Zn) and cadmium (Cd) and the macronutrients nitrate (NO_3), nitrite (NO_2), silicic acid ($Si(OH)_4$) and phosphate (PO_4) in collaboration with the MBC group.

Dissolved and particulate trace metals (Fe, Mn, Co, Ni, Cu, Zn, Cd)

The Arctic Ocean is subject to considerable change due to anthropogenic climate forcing (Meredith et al., 2019). Although the Arctic Ocean has seen an increase in primary production of ~57% between 1998 and 2018 (Lewis et al., 2020), little is known about the factors that drive this increase in phytoplankton growth, including micronutrient availability. Enhanced riverine discharges (Feng et al., 2021), increased shelf erosion and offshore transport of sediment material (Kipp et al., 2018), sea-ice decline (Spreen et al., 2008) and an ‘Atlantification’ of large parts of the Eastern Arctic Ocean (Polyakov et al., 2017; Wang and Danilov, 2022) have ramifications on trace metal cycling and micronutrient availability also in the region downstream to the Arctic Ocean including the Greenland Sea (Krisch et al., 2022).

With PS144, we aim to assess the changes in sources, cycling and sinks of dissolved micronutrients against previous expeditions from 2007 (PS70) and 2015 (PS94, ‘TransArc 2’). By resampling station from PS70 and PS94, it is the aim of our work to extend the timeline of Arctic Ocean micronutrient cycling at a sub-decadal resolution which we deem is crucial for the projection of future ecosystem services including primary production, carbon sequestration and food web structure in the Central Arctic and high-latitude North Atlantic Ocean.

In the scope of PS144, our objectives were:

- Determining the horizontal and vertical distributions of the dissolved and particulate (labile and refractory) fractions of Fe, Mn, Co, Ni, Cu, Cd and Zn in the Eastern and Central Arctic Ocean to full depth.
- Investigating into sources, cycling and sinks of dissolved Fe, Mn, Co, Ni, Cu, Cd and Zn with particularly emphasis on the upper water column to 750 m depth.
- Quantifying lateral and vertical export fluxes of the dissolved trace metals dFe, dMn, dCo, dNi, dCu, dZn, dCd, and dPb across two sections following the advection of the Transpolar Drift.
- Quantifying nutrient stoichiometries and investigating the extent of late summer fixed N and dFe deficiencies in the Central and Eastern Arctic Ocean relative to typical phytoplankton requirements.

Dissolved Fe isotopic composition (δ^{56}dFe)

The Arctic Ocean is subject to considerable change due to anthropogenic climate forcing (Meredith et al., 2019). This change manifests itself in enhanced riverine discharges (Feng et al., 2021), increased shelf erosion and offshore transport of sediment material (Kipp et al., 2018), sea ice decline (Spreen et al., 2008) and an 'Atlantification' of large parts of the Eastern Arctic Ocean (Polyakov et al., 2017) all of which have ramifications on Fe cycling and Fe availability. Through the use of the natural isotopes ^{54}Fe, ^{56}Fe, ^{57}Fe and ^{58}Fe, it is possible to investigate the provenance of dFe to the water column and trace key aspects of oceanic Fe cycling such as biological uptake, particle scavenging and speciation changes (Fitzsimmons & Conway, 2023).

In the scope of PS144 we aim to

- Characterise surface Fe-transport,
- Investigate biological drawdown and abiotic scavenging of dFe
- Calculate the relative contribution of hydrothermal venting, reductive and non-reductive sedimentary release to the dissolved pool in the Eastern and Central Arctic Ocean.

Special emphasis is put on the characterisation of sources and Fe cycling to the Nansen Basin and surface waters of the Transpolar Drift. Sampling for dFe isotope composition is focussing on the upper water column to 500-750 m depth to investigate into internal cycling of dFe related to primary production at stations that cover the interplay between the two diverse nutrient regimes.

Rare earth element concentrations and neodymium isotopes

The unique conditions in the Arctic of input, removal, and exchange processes in relation to particle composition, particle fluxes, and circulation are acting on trace element and isotope distributions in the Arctic Ocean. Particularly, cruise PS94 to the Central Arctic showed that dissolved rare earth element (REE) concentrations are exceptionally high in the Transpolar Drift (TPD), and the dissolved Nd isotope composition allows differentiation of the freshwater contributions to the TPD from the different Siberian rivers and Atlantic water (Paffrath et al., 2021a). These contributions and trace metal and isotope distributions are potentially sensitive to the environmental changes affecting the Arctic. We propose, that the increasing influence of Atlantic water in the Arctic ('Atlantification') will be visible in the Nd isotope signature in the Central Arctic in 2024 in comparison to 2015. Additionally, the catchment areas of the large Siberian rivers Lena, Yenisei and Ob are marked by different permafrost conditions that will react differently to increasing warming. We suggest that Nd isotopes and REE in the TPD will

trace these changes (in comparison to 2015). In the scope of PS144, we aimed at resampling key stations from PS94 to track changes in river input and surface transport in the TPD using REE and Nd isotopes.

Gallium

The Arctic Ocean is responding to changes in Atlantic water inflow, the effects of which have resulted in destabilization of the halocline in some regions of the Eurasian basin (Polyakov et al., 2023). During PS144, we plan to collect samples for dissolved gallium. We will combine these new samples with analysis of stored samples to build and interpret a pan-Arctic, temporally rigorous gallium dataset. Gallium was demonstrated to have significant differences in Pacific and Atlantic waters (McAlister and Orians, 2015; Whitmore et al., 2020). These differences (low concentrations in Pacific-derived waters and high in Atlantic-derived waters) were utilized to predict the fractions and distribution of water masses in the western Arctic Ocean (Whitmore et al., 2020), with the result that the Ga method predicted greater abundance of Pacific-derived seawater than the traditionally used nutrient deconvolutions (e.g., Whitmore et al., 2020; Newton et al., 2013). This project will address the primary questions: Does gallium distribution in the Eurasian basin indicate any substantive change over a decadal fingerprint (i.e., compare spatial distribution and concentration between 2015 and 2024 data)?

Mercury

Arctic biota is highly contaminated with mercury (Hg), when compared to mid-latitude biota, putting the health of the ecosystem and indigenous peoples at risk (AMAP Assessment 2021, 2021). This is a surprising fact, since no known anthropogenic Hg sources exist in the Arctic. Fisher et al. (2012) questioned the role of the Siberian rivers in Hg supply to the Arctic Ocean and Sonke et al. (2018) constrained a river flux to 44 t/y. In the following, the Arctic Hg budget was evaluated with 1900 Mg and about 200 Mg/y inputs and outputs (Petrova et al., 2020). Many of the estimates are associated with large uncertainties that require further research. It is clear though, that the short Hg residence time (10 years) makes the Arctic Ocean particularly sensitive to external changes. The Arctic Ocean receives Hg from the atmosphere (Steffen et al., 2008), rivers (Sonke et al., 2018), exchange with other oceans (Petrova et al., 2020). The largest removal mechanism is the vertical export to depth with settling particles (Tesán-Onrubia et al., 2020).

The Arctic Ocean is the only ocean with elevated Hg levels in surface waters and elevated levels of Methylmercury (MeHg) shallow waters (Heimbürger et al., 2015). The shallow MeHg may explain in part the elevated biota Hg levels (Wang et al., 2019). The shift from multi-year ice (MYI) to first year ice (FYI) has increased sea ice MeHg concentrations (Schartup et al., 2020). Preliminary data from 2018/19 show higher total Hg concentrations in the MYI and a large accumulation of MeHg in the seawater under the MYI, possibly enhancing MeHg bioaccumulation locally. Kohler et al. (2023) refined the Arctic budget with a seasonal cycle of Hg in the Arctic budget questioning the previously established arctic Hg budget. Adding to this uncertainty of the current state of Hg biogeochemistry, climate change is expected to affect the Arctic Ocean Hg budget by reducing sea ice cover, permafrost, and increasing riverine discharge. PS144 will allow us to get the first ever long-term observations starting in 2011 (Dastoor et al., 2022; Heimbürger et al., 2015; Petrova et al., 2020), allowing us to investigate possible changes over time.

In the scope of PS144, our objectives are:

- Determine the horizontal and vertical distributions of total, dissolved, and particulate Hg, and MeHg.

- Investigating Hg sources, cycling, and sinks across the three sections in the Central and Eastern Arctic Ocean.
- Quantifying Hg speciation and transfer along the different compartments.
- Test for possible long-term trends in Hg burden in the AO.

Natural radionuclides (^{230}Th, ^{231}Pa, ^{232}Th, ^{226}Ra, ^{228}Ra)

The naturally occurring radionuclides of the uranium and thorium (U/Th) decay series are unique tools in oceanography because of their exactly known source and loss terms from laws of radioactive decay. Therefore, they can serve as a time marker whenever they are re-distributed in the ocean, measuring their integrated response to marine processes. This has made some of them key parameters of the GEOTRACES programme, for example as tracers of ocean circulation, shelf-ocean exchange, or export production. In the Arctic Ocean, which is hardly or not at all accessible to continuous observation, they have proven to be particularly useful tracers for constraining the integrated rate of processes.

In particular, these U/Th series tracers are of use in the Arctic Ocean:

- ^{230}Th and ^{231}Pa serve as markers for deep water circulation and particle flux in the Central Arctic Ocean (Valk et al., 2020). In addition, they are used as proxies for past ocean circulation in sediments.
- ^{232}Th as a tracer for terrigenous input, providing information similar to other lithogenic trace metals like Al or Ti, but chemically identical to ^{230}Th that has a known source.
- ^{228}Ra as a tracer for shelf input, which has been shown to increase substantially due to the warming Arctic (Rutgers van der Loeff et al., 2018; Rutgers van der Loeff et al., 1995);
- ^{226}Ra provides information on deep water circulation, particularly when combined with Ba that can serve as a stable analogue (Le Roy et al., 2018). With newly achievable precision analyses (Vieira et al., 2021), ^{226}Ra may also trace slope contact. It also serves as a yield tracer for ^{228}Ra. Ba is also delivered by riverine input (Roeske et al., 2012), possibly ^{226}Ra as well.

Our aim was therefore to sample the dissolved distribution of ^{230}Th, ^{231}Pa, ^{232}Th, and the distribution of total ^{226}Ra and Ba in full depth profiles; the total ^{228}Ra/^{226}Ra ratio on surface samples and selected large-volume stations. Additionally, the particulate ^{230}Th, ^{231}Pa and ^{232}Th profiles on selected deep-water stations. This work includes to the determination of C-export via ^{234}Th by beta-counting following methods of Roca-Martí et al. (2016). Our objective it to compare these data to existing analyses to investigate the presence of absence of recent changes.

Dissolved Pb, particulate Pb (labile, refractory) and Pb isotopic composition

Pb is a toxic element (Wani et al., 2015), the natural cycling of which has been markedly affected by anthropogenic emissions such as from burning coal and leaded gasoline (Boyle et al., 2014). The North Atlantic Ocean is among the regions most affected by aerosol Pb deposition (Boyle et al., 2014; Zurbrick et al., 2018). Northward advection of Atlantic Waters (Tsubouchi et al., 2021), enriched in dPb (Schlosser & Garbe-Schönberg, 2019), may cross into the Arctic Ocean and lead to widespread Pb deposition along its flow path (Carignan et al., 2008; Gobeil et al., 2001). An additional source of Pb to the surface Arctic Ocean is derived from atmospheric deposition (Conca et al., 2019). Both sources, marine and atmospheric, may result in elevated Pb levels in Arctic marine biota (Schulz-Baldes & Lewin, 1976; Zimmer et al., 2011).

PS144 (“TransArc III”) aims to investigate the Pb cycling in the Eastern and Central Arctic Ocean and the current extent of perturbations from past Pb emissions. Specific emphasis is put on the investigation into the areal extent and changes to the northward advection of dPb from Atlantic Water between 2015 (“TransArc II”) and 2024 (“TransArc III”). This will be achieved by reoccupying stations from the previous 2015 campaign. We will investigate the efficiency of dPb transport from Siberian Shelf sources towards the Central Arctic Ocean by sampling transects in the Transpolar Drift at various distances from the shelf break. Through analyses of Pb isotopic composition, we aim to identify natural and anthropogenic sources of Pb to the water column, as has been previously achieved for the Western Arctic Ocean (De Vera et al., 2021).

Radionuclide Transient Tracers (^{14}C, ^{39}Ar, ^{129}I, ^{236}U)

The world’s oceans are responding to the anthropogenically induced climate change, with the Arctic Ocean standing out as one of the most rapidly changing regions (Meredith et al., 2019). A phenomenon known as Arctic ‘Atlantification’, linked to the melting sea-ice and influencing the Atlantic Meridional Overturning Circulation (AMOC), remains poorly understood. Bridging this knowledge gap requires intensified measurement and modelling efforts. To address this need, radionuclides of both natural and artificial origin (i.e. ^{129}I, ^{236}U, ^{14}C and ^{39}Ar) are excellent tools that bring insight to ocean circulation (i.e. transport and mixing) and ventilation processes. PS144 offers the unique opportunity to sample water masses in the Central Arctic Ocean one decade after TransArc2 providing valuable insights into alteration in water mass circulation and its relation to climate change.

In the scope of PS144, we will tackle the follow research questions:

1. What is the distribution of ^{129}I, ^{236}U, ^{14}C and ^{39}Ar in the central Arctic Ocean (2024)?
2. What are the pathways, circulation timescales and mixing regimes of Atlantic-origin waters in 2024 and how do they compare to 2015?
3. What are the ventilation timescales of deep water in the Central Arctic Ocean and how do these compare to previous estimates done in the 1990s?
4. What is the rate of increase of anthropogenic carbon in the Arctic Ocean?
5. How do changes (if any) relate to Arctic Atlantification?

Work at Sea

Aerosol trace metals and major ions

The high-volume aerosol sampler (Tisch Environmental Inc.) was placed on the A-deck directly at the front railing for collection of trace elements and major ions. In the absence of snow events, the unit was operated full-time and sampled for aerosols with a flow rate of 1 m^3/min along the cruise track at a time resolution of 3-5 days. In total, we collected 10 aerosol samples (Table 2.3). An automatic control system (‘wind sector controller’) checked the wind direction and wind speed (shutting down the collector if wind direction was between 140 – 250° of the ship’s bow or speed was less than 2 $m \cdot s^{-1}$) and prevented from the risk of contamination through the ship’s exhausts. Acid-washed ~20 x 25 cm Whatman 41 filters were used to collect aerosol particles. Handling of filters were conducted with vinyl gloves and the use of an aluminium cover in a plastic bag to protect the cassette from contamination during transport. Exchange of filters were conducted in the AWI class-100 clean-room container under a laminar flow cabinet. After

collection, the filter paper was folded in half, so that the two faces of the aerosol touch each other and was put the paper into the zip-lock plastic bag provided by the UEA. Samples were frozen immediately after collection and stored at -20°C in the dark until analysis. Additionally, three blanks were conducted: (a) a cassette blank, (b) motor blank and (c) exposure blank. For the cassette blank, a filter was loaded into the cassette, covered, placed in a plastic bag, and left for ~24 hours. The motor blank was treated exactly the same as normal samples, except that once the cassette was loaded in the sampler, the motor was only switched for 10 seconds. For the exposure blank, the filter was treated like a normal sample, but left in the collector for ~48 hours without switching the collector on. The cassette blank was conducted during sample collection in the study area. The motor and exposure blanks were conducted on the way into port.

Tab. 2.3: For further information please see the end of this chapter.

Nutrient addition bioassay experiments

The incubation experiments at sea were conducted following the procedure previously established on PS100 in Fram Strait (Krisch et al., 2020). A variation to this method was established due to light constraints when approaching polar night, and used artificial light and controlled temperatures using the set-up provided by the BTM group.

Seawater for the conduction of incubation experiments were collected at 15 m depth using the AWI trace metal clean CTD rosette equipped with trace metal clean Go-Flo bottles following GEOTRACES sampling protocols (Cutter et al., 2017). Incubation experiments were carried out in 1L trace-metal clean polycarbonate bottles. Each set of nutrient amendments (+N, +Fe, +N+Fe) was carried out in triplicate. One set of triplicate bottles was incubated without any nutrient addition and functioned as control. Three additional bottles without nutrient addition were sampled immediately after bottling to record the initial conditions. In total, 10 incubation experiments were conducted along the cruise track (Fig. 2.1). The first three incubation experiments (at stations PS144_009_01, PS144_018_02 and PS144_039_01) were conducted using an on-deck incubator (shaded with blue screening to yield incubator light intensities of ~35% of surface values) and was connected to the ships underway flow-through system to maintain the temperatures as in surface waters. These incubations were carried out for 96 hours. Bottles were manually stirred every 6h to mirror ocean wave action. The following seven incubation experiments were conducted using an in-door set-up provided by the BTM group. This set-up utilized artificial light (24h radiation, 40 µmol photons·s^{-1}) and controlled temperature (0°C) and mirrored surface conditions in polar summer. After incubation, bottles (initial and incubated) were filtered on glass fibre filters (0.7µm pore size, 25mm diameter, Fisher Scientific MF 300) to retain Chlorophyll-a. In addition, all remaining seawater in the triplicate replicate bottles were pooled and filtered onto a glass fibre filter to be analysed for phytoplankton pigment concentrations by HPLC (that is producing one sample per treatment). The filters were stored in the dark and frozen at -80°C immediately after sampling. Concentrations of chlorophyll-a (measured by fluorometry following acetone extraction), and pigment composition (indicative of phytoplankton species contributions; measured by HPLC) will be measured at GEOMAR.

Dissolved and particulate trace metals (Fe, Mn, Co, Ni, Cu, Zn, Cd)

During PS144, we sampled a total of 31 stations (Fig. 2.1), 8 of which focussed on the upper 500 m or 750 m to provide high resolution in surface waters. 23 stations sampled the water column to full depth. Stations mostly reoccupied PS94 stations to establish a timeline from

2007 (PS70), 2015 (PS94) to 2024 (PS144). Depths were selected based on *in situ* water mass properties (e. g. nutrient regimes, prevailing currents), occurrence of phytoplankton blooms or post-bloom conditions, or important trace metal sources and sinks (e.g. hydrothermal, shelf slope, sea-ice, riverine signals). Stations were sampled at high-resolution and to full depth for soluble, dissolved, and labile particulate and refractory particulate trace metals using the AWI contamination-free titanium CTD rosette (KUM, equipped with a SBE 911 CTD) equipped with 24 trace metal clean Go-Flo bottles and a clean winch (KleyFrance) following GEOTRACES sampling protocols (Cutter et al., 2017). Due to a failure of the clean winch after the 21st cast, stations 22 (PS144_130_01) to 31 (PS144_158_02) utilized a dyneema winch and an auto-fire module. This set-up however failed to provide in-situ CTD profiles. Sampling depths with the auto-fire module were then chosen according to water mass properties observed in the regular CTD casts which was deployed prior to the cleanCTD.

Subsampling from GoFlo bottles was conducted in AWI's class-100 clean-room container immediately after the CTD deployment. Samples for dissolved, particulate and macronutrients were taken at every station and every depth (usually 20-22 depth intervals). Samples for soluble trace metals were taken from every station and every other depth (usually 10 depth intervals). Samples for dissolved trace metals were filtered through 0.8/0.2 µm Acropak cartridge filters (Pall corporation) into 125 mL trace metal clean LDPE bottles and acidified to pH 1.9 through addition of ultra-pure hydrochloric acid (ROMIL) immediately after sampling. Triplicate samples for intercalibration of dTM data were taken at two stations (PS144_050_03, PS144_085_03) from 9 depths. A further filtered (0.8/0.2 µm) sample was retained, passed through a Whatman Anotop syringe filters (0.02 µm) using a peristaltic pump within 4 h of sample collection, and then acidified to obtain the soluble TM fraction (<0.02µm). Samples for the particulate trace metal fractions were collected on 0.2µm polythersulfone (PES) membrane filters (Whatman) using Savillex filter holders and slight over-pressure (0.3 bar) with clean-air filtering at least 4 L of seawater. Field blanks were taken at 2 stations from 6 depths each to determine trace metal contributions from the use of filters and filter holders. Field blanks used a second set of 0.2 µm filters (in Savillex filter holders) that was then connected in tandem so that 0.5 L filtrate from particulate trace metal sampling passed through. Particulate samples (incl. blanks) were frozen at -20°C immediately after sampling. In total, we collected 570 samples for dissolved and particulate trace metals each, and 340 samples for soluble trace metals. Soluble, dissolved and particulate samples are shipped to GEOMAR for analysis.

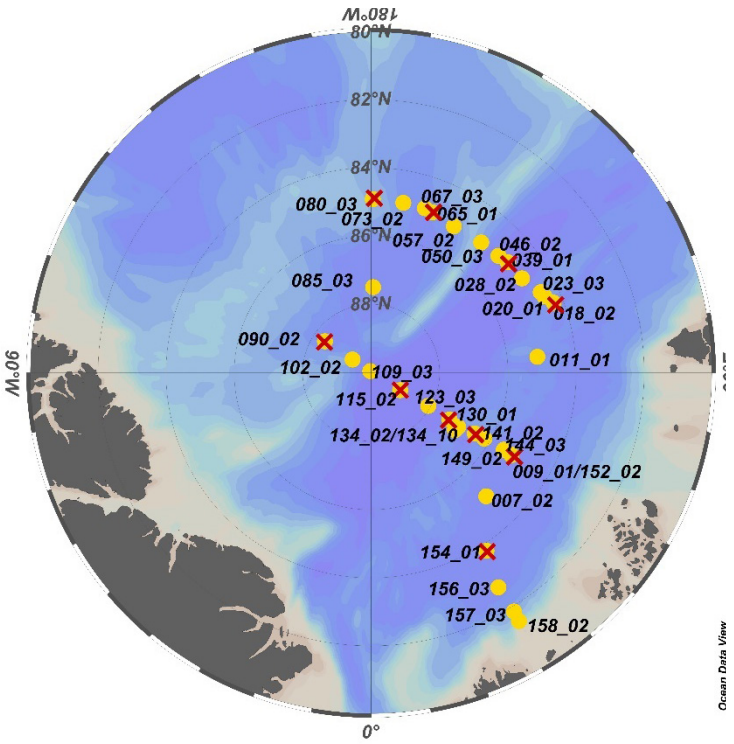

Fig. 2.1: Bathymetry and location of clean CTD stations sampled in the Central and Eastern Arctic Ocean during PS144 ('ArcWatch 2'). Stations with red crosses indicate location of nutrient addition bioassay experiments.

Tab 2.4: Tab 2.3: For further information please see the end of this chapter.

Dissolved Fe isotope composition (δ^{56}dFe)

During PS144, we collected 260 samples at 28 stations for the determination of dFe isotope composition. Samples for dFe isotope composition, usually at 10 depth intervals per cast, were collected using the AWI trace metal clean CTD rosette equipped with trace metal clean Go-Flo bottles following GEOTRACES sampling protocols (Cutter et al., 2017). 25 stations were samples to full depth, however, with a focus on the upper water column (<200 m depth). Additionally, 3 stations sampled the upper water column (500-750 m depth) exclusively. Greater vertical resolution of the upper water column will help us to constrain the provenance and internal cycling processes of dFe such as biological uptake and scavenging (Fitzsimmons & Conway, 2023). Samples were filtered through 0.8/0.2 µm Acropak cartridges (Pall corporation) into 250 mL, 1 L or 2 L trace metal clean LDPE bottles and acidified to pH 1.9 through addition of ultra-pure hydrochloric acid (ROMIL) immediately after sampling. Triplicate samples for intercalibration of Fe isotope composition were taken at station PS144_152_02 from 8 depths covering the full water column. Samples are stored in the dark and will be shipped to the University of South Florida for analysis.

Rare earth element concentrations and neodymium isotopes

Water column sampling was conducted and focussed on the upper 1,000 m at the GEOTRACES stations of PS94 and additional stations to extend the spatial resolution (Tab. 2.5, Fig. 2.2). Full depth sampling was conducted at selected locations. At each station, samples for dissolved REE and Nd isotopes were filtered directly from the Niskin bottles through AcroPak500 cartridges (0.8/0.2 µm pore size) into acid pre-cleaned LDPE sample containers. For REE, 100 mL of filtered seawater were collected and acidified to pH ~2 using 6N ultra-clean self-distilled hydrochloric acid immediately after sampling. For dissolved Nd isotopes, 5 L per sample were collected into LDPE cubitainers, acidified to pH = 3.5 + 0.05 with 6N ultra-clean hydrochloric acid and preconcentrated onboard within 12 hrs of sampling using C18 cartridges (Waters Inc.) pre-loaded with a complexing agent. In total, 284 samples for REE and 283 samples for Nd isotopes were collected at 20 stations. Particulate samples for REE and Nd isotope measurements will be obtained from a subsamples of particle filters collected for Th isotopes.

Tab. 2.5: Overview of stations sampled for dissolved REE and Nd isotopes from the regular CTD water sampling system during PS144

Event Label	Date	Latitude	Longitude	Bottom Depth [m]	Cast Depth [m]
PS144_003_01	14.08.2024	83° 02.427‘ N	29° 45.555‘ E	3836	3836
PS144_003_03	14.08.2024	83° 02.427‘ N	29° 45.555‘ E	3836	400
PS144_007_01	16.08.2024	85° 02.210‘ N	42° 42.200‘ E	3929	3951
PS144_007_07	16.08.2024	85° 02.210‘ N	42° 42.200‘ E	3929	400
PS144_011_02	20.08.2024	85° 06.800‘ N	95° 22.000‘ E	4570	4525
PS144_018-01	28.08.2024	84° 16.673‘ N	110° 46.984‘ E	3987	1000
PS144_023_02	29.08.2024	84° 29.353‘ N	115° 20.056‘ E	4111	3500
PS144_023_09	30.08.2024	84° 24.447‘ N	115° 49.294‘ E	4111	398
PS144_031_01	31.08.2024	84° 50.232‘ N	125° 34.651‘ E	4375	4375
PS144_050_02	04.09.2024	85° 01.866‘ N	139° 34.962‘ E	3951	3892
PS144_050_09	05.09.2024	85° 01.415‘ N	140° 05.026‘ E	3494	994
PS144_065_02	07.09.2024	84° 59.020‘ N	159° 02.627‘ E	3428	3358
PS144_080_02	10.09.2024	84° 55.239‘ N	179° 33.312‘ E	1974	1913

Event Label	Date	Latitude	Longitude	Bottom Depth [m]	Cast Depth [m]
PS144_080_04	11.09.2024	84° 56.514‘ N	179° 24.890‘ E	2118	2050
PS144_085_06	13.09.2024	87° 29.169‘ N	178° 16.708‘ E	3994	3923
PS144_090_01	16.09.2024	88° 21.978‘ N	124° 31.855‘ W	3560	3486
PS144_090_03	16.09.2024	88° 22.344‘ N	124° 05.821‘ W	3529	994
PS144_102_03	17.09.2024	89° 20.099‘ N	125° 23.579‘ W	1671	995
PS144_109_02	18.09.2024	89° 56.603‘ N	150° 53.320‘ W	4263	995
PS144_109_03	19.09.2024	89° 56.603‘ N	150° 53.320‘ W	4263	4192
PS144_115_03	21.09.2024	89° 00.679‘ N	58° 58.437‘ E	4396	995
PS144_123_01	23.09.2024	88° 04.732‘ N	60° 11.094‘ E	4416	995
PS144_134_06	25.09.2024	87° 02.496‘ N	57° 16.479‘ E	4223	996
PS144_134_09	25.09.2024	86° 59.372‘ N	58° 34.372‘ E	4846	4290
PS144_144_02	28.09.2024	86° 10.173‘ N	60° 01.384‘ E	3910	3836
PS144_144_04	29.09.2024	86° 10.067‘ N	59° 47.054‘ E	3911	995
PS144_153_01	30.09.2024	85° 14.658‘ N	59° 38.935‘ E	3926	3851
PS144_156_02	04.10.2024	82° 42.006‘ N	30° 47.318‘ E	3689	3617
PS144_157_02	04.10.2024	81° 51.211‘ N	30° 53.657‘ E	3165	3090

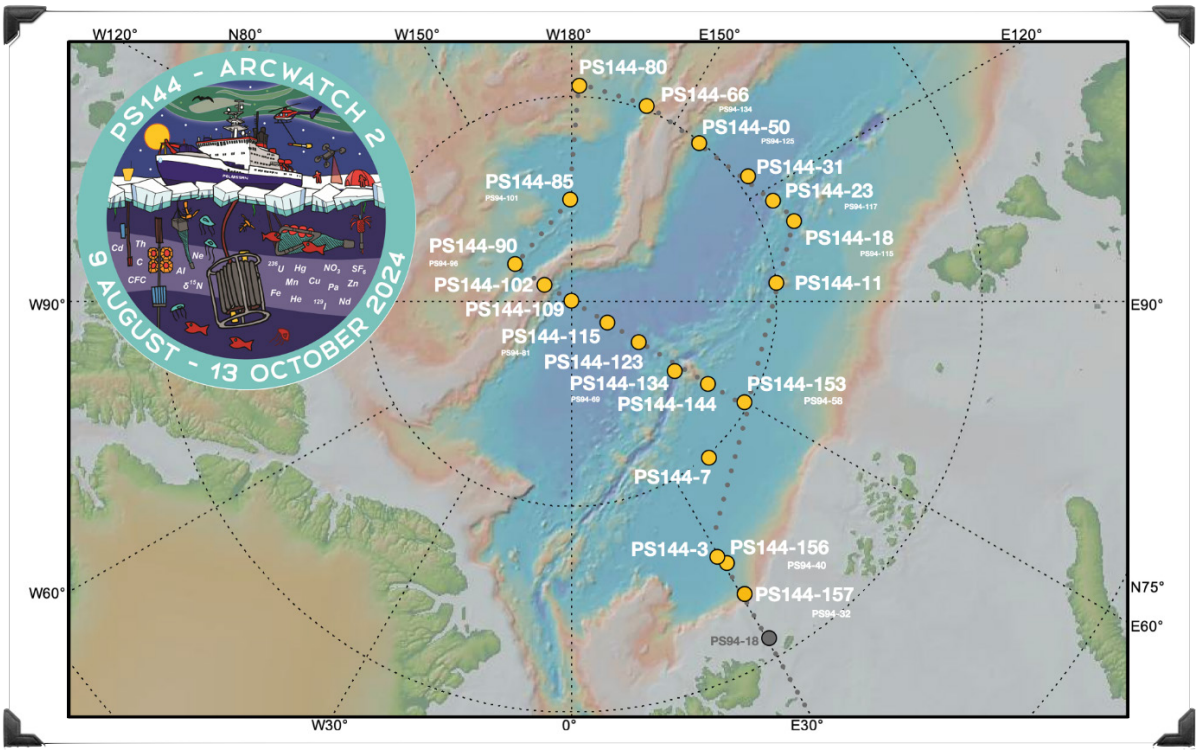

Fig. 2.2: Cruise track of PS144 (‘ArcWatch 2’) with stations sampled for dissolved REE and Nd isotopes highlighted by yellow symbols.

Gallium

To be able to establish a timeline of change, we aimed to resample as many PS94 stations as possible. Samples were from 29 stations at all depth intervals (usually 20-22) to full depth using AWI's trace metal clean CTD equipped with GoFlo bottles (Table 2.4). 6 stations focussed on the upper water column (500 m or 750 m depth). Sample handling was conducted entirely in the AWI clean-room container and followed GEOTRACES protocols (Cutter et al., 2017). Samples were filtered using 0.8/0.2 µm Acropak catridges (Pall cooperation) into 60 mL HDPE bottles provided by Laura Withmore (US.UAlaskaFairbanks). Sample bottles were closed tightly, doubled-bagged and stored in the dark until return to the shore-based laboratory at US.UAlaskaFairbanks. In total, 570 samples were collected along the entire cruise track. Sample preservation will be conducted at US.UAlaskaFairbanks through addition of ultra-pure HCl.

Mercury

Seawater was sampled from the AWI trace metal clean carousel at 27 station (Tab. 2.6). In total, 338 samples for total mercury (tHg), 338 samples for methylmercury (MeHg), 105 samples for monomethylmercury (MMHg), and 134 samples for particulate Hg (pHg) were obtained. Subsampling from GoFlo bottles was conducted in AWI's class-100 clean room container.

Unfiltered tHg was collected into pre-combusted glass vials. These samples will be measured via cold vapor atomic fluorescence spectroscopy (CVAFS; BROOKS Rand Model 3) at MIO. From an aliquot of tHg samples, we purged off dissolved gaseous mercury (DGM = Hg0 + DMHg) using compressed air. The DGM-purged sample was acidified with ultra-pure double distilled hydrochloric acid (HCl), immediately after sampling, for MMHg analysis back at MIO. Total methylmercury (MeHg = MMHg + DMHg) was sampled into PET bottles and acidified with above stated double-distilled HCl immediately after sampling. From selected depths, samples for pHg were collected onto GFF filters using in line bottle-filtration applying slight overpressure (0.3 bar). pHg will be measured via cold vapor atomic absorption spectroscopy (CVAAS; LECO AMA254) at MIO. MeHg and MMHg will be analyzed via species specific isotope dilution gas chromatography sector field ICP-MS (THERMO GC 1300 with Element XR). At three stations, extra samples were collected into the pre-combusted glass vials and were spiked with known concentrations of $i^{119}Hg$ and $MM^{201}Hg$, half of the samples were acidided after collection, the other half were incubated during 24h and then acidified, to investigate abiotic and biotic transformations regarding Hg methylation and MeHg demethylation.

To investigate the role of sea ice on Arctic Hg and MeHg cycling, we collected ice cores at 8 sites (Tab. 2.7, Fig. 2.3) applying trace metal clean techniques utilizing a Kovacs ice corer with a diameter of 9 cm. Ice cores were cut every 10 cm, pieces scraped with a ceramic knife to remove any possible external contamination and allowed to melt in the dark at room temperature. After, aliquots for tHg, MeHg and MMHg were sampled as previously described for water samples.

Tab. 2.6: Clean-CTD stations from PS144 sampled for mercury analysis

Event Label	Date	Lat [°N]	Lon [°E]	Depth [m]	Cast depth [m]
PS144_007-02	16.08.2024	85.07	42.99	3927	3948
PS144_009-01	18.08.2024	85.36	59.96	3841	500
PS144_011-01	20.08.2024	85.37	95.58	4577	4522
PS144_018-02	28.08.2024	84.48	111.02	4056	3988

Event Label	Date	Lat [°N]	Lon [°E]	Depth [m]	Cast depth [m]
PS144_023-03	29.08.2024	84.76	115.33	4135	4068
PS144_023-08	30.08.2024	84.48	115.53	3330	3351
PS144_028-02	31.08.2024	84.89	122.00	4388	4324
PS144_039-01	02.09.2024	84.90	129.14	4351	750
PS144_046-02	03.09.2024	85.03	132.71	4320	4251
PS144_050-07	05.09.2024	85.17	140.26	3463	3358
PS144_057-02	06.09.2024	85.32	150.63	958	916
PS144_067-08	08.09.2024	84.94	162.23	3559	3493
PS144_080-03	11.09.2024	84.99	179.74	1981	1927
PS144_0850-8	13.09.2024	87.56	178.12	3995	3934
PS144_090-02	16.09.2024	88.40	-123.63	3543	3478
PS144_102-02	17.09.2024	89.36	-124.56	1676	1623
PS144_109-07	19.09.2024	89.68	-138.51	4264	4201
PS144_115-02	21.09.2024	89.03	59.31	4395	4336
PS144_123-03	23.09.2024	88.15	59.81	4416	4356
PS144_134-10	26.09.2024	87.05	55.94	4530	4465
PS144_141-02	28.09.2024	86.57	59.90	2119	2062
PS144_144-03	28.09.2024	86.22	60.07	3910	3820
PS144_149-02	30.09.2024	85.73	60.00	3936	842
PS144_152-02	30.09.2024	85.39	59.76	3926	3813
PS144_156-03	04.10.2024	82.86	30.84	3695	3556
PS144_157-03	04.10.2024	81.91	31.15	3162	3063
PS144_158-02	05.10.2024	81.74	30.95	830	754

Tab. 2.7: Ice cores sampled for mercury analysis

Event Label	Date	Lat [°N]	Lon [°E]	Core Length [cm]
PS144_023_icec_01	29.08.2024	84.50	115.72	121
PS144_042_icec_02	02.09.2024	84.83	128.87	121
PS144_050_icec_03	05.09.2024	85.02	139.94	80
PS144_067_icec_04	08.09.2024	84.94	162.09	118
PS144_080_icec_05	11.09.2024	84.93	179.41	100
PS144_085_icec_06	13.09.2024	87.50	178.72	132
PS144_109_icec_07	19.09.2024	89.99	-142.69	128
PS144_134_icec_08	25.09.2024	87.04	57.07	114

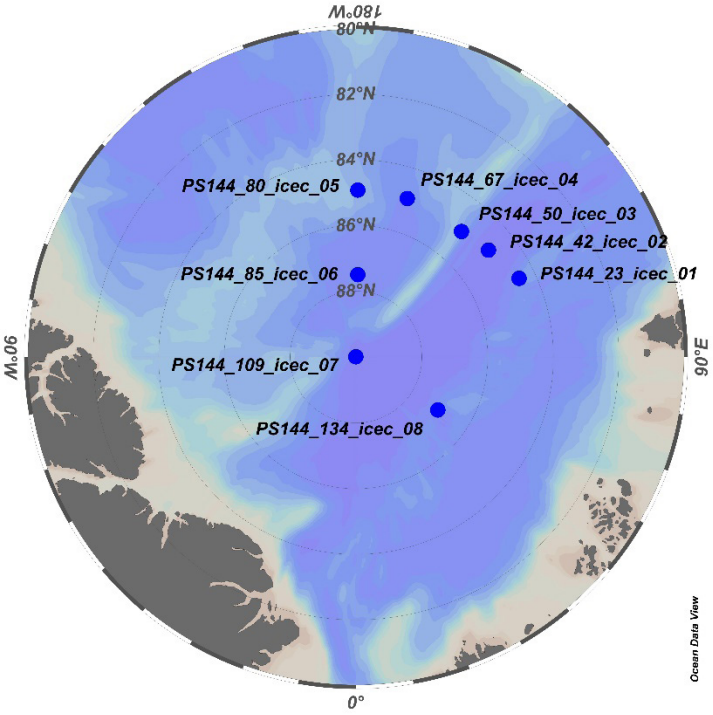

Fig. 2.3: Bathymetry and location of ice core stations sampled in the Central and Eastern Arctic Ocean during PS144 ('ArcWatch 2') for Hg and Hg speciation analysis.

Natural radionuclides (^{230}Th, ^{231}Pa, ^{232}Th, ^{226}Ra, ^{228}Ra)

Sampling for radium isotopes consisted in three different sample types:

- One-litre samples from the regular CTD, unfiltered and acidified with 1 mL of double-distilled HCl, for total ^{226}Ra via ICP-MS. Of these samples, 297 were taken in total.
- Large-volume samples (several hundred litres) of ^{228}Ra/^{226}Ra ratio, extracted onto manganese dioxide-coated filter cartridges directly from the seawater supply. 29 of these samples were taken throughout the expedition.
- On selected stations, samples of approximately 20 L for ^{228}Ra/^{226}Ra were taken from the regular CTD and extracted onto manganese dioxide-coated acrylic fibre in order to get an impression of the depth distribution of ^{228}Ra. 38 samples of this type were taken. The ^{228}Ra/^{226}Ra ratios can later be converted to ^{228}Ra concentrations, once the absolute ^{226}Ra values are known from the 1 L samples.

Complementary to the ^{226}Ra samples, dissolved barium (Ba) was taken from the clean CTD in 297 separate 30 mL samples. Ba is somewhat contamination-prone, while at the same time not being concentrated with the typical trace element preconcentration procedure on a Seafast-system, so it requires an extra subsample here. The sampling locations are identical with ^{232}Th samples, shown below. Please note that the exact agreement of 297 Ba samples and 297 ^{226}Ra samples is a coincidence and does not imply that all sample depths are matching. The distribution of all Ra samples is shown in Figure 2.4.

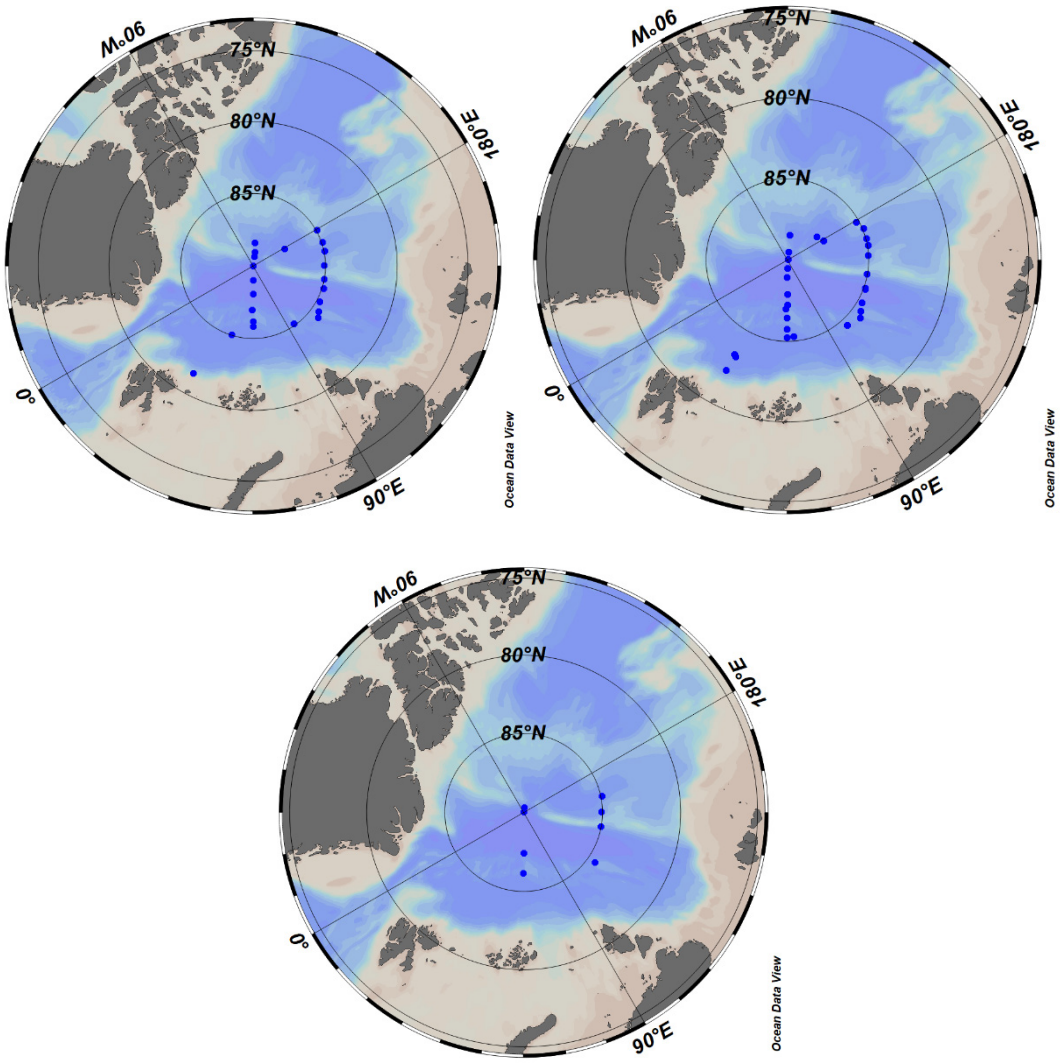

Fig. 2.4: Overview map of sampling locations for one litre ^{226}Ra samples (upper left), ^{228}Ra/^{226}Ra in surface waters (integrated samples from the seawater supply, upper right) and ^{228}Ra/^{226}Ra samples from the regular CTD from subsurface waters (lower right).

For dissolved ^{230}Th and ^{231}Pa, samples of typically ten litres volume were taken from the regular CTD, in total 133 samples. These samples were filtered through Acropak-Filters directly on the CTD into previously acid-cleaned sample containers (10 L cubitainer). The filters were re-used several times for water from the same depth range and stored refrigerated between sampling events. After sampling, the seawater was acidified with 10 mL double-distilled HCl, irrespective of the exact sample volume. Each sample was sealed with Parafilm ® and packed into a protective plastic bag for transport to the home institute.

As no *in-situ* pump samples were taken, large-volume samples for particulate ^{230}Th and ^{231}Pa were taken from the clean CTD on superstations as a replacement. Here, three bottles of 14 L each (= 42 L) from four different depths were filtered over one 142 mm Supor®-filter that had previously been stored in HCl for cleaning. The filtrate was collected in two 20-L cubitainers per depth and is available for comparisons between clean CTD/regular CTD sampling and for intercalibration. Twenty such particulate ^{231}Pa/^{230}Th samples were taken, with accompanying dissolved samples in duplicate. The separation procedure for ^{231}Pa/^{230}Th can be adapted to

sample other particulate TEIs as well, e.g. εNd or rare earth elements (REE). An overview of sample locations for ^{230}Th and ^{231}Pa is shown in Figure 2.5.

In addition to the large-volume ^{230}Th and ^{231}Pa samples, small-volume dissolved ^{232}Th samples were taken from the clean CTD, 276 in total. These can later be analysed by isotope-dilution ICP-MS.

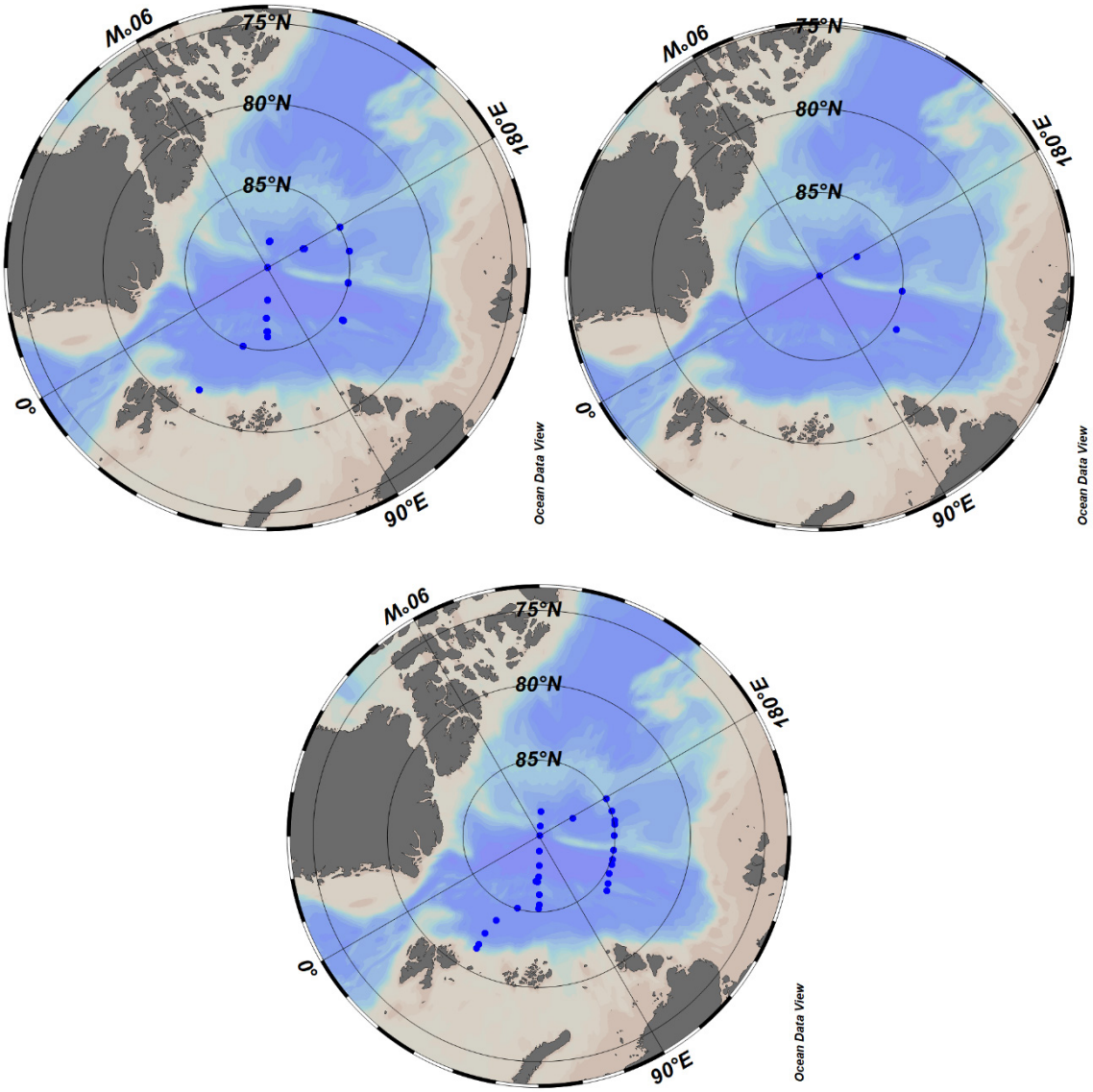

Fig. 2.5: Overview map of sampling locations for dissolved ^{230}Th/^{231}Pa samples from the regular CTD (upper left), particulate ^{230}Th/^{231}Pa samples from the clean CTD with accompanying duplicates of dissolved ^{230}Th/^{231}Pa and sampling locations for ^{232}Th-profiles from the clean CTD (bottom left).

For ^{234}Th, three different sample types were taken. For determining the total ^{234}Th deficit compared to ^{238}U, 138 samples from 21 stations were taken, with typically six depths. Several deep samples (1000 or 2000 m) were taken to determine ^{234}Th in equilibrium with ^{238}U as a means of data validation. Sample processing consisted in adding 5 mL of concentrated nitric acid to 4 L unfiltered water from the regular CTD, plus the addition of 0.5 mL a ^{230}Th spike with close to 0.1 Bq/g ^{230}Th for later determination of chemical yield. After at least 8h waiting, pH of

the sample was raised by adding 6.1 mL of conc. NH_3 solution, the 50 µL of a $KMnO_4$ solution and 50 µL of a $MnCl_2$-solution were added according to the RiOS method. The resulting MnO_2 precipitate extracting Th from solution was collected after another >8h waiting by filtration over QMA filters. The precipitate was then dried for 5 hours at 50 degrees, and sealed under a layer of cling film and thick aluminium foil. Samples were counted for beta activity onboard in the Risoe beta counter brought to the expedition in a lab container. They will be re-counted in the home lab for supported ^{234}Th, spiked with ^{229}Th and the Th yield will be determined with isotope dilution ICP-MS using the ^{230}Th spike added earlier.

To convert a ^{234}Th deficit to a value of carbon export, a ^{234}Th/carbon ratio on exported particles is required. In the absence of a direct access to exported particles, particulate ^{234}Th was sampled on a subset of the ^{234}Th total samples, in total 61 samples from 14 stations. 4 L unfiltered water from the regular CTD were filtered over pre-combusted QMA filters, dried for 5 hours at 50 degrees, and sealed under a layer of cling film and thick aluminium foil. These samples were measured onboard in a Risoe beta-counting system. After recounting them in the home-laboratory for supported ^{234}Th, they will be analysed for POC. Maps of the sampling locations for ^{234}Th are shown in Figure 2.6.

In addition to the particulate ^{234}Th/POC ratios, an experimental sampling of sinking particles was tried on two occasions. Here, a complete CTD bottle was sampled in 2 L increments, assuming that sinking particles would have settled within the bottle whereas small suspended particles would remain distributed evenly throughout the bottle content. However, after two attempts of sampling and measuring ^{234}Th in these samples, it was concluded that at least for this particle-poor environment, no significant difference could be measured with the small 2 L samples.

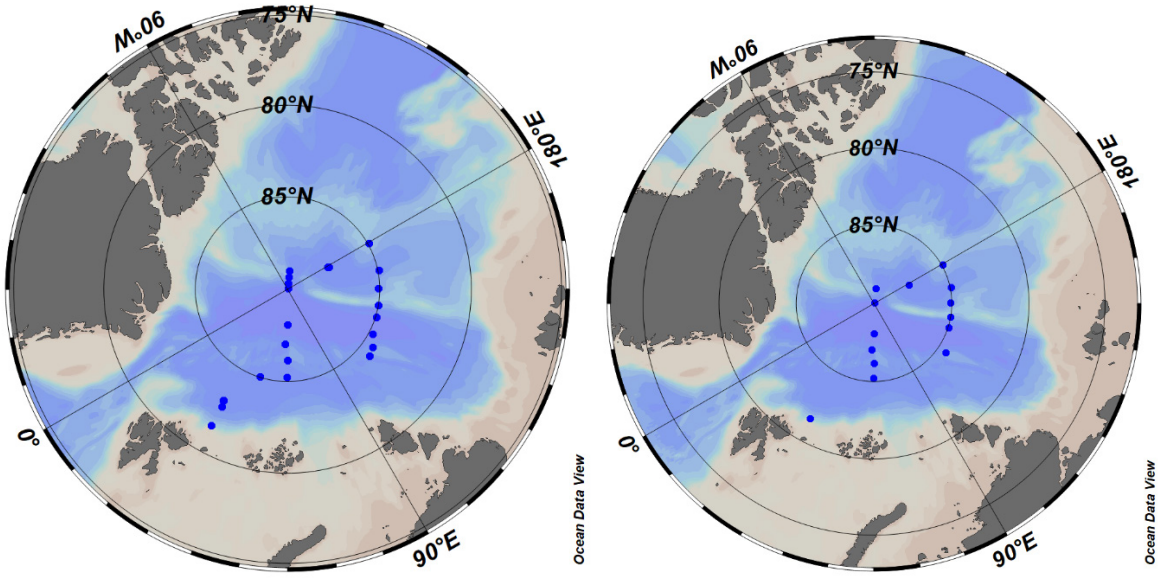

Fig. 2.6: Overview map of sampling locations for total ^{234}Th from the regular CTD, each typically with six depths of 4 L each (left) and of particulate ^{234}Th and POC from the regular CTD, typically with three to four depths of 4 L each (right).

A full overview of the samples of the natural radionuclide group is given below in Table 2.8. Triplicate samples for intercalibration of ^{232}Th and Ba were taken at two stations (PS144_050_03, PS144_085_03) to full depth from 9 depth intervals.

In addition to the water sampling work, the expedition was used to explore the possibilities of a new device for measuring spatially resolved ionizing radiation in a digital format. This device is eventually intended to be used for analysing radiation in environmental samples, in particular manganese nodules for the Volkswagen Stiftung funded project “radiotrophic life”. This project provided the funding for the device used here. An Advacam MiniPIX TPX3 Flex in a custom-built base was used in parallel to the beta counter to compare established quantitative techniques with spatially resolved analyses, to learn about the system.

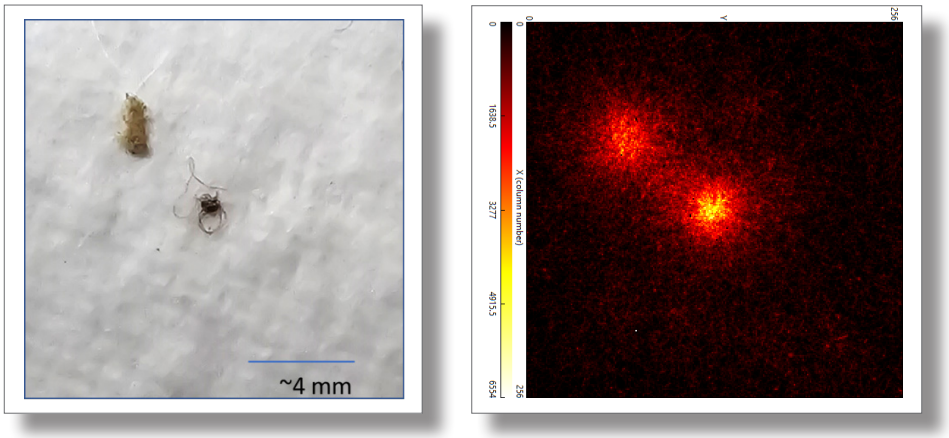

Fig. 2.7: Aggregates from the experiments in a roller tank by A. Bettinelli as seen in optical magnification (left) on a filter, and the spatially resolved signal of 234Th from a fortified seawater solution as seen in the customized Advacam MiniPIX TPX3 Flex camera in the same sample (right). The colour scale reflects the cumulated received energy for each pixel in non-calibrated units. The system has the capacity to separate radioisotope-bearing particles in a 2D-image, with the spatial resolution depending on the reach of the emissions, i.e. radiation type and energy.

The MiniPIX was then also used to study the distribution of ^{234}Th between particles and solution in the aggregation experiments of Alexandra Bettinelli (BTM team). To do this, the ^{234}Th content of seawater was fortified by adding ^{234}Th extracted from 33 mL of a commercial 1000 ppm U solution (ICP standard). This signal was high enough to detect and localize the ^{234}Th-containing particles on a sub-mm scale in some samples. However, in large parts of the aggregation experiments, the particle concentration was too low to lead to a significant fraction of ^{234}Th in particles. A full evaluation of the temporal evolution of ^{234}Th in the beta counter as well as in the MiniPIX system will be done in the home laboratory. In brief, the system worked well and has a large potential for spatially resolved analysis of radioisotopes.

Tab. 2.8: Overview of samples for radionuclides and accompanying parameters. *Latitude and Longitude reflect the time when hoisting the CTD cast for CTD samples and the mean position between start and end of sampling for underway samples (see next pages).

Event Label	Date	Lat*	Lon*	Water samples									
				Niskin						GoFlo	GoFlo	GoFlo	Seawater line
				234_Th	234_ThPOC	226Ra1L	DIC	228Ra_226Ra_CTD	231Pa_239Thdiss	231Pa_230Thpar	Ba_Clean	232Th_Clean	226Ra/228Ra
PS144-003-01	14.08.2024	83.039071	29.80872	x									
PS144-003-03	14.08.2024	83.045224	29.98308	x									
PS144-006-01	16.08.2024	85.037378	42.7011			x			x				
PS144-007-02	16.08.2024	85.062954	42.98625								x	X	
PS144-007-07	17.08.2024	85.048709	42.32191	x									
PS144-011-01	20.08.2024	85.117899	95.48505								x		
PS144-011-02	20.08.2024	85.11739	95.37954			x							
PS144-018-01	28.08.2024	84.272474	110.7122	x									
PS144-018-02	28.08.2024	84.28521	111.0113								x	X	
PS144-018-03	28.08.2024	84.272552	111.4426			x							
PS144-023-02	29.08.2024	84.487611	115.2514			x		x	x				
PS144-023-03	29.08.2024	84.508135	115.3636								x	X	
PS144-023-08	29.08.2024	84.421739	115.5755						x	x			
PS144-023-09	29.08.2024	84.407447	115.8216	x	x								
PS144-028-01	31.08.2024	84.77121	121.9011			x	x						
PS144-028-02	31.08.2024	84.794726	122.0135								x	X	
PS144-028-03	31.08.2024	84.781624	122.1323	x									
PS144-039-01	02.09.2024	84.863615	128.9579								x	X	
PS144-046-01	03.09.2024	84.955269	132.4262	x	x								
PS144-046-02	04.09.2024	84.947034	132.5428								x	X	
PS144-046-03	04.09.2024	84.91276	132.4851			x	x						
PS144-050-02	05.09.2024	85.026048	139.6784			x	x	x	x				
PS144-050-03	05.09.2024	85.014958	139.7659								x	X	
PS144-050-07	05.09.2024	85.023299	140.1292						x	x			
PS144-050-09	05.09.2024	85.023607	140.0835	x	x								
PS144-057-03	06.09.2024	85.080413	150.4793			x		x					
PS144-057-02	06.09.2024	85.081426	150.5148								x	X	

Event Label	Date	Lat*	Lon*	Water samples									
				Niskin						GoFlo	GoFlo	GoFlo	Seawater line
				234_Th	234_ThPOC	226Ra1L	DIC	228Ra_226Ra_CTD	231Pa_239Thdiss	231Pa_230Thpar	Ba_Clean	232Th_Clean	226Ra/228Ra
PS144-057-01	06.09.2024	85.084041	150.502	x	x								
PS144-065-01	07.09.2024	84.98076	159.073								x	X	
PS144-067-02	08.09.2024	84.943149	161.9011	x	x								
PS144-067-03	08.09.2024	84.939212	161.8892								x	X	
PS144-067-04	08.09.2024	84.944872	161.9534	x	x	x		x	x				x
PS144-073-02	09.09.2024	84.94324	169.2645								x	X	
PS144-073-03	09.09.2024	84.948634	169.2668			x							
PS144-080-02	10.09.2024	84.920643	179.555	x	x								
PS144-080-03	10.09.2024	84.923307	179.4683								x	X	
PS144-080-04	11.09.2024	84.942078	179.4151	x		x			x				
PS144-085-02	13.09.2024	87.518932	178.8489	x		x			x				
PS144-085-03	13.09.2024	87.501219	178.6992								x	X	
PS144-085-08	13.09.2024	87.468465	177.9871						x	x			
PS144-085-09	13.09.2024	87.461716	177.8681	x	x								
PS144-090-01	16.09.2024	88.366331	-124.529			x			x				
PS144-090-02	16.09.2024	88.369671	-124.256								x	X	
PS144-090-03	16.09.2024	88.372414	-124.096						x				
PS144-097-01	17.09.2024	89.011088	-125.736	x	x	x							
PS144-102-01	17.09.2024	89.335599	-125.424			x							
PS144-102-02	17.09.2024	89.33479	-125.382								x	X	
PS144-102-03	18.09.2024	89.334976	-125.393	x									
PS144-105-01	18.09.2024	89.661802	-126.49	x				x					
PS144-109-02	19.09.2024	89.944758	-151.124	x	x								
PS144-109-03	19.09.2024	89.947455	-150.459								x	X	
PS144-109-07	19.09.2024	89.958721	-135.707						x	x			
PS144-109-08	19.09.2024	89.963881	-128.004			x		x	x				
PS144-115-01	21.09.2024	89.02537	59.44834			x	x						
PS144-115-02	21.09.2024	89.013231	59.0085								x	X	
PS144-123-01	23.09.2024	88.078812	60.18708	x	x								
PS144-123-03	23.09.2024	88.071504	59.82912								x	X	

Event Label	Date	Lat*	Lon*	Water samples									
				Niskin						GoFlo	GoFlo	GoFlo	Seawater line
				234_Th	234_ThPOC	226Ra1L	DIC	228Ra_226Ra_CTD	231Pa_239Thdiss	231Pa_230Thpar	Ba_Clean	232Th_Clean	226Ra/228Ra
PS144-123-04	23.09.2024	88.064437	59.96141			x			x				
PS144-127-01	24.09.2024	87.430227	60.18741					x					
PS144-130-01	24.09.2024	87.332562	59.1921								x	X	
PS144-134-04	25.09.2024	87.004637	58.11287								x	X	
PS144-134-06	26.09.2024	87.040377	57.32827	x	x								
PS144-134-08	26.09.2024	86.983928	58.36968			x	x		x				
PS144-134-10	26.09.2024	87.034589	55.68046								x	X	
PS144-141-01	28.09.2024	86.483746	59.92445										
PS144-141-02	28.09.2024	86.488439	59.6467										
PS144-141-03	28.09.2024	86.492165	59.493										
PS144-144-01	29.09.2024	86.169568	60.02221			x			x				
PS144-144-02	30.09.2024	86.169877	59.87813								x	X	
PS144-144-03	30.09.2024	86.167776	59.78424	x	x			x	x				
PS144-149-01	30.09.2024	85.826752	59.81146			x			x				
PS144-149-02	30.09.2024	85.516704	59.95899								x	X	
PS144-152-02	30.09.2024	85.242844	59.59223								x	X	
PS144-152-03	30.09.2024	85.240475	59.50711	x	x								
PS144-154-01	03.10.2024	83.798611	32.9454								x	X	
PS144-156-02	04.10.2024	82.705758	30.82653	x									
PS144-156-03	04.10.2024	82.693959	30.68898								x	X	
PS144-157-02	05.10.2024	81.853254	30.8927								x	X	
PS144-158-01	05.10.2024	81.529469	30.79433	x	x	x	x		x				
PS144-158-02	05.10.2024	81.52984	30.79266								x	X	
UWAYSWL1	14.08.2024	83.345455	30.86989										x
UWAYSWL2	19.08.2024	85.284125	64.52801										x
UWAYSWL3	21.08.2024	84.573905	102.734										x
UWAYSWL4	28.08.2024	84.302	111.4911										x
UWAYSWL5	29.08.2024	84.499465	115.343										x
UWAYSWL6	30.08.2024	84.722725	120.4569										x
UWAYSWL7	01.09.2024	84.900965	129.4898										x
UWAYSWL8	03.09.2024	84.92899	130.0604										x

Event Label	Date	Lat*	Lon*	Water samples									
				Niskin						GoFlo	GoFlo	GoFlo	Seawater line
				234_Th	234_ThPOC	226Ra1L	DIC	228Ra_226Ra_CTD	231Pa_239Thdiss	231Pa_230Thpar	Ba_Clean	232Th_Clean	226Ra/228Ra
UWAYSWL9	05.09.2024	85.032175	140.0982										x
UWAYSWL10	07.09.2024	85.0421	153.3586										x
UWAYSWL11	07.09.2024	84.96207	160.4982										x
UWAYSWL12	09.09.2024	84.952615	165.4588										x
UWAYSWL13	10.09.2024	84.9236	172.9042										x
UWAYSWL14	11.09.2024	85.15405	178.9695										x
UWAYSWL15	13.09.2024	87.4929	178.4864										x
UWAYSWL16	14.09.2024	87.703265	-171.355										x
UWAYSWL17	16.09.2024	88.44826	-125.16										x
UWAYSWL18	17.09.2024	89.498625	-125.992										x
UWAYSWL19	18.09.2024	89.948575	-145.318										x
UWAYSWL20	20.09.2024	89.503275	60.14867										x
UWAYSWL21	21.09.2024	88.94587	58.90806										x
UWAYSWL22	23.09.2024	87.91425	59.92512										x
UWAYSWL23	24.09.2024	87.240985	59.96614										x
UWAYSWL24	25.09.2024	86.99836	58.22241										x
UWAYSWL25	28.09.2024	86.459745	59.58478										x
UWAYSWL26	29.09.2024	85.77216	59.48465										x
UWAYSWL27	30.09.2024	85.240655	59.4685										x
UWAYSWL28	03.10.2024	83.24886	31.86173										x
UWAYSWL29	04.10.2024	82.24245	30.84611										x

Triplicate samples for intercalibration of ^{232}Th and Ba were taken at two stations (PS144_050_03, PS144_085_03) to full depth from 9 depth intervals.

Dissolved Pb, particulate Pb (labile, refractory) and Pb isotopic composition

Samples for dissolved and particulate Pb were obtained using the AWI trace metal clean CTD rosette equipped with trace metal clean Go-Flo bottles following GEOTRACES sampling protocols (Cutter et al., 2017). To monitor change in Pb cycling between 2015 and 2024, we aimed to reoccupy as many stations from PS94 (TransArc II) as possible. Samples for dPb were filtered through a 0.8/0.2 µm Acropak cartridge filter (Pall corporation) into 125 mL trace metal clean LDPE bottles and acidified to pH 1.9 through addition of ultra-pure hydrochloric

acid (ROMIL) immediately after sampling. Samples for measurements of dissolved Pb isotopic composition were passed through the 0.8/0.2 µm Acropak cartridge filter (Pall corporation) into 1 L or 2 L trace metal clean LDPE bottles and acidified to pH 1.9 through addition of ultra-pure hydrochloric acid (ROMIL) immediately after sampling. Samples for the particulate fractions of Pb (labile particulate, refractory) and for measurements of isotopic composition of particulate Pb were collected on 0.2 µm filters (Millipore) filtering at least 4 L of seawater. Particulate samples are stored in the dark at 20°C.

In total, 31 stations were occupied and sampled for dissolved Pb (dPb, determined together with dissolved bio-essential trace metals) and particulate Pb (pPb, determined together with particulate bio-essential trace metals) (Tab. 2.4). 23 stations were sampled to full depth at 20-22 depth intervals. An additional 8 stations were sampled to 500 or 750 m depth only, respectively, to yield higher resolution in Atlantic Water masses, low salinity surface waters from the East Siberian Shelf (Transpolar Drift) and regions of elevated productivity (as indicated by *in-situ* fluorescence measurements). We obtained a total of 570 samples for determination of dissolved and particulate Pb. 17 stations were sampled for Pb isotopic composition and yielded a total of 131 samples.

Radionuclide Transient Tracers (^{14}C, ^{39}Ar, ^{129}I, ^{236}U)

We collected water samples from Niskin bottles that are attached to a Conductivity-Temperature-Depth (CTD) rosette. The first priority was to sample stations that have been occupied in 2015 (PS94), whenever possible, and in the same vertical resolution. Additionally, we collected more samples on the third transect to cover the Transpolar Drift at a higher resolution (see Fig. 2.8). Generally, sampling for ^{129}I and ^{236}U focused on the upper 1500-2000m. For ^{39}Ar and ^{14}C, we concentrated our sampling effort to intermediate and bottom waters (from 1500 down to 4500 m).

All samples were collected without filtration. We collected ~3L water samples for the analysis of ^{236}U and ^{129}I in plastic cubitainers. We collected ~10L seawater in propane bottles for ^{39}Ar that we filled with nitrogen gas beforehand to have an overpressure inside the bottles and avoid contamination with atmospheric argon. We used 120ml glass bottles to collect ^{14}C samples that were sealed air-tight with a septa, immediately after sampling. All ^{14}C samples were poisoned within one hour with 200 µl mercury chloride solution (37 g/l $HgCl_2$) to avoid organisms to grow inside the samples and modify the DI^{14}C-content.

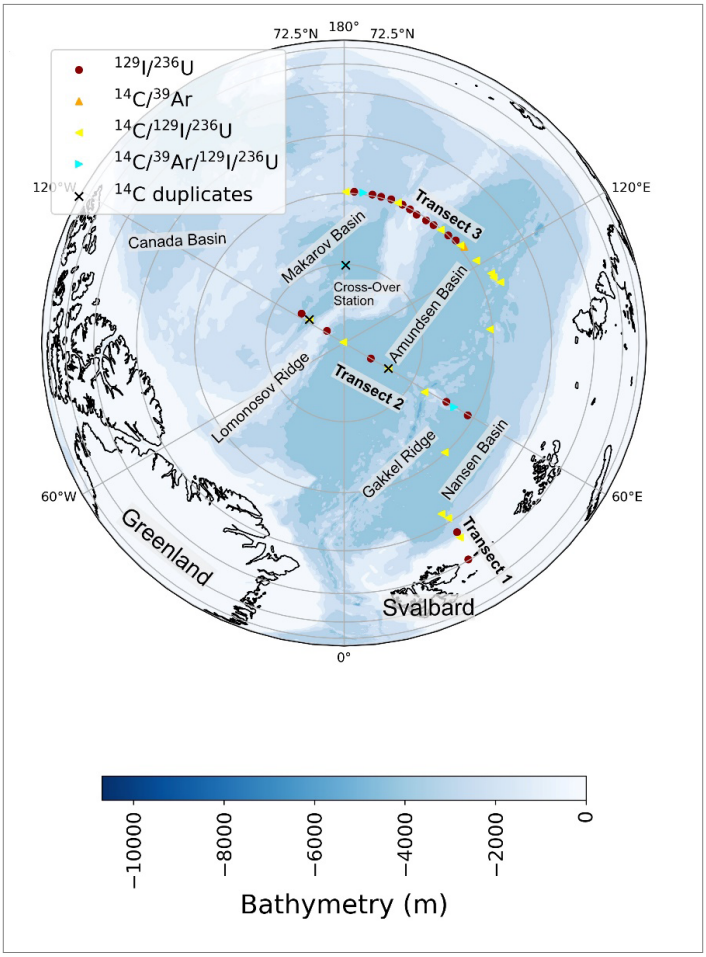

Fig. 2.8: Overview map of sampling location for transient tracers ^{14}C, ^{39}Ar, ^{129}I and ^{236}U during the PS144 expedition to the Central and Eastern Arctic Ocean in 2024.

Tab. 2.9 List of stations from PS144 sampled with the regular CTD water sampling system for transient tracer analysis.

Event Label	Date	Latitude [°N]	Longitude [°E]	Depth [m]	Cast Depth [m]	14C	39Ar	129I	236U
PS144_3_1	14.08.2024	83° 02.066‘	029° 41.883‘	3856.1	3876	X		X	X
PS144_003_03	14.08.2024	83° 02.638‘	029° 57.773‘	3852.2	397	X		X	X
PS144_006_01	16.08.2024	85° 02.145‘	042° 42.291‘	3928.9	3940	X		X	X
PS144_011_02	20.08.2024	85° 06.727‘	095° 22.350‘	4580.9	4515	X		X	X
PS144_018_03	28.08.2024	84° 16.842‘	111° 19.869‘	4045.9	3988	X		X	X
PS144_020_02	28.08.2024	84° 27.685‘	113° 48.383‘	2493.4	2609	X		X	X
PS144_023_02	29.08.2024	84° 29.353‘	115° 20.056‘	4111.8	4018	X		X	X
PS144_028_01	31.08.2024	84° 45.680‘	121° 58.425‘	4383.9	4337	X		X	X
PS144_035_01	01.09.2024	84° 54.616‘	130° 01.961‘	4343.4	4371	X		X	X
PS144_041_01	02.09.2024	84° 49.494‘	128° 42.124‘	4352.3	4323	X	X		
PS144_046_03	04.09.2024	84° 55.711‘	132° 34.335‘	4319.1	4304			X	X
PS144_048_01	04.09.2024	84° 59.904‘	135° 55.436‘	4256.2	4218			X	X
PS144_050_02	04.09.2024	85° 01.866‘	139° 34.962‘	3951	3892	X		X	X

Event Label	Date	Latitude [°N]	Longitude [°E]	Depth [m]	Cast Depth [m]	14C	39Ar	129I	236U
PS144_050_07	05.09.2024	85° 01.542‘	140° 06.527‘	3463.6	3363			X	X
PS144_052_01	05.09.2024	85° 03.885‘	142° 49.429‘	3387.6	3325			X	X
PS144_054_01	06.09.2024	85° 04.874‘	146° 20.084‘	2169.7	2095			X	X
PS144_057_03	06.09.2024	85° 04.977‘	150° 30.550‘	949.9	908			X	X
PS144_059_01	07.09.2024	85° 01.592‘	153° 44.574‘	1542.3	1491			X	X
PS144_064_01	07.09.2024	84° 58.544‘	157° 08.390‘	2510.4	2453			X	X
PS144_065_02	07.09.2024	84° 58.967‘	159° 02.541‘	3434.3	3358	X		X	X
PS144_067_04	08.09.2024	84° 56.537‘	161° 54.287‘	3560.1	3487			X	X
PS144_069_01	09.09.2024	84° 57.320‘	165° 44.451‘	3501	3426			X	X
PS144_073_04	09.09.2024	84° 56.810‘	169° 15.580‘	3424.4	3350			X	X
PS144_075_01	10.09.2024	84° 55.642‘	172° 46.561‘	3174.9	3122	X	X	X	X
PS144_077_01	10.09.2024	84° 55.196‘	176° 15.053‘	2634	2567			X	X
PS144_080_04	11.09.2024	84° 56.091‘	179° 24.891‘	2069.6	2050	X		X	X
PS144_085_02	13.09.2024	87° 31.237‘	178° 53.587‘	3995.9	3923	X	X	X	X
PS144_085_06	13.09.2024	87° 29.439‘	178° 22.565‘	3994.1	3923			X	X
PS144_090_01	16.09.2024	88° 21.823‘	124° 42.572‘ W	3571.2	3486			X	X
PS144_094_01	16.09.2024	88° 40.935‘	123° 53.548‘ W	3995.7	3922	X		X	X
PS144_102_01	17.09.2024	89° 20.159‘	125° 29.274‘ W	1683.6	1626			X	X
PS144_109_08	19.09.2024	89° 57.692‘	131° 55.741‘ W	4265.4	4194	X		X	X
PS144_115_01	21.09.2024	89° 02.279‘	059° 55.955‘	4383.8	4333			X	X
PS144_121_01	22.09.2024	88° 23.805‘	060° 11.076‘	4393.5	4345	X		X	X
PS144_134_09	26.09.2024	86° 59.372‘	058° 34.250‘	4846.1	4790	X		X	X
PS144_144_02	28.09.2024	86° 10.061‘	060° 06.685‘	3908.7	3836			X	X
PS144_147_01	29.09.2024	85° 49.800‘	059° 51.312‘	3926.9	3852	X	X	X	X
PS144_152_01	30.09.2024	85° 14.943‘	059° 46.694‘	3925.2	3851			X	X
PS144_156_02	04.10.2024	82° 42.224‘	030° 49.438‘	3691.7	3617	X		X	X
PS144_157_02	04.10.2024	81° 51.237‘	030° 53.378‘	3166.1	3090			X	X
PS144_158_01	05.10.2024	81° 31.824‘	030° 48.552‘	834.9	793	X		X	X
PS144_159_01	05.10.2024	80° 05.095‘	029° 54.372‘	307.8	293			X	X

Tab. 2.10: Overview of all samples collected during the PS144 expedition to the Central and Eastern Arctic Ocean in 2024.

Parameter	# of Stations	Samples per Station	Total # of Samples
^{14}C	22	5-12	198
^{39}Ar	4	7-8	30
^{129}I	41	1-15	379
^{236}U	41	1-15	379

Ancillary Parameters (Macronutrients, DOP/DON, DIC/TA, DOC, $\delta^{18}O$, Salinity)

Samples for macronutrients (nitrate, nitrite, ammonium, phosphate, and silicic acid), dissolved organic phosphorus and dissolved organic nitrogen (DOP/DON), dissolved inorganic carbon and total alkalinity (DIC/TA), stable oxygen isotopes ($\delta^{18}O$) and salinity were taken using the AWI contamination-free titanium CTD rosette (KUM, equipped with a SBE 911 CTD) equipped with trace metal clean Go-Flo bottles and a clean winch (KleyFrance).

Samples for surface macronutrients (100-200 m depth) remained unfiltered, and were refrigerated until analysis on-board by the MBC group (within 12-24h after collection) following well-established methods (see Chapter 5). 240 samples were analysed on-board. Additional macronutrient samples (350 samples for deep and surface waters) were filtered to 0.2 µm using Acropak cartridges (Pall Cooperation) into acid-clean 15 mL centrifuge tubes and frozen (-20°C) immediately after sampling, stored in the dark and were transported to GEOMAR for analysis (QuAAtro).

Samples for DOP/DON were filtered to 0.8/0.2 µm using Acropak cartridges (Pall Cooperation) into 50 mL centrifuge tubes. Samples were frozen immediately after sampling (-20°C) and stored in the dark until analysis at GEOMAR.

Samples for DIC and TA were taken together and remained unfiltered. DIC/TA samples were collected from the surface 75 m (usually from 15 m, 25 m, 50 m and 75 m depth) into 250 mL brown glass bottles (DURA) immediately after CTD recovery. Care was taken to avoid changes in the gas equilibrium since this may impact the carbonate system. Flexible tubing was used and went to the bottom of the glass bottle. The bottle was filled to the top whilst turning it to avoid bubble formation on the side of the bottle. The tubing was then gently withdrawn (still with sample flowing into the bottle and turning the bottle) and the bottle caped. Care was taken that the bottle had little to no air inside. Samples were then spiked with 250 µL of HgCl2 solution (37g/L) whilst minimising exposure of the sample to the atmosphere. The bottles were then closed tightly and firmly shaken, stored in the dark and shipped to GEOMAR for analysis. In total, 44 samples were taken for DIC abd TA.

Samples for DOC and $\delta^{18}O$ and were taken for Rainer Amon and Dorothea Bauch (MBC group) from selected stations and depth to increase the resolution of the regular CTD DOC profile. Samples were taken exactly as described in chapter 5. The stations and depths at which DOC and $\delta^{18}O$ samples were taken are found in the cleanCTD station log sheets ('water budget').

Samples for salinity were taken to calibrate the CTD sensor immediately after clean CTD recovery and transfer of bottles into the clean room container. In total, 20 stations were sampled in duplicate at two depths for salinity. 250 mL bottles were used and filled three times to overflow using a flexible tubing reaching to the bottom of the bottle. The rubber stopper lid was rinsed three times. After a final refill of the salinity bottle, approximately 50 mL was discarded and used to rinse the lid a final time before closing the bottle with the rubber stopper. The bottles were then rinsed with tap water and clamped with a metal cover immediately thereafter to avoid evaporation. Samples were measured directly onboard as described in chapter 4.

Preliminary (expected) results

Aerosol trace metals and major ions

Sample analysis will be done using methods applied to several other GEOTRACES cruises (e.g. Chance et al., 2015; Baker et al., 2020). This will allow us to estimate the contributions of different aerosol sources (e.g. combustion, mineral dust) to the atmospheric nutrient input to the Eastern Arctic Ocean, and (together with air mass trajectory analysis) to examine the

spatial distribution of these sources. Detailed chemical analysis will also provide information on the factors that control micronutrient solubility and hence influence bioavailable nutrient supply. We expect higher concentrations of aerosol trace metals in the Eurasian Basin owing to their proximity to sources which includes Siberian Forest fires, smelters, and urban emissions. Much lower concentrations, particularly in atmospheric inorganic pollutants are expected for the more Central Arctic Ocean owing to increasing precipitation (by rain and snow) with increasing distance from the shore.

Nutrient addition bioassay experiments

We expect that the Eastern and Central Arctic Ocean surface waters hosts two contrasting nutrient regimes in late summer: a.) Fe-replete, but fixed N-scarce conditions in surface waters of the Central Arctic Ocean Transpolar Drift, with low initial biomass owing to light limitation, and b.) Fe-scarce conditions, with a standing stock of fixed N and comparatively elevated phytoplankton concentrations in surface waters of the Eastern Arctic Ocean Nansen Basin. We expect that the interplay between Transpolar Drift and Atlantic Waters has a profound impact on late summer primary production in the region.

Dissolved and particulate trace metals (Fe, Mn, Co, Ni, Cu, Zn, Cd)

We expect comparatively low concentrations of dissolved and particulate trace metals in the Eastern Arctic Ocean, particularly the Nansen Basin, compared to the Central Arctic Ocean which is under the influence from surface offshore advection of shelf-derived material with the Transpolar Drift. Concentrations of dissolved micronutrients are expected to increase with depth in the Eastern Arctic Ocean due to phytoplankton uptake in surface waters and remineralisation at depth. Conversely, we anticipate dissolved micronutrient concentration to be considerably lower than surface concentrations in the water column beneath the Transpolar Drift.

We expect dissolved micronutrient transport with the Transpolar Drift to have increased between 2007, 2015 and 2024 owing to increased fluxes of shelf-derived material across the East Siberian Shelf break. Yet, the decline in Central Arctic Ocean sea-ice cover may have resulted in increasing destabilisation of the underlying dissolved micronutrient-enriched Polar Surface Water and a less efficient micronutrient transport (‘patchy’) towards Fram Strait. We expect that Arctic Ocean surface primary production is thus increasingly depended on mixing between dFe-replete waters of the Transpolar Drift, and macronutrients (i.e. fixed N) supplied by Atlantic Water.

Dissolved Fe isotopic composition (δ^{56}dFe)

We expect changes in the relative importance of different iron sources along a south-to-north gradient between surface waters influenced by Atlantic Water (Eastern Arctic Ocean) and those influenced by the pronounced offshore transport of dFe with the Transpolar Drift. We expect the flow path of the Transpolar Drift low salinity waters to be characterised by near-crustal δ^{56}Fe signature as has previously been observed (around +0.1‰, but “ranging from −0.4‰ to +0.5‰” (Charette et al., 2020)). Regions and water layers of elevated primary production such as the Nansen Basin and the Barents Sea shelf break may show a heavy residual δ^{56}dFe, owing to preferential uptake of light Fe-isotopes by phytoplankton (Fitzsimmons & Conway, 2023). Vice versa, remineralisation of organic matter at depth or in sediments is expected to result in a low δ^{56}dFe pool. Dissolved Fe in the deep waters of the Eurasian Basin (> 1,200 m depth) is likely sourced from offshore advection of shelf material (Rutgers van der Loeff et al., 2018), likely with an isotopically light to crustal signature, with the effect of reversible scavenging with sinking particles modifying δ^{56}dFe (Fitzsimmons et al., 2017). More locally, the deep Arctic Ocean basin will also receive dFe inputs from hydrothermal sources (Klunder et al., 2012)

which may be characterised by low δ^{56}dFe in the case of high-temperature hydrothermal fluid venting (Fitzsimmons & Conway, 2023).

Rare earth element concentrations and neodymium isotopes

Deep samples (> 1,500 m water depth) from reoccupied stations of cruise PS94 will be used for quality control since the deep-water column is not expected to have changed in REE and Nd isotope compositions.

Gallium

With samples collected during PS144, we will affirm the conservative nature of gallium in the region and leverage it in a multi-tracer approach to deconvolve different water masses in the Eurasian basin. The section in the Makarov Basin will be among the first Ga sections in the region, we expect that this area is highly influenced by decadal, atmospheric-oceanic coupling and switchgear mechanisms. We anticipate finding that distributions of gallium in the Eurasian basin is stable in deeper waters, but waters near the surface influenced by freshwater and greater vertical mixing may differ between 2015 and 2024.

Mercury

We expect to measure higher concentrations of total Hg and MeHg due to the increased mean temperature during the summer, the decrease in MYI, and possibly higher inputs from rivers and thawing permafrost. We expect to observe and quantify the vertical transport of MMHg methylated at the bottom of the AO to the lower levels of marine trophic chains, namely phyto- and zooplankton. Combining the data from 2007, 2015, and 2024, we expect to have robust evidence of the possible temporal evolution of the Arctic Ocean Hg reservoir.

Natural radionuclides (^{230}Th, ^{231}Pa, ^{232}Th, ^{226}Ra, ^{228}Ra)

For ^{231}Pa and ^{230}Th, we expect to produce full water depth profiles from stations that were previously occupied during GEOTRACES, in order to assess temporal variability, e.g. trends in particle flux and advection due to changing climate, or at sites where previously hydrothermal removal aspects were seen. For ^{226}Ra, we expect to produce one or more sections with the best possible precision, in order to see scavenging effects and possibly release from slopes. ^{228}Ra/^{226}Ra will be sampled in surface waters to see if the trends that were previously observed and attributed to enhanced release from warming shelves continue. This is part of the international ARION partnership (AWI/ WHOI/ 1st Institute of Oceanography China). Ba will be assessed in context with previous analyses of freshwater systems. In total, we expect to cover possible changes in a broad range of sources to Arctic biogeochemistry, in line with the Arcwatch missions.

Dissolved Pb, particulate Pb (labile, refractory) and Pb isotopic composition

We expect dPb concentrations and fractions of anthropogenic vs. natural dPb in the Eastern Arctic Ocean to have declined between 2015 and 2024, owing to continuous scavenging of dPb from the water column (Cochran et al., 1990) in response to the phase-out of leaded gasoline and restriction to industrial emissions of Pb (Nriagu, 1990; Pacyna et al., 2009). During the same time interval, dPb concentrations in the Central Arctic Ocean may have increased, related to increased freshwater discharge to the East Siberian Shelf (Feng et al., 2021), enriched in natural Pb (Guay et al., 2010), and transport with the Transpolar Drift (Charette et al., 2020). We anticipate that Pb with anthropogenic signature penetrated into deep waters of the Eurasian basins (> 1,500 m). Primary production and (reversible) scavenging with/on sinking particles, particularly along the Arctic Ocean boundaries, are major factors in Pb export and burial at depth.

Radionuclide Transient Tracers (^{14}C, ^{39}Ar, ^{129}I, ^{236}U)

After the expedition ^{39}Ar samples will be sent to the University of Heidelberg for measurements. Traditional low-level counting would require very large volumes due to the low abundance of 10^{-16} moles of ^{39}Ar in seawater. Therefore, the new technique Atom Trap Trace Analysis (ATTA) is applied. With this method, single atoms are caught with a magneto-optical trap, counted and the ratio of dissolved $^{39}Ar/Ar$ is deduced for each sample.

^{39}Ar is produced in the atmosphere and becomes isolated from its source as it enters the ocean through air-sea gas exchange. ^{39}Ar decays thereafter with a half-life of 269 years leading to lower concentrations in water masses that have not been in contact with the atmosphere for a long time. This can be used to calculate isolation ages and residence times of the seawater samples.

^{14}C, ^{129}I and ^{236}U samples will be sent to ETH Zurich for further processing in the laboratory and measurements with Accelerator Mass Spectrometry (AMS). Samples for ^{14}C in DIC will be degassed. $^{14}CO_2$ is then graphitized and measured via AMS. The radioisotopes ^{129}I and ^{236}U are present as dissolved ions in seawater, hence, these two tracers have to undergo a pre-concentration step in the laboratory leading to silver and iron participates for ^{129}I and ^{236}U, respectively, and will be measured via AMS as well. We will conduct the measurements of ^{236}U and ^{129}I at the Laboratory of Ion Beam Physics (ETH Zurich), using the Tandy and MILEA Accelerator Mass Spectrometry (AMS) systems for ^{129}I and ^{236}U, respectively. For the measurement of ^{14}C, we will use the Mini radiocarbon Dating System (MICADAS).

We will apply the Transit Time Distribution (TTD) model to the dataset by combining ^{129}I and ^{236}U concentrations, and ^{14}C and ^{39}Ar, separately. The model yields a probability function of different tracer ages for each water sample. This model enables us to calculate water mass transport timescales from the entrance of the Arctic Ocean to the specific station and depth where we collected the sample. With the TTD results from ^{39}Ar and ^{14}C we will infer the age of the intermediate and deep-water samples i.e. the time when it was last in contact with the atmosphere. This will give us ventilation timescales of these intermediate and deep-water samples.

As for results, we expect higher concentrations of ^{129}I and ^{236}U in the Polar Surface Water and Arctic Atlantic Waters. These water masses carry the tracer signal coming from two Reprocessing Plants in Europe into the Arctic Ocean through Fram Strait and the Barents Sea Opening. Deeper and old water masses have not been labeled by this signal and therefore are expected to have lower concentrations. For ^{14}C and ^{39}Ar, we expect higher concentrations in the upper water column decreasing with depth. These two radionuclides have their origin in the atmosphere which injects the tracer signal into the ocean via air-sea gas exchange. Deep and old water masses are therefore depleted with ^{14}C and ^{39}Ar as they have not been in contact with the atmosphere for a longer period and lost parts of the initial concentration through radioactive decay.

Data Management

Aerosol trace metals and major ions

The samples will be analysed by Alex Baker at the University of East Anglia. Quality control will be achieved through analysis of liquid- and solid phase certified reference materials. Results will be submitted to the international GEOTRACES data management office (BODC, www.bodc.ac.uk/geotraces) under the data management scheme agreed upon in the GEOTRACES programme available at http://www.geotraces.org.

Nutrient addition bioassay experiments

The results will be published on the PANGAEA Database and submitted to the international GEOTRACES data management office (BODC, www.bodc.ac.uk/geotraces) under the data management scheme agreed upon in the GEOTRACES programme available at http://www.geotraces.org.

Dissolved and particulate trace metals (Fe, Mn, Co, Ni, Cu, Zn, Cd)

The samples will be analysed at GEOMAR. Quality control will be achieved through intercalibration from triplicate samples of stations PS144_050_03 and PS144_085_03 which were previously occupied in 2015. Analytical runs are validated through the analysis of reference materials. The GEOTRACES Standards and Intercalibrations Committee will be asked for evaluation and approval. Results will be made available to the public within 2 years after the expedition.

The results will be published on the PANGAEA Database and submitted to the international GEOTRACES data management office (BODC, www.bodc.ac.uk/geotraces) under the data management scheme agreed upon in the GEOTRACES programme available at http://www.geotraces.org.

Dissolved Fe isotopic composition (δ^{56}dFe)

Dissolved Fe isotope ratios will be measured at Tampa Bay Plasma Facility at the University of South Florida following well-established chemical processing methods via multi-collector ICPMS (Conway et al., 2013). The samples will be analysed by Stephan Krisch and Tim M. Conway within two years after completion of the expedition. Quality control will be achieved through intercalibration from triplicate samples of stations PS144_152_02 and through the use of reference materials. The data will be submitted to Pangaea and the international GEOTRACES data management office (BODC, www.bodc.ac.uk/geotraces) under the data management scheme agreed upon in the GEOTRACES programme available at http://www.geotraces.org.

Rare earth element concentrations and neodymium isotopes

These results will be submitted to the GEOTRACES Intercalibration and Standards Committee for evaluation and approval. All data and metadata will be submitted to Pangaea and the international GEOTRACES data management office (BODC, www.bodc.ac.uk/geotraces) under the data management scheme agreed upon in the GEOTRACES programme available at http://www.geotraces.org.

Gallium

Deep samples (> 1,500 m water depth) from reoccupied stations of cruise PS94 will be used for quality control since the deep-water column is not expected to have changed in Ga concentrations. These results will be submitted to the GEOTRACES Intercalibration and Standards Committee for evaluation and approval. All data and metadata will be submitted to the Arctic Data Center and the international GEOTRACES data management office (BODC, www.bodc.ac.uk/geotraces) under the data management scheme agreed upon in the GEOTRACES programme available at http://www.geotraces.org.

Mercury

Reference materials will be used to validate all analytical runs through analysis. Quality control measures will include intercalibration with triplicate samples from two stations that

were also targeted in 2015. The evaluation and approval of the GEOTRACES Standards and Intercalibrations Committee will be sought. The results will be available to the public within a two-year time frame after the expedition. The PANGAEA Database will be the primary repository for the obtained results, submitted to the international GEOTRACES data management office (BODC, www.bodc.ac.uk/geotraces) under the data management scheme agreed upon in the GEOTRACES programme (http://www.geotraces.org).

Natural radionuclides (^{230}Th, ^{231}Pa, ^{232}Th, ^{226}Ra, ^{228}Ra)

Data acquired will be part of the international GEOTRACES programme, which has a dedicated data management plan, including standardized quality management, standardized variables and units, data curation, a database hosted at the British Oceanography Data Centre, and defined open data/accessibility plans.

Dissolved Pb, particulate Pb (labile, refractory) and Pb isotopic composition

Quality control for dissolved Pb analysis will be achieved through intercalibration from triplicate samples of stations PS144_050_03 and PS144_085_03. Analytical runs are validated through the analysis of reference materials. The GEOTRACES Standards and Intercalibrations Committee will be asked for evaluation and approval. The samples for dPb, labile particulate and refractory Pb will be analysed by Yaqing Ruan at GEOMAR. Measurements of isotopic composition of dPb and particulate Pb will be conducted by Mengli Chen and Xianfeng Wang in Singapore. Results will be made available to the public within 2 years after the expedition. The results will be published on the PANGAEA Database and submitted to the international GEOTRACES data management office (BODC, www.bodc.ac.uk/geotraces) under the data management scheme agreed upon in the GEOTRACES programme available at http://www.geotraces.org.

Radionuclide Transient Tracers (^{14}C, ^{39}Ar, ^{129}I, ^{236}U)

The results will be published on the MARIS Database and submitted to the international GEOTRACES data management office (BODC, www.bodc.ac.uk/geotraces) under the data management scheme agreed upon in the GEOTRACES programme available at http://www.geotraces.org. Data will be archived, published and disseminated according to international standards by the World Data Center PANGAEA Data Publisher for Earth & Environmental Science (https://www.pangaea.de) within two years after the end of the expedition at the latest. By default, the CC-BY license will be applied.

Data to be archived according to international standards by the World Data Center PANGAEA Data Publisher for Earth & Environmental Science (https://www.pangaea.de) will be published and disseminated within two years after the end of the expedition at the latest. By default, the CC-BY license will be applied.

This expedition was supported by the Helmholtz Research Programme “Changing Earth – Sustaining our Future”, Topics 2 and 6, Subtopics 2.1, 2.4 and 6.1, 6.3.

In all publications based on this expedition, the **Grant No. AWI_PS144_01** will be quoted and the following publication will be cited:

Alfred-Wegener-Institut Helmholtz-Zentrum für Polar- und Meeresforschung (2017) Polar Research and Supply Vessel POLARSTERN Operated by the Alfred-Wegener-Institute. Journal of large-scale research facilities, 3, A119. http://dx.doi.org/10.17815/jlsrf-3-163.

References

Achterberg EP (2022) Arctic – Atlantic Exchange of the Dissolved Micronutrients Iron, Manganese, Cobalt, Nickel, Copper and Zinc With a Focus on Fram Strait. Global Biogeochem. Cycles 36: e2021GB007191. https://doi.org/10.1029/2021GB007191

AMAP Assessment (2021) Mercury in the Arctic | AMAP, 2021. Tromsø, Norway.

Ardyna M, Hamilton DS, Harmel T, Lacour L, Bernstein DN, Laliberté J, Horvat C, Laxenaire R, Mills MM, van Dijken G, Polyakov I, Claustre H, Mahowald N, Arrigo KR (2022) Wildfire aerosol deposition likely amplified a summertime Arctic phytoplankton bloom. Commun. Earth Environ. 3:201. https://doi.org/10.1038/s43247-022-00511-9

Baker AR, Li M, Chance RJ (2020) Trace metal fractional solubility in size-segregated aerosols from the tropical eastern Atlantic Ocean, Global Biogeochemical Cycles 34:e2019GB006510. https://doi.org/10.1029/2019GB006510

Boyle E A, Lee J M, Echegoyen Y, Noble A, Moos S, Carrasco G, et al. (2014) Anthropogenic lead emissions in the ocean: The evolving global experiment. Oceanography 27(1):69–75. https://doi.org/10.5670/oceanog.2014.10

Carignan J, Hillaire-Marcel C, De Vernal A (2008) Arctic vs. North Atlantic water mass exchanges in Fram Strait from Pb isotopes in sediments, Canadian Journal of Earth Sciences 45(11):1253–1263. https://doi.org/10.1139/E08-050

Casacuberta N, Christl M, Vockenhuber C, Wefing A M, Wacker L, Masqué P, Synal H A & Rutgers van der Loeff M (2018) Tracing the Three Atlantic Branches Entering the Arctic Ocean With ^{129}I and ^{236}U. Journal of Geophysical Research: Oceans 123(9): 6909–6921. https://doi.org/10.1029/2018JC014168

Chance RJ, Jickells TD, Baker AR (2015) Atmospheric trace metal concentrations, solubility and deposition fluxes in remote marine air over the south-east Atlantic, Marine Chemistry 177:45–56. https://doi.org/10.1016/j.marchem.2015.06.028

Charette MA, Kipp LE, Jensen LT, Dabrowski JS, Whitmore LM, Fitzsimmons JN, et al. (2020) The Transpolar Drift as a Source of Riverine and Shelf-Derived Trace Elements to the Central Arctic Ocean. Journal of Geophysical Research: Oceans 125(5):e2019JC015920. https://doi.org/10.1029/2019JC015920

Cochran JK, McKibbin-Vaughan T, Dornblaser, MM, Hirschberg D, Livingston HD, & Buesseler KO (1990) ^{210}Pb scavenging in the North Atlantic and North Pacific Oceans. Earth and Planetary Science Letters 97(3–4):332–352. https://doi.org/10.1016/0012-821X(90)90050-8

Conca E, Abollino O, Giacomino A, Buoso S, Traversi R, Becagli S, Grotti M, Malandrino M (2019) Source identification and temporal evolution of trace elements in PM10 collected near to Ny-Ålesund (Norwegian Arctic). Atmos. Environ. 203:153–165. https://doi.org/10.1016/j.atmosenv.2019.02.001

Conway TM, Rosenberg AD, Adkins JF & John SG (2013) A new method for precise determination of iron, zinc and cadmium stable isotope ratios in seawater by double-spike mass spectrometry. Analytica Chimica Acta 793:44–52. https://doi.org/10.1016/j.aca.2013.07.025

Cutter G, Casciotti K, Croot P, Geibert W, Heimbürger LE, Lohan M, et al. (2017) Sampling and Sample-handling Protocols for GEOTRACES Cruises. GEOTRACES Standards and Intercalibration Committee. Retrieved from http://www.geotraces.org/science/intercalibration/222-sampling-and-sample-handling-protocols-for-geotraces-cruises

Feng D, Gleason CJ, Lin P, Yang X, Pan M, Ishitsuka Y (2021) Recent changes to Arctic river discharge. Nat. Commun. 12:6917. https://doi.org/10.1038/s41467-021-27228-1

Dastoor A, Angot H, Bieser J, Christensen JH, Douglas TA, Heimbürger-Boavida LE, Jiskra M, Mason RP, McLagan DS, Obrist D, Outridge M., Petrova MV, Ryjkov A, St. Pierre KA, Schartup AT, Soerensen AL, Toyota K, Travnikov O, Wilson SJ, Zdanowicz C (2022) Arctic mercury cycling. Nat Rev Earth Environ 3:270–286. https://doi.org/10.1038/s43017-022-00269-w

De Vera J, Chandan P, Landing WM, Stupple GW, Steffen A, Bergquist BA (2021) Amount, Sources, and Dissolution of Aerosol Trace Elements in the Canadian Arctic. ACS Earth Sp. Chem. 5:2686–2699. https://doi.org/10.1021/acsearthspacechem.1c00132

De Vera J, Chandan P, Pinedo-González P, John SG, Jackson S, Cullen JT, et al. (2021) Anthropogenic lead pervasive in Canadian Arctic seawater. Proceedings of the National Academy of Sciences of the United States of America 118(24):e2100023118. https://doi.org/10.1073/pnas.2100023118

Feng D, Gleason CJ, Lin P, Yang X, Pan M, & Ishitsuka Y (2021) Recent changes to Arctic river discharge. Nature Communications 12:6917. https://doi.org/10.1038/s41467-021-27228-1

Fisher JA, Jacob DJ, Soerensen AL, Amos HM, Steffen A, Sunderland EM (2012) Riverine source of Arctic Ocean mercury inferred from atmospheric observations. Nature Geosci 5:499–504. https://doi.org/10.1038/ngeo1478

Fitzsimmons J N, John SG, Marsay CM, Hoffman CL, Nicholas SL, Toner BM, et al. (2017) Iron persistence in a distal hydrothermal plume supported by dissolved-particulate exchange. Nature Geoscience 10(3):195–201. https://doi.org/10.1038/ngeo2900

Fitzsimmons JN & Conway TM (2023) Novel Insights into Marine Iron Biogeochemistry from Iron Isotopes. Annu. Rev. Mar. Sci. 15:383–406. https://doi.org/10.1146/annurev-marine-032822

García-Ibáñez M and Jeandel C (2018) The ^{226}Ra–Ba relationship in the North Atlantic during GEOTRACES-GA01. Biogeosciences 15:3027–3048.

Gobeil C, Macdonald R W, Smith J N, Beaudin L (2001) Atlantic Water Flow Pathways Revealed by Lead Contamination in Arctic Basin Sediments. Science 293(5533):1301–1304. https://doi.org/10.1126/science.1062167

Gong SL, Barrie LA (2005) Trends of heavy metal components in the Arctic aerosols and their relationship to the emissions in the Northern Hemisphere. Sci. Total Environ. 342:175–183. https://doi.org/10.1016/j.scitotenv.2004.12.031

Guay CKH, Zhulidov AV, Robarts RD, Zhulidov DA, Gurtovaya TY, Holmes RM, Headley, JV (2010) Measurements of Cd, Cu, Pb and Zn in the lower reaches of major Eurasian arctic rivers using trace metal clean techniques. Environmental Pollution 158(2):624–630. https://doi.org/10.1016/j.envpol.2009.08.039

Hamilton DS, Perron MMG, Bond TC, Bowie AR, Buchholz RR, Guieu C, Ito A, Maenhaut W, Myriokefalitakis S, Olgun N, Rathod SD, Schepanski K, Tagliabue A, Wagner R, Mahowald NM (2022) Earth, Wind, Fire, and Pollution: Aerosol Nutrient Sources and Impacts on Ocean Biogeochemistry. Ann. Rev. Mar. Sci. 14:303–330. https://doi.org/10.1146/annurev-marine-031921-013612

Hawkings JR, Linhoff BS, Wadham JL, Stibal M, Lamborg CH, Carling GT, Lamarche-Gagnon G, Kohler TJ, Ward R, Hendry KR, Falteisek L, Kellerman AM, Cameron KA, Hatton JE, Tingey S, Holt AD, Vinšová P, Hofer S, Bulínová M, Větrovský T, Meire L, Spencer RGM (2021) Large subglacial source of mercury from the southwestern margin of the Greenland Ice Sheet. Nat. Geosci. 14, 496–502. https://doi.org/10.1038/s41561-021-00753-w

Heimbürger LE, Sonke JE, Cossa D, Point D, Lagane C, Laffont L, Galfond BT, Nicolaus M, Rabe B, Rutgers van der Loeff MM (2015) Shallow methylmercury production in the marginal sea ice zone of the central Arctic Ocean. Sci Rep 5, 10318. https://doi.org/10.1038/srep10318

Ingvaldsen RB, Assmann KM, Primicerio R, Fossheim M, Polyakov IV & Dolgov AV (2021) Physical manifestations and ecological implications of Arctic Atlantification. Nature Reviews Earth & Environment 2(12):874–889. https://doi.org/10.1038/s43017-021-00228-x

Jiskra M, Heimbürger-Boavida LE, Desgranges M-M, Petrova MV, Dufour A, Ferreira-Araujo B, Masbou J, Chmeleff J, Thyssen M, Point D, Sonke JE (2021) Mercury stable isotopes constrain atmospheric sources to the ocean. Nature 597:678–682. https://doi.org/10.1038/s41586-021-03859-8

Jørgensen CJ, Søndergaard J, Larsen MM, Kjeldsen KK, Rosa D, Sapper SE, Heimbürger-Boavida L-E, Kohler SG, Wang F, Gao Z, Armstrong D and Albers CN (2024) Large mercury release from the Greenland Ice Sheet invalidated, Sci. Adv., 10: eadi7760. https://doi.org/10.1126/sciadv.adi7760 .

Kipp LE, Charette MA, Moore WS, Henderson PB, Rigor IG (2018) Increased fluxes of shelf-derived materials to the central Arctic Ocean. Sci. Adv. 4:eaao1302. https://doi.org/10.1126/sciadv.aao1302

Klunder MB, Laan P, Middag R, De Baar HJW & Bakker K (2012) Dissolved iron in the Arctic Ocean: Important role of hydrothermal sources, shelf input and scavenging removal. Journal of Geophysical Research 117:C04014. https://doi.org/10.1029/2011JC007135

Kohler SG, Heimbürger-Boavida LE, Petrova MV, Digernes MG, Sanchez N, Dufour A, Simić A, Ndungu K, Ardelan MV (2023) Arctic Ocean's wintertime mercury concentrations limited by seasonal loss on the shelf | Nature Geoscience. Nat. Geosci. 15:621–626. https://doi.org/10.1038/s41561-022-00986-3

Krisch S, Browning TJ, Graeve M, Ludwichowski KU, Lodeiro P, Hopwood MJ, Roig S, Yong JC, Kanzow T, Achterberg EP (2020) The influence of Arctic Fe and Atlantic fixed N on summertime primary production in Fram Strait, North Greenland Sea. Sci. Rep. 10:15230. https://doi.org/10.1038/s41598-020-72100-9

Krisch S, Hopwood MJ, Roig S, Gerringa LJA, Middag R, Rutgers van der Loeff MM, Petrova MV, Lodeiro P, Colombo M, Cullen JT, Jackson SL, Heimbürger-Boavida L, Law KS, Stohl A (2007) Arctic air pollution: Origins and impacts. Science (80) 315:1537–1540. https://doi.org/10.1126/science.1137695

Lewis KM, Van Dijken GL, Arrigo KR (2020) Changes in phytoplankton concentration now drive increased Arctic Ocean primary production. Science (80) 369:198–202. https://doi.org/10.1126/science.aay8380

McAlister JA, Orians KJ (2015) Dissolved gallium in the Beaufort Sea of the Western Arctic Ocean: A GEOTRACES cruise in the International Polar Year. Marine Chemistry 177:101–109. https://doi.org/10.1016/j.marchem.2015.05.007

Meredith M, Sommerkorn M, Cassotta S, Derksen C, Ekaykin A, Hollowed A, Kofinas G, Mackintosh A, Melbourne-Thomas J, Muelbert MMC, Ottersen G, Pritchard H, Schuur, EAG (2019) Polar Regions, in: IPCC Special Report on the Ocean and Cryosphere in a Changing Climate. pp. 203–320.

Mills MM, Brown ZW, Laney SR, Ortega-Retuerta E, Lowry KE, van Dijken GL, Arrigo KR (2018) Nitrogen Limitation of the Summer Phytoplankton and Heterotrophic Prokaryote Communities in the Chukchi Sea. Front. Mar. Sci. 5:362. https://doi.org/10.3389/fmars.2018.00362

Nriagu JO (1990) The rise and fall of leaded gasoline. Science of The Total Environment 92(C):13–28. https://doi.org/10.1016/0048-9697(90)90318-O

Ortega-Retuerta E, Jeffrey WH, Ghiglione JF, Joux F (2012) Evidence of heterotrophic prokaryotic activity limitation by nitrogen in the Western Arctic Ocean during summer. Polar Biol. 35:785–794. https://doi.org/10.1007/s00300-011-1109-8

Pacyna JM, Pacyna EG, & Aas W (2009) Changes of emissions and atmospheric deposition of mercury , lead , and cadmium. Atmospheric Environment 43(1):117–127. https://doi.org/10.1016/j.atmosenv.2008.09.066

Paffrath R, Laukert G, Bauch D, Rutgers van der Loeff M, Pahnke K (2021) Separating individual contributions of major Siberian rivers in the Transpolar Drift of the Arctic Ocean. Scientific Reports 11:8216. https://doi.org/10.1038/s41598-021-86948-y

Paffrath R, Pahnke K, Böning P, Rutgers van der Loeff M, Valk O, Gdaniec S, Planquette H (2021) Seawater-Particle Interactions of Rare Earth Elements and Neodymium Isotopes in the Deep Central Arctic Ocean. Journal of Geophysical Research: Oceans 126:e2021JC017423. https://doi.org/10.1029/2021JC017423

Petrova MV, Krisch S, Lodeiro P, Valk O, Dufour A, Rijkenberg MJA, Achterberg EP, Rabe B, Rutgers van der Loeff M, Hamelin B, Sonke JE, Garnier C, Heimbürger-Boavida LE (2020) Mercury species export from the Arctic to the Atlantic Ocean. Marine Chemistry 225:103855. https://doi.org/10.1016/j.marchem.2020.103855

Polyakov IV, Pnyushkov AV, Alkire MB, Ashik IM, Baumann TM, Carmack EC, Goszczko I, Guthrie J, Ivanov VV, Kanzow T, Krishfield R, Kwok R, Sundfjord A, Morison J, Rember R, Yulin A (2017) Greater role for Atlantic inflows on sea-ice loss in the Eurasian Basin of the Arctic Ocean. Science (80) 356:285–291. https://doi.org/10.1126/science.aai8204

Polyakov IV, Alkire MB, Bluhm BA, Brown KA, Carmack EC, Chierici M, Danielson SL, Ellingsen I, Ershova EA, Gårdfeldt K, Ingvaldsen RB, Pnyushkov AV, Slagstad D, Wassmann P (2020) Borealization of the Arctic Ocean in Response to Anomalous Advection From Sub-Arctic Seas. Frontiers in Marine Science 7.

Rijkenberg MJA, Slagter HA, Rutgers Van Der Loeff MM, Ooijen JV & Gerringa LJA (2018). Dissolved Fe in the deep and upper Arctic Ocean with a focus on Fe limitation in the Nansen Basin. Frontiers in Marine Science 5:88. https://doi.org/10.3389/fmars.2018.00088

Roca-Martí M, Puigcorbé V, Rutgers van der Loeff MM, Katlein C, Fernández-Méndez M, Peeken I and Masqué P (2016) Carbon export fluxes and export efficiency in the central Arctic during the record sea-ice minimum in 2012: a joint $^{234}Th/^{238}U$ and $^{210}Po/^{210}Pb$ study. Journal of Geophysical Research: Oceans 121:5030–5049.

Roeske T, Bauch D, Rutgers VD, Loeff M and Rabe B (2012) Utility of dissolved barium in distinguishing North American from Eurasian runoff in the Arctic Ocean. Marine Chemistry 132–133:1-14.

Rutgers van der Loeff MM, Key RM, Scholten J, Bauch D and Michel A (1995) ^{228}Ra as a tracer for shelf water in the arctic ocean. Deep Sea Research Part II: Topical Studies in Oceanography 42, 1533-1553.

Rutgers van der Loeff MM, Kipp L, Charette MA, Moore WS, Black E, Stimac I, et al. (2018) Radium Isotopes Across the Arctic Ocean Show Time Scales of Water Mass Ventilation and Increasing Shelf Inputs. Journal of Geophysical Research: Oceans 123(7):4853–4873. https://doi.org/10.1029/2018JC013888

Schartup AT, Soerensen AL, Heimbürger-Boavida LE (2020) Influence of the Arctic Sea-Ice Regime Shift on Sea-Ice Methylated Mercury Trends. Environ. Sci. Technol. Lett. 7:708–713. https://doi.org/10.1021/acs.estlett.0c00465

Schauer, U (2016) The Expedition PS94 of the Research Vessel POLARSTERN to the central Arctic Ocean in 2015. In EPIC3 Berichte zur Polar- und Meeresforschung = Reports on polar and marine research, Bremerhaven, Alfred Wegener Institute for Polar and Marine Research, 703, 170 p., ISSN: 1866-3192. Alfred Wegener Institute for Polar and Marine Research. https://doi.org/10.2312/BZPM_0703_2016

Schlosser P, Bönisch G, Kromer B, Münnich KO, & Koltermann KP (1990) Ventilation rates of the waters in the Nansen Basin of the Arctic Ocean derived from a multitracer approach. Journal of Geophysical Research: Oceans 95(C3):3265–3272. https://doi.org/https://doi.org/10.1029/JC095iC03p03265

Schulz-Baldes M & Lewin RA (1976) Lead uptake in two marine phytoplankton organisms. Biological Bulletin 150(1):118–127. https://doi.org/10.2307/1540593

Schlosser C & Garbe-Schönberg D (2019) Mechanisms of Pb supply and removal in two remote (sub)polar ocean regions. Marine Pollution Bulletin 149:110659. https://doi.org/10.1016/j.marpolbul.2019.110659

Sonke JE, Teisserenc R, Heimbürger-Boavida LE, Petrova MV, Marusczak N, Dantec TL, Chupakov AV, LI C, Thackray CP, Sunderland EM, Tananaev N, Pokrovsky OS (2018) Eurasian river spring flood observations support net Arctic Ocean mercury export to the atmosphere and Atlantic Ocean. PNAS 115:E11586–E11594. https://doi.org/10.1073/pnas.1811957115

Spreen G, Kaleschke L & Heygster G (2008) Sea ice remote sensing using AMSR-E 89-GHz channels. Journal of Geophysical Research 113:C02S03. https://doi.org/10.1029/2005JC003384

Steffen A, Douglas T, Amyot M, Ariya P, Aspmo K, Berg T, Bottenheim J, Brooks S, Cobbett F, Dastoor A, Dommergue A, Ebinghaus R, Ferrari C, Gardfeldt K, Goodsite ME, Lean D, Poulain AJ, Scherz C, Skov H, Sommar J, Temme C (2008) A synthesis of atmospheric mercury depletion event

chemistry in the atmosphere and snow. Atmospheric Chemistry and Physics 8:1445–1482. https://doi.org/10.5194/acp-8-1445-2008

Taylor RL, Semeniuk DM, Payne CD, Zhou J, Tremblay J-É, Cullen JT, Maldonado MT, (2013) Colimitation by light, nitrate, and iron in the Beaufort Sea in late summer. J. Geophys. Res. Ocean. 118:3260–3277. https://doi.org/10.1002/jgrc.20244

Tesán-Onrubia JA, Petrova MV, Puigcorbé V, Black EE, Valk O, Dufour A, Hamelin B, Buesseler KO, Masqué P, Le Moigne FAC, Sonke JE, Rutgers van der Loeff M, Heimbürger-Boavida LE (2020) Mercury Export Flux in the Arctic Ocean Estimated from $^{234}Th/^{238}U$ Disequilibria. ACS Earth Space Chem. 4:795–801.

Tsubouchi T, Våge K, Hansen B, Larsen KMH, Østerhus S, Johnson C, et al. (2021) Increased ocean heat transport into the Nordic Seas and Arctic Ocean over the period 1993–2016. Nature Climate Change 11(1):21–26.

Valk O, Rutgers Van Der Loeff MM, Geibert W, Gdaniec S, Moran SB, Lepore K, Edwards RL, Lu Y, Puigcorbé V and Casacuberta N (2020) Decrease in ^{230}Th in the Amundsen Basin since 2007: far-field effect of increased scavenging on the shelf? Ocean Science 16:221–234.

Vieira LH, Geibert W, Stimac I, Koehler D and Rutgers van der Loeff MM (2021) The analysis of ^{226}Ra in 1-liter seawater by isotope dilution via single-collector sector-field ICP-MS. Limnology and Oceanography: Methods.

Wang F, Outridge PM, Feng X, Meng B, Heimbürger-Boavida LE, Mason RP (2019) How closely do mercury trends in fish and other aquatic wildlife track those in the atmosphere? – Implications for evaluating the effectiveness of the Minamata Convention. Science of The Total Environment 674: 58–70. https://doi.org/10.1016/j.scitotenv.2019.04.101

Wang Q, Danilov S (2022) A Synthesis of the Upper Arctic Ocean Circulation During 2000–2019: Understanding the Roles of Wind Forcing and Sea Ice Decline. Front. Mar. Sci. 9:863204. https://doi.org/10.3389/fmars.2022.86320

Wani AL, Ara A & Usmani JA (2015) Lead toxicity: A review. Interdisciplinary Toxicology 8(2):55–64. https://doi.org/10.1515/intox-2015-0009

Wefing A-M, Casacuberta N, Christl M & Dodd PA (2022) Water mass composition in Fram Strait determined from the combination of ^{129}I and ^{236}U: Changes between 2016, 2018, and 2019. Frontiers in Marine Science 1598.

Wefing, A-M, Casacuberta N, Christl M, Gruber N & Smith J N (2021) Circulation timescales of Atlantic Water in the Arctic Ocean determined from anthropogenic radionuclides. Ocean Science 17(1):111–129. https://doi.org/10.5194/OS-17-111-2021

Wefing A-M, Christl M, Vockenhuber C, Rutgers van der Loeff M & Casacuberta N (2019) Tracing Atlantic Waters Using ^{129}I and ^{236}U in the Fram Strait in 2016. Journal of Geophysical Research: Oceans 124(2):882–896. https://doi.org/10.1029/2018JC014399

Whitmore LM, Pasqualini A, Newton R, Shiller AM (2020) Gallium: A New Tracer of Pacific Water in the Arctic Ocean. J. Geophys. Res. Oceans 125. https://doi.org/10.1029/2019JC015842

Zimmer LA, Asmund G, Johansen P, Mortensen J & Hansen BW (2011) Pollution from mining in South Greenland: Uptake and release of Pb by blue mussels (*Mytilus edulis* L.) documented by transplantation experiments. Polar Biology 34(3):431–439. https://doi.org/10.1007/s00300-010-0898-5

Zurbrick CM, Boyle EA, Kayser R, Reuer MK, Wu J, Planquette H, et al. (2018) Dissolved Pb and Pb isotopes in the North Atlantic from the GEOVIDE transect (GEOTRACES GA01) and their decadal evolution. Biogeosciences 15:4995–5014. https://doi.org/10.5194/bg-2018-29

Tab. 2.3: Sampling information for underway collection of aerosols during PS144 Expedition to the Central and Eastern Arctic Ocean.

	Start					End					
Sample ID	Date	Time (UTC)	Lat [°N]	Lon [°E]	Reading (h)	Date	Time (UTC)	Lat [°N]	Lon [°E]	Reading (h)	Sampling time (h)
PS144-TM01	13.08.2024	08:25	81° 24.347'	22° 17.228'	27879,9	17.08.2024	10:49	85° 05.082'	43° 29.406'	27920,1	40,2
PS144-TM02	17.08.2024	12:50	85° 06.375'	44° 55.713'	27920,1	21.08.2024	10:35	84° 34.023'	107° 41.659'	27966,4	46,4
PS144-TM03	21.08.2024	11:15	84° 32.977‘	108° 23.872'	27966,4	24.08.2024	20:00	84° 52.245'	42° 58.947'	28020,2	53,7
PS144-TM04	25.08.2024	11:50	85° 15.432'	56° 08.972'	28020,2	29.08.2024	15:00	84° 29.295'	115° 19.270'	28061,1	40,9
Cassette Blank	29.08.2024	17:00	84° 30.541'	115° 24.875'	28061,1	30.08.2024	15:00	84° 34.090'	117° 02.981'	28061,1	NA
PS144-TM05*	30.08.2024	16:40	84° 35.475'	116° 55.926'	28061,1	03.09.2024	19:00	85° 00.252'	130° 50.290'	28100,7	39,6
PS144-TM06**	14.09.2024	16:30	87° 43.660'	169° 04.508' W	28100,7	20.09.2024	06:00	89° 40.357'	59° 48.992'	28156,7	56,0
PS144-TM07***	21.09.2024	14:15	88° 57.239'	57° 27.877'	28156,7	26.09.2024	06:24	87° 02.815'	57° 06.440'	28169,3	12,6
PS144-TM08***	28.09.2024	05:30	86° 29.273'	59° 40.327'	28169,3	02.10.2024	07:45	84° 55,110'	46° 27,763'	28188,1	18,8
PS144-TM09***	02.10.2024	08:50	84° 52,939'	045° 46,068'	28188,1	06.10.2024	09:00	77° 34,499'	027° 58,676'	28204,5	16,4
PS144-TM10	06.10.2024	09:45	77° 30,378'	027° 29,298'	28204,5	09.10.2024	10:50	67° 13,576'	008° 41,920'	28259,8	55,3
Motor Blank	09.10.2024	11:15	67° 09,812'	008° 37,451'	28259,8	09.10.2024	11:16	67° 09,664'	008° 37,268'	28259,8	NA
Exposure Blank	09.10.2024	11:45	67° 05,308'	008° 32,064'	28259,8	11.10.2024	11:15	59° 51,876'	004° 00,286'	28259,8	NA

* Filter completely snow-covered by recovery. Snow carefully removed. Wet filter paper including some meltwater frozen.

** Occasionally snowing during sampling period. Then sampler manually turned off. Light snow cover at removal (<1cm) and gently knocked off before storage.

***Sampling stopped several times due to heavy snowing.

Tab. 2.4: Overview of samples taken from the ucCTD water sampling system on stations during PS144

Event Label	Date	Latitude* [°N]	Longitude*	Depth* [m]	Cast Depth [m]	Macronuts	DOP/DON	DIC/TA	sTM	dTM	pTM	Fe iso	Pb iso	tHg	pHg	MeHg	Ga	^{232}Th	Ba	Incubations
PS144_007_02	16.08.2024	85° 03.778'	42° 59.175' E	4135	3948	X			X	X	X	X	X	X	X	X	X	X	X	
PS144_009_01	18.08.2024	85° 15.386'	59° 44.050' E	3841	500	X			X	X	X	X		X	X	X				X
PS144_011_01	20.08.2024	85° 07.087'	95° 29.230' E	4546	4521	X			X	X	X	X	X	X	X	X	X		X	
PS144_018_02	28.08.2024	84° 17.113'	111° 00.643' E	4049	3988	X			X	X	X	X	X	X		X	X	X	X	X
PS144_020_01	28.08.2024	84° 27.791'	113° 44.976' E	2518	500	X			X	X	X									
PS144_023_03	29.08.2024	84° 30.482'	115° 21.581' E	4137	4068	X			X	X	X	X	X	X		X	X	X	X	
PS144_028_02	31.08.2024	84° 47.684'	122° 00.787' E	4385	4324	X			X	X	X	X	X	X		X	X	X	X	
PS144_039_01	02.09.2024	84° 51.821'	128° 57.479' E	4351	750	X			X	X	X	X		X	X	X	X	X	X	X
PS144_046_02	03.09.2024	84° 56.824'	132° 32.556' E	4320	4251	X			X	X	X	X	X	X		X	X	X	X	
PS144_050_03	05.09.2024	85° 00.900'	139° 44.982' E	3961	3892	X	X		X	X	X	X	X				X	X	X	
PS144_057_02	06.09.2024	85° 04.886'	150° 30.882' E	954	916	X	X		X	X	X	X		X	X	X	X	X	X	
PS144_065_01	07.09.2024	84° 58.839'	159° 04.470' E	3443	750	X	X	X	X	X	X	X		X		X	X	X	X	X
PS144_067_03	08.09.2024	84° 56.352'	161° 53.356' E	3560	3494	X	X	X	X	X	X	X	X				X	X	X	
PS144_073_02	09.09.2024	84° 56.590'	169° 15.863' E	3424	750	X	X	X	X	X	X	X		X		X	X	X	X	
PS144_080_03	10.09.2024	84° 55.395'	179° 28.140' E	1982	1920	X	X	X	X	X	X	X	X	X		X	X	X	X	X
PS144_085_03	13.09.2024	87° 30.075'	178° 41.988' E	3996	3932	X	X		X	X	X	X	X				X	X	X	
PS144_090_02	16.09.2024	88° 22.179'	124° 15.447' W	3543	3478	X	X		X	X	X	X	X	X		X	X	X	X	X
PS144_102_02	17.09.2024	89° 20.087'	125° 22.942' W	1664	1623	X		X	X	X	X	X		X	X	X	X	X	X	
PS144_109_03	19.09.2024	89° 56.844'	150° 29.492' W	4265	4203	X	X	X	X	X	X	X	X				X	X	X	
PS144_115_02	21.09.2024	89° 00.798'	59° 00.594' E	4396	4336	X	X	X	X	X	X	X			X	X	X	X	X	X
PS144_123_03	23.09.2024	88° 04.291'	59° 49.680' E	4416	4356	X	X	X	X	X	X	X	X	X	X	X	X	X	X	
PS144_130_01	24.09.2024	87° 19,946'	59° 11,923' E	3698	790	X	X		X	X	X	X					X	X	X	X
PS144_134_04	25.09.2024	87° 00.271'	58° 06.855' E	4761	4633	X			X	X	X	X					X	X	X	
PS144_134_10	26.09.2024	87° 02.076'	55° 40.989' E	NA	4465	X	X	X	X	X	X	X		X	X	X	X	X	X	
PS144_141_02	28.09.2024	86° 29.301'	59° 39.042' E	2118	2062	X	X	X	X	X	X	X		X		X	X	X	X	X
PS144_144_03	28.09.2024	86° 10.193'	59° 52.736' E	3910	3820	X	X	X	X	X	X	X					X	X	X	
PS144_149_02	29.09.2024	85° 30.840'	59° 52.445' E	3936	850	X	X		X	X	X			X		X	X	X	X	
PS144_152_02	30.09.2024	85° 14,573'	59° 35,629' E	3926	3813	X	X		X	X	X	X	X	X		X	X	X	X	
PS144_154_01	03.10.2024	83° 47,920'	32° 56,757' E	4027	748	X	X		X	X	X						X	X	X	X
PS144_156_03	04.10.2024	82° 41,645'	30° 41,536' E	3695	3554	X	X		X	X	X	X	X	X	X	X	X	X	X	
PS144_157_03	04.10.2024	81° 51,222'	30° 53,981' E	3162	3063	X	X		X	X	X	X	X	X	X		X	X	X	
PS144_158_02	05.10.2024	81° 31,793'	30° 47,603' E	830	754	X	X		X	X	X	X	X				X	X	X	

*at maximum depth

NA: not applicable due to misreading of echo-sounding during cast.

3. IMPACT OF ICE DRIFT ON NUTRIENT AND TRACE-METAL DISTRIBUTION, OCEAN PRODUCTIVITY, AND CARBON EXPORT (BIOLOGICAL TRACE METALS – BTM)

Alexandra Bettinelli[1], Christian Völkner[1], [1]DE.AWI
Ingrid Stimac[1], Walter Geibert[1] [2]FR.UBO
not on board: Scarlett Trimborn[1], Morten Iversen[1],
Lois Maignien[2]

Grant-No. AWI_PS144_02

Objectives

Arctic phytoplankton is known to be primarily limited by nitrogen availability (Ko et al., 2020). However, investigations of potential co-limiting factors, such as iron, remain limited. While research indicates that ice originating from the Siberian shelves and transported via the Transpolar Drift serves as a source of nutrients and trace metals to the central Arctic (Charette et al., 2020), the precise contribution of these ice-derived elements to Arctic Ocean productivity and carbon sequestration, and the implications of different ice types remain uncertain. Additionally, global warming foresees increased ice-melt and freshwater inputs to the Arctic Ocean, potentially reshaping seawater biogeochemistry, thereby potentially affecting primary productivity, phytoplankton community structure, and CO_2 export to the depth (Krumpen et al., 2019). The predicted increased Arctic stratification due to global warming may further disrupt the upwelling of nutrients and trace metals, potentially increasing their significance as a result of sea ice melting (Krisch et al., 2020). Augmented primary production resulting from ice melt could alter the biological carbon pump and the Arctic carbon sink. Our research aimed to shed light on these complex interactions and their potential implications for primary production and carbon sequestration by Arctic phytoplankton.

Our overall goals were to:

- characterise the trace metal and nutrient distribution in bottom ice, surface water, and under ice water,
- estimate and map trace metals within the phytoplankton community and within single cells, assess the photophysiological state and determine the community composition of the surface and under ice water phytoplankton,
- assess primary production rates of the surface water, the chlorophyll maximum and the under-ice water,
- conduct bottle incubation experiments amended with either melted sea ice, nutrients and dissolved iron to elucidate the impact of ice-associated trace elements and nutrients on Arctic phytoplankton growth and productivity as well as ice and nutrient-induced changes in the carbon content and export of the newly formed aggregates through roller tank incubation experiments.

Work at sea

The work at sea consisted of water and ice sampling as well as the performance of onboard phytoplankton nutrient amendment incubation and roller tank experiments. Surface seawater (15 m depth) was sampled at 28 stations using a trace metal-clean Teflon CTD rosette. Additionally, under-ice water was collected using clean sampling techniques at six stations. Ice cores or ice samples were taken trace metal clean at seven super ice stations, where water work was conducted in parallel, and at two short stations, where sediment-loaded ice was explicitly targeted. During the expedition, three phytoplankton bottle incubation experiments were conducted to assess the impact of trace elements and nutrients released from melted sea ice. The treatments comprised melted bottom sea ice and sediment-loaded sea, as well as macronutrient and iron additions that allowed the identification of key limiting nutrients. Subsequently, 1.2 L of the final community of each treatment was incubated in the dark in roller tanks to promote aggregate formation and identify potential treatment-induced changes in carbon export.

The work at sea is described in more detail in the following.

Clean CTD operation

The sensors and rosette of the Clean-CTD were provided by the Ecological Chemistry group from DE.AWI. The characterisation of the water chemistry and sampling for trace elements was possible through the use of titanium and plastic instead of steel. For water sampling, 24 14 L bottles made of PVC and titanium with butterfly closures, based on the NIOZ PRISTINE bottles, were used. The Clean-CTD setup has its own winch equipped with 8000 m synthetic cable and a clean room container for sampling. The sensor configuration of the Clean-CTD during the cruise consisted of two temperature sensors, two conductivity cells, a pressure sensor, two oxygen sensors, a transmissometer, two fluorescence sensors, a photosynthetically active radiation (PAR) sensor and an altimeter, see Table 3.1 for more details. The CTD was operated using a Seabird 11 plus Deckunit. Due to a malfunction of the Clean-CTD winch at station PS144_130-1, we needed to switch to the EL030 winch equipped with an 11 mm Dyneema rope until the end of the cruise. During that time, bottles were closed on a pre-set depth using a Seabird SBE 17plus V2 Searam Recorder and Auto Fire Module. To better estimate the CTD's actual depth, the ship's POSIDONIA transmitter was wrapped in plastic and attached to the CTD. This allowed us to go closer to the sea floor, as with the POSIDONIA reading, we no longer had to rely purely on the cable length to estimate the depth.

Tab 3.1: Sensor configuration of the Clean-CTD during PS144

Parameter	SN	Calibration Date	Channel	Sensor type
	1229	-	Deckunit Seabird 11plus	
	398	-	Searam Recorder & Auto Fire Module SBE17plus V2	later, after changing the winch
Temperature 1	6519	11-Jul-23	F0	Seabird SBE3plus
Conductivity 1	4964	11-Jul-23	F1	Seabird SBE4c
Pressure	1557	30-Nov-23	F2	Seabird SBE9plus
Temperature 2	6491	14-Jul-23	F3	Seabird SBE3plus
Conductivity 2	4982	11-Jul-23	F4	Seabird SBE4c

Parameter	SN	Calibration Date	Channel	Sensor type
Oxygen 1	4047	29-Aug-23	V0	Seabird SBE43
Oxygen 2	1834	15-Feb-24	V1	Seabird SBE43
	10510	-	pump	Seabird SBE5T
	10517	-	pump	Seabird SBE5T
Chl-a fluorescence	6450	12-Aug-20	V2	WETlabs ECO-AFL/FL
Beam Transmission	2064	20-Nov-20	V3	WETlabs C-Star
Altimeter	74480	06-Mar-20	V4	Valeport VA-500
PAR	2067	11-Nov-20	V5	PAR/Logarithmic, Satlantic
CDOM fluorescence	7239	12-Sep-21	V6	Wetlabs ECO CDOM

Tab 3.2: Meta-data of all Clean-CTD stations from PS144. Bold fronts highlight the casts where the SBE 17plus V2 Searam Recorder and Auto Fire Module were used.

Event Label	Date	Time (UTC)	Latitude	Longitude	Water depth [m]	Profile depth [m]
PS144_7-2	16.08.2024	12:44	85.07	42.99	3927	3948
PS144_9-1	18.08.2024	06:41	85.36	59.96	3841	500
PS144_11-1	20.08.2024	01:28	85.37	95.58	4577	4522
PS144_18-2	28.08.2024	08:01	84.48	111.02	4056	3988
PS144_20-1	28.08.2024	21:36	85.67	113.84	2545	500
PS144_23-3	29.08.2024	18:14	84.76	115.33	4135	4068
PS144_23-8	30.08.2024	07:32	84.48	115.53	3330	3351
PS144_28-2	31.08.2024	07:49	84.89	122.00	4388	4324
PS144_39-1	02.09.2024	12:14	84.90	129.14	4351	750
PS144_46-2	03.09.2024	21:58	85.03	132.71	4320	4251
PS144_50-3	05.09.2024	01:57	85.05	139.76	3960	3892
PS144_50-7	05.09.2024	12:16	85.17	140.26	3463	3358
PS144_57-2	06.09.2024	20:10	85.32	150.63	958	916
PS144_65-1	07.09.2024	21:55	85.20	159.12	3445	750
PS144_67-3	08.09.2024	08:34	85.06	162.09	3561	3494
PS144_67-8	08.09.2024	21:33	84.94	162.23	3559	3493
PS144_73-2	09.09.2024	16:22	85.08	169.28	3424	750
PS144_80-3	11.09.2024	22:50	84.99	179.74	1981	1927
PS144_85-3	13.09.2024	08:31	87.57	178.79	3996	3932
PS144_85-8	13.09.2024	19:37	87.56	178.12	3995	3934
PS144_90-2	16.09.2024	06:08	88.40	-123.63	3543	3478
PS144_102-2	17.09.2024	20:00	89.36	-124.56	1676	1623
PS144_109-3	18.09.2024	23:47	89.55	-150.86	4264	4203
PS144_109-7	19.09.2024	11:13	89.68	-138.51	4264	4201
PS144_115-2	21.09.2024	06:31	89.03	59.31	4395	4336
PS144_123-3	23.09.2024	06:31	88.15	59.81	4416	4356

Event Label	Date	Time (UTC)	Latitude	Longitude	Water depth [m]	Profile depth [m]
PS144_130-1	24.09.2024	16:07	87.58	59.44	3698	791
PS144_134-4	25.09.2024	17:40	87.08	58.34	4761	4633
PS144_134-10	26.09.2024	21:14	87.05	55.94	4530	4465
PS144_141-2	28.09.2024	07:00	86.57	59.90	2119	2062
PS144_144-3	28.09.2024	21:57	86.22	60.07	3910	3820
PS144_149-2	30.09.2024	00:08	85.73	60.00	3936	842
PS144_152-2	30.09.2024	19:33	85.39	59.76	3926	3813
PS144_154-1	03.10.2024	13:54	83.93	33.14	4027	856
PS144_156-3	04.10.2024	08:14	82.86	30.84	3695	3556
PS144_157-3	04.10.2024	21:12	81.91	31.15	3162	3063
PS144_158-2	05.10.2024	03:34	81.74	30.95	830	754

Trace Metal Clean Surface Seawater and Under Ice Water Sampling

At 28 clean stations, surface seawater (15m depth), and at 12 stations the chlorophyll maximum was collected using the trace metal clean CTD rosette. Under-ice water was collected at six ice stations using an under-ice water pump. To estimate biomass and to characterise the phytoplankton community composition, samples were taken for light microscopy, pigments (HPLC), particulate organic carbon (POC), flow cytometry as well as size-fractionated metatranscriptomics and metagenomics (0.2-3 µm, >3 µm). The photophysiological status of the sampled phytoplankton community was assessed using a Fast Repetition Rate fluorometer (FRRf).

Furthermore, to determine the plankton community's trace metal limitation, surface and under-ice water samples were taken for dissolved trace metals (dTM) (Fe, Mn, Co, Cu, and Zn), intracellular macronutrient and trace metal distribution, and trace metal quotas. Samples were collected and processed according to the Sampling and Sample Handling Protocols for GEOTRACES Cruises. In Addition, salinity, pH, dissolved inorganic carbon (DIC), and dissolved organic carbon (DOC) were sampled for analysis at AWI. Onboard, Siué Torres and his team analysed macronutrients (NO_3+NO_2, NO_2, $Si(OH)_4$, PO4, NH_4, TN, TP), which will complete the data set.

Lastly, primary production rates were determined using ^{14}C-bicarbonate at each site. ^{14}C removal rates were measured using 125 ml triplicate bottles spiked with 0.1 µC ^{14}C-bicarbonate. The bottles were incubated under a constant light of 40 µE at 0 °C throughout the whole expedition to obtain relative primary production rates. The primary production rates were calculated as

$$PrimaryProduction\left[\frac{mgC}{m^3 * d}\right] = SDPM\frac{\frac{\frac{SDPM}{V} * W * 0.05 * 10^3}{TADPM} * 1.05}{T}$$

With SDPM = DPMs in the filtered sample, V = volume of the filtered sample [L], TADPM = Total activity ^{14}C DPMs in 50 µl, W= DIC concentration in the sample (25000 mgCm^{-3}), 1.05 = correction for the lower uptake of ^{14}C compared to ^{12}C, T = incubation time [days].

Tab 3.3: Biological and chemical samples taken from surface seawater at each clean CTD station. X indicates single measurements, X* duplicate and X** triplicate measurements.

Event Label	Depth [m]	pH	Salinity	Photophysiology	Taxonomy	Flow Cytometry	POC	Pigments	DIC	Intracellular Nutrient Distribution	Metatranscriptomics	Nutrients	dTM	TM quota	Primary Production
PS144-09-01	15				X	X*	X*	X*	X	X	X**		X*	X*	
PS144-11-01	15	X		X	X	X*	X*	X*	X	X	X**		X		
PS144-18-02	14	X		X	X	X*	X*	X*	X*	X	X**		X*	X*	X**
PS144-20-01	14.6	X	X	X	X	X**	X*	X*	X**	X*	X**	X*	X*	X*	X**
PS144-23-03	15	X	X	X	X	X*	X*	X*	X	X	X**		X*	X**	X**
PS144-28-02	15	X		X	X	X*	X*	X*	X	X	X**		X*	X*	X**
PS144-39-01	15	X		X	X	X*	X*	X*	X	X	X**		X*	X**	X**
PS144-46-02	15	X		X	X	X*	X*	X*	X	X	X**		X*	X**	X**
PS144-50-03	15	X		X	X	X*	X*	X*	X	X	X**		X*	X**	X**
PS144-57-02	15	X		X	X	X*	X*	X*	X	X	X**		X*	X**	X**
PS144-67-03	15	X	X	X	X	X*	X*	X*	X	X	X**		X*	X**	X**
PS144-73-02	15	X		X	X	X*	X*	X*	X	X	X**		X*	X**	X**
PS144-80-03	15	X	X	X	X	X**	X*	X*	X**	X*	X**	X*	X**	X*	X**
PS144-85-03	15	X		X	X	X*	X*	X*	X	X	X**		X*	X*	X**
PS144-90-02	15	X		X	X	X*	X*	X*	X	X	X**		X*	X*	X**
PS144-102-02	15	X		X	X	X*	X*	X*	X	X	X**		X*	X*	X**
PS144-109-03	17	X		X	X	X*	X*	X*	X	X	X**		X*	X*	X**
PS144-115-02	15	X		X	X	X*	X*	X*	X	X	X**		X*	X*	X**
PS144-123-03	13	X		X	X	X*	X*	X*	X	X	X**		X*	X*	X**
PS144-134-04	-	X		X	X	X*	X*	X*	X	X	X**		X*	X*	X**
PS144-134-10	15	X			X	X*	X*	X*	X	X			X*		X**
PS144-141-03	15	X		X	X	X*	X*	X*	X	X	X**		X*	X*	X**
PS144-144-03	18	X		X	X	X*	X*	X*	X	X	X**		X*	X*	X**
PS144-149-02	23.7	X		X	X	X**	X*	X*	X**	X*	X**	X*	X**	X*	X**
PS144-152-02	15	X		X	X	X*	X*	X*	X	X	X**		X*	X*	X**
PS144-156-03	14	X		X	X	X*	X*	X*	X	X	X**		X*		
PS144-157-03	15	X		X	X	X*	X*	X*	X	X	X**		X*		
PS144-158-02	15	X		X	X	X*	X*	X*	X	X	X**		X*		

Tab 3.4: Biological and chemical samples taken from under-ice water at ice stations. X indicates single measurements, X* duplicate and X** triplicate measurements.

Event Label	Depth [m]	pH	Salinity	Fv/Fm	PI curves	Taxonomy	Flow Cytometry	POC	Pigments	DIC	Intracellular Nutrient Distribution	Metatranscriptomics	Nutrients	dTM	TM quota	Primary Production
PS144-23-01	0.1	X	X	X		X	X*	X*	X*	X*	X	X**	X	X*	X*	X**
PS144-42-01	0.1	X		X		X	X*	X*	X*	X	X	X**	X	X*	X**	X**
PS144-80-01	0.1	X	X	X		X	X*	X*	X*	X	X	X**	X	X*	X**	X**
PS144-85-01	0.1	X	X	X	X	X	X*	X*	X*	X	X	X**	X	X*	X*	X**
PS144-109-01	0.1	X	X	X	X	X	X*	X*	X*	X	X	X**	X	X*	X*	X**
PS144-134-01	0.1	X		X	X	X	X*	X*	X*	X	X	X**	X	X*	X*	X**

Trace Metal Clean Ice Sampling

Ice samples were collected together with surface and under-ice water samples to elucidate the role of chemical and biological processes at the ice-water interface and better understand the impact of trace elements and nutrients released from the melting sea ice. Ice cores were primarily collected for ice-addition phytoplankton incubation experiments. The goal was, therefore, to obtain ice material from different origins and with different chemical compositions, e.g., ice containing terrigenous material and marine sea ice with no terrigenous input. Thomas Krumpen and his team will perform sea ice back-tracking, allowing us to subsequently determine the ice sources/origin.

Ice cores were collected using a Kovacs ice corer with a 9 cm diameter, following the indications for trace metal clean ice coring in the Nansen Legacy Sampling Protocols Version 10. In brief, the sampling site was located against the wind and at a distance of at least 100 m from other activities to avoid contamination from the ship and other working groups. Care was taken to be the first group to start sampling before other ice work started. Clean room garments, overshoes, and gloves were put on 10 m away from the final ice sampling site. The bottom 15 cm of collected ice cores were sampled at three ice stations for the incubation experiments. 1 cm of the outer ice was removed still on the ice floe using a trace metal clean ceramic knife. The scraped bottom ice core sections were placed into trace metal clean containers and double-packed for melting. On four additional ice stations, 3 to 4 ice cores were sampled, packed, and frozen at -20 °C for further trace metal, mercury, and other analyses in the home lab and associated institutes (AWI, GEOMAR, MIO).

Additionally, sediment-loaded ice was explicitly targeted and collected during two short deployments. At station PS144_10-1, a mammy chair was used to access a sediment-loaded ice floe. Five ice cores were drilled, and only the top 15 cm containing the sediment layers were sampled. At station PS144_58-2, ice pieces were collected using an ice bucket, which was lowered from the ship. In both cases, the ice cores/pieces were stored at -20 °C and processed under the clean hood the following day. Again, the outer part of the ice (at least 1 cm) was scraped off using a ceramic knife and afterwards placed in trace metal clean boxes, double-packed, and left to melt.

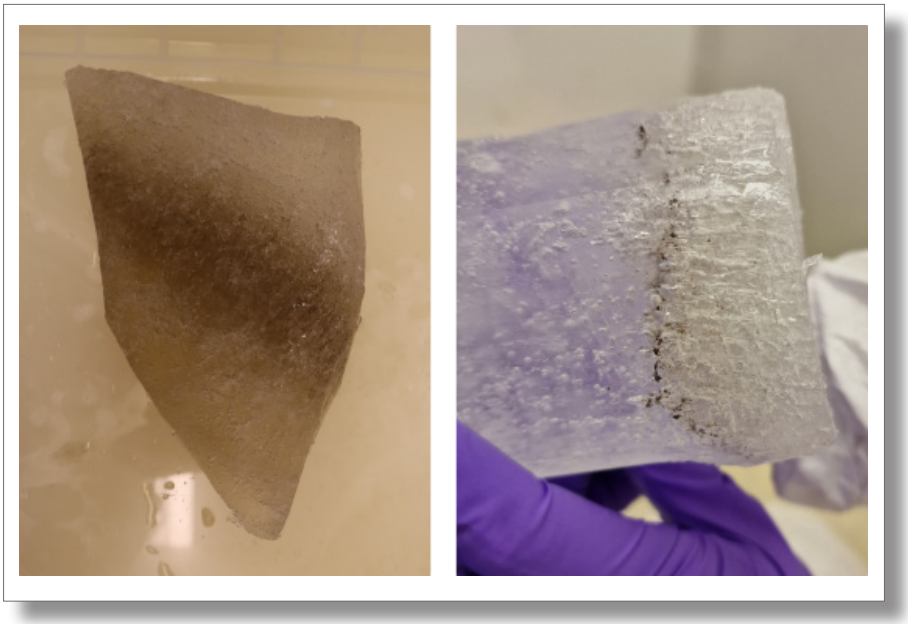

Fig. 3.1: Examples of sediment-loaded sea ice sampled during PS144. Left: Sediment layer in ice piece sampled at station PS144_58-2. Right: Sediment layer in top 15 cm of an ice core sampled at station PS144_10-1

The dissolved iron concentration of the melted ice samples was analysed onboard via flow injection analysis (FIA) with luminol chemiluminescence detection. The pH and salinity were measured, and macronutrients were again analysed by Sinhué Torre's team onboard.

Also, samples of dissolved organic carbon (DOC), dissolved inorganic carbon (DIC), and dissolved and particulate trace metals (dTM, pTM) (Fe, Mn, Co, Cu, and Zn) were taken for later analysis at the AWI. Oxygen isotope ($\delta^{18}O$) samples were taken to quantify freshwater sections and will be analysed at the Leibniz Laboratory at Kiel University.

Tab 3.5: Samples taken from ice. X indicates single measurements, X* duplicate and X** triplicate measurements.

Event Label	Cores	pH	Salinity	DOC	DIC	Nutrients	δ18O	dTM	dFe (FIA)	pTM
PS144-10-01	5	X	X	X*	X*	X*		X*	X	X**
PS144-23-01	10	X	X	X*	X**	X*	X	X*	X	X**
PS144-42-01	11	X	X	X*	X**	X*	X	X*	X	X**
PS144-50-01	12	X	X	X*	X**	X*	X	X*	X	X**
PS144-58-02	-	X	X	X*	X**	X*	X	X*	X	X**
PS144-80-01	2	frozen at -20 °C								
PS144-85-01	4	frozen at -20 °C								
PS144-109-01	3	frozen at -20 °C								
PS144-134-01	3	frozen at -20 °C								

Ice Incubation Experiments: Assessing the Impacts of Trace Metals on Plankton Community Composition

At three sampling stations, PS144_20-1, PS144-80-3, and PS144_149-2, half an ultra-clean CTD cast (~120 L) were required to sample surface seawater with the local phytoplankton community for three bottle incubation experiments. Three sets of trace metal clean 4 L polycarbonated bottles were filled with seawater containing the local phytoplankton community and amended, in triplicates, with different ice types and nutrients. To avoid a co-limitation of phosphate with other macronutrients, 1 µM of PO_4^{3-} was added to all treatments, including the control. The seawater was left to grow in a climate-controlled room at 0 °C.

In the following, the three experiments will be referred to as IcyMetal 1- 3.

For IcyMetal 1, water was collected at 15 m depth at station PS144_20-1, filled into trace metal-clean 4 L polycarbonate bottles, and, in triplicates, amended with seven different treatments: NO_3 (10 µM), Fe (10 nM), Si (10 µM), NO_3+Fe, NO_3+Si, and 400 ml melted sediment-loaded sea ice from station PS144_10-1 (Sed Ice 1) or remained unamended serving as Control. The bottles were left to grow for seven days at a constant light of 40 µE.

A second set of 4 L bottles (Icy Metal 3) was filled with seawater from station PS144_80-3 (15 m) and amended with NO_3 (10 µM), Fe (10 nM), and NO_3+Fe, 400 ml of melted bottom ice collected at station PS144_42-1 (Mar Ice) that did not contain visible terrigenous input, and 400 ml melted sediment-loaded sea ice sampled from station PS144-58-2 (Sed Ice 2). No addition was made to the last set of bottles (Control). The bottles were left to grow for nine days at a constant light intensity of 30 µE.

For Ice Metal 3, ice was sampled at 24 m depth at station PS144_49-2 and incubated for six days with the same treatments as in Icy Metal 2. However, the light settings were adjusted to the decreasing light intensity of 20 µE light and adjusted to a 9:15 h light/dark cycle.

In all experiments, macronutrient concentrations were determined every second/third day by Sinhué Torres to follow macronutrient drawdown as an indirect indicator for phytoplankton growth. At the same time, the photophysiological status of the cells was determined by measuring the F_v/F_m.

At the experiments' start and end, samples were collected and analysed as described above to characterise the plankton community, estimate primary production and determine water chemistry.

Aggregation Experiments

To study the effects of each treatment on aggregate formation and carbon export, 1.2 L of the final communities from Icy Metal 1 and Icy Metal 2 were incubated in roller tanks. There was no aggregation experiment for Icy Metal 3 due to time constraints. The tanks were set to approximately 20 seconds/rotation and placed at 0 °C in the dark to avoid further phytoplankton growth. Sinking velocity, particle abundance, and size were monitored by video analysis 1-2 times daily. Finally, the aggregates were let to sink to the tank bottom and, if possible, picked using a glass Pasteur pipette to determine their POC content. However, as aggregates were very small but plentiful, picking was challenging. Hence, the method was changed for Icy Metal 2. Instead of picking aggregates after letting them settle, the background surface water was slowly removed from the water surface using a peristaltic pump and filtered through a GFF filter. The last 50 to 100 ml contained the most settled aggregates and were filtered through a separate GFF filter for POC analysis.

Thorium^{234} spike aggregation experiment

One additional control roller tank (IcyMetal 2) was spiked with thorium^{234} to investigate its time-related absorption on forming particles. A 5 ml sample was taken from the tank twice a day and let seep through a 2 µm QM-A filter to collect the aggregates. After four days, the particles were specifically picked and put on a QM-A filter; the remaining background seawater was filtered separately. The filters were then analysed using a Timepix low-power radiation camera equipped with a particle tracking and imaging detector (see Chapter 2 for more details).

Preliminary results

Characterisation of the Arctic Surface Phytoplankton Community and Biogeochemistry

Most samples collected during the PS144 cruise will be analysed at the AWI. However, some preliminary data were generated on board, including the photophysiological status of the sampled phytoplankton and primary production data. Macronutrient data obtained from station work during the cruise, including surface data, will be discussed in further detail in Chapter 5. The preliminary results of the Thorium^{234} spike aggregation experiment are described in Chapter 2.

Primary production rates were assessed at 22 clean CTD stations, 22 times from surface water, and 12 times from the chlorophyll maximum. At six ice stations, primary production rates were also assessed from under-ice water samples (Fig. 3.2).

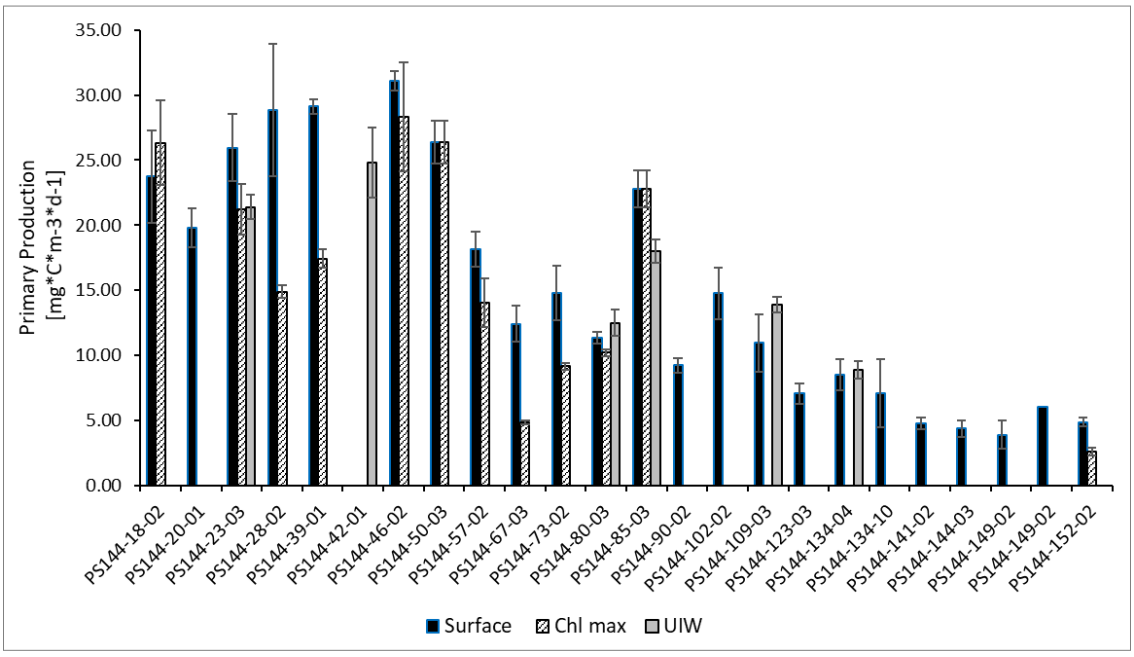

Fig. 3.2: PS144 station primary production rates in surface water from 15 m depth (surface)), the chlorophyll maximum (Chl max) and under ice water (UIW).

Ice Incubation Experiments: Assessing the Impacts of Trace Metals on Plankton Community Composition

The photosynthetic efficiency of phytoplankton (F_v/F_m) is a quick proxy in the field to assess potential stressors and limitations of the cells. At the start of all experiments, F_v/F_m ranged between 0.24 and 0.30, indicating potential nutrient and/or light stress. The F_v/F_m data of the

incubation experiments must be further processed to obtain valuable information. Hence, no data are presented here.

At the end of the incubation time of each experiment, primary production rates were estimated (Fig 3.3). The results for the silicate treatments in Icy Metal 1 are not displayed, as there was a problem in sample preparation. The preliminary primary production rates for Icy Metal 1 (Fig. 3.3 a) show a strong response to Fe and NO_3+Fe addition. In contrast, rates of the NO_3 addition alone were even lower than the Control, suggesting a potential relief of iron limitation rather than a response driven by NO_3. Analysing the other parameters at AWI will give more insights into the phytoplankton dynamics. In Icy Metal 2, NO_3 and NO_3+Fe caused a similar increase in primary production, while rates after the Fe addition were similar to the one of the Control, suggesting that NO_3 is primarily limiting in the community. The primary production rates of Icy Metal 3 are very low compared to the previous experiments, which could be attributed to limited light availability and low biomass. There are no apparent differences in production rates between the different treatments. In Icy Metal 1 and 2, primary production seems to be enhanced in the Sed Ice treatment compared to the Control, whereas this was not the case for the Mar Ice treatment. In Icy Metal 3, primary production seems to be increased in both ice treatments compared to the Control. The statistical significance of the results and a more in-depth analysis of the community and elemental composition at AWI will be necessary to dismantle the single and combined effects of the different treatments in all three experiments.

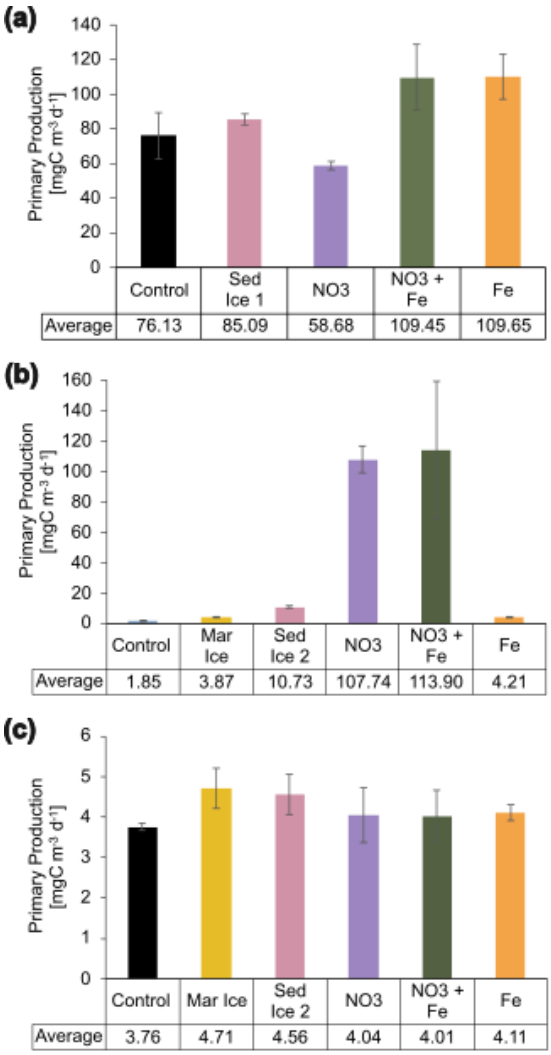

Fig. 3.3: Primary production rates of 4L bottle incubation experiments. (a) Icy Metal 1 after 7 days, (b) Icy Metal 2 after 9 days incubation, (c) Icy Metal 3 after 9 days incubation.

Aggregation Experiments

Aggregation experiments were conducted with the final community of Icy Metal 1 and Icy Metal 2 and lasted three days. Very low biomass was observed in both experiment sets, and only small aggregates were formed. There was no visual difference between the treatments. However, further analysis of the particle size, POC content, and sinking velocity will be conducted at the AWI, providing more information.

Data management

Environmental data will be archived, published, and disseminated according to international standards by the World Data Center PANGAEA Data Publisher for Earth & Environmental Science (www.pangaea.de) within two years of the end of the cruise. By default, the CC-BY license will be applied.

Molecular data (DNA and RNA data) will be archived, published, and disseminated within one of the repositories of the International Nucleotide Sequence Data Collaboration (INSDC, www.insdc.org) comprising EMBL-EBI/ENA, GenBank, and DDBJ). Environmental proteome data will be deposited in the publicly accessible Ocean Protein Portal (https://proteinportal.whoi.edu).

Any other data will be submitted to an appropriate long-term archive that provides unique and stable identifiers for the datasets and allows open online access to the data.

This expedition was supported by the Helmholtz Research Programme “Changing Earth – Sustaining our Future” Topic 2 Subtopic 1 and Topic 6 Subtopic 3.

In all publications based on this expedition, the **Grant No. AWI_ PS144_02** will be quoted, and the following publication will be cited:

Alfred-Wegener-Institut Helmholtz-Zentrum für Polar- und Meeresforschung (2017) Polar Research and Supply Vessel POLARSTERN Operated by the Alfred-Wegener-Institute. Journal of large-scale research facilities, 3, A119. http://dx.doi.org/10.17815/jlsrf-3-163.

References

Charette MA, Kipp LE, Jensen LT, Dabrowski JS, Whitmore LM, Fitzsimmons JN, Williford T, Ulfsbo A, Jones E, Bundy RM, Vivancos SM, Pahnke K, John SG, Xiang Y, Hatta M, Petrova MV., Heimbürger-Boavida LE, Bauch D, Newton R, . . . Zhang R (2020) The Transpolar Drift as a Source of Riverine and Shelf-Derived Trace Elements to the Central Arctic Ocean. Journal of Geophysical Research: Oceans 125(5). https://doi.org/10.1029/2019jc015920

Ko E, Gorbunov MY, Jung J, Joo HM, Lee Y, Cho KH, Yang EJ, Kang SH & Park J (2020) Effects of Nitrogen Limitation on Phytoplankton Physiology in the Western Arctic Ocean in Summer. Journal of Geophysical Research: Oceans 125(11). https://doi.org/10.1029/2020jc016501

Krisch S, Browning TJ, Graeve M, Ludwichowski, KU, Lodeiro P, Hopwood MJ, Roig S, Yong JC, Kanzow T & Achterberg EP (2020) The influence of Arctic Fe and Atlantic fixed N on summertime primary production in Fram Strait, North Greenland Sea. Sci Rep 10(1):15230. https://doi.org/10.1038/s41598-020-72100-9

Krumpen T, Belter HJ, Boetius A, Damm E, Haas C, Hendricks S, Nicolaus M, Nothig EM, Paul S, Peeken I, Ricker R & Stein R (2019) Arctic warming interrupts the Transpolar Drift and affects long-range transport of sea ice and ice-rafted matter. Sci Rep 9(1):5459. https://doi.org/10.1038/s41598-019-41456-y

Roca-Martí M, Puigcorbé V, Rutgers van der Loeff MM, Katlein C, Fernández-Méndez M, Peeken I & Masqué P (2016) Carbon export fluxes and export efficiency in the central Arctic during the record sea-ice minimum in 2012: a joint 234Th/238U and 210Po/210Pb study. Journal of Geophysical Research: Oceans 121(7):5030–5049. https://doi.org/10.1002/2016jc011816

4. PHYSICAL OCEANOGRAPHY – PO

Jacob Allerholt[1], Ke-Hsien Fu[2], Céline Heuzé[3], Mario Hoppmann[1], Oliver Huhn[4], Benjamin Rabe[1], Simran Suresh[1], Sandra Tippenhauer[1], Hau-Man Wong[3], Jialiang Zhu[5]
Not on board: Ying-Chi Fang[6], Tao Li[5], Maren Walter[4], Birgit Klein[7], Meike Martins[7]

[1]DE.AWI
[2]TW.NAMR
[3]SW.UGOT
[4]DE.UHB.UIP
[5]CN.OUC
[6]TW.SUNYAT-SEN
[7]DE.BSH

Grant-No. AWI_PS144_03

Outline

The observational program of the Physical Oceanography (PO) Team includes research from the AWI and the University of Gothenburg, and under the secondary user proposals A2A (University of Bremen, Germany), IPA-ArcWatch 2 (Sun Yat Sen University, Taiwan) and DTOP-AW2/TA3 (Ocean University of China, China).

Objectives

The central Arctic Ocean is a crucial part of the global climate system, yet it is notoriously under-observed. Decades of repeated surveys using icebreakers and autonomous instrumentation and, to some extent, remote sensing, covering most of the Eurasian and Amerasian basins (e.g. Behrendt et al., 2018), have allowed to identify its variability on interannual to decadal time scales. Large-scale changes have been identified by temperature and salinity profile data (e.g. Rabe et al., 2014), while water sample analysis has led to further insight into water mass pathways by using various tracers (e.g. Huhn et al., 2018).

Waters imported to the Arctic Ocean are subject to cooling, freezing and melting, altering the properties of these water masses (e.g. Rudels et al., 2021; Timmermans and Marshall, 2020). The warm inflow of waters of Atlantic origin occurs via two pathways: the eastern Fram Strait and the Barents Sea. These two branches are subject to transformation by surface processes and lateral mixing before and after entering the Nansen Basin. Continental runoff enters the Eurasian and Makarov basins via the extensive shelf regions north of Eurasia, before advected within the Transpolar Drift and, at times, the Beaufort Gyre. In the central Arctic, stratification due to fresh water in the mixed layer and the halocline inhibits the release of heat from underlying waters to the atmosphere. This stratification is maintained by continental runoff, and ice or meltwater. However, changes may occur from the different wind mixing with and without ice cover, and the fact that now large areas have longer seasons without sea ice.

To identify further development of the variability, in particular, in the light of the “new Arctic” (e.g. Weingartner et al., 2022, and references therein) it requires repeated hydrographic surveys and deployment of autonomous instrumentation. Further attention has been paid to local process studies on the scale of one ice floe and the surrounding region, e.g. MOSAiC (Rabe et al., 2022; Nicolaus et al., 2022; Shupe et al., 2022) and N-ICE2015 (Granskog et al., 2018). However, further research and *in-situ* observation is needed to shed light on these

processes and, ultimately, improve model parameterisation and our understanding of the Arctic and global climate system.

Besides, in the absence of sustained time series of observations in the Arctic, trace gases provide a unique tool to observe ventilation time scales and circulation changes by estimating tracer ages (e.g., Karcher et al., 2012; Smith et al., 2021, 2022). During the MOSAiC expedition, we acquired a data set of anthropogenic trace gases and noble gas isotopes (Rabe et al.,, 2022; Heuzé et al., 2023) of the upper ocean along the drift track. This data set offers a unique opportunity to study a diverse set of processes, for example water mass ventilation (Huhn et al., 2013), ice melt (Huhn et al., 2018; Rhein et al., 2018), air-sea gas exchange (Wanninkhof et al., 2004), upwelling (Jenkins, 2020), or dispersal of hydrothermal input (German et al., 2022) that affect concentrations and isotopic ratios. However, the new data set has the inherent problem that the observations during the MOSAiC drift show a mixed temporal-spatial signal. Especially for the upper ocean and mixed layer, seasonal and regional variability are difficult to disentangle. During PS144 we will complement the MOSAiC winter data with a data set from the same region, but during summer, which will facilitate to identify individual processes. Additionally, we will extend the vertical scope of the sampling towards the deep water (that is not affected by seasonal variability) to study the age distribution, renewal times and the role of slope convection of the deep water masses of the Arctic Ocean.

The team aims to improve the temporal and spatial oceanographic data coverage on the basin scale in the Eurasian and Makarov basins, as well as to use the ice station time to study local processes, such as leads, shallow ocean stratification, turbulence, and feedback with the ice, snow and atmosphere system. Several hydrographic sections will improve our understanding of changes in time by repeating work from earlier cruises the have been conducted since the early 1990s with the icebreakers *Polarstern* and *Oden*, and within the NABOS (Nansen-Amundsen Basin Observation System) project. These observations will be augmented by upper-water-column hydrography perpendicular to the sections to capture horizontal gradients in all directions. We will run continuous and on-station measurements of current velocity to aid the interpretation of the hydrographic data and estimate transports. To extend the observational range of the ship survey in space and time, we plan to deploy autonomous, ice-based buoys, and deploy and recover bottom-moored observatories. From the sea ice, we will use a turbulence profiler to obtain estimates of fine structure and turbulent energy dissipation in the upper water column. This will improve our understanding of vertical mixing processes in the context of large-scale hydrography. The study is part of the ArcWatch series of *Polarstern* expeditions and embedded in wider frameworks, such as the International Arctic Buoy Programme (IABP; https://iabp.apl.uw.edu/) and especially GEOTRACES (e.g. Charette et al., 2020).

Work at sea

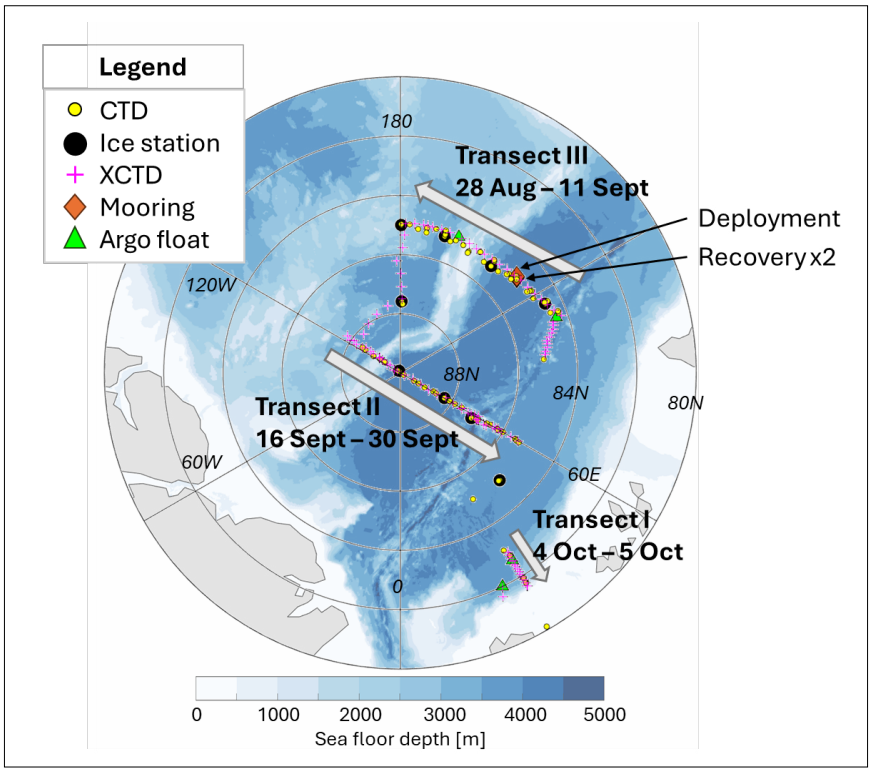

Fig. 4.1: Overview of the ship-based work of the Physical Oceanography group

Lowered Conductivity Temperature Depth (CTD) rosette and mounted sensors

The CTD/Rosette was operated using the standard SeaBird SBE911plus setup, equipped with double sensors for temperature, salinity, and oxygen and one sensor each for pressure, substance fluorescence Chl-a (WET Labs ECO-AFL/FL), substance fluorescence of coloured dissolved organic matter (CDOM, WET Labs ECO CDOM), yellow substance fluorescence (Dr. Haardt), beam transmission (WET Labs C-Star), photosynthetically active radiation (PAR/Logarithmic, Satlantic), and surface photosynthetically active radiation (SPAR/Linear, Satlantic). The sensor configuration is summarised in Tab. 4.1. In addition, 24 12-liter Niskin bottles for water sampling were attached. An altimeter was mounted to monitor the distance to the seafloor. The C-Star transmissiometer was calibrated following the procedure described in Seabird application-note-07 in the beginning of the cruise.

The altimeters performed overall well, giving reliable values from about 50 m above the seafloor on most casts, sometimes 90 m even. For all casts we limited our distance to the seafloor to 10 m.

The CDOM sensor on the CTD/rosette did not work properly. It was an old sensor, borrowed from Marine Biogeochemistry (MBC) Team.

The SPAR sensor was installed from profile PS144_007_04 onward.

Additionally, two 300 kHz RDI Workhorse up and downward looking ADCPs were mounted on the CTD/rosette to act as lowered ADCPs (LADCP): ADCP SN 23293 (sw1309) as master, looking down and ADCP SN 23292 (sw1258) as slave, looking up. The LADCP assembly also had a battery container. The ADCPs were operated using the GUI of the LADCP tool V1.7 from

GEOMAR. LADCP measurements were conducted at all CTD stations except those where the Pelagic and Seaice Biology team's WBAT was operated or other issues prevented data recording (see Tab. 4.2). The battery was changed on 23.09.2024. The settings are:

[LADCP]
last_profile_number=73
base_path=C:\ladcp\scripts\..\
network_path=C:\ladcp\data\PS144\
cruise_id=PS144
up_installed=1
down_installed=1
total_pings=372186
total_ping_time=68.8
erase_button=enabled
download_files=all
last_action=erase
ntp_server=192.168.20.3
[Master-Commands]
mode_15=1
ambiguity_velocity=250
bin_number=20
bin_length=1000
blank_after_transmit=0
broadband=1
sensor_source=0111101
coordinate_transformation=00111
flow_control=11101
pings_per_ensemble=1
time_between_pings=0
time_per_ensemble=1.2
master_slave=1
wait_ensembles_before_sync=0
master_slave_when_to_sync=011
wait_time_before_sync=5500
power_output=255
[Slave-Commands]
mode_15=1
ambiguity_velocity=250
bin_number=20
bin_length=1000
blank_after_transmit=0
broadband=1
sensor_source=0111101
coordinate_transformation=00111
flow_control=11101
pings_per_ensemble=1

time_between_pings=0
time_per_ensemble=1.2
master_slave=2
master_slave_when_to_sync=011
wait_time_before_start_without_sync=200
power_output=255

A SUNA nitrate sensor (SN1472) was installed on the CTD/rosette during casts shallower than 2000 m. The instrument was deployed on 24 casts to obtain high-resolution nitrate profiles (Tab. 4.3) and recorded the data internally as soon as power was supplied by the SBE911plus.

An Underwater Vision Profiler (UVP) was attached to the rosette to continuously record Plankton and particle images during the CTD downcast, recording data internally. The instrument was operated by the Pelagic and Seaice Biology group.

A WBAT Single beam transduce (200 kHz) was occasionally mounted to the CTD to record hydroacoustic backscatter. The instrument was operated by the Pelagic and Seaice Biology group.

The initial configuration (*conf1*) of the SBE911+ CTD on the rosette remained unchanged throughout the cruise.

Water samples were taken throughout and analysed for the correction of temporal drift and pressure effects of the conductivity and oxygen sensors. For the salinity samples the respective bottles were closed after at least a 60 s wait at the sampling depth. The samples will be used to finalise the data sets after the expedition using those bottle sample data as well as the manufacturer's calibration pre- and post-expedition. Additional samples for chemical and biological variables, such as nitrate and Chl-a, will be used to correct the Chl-a fluorescence and nitrate sensors after the expedition. The oxygen sampling and titration was performed by the Marine Biogeochemistry group.

For calibration of the conductivity sensors, salinity samples were taken regularly (Fig. 4.2 and Tab. 4.4) and measured with the Optimare Precision Salinometer (OPS). Before measurement, samples were degassed by heating them to 30 degrees for one hour, letting out the overpressure, and letting them adjust to room temperature again.

The in total 212 salinity samples were measured using the OPS-006 or OPS-007. As a standard the OPS-006 is the one to be used by scientists while OPS-007 is to be used by crew. As OPS-006 showed unstable readings during the first measurement session OPS-007 was used instead while 006 was rinsed for several times. Since then, OPS-006 showed stable readings and was used for the remaining measurements.

The final calibration of the CTD data will be done based on the salinometer results in combination with the post-cruise manufacturer calibration of the sensors.

We collected full-depth profiles from 502 water samples at 33 stations for anthropogenic transient tracers CFC-12 and SF_6, 383 water samples at 29 stations for noble gas isotopes He (^{3}He and total He) and total Ne, and 148 water samples at 11 stations for tritium from the ship deployed full depth profiling CTD and water sample system (Fig. 4.2. and Tab. 4.4). We collected an additional seven snow samples for tritium (Tab. 4.5).

Water samples for CFC-12 and SF_6 measurements have been stored from the ship deployed water samplers into 200 ml glass ampoules and sealed off after a CFC and SF_6 free headspace of pure nitrogen has been applied. The samples will be analysed post-cruise in the CFC and SF_6 laboratory at the IUP Bremen. The determination of CFC-12 and SF_6 concentrations is accomplished by purge and trap sample pre-treatment followed by gas chromatographic (GC) separation on a capillary column and electron capture detection (ECD). The amount of CFC-12 and SF_6 degassing into the headspace is accounted for during the measurement procedure in the lab. The system is calibrated by analysing several different volumes of a known standard gas. Additionally, the blank of the system is analysed regularly. For details see Bulsiewicz et al. (1998).

The oceanic water samples for helium and neon isotopes have been stored from the CTD and water bottle system into 50 ml gas tight copper tubes, clamped of at both sides. The noble gas samples are to be analysed post-cruise in the IUP Bremen noble gas mass spectrometry lab. The copper tube water samples will be processed in a first step with an ultra-high vacuum gas extraction system. Sample gases are transferred via water vapor into a glass ampoule kept at liquid nitrogen temperature. For analysis of the noble gas isotopes the glass ampoules are connected to an ultra-high vacuum mass spectrometric system equipped with a two-stage cryogenic trap system. The system is regularly calibrated with atmospheric air standards. Measurement of blanks and linearity are done as well. The tritium samples will be gas extracted and stored for about half a year, in which a sufficient amount of tritium will decay to ^3He, which is then analysed in the same manor described above. For details regarding noble gases and tritium analysis see Sültenfuß et al. (2009).

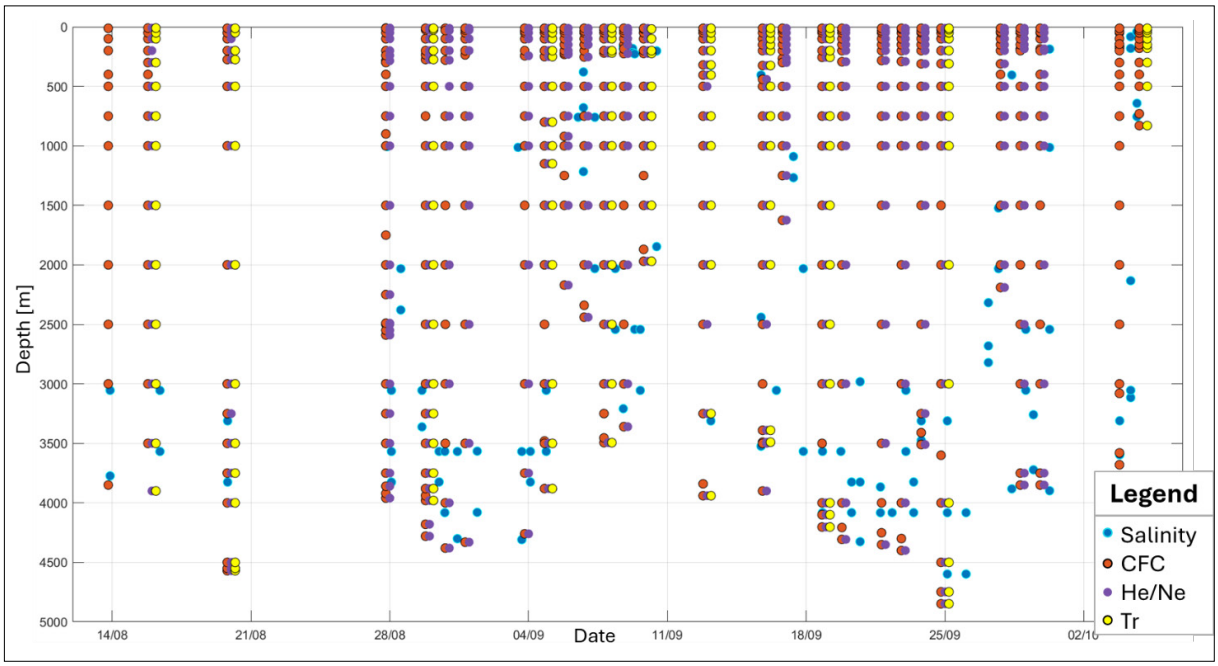

Fig. 4.2: Overview of the water samples collected from the CTD-rosette for salinity (blue), CFC12-SF_6 (red), noble gases (purple), and tritium (yellow).

Finally, for a feasibility study, we collected 49 opportunistic “PFAS” samples during transect III in the so-called “surface”, CDOM max” and “Atlantic Water core” depth levels, if there was water left in the Niskin bottles after all teams had taken their samples. The sampling protocol

was unclearly communicated and probably too simplistic given the many possible sources of contamination (“small rinsing 3 times, then collect 800 ml in a plastic bottle”), so it is most likely that these samples, once analysed, will only show a correlation with who the sampler was and what they were wearing on this day.

Tab. 4.1: Sensor configuration for the ship-based CTD rosette used during PS144

Parameter	**SN**	**Calibration Date**	**Channel**	**Sensor type**
	525	-	Deckunit Seabird11plus	
Temperature 1	4127	16-Jan-24	F0	Seabird SBE3plus
Conductivity 1	2618	09-Jan-24	F1	Seabird SBE4c
Pressure	287	14-Nov-17	F2	Seabird SBE9plus
Temperature 2	5101	10-Aug-21	F3	Seabird SBE3plus
Conductivity 2	3238	10-Aug-21	F4	Seabird SBE4c
Oxygen 1	467	20-Mar-21	V0	Seabird SBE43
Oxygen 2	48	09-Sep-21	V1	Seabird SBE43
	2544	--	pump	Seabird SBE5T
	4317	--	pump	Seabird SBE5T
Chl-a fluorescence	8103	20-Apr-2023	V2	WETlabs ECO Chl-a
Beam Transmission	1220	25-Aug-24	V3	WETlabs C-Star
Altimeter	46611/ 86344	--	V4	Teledyne Benthos PSA916, later Valeport
CDOM fluorescence	742	--	V5	WETlabs ECO CDOM
Yellow Sub. fluorescence	3	--	V6	Dr. Haardt
PAR	2197	30-Nov-21	V7	PAR/Logarithmic, Satlantic
SPAR	2335	9-Jan-2024	SPAR	SPAR/Linear, Satlantic
Additional Sensor:				
Current velocity	23293/ 23292	--	--	RDI Workhorse ADCPs 300 kHz
Nitrate	1472			Satlantics Deep SUNA V2
underwater vision	202	--	--	UVP, Hydroptic
Hydroacoustic backscatter	11000	--	--	WBAT, Simrad, Single beam transduce ES200-7CDKr (200 khz)

Tab. 4.2: Metadata of all CTD station and casts. “Station” refers to the final part of the respective file name, starting with “PS144_” and equivalent to the corresponding Event Label. Also indicated are the LADCP profile numbers. Bold fonts highlight the casts used for the mooring sensor calibrations (see subsection “Instrument calibration casts” in this chapter). Asterisk * highlights the cast with the suspected plume during the upcast (see "Preliminary results").

Station	Date	Time (UTC)	Latitude [°]	Longitude [°]	Water depth [m]	Profile depth [m]	LADCP
003_01	14.08.2024	7:03	83.04	29.73	3858	3877	1
003_03	14.08.2024	11:54	83.04	29.96	3851	3996	2
006_01	14.08.2024	5:57	85.04	42.70	3929	3954	3
007_04	16.08.2024	19:23	85.06	42.80	3929	3951	4
007_07	17.08.2024	2:57	85.05	42.36	3685	400	-
***011_02**	**20.08.2024**	**5:18**	**85.11**	**95.37**	**4584**	**4525**	**5**
018_01	**28.08.2024**	**6:39**	**84.27**	**110.66**	**3985**	**1000**	**6**
018_03	28.08.2024	11:34	84.28	111.33	4045	3960	7
020_02	28.08.2024	22:53	84.46	113.81	2680	2569	8
023_02	29.08.2024	14:01	84.49	115.33	4067	4022	9
023_05	30.08.2024	0:34	84.46	115.88	3790	3794	10
023_09	30.08.2024	10:29	84.41	115.79	3247	400	11
026_01	30.08.2024	21:16	84.67	119.06	4391	4331	12
028_01	31.08.2024	4:13	84.76	121.97	4385	4326	13
028_03	31.08.2024	11:22	84.79	122.13	4384	1001	14
031_01	31.08.2024	19:27	84.84	125.58	4375	4313	15
035_01	01.09.2024	19:27	84.91	130.04	4343	4282	16
037_01	02.09.2024	2:13	84.88	129.83	4346	4286	17
041_01	02.09.2024	15:50	84.82	128.70	4353	4292	18
046_01	03.09.2024	20:50	84.95	132.40	4322	1000	19
046_03	04.09.2024	1:19	84.93	132.57	4319	4259	20
048_01	04.09.2024	11:47	85.00	135.92	4256	4192	21
050_02	04.09.2024	22:44	85.03	139.58	3951	3889	23
050_05	05.09.2024	6:59	85.02	139.80	3960	3893	24
050_09	05.09.2024	15:18	85.02	140.10	3465	1000	-
052_01	05.09.2024	22:32	85.06	142.83	3388	3326	25
054_01	06.09.2024	6:20	85.08	146.34	2196	2100	26
057_01	06.09.2024	19:03	85.08	150.46	958	917	27
057_03	06.09.2024	21:35	85.08	150.51	950	913	28
059_01	07.09.2024	3:58	85.03	153.75	1549	1497	29
064_01	07.09.2024	17:46	84.98	157.14	2510	2448	30
065_02	07.09.2024	23:09	84.98	159.04	3434	3367	31
067_02	08.09.2024	7:29	84.95	161.90	3560	1000	-
067_04	08.09.2024	11:37	84.94	161.90	3560	3495	32
067_07	08.09.2024	18:35	84.93	162.19	3559	3494	33
069_01	09.09.2024	4:14	84.95	165.76	3501	3437	34
073_01	09.09.2024	15:32	84.94	169.28	3423	400	-
073_04	09.09.2024	18:05	84.95	169.26	3424	3360	35

Station	Date	Time (UTC)	Latitude [°]	Longitude [°]	Water depth [m]	Profile depth [m]	LADCP
075_01	10.09.2024	0:49	84.93	172.78	3175	3122	36
077_01	10.09.2024	7:32	84.92	176.26	2630	2575	37
080_02	10.09.2024	20:38	84.92	179.57	1977	1919	38
080_04	11.09.2024	1:33	84.94	179.41	2072	2054	39
085_02	12.09.2024	3:11	87.52	178.89	3996	3934	40
085_06	13.09.2024	14:13	87.49	178.37	3994	3932	41
085_09	13.09.2024	22:33	87.46	177.90	3994	1000	42
090_01	16.09.2024	3:03	88.36	-124.66	3560	3437	43
090_03	16.09.2024	9:20	88.37	-124.12	3529	1000	-
094_01	16.09.2024	21:33	88.68	-123.89	3996	3933	44
097_01	17.09.2024	7:20	89.01	-125.76	1664	1619	45
102_01	17.09.2024	18:14	89.34	-125.48	1656	1632	46
102_03	17.09.2024	22:31	89.33	-125.39	1668	1000	47
105_01	18.09.2024	6:09	89.66	-126.38	4250	4189	48
109_02	18.09.2024	22:36	89.94	-151.08	4264	1000	49
109_05	19.09.2024	5:25	89.95	-144.85	4264	4203	50
109_08	19.09.2024	15:27	89.96	-131.63	4266	4205	51
111_01	20.09.2024	3:37	89.68	59.73	4324	4264	52
113_01	20.09.2024	16:35	89.36	59.90	4366	4308	53
115_01	21.09.2024	2:55	89.03	59.73	4395	4336	54
115_03	**21.09.2024**	**10:26**	**89.00**	**58.88**	**4396**	**1000**	**-**
118_01	22.09.2024	3:31	88.70	60.66	4410	4351	55
121_01	22.09.2024	17:39	88.40	59.97	4415	4357	56
123_01	23.09.2024	3:56	88.08	60.17	4416	1000	-
123_04	**23.09.2024**	**10:17**	**88.07**	**59.93**	**4416**	**4359**	**-**
125_01	23.09.2024	19:43	87.76	60.03	4365	4320	57
127_01	24.09.2024	4:58	87.43	60.25	3521	3510	58
134_03	25.09.2024	12:24	86.98	58.64	4896	4848	59
134_06	26.09.2024	2:41	87.04	57.38	4243	1000	60
134_09	26.09.2024	11:08	86.99	58.57	4845	4794	61
138_01	27.09.2024	14:10	86.74	59.10	2942	2872	62
141_01	28.09.2024	2:25	86.48	60.03	2122	2109	63
141_03	28.09.2024	6:58	86.49	59.53	2094	1000	64
144_02	28.09.2024	18:30	86.17	60.10	3909	3846	65
144_04	29.09.2024	0:55	86.17	59.81	3911	1000	66
147_01	29.09.2024	11:26	85.83	59.86	3927	3863	67
149_01	29.09.2024	20:42	85.52	60.01	3936	3871	68
152_01	30.09.2024	16:17	85.25	59.77	3926	3861	69
152_03	30.09.2024	22:17	85.24	59.53	3927	1000	70
156_02	04.10.2024	5:08	82.70	30.82	3692	3629	71
157_02	04.10.2024	18:25	81.85	30.89	3166	3102	72
158_01	05.10.2024	2:03	81.53	30.81	828	798	73
159_01	05.10.2024	14:24	80.09	29.91	306	297	74

Tab. 4.3: Metadata of all PS144 ship-based nitrate profiles, using the same nomenclature as Table 4.2

Station	Date	Time (UTC)	Latitude [°]	Longitude [°]	Water depth [m]	Profile depth [m]	Profile number
007_07	17.08.2024	2:57	85.05	42.36	3685	400	A0002608
018_01	28.08.2024	6:39	84.27	110.66	3985	1000	A0002609
023_09	30.08.2024	10:29	84.41	115.79	3247	400	A0002610
046_01	03.09.2024	20:50	84.95	132.40	4322	1000	A0002611
050_09	05.09.2024	15:18	85.02	140.10	3465	1000	A0002612
057_01	06.09.2024	19:03	85.08	150.46	958	917	A0002613
057_03	06.09.2024	21:35	85.08	150.51	950	913	A0002614
059_01	07.09.2024	3:58	85.03	153.75	1549	1497	A0002615
067_02	08.09.2024	7:29	84.95	161.90	3560	1000	A0002616
073_01	09.09.2024	15:32	84.94	169.28	3423	400	A0002617
085_09	13.09.2024	22:33	87.46	177.90	3994	1000	A0002618
090_03	16.09.2024	9:20	88.37	-124.12	3529	1000	A0002619
097_01	17.09.2024	7:20	89.01	-125.76	1664	1619	A0002620
102_01	17.09.2024	18:14	89.34	-125.48	1656	1632	A0002621
102_03	17.09.2024	22:31	89.33	-125.39	1668	1000	A0002622
109_02	18.09.2024	22:36	89.94	-151.08	4264	1000	A0002623
115_03	21.09.2024	10:26	89.00	58.88	4396	1000	A0002624
123_01	23.09.2024	3:56	88.08	60.17	4416	1000	A0002625
134_06	26.09.2024	2:41	87.04	57.38	4243	1000	A0002626
141_03	28.09.2024	6:58	86.49	59.53	2094	1000	A0002627
144_04	29.09.2024	0:55	86.17	59.81	3911	1000	A0002628
152_03	30.09.2024	22:17	85.24	59.53	3927	1000	A0002629
158_01	05.10.2024	2:03	81.53	30.81	828	798	A0002630
159_01	05.10.2024	14:24	80.09	29.91	306	297	A0002631

Tab. 4.4: Overview of water sampling from the CTD-rosette for salinity, CFC12-SF_6 (“CFC”), noble gases (“He/Ne”), and Tritium (“Tr”)

Station	Date	Time	Latitude	Longitude	Salinity	CFC	He/Ne	Tr
003_01	14.08.2024	7:03	83.04	29.73	x	x		
003_03	14.08.2024	11:54	83.04	29.96		x		
007_04	16.08.2024	19:23	85.06	42.80	x	x	x	x
011_02	20.08.2024	5:18	85.11	95.37	x	x	x	x
018_01	28.08.2024	6:39	84.27	110.66	x			
018_03	28.08.2024	11:34	84.28	111.33	x	x	x	
020_02	28.08.2024	22:53	84.46	113.81	x	x	x	
023_05	30.08.2024	0:34	84.46	115.88	x	x	x	x
026_01	30.08.2024	21:16	84.67	119.06	x	x	x	
028_01	31.08.2024	4:13	84.76	121.97	x	x	x	
031_01	31.08.2024	19:27	84.84	125.58	x			

Station	Date	Time	Latitude	Longitude	Salinity	CFC	He/Ne	Tr
035_01	01.09.2024	19:27	84.91	130.04	x	x	x	
046_01	03.09.2024	20:50	84.95	132.40	x			
046_03	04.09.2024	1:19	84.93	132.57	x	x	x	
048_01	04.09.2024	11:47	85.00	135.92	x			
050_05	05.09.2024	6:59	85.02	139.80	x	x	x	x
054_01	06.09.2024	6:20	85.08	146.34		x	x	
057_03	06.09.2024	21:35	85.08	150.51	x	x	x	
059_01	07.09.2024	3:58	85.03	153.75	x			
064_01	07.09.2024	17:46	84.98	157.14	x	x	x	
067_07	08.09.2024	18:35	84.93	162.19	x	x	x	x
069_01	09.09.2024	4:14	84.95	165.76	x			
073_01	09.09.2024	15:32	84.94	169.28	x			
073_04	09.09.2024	18:05	84.95	169.26	x	x	x	
075_01	10.09.2024	0:49	84.93	172.78	x			
080_02	10.09.2024	20:38	84.92	179.57	x	x	x	x
085_06	13.09.2024	14:13	87.49	178.37	x	x	x	x
090_01	16.09.2024	3:03	88.36	-124.66	x	x	x	x
094_01	16.09.2024	21:33	88.68	-123.89	x	x	x	
102_01	17.09.2024	18:14	89.34	-125.48	x	x	x	
105_01	18.09.2024	6:09	89.66	-126.38	x			
109_05	19.09.2024	5:25	89.95	-144.85	x	x	x	x
111_01	20.09.2024	3:37	89.68	59.73	x			
113_01	20.09.2024	16:35	89.36	59.90	x	x	x	
115_01	21.09.2024	2:55	89.03	59.73	x			
118_01	22.09.2024	3:31	88.70	60.66	x	x	x	
121_01	22.09.2024	17:39	88.40	59.97	x			
123_04	23.09.2024	10:17	88.07	59.93	x	x	x	
125_01	23.09.2024	19:43	87.76	60.03	x			
127_01	24.09.2024	4:58	87.43	60.25	x	x	x	
134_03	25.09.2024	12:24	86.98	58.64	x	x	x	x
134_09	26.09.2024	11:08	86.99	58.57	x			
138_01	27.09.2024	14:10	86.74	59.10	x			
141_01	28.09.2024	2:25	86.48	60.03	x	x	x	
144_02	28.09.2024	18:30	86.17	60.10	x			
147_01	29.09.2024	11:26	85.83	59.86	x	x	x	
149_01	29.09.2024	20:42	85.52	60.01	x			
152_01	30.09.2024	16:17	85.25	59.77	x	x	x	
156_02	04.10.2024	5:08	82.70	30.82	x	x		
157_02	04.10.2024	18:25	81.85	30.89	x	x		
158_01	05.10.2024	2:03	81.53	30.81	x	x		x

Tab. 4.5: Overview of snow sampling for Tritium

Station	Date	Latitude	Longitude
042_02	02.09.2024	84.84	128.65
042_02	02.09.2024	84.84	128.65
044_01	03.09.2024	84.87	129.57
044_01	03.09.2024	84.87	129.57
067_04	08.09.2024	84.95	162.04
067_04	08.09.2024	84.95	162.04
085_01	12.09.2024	87.52	179.10
085_01	12.09.2024	87.52	179.10
109_08	19.09.2024	89.96	-128.04
109_08	19.09.2024	89.96	-128.04
123_02	23.09.2024	88.07	59.72
123_02	23.09.2024	88.07	59.72
134_01	26.09.2024	87.04	57.46
134_01	26.09.2024	87.04	57.46

Underway observations

Polarstern is equipped with an Ocean Surveyor 150kHz (RD-Instruments) Acoustic Doppler Current Profiler (SADCP) to monitor ocean currents. The SADCP was operated using these settings:

; Restore factory default settings in the ADCP
cr1

; set the data collection baud rate to 9600 bps,
; no parity, one stop bit, 8 data bits
; NOTE: VmDas sends baud rate change command after all other commands in
; this file, so that it is not made permanent by a CK command.
cb411

; Set for narrowband single-ping profile mode (NP), 80 (NN), 4 meter bins (NS),
; 4 meter blanking distance (NF)
WP000
NP001
NN080
NS0400
NF0400
;WV390 (default)

; Disable single-ping bottom track (BP),
BP000

; output velocity, correlation, echo intensity, percent good
ND111100000

; Ping as fast as possible
TP000000

; Since VmDas uses manual pinging, TE is ignored by the ADCP
; and should not be set.
;TE0000000

; Set to calculate speed-of-sound, no depth sensor, external synchro heading
; sensor, pitch or roll being used, no salinity sensor, use internal transducer
; temperature sensor
EZ1011101

; Output beam data (rotations are done in software)
EX00000

; Set transducer misalignment (hundredths of degrees).
; Ignored here but set in VmDAS options.
;EA00000

; Set transducer depth (decimeters)
ED00110

; Set Salinity (ppt)
ES35

;set external triggering and output trigger; no trigger
CX0,0 (either on or off)

;set external triggering and output trigger
;CX1,3 (either on or off)

; save this setup to non-volatile memory in the ADCP
CK

During most of the cruise the SADCP was operated in parallel with the EK-80 without using the K-Synch unit. The EK-80 was running with four different frequencies (38Hz, 70Hz, 120Hz, 200k Hz) in FM-mode (broadband) as well as the single ping 18 kHz depth sound. For protection against ice, the Ocean Surveyor is mounted behind a window, flooded with water, in the ship's hull. When steaming through ice, air can accumulate inside the window over time, which negatively affects the data quality. During PS144 the air was regularly released by the laboratory electrician but only very little air did accumulate. The data from the SADCP was merged online with the corresponding navigation data (i.e., the vessel's GPS system) and stored on the hard disk using the program VMDAS. Pitch, roll and heading data are converted from NMEA. Current speed data were collected in beam coordinates to apply corrections during post processing. Processing during the cruise was conducted using GEOMAR sadcp

software (OSSI19). Final data processing and quality control will be done at AWI after the field campaign.

Onboard *Polarstern* there are two SBE21 SeaCAT Thermosalinograph with additional external thermometer SBE38 for minimum thermal contamination from the ship. The two systems are operated in parallel on the same seawater intake. The pumped system is equipped with a flow meter and set to pump 60 L/min. Position and time information are added via NMEA telegram. The system is located in the ship's keel with the water intake at about 11 m depth, depending on the ship's draft. During PS144 the system was running continuously without any maintenance or cleaning being necessary. For calibration, salinity samples are taken irregularly, depending on the ice conditions. On average, samples are taken every other week and measured with an Optimare Precision Salinometer on board by the ship's laboratory-electrician. The sensors are usually operated for one full season (about half a year, depending on expedition schedule) and changed during time in port in Bremerhaven. After post-cruise calibration of sensors, the data is processed and calibrated by Fielax GmbH and stored in the PANGAEA data repository.

During transits through ice-covered seas we used eXpendable CTDs (XCTD; deck unit MK150 by TSK, probes TSK/Lokheed-Martin Sippican XCTD 4) to increase the spatial resolution of the regular CTD sections in the upper water column. A total of 107 XCTD-4 probes were deployed during PS144 (Tab. 4.6) to collect profiles of temperature and salinity along the cruise track as a complement to the regular CTD stations. The probes were launched from the aft of the ship using a standard hand-held launcher connected to the MK150 deck unit (Fig. 4.3). Most profiles achieved a full depth of 2000 m. Three probes were defect or did not reach critical depth before ceasing to respond.

Tab. 4.6: Overview of XCTD deployments

XCTD Event Label	Date	Time (UTC)	Latitude [°]	Longitude [°]	Max. Depth [m]	SN
PS144_1-2	13.08.2024	16:10	81.68	24.68	473	22031244
PS144_2-1	13.08.2024	20:22	81.98	25.56	1085	22031247
PS144_13-1-1	20.08.2024	17:55	85.07	97.13	178.5	23117946
PS144_13-1-2	20.08.2024	18:01	85.07	97.12	31	23117947
PS144_13-2	20.08.2024	19:28	85.02	98.30	2000	23117948
PS144_13-3	20.08.2024	21:05	84.95	99.77	2000	23117949
PS144_13-4	20.08.2024	22:43	84.92	101.10	2000	23117951
PS144_13-5	21.08.2023	0:31	84.92	102.32	2000	23117950
PS144_13-6	21.08.2024	2:18	84.81	103.54	2000	23117952
PS144_13-7	21.08.2024	5:52	84.70	104.77	2000	23117953
PS144_13-8	21.08.2024	7:39	84.63	105.83	1853.5	23117954
PS144_13-9-1	21.08.2024	9:48	84.58	107.23	218.5	23117956
PS144_13-9-2	21.08.2024	9:56	84.58	107.24	1359.5	23117957
PS144_13-1	21.08.2024	11:23	84.55	108.46	2000	23128654
PS144_17-1	28.08.2024	4:49	84.22	109.68	1226	23128655
PS144_19-1	28.08.2024	19:33	84.38	112.26	1124	23117955
PS144_21-1-1	29.08.2024	2:49	84.51	114.84	223.8	23128656
PS144_21-1-2	29.08.2024	2:58	84.52	114.83	2000	23128657
PS144_25-1	30.08.2024	18:52	84.62	117.44	1776.5	23128659

XCTD Event Label	Date	Time (UTC)	Latitude [°]	Longitude [°]	Max. Depth [m]	SN
PS144_27-1	31.08.2024	2:15	84.72	120.38	1080.5	23128660
PS144_3-1	31.08.2024	17:01	84.81	123.82	2000	23128661
PS144_32-1	01.09.2024	0:17	84.85	127.50	2000	23128662
PS144_45-1	03.09.2024	15:57	84.93	130.58	2000	23128658
PS144_47-1	04.09.2024	6:50	84.96	134.22	1325.5	23128664
PS144_49-1	04.09.2024	17:49	85.03	137.64	1281.5	23128665
PS144_51-1	05.09.2024	20:27	85.05	141.10	2000	23128644
PS144_53-1	06.09.2024	3:31	85.07	144.74	2000	23128647
PS144_56-1	06.09.2024	16:09	85.07	148.48	1759	23128646
PS144_58-1	07.09.2024	0:40	85.04	151.89	807	22031201
PS144_6-1	07.09.2024	7:11	85.01	155.42	2000	23128642
PS144_66-1	08.09.2024	3:09	84.97	160.52	2000	23128645
PS144_68-1	09.09.2024	2:06	84.95	163.96	1908.5	23128643
PS144_72-1	09.09.2024	13:11	84.95	167.39	2000	23128649
PS144_73-3	09.09.2024	17:42	84.95	169.26	2000	23128648
PS144_74-1	09.09.2024	23:03	84.93	171.01	2000	23128650
PS144_76-1	10.09.2024	5:23	84.93	174.40	2000	23128651
PS144_79-2	10.09.2024	17:50	84.94	177.88	2000	23117991
PS144_82-1	11.09.2024	14:33	85.33	178.16	988	23118653
PS144_82-2	11.09.2023	19:20	85.77	178.94	2000	23117992
PS144_82-3	12.09.2023	0:23	86.22	-178.06	609	23117993
PS144_82-4	12.09.2024	4:43	86.63	179.58	2000	23117989
PS144_82-5	12.09.2024	11:30	87.08	179.20	922	23117988
PS144_85-5	13.09.2024	13:53	87.49	178.39	2000	23117986
PS144_87-1	14.09.2024	14:46	87.69	-169.39	1433.5	23117990
PS144_87-2	15.09.2024	0:25	87.86	-158.09	2000	23117985
PS144_87-3	15.09.2024	7:43	88.02	-147.00	2000	23117983
PS144_87-4	15.09.2024	17:13	88.20	-136.26	2000	23117982
PS144_Heli_XCTD-1	16.09.2024	10:12	87.82	-124.97	2000	23117994
PS144_Heli_XCTD-2	16.09.2024	10:43	87.96	-123.00	2000	23117984
PS144_Heli_XCTD-3	16.09.2024	11:13	88.09	-124.93	2000	23128601
PS144_Heli_XCTD-4	16.09.2024	11:43	88.23	-123.03	2000	23117999
PS144_92-1	16.09.2024	17:42	88.47	-123.33	2000	23128605
PS144_93-1	16.09.2024	19:31	88.57	-125.80	2000	23128602
PS144_95-1	17.09.2024	2:05	88.77	-125.82	1150	23118000
PS144_96-1	17.09.2024	4:18	88.88	-124.53	2000	23117997
PS144_99-1-1	17.09.2024	11:07	89.13	-125.11	645	23117998
PS144_99-1-2	17.09.2024	11:16	89.13	-126.80	879	23117996
PS144_1-1	17.09.2024	14:17	89.25	-126.00	1610	23128604
PS144_13-1	18.09.2024	2:22	89.45	-123.38	1152	23117995
PS144_14-1-1	18.09.2024	4:02	89.57	-125.72	426	23128603

XCTD Event Label	Date	Time (UTC)	Latitude [°]	Longitude [°]	Max. Depth [m]	SN
PS144_14-1-2	18.09.2024	4:14	89.58	-125.48	910	23117968
PS144_16-1	18.09.2024	11:09	89.78	-114.41	2000	23117967
PS144_17-1	18.09.2024	13:10	89.90	-115.20	1276	23117964
PS144_11-1	20.09.2024	1:06	89.84	63.29	1171	23128630
PS144_112-1	20.09.2024	13:18	89.53	63.18	2000	23128631
PS144_114-1	20.09.2024	22:23	89.21	60.43	106	23117969
PS144_117-1	21.09.2024	23:27	88.88	59.42	828	23128633
PS144_119-1	22.09.2024	9:44	88.56	59.99	2000	23128634
PS144_122-1-1	23.09.2024	0:17	88.24	61.40	656.5	23128635
PS144_122-1-2	23.09.2024	0:23	88.24	61.44	755.5	23128632
PS144_124-1	23.09.2024	16:24	87.93	60.05	933	23128637
PS144_126-1	24.09.2024	2:00	87.60	60.03	74	23128638
PS144_126-2	24.09.2024	2:13	87.60	60.01	64	23128636
PS144_129-1	24.09.2024	11:23	87.34	59.63	389	23128639
PS144_129-2	24.09.2024	11:26	87.33	59.63	2000	23128640
PS144_131-1	24.09.2024	18:25	87.23	59.73	1784	23128615
PS144_132-1	24.09.2024	21:41	87.10	60.46	2000	23128616
PS144_133-1	25.09.2024	0:35	86.97	61.03	2000	23128614
PS144_134-2	25.09.2024	12:09	86.98	58.65	2000	23128617
PS144_134-8	26.09.2024	10:51	86.99	58.59	2000	23128612
PS144_136-1	27.09.2024	6:00	86.92	58.64	439	23128613
PS144_136-2	27.09.2024	6:13	86.91	58.67	2000	23128611
PS144_139-1	27.09.2024	18:12	86.69	58.50	635	23128609
PS144_14-1	27.09.2024	21:12	86.59	58.38	832	23128608
PS144_142-1	28.09.2024	11:09	86.38	60.00	2000	23128610
PS144_143-1	28.09.2024	13:40	86.26	59.75	422	23128607
PS144_143-2	28.09.2024	13:45	86.26	59.72	2000	23128606
PS144_144-1	28.09.2024	18:06	86.17	60.13	2000	23128628
PS144_145-1	29.09.2024	5:26	86.01	59.54	2000	23128627
PS144_148-1	29.09.2024	17:28	85.68	60.04	2000	23128624
PS144_15-1	30.09.2024	3:08	85.40	59.83	1630	23128625
PS144_155-1	04.10.2024	2:20	82.93	30.98	2000	23128622
PS144_155-2	04.10.2024	3:26	82.83	30.85	2000	23128626
PS144_156-1	04.10.2024	4:44	82.70	30.82	2000	23128629
PS144_155-3-1	04.10.2024	11:30	82.60	30.87	669	23128621
PS144_155-3-2	04.10.2024	11:35	82.59	30.86	2000	23128618
PS144_155-4	04.10.2024	12:28	82.48	30.80	1920	23128619
PS144_155-5	04.10.2024	13:22	82.39	30.86	2000	23117966
PS144_155-6	04.10.2024	14:20	82.28	30.85	2000	23128623
PS144_155-7	04.10.2024	15:21	82.17	30.86	2000	23128620
PS144_155-8	04.10.2024	16:13	82.07	30.87	754	23117962

XCTD Event Label	Date	Time (UTC)	Latitude [°]	Longitude [°]	Max. Depth [m]	SN
PS144_155-9	04.10.2024	16:59	81.96	30.89	2000	23117961
PS144_157-1	04.10.2024	18:01	81.85	30.89	2000	23117959
PS144_155-1	04.10.2024	23:53	81.73	30.86	2000	23117960
PS144_155-11-1	05.10.2024	0:44	81.63	30.82	1015.5	23117965
PS144_155-11-2	05.10.2024	0:51	81.62	30.82	480	23117963
PS144_155-11-3	05.10.2024	0:57	81.62	30.83	1975	23117958

Fig. 4.3: XCTD deployment using a hand-held launcher from the aft of the ship; photo credit: Jialiang Zhu

Mooring recoveries

We successfully recovered the two seafloor-based moorings CAO1-01 and CAO2-01 that were co-deployed during PS138 in the eastern Amundsen Basin on 31 August 2023 (Tab. 4.7). They were spaced approximately 3.5 km apart from each other. Mooring CAO1-01 was equipped with 7 Seabird SBE56 temperature loggers, 9 Seabird SBE37 MicroCats, one RDI Longranger 75 kHz ADCP, one Develogic Sonovault and one Nortek S500 ADCP. The upper 27 m of the mooring were equipped with several interconnected segments of a solid plastic pipe, to protect the comparably shallow mooring against sea ice keels and icebergs. Mooring CAO2-01 was equipped with 3 SBE37 Microcats, 2 Aanderaa RCM11 current meters, one RDI 300kHz Workhorse ADCP, one ASL Acoustic Zooplankton Fish Recorder (AZFP), one AURAL Acoustic Recorder, 2 Sediment Traps, one BoP trap, and 2 Remote Access Samplers (RAS) including sets of SBE37 Microcats, Satlantics SUNA nitrate sensors, Sunburst SAMI pH and CO2 sensors, and additional Wetlabs ECO PAR & ECO Triplet sensors on the upper RAS. The RAS were programmed to collect seawater samples at weekly intervals for the measurement of dissolved nutrients in seawater and SUNA calibration (D. Scholz and S. Torres-Valdés), and for genetic analyses (K. Metfies, M. Wietz, C. Bienhold). The mooring diagrams are shown in Figs 4.7 and 4.8 at the end of this subsection.

Tab. 4.7: Overview of the two moorings recovered

Mooring ID	Date	Time (UTC)	Rec. Latitude	Rec. Longitude	Water depth [m]	Device Operation	Deployment
CAO1-01	01.09.2024	7:05	84.91	129.29	4343	PS144_34-1	PS138_118-1
CAO2-01	02.09.2024	6:40	84.89	129.64	3762	PS144_38-1	PS138_119-1

Both recoveries were challenging due to heavy ice conditions. CAO1-01's ET861 Posidonia transponder at ~280 m was successfully pinged from the bridge upon arrival at the site on 01 September 2024 at 3:30 UTC. The presence of this mooring was already a big success, given that the only two other tube moorings had been lost in the past. No echo was received from both bottom releasers, which was however expected due to the density gradient present in the central Arctic in summer. The mooring was released multiple times between 6:40 and 7:40 UTC, when small holes of open water were present above the expected location, but neither the tube nor the 3 floatation packages could be found until 8:10 UTC, when after 1.5 hour of search, a part of the tube was discovered in a patch of nearby open water. When the ship was getting ready to pick up the tube, it was dragged below a giant ice floe by the strong currents. Also, no additional floatation package had showed up yet, which raised the suspicion that the floats could have been damaged. What followed was a 7-hour long dramatic hunt for the tube that would subsequently sometimes show up in downstream leads, only to disappear again under an ice floe before it could be reached. Keeping track of its approximate location and course was only possible due to the transponder, which continuously provided realistic heading and distance. Without this transponder, the entire mooring would have been lost immediately. Eventually, after unsuccessfully trying to use the Zodiac for recovery, the tube got stuck on a ridge close to a floe edge, which gave us enough time to prepare the mummy chair and to attach a rope to the top segment at 14:50 UTC (Fig. 4.4a). The 27-meter long tube was picked up in one piece over the side with the help of the aft crane (Fig. 4.4b), and the rest of the mooring could be safely recovered using the standard procedure until the station ended at 19:10 UTC. The bottom floatation package was completely destroyed/gone, as initially suspected. The instruments generally performed well, with the exception of just one SBE56 (see Tab. 4.8).

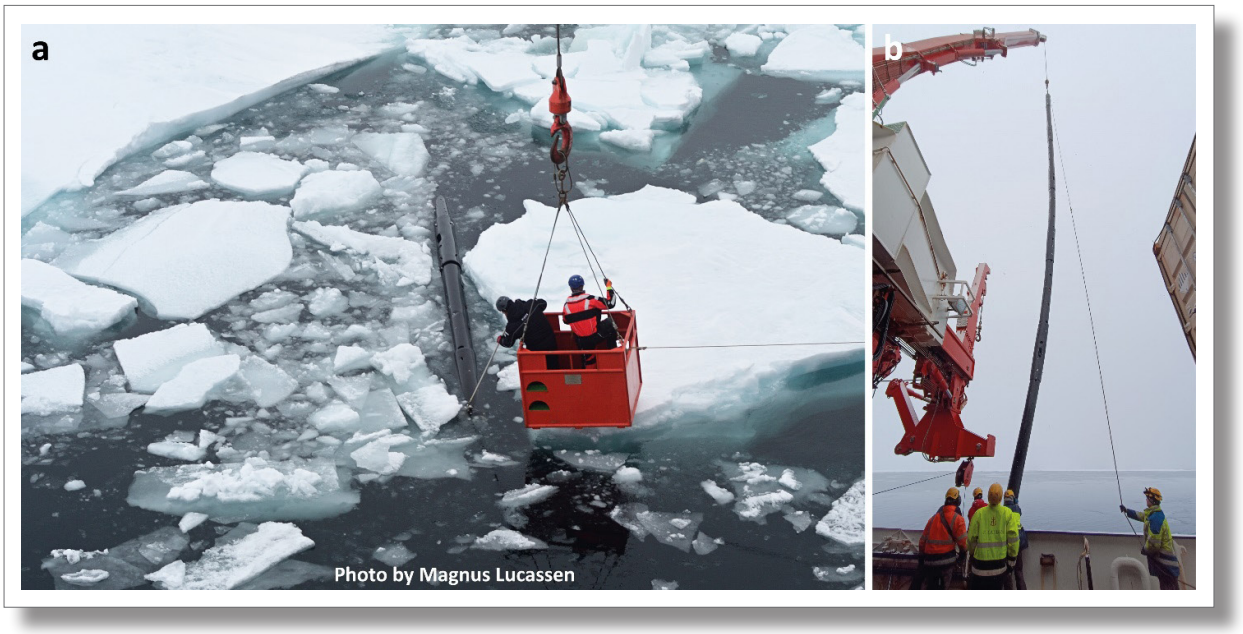

Fig. 4.4: CAO1-01 tube mooring recovery. a) Attaching a recovery rope to the top segment of the tube using the mummy chair. b) The aft crane is lifting the entire 27-meter tube over the side of the ship. Photo credit: a) Magnus Lucassen; b) Mario Hoppmann

Tab. 4.8: Overview of recovered mooring instruments and performance

Mooring	Instrument	Serial number	Nominal depth	Prelim. data check
CAO1-01	Nortek S500 ADCP	103942	6 m	tbd
CAO1-01	SeaBird SBE37-ODO	13488	7 m	ok
CAO1-01	SeaBird SBE37-ODO	13489	14 m	ok
CAO1-01	SeaBird SBE56	6257	19 m	ok
CAO1-01	SeaBird SBE37-ODO	13491	24 m	ok
CAO1-01	SeaBird SBE37-ODO	13005	29 m	ok
CAO1-01	SeaBird SBE37	2388	34 m	ok
CAO1-01	SeaBird SBE37	2389	45 m	ok
CAO1-01	SeaBird SBE37	1603	50 m	ok
CAO1-01	SeaBird SBE56	6358	55 m	ok
CAO1-01	SeaBird SBE37	11422	60 m	ok
CAO1-01	SeaBird SBE56	6359	65 m	no data
CAO1-01	SeaBird SBE37	2091	85 m	ok
CAO1-01	SeaBird SBE56	6360	135 m	ok
CAO1-01	SeaBird SBE56	6361	185 m	ok
CAO1-01	SeaBird SBE56	6335	242 m	ok
CAO1-01	Develogic Sonovault	1091	265 m	tbd
CAO1-01	RDI LRADCP	5373	290 m	ok
CAO1-01	SeaBird SBE56	6362	390 m	ok
CAO2-01	McLane RAS	13464	25 m	only 50 ml volume per bottle
CAO2-01	SeaBird SBE37-ODO	20522	25 m	ok

Mooring	Instrument	Serial number	Nominal depth	Prelim. data check
CAO2-01	Wetlabs EcoPAR	7874	25 m	ok
CAO2-01	Wetlabs EcoTriplet	6483	25 m	ok
CAO2-01	Satlantic SUNA	1155	25 m	ok
CAO2-01	Sunburst SAMI pCO2	144	25 m	tbd
CAO2-01	Sunburst SAMI PH	193	25 m	no data due to power issues
CAO2-01	RDI 300kHz WH ADCP	15085	45 m	ok
CAO2-01	ASL AZFP	55113	142 m	tbd
CAO2-01	Sediment Trap	2021492	201 m	ok
CAO2-01	AADI RCM11	568	202 m	ok
CAO2-01	SeaBird SBE37	2817	203 m	ok
CAO2-01	MTE AURAL M2	319	226 m	tbd
CAO2-01	McLane RAS	15348	254 m	ok
CAO2-01	SeaBird SBE37-ODO	16389	254 m	ok
CAO2-01	Satlantic SUNA	1473	254 m	ok
CAO2-01	Sunburst SAMI pCO2	145	254 m	tbd
CAO2-01	Sunburst SAMI PH	175	254 m	tbd
CAO2-01	BOP Trap	2015428	857 m	several vials destroyed during recovery
CAO2-01	Sediment Trap	2021493	3782 m	ok
CAO2-01	AADI RCM11	619	3783 m	ok
CAO2-01	SeaBird SBE37	2097	3784 m	ok
CAO2-01	SeaBird SBE37	2087	4278 m	ok

The recovery of CAO2-01 was much easier in comparison, but not without problems. The mooring was released in a wide area of open water, and the steel float was found quickly. The recovery procedure went smoothly, until the rope was found severely entangled at roughly 500 m. The samples of the Bio-Optical trap suffered some damage, and 12 vials were destroyed (Fig. 4.5 a,b). The sediment traps needed to be taken upside-down (Fig. 4.5c) which usually does not affect the samples. The instruments generally performed well, with some exceptions. One pH sensor failed upon deployment due to power issues. The lower RAS (250 m depth) only pumped 50 ml instead of 500 ml per sample, for yet-to-be-determined reasons. All other sensors worked as expected, pending a more comprehensive data analysis.

Fig. 4.5: Photos of CAO2-01 mooring recovery. a) Bio-Optical trap; b) close-up of damaged samples due to entanglement; c) sediment trap recovered upside-down. Photo credits: Mario Hoppmann

Mooring deployment

Tube mooring CAO1-02 was deployed on 03 September 2024 as a follow-up of the recently recovered CAO1-01 (Fig. 4.7, Tab. 4.9). Due to the uncertainty of future recovery logistics, the number and types of sensors were significantly reduced (Fig. 4.9, Tab. 4.10). CAO2 was not redeployed at all for the same reason. SBE56 were configured to measure every 60 s. Regular SBE37 were configured to sample every 1 h, whereas SBE37-ODO were configured to 2 h.

The holes in the tube prepared to mount the SBE37 instruments had to be enlarged because the older models (with external pump) did not fit in. 4 + 40 m of rope were substituted by 5 + 20 m after manual plumbing, which also matched the lengths of the previous deployment. The deployment itself went well and no bigger challenges were encountered. The ET861 transponder was successfully pinged before leaving the site.

Tab. 4.9: Overview of mooring deployments.

Mooring ID	Date	Time (UTC)	Depl. Latitude	Depl. Longitude	Water depth [m]	Device Operation
CAO1-02	03.09.2024	10:15	84.91	129.26	4349	PS144_43-1

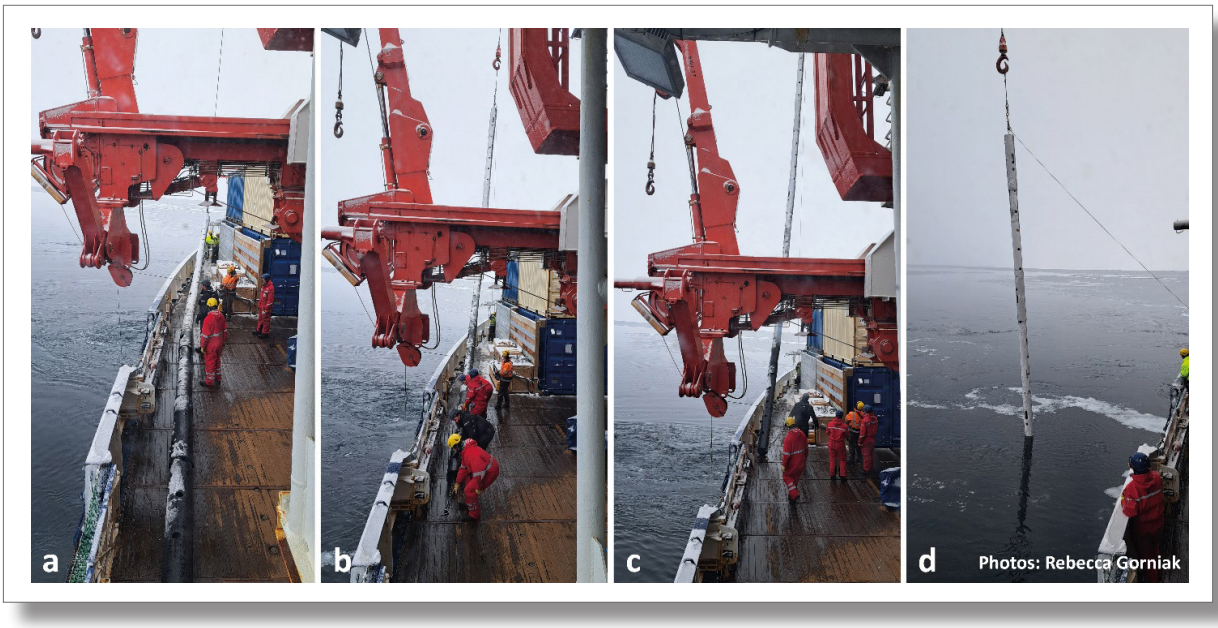

Fig. 4.6: Photo series of CAO1-02 tube mooring deployment. Photo credits: Rebecca Gorniak

Tab. 4.10: Overview of deployed mooring instruments. Asterisks (*) denote sensors not recently calibrated by the manufacturer SeaBird.

Mooring	Instrument	Serial number	Nominal depth
CAO1-02	SeaBird SBE37-ODO	13987	7 m
CAO1-02	SeaBird SBE37-ODO	13902	14 m
CAO1-02	SeaBird SBE56	7082	19 m
CAO1-02	SeaBird SBE37*	437	24 m
CAO1-02	SeaBird SBE37*	1607	29 m
CAO1-02	SeaBird SBE37-ODO	13908	34 m
CAO1-02	SeaBird SBE37	1564	45 m
CAO1-02	SeaBird SBE37	2100	50 m
CAO1-02	SeaBird SBE56	7090	55 m
CAO1-02	SeaBird SBE37	2096	60 m
CAO1-02	SeaBird SBE56	8480	65 m
CAO1-02	SeaBird SBE56	6364	85 m
CAO1-02	SeaBird SBE37	10934	135 m
CAO1-02	SeaBird SBE56	8482	185 m
CAO1-02	SeaBird SBE56	10416	225 m
CAO1-02	SeaBird SBE56?	8481	?
CAO1-02	Develogic Sonovault	1091	290 m

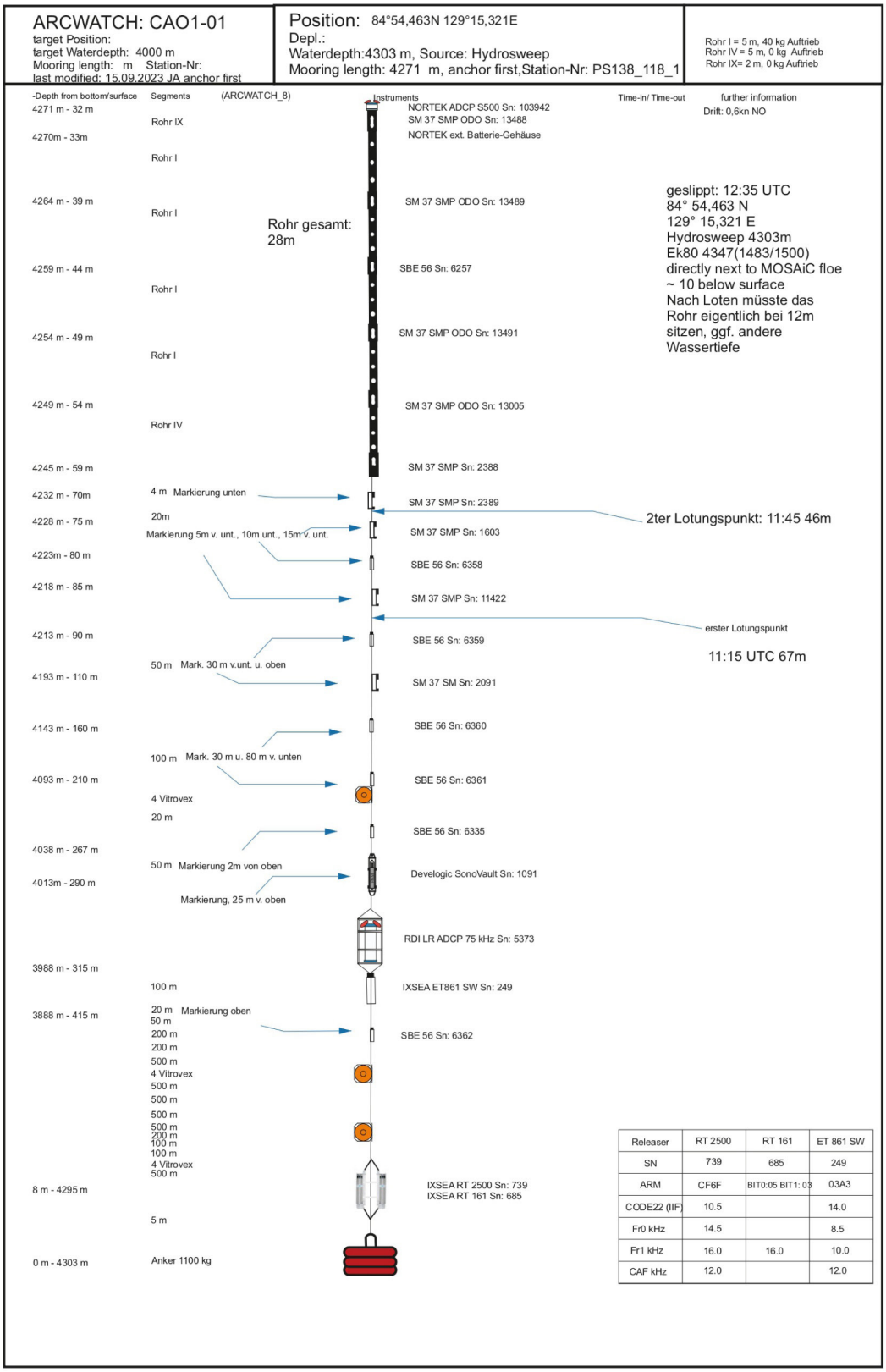

Fig. 4.7: Diagram of recovered mooring CAO1-01

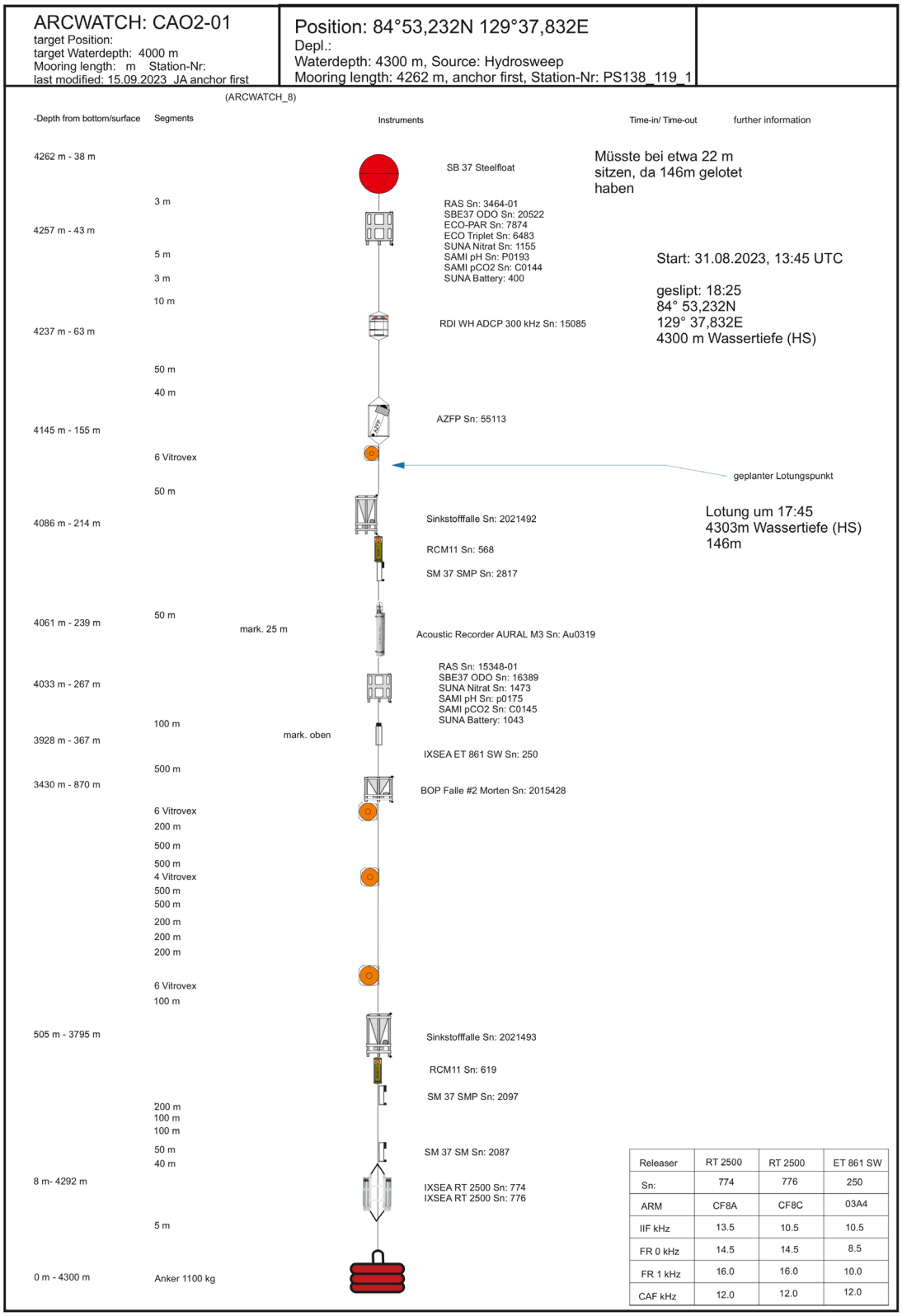

Fig. 4.8: Diagram of recovered mooring CAO2-01

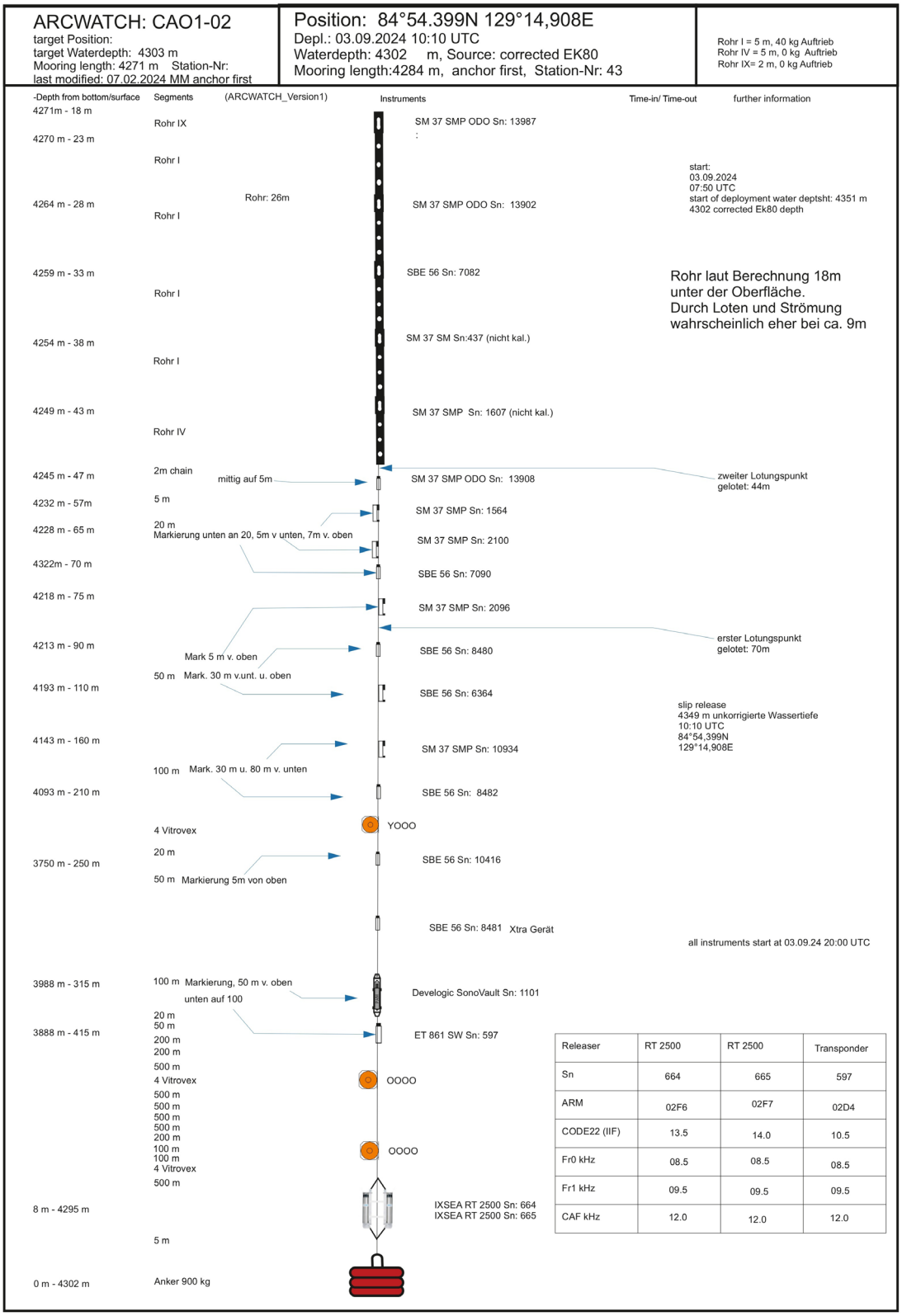

Fig. 4.9: Diagram of deployed mooring CAO1-02

Instrument calibration casts

Mooring and ice station instruments were calibrated *in-situ* using the ship-based CTD/Rosette system during 4 casts (Tabs. 4.2 and 4.11). The regular SBE37 microcats, SBE37-ODO and SBE56 temperature loggers were mounted on dedicated metal rods with a total space for up to 14 instruments (Fig. 4.10). The batches were separated into to-be-deployed instruments, recovered instruments, as well as into SBE56/SBE37 due to their different depth ratings. The sampling interval was set to 10 s for regular SBE37, 20 s for SBE37-ODO, and 10 s for SBE56. Stops of 5-10 minutes were done at 1-3 depths (Fig. 4.11) that exhibited minimal gradients. Salinity samples were taken at these depths as well. The respective bottles were closed at the end of each stop.

In the context of the calibration casts, a recurring problem with the SBE56 temperature loggers emerged. Despite being configured to sampling intervals of e.g. 10 s with a specific starting time in the future, some older instruments would always start with a default sampling interval of 60 s. After contacting the technical support, it was confirmed that instruments with serial numbers below 56-09381 and with firmware versions 0.96, 0.97, 1.0, and 1.01 were affected by this bug (see SeaBird Field Service Bulletin 35, June 2019). A new firmware version was provided and will be tested back in Bremerhaven.

Tab. 4.11: Overview of instrument calibration casts for the mooring deployment and recoveries, and ice station instruments. “CTD Cast” refers to the latter part of the corresponding event label, after “PS144_”.

CTD Cast	Date	Time (UTC)	CTD depth (m)	Instrument type	Instrument serial numbers
011_02	20.08.2024	05:15	4515	SBE37 (mooring deployments, ice station instruments)	0437, 1564, 1607, 2096, 2100, 10934, 13902, 13908, 13987, 23786
018_01	28.08.2024	06:34	1005	SBE56 (mooring deployments, ice station instruments)	6300, 6364, 6398, 6403, 7065, 7082, 7090, 7824, 7825, 8477, 8478, 8479, 8480, 8481, 8482, 10416, 11209, 11210
115_03	21.09.2024	10:20	995	SBE56 (mooring recoveries)	6257, 6335, 6358, 6359, 6360, 6361, 6362
123_04	23.09.2024	10:15	4350	SBE37 (mooring recoveries)	1603, 2087, 2091, 2097, 2388, 2389, 2817, 11422 13005, 13488, 13489, 13491, 16389, 29522

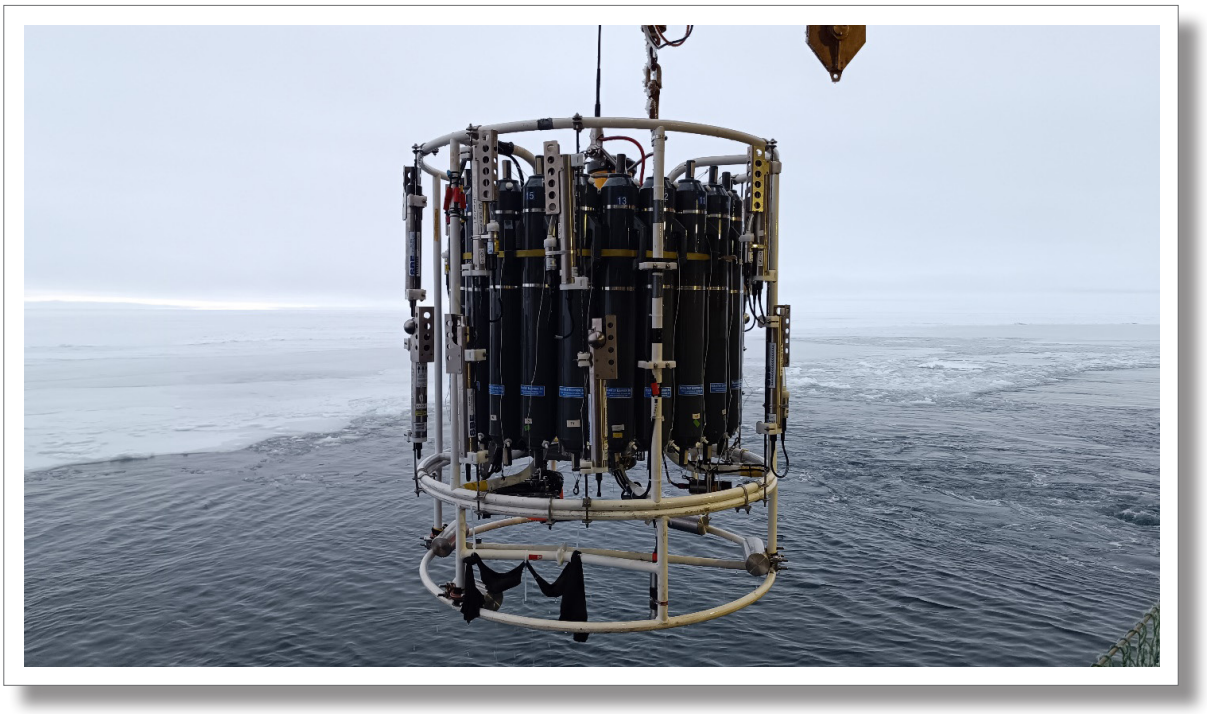

Fig. 4.10: Photo of the CTD/Rosette calibration cast PS144_123_04, showing 14 SBE37 microcats mounted onto dedicated steel rods on the outer frame. Photo credit: Mario Hoppmann.

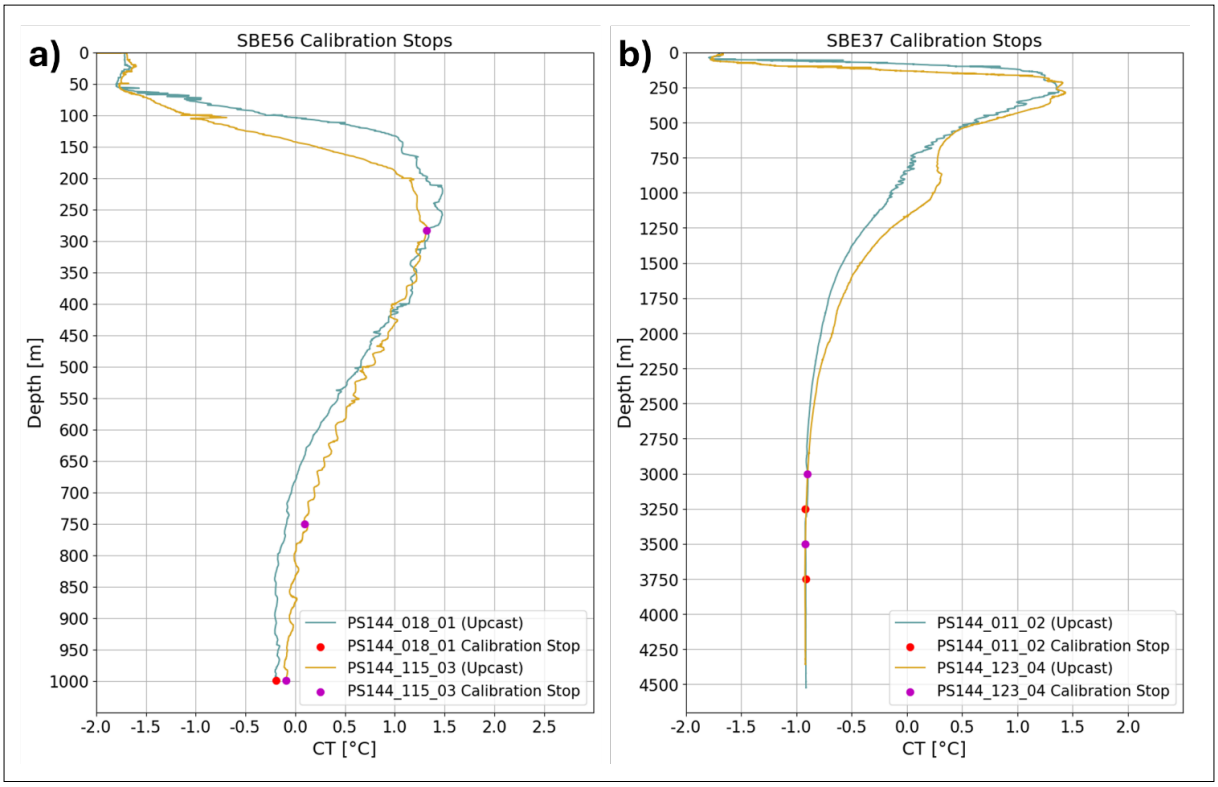

Fig. 4.11: CTD temperature profiles and calibration stops during the 4 CTD/Rosette calibration casts

Argo Float deployments

In collaboration with the German Federal Maritime and Hydrographic Agency (BSH) we deployed four ARGO floats in the Nansen Basin near Svalbard and in the eastern Amundsen Basin, north of the Laptev Sea, to further improve the use of this technology in the (partly) ice-covered Arctic Ocean (see Tab. 4.12). The floats were successfully started using a BSH standard procedure and thrown overboard from 3 m height in the aft of the ship (Fig. 4.12). All floats were equipped with an active ice avoidance algorithm. Although they were all deployed in regions of largely open water of at least 5.5 km diameter, 24DE007 and 24DE008 did not report their first profile in the weeks after the deployment. Post-deployment inspection of the initial starting messages was inconspicuous. We suspect they drifted under the sea ice already after their first dive. 24DE006 and 24DE009 did report back as expected the following day.

Fig. 4.12: Deployment of ArgoFloat 24DE007 on 21 August 2024. Photo credit: Mario Hoppmann.

Tab. 4.12: For further information please see the end of this chapter.

Autonomous ice-tethered buoys

Various autonomous ice-tethered buoys were deployed as part of our work program. Details are given in Chapter *8*.

Repeated under-ice profiling for Microstructure Turbulence (MSS)

During most ice stations, a microstructure profiler (type MSS90L, Sea&Sun Technologies, Germany) was deployed through holes in the ice to measure temperature, salinity, oxygen, Chl-a fluorescence as well as shear, to study turbulent exchange processes. We used two

microstructure profilers (SN 075 and 097), which were equipped with an identical sensor setup (see Tab. 4.13): two airfoil probes aligned parallel to each other (shear probes type PNS6) a fast-tip thermistor (FP07, with a small sensor guard), an acceleration sensor (for body vibration measurements), conventional CTD sensors (SST) for precision measurements, a Turner Design Cyclops-7 in Vivo Chlorophyll/Blue sensor for Chl-a fluorescence, and a fast optical dissolved oxygen sensor (SST). All channels sampled at 512 Hz. All sensors were checked and, if necessary, re-calibrated by SST shorty before the expedition. An additional set of shear sensors was calibrated at IOW before as well.

Tab. 4.13: Overview of shear sensors mounted on the MSS profilers 075 and 097.

MSS SN	Sensor	Sensor SN	Time of operation	Comment
075	Shear 1	6184	Before 22.09.2024	
	Shear 2	6185	Whole expedition	
	Shear 1	6104	From 22.09.2024	Solved higher values >250m of sensor 6184
097	Shear 1	6183	Whole expedition	
	Shear 2	6180	Whole expedition	

A typical MSS deployment was done using a mobile setup mounted to a Nansen sledge, and through a hole opened by joining 4 – 5 augered holes, usually located approximately 150 – 300 m away from the ship. A pop-up tent was erected over the hole as a shelter (Fig. 4.13). The profiling was carried out with the probe in free-fall by laying out slack cable (“loops”) before being winched back to the surface by a SWM400 electrical winch system. The setup on the ice was powered by a Honda EU22 generator. The protective cage around the MSS sensor array was removed for most of the profiles to reduce noise and, thus, facilitate higher sensitivity to low-level turbulence. The cage was only present during casts 1 to 5 of the first ice station (ICE1). We also note that the sensor guard of the FP07 likely limited the size of the eddies resolved by this sensor. The instrument was ballasted for a typical fall speed of ~ 0.5 m s^{-1}. All sensors pointed downward during profiling. Data were transmitted in real-time to a field laptop on the ice. We collected profiles down to ~400 m, depending on the ice drift that caused the probe to displace laterally relative to the ice hole. The MSS profiler was left in the water between casts. Different series of consecutive profiles were carried out during longer ice stations. Instrument data was pre-processed using the MSP toolbox (Schulz, 2022), and the performance of the sensors was constantly evaluated after each station using for example the shear. See Tab. 4.14 for an overview of all casts during PS144.

During the last ice station, a newly acquired self-recording module (SST) was tested in conjunction with the second profiler, MSS097. We were originally planning to use this more mobile setup much earlier during the expedition, but a number of technical challenges with the module’s charging circuit made it necessary to postpone its use. After successful removal of the latter, and rewiring the controller, 2 profiles were obtained during the last ice station, ICE10, using the now self-recording MSS097. The measurements were generally successful, although the data of individual sensors need to be double-checked.

Fig. 4.13: Setup for repeated microstructure profiling a) Outside view of exemplary MSS site; b) view of MSS on winch setup in the tent
Photo credits: a) Mario Hoppmann; b) Céline Heuzé

Tab. 4.14: Overview of MSS measurements during ice stations. All profiles were run with the protective cage detached from the profiler, unless noted otherwise. Start / end times and geographic positions of each time series of profiles are given for each day and station.

Event Label	MSS SN	Date	Time	Long. [°E]	Lat. [°N]	Number of Profiles	Comment
PS144_7_MSS_1	75	16.08.2024	14:57	42.9897	85.0603	9	1-5 with cage
			19:03	42.8429	85.0541		
PS144_23_MSS_1	75	29.08.2024	16:19	115.2578	84.4895	16	
			22:52	115.8123	84.4899		
PS144_23_MSS_2	75	30.08.2024	8:50	115.6081	84.4231	2	
			9:23	115.651	84.422		
PS144_50_MSS_1	75	05.09.2024	12:21	140.1361	85.025	10	
			16:45	140.0861	85.0258		
PS144_67_MSS_1	75	08.09.2024	17:09	162.1845	84.9396	8	
			19:51	162.2059	84.9333		
PS144_85_MSS_1	75	12.09.2024	21:14	179.0365	87.5131	10	
			01:37 +1	178.9297	87.5132		
PS144_85_MSS_2	75	13.09.2024	8:29	178.7515	87.5029	21	
			16:40	178.2083	87.4816		
PS144_109_MSS_1	75	18.09.2024	23:49	-153.4956	89.9461	8	
			03:23 +1	-150.6759	89.9502		
PS144_109_MSS_2	75	19.09.2024	12:45	-140.4209	89.9577	5	
			14:33	-137.2716	89.9611		

Event Label	MSS SN	Date	Time	Long. [°E]	Lat. [°N]	Number of Profiles	Comment
PS144_134_MSS_1	75	25.09.2024	6:35	58.5047	86.9882	4	Sensor SH1 changed
			8:01	58.4245	86.9933		
PS144_134_MSS_2	75	25.09.2024	23:59	57.498	87.0378	13	
			05:03 +1	57.1448	87.0446		
PS144_134_MSS_3	75	26.09.2024	18:06	56.0798	87.0364	3	
			19:13	55.9763	87.0362		
PS144_134_MSS_4	97	26.09.2024	19:45	55.9763	87.0362	2	Auto-MSS without GPS
			20:01	55.8589	87.0353		

Under-ice continuous observations

Using a high-resolving ADCP (Nortek Signature 1000 SN 104403) we aimed to obtain direct observations of turbulent fluxes in the ice-ocean boundary layer (IOBL) at most ice stations (Fig. 4.14). The instrument was configured to take average current measurements in the upper 18 m with a bin size of 0.5 m every 2 minutes, using an average interval of 60 s. In addition, the instrument ran in continuous Burst mode with a sampling rate of 4 Hz. In addition, the High Resolution (HR) firmware was active and configured to 2.5 m with a cell size of 0.05 m.

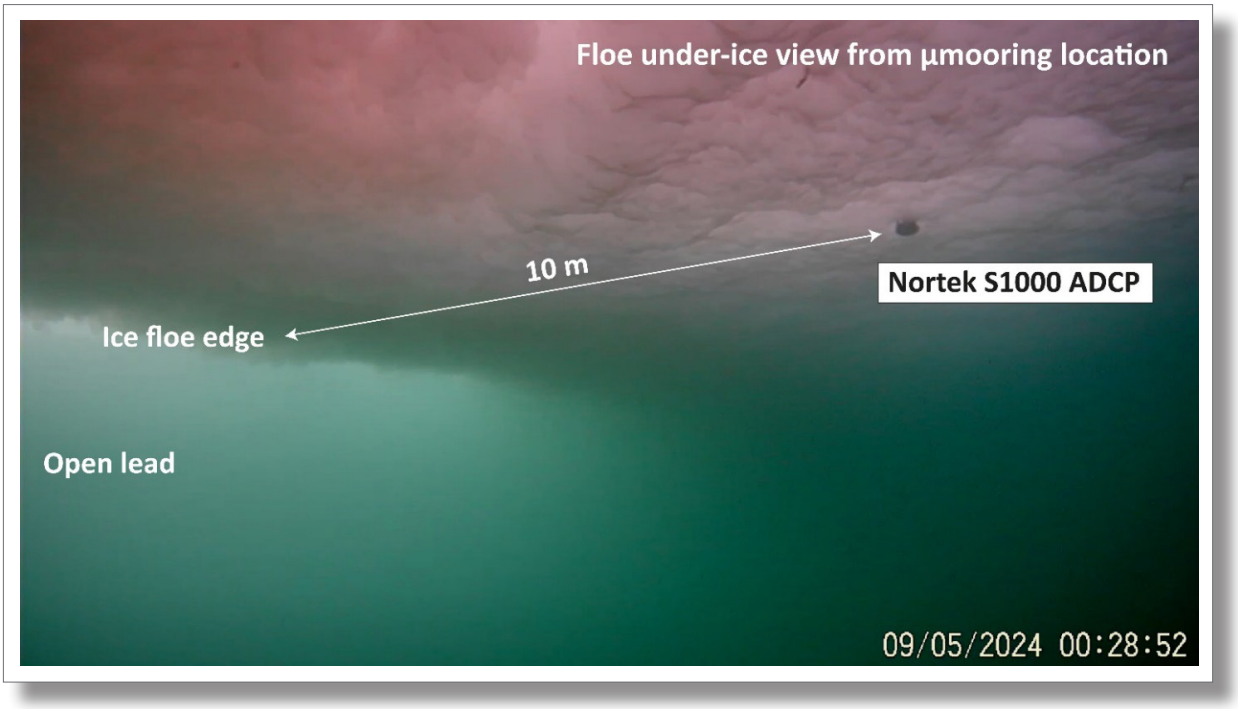

Fig. 4.14: Under-ice view of the Nortek S1000 ADCP from the perspective of the micro-mooring ice hole during ice station ICE4 on 05 September 2024. The brighter area to the left is the lead next to the floe edge. Photo credit: Mario Hoppmann

Alongside the MSS casts, an RDI WH-300 kHz ADCP (SN 9271) was suspended through a separate hole in the ice, typically 10 to 20 m away from the microstructure profiling hole (Fig. 4.15), sampling continuously at 1-s intervals, and with a 2-m vertical bin size. The output was set to give velocity in instrument coordinates with additional compass heading. The data will later be averaged to larger time intervals after analysing compass performance during our expedition close to the magnetic north pole. This ADCP was deployed at most ice stations.

Fig. 4.15: Setup of the RDI 300kHz ADCP to complement the MSS measurements. Photo credit: Mario Hoppmann

In addition to the standard instrumentation described above, we deployed a “mini mooring” consisting of up to 10 SBE37 microcats and SBE56 temperature loggers either close to the floe edge (ICE2, ICE4), or at the MSS site (ICE1). We opportunistically deployed a 600kHz ADCP close to a lead during ice station ICE2. Finally, we deployed a “micro-mooring” consisting of 2 RBRduo 16Hz wave recorders (Sns 208478 and 208479) at 0 and 2 below the ice base, and one 16Hz RBRconcerto CTD (SN 210909) at 1 m below the ice base, at the floe edge (ICE4) or at the MSS site (ICE10). See Tab. 4.15 for an overview of all instruments that provided under-ice continuous observations during ice stations.

A number of GPS stations deployed by the Sea Ice Physics team recorded the floe movement during ice stations continuously. These data will subsequently be used to obtain floe translation and rotation to obtain geographically referenced velocity from and / or check the performance of the compass of the under-ice ADCP.

Tab. 4.15: Overview of under-ice measurements during ice stations. No instruments were deployed during ICE3, 6 and 9.

Ice station	Instrument	Event label	Date	Time (UTC)	Site	Latitude [°]	Longitude [°]
ICE1	RDI WH300kHz ADCP SN 9271	PS144_7_RDI300	16.08.2024	14:20:00	MSS	85.060	42.990
			16.08.2024	19:24:00	MSS	85.054	42.843
	Nortek S1000 ADCP SN 104403	PS144_7_ Nortek1000	16.08.2024	15:34	MSS	85.060	42.990
			16.08.2024	19:00	MSS	85.054	42.843
	SeaBird SBE37 + SBE56 mini mooring*	PS144_7_ miniMooring	16.08.2024	15:34	MSS	85.060	42.990
			16.08.2024	19:00	MSS	85.054	42.843
ICE2	RDI WH300kHz ADCP SN 9271	PS144_23_ RDI300	29.08.2024	15:21	MSS	84.423	115.608
			30.08.2024	9:59	MSS	84.422	115.651
	RDI WH600kHz ADCP SN 19316	PS144_23_ RDI600	29.08.2024	18:17	floe edge	84.423	115.608
			30.08.2024	9:18	floe edge	84.422	115.651
	Nortek S1000 ADCP SN 104403	PS144_23_ Nortek1000	29.08.2024	17:10	floe edge	84.423	115.608
			30.08.2024	9:15	floe edge	84.422	115.651
	SeaBird SBE37 + SBE56 mini mooring	PS144_23_ miniMooring	29.08.2024	18:17	floe edge	84.423	115.608
			30.08.2024	9:18	floe edge	84.422	115.651

Ice station	Instrument	Event label	Date	Time (UTC)	Site	Latitude [°]	Longitude [°]
ICE4	RDI WH300kHz ADCP SN 9271	PS144_50_ RDI300	05.09.2024	11:16	MSS	85.025	140.136
			05.09.2024	17:33	MSS	85.026	140.086
	Nortek S1000 ADCP SN 104403	PS144_50_ Nortek1000	05.09.2024	1:43	floe edge	85.025	140.136
			05.09.2024	18:53	floe edge	85.026	140.086
	SeaBird SBE37 + SBE56 mini mooring	PS144_50_ miniMooring	05.09.2024	2:00	floe edge	85.025	140.136
			05.09.2024	18:30	floe edge	85.026	140.086
	RBRduo + RBRconcerto micro mooring	PS144_50_ µMooring	05.09.2024	2:00	floe edge	85.025	140.136
			05.09.2024	18:30	floe edge	85.026	140.086
ICE5	RDI WH300kHz ADCP SN 9271	PS144_67_ RDI300	08.09.2024	11:02	MSS	84.940	162.185
			08.09.2024	20:01	MSS	84.950	162.206
	Nortek S1000 ADCP SN 104403	PS144_67_ Nortek1000	08.09.2024	14:56	MSS	84.940	162.185
			08.09.2024	19:57	MSS	84.950	162.206
ICE7	RDI WH300kHz ADCP SN 9271	PS144_85_ RDI300	12.09.2024	20:43	MSS	87.513	179.037
			13.09.2024	17:09	MSS	87.208	178.930
ICE8	RDI WH300kHz ADCP SN 9271	PS144_109_ RDI300	18.09.2024	22:30	MSS	89.946	-153.496
			19.09.2024	20:05	MSS	89.961	-137.272
	Nortek S1000 ADCP SN 104403	PS144_109_ Nortek1000	18.09.2024	22:35	MSS	89.946	-153.496
			19.09.2024	20:03	MSS	89.961	-137.272

Ice station	Instrument	Event label	Date	Time (UTC)	Site	Latitude [°]	Longitude [°]
ICE10	RDI WH300kHz ADCP SN 9271	PS144_134_ RDI300	25.09.2024	6:13	MSS	86.988	58.505
			26.09.2024	20:11	MSS	87.035	55.859
	Nortek S1000 ADCP SN 104403	PS144_134_ Nortek1000	25.09.2024	6:04	MSS	86.988	58.505
			26.09.2024	20:13	MSS	87.035	55.859
	RBRduo + RBRconcerto micro mooring	PS144_134_ µMooring	25.09.2024	6:00	MSS	86.988	58.505
			26.09.2024	20:13	MSS	87.035	55.859

Other plans that were not realised

One of the focii of our ice work had originally been to investigate the spatio-temporal variability of the thin melt water layer beneath the sea ice. However, we did not get the opportunity to test a number of new methods and measurement protocols that we originally planned to conduct, for different reasons. For example, we neither used our small boat to obtain CTD and MSS profiles in open leads, nor did we deploy a floating ADCP in a lead, due to environmental conditions (fog, freezing), personnel challenges, and lack of time. It is worth pointing out that all ice stations had a simultaneous heavy ship-based component (the so-called “super stations”) that forced us to split our team. This was particularly demanding during transect III as the team members were not fully trained yet and all ice stations featured the deployment of large buoys (see Chapter 8).

On a few occasions, shallow stratification close to the ice base was observed by a custom-made, hand-held uprising CTD system, consisting of a stand-alone CTD (RBR SN 235669; inductive conductivity) attached to a rope with a length of 15 meters. This instrument had however some initial problems with the calibration due to a manufacturer mistake. By the time this issue was fixed, the meltwater layer had gone and no more profiles were taken.

Preliminary results

Suspected plume by Gakkel Ridge

On 20 August 2024, we performed two casts over the Gakkel Ridge. The first cast 011_01, using the clean CTD, had a clear anomaly in all properties recorded from approximately 2900 dbar to 3600 dbar (shown on Fig. 4.16 for the temperature). Given the proximity to Gakkel Ridge, hydrothermal activity was suspected. The ship was drifting a lot on that day, so when the regular CTD reached the same depth about 3h later, there was only a small anomaly centred on 3200 dbar (Fig. 4.16, brown). The ship kept on drifting though, so the anomaly was clearly visible again during the upcast, albeit less strong than during the clean cast and over a narrower pressure range (Fig. 4.16, cyan). Preliminary analysis of the ship's trajectory was inconclusive regarding the possible location of the source of the plume (not shown). Many tracers were collected in the depth range of this suspected plume, both from the clean and regular CTDs; further analyses combining the hydrography with these tracers are needed.

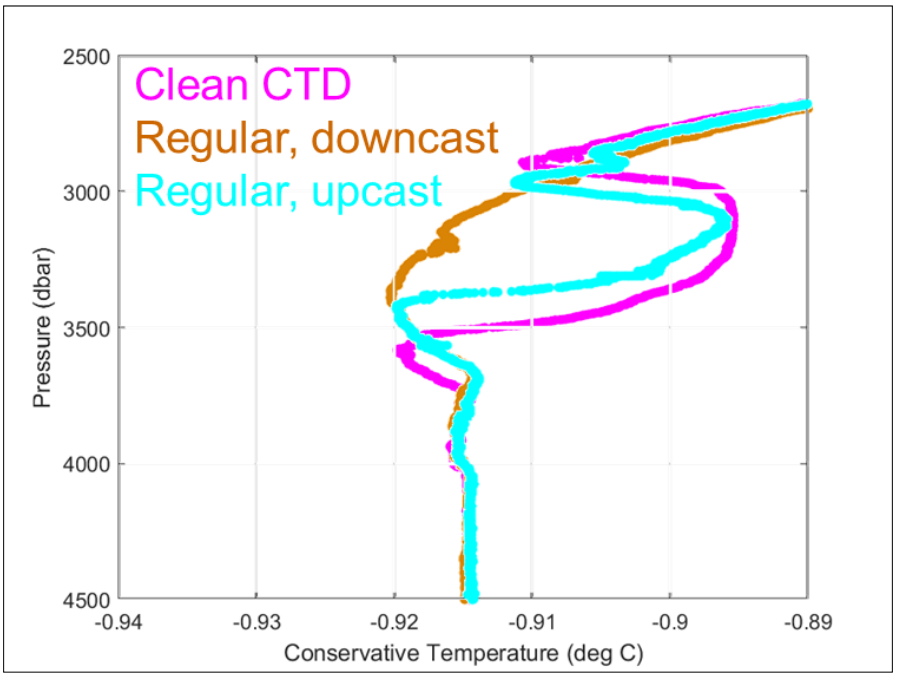

Fig. 4.16: Profile of Conservative Temperature with pressure from 2500 dbar down for casts 011_01 (clean CTD, magenta) and 011_02 (regular CTD: orange is the downcast, cyan the upcast). Values are preliminary.

A first look at Transect III

Transect III went across the Amundsen basin, on top of Lomonosov Ridge, and across the Makarov Basin until the Alpha-Mendeleev Ridge. A comparison of the CTD profiles on either side of the Lomonosov Ridge reveals both expected and intriguing findings:

- The mixed layer was warmer and fresher in the Amerasian basin (Fig. 4.17a,b). This could indicate that we were in Transpolar Drift, maybe reached the Beaufort Gyre even, but the different steepness of the "knee" in the T-S diagram suggests that the difference could just be sea ice melt-induced.

- The Atlantic Water layer sat higher in the water column in the Eurasian basin, where its core was warmer by more than 0.3 deg C. In both basins, the layer's lower limit was at approximately 800 m depth.
- We detected a cold anomaly centered around 900 m depth in the Eurasian basin. The anomaly became most pronounced as we approached Lomonosov Ridge. Its oxygen concentration was high compared to the waters both above and below it, and it increased as the temperature anomaly increased as well, suggesting a young water. There was no consensus onboard regarding what this anomaly could be; further analyses, using the water samples collected by the various teams, are required.
- As expected, the deep waters were warmer by approximately 0.5 deg C (and saltier) in the Amerasian basin.

Note that the values on the profiles and T-S diagrams are preliminary; they all require post-cruise calibration of the salinity and oxygen sensors.

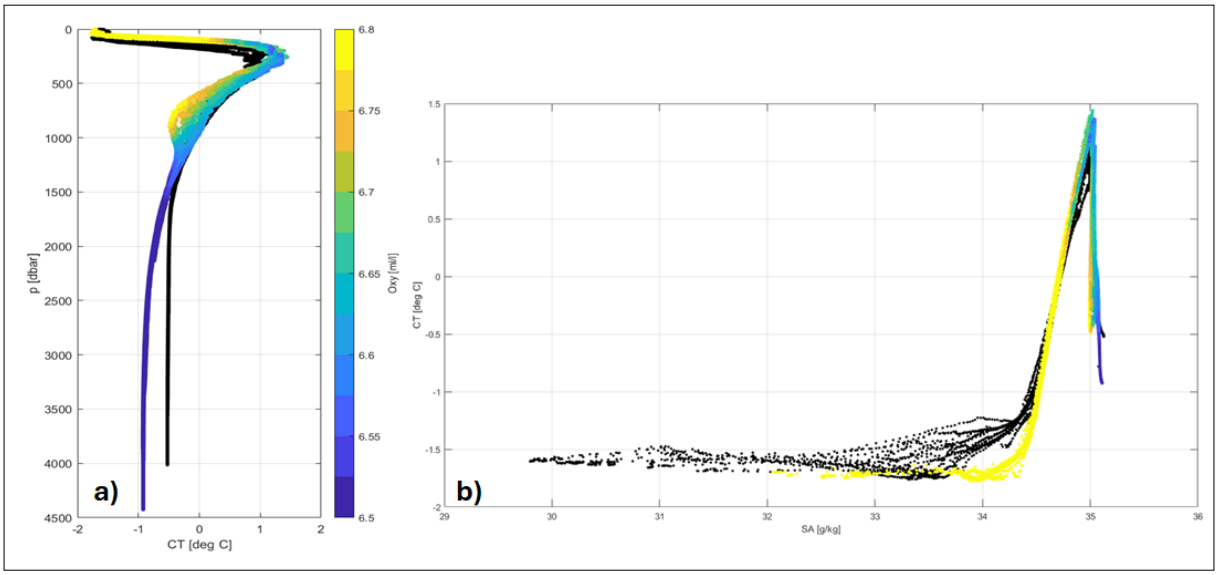

Fig. 4.17: a) Profile of Conservative Temperature with pressure and b) T-S diagram of all the casts of Transect III. On the Eurasian side, dots are coloured by the dissolved oxygen concentration, in ml/l; on the Amerasian side, dots are black.

A proof of concept for the first tube mooring in the Arctic

Preliminary assessment of the top instruments in the tube revealed that its top segment was as shallow as 8 m depth on average, which is even better than the already optimistic 12 m we were initially aiming for during deployment (Fig. 4.18, top). Tube motion and downdrag were generally most pronounced between August and October, and during several short events in between, as confirmed by Fig. 4.18, which shows preliminary instrument orientation data of the Nortek S500 ADCP mounted in the top of the tube, and by Fig. 4.19, which shows higher ocean current velocity during the same periods. Overall, CAO1-01 was the first proof that the concept of a tube mooring works in heavily ice-covered waters such as the central Arctic. One immediate implication of the successful recovery was the subsequent re-deployment of a similar tube-mooring (CAO1-02) as a follow-up mooring at the same location, a decision that depended on the success of CAO1-01.

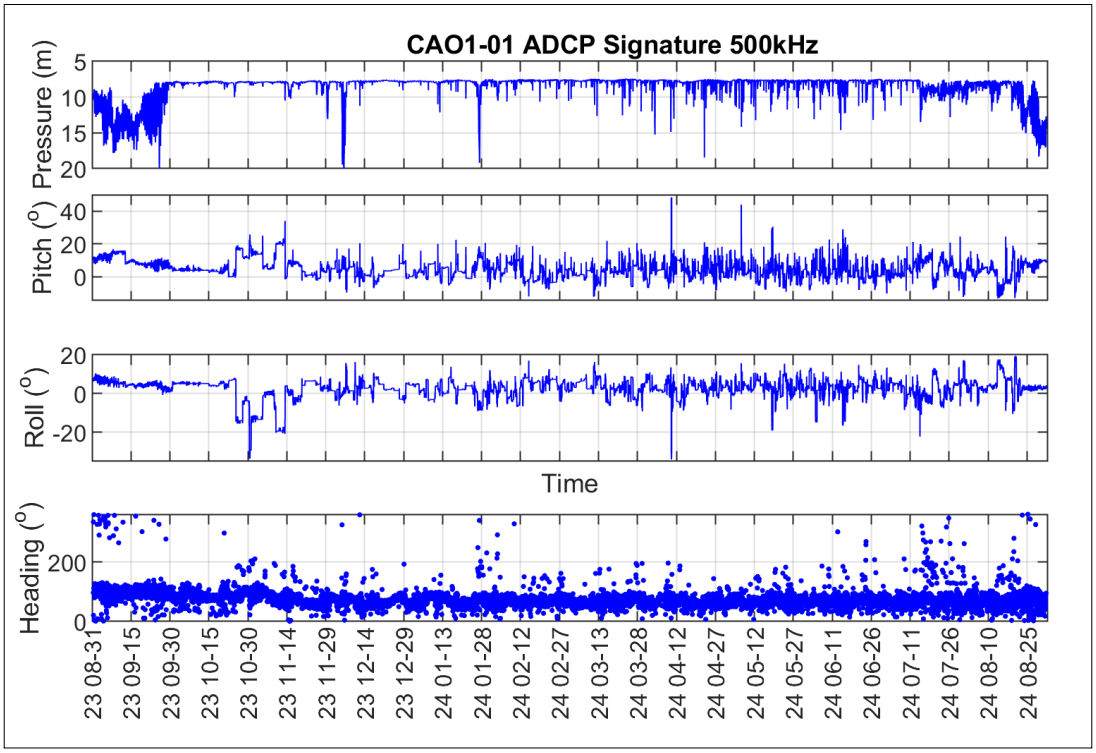

Fig. 4.18: Preliminary plot of Nortek S500 ADCP pressure, pitch, roll and heading data. The sensor was mounted upward-looking in the top of CAO1-01's tube using a gimbal suspension system, and was located at a nominal water depth of ~8 m.

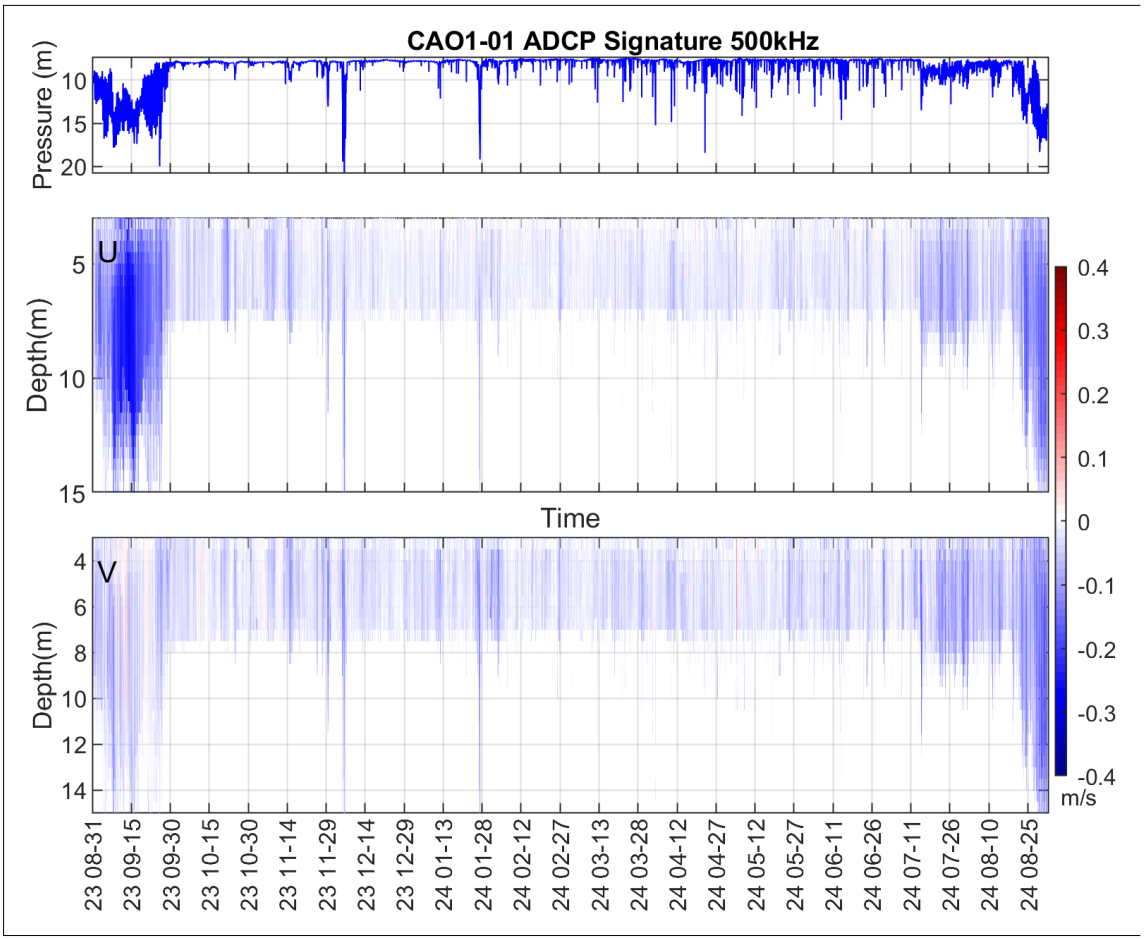

Fig. 4.19: Preliminary plot of Nortek S500 ADCP instrument pressure, along with the meridional (u) and zonal (v) components of ocean current velocity

We do not present further preliminary results as further processing on land is needed for in-depth analysis.

A first look at the XCTD data of transect I:

Transect I extended along 30°E southward, from the Nansen basin to the Barents Sea slope. A total of 15 XCTDs were deployed over a distance of 145 km, with a spatial resolution of approximately 12 km. Fig. 4.20 shows the cross-sections of conservative temperature (CT, panel a) and absolute salinity (SA, panel b) within the upper 400 meters. Intrusions and interleaving structures are clearly visible between the distances of 60 – 120 km. The T-S diagram (panel c) further highlights how properties in the upper 80 meters drastically change as we traveled on the slope, into the Atlantic Water core: CT increases from freezing (approx. -1.7°C) to 3°C, and SA from 32.2 g/kg to 34.1 g/kg. Further post-processing on land is needed for a more in-depth analysis.

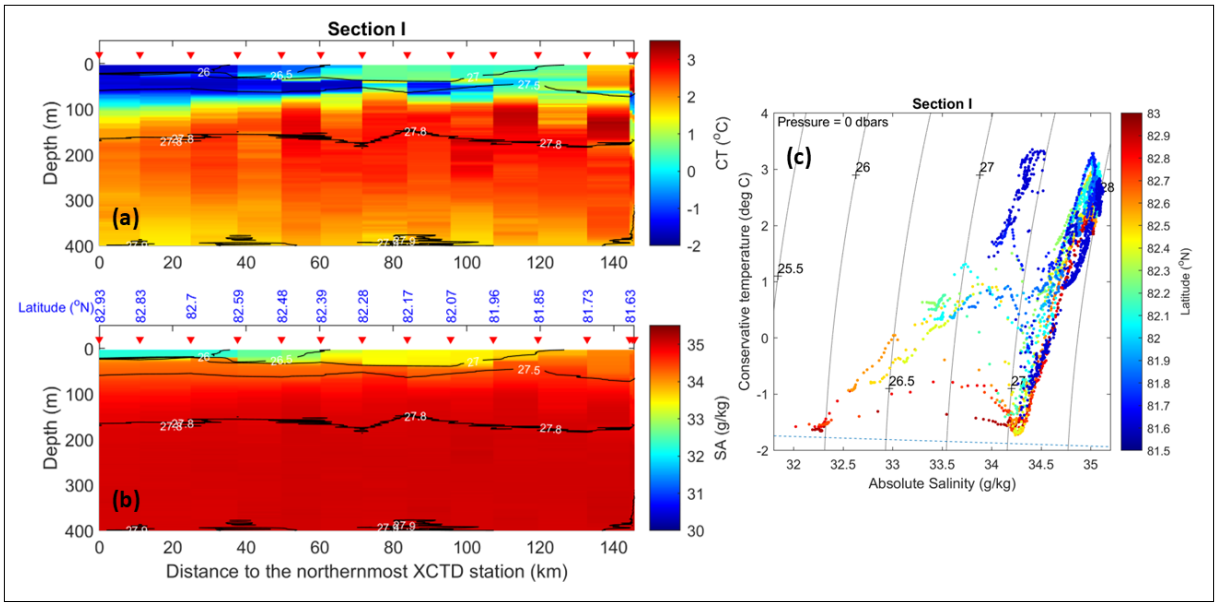

Fig. 4.20: The upper 400 metres of Conservative Temperature (a) and Absolute Salinity (b) of transect I; x-axis is the distance to the northernmost XCTD station (c) T-S diagram, where dots are coloured by the latitude.

Data management

Environmental data will be archived, published and disseminated according to the FAIR principles at the World Data Center PANGAEA, Data Publisher for Earth & Environmental Science (https://www.pangaea.de), within two years after the end of the expedition. By default, the CC-BY license will be applied.

The iridium buoy data have been stored on the server infrastructure of the respective manufacturer by default. These data have also been fed into the database of the International Arctic Buoy Programme IABP at https://iabp.apl.uw.edu/index.html, and have been made available in near-real time on www.meereisportal.de. Selected buoys have also been reporting their data directly to the WMO's Global Telecommunication System (GTS), thereby contributing to improved global numerical weather predictions. Buoy data will also be made available on PANGAEA within two years after a buoy ceased operation.

This part of the expedition is supported by the Helmholtz Research Programme "Changing Earth – Sustaining our Future" Topic 2, Subtopics 1, 3 and 4, and Topic 6, Subtopics 1, 2 and 3. Trace gas observations are supported by the DFG CRC 172 (AC)3 – Arctic Amplification.

In all publications based on this expedition, the **Grant No. AWI_ PS144_03** will be quoted and the following publication will be cited:

Alfred-Wegener-Institut Helmholtz-Zentrum für Polar- und Meeresforschung (2017) Polar Research and Supply Vessel POLARSTERN Operated by the Alfred-Wegener-Institute. Journal of large-scale research facilities, 3, A119. http://dx.doi.org/10.17815/jlsrf-3-163.

References

Behrendt A, Sumata H, Rabe B, Schauer U (2018) UDASH – Unified Database for Arctic and Subarctic Hydrography. Earth Syst Sci Data 10:1119–1138. https://doi.org/10.5194/essd-10-1119-2018

Bulsiewicz K, Rose H, Klatt O, Putzka A, Roether W (1998) A capillary-column chromatographic system for efficient chlorofluorocarbon measurement in ocean waters. J. Geophys. Res. Oceans 103(C8):15959–15970. https://doi.org/10.1029/98JC00140

Charette MA, Kipp LE, Jensen LT, et al (2020) The Transpolar Drift as a Source of Riverine and Shelf-Derived Trace Elements to the Central Arctic Ocean. JGR Oceans 125. https://doi.org/10.1029/2019JC015920

German CR, Reeves EP, Türke A, Diehl A, Albers E, Bach W, Purser A, Ramalho SP, Suman S, Mertens C, Walter M, Ramirez-Llodra E, Schlindwein V, Bünz S, Boetius A (2022) Volcanically hosted venting with indications of ultramafic influence at Aurora hydrothermal field on Gakkel Ridge. Nat Comm. 13:6517. https://doi.org/10.1038/s41467-022-34014-0

Granskog MA, Fer I, Rinke A, Steen H (2018) Atmosphere-Ice-Ocean-Ecosystem Processes in a Thinner Arctic Sea Ice Regime: The Norwegian Young Sea ICE (N-ICE2015) Expedition. J Geophys Res Oceans 123:1586–1594. https://doi.org/10.1002/2017JC013328

Heuzé C, Huhn O, Walter M, et al., (2023) A year of transient tracers (chlorofluorocarbon 12 and sulfur hexafluoride), noble gases (helium and neon), and tritium in the Arctic Ocean from the MOSAiC expedition (2019-2020). Earth Syst. Sci. Data 15:5517–5534. https://doi.org/10.5194/essd-15-5517-2023

Huhn OM, Rhein M, Hoppema M, van Heuven S (2013) Decline of deep and bottom water ventilation and slowing down of anthropogenic carbon storage in the Weddell Sea, 1984-2011. Deep-Sea Res. I 76:66–84. https://doi.org/10.1016/j.dsr.2013.01.005

Huhn O, Hattermann T, Davis PED, Dunker E, Hellmer HH, Nicholls KW, Østerhus S, Rhein M, Schröder M, Sültenfuß J (2018) Basal melt and freezing rates from first noble gas samples beneath an ice shelf. Geophys. Res. Lett. 45. https://doi.org/doi:10.1029/2018GL079706

Jenkins WJ (2020) Using excess ^{3}He to estimate Southern Ocean upwelling time scales. Geophys. Res. Lett. 47:e2020GL087266. https://doi.org/10.1029/2020GL087266

Nicolaus M, Perovich DK, Spreen G, et al (2022) Overview of the MOSAiC expedition: Snow and sea ice. Elementa: Science of the Anthropocene 10:000046. https://doi.org/10.1525/elementa.2021.000046

Rabe B, Heuzé C, Regnery J, et al (2022) Overview of the MOSAiC expedition: Physical oceanography. Elementa: Science of the Anthropocene 10. https://doi.org/10.1525/elementa.2021.00062

Rabe B, Karcher M, Kauker F, et al (2014) Arctic Ocean basin liquid freshwater storage trend 1992-2012. Geophys Res Lett 41:961–968. https://doi.org/10.1002/2013GL058121

Rhein M, Steinfeldt R, Huhn O, Sültenfuß J, Breckenfelder T (2018) Greenland submarine melt water observed in the Labrador and Irminger Sea. Greenland submarine melt water observed in the Labrador and Irminger Sea. Geophys. Res. Lett 45:10,570-10,578. https://doi.org/10.1029/2018GL079110

Rudels B (2021) The Physical Oceanography of the Arctic Mediterranean Sea. Elsevier. https://doi.org/10.1016/C2018-0-01360-2

Schulz K, Mohrholz V, Fer I et al. (2022) A full year of turbulence measurements from a drift campaign in the Arctic Ocean 2019–2020. Sci Data 9:472. https://doi.org/10.1038/s41597-022-01574-1

Shupe MD, Rex M, Blomquist B, et al (2022) Overview of the MOSAiC expedition: Atmosphere. Elementa: Science of the Anthropocene 10:00060. https://doi.org/10.1525/elementa.2021.00060

Smith JN, Karcher M, Casacuberta N, Williams WJ, Kenna T, Smethie Jr. WM (2021) A Changing Arctic Ocean: How Measured and Modeled ^{129}I Distributions Indicate Fundamental Shifts in Circulation Between 1994 and 2015. J. Geophys. Res. Oceans 126:e2020JC016740. https://doi.org/10.1029/2020JC016740

Smith JN, Smethie Jr. WM, Casacuberta N (2022) Synoptic ^{129}I and CFC–SF_6 transit time distribution (TTD) sections across the central Arctic Ocean from the 2015 GEOTRACES cruises. J. Geophys. Res. Oceans 127:e2021JC018120. https://doi.org/10.1029/2021JC018120

Sültenfuß J, Rhein M, Roether W (2009) The Bremen mass spectrometric facility for the measurement of helium isotopes, neon, and tritium in water. Isotopes Environ. Health Stud. 45(2):1–13. https://doi.org/10.1080/10256010902871929

Timmermans M, Marshall J (2020) Understanding Arctic Ocean Circulation: A Review of Ocean Dynamics in a Changing Climate. J. Geophys. Res. Oceans 125. https://doi.org/10.1029/2018JC014378

Weingartner T, Ashjian C, et al (2022) Introduction to the Special Issue on the New Arctic Ocean. Oceanog. https://doi.org/10.5670/oceanog.2022.132

Wanninkhof R, Sullivan KF, Top Z (2004) Air-sea gas transfer in the Southern Ocean. J. Geophys. Res. 109:C08S19. https://doi.org/10.1029/2003JC001767

Tab. 4.12: Overview of ArgoFloat deployments

Float ID	WMO ID	Event Label	Depl. Date	Time (UTC)	Depl. latitude	Depl. longitude	Water depth (m)	CTD profile	Additional information
AI2600_24DE006	7901144	PS144_2-2	13.08.2024	20:38	82.00	25.59	3598	XCTD PS144_002_01	calm sea, very small amount of ice floes
AI2600_24DE007	7901145	PS144_16-1	21.08.2024	17:25	84.39	109.56	4025	XCTD PS144_013_10	calm sea, big hole of open ocean in the ice cover, diameter 5nm, float deployed in the middle
AI2600_24DE008	7902188	PS144_61-1	07.09.2024	09:22	84.99	156.67	2534	XCTD PS144_060_01, CTD PS144_059_01	calm sea, 10-20% ice concentration, some big floes in vast area of open water
AI2600_24DE009	7902189	PS144_156-4	04.10.2024	11:20	82.61	30.88	3640	CTD PS144_156_02	calm sea, big area of open water within pancake ice

5. NUTRIENT BIOGEOCHEMISTRY, NITROGEN ISOTOPES, DISSOLVED ORGANIC MATTER (DOM), AND WATER ISOTOPES (MARINE BIOGEOCHEMISTRY – MBC)

Rainer Amon[1], Rebecca Gorniak[2];
Kari Kaphegy[3]; Zoe Neumann[4];
Freya Palmer[5]; Sinhué Torres-Valdés[2];
Sunke Trace-Kleeberg[6];
not on board: Raja Ganeshram[5], Marta Santos Garcia[5]; Dorothea Bauch[4,7], Boris Koch[2]

[1]US.ATM
[2]DE.AWI
[3]AT.UIBK.AC
[4]DE.CAU
[5]UK.ED
[6]UK.UNI-SOUTHAMPTON-SOES
[7]DE.GEOMAR

Grant-No. AWI_ PS144_04

Outline

The observational programme of the Marine Biogeochemistry (MBC) Team includes research from the AWI, University of Edinburgh and by Texas A&M University, Christian-Albrechts-Universität zu Kiel and GEOMAR, under the secondary user proposal DOMAHAWK.

Objectives

Nutrient biogeochemistry

Due to a rapidly changing Arctic Ocean, monitoring key processes over long time scales is important to determine how changes in ocean dynamics affect biogeochemical cycles and ocean productivity. Atlantic Water entering via Fram Strait and the Barents Sea Opening supply nutrients to the Nansen and Amundsen basins, contributing to the Arctic Ocean nutrient budget providing rich nutrient waters at depth. With current changes in sea ice decline, the resulting stratification and changes in the Atlantic Water inflow, it is important to investigate how these may impact on the nutrient supply to the sunlit layers of the Arctic Ocean and how the interaction between physical and biological processes modify nutrients along the pathway of Atlantic Water, which will eventually be reflected in the wider nutrient budget. Our global aim was therefore to measure nutrient fields during PS144 in order to assess them in relation to previous observations within the context of ArcWatch objectives (i.e., long term observations). As part of a wider sampling strategy starting back in 2018, the data collected on this expedition will be merged with previous FRAM/HAUSGARTEN, MOSAiC and Central Arctic expeditions, as well as further expeditions in 2025 and 2026, as part of an INSPIRES PhD project addressing nutrient exchange across Fram Strait and its link to the Central Arctic Ocean in relation to the wider Arctic Ocean nutrient budget. This includes an assessment of temporal variability, water mass nutrient content, nutrient finer vertical structure, nutrient relative abundance (stoichiometry), denitrification, winter time nutrient resupply (convection and lateral transport). Additionally, we also aim to evaluate the role of snow fall as an additional source of nitrogen. This was done via the collection of snow samples during ice stations, complemented with measurements of snow depth.

Nitrogen isotopes

Primary productivity in the Arctic Ocean appears to be limited by the availability of nitrogen (Yamamoto-Kawai et al., 2006). Biologically available nitrogen is lost in the Arctic Ocean through shelf productivity (i.e., phytoplankton uptake and sediment burial) and sediment denitrification. Denitrification in shelf sediments, such as that occurring off Siberia, leads to significant N losses in the upper water column of the Arctic Ocean (Yamamoto-Kawai et al., 2006). This process is thought to be responsible for the N limitation in the Arctic Ocean. Denitrification is particularly sensitive to shelf processes such as changes in shelf productivity, circulation, and diapycnal mixing, which result from the reduced sea-ice cover (Codispoti et al., 2013). Primary productivity along the shelf edge bordering the Siberian shelves has increased by 96-117% over the last two decades (Lewis et al., 2020) which in turn should have driven an increase in denitrification rates as these processes are proportional (Chang and Devol, 2009). This is expected to have biogeochemical implications at a pan-Arctic scale as the shelves are connected to the Fram Strait outflow gateway via the Transpolar Drift (Debyser et al., 2022). It is postulated that the balance between N inputs and outputs which was in delicate balance (Torres-Valdés et al., 2013) might have transitioned to an N deficit. This work aims to quantify this N loss in the Transpolar Drift through the use of stable isotopes and inverse modelling.

The main objective is to understand the role of various N cycling processes in determining loss of nitrate in the N-limited Arctic Ocean. To this end, we will disentangle the influences of biogeochemical processes, horizontal transport and vertical mixing in the chemical and isotopic compositions of waters in the upper water column in the central Arctic which are under the influence of the Transpolar Drift. These processes will be evaluated from an analysis of measurements of nitrate concentrations and isotopic measurements and from the development and application of mathematical models describing the cycling of nitrogen in the upper Arctic.

Dual isotope signatures of $\delta^{15}N\text{-}NO_3$ and $\delta^{18}O\text{-}NO_3$ allow tracing nitrogen cycling processes as they exhibit characteristic isotopic fractionation trends (Sigman and Casciotti, 2001). Quantification of N cycling processes along the Transpolar Drift would allow untangling the N deficit signal associated with shelf denitrification. This is possible as, during denitrification, the $^{15}N/^{14}N$ ratio of nitrate tends to increase due to the preferential uptake of the light isotope by denitrifying bacteria, leaving the residual nitrate enriched in the heavy isotope, while $^{18}O/^{16}O$ decreases due to isotopic exchange with ambient seawater (Fripiat et al., 2018).

Our first aim is to compare nutrient stoichiometry and N isotope values we obtain from this cruise with previous measurements (TransARC II, 2015; MOSAiC, 2019/20; ArcWatch I, 2023) to see if there are discernible changes in N cycling/deficit. Our second aim is to improve the coverage of isotopic data in the central Arctic Ocean to a density that will allow us to use inverse methods to address present and future changes in N cycling and N availability.

The dataset collected will be interpreted in the context of a wide range of oceanographic and biogeochemical data collected during the cruise. Specific questions to be addressed are:

1. What is the magnitude of various sources and sinks of N in the central Arctic Ocean and how are they changing (including shelf denitrification N losses)?
2. How are these changes impacting nitrate levels in various Arctic water masses?
3. Ultimately, what are the likely consequences of current climate change on the future Arctic Ocean N budget and productivity?

DOMAHAWK

The overall purpose of the project is to further understand the effects of sea-ice processes on the water mass structure of the central Arctic Ocean halocline in order to get a basis to estimate future and ongoing effects of climate changes on the distribution and transport of constituents such as of carbon, nutrients and trace elements (TE) within the upper water column of the Transpolar Drift (TPD). The wind-driven TPD in the central Arctic Ocean is the main transport pathway connecting the Siberian shelves to Fram Strait and enabling the transfer of Siberian river water and constituents to the North Atlantic. However, a comprehensive understanding of the actual influence of the TPD remains elusive, particularly due to the complex seasonal ice-ocean interactions. Recent studies (Slagter et al., 2017, 2019; Charette et al., 2020, Williford et al., 2021, 2022) in the Arctic Ocean suggest the transport, distribution and fate of DOM, water isotopes and TE are closely intertwined, and the ArcWatch2 programme provides a unique opportunity to further explore the interactions between DOM, water isotopes and TE. The proposed research builds and expands on our previous research on the origins, transformations and fate of DOM in the Arctic and will provide an unprecedented comparison of DOM and TE biogeochemistry in large parts of the central Arctic Ocean. We propose a suite of chemical and optical characterizations of DOM that will distinguish terrigenous and marine DOM as well as its bioavailability and extent of diagenetic alteration. In order to address the role of DOM for the distribution and cycling of TE, and to understand potential changes due to increasing freshwater discharge and receding summer sea-ice cover, we have the following goals, objectives.

1. To assist and provide the international Arctic Geotraces community with data on water isotopes ($\delta^{18}O$) and on the abundance, distribution, origin and composition of dissolved organic matter in the central Arctic Ocean.

2. To understand the effects of increasing continental runoff and declining sea ice on carbon and trace element cycling and hydrography of the central upper Arctic Ocean.

Work at sea

The next section is divided into the following subsections: Nutrients (Section 5.1), Dissolved Oxygen (Section 5.2), Nitrogen Isotopes (Section 5.3), Dissolved Organic Matter (DOM) and Water Isotopes (Section 5.4), and terrestrial dissolved organic matter (Section 5.5).

5.1 Nutrients

Lab Set up

For PS144 a 7-channel Seal Analytical AA-500 autoanalyser was set up in the chemistry lab for the analysis of micro-molar concentrations of 1) dissolved inorganic nutrients; nitrate plus nitrite (NO_3^-+NO_2^-) – hereafter referred to as nitrate –, nitrite (NO_2^-), silicate ($Si(OH)_4$), phosphate (PO_4^{3-}), and ammonium (NH_4^+) and 2) total nutrients; total phosphorus (TP) and total nitrogen (TN). Installation of the AA-500 involved the fitting of new pump tubing and new cadmium columns for TN and nitrate. The nutrient analyser was controlled by the Seal Analytical Software AACE version 8.03 SP1, which allows for automated and simultaneous analysis of up to 7 channels. Following analyser set up, analytical reagents (stock and working solutions), standards (stock solutions and calibrants) and lab-made quality control solutions were prepared. ‘Stocks’ are concentrated solutions from which ‘working’ reagents/standards are prepared as required by solution stability or usage. Pump tubing in the analyser were replaced three times during the expedition, having started already with a new set installed. Analyses were carried out following current Seal Analytical Methods, which are based on

standard and widely used colorimetric techniques for the analysis of nutrients in water and seawater. The methods used during PS144 are listed below:

1. Total dissolved nitrogen in seawater No. G-218-98 revision 14 (MT23).
2. Nitrate and nitrite in water and seawater No. A-044-19 revision 5 (MT519A).
3. Nitrite in water and seawater No. A-003-18 revision 3 (MT518).
4. Total dissolved phosphorus in seawater No. G-439-16 revision 2 (MT33).
5. Phosphate in water and seawater No. A-004-18 revision 4 (MT518).
6. Silicate in water and seawater No. A-006-19 revision 3 (MT519).
7. Ammonium in water and seawater No. G-327-05 revision 8

Best practices procedures for the analyses of nutrients in seawater following GO-SHIP recommendations, as described in Hydes et al. (2010) and Becker et al. (2020) were adopted.

Calibrants

Calibration standards for the analysis were prepared using 1000 mg/L NO_3^-, NO_2^-, PO_4^{3-}, Si and NH_4^+ MERCK solutions. An intermediate standard containing 4.032, 0.152, 3.560, 0.947 and 0.5266 µmol/mL of nitrate, nitrite, silicate, phosphate and ammonium was prepared in Milli-Q water using a 100 mL volumetric flask. Although working calibration standards are typically prepared in a saline solution or "artificial seawater" (35 g NaCl in 1 L of Milli-Q water), which is also used as a matrix for the analysis, in later years the so called "ultra clean or analytical grade reagents" have been found to be contaminated with a given nutrient (usually phosphate, nitrate and organic nitrogen, and even silicate). In our case, the analytical grade NaCl was found to be contaminated with nitrate and organic nitrogen. Therefore, standards and the analysis matrix were based on Milli-Q water instead. From the intermediate standards, five calibration standards were prepared regularly using either 500 mL or 250 mL flasks to yield the target concentrations shown in Table 5.1.1. These values were then put into an analysis template file in the AACE software, from which all consecutive runs were then built. For each analysis, standards were measured in triplicate, with the first measurement intended as preconditioning and thus ignored as calibrant. It is good practice to adapt calibration concentration ranges for the particular system being measured, in this case, the Arctic Ocean. Here though, we used a rather high range for phosphate. This was imposed by the method to measure TP, which is designed to work efficiently with a top standard of 5 µmol L^{-1}. A calibration range with a top standard lower than this is likely to yield high noise in the signal.

Tab. 5.1.1: Set of calibration standards (*Std*) used for dissolved inorganic nutrient analysis. Concentration units are µmol L^{-1}. Concentrations in the first column are the sum of NO_3^- and NO_2^-, hence NO_3^-+NO_2^-. This concentration also applies for TN. Likewise, the concentration range for phosphate applies to TP.

	NO_3^-+NO_2^-	NO_2^-	$Si(OH)_4$	PO_4^{3-}	NH_4^+	TN	TP
Std 1	0.469	0.017	0.399	0.106	0.059	0.528	0.106
Std 2	6.209	0.226	5.284	1.406	0.782	6.991	1.406
Std 3	11.950	0.435	10.169	2.707	1.504	13.454	2.707
Std 4	17.961	0.643	15.054	4.007	2.227	19.917	4.007
Std 5	23.431	0.852	19.939	5.307	2.949	26.381	5.307

All primary, secondary and working standards, CRMs and quality control solutions were kept in moisturised and dark conditions within a high-quality grade cool box when not in use and right after preparations.

Figure 5.1.1 shows the run-to-run spread (noise) of calibration standards. This information was used to assess the precision of measurements at each concentration level. The cruise-mean, standard deviation and precision of the analysis at the different concentration levels are presented in Table 5.1.2.a & b. Calibration standards show good consistency through out the expedition. As is common, precision is reduced at low concentration levels. The limits of detection, taken as twice the standard deviation of the lowest concentration standard (cruise-long standard deviation) were: 0.09, 0.005, 0.05, 0.01, 0.03, 0.07 and 0.02 µmol L^{-1} for NO_3^- +NO_2^-, NO_2^-, $Si(OH)_4$, PO_4^{3-}, NH_4^+, TN and TP, respectively.

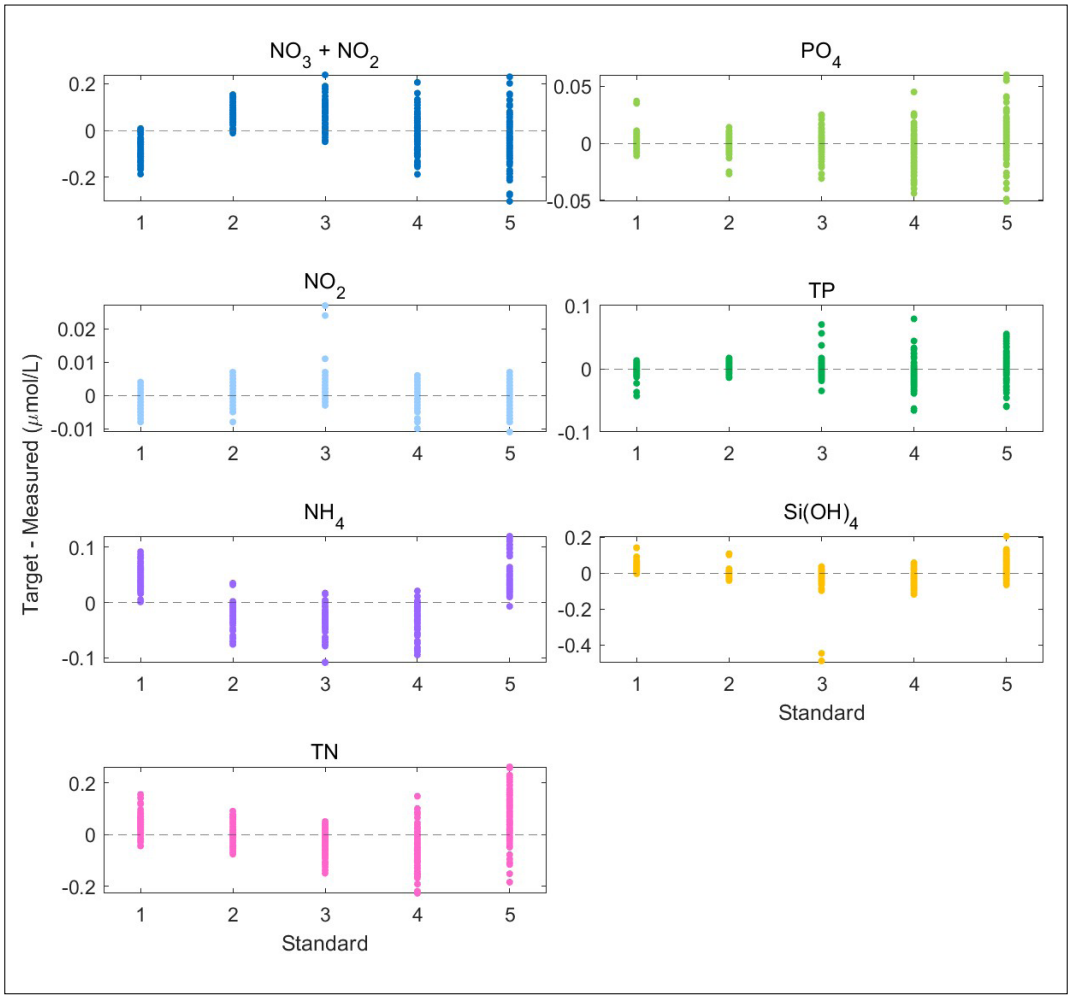

Fig. 5.1.1: Calibration standards for each nutrient measured, showing the spread of data point on a run-by-run basis. Precision at the different concentration levels derives from this assessment.

Tab. 5.1.2 a & b: For further information please see the end of this chapter.

Quality controls (QCs)

There are various products and lab-made solutions that are used for quality control of the analysis; low nutrient seawater, recovery standards and certified reference materials (CRMs). Below we describe how and what we used them for. All quality control standards and CRMs were measured in duplicate in every analysis run.

Low Nutrient Seawater (LNSW) from OSIL Scientific

LNSW can have multiple uses. It can be used as a saline matrix, as a low concentration standard or, as in our case, to determine whether contamination with any given nutrient occurred during sample collection or preparation of reagents. It is expected that the signal produced is close to the baseline (i.e., blank) or above, and remain constant throughout analyses. LNSW is also useful in assessing the effect of measuring saline samples within a Milli-Q based matrix (the so-called salt effect). Seal Analytical analysers are made to account for this effect and so any impact on the analysis is minimised. During PS144, LNSW measured for the various nutrients yielded consistent results within the expected analytical error associated with low nutrient concentrations and/or the precision as estimated for different concentration levels. Figure 5.1.2 shows time series of these measurements, including mean and standard deviation.

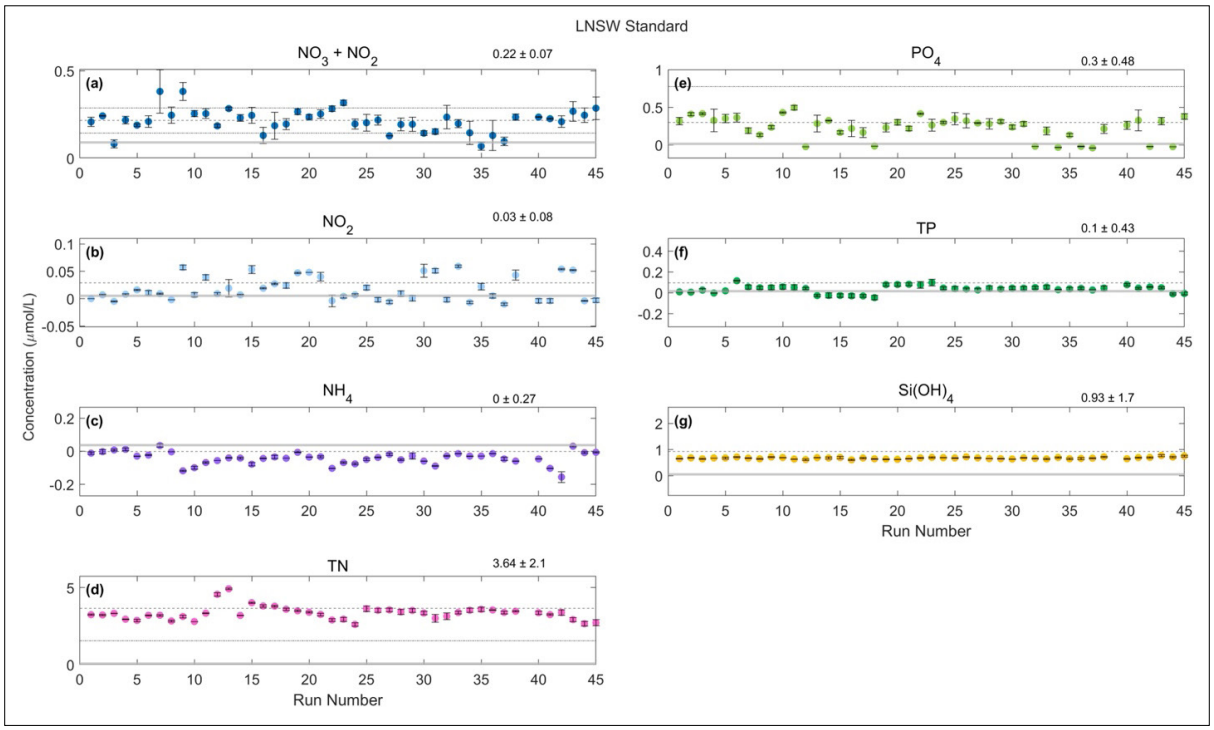

Fig. 5.1.2: Time series (shown as per run number) of OSIL Scientific certified Low Nutrient SeaWater measurements. This additional QC was measured in duplicate in every analysis run. Grey lines show the limit of detection for every variable. The dotted line shows the mean and dashed/dotted line the standard deviation.

Recovery Standards: Cadmium coil and column reduction efficiency

The measurement of some nutrients such as NO_3^-+NO_2^- and TN require continuous monitoring of the reduction efficiency of the Cadmium (Cd) column. The colorimetric method upon which the measurement of these two nutrients is based, relies on the chemical reaction between reagents and NO_2^-. Thus, in order to measure NO_3^-, this has to be reduced to NO_2^- (the Cd is oxidised and the NO_3^- is reduced). In the case of TN, the reaction is slightly more complex, as all dissolved nitrogen present in the water first needs to be oxidised to NO_3^-+NO_2^- and then reduced to NO_2^-. For TN there is thus an extra step to monitor; the oxidation efficiency, which is dealt with in the next subsection. In order to monitor the reduction efficiency, two lab-made standards containing only NO_2^- and only NO_3^- were prepared, both at a concentration of 23.31 µmol L^{-1}. The concentration yielded by measuring both recovery standards should be equal within the precision of the analyses. The reduction efficiency is the ratio of the NO_3^- standard to the NO_2^- standard in percentage. As per best practice recommendations, the Cd columns were reactivated or replaced when the reduction efficiency reached or was close to 95%. Figure 5.1.3 shows time series of the Cd reduction efficiency of the NO_3^- + NO_2^- (Fig. 5.1.3a) and TN (Fig. 5.1.3b) columns. Recovery standards were measured in duplicate at the beginning and at the end of each run. This is particularly useful as the efficiency can potentially be reduced during the analysis, in particular with long runs. This way, we were able to assess whether the efficiency was still within expected values at the end of a given analysis run. Therefore, when required, we reactivated the column and tested its reduction efficiency before starting a new run. This was done by measuring -in duplicate- the top standard, the NO_3^- standard and the NO_2 and making sure peaks were of similar height.

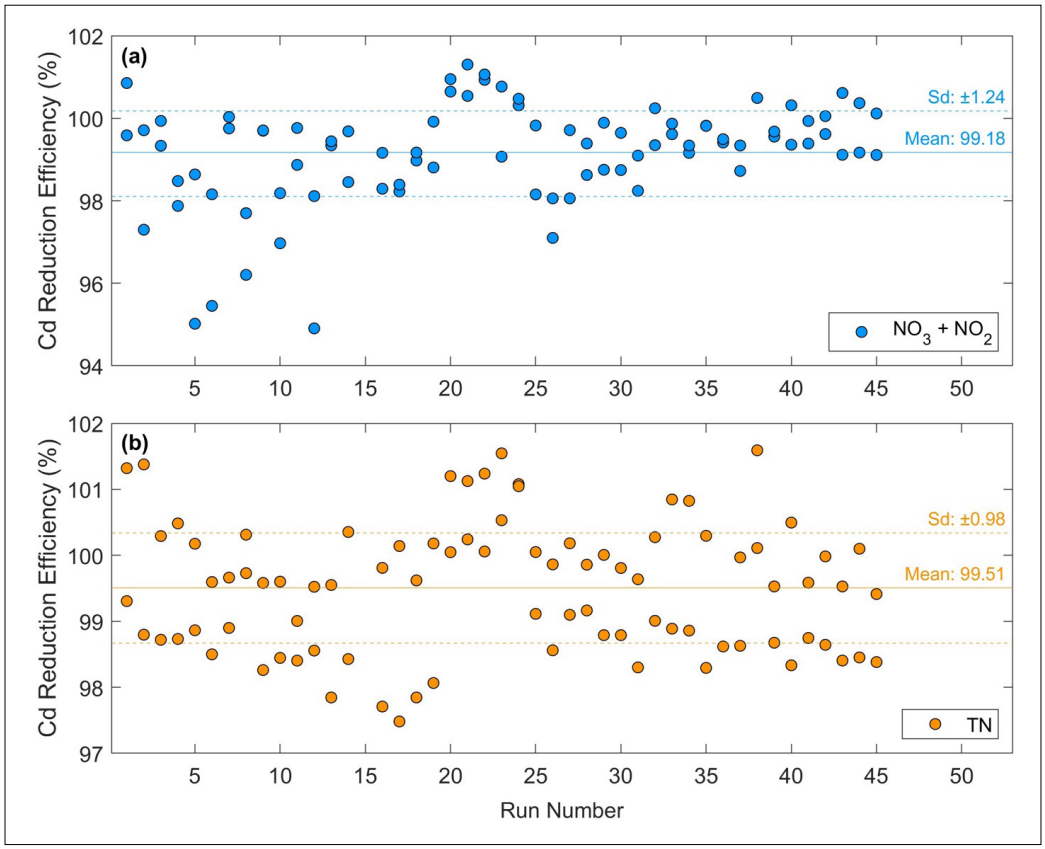

Fig. 5.1.3: Cd column reduction efficiency for the measurement of (a) NO_3^-+NO_2^- and (b) TN during PS144. The cruise-long average reduction efficiency is indicated in the plots. Solid and dash lines show the mean and standard deviation, respectively.

Recovery Standards: TN oxidation efficiency

As mentioned above, the measurement of TN requires the oxidation of all nitrogenous compounds present in the sample. There are no certified reference materials available in the market to test the oxidation efficiency and the accuracy of the method. However, there are steps that can be taken. During PS144 we used an OSIL Scientific 10 µmol L^{-1} ammonium (NH_4^+) certified standard, from which we prepared a 15 µmol-NH_4^+ L^{-1} solution. This standard was measured in duplicate in every run. Although this standard is not an organic compound, it is most useful as the NH_4^+ first needs to be oxidised to NO_3^-+NO_2^- and then reduced to NO_2^-. Figure 5.1.4 shows time series of the oxidation efficiency and recovery of NH_4^+.

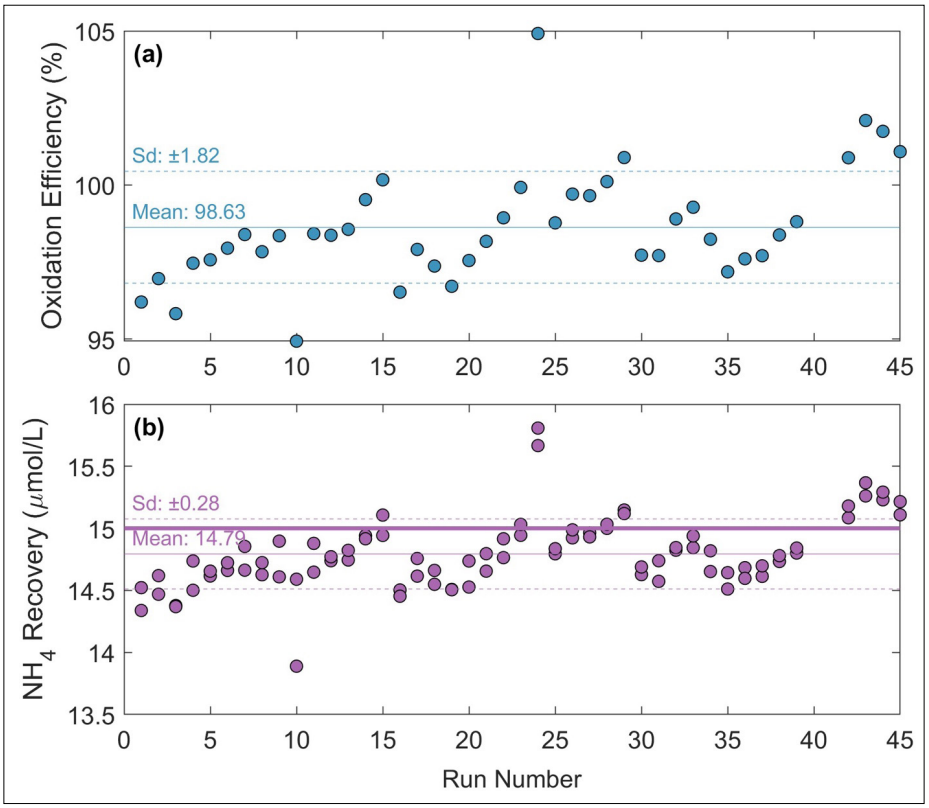

Fig. 5.1.4: Time series of the NH_4^+ recovery standard used during PS144 to test the oxidation efficiency of the TN channel. (a) Percent efficiency and (b) recovery relative to the NH_4^+ standard prepared (15 µmol L^{-1}shown as a thick solid line). Cruise mean (thin solid lines) and standard deviation (dashed lines) are also shown.

The oxidation efficiency also needs to be tested for TP, as phosphorous bound to organic compounds has to be oxidised to PO_4^{3-} to be measured. There is a second way in which we monitored both, the oxidation efficiency of TN and TP, and we present this in the following section.

Certified reference materials (KANSO and OSIL Scientific)

In order to assess the accuracy and consistency of the methods employed, we used two types of certified reference materials (CRMs); 1) KANSO Technos Co., LTD, Japan, lots CL and CJ, and 2) OSIL Scientific, UK, nutrient standards. KANSO are also known as 'RMNS or reference materials for the measurement of nutrients in seawater'. These are made from

natural seawater, typically by combining deep and surface water from selected ocean regions to yield target concentrations, plus further processing (e.g., sterilisation). Certified values are reported in units of µmol kg^{-1}, so for our work we converted them to µmol L^{-1} using the reported CRM salinity and an average lab temperature of 22°C. KANSO CRM concentrations are shown in Table 5.1.3. The reported salinity of the CRMs is as follows: 36.619, 34.991, 34.685, 34.520 and 35.654 for CR, CH, CL, CS and CI respectively.

For our work we use the sum of NO_3^- and NO_2^-, with the uncertainty propagated from the respective uncertainties. OSIL Scientific standards are concentrated solutions distilled-water-based and certified to 100 µmol-PO_4^{3-} L^{-1}, 100 µmol-NO_2^- L^{-1}, 1000 µmol-NO_3^- L^{-1}, 1000 µmol-$Si(OH)_4$ L^{-1} and 1000 µmol-NH_4 L^{-1}. These concentrated solutions were used to prepare an additional quality control standard with concentrations equal to our top calibration standard (STD 5, Tab. 5.1.1). This standard was measured in duplicate at the beginning of each run. Table 5.1.4 shows the cruise-long-mean of measurements of certified materials and Figures 5.1.5 to 5.1.10 show time series of measurements, as carried out in individual runs. The idea behind the measurement of KANSO CRMs is to assess whether the methods used are accurate or whether corrections need to be applied. As these are internationally used CRMs, the aim is to provide traceability and render data comparable to measurements carried out by other laboratories. Data are adjusted based on the CRM measurements. A correction factor is obtained as $CRM_{certified}$:$CRM_{measured}$. Data is then multiplied by this correction factor. Corrections were applied on a run-by-run basis. The main assumption and “big leap of faith” here, is that the result of the CRM measured is representative of the whole run where it was analysed. Note that the implied correction factor is slightly different depending on the CRM Lot used. As per best practice procedures, a CRM concentration closest to the top calibration standard are to be used. Ideally one would like to use the same CRM throughout an expedition. However, CRMs do not always contain concentrations that are useful for all nutrients and so a combination of CRMs are typically used. During PS144 we started our analysis with a combination of CRMs of lots CR and CH. The former contains $Si(OH)_4$ at a concentration close to our top standard and it is the only CRM with certified NH_4^+. The later contains concentrations suitable for the remaining inorganic nutrients (NO_3^-+NO_2^-, PO_4^{3-} and NO_2^-,). Once we ran out of CRM CH, we used a combination of CRMs CR and CI, and finally CL and CS. Data was thus processed in three different batches depending on the combination of CRMs. By the time we used the combination CL and CS there were only 2 bottles of CRM CR left. We continued to measure this CRM in a single measurement so as to continue monitoring NH_4^+.

None of the CRMs used have certified values for TN and TP, so what we do to standardise the data and avoid noise is to obtain the mean of all measurements carried out for a given CRM (excluding outliers), in particular those with concentrations closest to our top standards. Then each run is normalised to this mean. The OSIL standard was used as an additional and independent quality control to assess run-to-run noise.

Tab. 5.1.3: CRM certified nutrient concentrations (in µmol L^{-1}).

CRM lot	NO_3^-	NO_2-	NOX	$Si(OH)_4$	PO_4^{3-}	NH_4^+
CR	5.591±0.164	0.993±0.072	6.584±0.179	14.335±0.307	0.403±0.014	0.973±0.154
CH	17.35±0.154	0.184±0.041	17.535±0.159	30.608±0.164	1.2±0.015	---
CL	5.601±0.154	0.015±0.006	5.617±0.154	14.131±0.031	0.435±0.019	---
CS	17.047±0.164	0.184±0.072	17.231±0.179	34.606±0.41	1.095±0.179	---
CI	14.11±0.133	0.42±0.041	14.53±0.139	8.864±0.174	0.971±0.013	---

Tab. 5.1.4: Cruise-long-mean and standard deviation of measured CRMs for the 7 analyser channels (µmol L^{-1}). Number of runs analysed with each CRM lot were as follows: CR (n=35), CH (n=20), CI (n=15), CL (n=10) and CS (n=10). Cells under NH_4^+, TN and TP are shaded in orange to indicate variables for which there are no KANSO CRM values reported. In the case of the OSIL CRM, TN is given by NO_3^-+NO_2^-+NH_4^+ and TP only by PO_4^{3-} (i.e., there is no organic nitrogen or organic phosphorus).

CRM	NO_3^-+ NO_2^-	NO_2^-	$Si(OH)_4$	PO_4^{3-}	NH_4^+	TN	TP
CR	5.61±0.94	1.007±0.128	12.82±0.12	0.528±0.133	0.83±0.26	9.93±0.74	0.581±0.054
CH	13.32±2.91	0.185±0.036	26.31±1.79	1.184±0.022	1.54±0.21	20.03±1.25	1.576±0.046
CL	5.48±0.45	0.041±0.024	12.85±0.07	0.514±0.142	1.75±0.35	9.89±0.89	0.436±0.042
CS	17.22±1.14	0.184±0.006	31.06±0.15	1.093±0.037	0.67±0.11	18.94±1.28	1.129±0.033
CI	11.9±2.16	0.447±0.071	7.62±0.05	0.935±0.098	1.79±0.42	19.01±1.35	1.408±0.073
OSIL	23.37±0.48	1.019±0.372	20.06±0.26	5.276±0.046	3.02±0.09	26.69±0.48	5.222±0.565

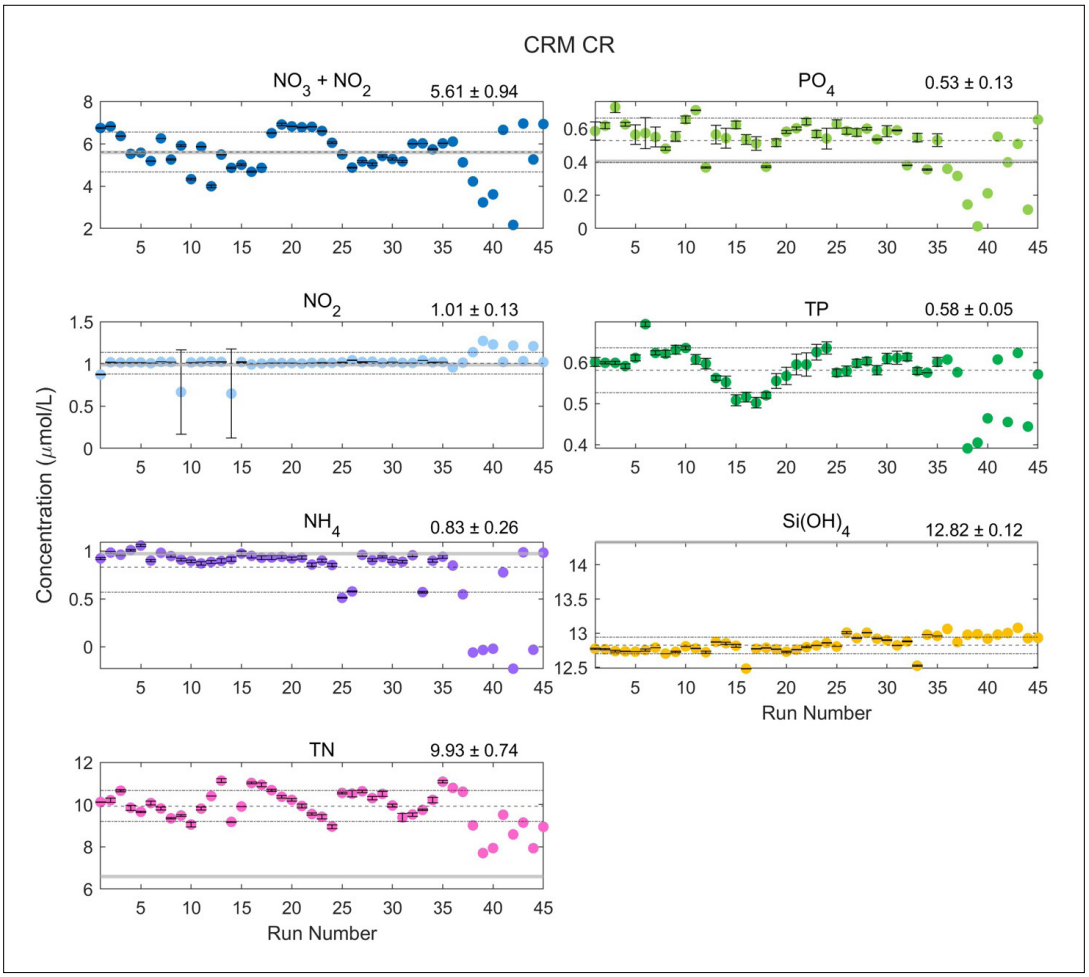

Fig. 5.1.5: Time series of KANSO CRM Lot CR measured on 35 runs during PS144. Solid and dashed lines show cruise mean and standard deviation (displayed also on top of each panel). Thick grey line shows certified value. Error bars in symbols show standard deviation. From and including run 36, a single measurement of CRM CR was done per run (hence there are no error bars).

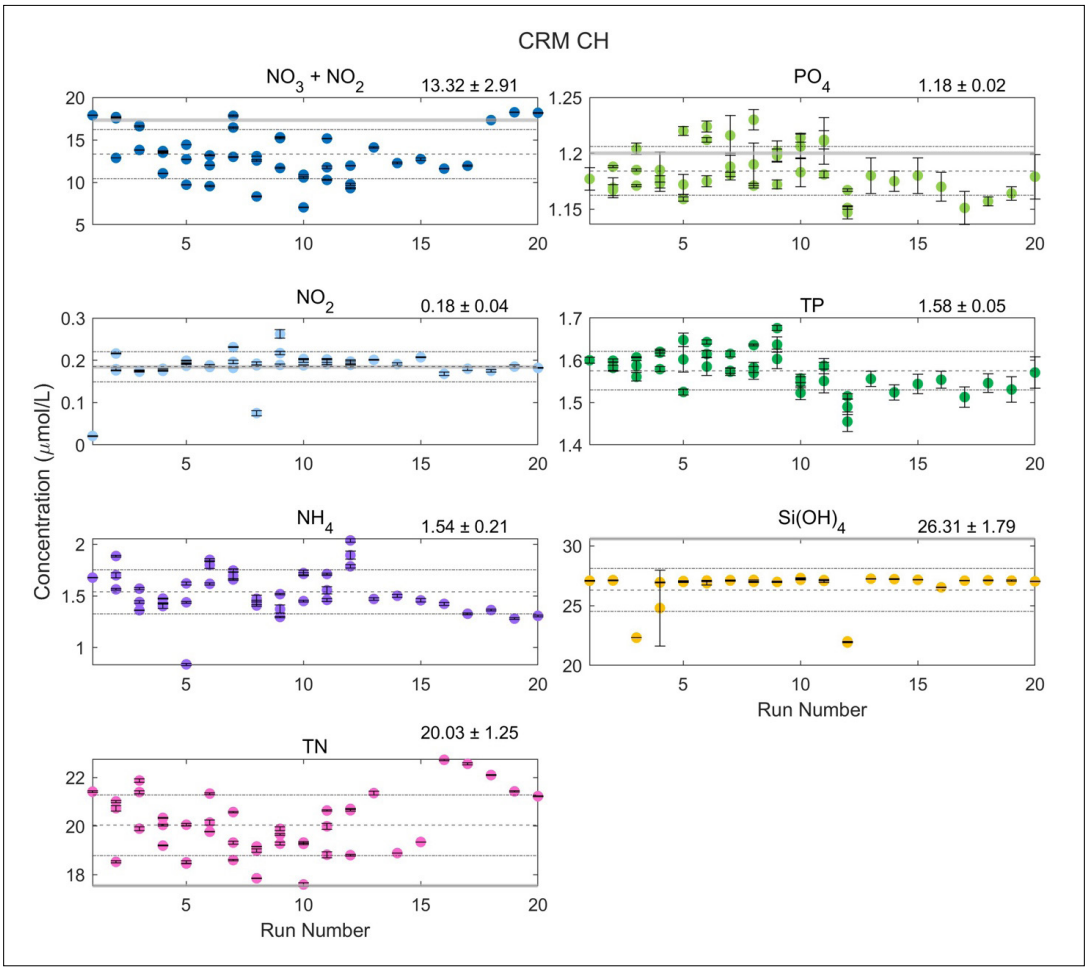

Fig. 5.1.6: Time series of KANSO CRM Lot CH measured on 20 runs during PS144. Solid and dashed lines show cruise mean and standard deviation (displayed also on top of each panel). Thick grey line shows certified value. Error bars in symbols show standard deviation.

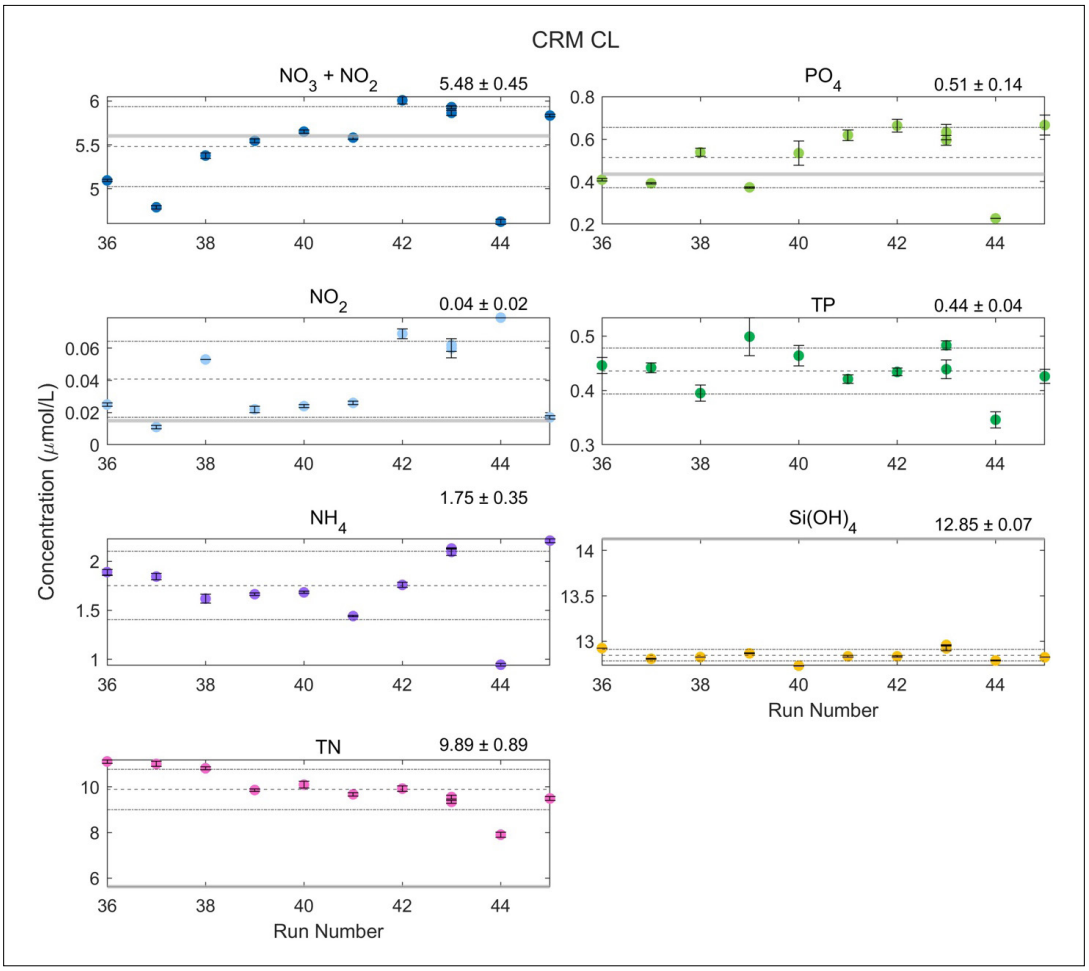

Fig. 5.1.7: Time series of KANSO CRM Lot CL measured on 10 runs during PS144. Solid and dashed lines show cruise mean and standard deviation (displayed also on top of each panel). Thick grey line shows certified value. Error bars in symbols show standard deviation.

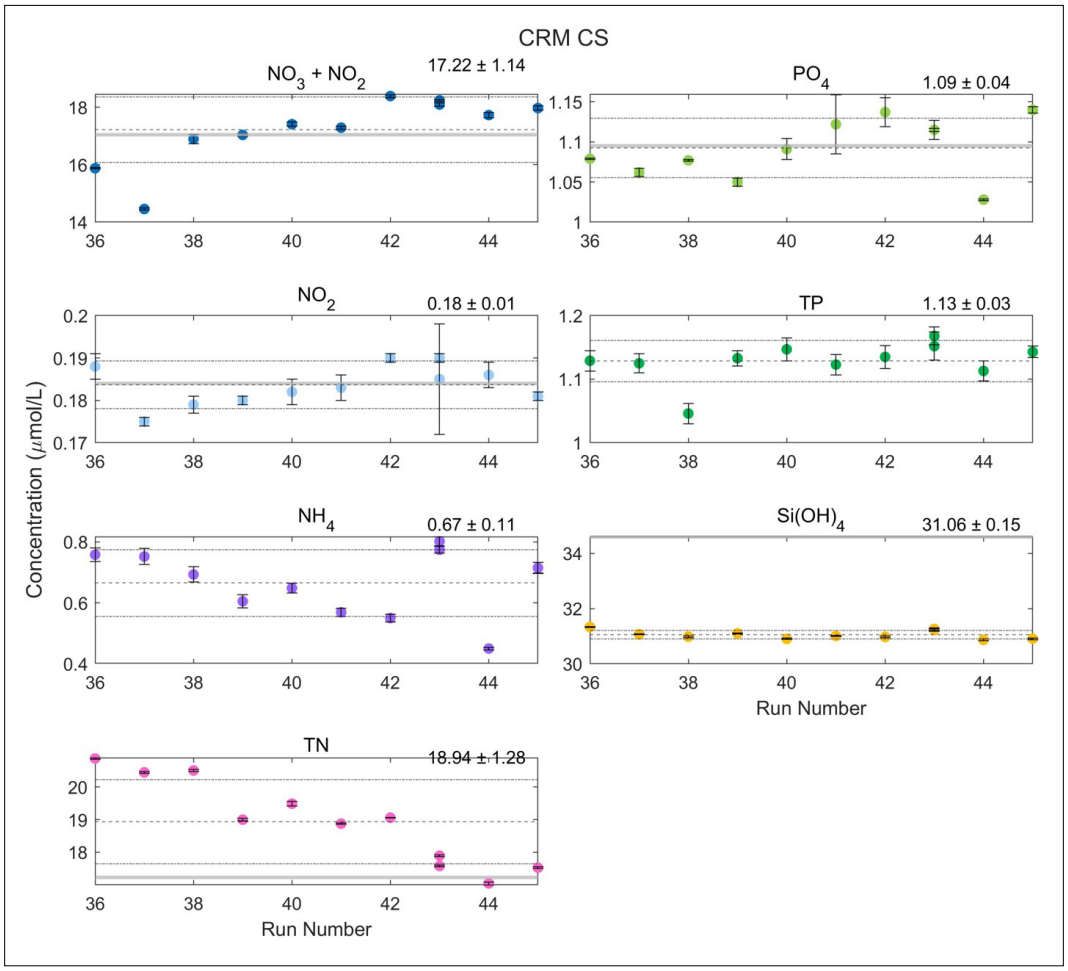

Fig. 5.1.8: Time series of KANSO CRM Lot CS measured on 10 runs during PS144. Solid and dashed lines show cruise mean and standard deviation (displayed also on top of each panel). Thick grey line shows certified value. Error bars in symbols show standard deviation.

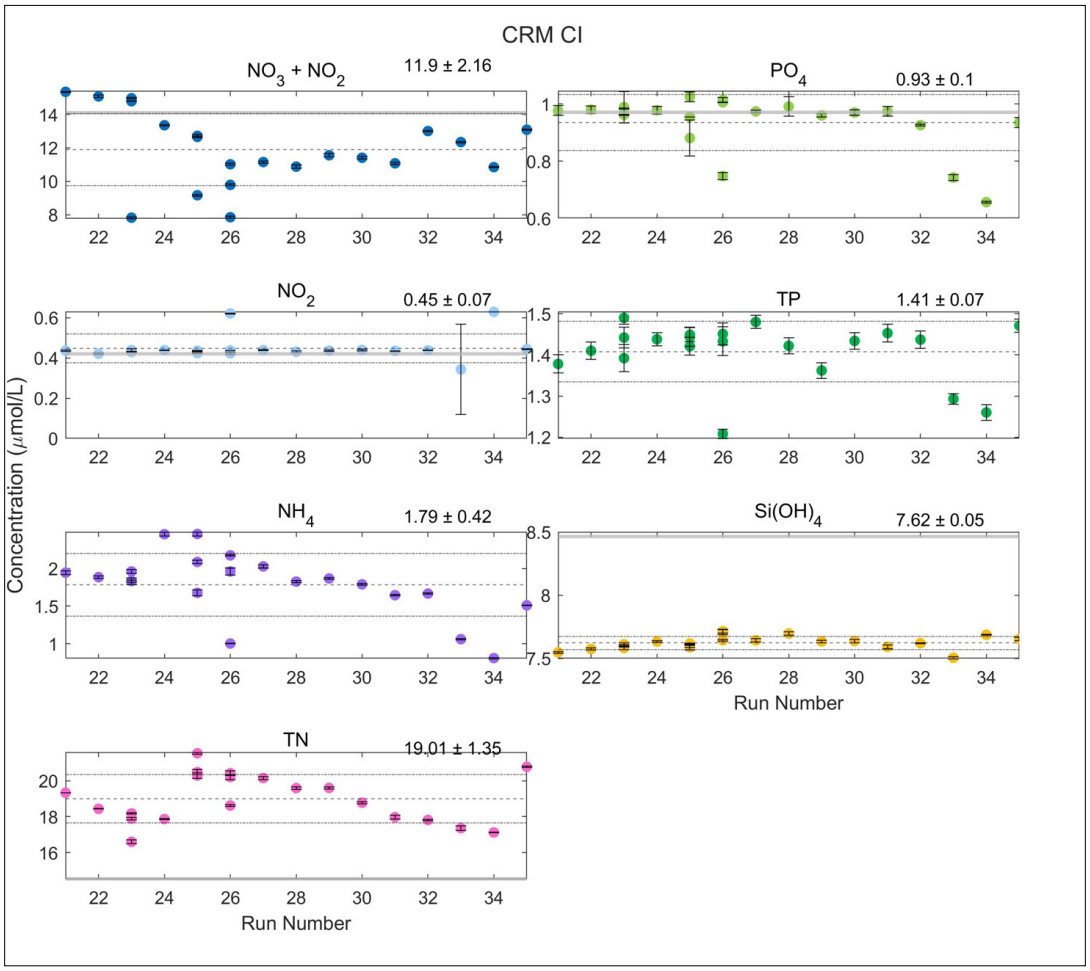

Fig. 5.1.9: Time series of KANSO CRM Lot CI measured on 15 runs during PS144. Solid and dashed lines show cruise mean and standard deviation (displayed also on top of each panel). Thick grey line shows certified value. Error bars in symbols show standard deviation.

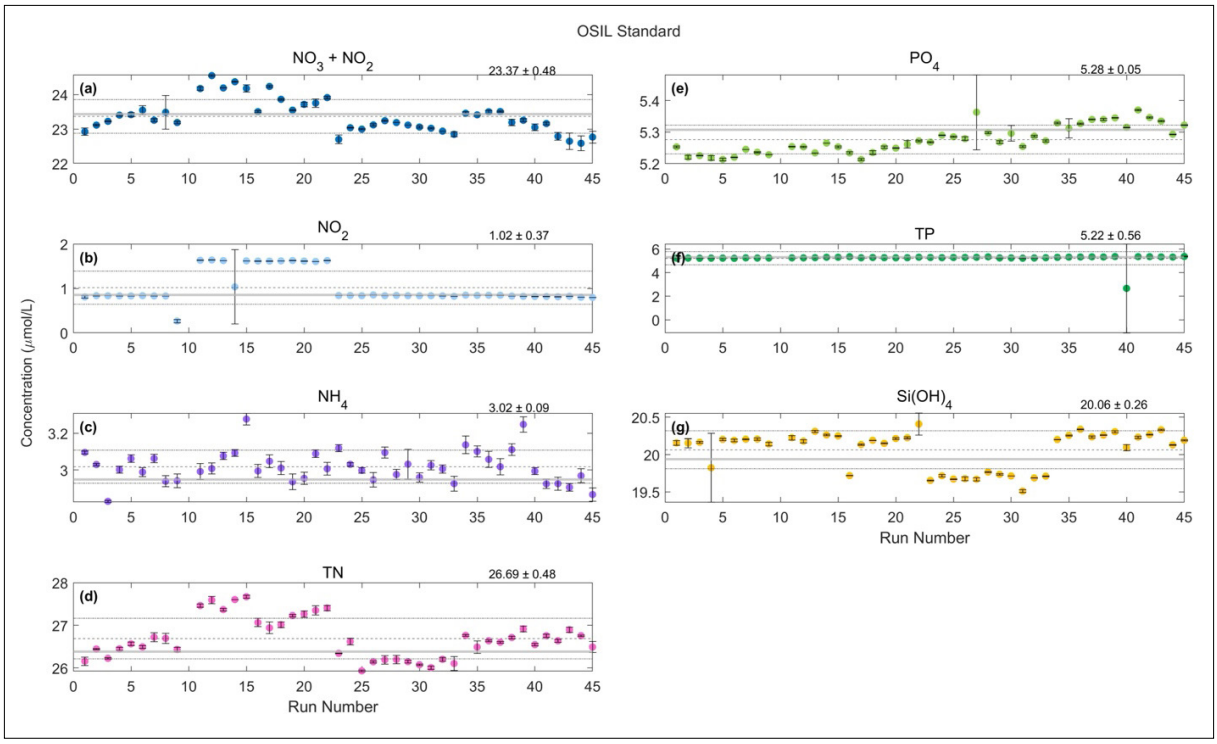

Fig. 5.1.10: Time series of standards prepared from OSIL Scientific concentrated CRMs. The solid grey line indicates the concentration at which each nutrient was prepared (top standard in Tab. 5.1.1). Dashed and dotted lines show cruise mean and standard deviation.

Sample collection and analysis

40 mL samples were collected directly into 50 mL sterile Falcon tubes for the analysis of nutrients. Tubes were rinsed three times with seawater before the sample was drawn. Two duplicate samples were randomly collected from each cast. In order to optimise labwork (e.g., number of samples analysed per run) and reduce the amount chemical waste produced, analyses were carried out when a minimum of 50-70 samples were available. Runs included samples from experiments (Alexandra Bettinelli), sea ice cores (Hauke Flores), Clean CTD (6-8 bottles/depths) remote access samplers from previous expeditions and recovered in the current expedition, samples from PS143-1 and PS143-2, snow samples as well as from shallow CTD casts, where our SUNA Nitrate sensor was deployed in order to obtain high vertical resolution nitrate profiles. Samples collected from shallow casts will be used to calibrate the SUNA Nitrate sensor. All samples, with the exception of some samples from experiments, were analysed in duplicate. All hydrographic stations occupied with the regular CTD were sampled and analysed onboard.

Ice Stations

During PS144 we collected data at 8 ice stations, this consisted of snow depth measurements (Tab. 5.1.5) and samples (Tab. 5.1.6) of mostly snow. Although at the first station where melt ponds were present this was also sampled. As well as frost flowers when they were present and accessible from the ice floe edge.

During the ice stations the method of collecting snow depth measurements changed. Initially a measurement was only taken at the locations where a sample was also collected. At station

PS144_085_01_ICE07, the sampling procedure was adjusted to a transect with snow depth measurements every 10 paces and snow samples collected every 100 paces. This method of data collection was continued for the remainder of the stations with the number of snow depth measurements varying due to the length of the transect. Figure 5.1.11 shows the location of the snow thickness measurements where the colours correspond to the depth. The positions of the snow thickness measurements have been drift corrected using the GNSS boxes that were deployed at each station by the sea ice physics team. The reference times and coordinates for each station are listed Table 5.1.5. The snow depths at each station are compared in Figure 5.1.12. Measurements show an increasing trend of snow thickness from the first ice station to the ninth. However, at the final ice station PS144_134_01_ICE10, the snow thickness was shallower, more in the range observed at the second station. At PS144_085_01_ICE07, the transect of snow thickness measurements ended early as it's likely the battery of the device was too low. As a result the locations of the snow samples were recorded using the GPS coordinates from a phone, these are not shown on the figure.

Once the snow samples were brought back into the lab on *Polarstern* they were defrosted before transferring 40 mL into falcon tubes for nutrient analysis as described in the sections above. From station PS144_067_01_ICE05 onwards, the volume of melted snow in each of the snow containers was measured. This was done by pouring 40 mL into a falcon tube for nutrient analysis and then measuring the volume of the remaining amount with a measuring cylinder.

Tab. 5.1.5: Transect measurements for snow depth

Event Label	Date	Time (UTC)	Latitude (°N)	Longitude (°E)	Device short name	Data Points
PS144_7_Magna-Kathrin	16.08.2024	17:00	85.058	42.934	Magnaprobe-katrin	15
PS144_23_Magna-Katrin	29.08.2024	22:00	84.500	115.720	Magnaprobe-katrin	15
PS144_50_Magna-Katrin	05.09.2024	09:09	85.025	139.943	Magnaprobe-katrin	20
PS144_67_Magna-Katrin	08.09.2024	15:00	84.946	162.094	Magnaprobe-katrin	21
PS144_85_Magna-Katrin	13.09.2024	09:00	87.500	178.725	Magnaprobe-katrin	97
PS144_109_Magna-Katrin	19.09.2024	09:20	89.951	-142.696	Magnaprobe-katrin	278
PS144_123_Magna-Katrin	23.09.2024	10:00	88.070	59.952	Magnaprobe-katrin	271
PS144_134_Magna-Katrin	25.09.2024	06:00	87.047	57.073	Magnaprobe-katrin	565

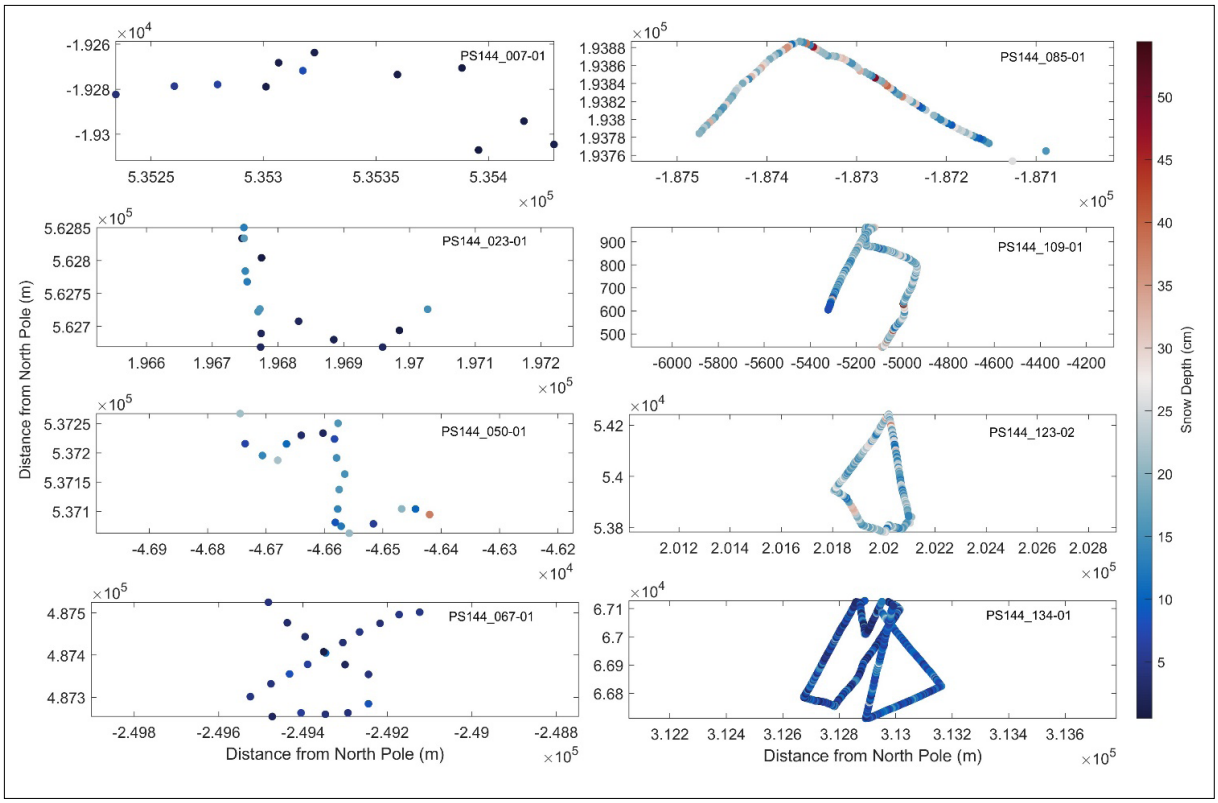

Fig. 5.1.11: Plots of snow thickness measurements taken with the magna probe. Colours correspond to the measured depth. These locations have been drift corrected to the reference times as defined in Table 5.1.5.

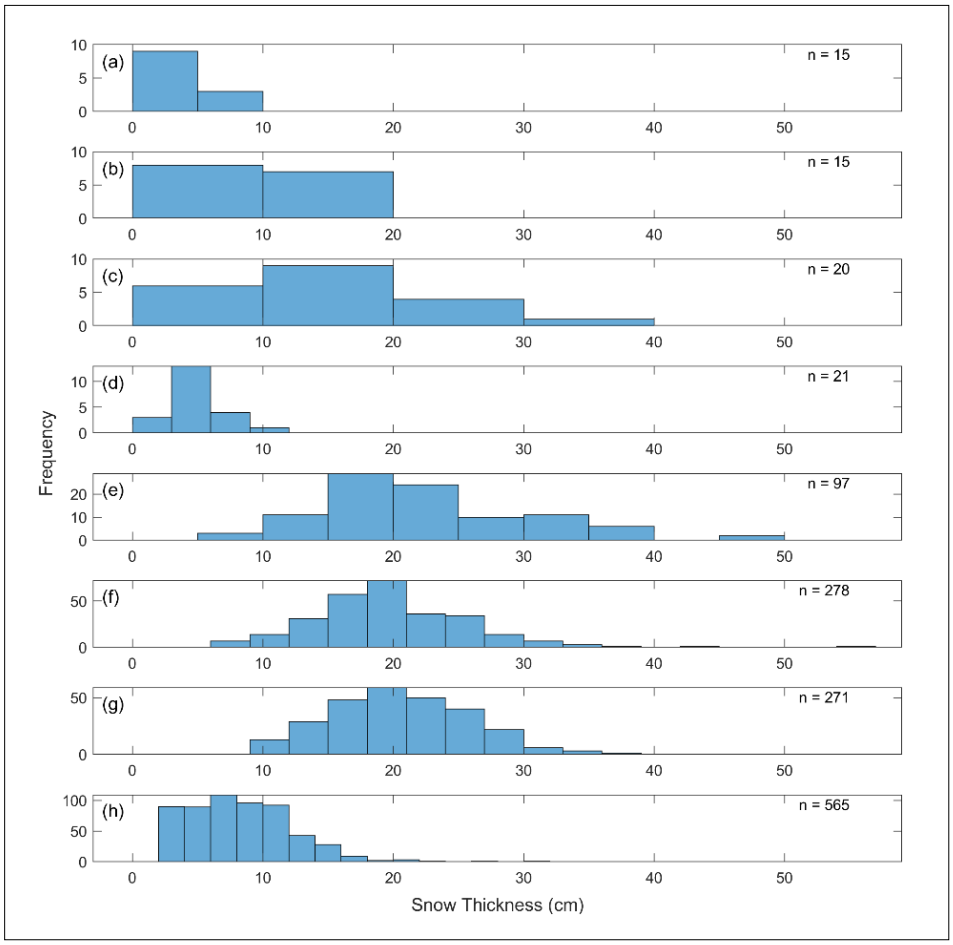

Fig. 5.1.12: Histogram of snow thickness measurements taken at the different ice stations. Panels (a) to (h) correspond to the stations listed in Table 5.1.5. On each penal the number of data points are shown by the value of n.

Tab. 5.1.6: Overview of samples collected at ice stations during PS144

Event Label	Date	Ice station	Samples collected	Comment
PS144_7_SnowCup	16.08.2024	1	15	12 snow samples 3 melt pond water samples
PS144_23_SnowCup	29.08.2024	2	15	15 snow samples
PS144_50_SnowCup	05.09.2024	4	21	20 snow samples 1 freshly falling snow
PS144_67_SnowCup	08.09.2024	5	21	21 snow samples
PS144_85_SnowCup	13.09.2024	7	21	20 snow samples 2 frost flower samples
PS144_109_SnowCup	19.09.2024	8	21	18 snow samples 6 lead water samples
PS144_123_SnowCup	23.09.2024	9	21	21 snow samples
PS144_134_SnowCup	25.09.2024	10	42	42 snow samples

Remote Access Sampler (RAS)

Mooring CAO2 (deployed on 31.08.2023 during PS138) was equipped with 2 RAS at roughly 43 m and 250 m depth. The RAS were programmed to collect seawater samples at weekly intervals for the measurement of dissolved nutrients in seawater and SUNA calibration (D. Scholz and S. Torres-Valdés), and for genetic analyses (K. Metfies, M. Wietz, C. BIenhold). One RAS only collected 60 mL samples; of this we subsampled 20 mL to take a single nutrient measurement. The other one collected the full 500 ml, but of 48 sample bags the last two were empty. An aliquot of 40 mL was taken from these samples before they were stored for transport back to AWI. Figure 5.1.13 shows one of the RAS packages being recovered.

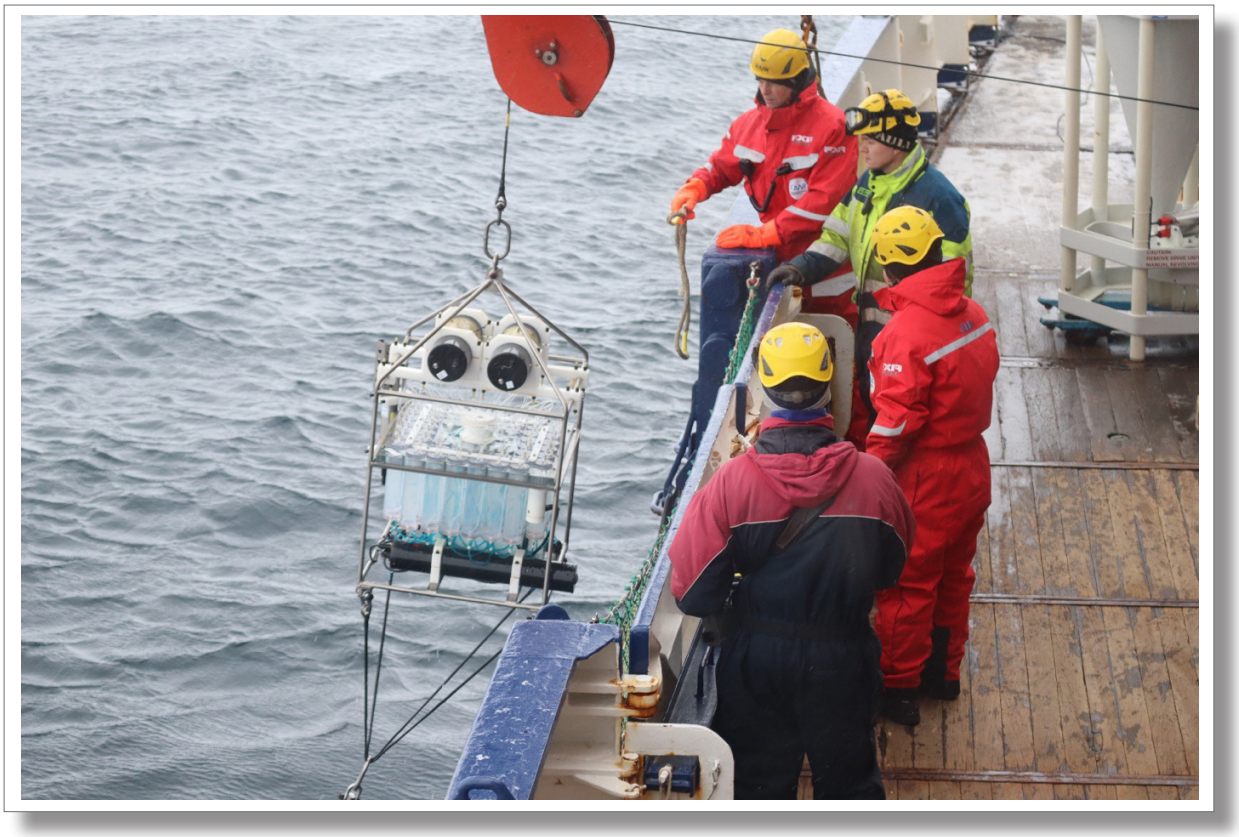

Fig. 5.1.13: Remote Access Sampler (RAS) recovered from mooring CAO02, deployed during PS138 in 2023. Visible are pH, pCO2, sample tubes, and a battery pack. Two RAS were deployed during PS138, one close to the surface (43 m) and another at about 250 m depth (approximately at the Atlantic Water core). The RAS close to the surface was equipped with the following sensors: PAR, EcoTriplet (backscatter, Chl-fluorescence, CDOM), CTD-O_2, SUNA-Nitrate, pH and pCO_2. The RAS at depth was equipped with a similar set of sensors, except PAR and EcoTriplet.

Problems encountered

Recurrent problems were mostly related to blockage of air lines, reagent lines and cadmium column lines. When identified soon, the problem was corrected, but there were multiple instances where samples for a given nutrient were affected. When this was the case, the remaining sample was reanalysed in the following run. We also experienced software crashes, where we needed to re-start the analysis. The autosampler failed a couple of times, also requiring restarting analysis. Two of the reagent valves of the analyser failed and were thus bypassed. These valves will need repair by the manufacturer at some stage once on back on

land. While simple to list the problems above, solving the issue requires hours of work and troubleshooting as sometimes identifying the problem requires diagnostic tests.

A final and surprising problem, was related to run-to-run noise, which was particularly high for the NO_3+NO_2 channel and PO_4 channel. As a result of these, data will need further quality control. If we cannot get it done before the expedition ends, it will take few months before the final QC data will be ready.

5.2 Dissolved oxygen

As for nutrients, samples were collected for the analysis of dissolved oxygen from CTD-Rosette casts from selected depths. We also aimed to have as best vertical resolution as possible. Dissolved oxygen was measured as an important biogeochemical variable linked to nutrient cycling and also in order to calibrate the CTD-O_2 sensors and to have reference values for the CTD-O_2 sensors attached to moorings. Whenever samples for helium and DIC were not collected, samples for dissolved oxygen were the first drawn from the Niskin bottles. Samples were collected using a tygon tube attached to the spigot of the Niskin bottles and placed directly into volume-calibrated borosilicate glass bottles with narrow necks. Care was taken to avoid bubbles inside the sampling tube and the sampling bottles. Water was left to spill over approximately three or more times the volume of the sampling bottle before the sample was drawn. A hand-held thermometer was used to measure the temperature of the seawater at the time of sample collection (i.e., fixing temperature) using a relatively fast-response temperature probe. Samples were immediately fixed by dispensing 1 mL of manganese chloride, followed by 1 mL of alkaline iodide, and then mixed thoroughly. When sampling was completed, the precipitate of the sample was let to settle to about a third of the volume (~1 hour). Then, samples were mixed thoroughly for a second time and the precipitate let to settle for a minimum of one hour more or until analysis. Analysis was carried out using a Metrohm Ti-Touch titration unit set up with the amperometric end point detection. Before analysis, 1 mL of 5 M sulphuric acid was added to a sample for titration. We followed the method and best practices procedures as described by Langdon (2010). All hydrographic stations were sampled. Samples were collected at the same vertical resolution as for nutrients, including two random duplicates.

Soon after laboratory set up, 1 L of thiosulphate solution (titrant) was prepared (50 g/L), as it takes one to two days to stabilise. Thiosulphate calibrations were carried out using 1.667 mM OSIL Scientific certified Iodate Standards. Calibrations are done by first measuring 5 blanks (involving 2 x 1 mL additions of iodate standard, each titrated one at a time) and then 5 standards (each with 10 mL of iodate standard). The first calibration was carried out 3 days after the thiosulphate solution was prepared. There on, calibrations were carried out approximately every 4 days, with a total of 10 calibrations carried out for the first thiosulfate solution and 5 for the second thiosulfate solution (Tab. 5.2.1) prepared during PS144. Every time a calibration was done; calculation sheets were updated with the blank and standard titration volumes. Thus, the concentrations of dissolved oxygen for a given number of CTD casts were calculated with the most recent calibration results. Provided calibrations are consistent with each other and show no trend which may suggest degradation of reagents, results from calibrations represent analytical ‘noise’, that is, the combination of human, reagents and titration unit error associated with each analysis.

We present the results from each calibration in Table 5.2.1 and Figure 5.2.1. Given there seemed to be no temporal trend, at the end of the expedition all calculation sheets were updated with the cruise-mean titration blank and standard volumes from the two batches of thiosulfate solution, and the dissolved oxygen concentration of all CTD casts sampled were thus recalculated. A comparison of profiles/data calculated from individual calibrations and from the cruise mean is presented in Figure 5.2.2. CTD profiles from station PS144_3-1 to

PS144_123-4 were analysed with the first thiosulfate solution. Stations PS144_125-1 to PS144_158-1 were analysed with the second thiosulfate solution.

As mentioned above, on every cast, a minimum of two randomly selected niskin bottles were sampled in duplicate to render confidence to single measurements. A total of 1084 samples were taken of which 99 (9.1%) were duplicates. The absolute difference between all duplicate samples taken during the expedition is shown in Figure 5.2.3. Absolute differences greater than 1µmol/L were considered outliers. The mean difference and standard deviation of all duplicates taken (n = 99) is 0.65 ±1.3 µmol/L, while without outliers (n=87) values are 0.32 ± 0.25 µmol/L.

The calibration carried out on the 20 August 2024 yielded anomalously high blank values. A repeat calibration on the 21 August 2024 did not reproduce these measurements so the values from the 8th calibration have been excluded from the calculation of the mean and standard deviation. It is not known what caused these higher blank measurements, but we think it was related to accumulation of small bubbles in the tubes dispensing thiosulphate and or iodate standard, from the electronic burettes into the bottles being titrated.

Tab. 5.2.1: Thiosulfate solution calibrations (titrations) done for the determination of dissolved oxygen. Blank (Blk), Standard (STD), STD minus Blk (STD-Blk) titration volume (mL), and calculated thiosulfate molarity.

	Calibration	Date	Blank (mL)	Standard (mL)	STD-Blk	Thiosulfate Molarity
Thiosulfate Batch 1	1	13.08.2024	0.0045	0.4988	0.4943	0.2024
	2	18.08.2024	0.0054	0.5017	0.4963	0.2015
	3	23.08.2024	0.0055	0.5038	0.4983	0.2007
	4	28.08.2024	0.0042	0.5007	0.4965	0.2015
	5	02.09.2024	0.0031	0.4990	0.4959	0.2017
	6	06.09.2024	0.0029	0.4998	0.4969	0.2013
	7	12.09.2024	0.0033	0.4985	0.4952	0.2020
	*8**	*20.09.2024*	*0.0100*	*0.5001*	*0.4901*	*0.2041*
	9	21.09.2024	0.0023	0.4977	0.4954	0.2019
	10	24.09.2024	0.0050	0.5000	0.4950	0.2021
	Average		**0.0040**	**0.5000**	**0.4960**	**0.2017**
	Standard deviation		**0.0012**	**0.0019**	**0.0012**	**0.0005**
Thiosulfate Batch 2	11	24.09.2024	0.0047	0.5055	0.5008	0.1997
	12	28.09.2024	0.0011	0.5010	0.4999	0.2001
	13	01.10.2024	0.0050	0.5030	0.4980	0.2008
	14	04.10.2024	0.0041	0.5017	0.4976	0.2010
	15	05.10.2024	0.0042	0.5027	0.4985	0.2006
	Average		**0.0038**	**0.5028**	**0.4990**	**0.2005**
	Standard deviation		**0.0016**	**0.0017**	**0.0013**	**0.0005**

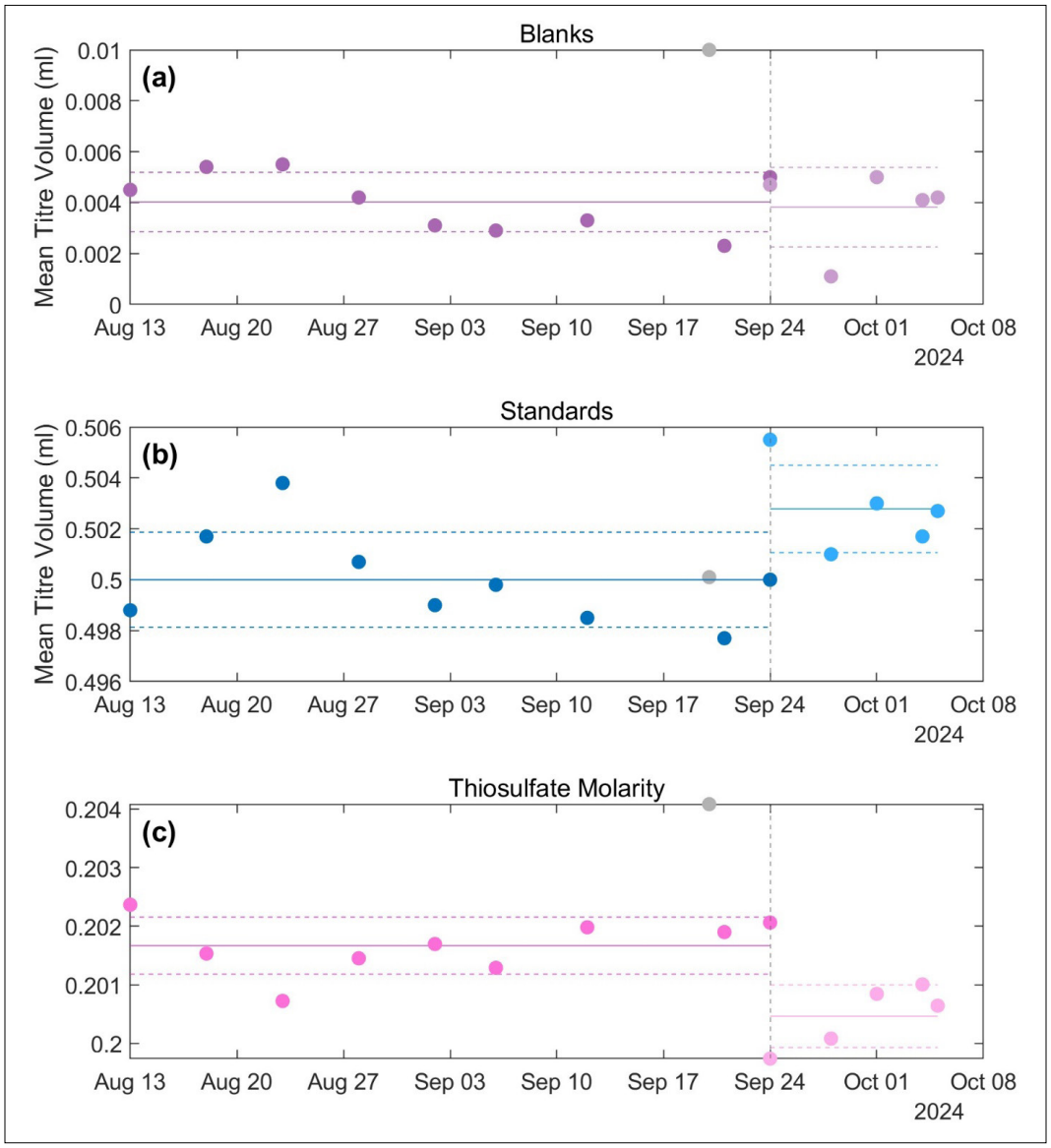

Fig. 5.2.1: Results from thiosulfate calibration carried out during PS144 for the determination of dissolved oxygen in seawater. The distribution of data over time does not show any significant trend that may suggest degradation/alteration of the reagents used. Solid and dashed horizontal lines show the mean and respective standard deviations, as indicated in the two bottom rows of Table 5.2.1. Vertical dashed line indicates swap from the first to second thiosulfate titre solution.

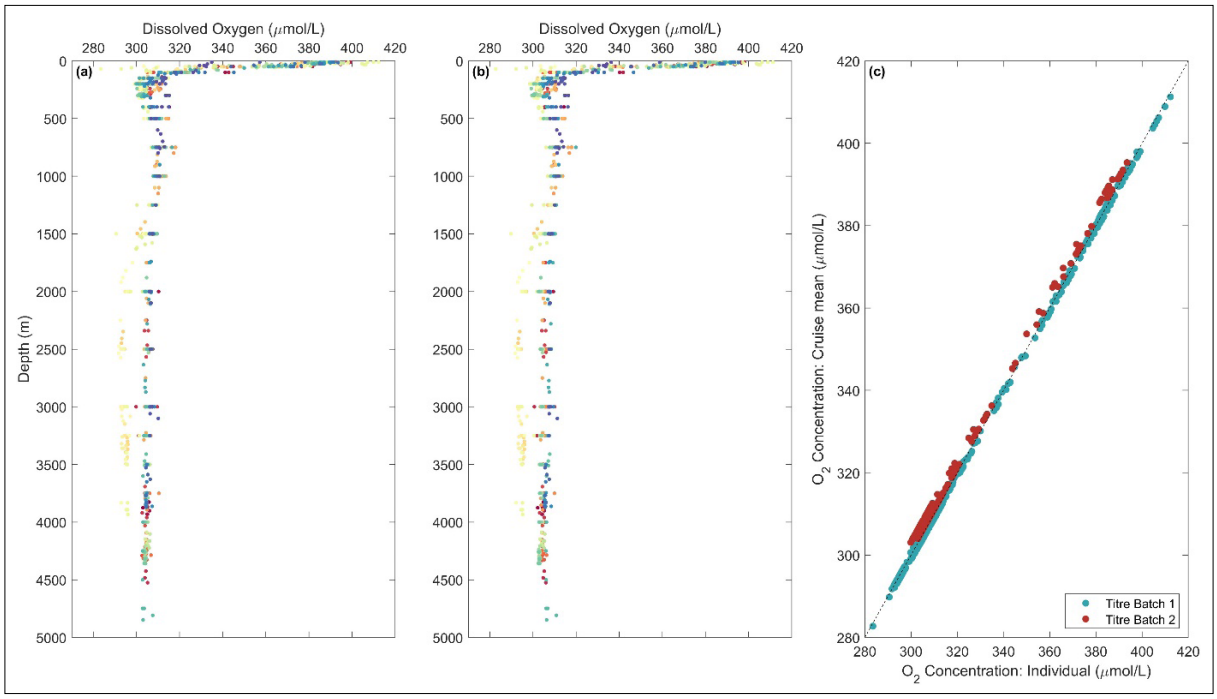

Fig. 5.2.2: (a) Dissolved oxygen profiles (data from all casts) as calculated with the respective calibration results (b) dissolved oxygen profiles (data from all casts) as calculated from the cruise-mean blank and standard titration volumes for the two thiosulfate batches. Colours represent individual casts. (c) Dissolved oxygen concentration measured with respective calibration results plotted against cruise mean. The black dotted line shows the 1:1 relation. Blue points correspond to first thiosulfate batch and red points are from the second titre batch.

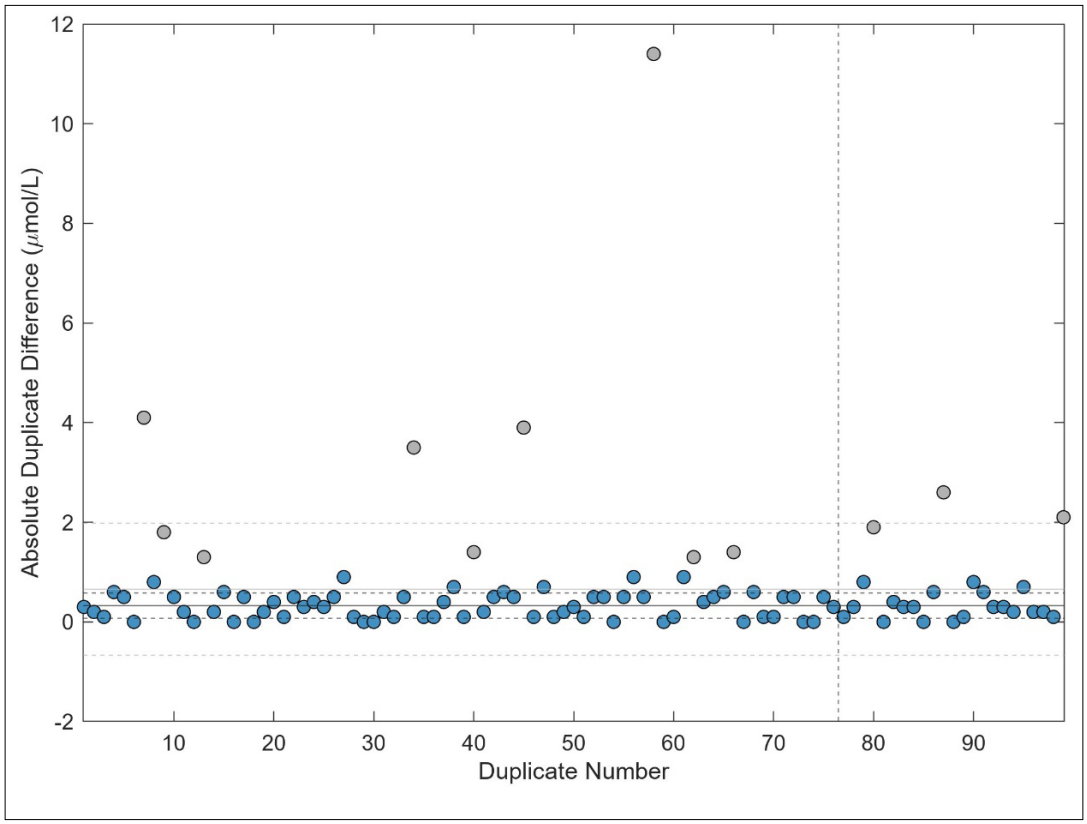

Fig. 5.2.3: Absolute difference between duplicate samples taken during PS144. Grey dots show outliers, here considered as difference between duplicates >1 μmol L^{-1}. Solid and dashed grey lines showed the mean difference of all duplicates taken (n=99; 0.65±1.3 μmol L^{-1}). Blue dots show the absolute difference of duplicates without outliers (<1 μmol/L). Solid and dashed black lines show the mean and standard deviation of the absolute difference between duplicates, without outliers 0.32 ± 0.25 µmol/L. Vertical dashed line indicates change from first to second thiosulfate solution.

5.3 Nitrogen Isotopes

A total of 929 water samples were obtained for stable isotope analyses of N and O of dissolved nitrate in the water column (upper, intermediate and deep-water column). Samples of 60 mL and 120 mL were taken at 46 CTD stations with 13 to 24 samples taken from each cast (alongside nutrients). All available depths were sampled and always included: Bottom, Bottom +20, Bottom +50, Atlantic water (AW), chromophoric dissolved organic matter (CDOM) max, chlorophyll (Chl) max, and surface backscatter maximum (SBM), when available. Stations and number of samples collected are listed in Table 5.3.1. When taking samples, an Acropak 500 filter was attached to the Niskin bottle, and left to flow for 10 to 20 seconds before rinsing a HDPE bottle thrice. Before sampling from the succeeding Niskin bottle, the previous sample water was drained by upturning the filter and unscrewing the valve. Samples were stored frozen at -20°C and will be shipped to the University of Edinburgh for analysis. An additional 2 sea ice brine samples were taken, but nutrient and salinity measurements indicated the liquid collected was not brine.

Station ID	No. Samples	Depth Range (m)	Longitude (deg)	Latitude (deg)
144_3-1	13	400.0 - 3876.0	29.806153	83.039262
144_7-4	20	12.0 - 3951.0	42.692052	85.054218
144_18-3	18	12.0 - 3960.0	111.442573	84.272552
144_20-2	22	12.0 - 2567.0	114.002882	84.444854
144_25-5	19	12.0 - 3794.0	115.787232	84.427868
144_26-1	19	12.0 - 4331.0	119.227729	84.659839
144_28-1	19	12.0 - 4326.0	121.902071	84.771044
144_31-1	19	12.0 - 4314.0	125.736793	84.847854
144_37-1	20	12.0 - 4286.0	129.656437	84.870021
144_46-3	19	12.0 - 4260.0	132.487222	84.912987
144_48-1	19	12.0 - 4192.0	135.959471	84.983955
144_50-5	19	12.0 - 3893.0	139.863824	85.024087
144_52-1	22	12.0 - 3285.0	142.927372	85.06451
144_54-1	18	12.0 - 2100.0	146.345478	85.087436
144_57-3	14	12.0 - 913.0	150.502043	85.084041
144_59-1	20	12.0 - 1496.0	153.749139	85.027372
144_64-1	17	12.0 - 2448.0	157.122581	84.969544
144_65-2	18	12.0 - 3367.0	159.043777	84.983672
144_67-7	22	12.0 - 3494.0	162.188041	84.932247
144_69-1	22	12.0 - 3437.0	165.784762	84.952761
144_73-4	18	13.0 - 3360.0	169.266762	84.948632
144_75-1	17	12.0 - 3723.0	172.703615	84.932694
144_77-1	22	12.0 - 2575.0	176.271108	84.919139
144_80-2	17	12.0 - 1919.0	179.555207	84.920654
144_85-6	21	11.0 - 3932.0	178.278467	87.48615
144_90-1	18	12.0 - 3497.0	-124.530915	88.366302
144_94-1	22	12.0 - 3933.0	-123.888731	88.683425
144_97-1	20	12.0 - 1619.0	-125.735801	89.011083
144_102-1	17	12.0 - 1631.0	-125.382363	89.334791
144_105-1	21	12.0 - 4188.0	-126.48511	89.661868
144_109-5	20	12.0 - 4203.0	-142.843007	89.950035
144_111-1	24	12.0 - 4264.0	59.726602	89.674836
144_113-1	23	12.0 - 4307.0	59.683275	89.350493
144_115-1	24	12.0 - 4336.0	59.450636	89.025424
144_118-1	24	12.0 - 4351.0	60.651107	88.699839
144_121-1	24	12.0 - 4357.0	60.160956	88.396842
144_123-4	23	12.0 - 4359.0	59.961268	88.064483
144_125-1	24	12.0 - 4320.0	60.059254	87.756732
144_127-1	21	12.0 - 3510.0	60.187613	87.430217
144_134-3	23	12.0 - 4848.0	58.47151	86.988225
144_138-1	23	12.0 - 2872.0	58.944794	86.744624
144_141-1	20	12.0 - 2705.0	59.926716	86.483724
144_144-2	24	12.0 - 3846.0	60.023064	86.169552
144_147-1	17	12.0 - 3863.0	59.811823	85.826778
144_149-1	24	12.0 - 8000.0	59.959155	85.516707
144_152-1	19	12.0 - 3869.0	59.718529	85.246457

Tab. 5.3.1 (left)**:**
A summary of all CTD casts where nitrate isotope samples were taken. The table shows station ID (equivalent to the Event Label without the leading “PS”), number of samples taken, the depth range for the samples taken, and the location.

5.4 Dissolved Organic Matter and Water Isotopes

Water samples and *in situ* fluorescence data were collected at approximately 50 hydrographic stations during PS144. From Each station, we collected 12 water samples for the analyses of dissolved organic carbon (DOC), optical properties (absorbance and fluorescence), and total dissolved lignin phenols (see DOM sample log in appendices). The *in situ* fluorometers were used at every station on both CTD units during the cruise. We used 2 different types of *in situ* fluorometers, the backscatter CDOM fluorometer of Dr. Haardt (excitation = 360 - 450nm, emission = 550nm) and the WetLabs CDOM fluorometer by Seabird (excitation = 370 nm, emission = 450 nm). For DOM we collected 1,250 mL for DOC (20 ml), optical properties (40 ml) and lignin phenols (1000 ml) from 12 depths at 50 stations. Samples for DOM were collected directly from the Niskin Bottles without filtration for depths below ~300m and samples above 300 m were filtered through precombusted glass fiber filters using Swinnex inline filter holders directly on the Niskin Bottles. Samples (1000 ml) for lignin phenols were extracted on PPL solid phase extraction (SPE) cartridges using a homemade SPE manifold on the ship. Samples for oxygen isotopes ($\delta^{18}O$) of water were collected from 16-24 depth levels per station. More specifically for water isotopes, we collected water samples for stable oxygen isotope analysis ($\delta^{18}O$) in parallel to CTD measurements and hydro-chemical parameters. Sampling focused on the halocline and the intermediate waters down to a depth of about 1,000 m. Sampling within the deep and bottom waters was conducted for a sub-selection of stations. Sampling was carried out along 2 sections (Section II and III) across the Transpolar Drift. A typical sample set from PS144 included the sampling depth levels at about: 12, 25, 50, 75, 100, 150, 200, 250, 300, 350, 400, 500, 600, 800, and 1,000 m. At selected stations further sampling down to the sea floor at additional depth levels: 1,250, 1,500, 1,750, 2,000, 2,250, 2,500, 3,000 m, to bottom depth, was included. We collected 50 mL of water for each $\delta^{18}O$ sample from the CTD-Rosette. Since $\delta^{18}O$ is measured on the oxygen of the H_2O itself, it is not a trace-element and its conservation is relatively easy. No poisoning of the water is necessary and some gas-exchange on a short time scale (e.g. bubbling while sampling) is of no harm. Tables 5.4.1 and 5.4.2 list all the samples collected during PS144, for organic matter variables and oxygen isotopes, respectively.

Identification and quantification of terrestrial dissolved organic matter (tDOM)

The work package aims at identifying and quantifying the contribution of terrestrial dissolved organic matter (tDOM) during ArcWatch 2. The results will be compared to previous similar efforts during the MOSAiC expedition (PS122, leg 1 to 5) and ArcWatch 1 (PS138). Together with the upcoming cruise ArcWatch 3, we will be able to evaluate a five-year time series, with the intention to detect interannual changes in tDOM, particularly in the transpolar drift (TPD).

We sampled original filtered seawater for the quantification of the bulk dissolved organic carbon concentration (DOC) and for the molecular DOM characterization by a new mass spectrometry method (Lechtenfeld et al., 2024). Fluorescent dissolved organic matter (Fluor) was sampled as an additional parameter that is suitable to track tDOM.

Sample collection and further analyses

At Transect III (85°N) every CTD was sampled at a high depth resolution, on Transect II (60°E) every fourth CTD was sampled for comparison to results from PS138. Additionally, the following segregated CTDs were sampled: 007-04 as a reference point outside the TPD, 011-02 to catch a Hydrothermal vent on the Gakkel ridge, 085-06 as an intercalibration as well as the North Pole 109-05 to verify data collected during PS138. The following CTD depths were chosen for sampling: bottom, bottom + 40 m, bottom + 100 m, 2000 m, 1000 m, 500 m, Atlantic water layer,

100 m, 50 m, CDOM max, Chl-max and surface (12 m) (Tab. 5.4.1). The higher resolution both at the bottom and in the upper 1000 m allowed a better examination of gradients.

Seawater samples were collected directly at the CTD-Rosette. Each sample was filtered through a HDPE inline filter connected that was connected with Teflon tubing to the Niskin bottles. Filters were pre-combusted (450° C, 5 h) glass fibre (Whatman, GFF, 42 mm diameter). Seawater samples were filled into pre-cleaned (10 % HCl acid bathing, subsequent ultrapure water rinsing) high-density polyethylene (HDPE) bottles (60 mL). To avoid absorption effects by the GFF filter and to rinse the HDPE bottle, the bottle was flushed with at least 200 mL of the respective sample before disconnecting it from the sampling device and closing it. The DOC sample was taken first, followed by the fluorescence samples using the same GFF filter. The tDOM sample (labelled as “DOM”) was taken as an aliquote from the Fluorescence sample in the chemistry lab of RV *Polarstern* under the fume hood (Tab. 5.4.2).

Additional samples from under the sea ice during ice stations were taken to analyse the Total Organic Carbon (TOC) content from the Surface Backscatter Maximum (SBM).

For quality control, at the stations 018-03, 026-01, 094-01, 125-01, 134-03 and 141-01 additional samples were not filtered to determine the TOC.

Blanks were taken as followed:

- Ultrapure water from *Polarstern* on different days for DOC, Fluor, DOM
- Ultrapure water brought from AWI on different days for DOC, Fluor, DOM
- Ultrapure water from *Polarstern* flushed through the sampling device equipped with a GFF filter on different days for DOC, Fluor, DOM
- Ultrapure water from *Polarstern* flushed through the sampling device not equipped with a GFF filter on different days for DOC, Fluor, DOM
- Ultrapure water from *Polarstern* filled in a previously rinsed 60 mL HDPE bottle and opened at the CTD sampling room for 20 seconds on different days for TOC and DOM
- SBM Blank following the complete sampling procedure with ultrapure water for TOC

The sampling device was pre-cleaned in a 10 % HCl acid bath and subsequently rinsed with ultrapure water in AWI laboratories before the expedition. It was thoroughly flushed with ultrapure water between the stations. For each depth, one sampling device was used for all sampled parameters. If the number of sample devices exceeded the number of sampling devices, the sampling device of depth 2000 m was taken repeatedly.

All samples were stored at -20°C until further analyses. DOC, Fluorescence and TOC measurements will be conducted at the AWI, Bremerhaven, Germany. tDOM analyses will be carried out at the Helmholtz Centre for Environmental Research (UFZ), Leipzig, Germany.

Anthropogenic contaminants

At ten selected stations that were equally distributed over the course of the expedition surface seawater (12 m water depth) was collected to track potential anthropogenic contaminants (EU project ONE-BLUE; Tab. 5.4.1, Tab. 5.4.2). This sampling is a follow-up of the efforts carried out during the expedition PS138 ‘ArcWatch 1’.

A volume of 1 L was directly collected from the Niskin bottle using the same inline filter sampling device as for DOC, Fluor and tDOM. Samples were collected in a pre-cleaned (10 % HCl acid bathing, subsequent ultrapure water rinsing) HDPE bottle and stored frozen at -20°C.

Tab. 5.4.1: For further information please see the end of this chapter.

Tab. 5.4.2: Number of samples taken for the different parameters.

Parameter	Number of samples
Dissolved organic carbon (DOC)	359
Fluorescence	358
Terrestrial dissolved organic matter (tDOM)	360
Total organic carbon (TOC)	18
Contaminants	10
Quality control	285

5.5 Preliminary results

Nutrients and dissolved oxygen

Due to multiple problems encountered during analysis throughout PS144, dissolved nutrient data will require further quality control. It is expected that this will be completed within 6-8 months after the expedition. As mentioned in the introduction, results from this expedition will be part of an AWI INSPIRES PhD project. It is expected that the selected candidate will work these data out as part of the training and data familiarisation process, and then will be used to address the scientific questions set out for this PhD project. Data will be eventually submitted to PANGAEA when fully quality controlled. Access will be granted to participants of the expedition upon request and agreement on data usage. Data will be made publicly available upon publication of research results.

Dissolved oxygen data is now fully quality controlled and shown above in the respective section. These data will be used to address scientific questions in combination with nutrient data, but also to calibrate the CTD sensors.

Nitrogen isotopes

We expect that horizontal advection from the Siberian shelves are essential to explain nutrient and isotopic distribution in the upper Central Arctic, specifically in Makarov and Amundsen basins. These basins are under the Transpolar Drift influence and are thus affected by riverine inputs and shelf denitrification occurring over the shelves. Despite increases in terrestrial inputs, we expect that riverine fixed N is predominantly lost on the shelves through denitrification and would have a limited role in alleviating N limitation in the upper Central Arctic.

Stable isotope analyses will be employed along with concentration parameters to better understand and quantify N cycling processes in the Arctic Ocean and its ongoing alterations as a result of climate change. Stable isotope analysis of nitrate will be carried out in the Wolfson's Mass Spectrometry Laboratory at the School of GeoSciences, University of Edinburgh, as part of the PhD of Marta Santos Garcia.

Stable isotope analyses from upper water column samples will be used to understand the role of various N cycling processes in determining N availability and the loss of nitrate in the N-limited Arctic Ocean. Nutrient stoichiometry and N isotope results we obtain from this cruise combined with previous measurements (TransARC II, 2015; MOSAiC, 2019/20; ArcWatch I, 2023) will help understand changes in nutrient limitation in the central Arctic under the influence of the Transpolar Drift.

To this end, nutrient imbalances in the Central Arctic will be explained through assessment of the influence of horizontal transport from the Siberian shelves (i.e., far-field processes) compared to vertical mixing and biological uptake (i.e., local processes). All processes will be evaluated using isotopic measurements and mathematical models which involve physical circulation. Specifically, a 1-D (vertical) model is developed using inverse and forward approaches to outline the processes required to explain the nutrient budgets observed in the Central Arctic. The modelling work is a result of an ongoing collaboration between the University of Edinburgh and Dr Olivier Marchal at Woods Hole Oceanographic Institution.

Stable isotope analyses from intermediate and deep-water column samples will be used – alongside nutrient stoichiometry and oxygen concentrations from three GEOTRACES cruises (2015, 2023 and 2024) - to investigate the factors influencing deep basin oxygenation and the fate of oxygenation in the deep Arctic basin. Specifically, the role of the Arctic shelf carbon pump modulating the deep Arctic oxygenation will be explored. We hypothesise that oxygen consumption is likely explained by remineralisation of organic matter (OM) laterally advected from the Siberian shelves as opposed to remineralisation of OM sourced from *in-situ* primary production. If, as proposed, most of the oxygen consumption in the Central Arctic is due to OM advected from the Siberian shelves, it is likely that oxygen concentrations will also decline in the future. This is because primary productivity in the Siberian shelves is currently increasing (Ardyna & Arrigo, 2020), hence leading to a higher export of OM and thus higher remineralisation in the Central Arctic. The significance of these results will focus on the potential mitigating effects on global warming as it involves the long-term carbon sequestration in the deep Arctic.

DOMAHAWK

Based on previous data (Amon et al., 2024) we used the *in-situ* fluorescence data to track the distribution of river water/shelf water and the halocline layers in the central Arctic Ocean. The fluorescence signal shown in Figures 5.5.1 and 5.5.2 helped guide sampling efforts for our group but also many other groups on board. Based on *in situ* fluorescence we selected sampling depths for the other DOM parameters and for water isotopes. With the newly developed method for lignin phenols, a specific biomarker for terrigenous DOM, we collected the first high resolution sample set, allowing to better constrain the distribution of river organics, halocline formation and freshwater source identification. In addition, this PS144 data set can be compared to previous efforts in 2005, 2007 and 2015 and allows to observe changes over the past 20 years.

The figures below show the distribution of *in situ* fluorescence in the upper 400 m on section 3, closer to the Eurasian shelf and on section 2, crossing the North Pole, during this expedition. Both sections indicate the prominent feature of the Transpolar Drift extending for about 350 km from the surface to about 100m depth. Most of the fluorescence signal comes from river dissolved organic matter but some of the fluorescence signal derives from shelf sediment. These different “vintages” of Chromophoric Dissolved Organic Matter (CDOM) will be characterized using the lignin phenol analysis done at TAMU. A glimpse of other CDOM sources, in addition to river DOM, can be seen by the Apparent Oxygen Utilization (AOU) plot below (Figure 5.4.1 b). AOU is always elevated in the upper halocline of the Canada Basin as a result of organic matter decomposition and the intrusion of upper halocline waters on the North American side of the sections is obvious (Willifort et al., 2021, 2022). This very obvious signal is not as strong in the Eurasian basins, but we were still able to observe smaller AOU peaks along with elevated CDOM at many stations near the bottom of the CDOM signal. One open question is the nature of the deep intrusion of Canada Basin water into the Makarov Basin seen during this expedition. Previous years have shown an extension of the TPD all the way to the Alpha Ridge and it is conceivable that the TPD continues further to the North American continent and that we were inside a mesoscale eddy or some other isolated intrusion

of Canada Basin water at the beginning of section 2. Further analysis of optical and biomarker samples will facilitate the interpretation of these results. Comparison to previous years will allow a deeper understanding of changes over the last 20 years. Did the density of halocline layers change, did the contribution of river DOM to the halocline change? Did the relationship between CDOM, lignin and oxygen isotopes change? These questions will be answered after this large sample set has been analysed in the laboratory and results have been integrated with hydrographic information and other tracers determined by colleagues on expedition PS 144.

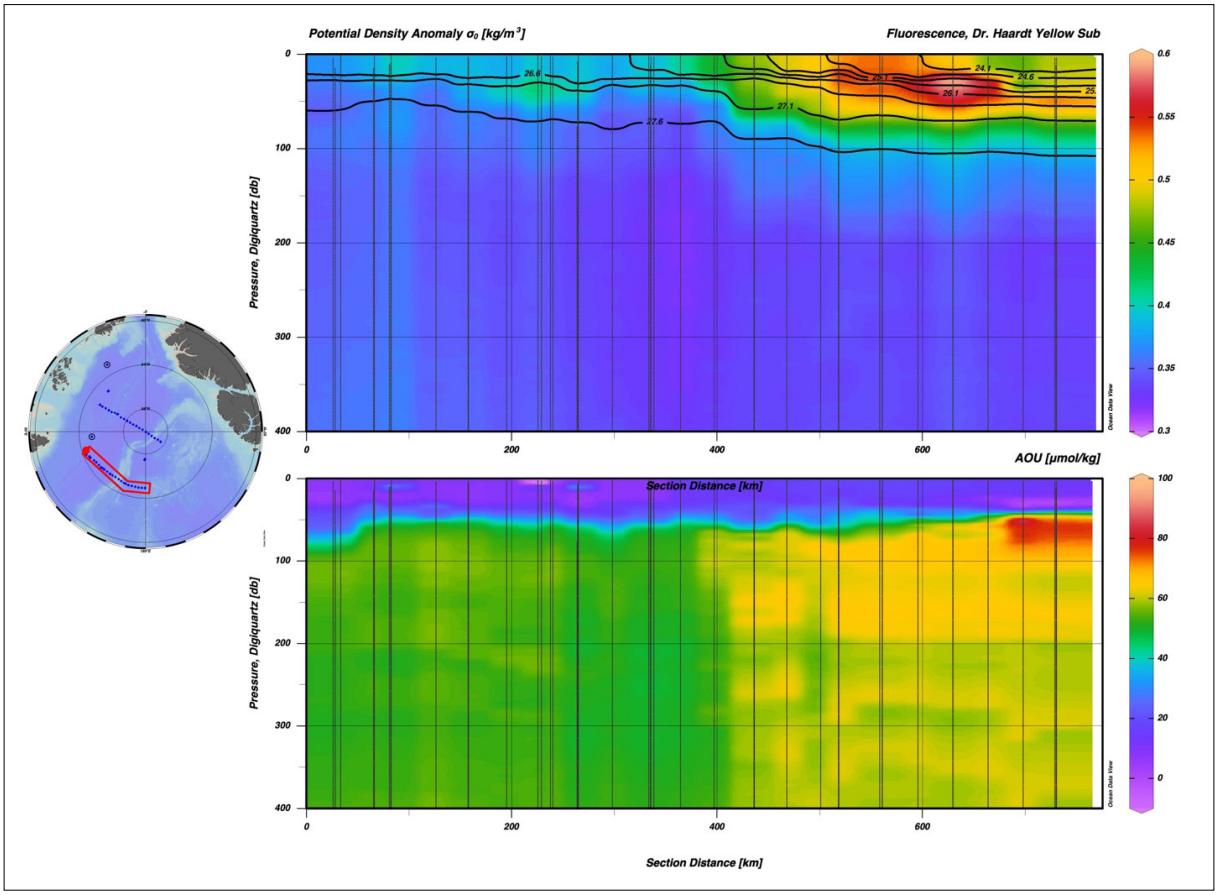

Fig. 5.5.1: (a) Top panel shows the in-situ backscatter fluorescence of CDOM (excitation 350-460 nm, emission 550 nm) along a section roughly parallel to 85°N stretching from the Gakkel Ridge (111°E) to the Mendeleev Ridge (180°E). The lower panel (b) shows the distribution of Apparent Oxygen Utilization on the same section.

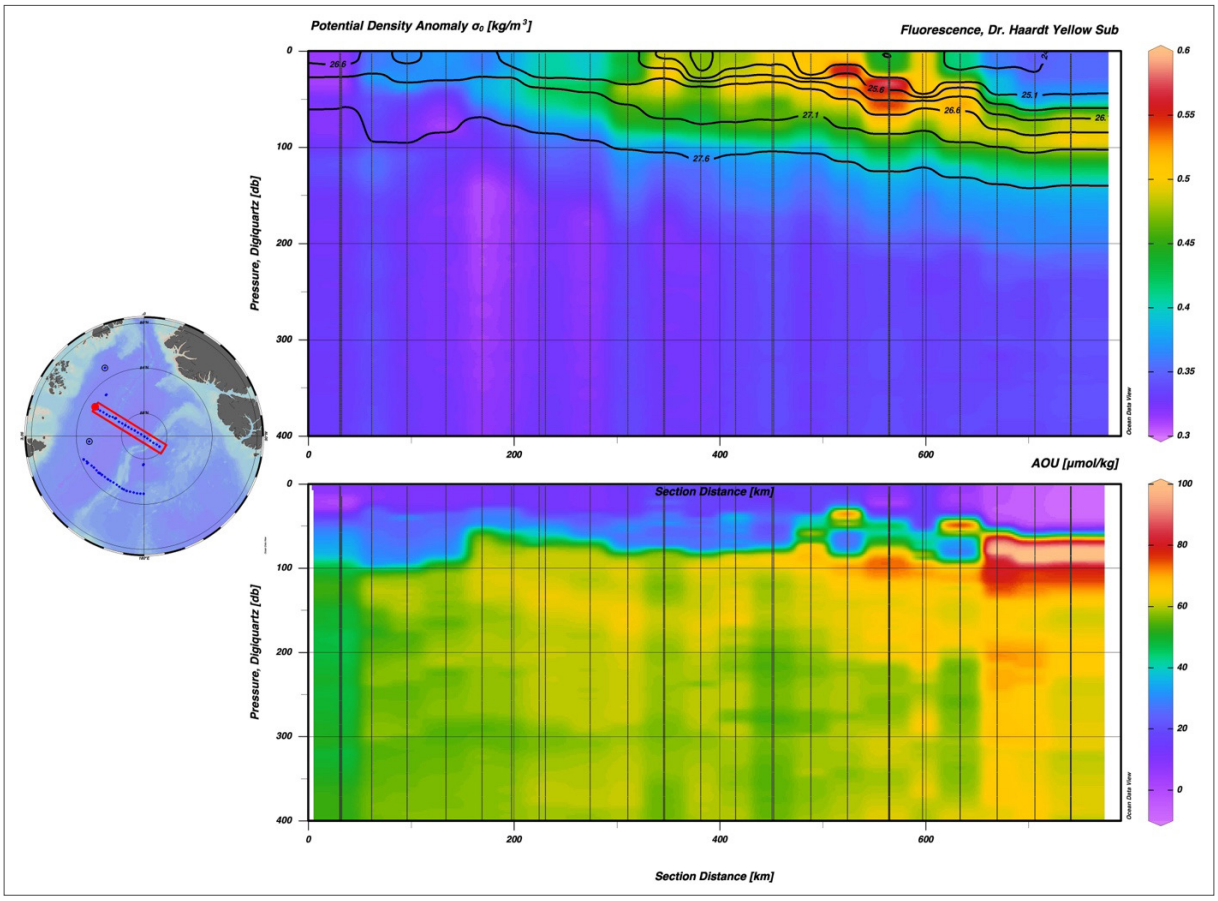

Fig. 5.5.2: Top panel shows the in-situ backscatter fluorescence of CDOM (excitation 350-460 nm, emission 550 nm) along a section crossing over the North Pole stretching from the Gakkel Ridge to the centre of the Makarov Basin. The lower panel shows the distribution of Apparent Oxygen Utilization on the same section.

For water isotopes specifically, samples will be transported to Kiel. Analysis will be conducted at the Leibniz Laboratory at Kiel University, Kiel, Germany and partly at the Stable Isotope Facility at CEOAS at Oregon State University, Oregon, USA. We will facilitate stable oxygen isotopes ($\delta^{18}O$) in a mass balance calculation together with salinity and hydro-chemical constituents to quantify freshwater fractions i.e. river water and sea-ice melt or formation. The water mass fractions will be compared to constituents such as carbon, nutrients and TE. This will allow to investigate the fate of e.g. the terrestrial carbon components but will also deliver additional information on the local freezing cycles. We hypothesize that during freezing events river water may be largely stripped of dissolved components. Comparison of expected versus observed concentrations of river derived constituent will allow to derive semi-quantitative information on refreezing effects. From previous investigations in the Central Arctic Ocean e.g. in summer 2007, 2015 and 2019/20 we know that there is spatial and temporal variation of freshwater distribution within the Arctic Ocean halocline on an interannual and seasonal timescale (Bauch et al., 2011; Paffrath et al., 2021; Bauch et al., in prep). Investigations within the TPD as covered by PS144 allow to capture (i) the transported signal from the Siberian shelves in which the local sea-ice modification of constituents is expected to be relatively low due to a relatively

short mean residence time (Schlosser et al., 1994) and (ii) the gradient between the TPD towards the Canadian side in which local sea-ice modification of river derived constituents is expected to be relatively strong due to considerably longer mean residence times (Schlosser et al., 1994; Charette et al., 2020; Pasqualini, 2021). In addition, the project will estimate the rate of local versus advected sea-ice signal within different parts of the TPD.

The results will provide further understanding of the impact of sea-ice processes on the structure of the Arctic halocline and the TPD. Understanding sea-ice processes in the TPD has a wide impact as these precondition Arctic surface waters to become incorporated in North Atlantic Deep Water at downstream convection sites. DOM parameters will be determined at Texas A&M University.

Terrestrial Dissolved Organic Matter (tDOM)

Using the recent mass spectrometry method in combination with 3D fluorescence analyses, we expect to identify molecular formulas that are particularly indicative for tDOM. Since the mass spectrometry method yields near quantitative results, we will acquire estimates for the concentration of terrestrial dissolved organic carbon in the water samples. In combination with the results of the previous cruises and an available collection of DOC concentration values, this will allow to establish a Central Arctic Ocean tDOM inventory.

Data management

Environmental data will be archived, published and disseminated according to international standards by the World Data Center PANGAEA Data Publisher for Earth & Environmental Science (https://www.pangaea.de) within two years after the end of the expedition at the latest. By default, the CC-BY license will be applied.

In situ fluorescence will be part of the CTD data set released by the physical oceanography group.

In addition, all DOM and $\delta^{18}O$ data and metadata will be submitted to the Arctic Data Center and the international GEOTRACES data management office (BODC, www.bodc.ac.uk/geotraces) under the data management scheme agreed upon in the GEOTRACES programme available at http://www.geotraces.org.

Any other data will be submitted to an appropriate long-term archive that provides unique and stable identifiers for the datasets and allows open online access to the data.

This expedition was supported by the Helmholtz Research Programme “Changing Earth – Sustaining our Future” Topics 2 and Topic 6, Subtopic 2.1 and Subtopic 6.3.

In all publications based on this expedition, the **Grant No. AWI_ PS144_04** will be quoted and the following publication will be cited:

Alfred-Wegener-Institut Helmholtz-Zentrum für Polar- und Meeresforschung (2017) Polar Research and Supply Vessel POLARSTERN Operated by the Alfred-Wegener-Institute. Journal of large-scale research facilities, 3, A119. http://dx.doi.org/10.17815/jlsrf-3-163.

References

Amon RMW, Kaiser K, Engel A (2024) Dissolved organic matter in the Arctic Ocean. In: Biogeochemistry of Marine Dissolved Organic Matter, 3rd edition. Elsevier (in press).

Ardyna M, Arrigo KR (2020) Phytoplankton dynamics in a changing Arctic Ocean. Nat. Clim. Chang. 10: 892–903. https://doi.org/10.1038/s41558-020-0905-y

Bauch D, Schlosser P, Fairbanks RF (1995) Freshwater balance and the sources of deep and bottom waters in the Arctic Ocean inferred from the distribution of $H_2{}^{18}O$. Progress in Oceanography 35:53-80.

Bauch D, Rutgers van der Loeff M, Andersen N, Torres-Valdes S, Bakker K and Abrahamsen EP (2011) Origin of freshwater and polynya water in the Arctic Ocean halocline in summer 2007. Progress in Oceanography 482-495. doi:10.1016/j.pocean.2011.1007.1017.

Becker S, Aoyama M, Woodward EMS, Coverly S, Mahaffey C, Tanhua T (2020) GO-SHIP Repeat Hydrography Nutrient Manual: the precise and accurate determination of dissolved inorganic nutrients in seawater, using continuos flow analysis methods. Frontiers in Marine Science 7:581790. https://doi.org/10.3389/fmars.2020.581790

Charette MA, Kipp LE, Jensen LT, Dabrowski JS, Whitmore LM, Fitzsimmons JN, Williford T, Ulfsbo A, Jones E, Bundy RM, Vivancos S, Pahnke K, John SG, Xiang Y, Hatta M, Petrova MV, Heimbürger-Boavida L, Bauch D, Newton R, Pasqualini A, Agather AM, Amon RMW, Anderson RF, Andersson PS, Benner R, Bowman KL, Edwards RL, Gdaniec S, Gerringa LJA, Aridane G, González, Granskog M, Haley B, Hammerschmidt CR, Hansell DA, Henderson PB, Kadko DC, Kaiser K, Laan P, Lam PJ, Lamborg CH, Levier M, Li X, Margolin AR, Measures C, Middag R, Millero FJ, Moore WS, Paffrath R, Planquette H, Rabe B, Reader H, Rember R, Rijkenberg MJA, Roy-Barman M, Rutgers van der Loeff M, Saito M, Schauer U, Schlosser P, Sherrell RM, Shiller AM, Slagter H, Sonke JE, Stedmon C, Woosley RJ, Valk O, van Ooijen J, Zhang R (2020) The Transpolar Drift as a source of riverine and shelf-derived trace elements to the central Arctic Ocean. Journal of Geophysical Research: Oceans 125(5):e2019JC015920.-

Chang BX, Devol A H (2009) Seasonal and spatial patterns of sedimentary denitrification rates in the Chukchi Sea. Deep Sea Research Part II: Topical Studies in Oceanography 56(17):339–1350. https://10.1016/j.dsr2.2008.10.024

Codispoti LA, Kelly V, Thessen A, Matrai P, Suttles S, Hill V, ... , Light B (2013) Synthesis of primary production in the Arctic Ocean: III. Nitrate and phosphate based estimates of net community production. Progress in Oceanography, 110:126–150. https://doi.org/10.1016/j.pocean.2012.11.006

Debyser M C, Pichevin L, Tuerena R E, Dodd P A, Doncila A, Ganeshram R S (2022) Tracing the role of Arctic shelf processes in Si and N cycling and export through the Fram Strait: Insights from combined silicon and nitrate isotopes. Biogeosciences, 19(23):5499–5520. https://doi.org/10.5194/bg-19-5499-2022

Fripiat F, Declercq M, Sapart C J, Anderson L G, Brüchert V, Deman F, ..., Dehairs F (2018) Influence of the bordering shelves on nutrient distribution in the Arctic halocline inferred from water column nitrate isotopes. Limnology and Oceanography 63(5):2154–2170. https://doi.org/10.1002/lno.10930

Hydes D, Aoyama M, Aminot A, Bakker K, Becker S (2010) Recommendations for the determination of nutrients in seawater to high levels of precision and inter-comparability using continuous flow auotoanalysers. The GO-SHIP repeat hydrography manual: a collection of expert reports and guidelines.

Langdon C (2010) Determination of dissolved oxygen in seawater by Winkler titration using the amperometric technique. The GO-SHIP Repeat Hydrography Manual: A Collection of Expert Reports and Guidelines. IOCCP Report No. 14, ICPO Publication Series No. 134.

Lechtenfeld O J, Kaesler J, Jennings E K, & Koch B P (2024). Direct analysis of marine dissolved organic matter using LC-FT-ICR MS. Environmental Science & Technology 58(10):4637–4647. https://doi.org/10.1021/acs.est.3c07219

Lewis K M, Van Dijken G L, Arrigo K R (2020) Changes in phytoplankton concentration now drive increased Arctic Ocean primary production. Science 369(6500):198–202. https://doi.org/10.1126/science.aay8380

Paffrath R, Lauker G, Bauch D, Rutgers van der Loeff M, & Pahnke K (2021) Separating individual contributions of major Siberian rivers in the Transpolar Drift of the Arctic Ocean. Scientific Reports 11(1):8216. https://doi.org/10.1038/s41598-021-86948-y

Pasqualini A (2021) Circulation pathways, time scales, and water mass composition in the Arctic Ocean: Results from 25 years of tracer observations. Columbia University.

Schlosser P, Bauch D, Bönisch G, Fairbanks RF (1994) Arctic river-runoff: mean residence time on the shelves and in the halocline. Deep-Sea Research I 41:1053–1068.

Sigman DM & Casciotti K L (2001) Nitrogen isotopes in the ocean. Encyclopedia of ocean sciences 3: 1884–1894. https://doi.org/10.1016/B978-012374473-9.00632-9

Slagter H A, Reader H E, Rijkenberg M J A, Van Der Loeff M R, de Baar H J W & Gerringa L J A (2017) Organic Fe speciation in the Eurasian Basins of the Arctic Ocean and its relation to terrestrial DOM. Marine Chemistry 197:11–25.

Slagter H A, Laglera LM, Sukekava C, Gerringa LJ, 2019. Fe-binding organic ligands in the humic-rich Trans Polar drift in the surface Arctic Ocean using multiple voltammetric methods. J. Geophys. Res. Oceans 124(3):1491–1508.

Torres-Valdés S, Tsubouchi T, Bacon S, Naveira-Garabato A C, Sanders R, McLaughlin F A , Whitledge T E (2013) Export of nutrients from the Arctic Ocean. Journal of Geophysical Research: Oceans 118(4): 1625–1644. https://doi.org/10.1002/jgrc.20063

Williford T, Amon R M W, Benner R, Kaiser K, Bauch D, Stedmon C, ... & Klunder M B. (2021) Insights into the origins, molecular characteristics and distribution of iron-binding ligands in the Arctic Ocean. Marine Chemistry 103936.

Williford T, Amon RMW, Kaiser K, Benner R, Stedmon C, Bauch D, Jessica N, Loes F, Gerringa JA, Newton R, Hansell DA, Granskog MA, Jensen L, Laglera LM, Pasqualini A, Rabe B, Reader H, Rutgers van der Loeff M, & Yan G (2022) Spatial complexity in dissolved organic matter and trace elements driven by hydrography and freshwater input across the Arctic Ocean during 2015 Arctic GEOTRACES expeditions. Journal of Geophysical Research: Oceans 127:e2022JC018917.

Yamamoto-Kawai M, Carmack E, McLaughlin F (2006) Nitrogen balance and Arctic throughflow. Nature 443(7107):43–43. https://doi.org/10.1038/443043a

Tab. 5.1.2.a: Cruise-mean, standard deviation and precision (%) of all calibration standards (Std). Concentration units are µmol L^{-1}.

Standard Number	$NO_3^-+NO_2^-$		NO_2^-		$Si(OH)_4$	
	Mean and Standard Deviation (µmol/L)	Precision (%)	Mean and Standard Deviation (µmol/L)	Precision (%)	Mean and Standard Deviation (µmol/L)	Precision (%)
1	0.555±0.045	8.10	0.018±0.003	13.9	0.367±0.025	6.9
2	6.141±0.036	0.60	0.225±0.003	1.2	5.293±0.022	0.4
3	11.872±0.058	0.50	0.432±0.004	1.0	10.202±0.072	0.7
4	17.706±0.076	0.40	0.644±0.003	0.4	15.093±0.039	0.3
5	23.476±0.101	0.40	0.853±0.004	0.4	19.892±0.049	0.2

Tab. 5.1.2.b: (Continued) Cruise-mean, standard deviation and precision (%) of all calibration standards (Std). Concentration units are µmol L^{-1}.

Standard Number	PO_4^{3-}		NH_4+		TN		TP	
	Mean and Standard Deviation (µmol/L)	Precision (%)	Mean and Standard Deviation (µmol/L)	Precision (%)	Mean and Standard Deviation (µmol/L)	Precision (%)	Mean and Standard Deviation (µmol/L)	Precision (%)
1	0.105±0.007	7	0.019±0.018	98.4	0.490±0.037	7.6	0.108±0.009	8.0
2	1.405±0.007	0.5	0.804±0.021	2.6	6.991±0.041	0.6	1.401±0.006	0.5
3	2.706±0.011	0.4	1.539±0.022	1.5	13.497±0.048	0.4	2.704±0.014	0.5
4	4.015±0.016	0.4	2.254±0.026	1.1	19.985±0.070	0.3	4.016±0.020	0.5
5	5.302±0.020	0.4	2.906±0.027	0.9	26.309±0.094	0.4	5.302±0.022	0.4

Tab. 5.4.1: Parameters and their associated sampled depths at each station, here equivalent to the Event label without the leading “PS144_”.

Station-Cast	Date	Lat [deg]	Long [deg]	Parameter	Sampled Depths [m]
007-04	16.08.2024	85.054218	42.692052	DOC, Fluor, DOM	3951, 3931, 3901, 2000, 1000, 500, 140, 100, 48, 20, 12
007-07	17.08.2024	85.049895	42.349853	DOC, Fluor, DOM	200, 30
011-02	20.08.2024	85.117298	95.378609	DOC, Fluor, DOM	4525, 4483, 4425, 4001, 3250, 2000, 1001, 500, 100, 50, 27, 12
018-01	28.08.2024	84.270833	110.689692	Contaminants	12
018-03	28.08.2024	84.272552	111.442573	DOC, Fluor, DOM, TOC	3960, 3920, 2000, 1000, 500, 285, 100, 20, 32, 12
020-02	29.08.2024	84.454446	113.930319	DOC, Fluor, DOM	2567, 2526, 2466, 2001, 1000, 500, 99, 48, 12
023-01	29.08.2024	84.507698	115.398806	TOC	26
023-05	30.08.2024	84.427868	115.787232	DOC, Fluor, DOM, Contaminants	3794, 3750, 3692, 2003, 1003, 501, 275, 100, 30, 25, 12
026-01	31.08.2024	84.659839	119.227729	DOC, Fluor, DOM, TOC	4331, 4289, 4230, 2002, 1001, 230, 500, 100, 24.6, 20, 12
028-01	31.08.2024	84.771044	121.902071	DOC, Fluor, DOM	4326, 4286, 4226, 2000, 1000, 500 (no Fluor), 280, 100, 30, 20, 12
031-01	01.09.2024	84.847854	125.736793	DOC, Fluor, DOM	4314, 4274, 4212, 2000, 1002, 500, 279, 201, 50, 39, 24, 12
037-01	02.09.2024	84.870021	129.656437	DOC, Fluor, DOM	4286, 4247, 4186, 2001, 1003, 500, 270, 100, 60, 40, 25, 12
046-03	04.09.2024	84.912987	132.487222	DOC, Fluor, DOM	4260, 4220, 4160, 2000, 1001, 500, 242, 100, 49, 35, 12
048-01	04.09.2024	84.983955	135.959471	DOC, Fluor, DOM	4192, 4152, 4092, 2000, 1000, 500, 240, 100, 49, 30, 12
050-01	04.09.2024	85.032701	139.446069	TOC	25
050-05	05.09.2024	85.024087	139.863824	DOC, Fluor, DOM	3893, 3853, 3793, 2000, 1000, 500, 250, 100, 55, 50, 27, 12
050-09	05.09.2024	85.023579	140.083771	Contaminants	12
052-01	06.09.2024	85.064510	142.927372	DOC, Fluor, DOM	3285, 3226, 2000, 1000, 500, 254, 100, 50, 28, 20, 12
054-01	06.09.2024	85.087436	146.345478	DOC, Fluor, DOM	2100, 2060, 2000, 1000, 500, 232, 100, 50, 25, 18, 12
057-03	07.09.2024	85.084041	150.502043	DOC, Fluor, DOM, Contaminants	913, 873, 813, 500, 222, 100, 60, 50, 30, 19, 12
059-01	07.09.2024	85.027372	153.749139	DOC, Fluor, DOM	1497, 1457, 1397, 1000, 500, 100, 50, 35, 22, 12
064-01	07.09.2024	84.969544	157.122581	DOC, Fluor, DOM	2448, 2408, 2348, 2000, 1000, 500, 252, 100, 50, 35, 25, 12
065-02	08.09.2024	84.983672	159.043777	DOC, Fluor, DOM	3367, 3327, 3267, 2000, 1000, 500, 224, 100, 50, 25, 22, 12
067-01	08.09.2024	84.946387	161.903856	TOC	25
067-07	08.09.2024	84.932247	162.188041	DOC, Fluor, DOM	3494, 3454, 3394, 2000, 1000, 500, 220, 100, 50, 28, 23, 12
069-01	09.09.2024	84.952761	165.784762	DOC, Fluor, DOM	3437, 3397, 3337, 2000, 1000, 500, 220, 100, 50, 30, 20, 12
073-04	09.09.2024	84.948632	169.266762	DOC, Fluor, DOM	3360, 3320, 3260, 2000, 1000, 500, 225, 100, 50, 28, 13, 12
075-01	10.09.2024	84.932694	172.703615	DOC, Fluor, DOM	3123, 3083, 3023, 2001, 1000, 500, 227, 100, 50, 31, 23, 12
077-01	10.09.2024	84.919139	176.271108	DOC, Fluor, DOM	2575, 2535, 2475, 2000, 1000, 500, 240, 100, 50, 26, 24, 12
080-01	10.09.2024	84.922594	179.577229	TOC	23

Station-Cast	Date	Lat [deg]	Long [deg]	Parameter	Sampled Depths [m]
080-02	11.09.2024	84.920654	179.555207	DOC, Fluor, DOM, Contaminants	1919, 1879, 1819, 1000, 500, 224, 100, 18, 12
085-01	12.09.2024	87.515029	179.097150	TOC	27
085-06	13.09.2024	87.486150	178.278467	DOC, Fluor, DOM	3932, 3892, 3832, 2000, 1000, 500, 405, 200, 100, 50, 29, 20, 11, 12
085-08	14.09.2024	87.463849	177.906714	Contaminants	12
094-01	16.09.2024	88.683425	-123.888731	DOC, Fluor, DOM, TOC	3933, 3893, 3833, 2000, 1000, 500, 441, 100, 90, 70, 50, 12
109-01	19.09.2024	89.944844	-150.666993	TOC	21
109-05	19.09.2024	89.950035	-142.843007	DOC, Fluor, DOM, Contaminants	4203, 4163, 4103, 2000, 1000, 500, 256, 100, 50, 32, 20, 12
118-01	22.09.2024	88.699839	60.651107	DOC, Fluor, DOM	4203, 4163, 4103, 2000, 1000, 500, 256, 100, 50, 32, 20, 12
125-01	24.09.2024	87.756732	60.059254	DOC, Fluor, DOM, TOC	4320, 4280, 4220, 2000, 1000, 500, 307, 100, 50, 35, 13, 12
134-01	25.09.2024	86.981690	58.673999	TOC	28
134-03	25.09.2024	86.988225	58.471510	DOC, Fluor, DOM, TOC	4848, 4808, 4748, 2000, 1000, 500, 310, 100, 50, 40, 24, 12
134-06	26.09.2024	87.040338	57.330179	Contaminants	12
141-01	28.09.2024	86.485727	59.785296	DOC, Fluor, DOM, TOC	2109, 2065, 2009, 2000, 1000, 500, 311, 100, 50, 40, 20, 12
141-03	28.09.2024	86.492032	59.495372	Contaminants	12
152-01	30.09.2024	85.246457	59.718529	Contaminants	12

6. SEA-ICE AND ATMOSPHERIC PHYSICS

Niklas Neckel[1], Janna Rückert[2], Thomas Kordes[1], Nils Risse[3], Jonathan Bahlmann[4], Linnea Bühler[3], Jonathan Kolar[2], Mario Mech[3], Sunke Trace-Kleeberg[5]
not on board: Thomas Krumpen[1], Kerstin Ebell[3], Sabrina Schnitt[3], Christine Eis[6], Gunnar Spreen[2], Marcel Nicolaus[1]

[1]DE.AWI
[2]DE.IUP
[3]DE.UNI-KOELN
[4]DE.DRIFT-NOISE
[5]UK.UNI-SOUTHAMPTON-SOES
[6]DE.ZETEM

Grant-No. AWI_PS144_05

Outline

The sea-ice and atmospheric physics program of ArcWatch-2 is composed of a standard sea-ice measuring program and two secondary-use projects. The standard sea-ice measuring program included numerous ice thickness and snow measurements acquired by helicopter and ice-based surveys, assistance for other groups working on the ice and gathering general information on sea ice from satellite data and from the bridge for nautical and scientific personal. Water vapor, properties of mixed-phase clouds, and microwave surface emissivities were measured and analyzed as part of the secondary-use project *Water Vapor, Mixed-Phase Clouds, and Sea Ice Emissivity over the Central Arctic Ocean* (VAMPIRE, see Sections 6.4 and 6.5). Dedicated Unmanned Aerial Vehicle (UAV) operations for ice navigation and for measuring sea ice related parameters were carried out as part of the secondary-use project *Drone and AI-based image solutions foR sciEnce and iCe navigaTion* (DIRECT).

Objectives

By reflecting most of the incoming solar radiation, sea ice keeps the Arctic Ocean cold and its decline has significant effects on the local and global climate. Therefore, one of the main objectives of ArcWatch-2 (PS144) was to closely monitor sea ice characteristic parameters and to extend time series from previous expeditions. A special focus of PS144 was on incorporating Unmanned Aerial Vehicle (UAV) systems in the sea ice measuring program and to test how drones can be used for more efficient ice navigation and survey planning. Also, *in situ* measurements to improve satellite retrievals of water vapor were conducted and new satellite-based tools and techniques for ice navigation were evaluated under real conditions. The sea ice measurements were complemented by atmospheric observations conducted by the VAMPIRE project, focusing on the essential climate variables water vapor and (mixed-phase) clouds. More specifically, our objectives can be divided into three sub-topics, contributing to (i) an improved understanding of the sea ice (Section 6.1, Section 6.3, and Section 6.4), (ii) supporting new ideas for ice navigation (Section 6.2), and (iii) the Arctic atmosphere and its interaction with sea ice (Section 6.5).

Monitoring of sea ice characteristic parameters

The results of ArcWatch-2 contribute to our Arctic-wide sea-ice thickness monitoring program performed from vessels and aircraft. In particular we compare our results to the ice thickness distribution and ice history evaluated during ArcWatch-1 (PS138, 2023), as both expeditions

sampled similar regions in the central Arctic at a similar time of the year. However, further comparisons will also include work with data from the International Arctic Buoy Program (IABP) and include the MOSAiC drift (Nicolaus et al., 2022) and aircraft campaigns (e.g., IceBird, Belter et al., 2021). During the cruise, we extensively measured the ice thickness distribution by helicopter accompanied by *in situ* measurements at higher spatial resolution when on ice station. In addition, instruments were deployed to cover seasonal mass balance parameters.

A special focus of ArcWatch-2 was on the implementation of drone-based measurements for sea ice surveys. In particular we conducted UAV based laser scans and implemented automated grid flights over drifting sea ice. From these data we can now draw conclusions about surface roughness (i.e., ridge frequency), ice thickness, melt pond distribution and their volumes. Furthermore, we evaluated the potential of state-of-the-art drone systems for ice navigational purposes which showed very promising results. We also show the potential of drones to directly plan, realize and optimize scientific operations and measurements in sea ice covered areas.

Synthetic Aperture Radar based ice navigation

Being able to accurately and safely navigate ice covered waters is the foundation for all kinds of polar marine operations. In addition to close-proximity ice monitoring from the ship, satellite radar imagery (Synthetic Aperture Radar, SAR) has developed into the most promising tool to identify potentially navigable open leads and impassable ice ridges even beyond the vessel's detection reach. While SAR images provide high spatial resolution and reliable images even during cloudy conditions and night-time, their coarse temporal resolution does not account for the dynamic nature of drifting sea ice, which can move up to several kilometers per day. The initial satellite image becomes outdated rather quickly. Ice motion taking place between consecutive satellite acquisitions remains unknown and can only be estimated once the new image arrives. To overcome the data gap between consecutive images, we tested two novel algorithms that produce drift-corrected SAR imagery. Sea ice drift data from various on-board sources was applied such that the temporal limits and spatial accuracy of both the algorithms and the various data products could be determined. Additionally, the drift-corrected SAR imagery was discussed with the nautical crew on board such that expectations and requirements for an operational product could be worked out. Secondly and as part of the ongoing FastCast-2 research project (https://bmdv.bund.de/SharedDocs/DE/Artikel/DG/mfund-projekte/fast-cast2.html) we tested AI-based optimized route suggestions under real-world conditions. Here, optimized routes are calculated using SAR imagery as well as sea ice drift forecast models. They provide valuable route estimates that go beyond the visual/radar range available to the nautical crew on board with the goal to make it easier for navigators to identify and choose safer, faster and more fuel-efficient pathways through the ice. During PS144 we shared the FastCast-2 route suggestions with the nautical crew for a qualified evaluation and followed some of them in order to test them and to learn more about the factors that build trust in these machine-generated routes. The details of this work are outlined in Section 6.2.

Surface emissivity in the microwave spectrum

Here we want to determine the spatio-temporal variability of microwave (MW) emissivity of sea ice in the Marginal Ice Zone (MIZ) and the pack ice in the central Arctic. Further we want to assess the accuracy of models, databases, and satellite retrievals in representing the MW emissivity measurements. Finally, we aim to evaluate the impact of surface condition-induced variability in surface emissivity on MWR satellite retrievals of IWV. Here, we measured the surface signal with two microwave radiometer along the vessel's track, covering satellites' footprint scales (Section 6.5) and performed sea ice and snow *in situ* observations within the radiometer footprint during ice stations (Section 6.4).

Water vapor in the summertime central Arctic

Here we aim to understand the spatio-temporal variability of summertime Integrated Water Vapor (IWV) and of the water vapor profile in the central Arctic region. Further we want to find answers on how surface conditions, i.e., open ocean, MIZ and sea ice drive the atmospheric water vapor content and its vertical distribution. Another research question is if we can identify a surface dependency or if the coupling to the surface is rather masked by large-scale transport mechanisms of water vapor. During PS144, we measured water vapor by microwave radiometers and additional radiosondes (Section 6.5).

Properties of Arctic mixed-phase clouds

This objective relates to the spatio-temporal variability of the liquid water path (LWP) of summertime Arctic clouds in the central Arctic. Further we want to better understand the processes that regulate the formation, properties, precipitation, and lifetime of Arctic clouds, in particular mixed-phase clouds and the properties of their supercooled liquid layers. Here, our main instruments that we deployed for this purpose were two cloud radars, complemented by precipitation and wind measurements, see Section 6.5.

6.1 Routine sea-ice observations and remote sensing

Work at sea

General ice conditions and Ice Watch

To create a continuous record of the sea ice conditions, all participants on the cruise conducted standardized visual observations from the ship's bridge, aiming for one observation every hour when the ship was not stationed. However, not all shifts were covered. In total, there were 287 observations out of a possible 1250 during the time spent in the ice (excluding station time), representing about 23% of the available observation time. The observations began when *Polarstern* approached the ice on 13 August 2024, and continued until the ship departed from the ice on 4 October 2024. The observations followed the standardized protocol of the *Ice Watch* program (https://icewatch.met.no/assist). The ASSIST software tool, a Java application, was installed on a notebook on the bridge, with version 4.1 used for data recording. A Canon Powershot GT-X camera was employed to capture three photographs per observation. Guidance from the Ice Watch Manual (Hutchings et al., 2018) and the World Meteorological Organization (WMO) sea ice nomenclature (WMO, 1989) assisted in conducting the observations. ASSIST can record 110 different parameters for each observation describing the conditions within a radius of 1.5 nautical miles around the vessel; however, only a limited set is consistently recorded: time, location, total ice concentration, ice types, ice thickness, floe size and meteorological conditions. Additional details, such as snow cover, ice topography, melt state, and other observations, were included when applicable.

Panorama camera

Fig. 6.1: Example image of Panomax camera acquired on 25 August 2024 06:15:00 UTC.

We operated a panorama camera (type Panomax, PS144_0_Underway-8, see Fig. 6.1) above the crow's nest during the entire expedition, taking regular photographs of the sea ice and weather conditions in 5 min intervals. The first photo was taken on 12 August 2024 19:00 UTC and the last photo on 7 October 2024 08:10 UTC (total 13.353 photos). The photos were available in the intranet on board for the entire cruise and frequently used for example by the DWD weather forecaster.

SAR

To ensure a safe and efficient navigation in the ice-covered polar waters, satellite data from multiple sources were available on this cruise. One to two daily images from the X-Band SAR satellite TerraSAR-X were ordered via the German Aerospace Center (DLR) in Bremen and made available in the MapViewer automatically. Additionally, to the standard data aboard *Polarstern*, namely C-Band data from Sentinel-1 and the Radarsat Constellation Mission (RCM), 14 additional scenes from the X-Band SAR Constellation of Small Satellites for Mediterranean basin Observation (Cosmo SkyMed) were ordered via the Italian Space Agency under the project card Polafstern144.

Backtracking

For certain locations along the cruise track the origin of the investigated ice is of particular interest. Therefore, we provided backward trajectories of the ice for all ice stations and certain other regions of interest (e.g. areas of (e.g. areas of Surface Under Ice Trawl (SUIT) application).

Preliminary results

These routine observations primarily serve as supplementary material for the other datasets and provide an overview of the changing ice conditions as the ship was travelling. Ice Watch observations, panorama images and satellite data can be used after the cruise to derive sea-ice conditions along track and to support improvements of satellite algorithms for different ice properties such as melt pond fractions, floe sizes or snow cover. Figure 6.2 shows a map of all Ice Watch sea ice thickness observations of the primary (i.e., the thickest) ice type observed during PS144. The map reflects the high variability of ice conditions that we encountered: low ice thickness and high open water fractions were observed at different times and locations during the cruise. The satellite data that were available on board also revealed low ice concentrations on the transit towards transect II. On the other hand, thick multi-year ice (confirmed by the backtracking analysis) was observed as well, e.g., towards the end of transect II. Overall, the ice thickness distribution agrees well with the ones obtained from electromagnetic induction sounding during helicopter survey (Section 6.3) and ice stations (Section 6.4).

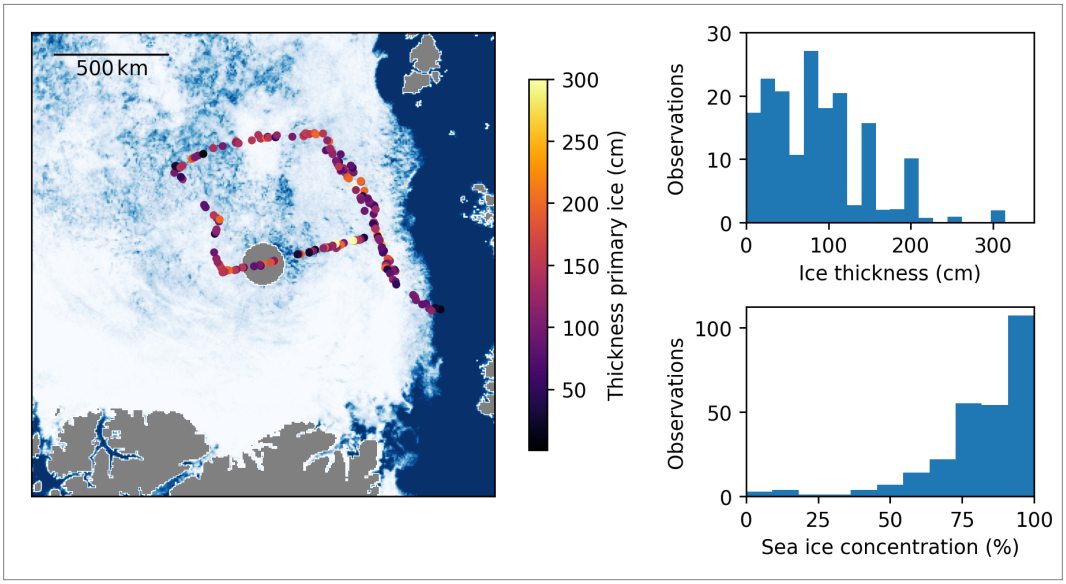

Fig. 6.2: Left panel: Thickness of primary (thickest) sea ice along the cruise track. Upper right panel: Distribution of ice thickness of primary, secondary and tertiary ice weighed by the respective concentration. Lower right panel: Distribution of observed total sea ice concentration

6.2 Ice navigation

Work at Sea

Drift-Corrected SAR Imagery

As part of the project „real-time drift correction for efficient navigation on *Polarstern*“ (EDEN), a computer program for displacing SAR imagery was prepared on land. The EDEN software was significantly improved and adapted to the data available on board of *Polarstern* during the cruise. Different possible sources for the derivation of sea-ice drift were investigated, implemented, tested and evaluated. Along with a framework for trying different methods and sources during the expedition, an entirely automatic workflow to display drifted imagery on the bridge (via the on-board map viewing system MapViewer) was established in close collaboration with the ship's system administrator Andreas Winter. The general architecture of that infrastructure is detailed in Figure 6.3. With a virtual machine that runs the EDEN code on board of *Polarstern*, imagery is automatically processed and made available to the MapViewer around the clock. The displaced SAR imagery is displayed in a newly added layer called “Drifted”. The quality of the drift correction as well as the visualization on the bridge was discussed with the nautical officers. Secondly, the Destination Earth project “DESIDE” allowed us to test ice drift and wind model data in order to displace an image. Manually, an algorithm to warp images was employed which considers not only a single but many drift trajectories over the area of the satellite scene. It was evaluated whether this way certain advantages or disadvantages arose over displacing the images only according to a simple translation.

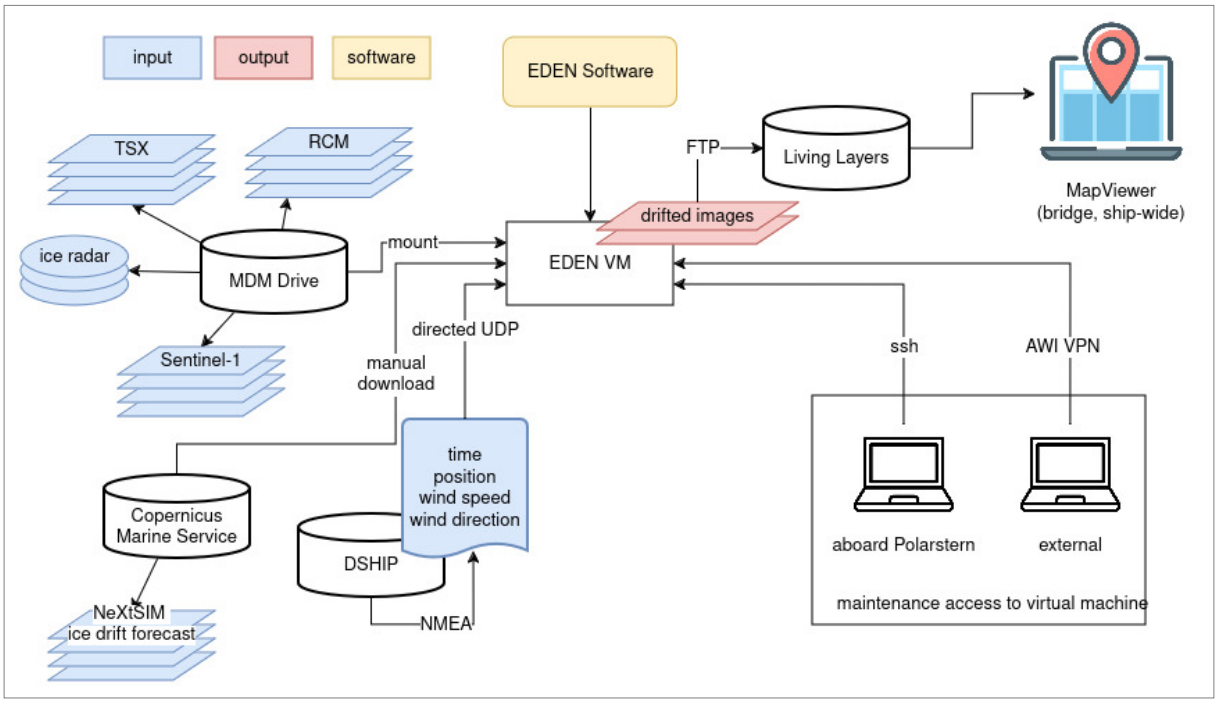

Fig. 6.3: EDEN infrastructure and data flow via the MapViewer to display the drift-corrected SAR imagery directly on the bridge of Polarstern. Input data as well as external access to the VM are outlined.

Route Optimization

The FASTCAST-II routing algorithm is able to use Sentinel-1 classified SAR imagery as it's main input. As the satellite constellation does not regularly take data over the planned research area, a region of extended Sentinel-1 coverage was organized via ESA previous to the routing test. As soon as this area was reached at a latitude of 87.5°N, station plan coordinates along with progress estimates were communicated to Christine Eis at the University of Bremen, who then provided the ice-drift-forecasted classifications, an optimized route through the ice, and an animation detailing the route progress against the progressing ice drift. On board, the classification and route data were then printed in an overview map for presentation on the bridge, as can be seen in Figure 6.4. Overall, six optimized routes between scientific waypoints and three routes between nautical waypoints were discussed on the bridge between 24.09.2024 and 02.10.2024. During these discussions, the overview route maps along with relevant ice information such as recent SAR images and ice radar images were considered. Two of the routes were evaluated as feasible and then followed with the ship by manually extracting route waypoints and entering them into the ship's Electronic Chart Display and Information System (ECDIS). For evaluating a route as feasible for navigation, the route had to be verified with a recent SAR image from the TerraSAR-X satellite. Nautical officers were approached with the principle to only navigate a route if it made sense in their professional opinion. Therefore, no route was navigated for scientific purposes only. Table 6.1 details all of the discussed routes. The second column "observation type" notes one of three possible scenarios. Some routes were discussed and dismissed without further observations ("discussion"), while other times, the actual navigation after a route discussion was observed ("observation"). The two routes that were navigated are denoted with "navigation". For all routes respective notes were taken directly onto the printed map, detailing the comments and decisions made by the nautical officers. On occasion, further material like more detailed notes, screenshots and photographs are provided.

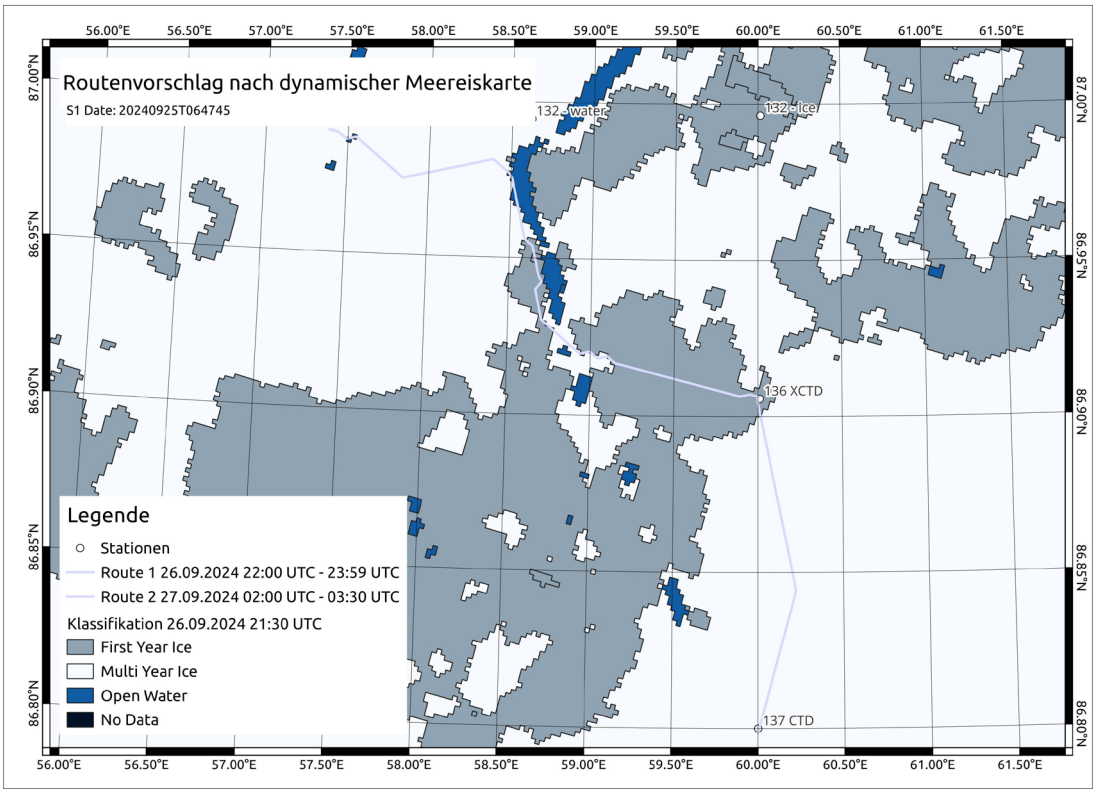

Fig. 6.4: Example of a map showing a classified Sentinel-1 image and an optimized route (in two parts) to the scientific station number 137

Tab. 6.1: Overview of FASTCAST II route optimization instances

#	Obs. Type	Date	Est. time of travel	Actual time of travel*	Distance	Classified Satellite Image	Comment
1	Observation	24.09.2024	2:45	4:45	6.3	S1 22.09.2024	d, dep
2	Discussion	27.09.2024	2:45	5:54	9.8	S1 25.09.2024	d, sta
3	Observation	27.09.2024	3:13	2:30	7.9	S1 25.09.2024	d, stp, dep
4	Discussion	27.09.2024	9	3:45	16.5	S1 25.09.2024	d
5	Observation	28.09.2024		6:18	12.8	S1 28.09.2024	s
6	Navigation	29.09.2024	4	3:40	9.1	S1 28.09.2024	d
7	Discussion	01.10.2024		20	45.8	S1 01.10.2024	s
8	Observation	01.10.2024	9:30	10	20	TSX 01.10.2024	d
9	Navigation	02.10.2024	36	14:06	69.9	S1 01.10.2024	d

* actual time of travel is calculated by the point of closest approach of the ship's GPS track to the originally planned route coordinates and may contain station work time

d dynamic route calculation (considering ice drift)

s static route calculation (considering only a single classified image)

stp start position changed

dep destination position changed during route

sta start time changed, route out of date

Drone based sea ice exploration

To ensure safe and efficient navigation of the vessel through the ice, regular ice reconnaissance flights are carried out by helicopter, e.g. to find open water areas in the ice to travel. This allows higher speeds during transfer trips, resulting in more ship time at stations and less fuel consumption on the way.

One question is whether drones can make a contribution to ice exploration and what conditions need to be created for effective use. A DJI Matrice 350 RTK multicopter platform was selected as a test system. As payload we selected the DJI H20T camera, which records both RGB and thermal infrared (TIR) data. The following two approaches were tested for navigational purposes:

Near-real time mapping in the Mapviewer system

In this scenario, the drone took off from the helicopter deck and climbed to the highest possible altitude in the vicinity of the ship. Nadir and oblique photos were taken, with oblique photos covering a 360° roundshot with a certain amount of overlap. The photos were downloaded to the controller (DJI RC Plus), which was connected to the vessels's Wi-Fi, during the flight. The image data were then transferred to the ship's network system via an FTP client installed on the controller. Prior to the cruise we developed a workflow to directly orthorectify the images using the positional and orientational data of the drone resulting in an orthorectified image for each data take, finally this could be read into Werum's customized Mapviewer software.

Integration of the drone's live image into the ship's video system

A different setup was used for this method. In addition to the main controller, which was employed for controlling the drone, a second controller was used to receive the live video stream of the drone. This controller was positioned inside the observation corridor and connected to external antennas mounted on the observation deck. The live video was send via HDMI output from the controller to a converter, which generated a video signal that could be fed into the vessel's system. This video signal could then be displayed on any monitor connected with a video switch (Kreuzschiene).

In addition to the work required to implement the above scenarios, a DJI Cloud Service was installed on a virtual machine on board. After some adjustments, it is now possible, to import the drone's live position data into the DShip system and display the drone track in the Mapviewer system.

Preliminary results

Drift-Corrected SAR Imagery

As expected, the data sources can be differentiated by certain trade-offs. While the wind data on board is available at the location of the ship around the clock, buoy data is strongly limited to the immediate vicinity of a couple nautical miles around the buoy location. However the latter is on average far more precise than the previous. Though it has to be noted that during the second transect of the expedition, wind-derived ice drift matched the real-world situation down to a hundred meters, which is about the visual threshold on what is perceived as an "exact match" on a map. Ice drift derived from the ice radar images showed some promising possibilities, yet the technique has to be further investigated to improve results. The wind as well as ice drift model data seemed to catch the general ice drift movements of an area but failed to achieve the same accuracy as buoy or (sometimes) wind-derived drift. Overall, the more basic image translation was found sufficient to display the drift-corrected SAR images. While the image

warping could potentially be beneficial in cases of inconsistent ice movements, this comes at the cost of image distortions, for example blurry patches, which can obstruct a clear view of the data. The usage uptake of the new “Drifted” layer (example in Fig. 6.5) was very good, with all nautical officers using the layer regularly by the end of the cruise. We’ve also received very positive feedback from the scientists involved in planning activities depending on the current ice situation. A major feedback was that the experimental layer came about a bit overloaded with different imagery, and that in times of hectic navigational efforts, the most relevant and up-to-date scene was hard to find. This can be improved upon during the further course of the project.

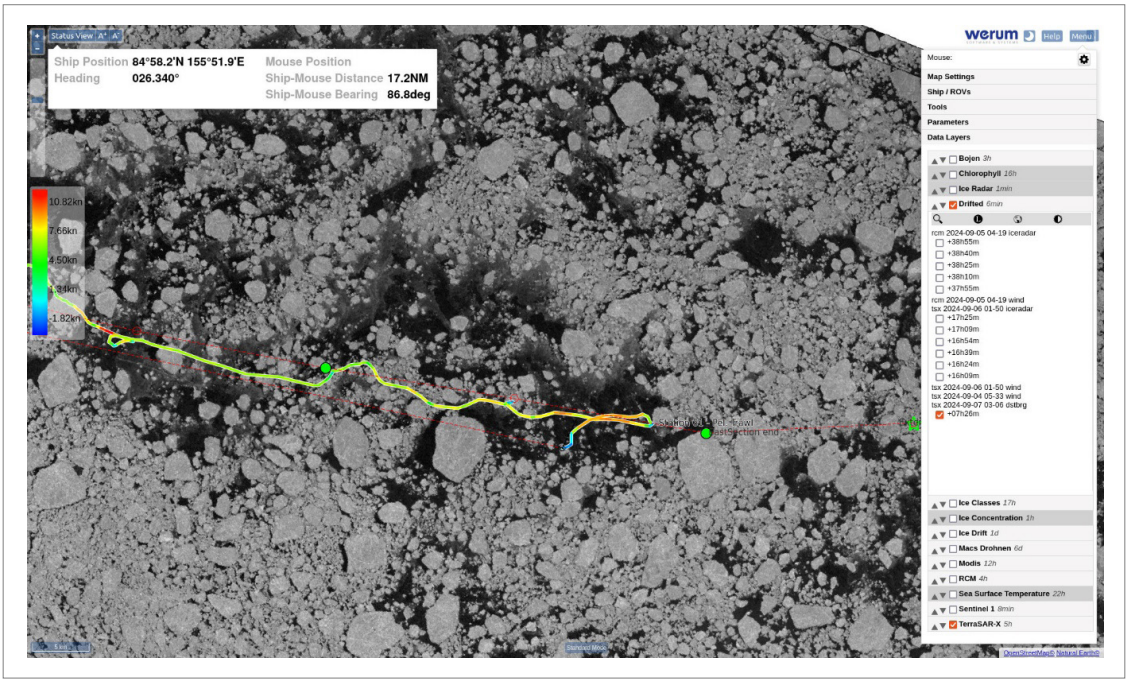

Fig. 6.5: Example scene from the new „Drifted“ layer in the MapViewer.
The figure shows a scene from the German TerraSAR-X satellite (via DLR), corrected for 7.5 hours since its acquisition to illustrate the ice drift.

Route Optimization

Optimized routes were calculated for nearly 200 nautical miles, of which 79 nm were actually travelled along route waypoints. Only when nautical officers were able to see that the displayed route could be followed all the way through to the next waypoint by taking into account a recent high-resolution SAR image, the navigation was initialized. The main factor hindering the navigation of routes was the presence of open leads only visible in said high resolution imagery. Those leads were often missing from the Sentinel-1-based classifications and could thus not be considered in the route calculations. Secondary factors were changes in the planned itinerary (route start or destination coordinates, route start time), and a mismatch in the forecasted sea-ice drift. All those factors either meant the route was not applicable anymore or was seen as a significant detour. Both cases where a route was deemed navigable and was followed via ECDIS waypoints, the routes received positive feedback by the nautical officers. The waypoints were said to be a good orientation while officers were busy with the immediate tactical navigation and ship steering in complicated situations. However, a mismatch was noticed in the information available to the nautical officers and to the routing algorithm. While officers take into account all information they can read from a SAR image like the size,

density and position of smaller and larger ice floes, possible gaps between them, the ridge density as well as the suggested smoothness indicating thinner ice and connect that larger scale information to the smaller scale ice radar display, the routing algorithms sole input is the classified ice age over multiple time steps. While in some situations this might be the critical factor, it often is not. This gap can lessen the confidence into the route, as it has not based on all relevant factors.

Near-real time display of orthorectified drone images in the Mapviewer system

Figure 6.6 shows the result of the method described above for displaying individual images in the Mapviewer system. In this example the individual images were taken from an altitude of 500 m. By adding oblique images, which were subsequently orthorectified, an area of approximately 10 km x 10 km could be mapped which equals the radius of the vessel's radar system (Fig. 6.7).

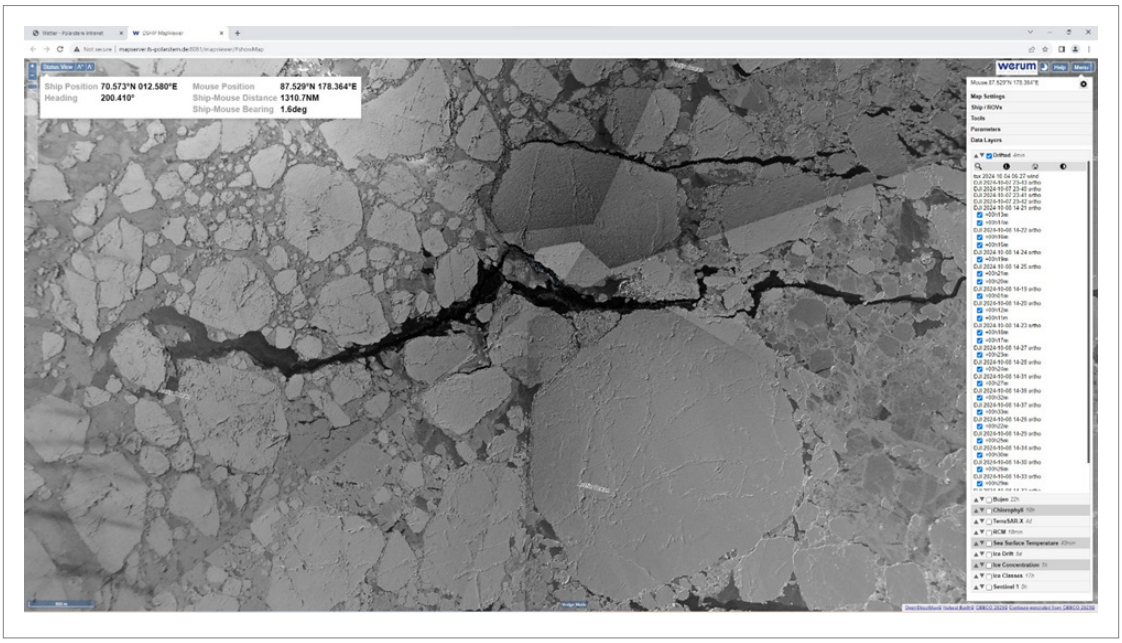

Fig. 6.6: Display of orthorectified individual images in the Mapviewer system on-board Polarstern. The vessel is located in the centre of the image with the drone flying approximately 500 m above the vessel. The x-axis scale of the image is approximately 5 km.

The corresponding flight to record the image data took approximately 15 minutes. Thanks to the methods described above, the processed images were available in the Mapviewer system just a few minutes after the images were taken. The described workflow was implemented and its functionality was successfully demonstrated. The results were rated to be very useful by the nautical officers to further improve vessel navigation through the ice.

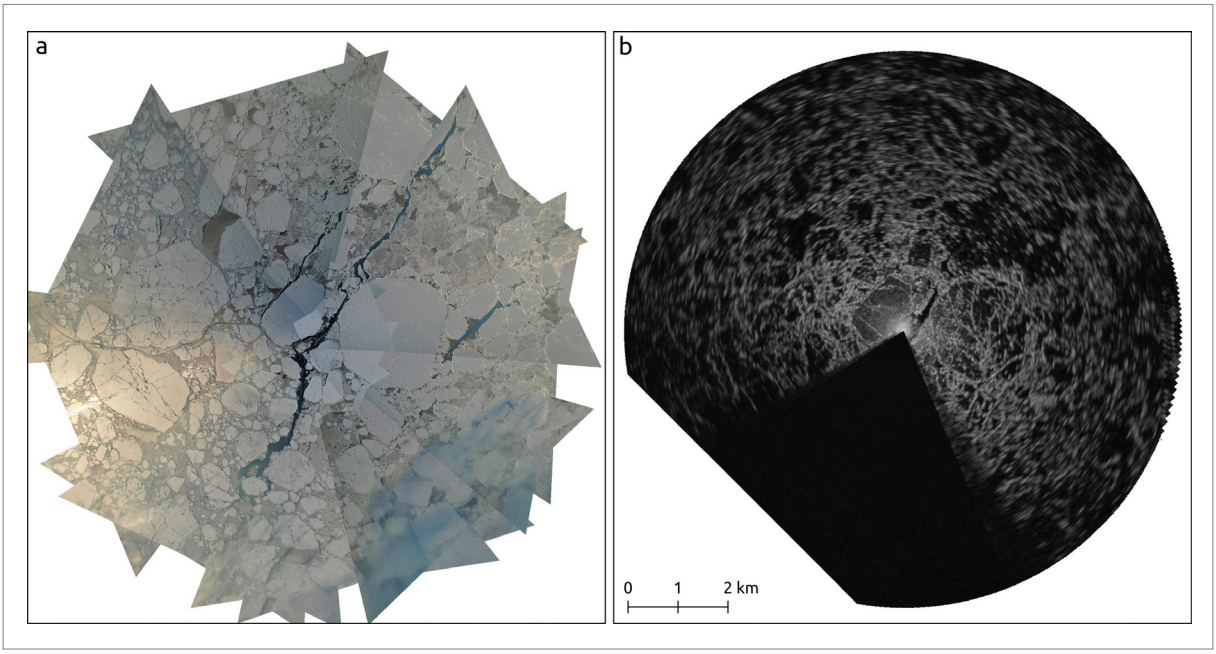

Fig. 6.7: Near real-time drone projections for the Mapviewer interface (a) compared to contemporary acquired ship radar data on 12 September 2024 (b). Drone altitude was ~500 m above the vessel, with oblique images acquired at different camera angles. The ship track is visible at the left side of the drone images.

Integration of drone live images into the video system of Polarstern

Figures 6.8 and 6.9 show examples of integrating the live video feed into the ship's system. The drone operator was located on the helicopter deck and controlled the drone while the live image was displayed on the bridge. The operator was in contact with the bridge via radio and received appropriate instructions for the reconnaissance from the bridge. In this example the mission was to search for open water areas suitable for fishing.

Fig. 6.8: Live drone video feed on the bridge,
here data from the thermal infrared (TIR) camera is shown.

Fig. 6.9: Live TIR and RGB images of the vessel‘s track through the ice

The advantage of this method is that the bridge receives a live image of the situation in real time and can react directly. The disadvantage compared to the single image method in the Mapviewer application is the comparatively small area that can be captured during a flight. Furthermore, orientation can be lost quickly whereas in the Mapviewer all data are orientated in same geographic reference system.

In summary, it can be said that both methods were successfully implemented and tested. For capturing large areas, the method of individual images from high altitudes appeared to be the more promising approach. For detailed and interactive reconnaissance at close range the use of a live video is very suitable.

Drone images and videos for public outreach

On 19 September 2024 we were able to broadcast a drone live stream directly from the North Pole. For this we also used the integration of the drone's video stream into the video system of the vessel. From here the data could be broadcasted via satellite to any place of the world. Such images and video feeds are important to sensitize the public for this fragil environment strongly affected by a changing climate.

6.3 Helicopter sea ice surveys

Work at sea

We used airborne electromagnetic induction sounding to measure the sea-ice thickness during helicopter surveys. During PS144 we used the new AWI EM-Bird which is towed on a 20 m long cable underneath the helicopter, flying 10-15 m above the ice surface. The distance between the EM-Bird and the seawater underneath the ice is measured by induction using a frequency of 4 kHz. A laser altimeter is integrated in the EM-Bird system, measuring the distance to the surface along the flight track. The difference between both distances results in the combined snow and ice thickness in the footprint of the system. Next to the need of the laser altimeter in the ice thickness calculation, the data can also be employed for surface roughness estimates and hence for estimates of ridge density and distribution. Ice conditions during the flights were documented by a GoPro camera mounted through the back window of the helicopter. In total, we carried out 11 EM-Bird flights. Due to bad weather conditions in August, 10 of the flights were conducted in September introducing a small spatial bias towards the end of the cruise. We conducted two flights during ice stations when we flew over the ice station floe and have therefore co-located ground measurements for validation purposes (stations 67 and 85). All helicopter EM-Bird surveys are summarized in Table 6.2 with their location shown in Figure 6.10.

Tab. 6.2: Overview of all conducted EM-Bird flights during PS144

Flight ID	Date	Start (UTC)	Stop (UTC)	Latitude	Longitude	Comments
PS144_Heli_EM-Bird_001	2024-08-25	11:09:26	12:25:32	85.25689	55.39796	Good triangle survey, fog came in at the western side of the survey
PS144_Heli_EM-Bird_002	2024-09-07	07:53:59	09:04:34	85.00958	155.4289	Foggy conditions towards the end
PS144_Heli_EM-Bird_003	2024-09-08	11:47:29	13:12:16	84.93682	161.8455	Ice station over flight (station 67, ice station 5)
PS144_Heli_EM-Bird_004	2024-09-09	09:46:26	10:23:20	84.94877	166.4991	Survey was ended due to fog (error 113 at ~10:11)

Flight ID	Date	Start (UTC)	Stop (UTC)	Latitude	Longitude	Comments
PS144_Heli_EM-Bird_005	2024-09-12	14:31:45	15:48:14	87.25851	179.4937	
PS144_Heli_EM-Bird_006	2024-09-13	15:21:19	16:27:57	87.49057	178.6436	Ice station over flight (station 85, ice station 7)
PS144_Heli_EM-Bird_007	2024-09-14	08:32:08	09:42:20	87.60901	-174.8826	First flight of the day
PS144_Heli_EM-Bird_008	2024-09-14	17:03:24	18:21:11	87.75826	-168.2509	Second flight of the day (error 113 occurred again, data receiving delay)
PS144_Heli_EM-Bird_009	2024-09-16	07:25:14	08:40:44	88.3637	-124.2224	Error 113 occurred again, bird needed restart
PS144_Heli_EM-Bird_010	2024-09-21	14:36:05	16:27:40	88.95821	56.79076	Data receiving delay, bird needed a restart
PS144_Heli_EM-Bird_011	2024-09-28	07:22:24	08:58:11	86.494	59.63479	

Preliminary results

As both PS144 (2024) and PS138 (2023) covered similar regions and both were conducted in August/September we describe the results of the EM-Bird measurements in the context of both expeditions. In late summer 2023 and 2024 we observe very similar motion patterns/ atmospheric conditions compared to the past decade, although drift velocities in 2023 were higher than in 2024 (results from satellite retrievals, not shown here). A comparison of 2023/2024 with motion patterns observed between 2010 and 2022 shows that the central Arctic Ocean was mainly supplied by Beaufort Sea ice in the last two years (Fig. 6.10). Ice that formed on the Russian shelves was suppressed, remained closer to the coast and probably melted completely during the summer. As a result, the proportion of shelf-sourced, potentially sediment-laden sea ice has probably been unusually low over the past two years.

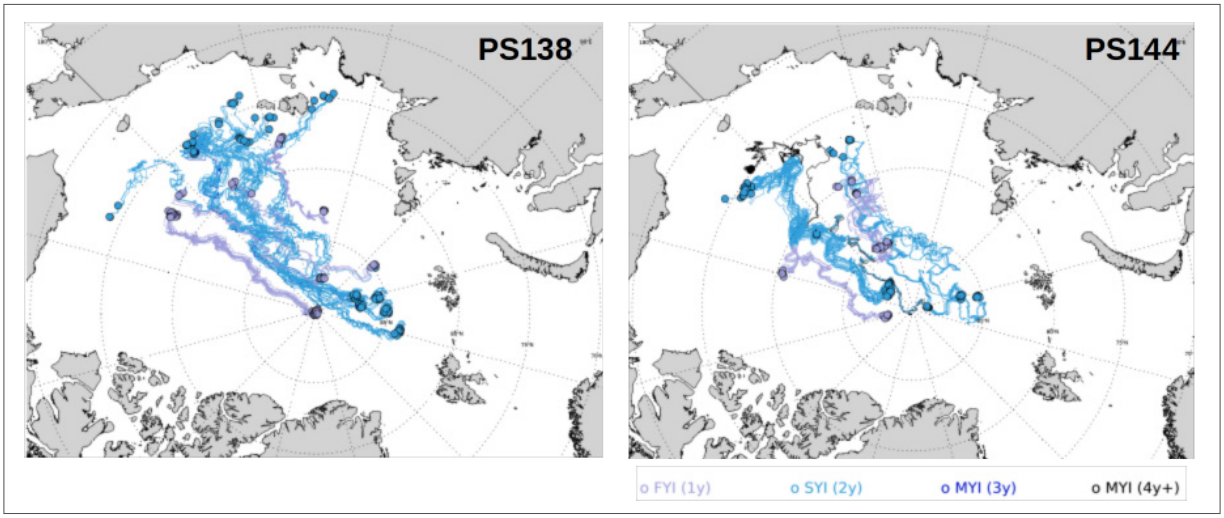

Fig. 6.10: Trajectories of sea ice measured at helicopter EM-Bird flights conducted during PS138 (in 2023, left) and PS144 (this expedition, right). For both years similar source regions are evident.

As a result the ice measured in 2023 and 2024 shows major similarities. We observe a similar modal and average ice thickness (Fig. 6.11), a similar ridge frequency and both years show an unusual large amount of open water fraction (~20% of all profiles). Within the context of previous years there is no significant change in the ice thickness in the study area, however there is evidence of significantly more open water fractions and a reduced frequency of ice ridges.

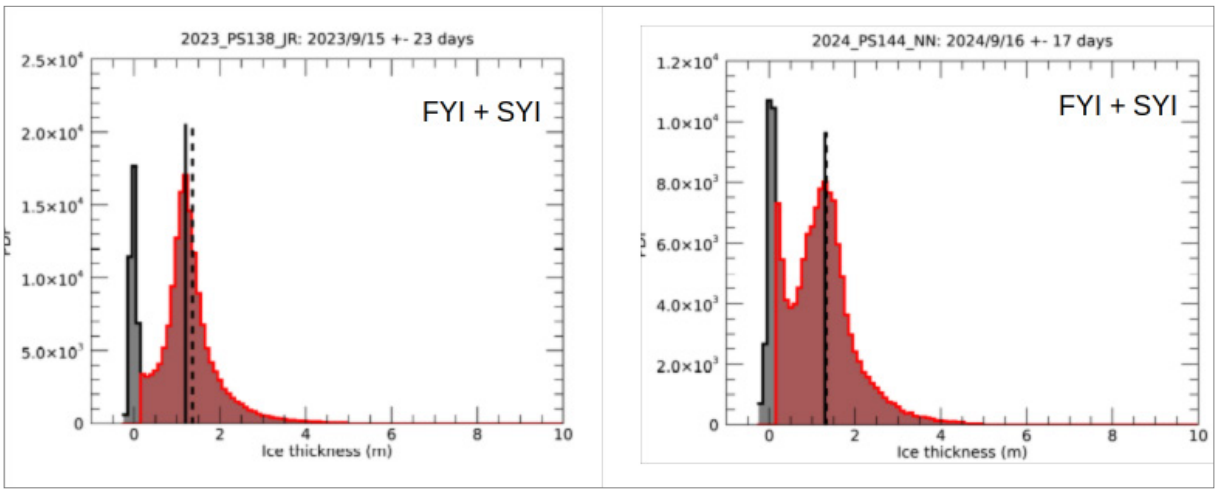

Fig. 6.11: Sea-ice thickness distribution of all EM-bird flights conducted during PS138 (in 2023, a) and PS144 (this expedition, b), the black lines mark the modal thickness of 1.2 m and 1.3 m and the dashed line the mean thickness of 1.37 m and 1.33 m for PS138 and PS144, respectively.

Figure 6.12 shows anomalies in ice divergence for PS138 and PS144. Here it becomes evident that all EM-Bird flights were conducted in regions of diverging sea ice. This fits well to the observations of high open water fractions. A possible explanation could be large scale anomalies in atmospheric pressure during August/September in the central Arctic.

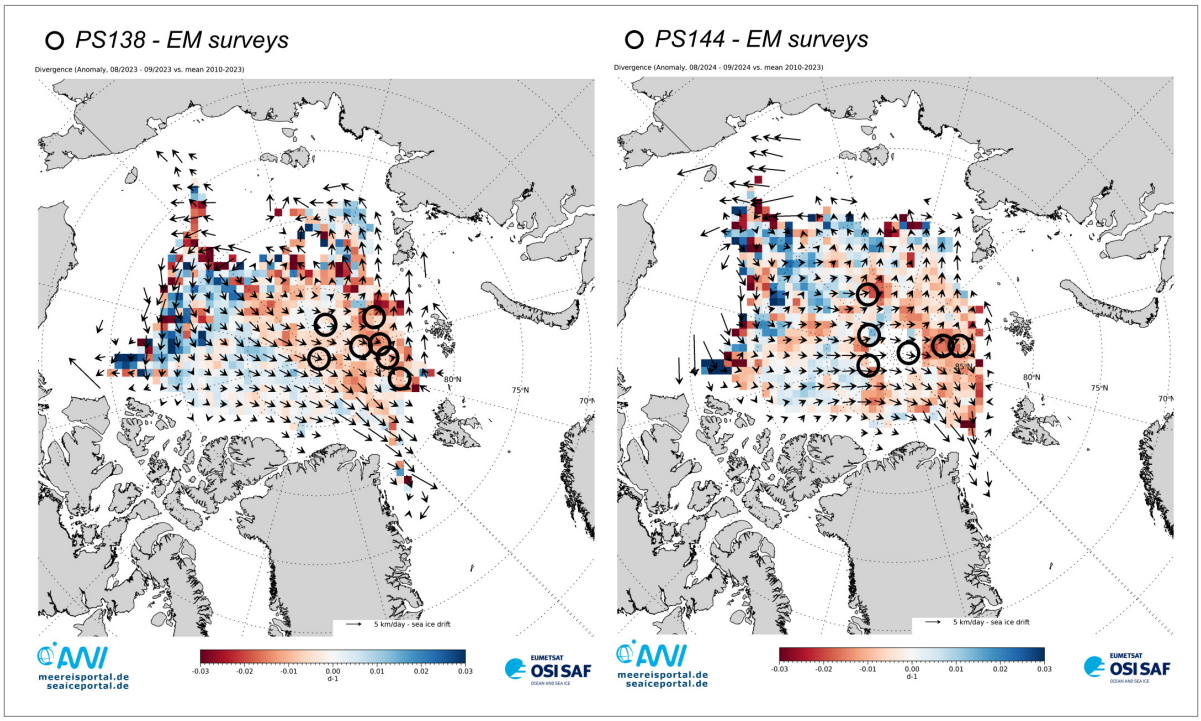

Fig. 6.12: Anomalies in ice divergence for PS138 (left) and PS144 (right). EM-Bird flights of both years are indicated by black circles. All flights were conducted in regions of ice divergence, implying a potentially higher fraction of open water.

6.4 Ice station work: physical sea-ice properties

During PS144 we performed measurements during 11 ice stations (Fig. 6.13 and Tab. 6.3). The measurements and deployments during ice stations included:

- Installation of autonomous platforms
- GNSS network for drift and reference measurements
- Drone measurements and validation (e.g. melt pond survey)
- Transect measurements of sea ice (total) thickness with GEM-2 sensor
- Transect measurements of snow depth with MagnaProbe sensors
- Ice and (snow) surface measurements in the radiometer footprint

An overview of the activities is given in Table 6.4. In addition, we supported other groups in drilling, probing and buoy deployment.

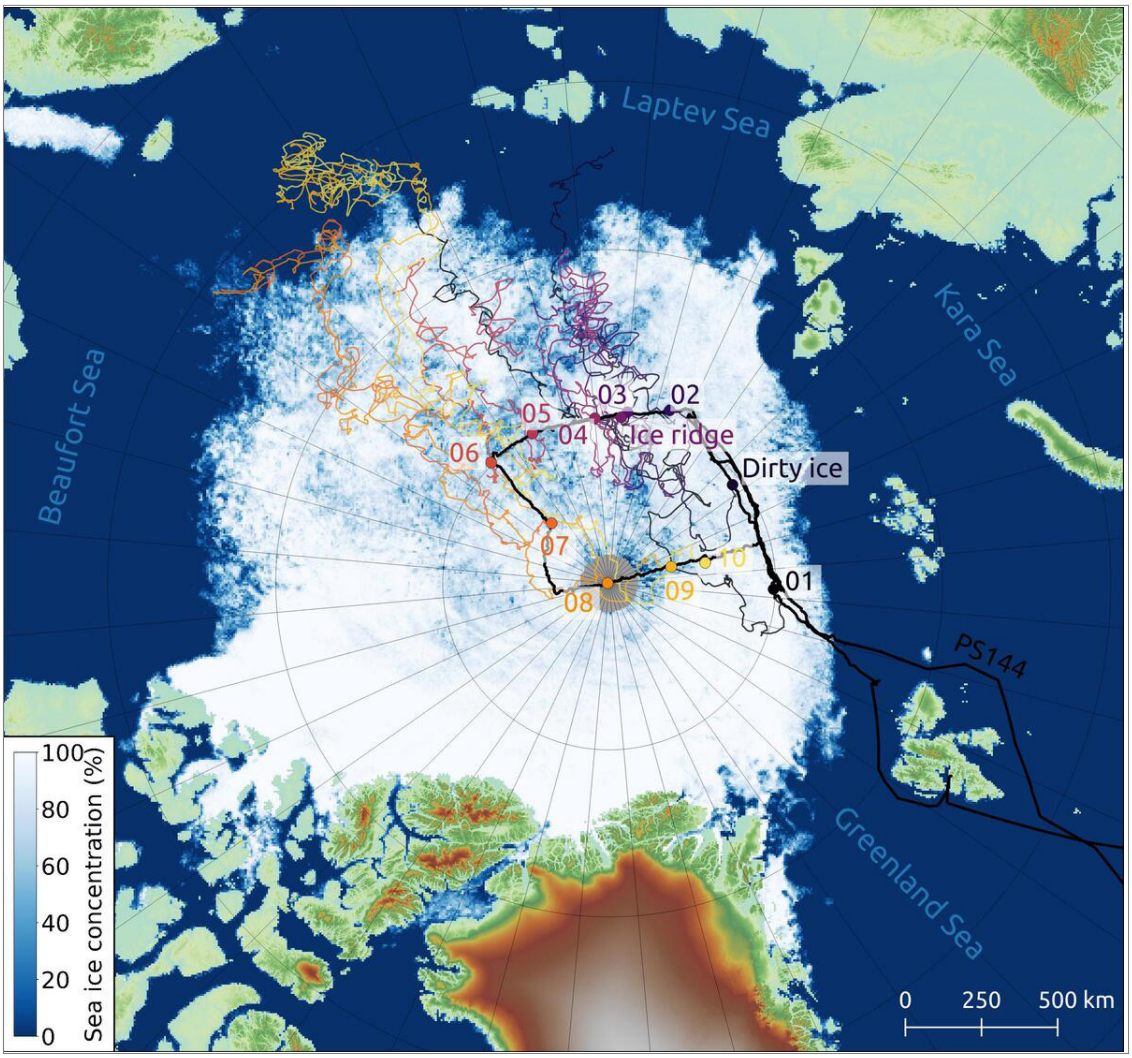

Fig. 6.13: Overview of all ice stations of PS144 including their corresponding drift trajectories. Sea ice concentration is shown at its annual minimum on 7 July 2024 (Spreen et al., 2008), from their original formation to the measurement location. Numbers on the map represent the ice station number, as given in Table 6.3: e.g. PS144_007_01_ICE01 => 01. Surface elevations originate from the World 3D - 30 m (AW3D30) Digital Elevation Model (Tadono et al., 2014, Takaku et al., 2020). The black line shows the cruise track of PS144.

Tab. 6.3: List of all ice stations of PS144.

For further information please see the end of this chapter.

Tab. 6.4: Detailed list of all devices employed during the ice stations listed in Table 6.3. Labels refer to the event labels listed in AWI‘s O2A database.

For further information please see the end of this chapter.

Autonomous ice-tethered buoys

Various autonomous ice-tethered buoys were deployed as part of our work program. Details are given in Chapter 8.

GNSS

Work at sea

We employed 3 to 6 GNSS receiving stations at each ice station. All GNSS receiving stations included one Novatel FlexPak6 L-Band GPS receiver, one Novatel choke ring GNSS antenna and one Avisaro data logger (Neckel et al., 2020). The antennas were mounted on top of the cases hosting the receiving and power unit. GNSS data were logged every second for ice stations PS144_007_01_ICE01 to PS144_050_01_ICE04 and every 5 seconds for ice stations PS144_067_01_ICE05 to PS144_134_01_ICE10. All data were processed using the Canadian Spatial Reference System Precise Point Positioning (CSRS-PPP) service (Tétreault et al., 2005) and serve as a reference frame for various instruments installed during the ice stations. Next to the GNSS derived surface elevations we measured ice thickness, freeboard and snow thickness at each GNSS station.

Preliminary results

All GNSS station data of the cruise were processed by the Canadian Spatial Reference System Precise Point Positioning (CSRS-PPP) service (Tétreault et al., 2005) being a fundamental data source for drift correcting GEM, EM-Bird, Drone, snow probe and borehole measurements to the reference times given in Table 6.3. Preliminary datasets of all ice stations are available in raw and post processed format and show an accuracy at cm scale. This also allows conclusions to be drawn on tidal cycles.

Tidal signals in GNSS timeseries

Initial plotting of GNSS station data measurements showed vertical displacements with magnitude and frequency indicative of tidal signals, this was looked into in more detail by carrying out harmonic analysis on the time series. The length of ice stations varied resulting in different lengths of GNSS station data. Stations PS144_007_01_ICE01, PS144_050_01_ICE04 and PS144_123_02_ICE09 had durations of less than 12 hours, meaning they are not suitable for tidal harmonic analysis. However, at the other stations the GNSS stations were deployed for between 18 and 37 hours. This allows for identification of tidal constituents through harmonic analysis. The following steps were carried out to achieve this:

1. The time series are quality controlled the remove outlier height values resulting from set up and set down of the sensors at the beginning and/or end of the time series. This was done manually, due to the small number of stations.

2. The high frequency variability is smoothed out by calculating the median height every 5-minutes.

3. The tidal components are calculated and reconstructed using the MATLAB Unified Tidal Analysis and Prediction Functions (*UTide*) (Codiga et al., 2021). Initially automatic constituent detection was selected to see which constituents would be identified. Then the harmonic analysis was repeated with the eight major tidal constituents (M2, S2, N2, K2, K1, O1, P1 and Q1). In the case of the longest DGPS record, additional constituents that were automatically identified were then added to the calculation to improve the fit of the reconstructed tide. The confidence interval information is based on the coloured Monte Carlo method, which is the default selection in *UTide*.

Ice station PS144_134_01_ICE10, had the longest time series from GPS5 at 37 hours and 9 minutes. This resulted in an automatic detection of 8 tidal constituents (from *UTide*), the fit was improved by specifying other constituents to analyse. The time series of raw data, 5-minute median and reconstructed tide are shown in Figure 6.14. The harmonic analysis results are shown in Table 6.5.

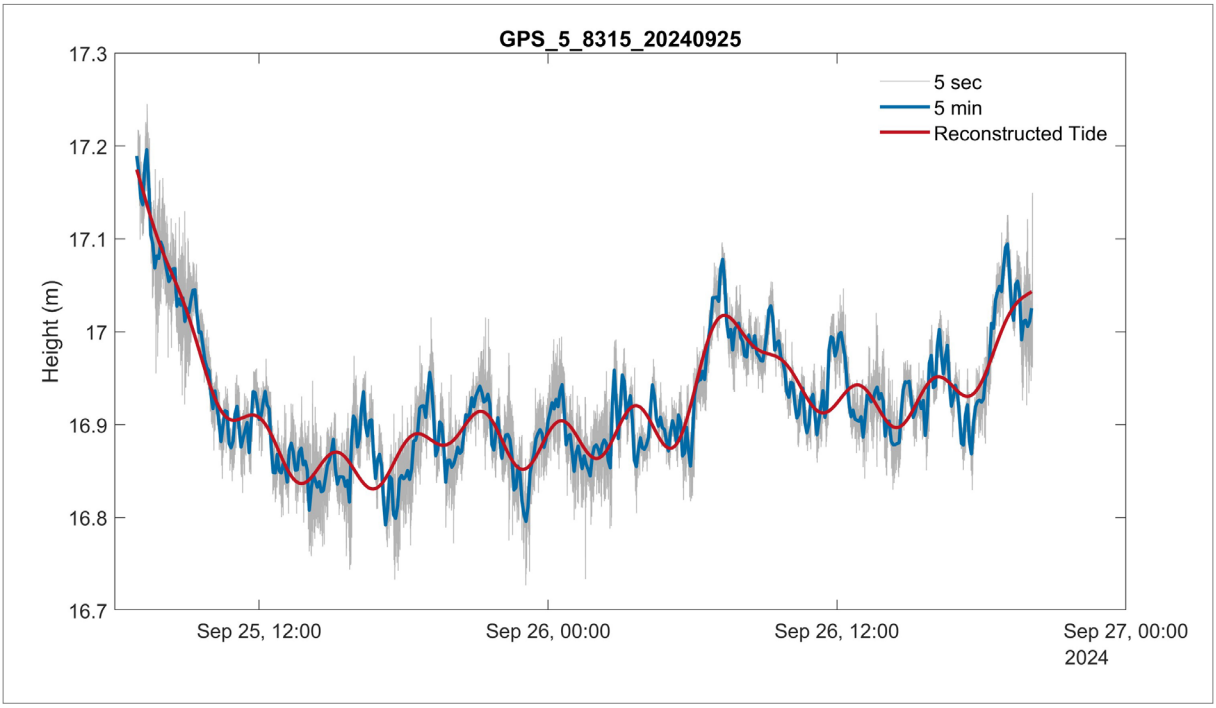

Fig. 6.14: Time series of GPS height relative to WGS-84 ellipsoid at station PS144_134_01_ICE10. The thin grey line shows the raw 5 second data. The thick blue line is the 5-minute median, with the reconstructed tidal signal shown in red.

Tab. 6.5: Tidal constituents with amplitude, phase and 95% confidence intervals identified by harmonic analysis using *UTide*

Constituent	Amplitude [m]	Amplitude 95% Confidence Interval	Phase Lag [°]	Phase Lag 95% Confidence Interval
O1	5.48	1.51	278	4.96
Q1	3.87	1.02	8.65	4.83
K1	1.71	0.422	121	11.0
M2	0.0276	0.00550	51.9	11.8
M8	0.0241	0.00416	20.4	9.9
M4	0.0173	0.00411	85.6	13,´.7
M3	0.00991	0.00403	49.9	23.3
M6	0.00960	0.00411	117	24.6
2MK5	0.00862	0.00353	74	24.1
3MK7	0.00528	0.00367	103	40.1

GEM

Work at sea

At all 10 ice stations, GEM-2 thickness surveys were carried out. The Geophex GEM-2 is a broadband electromagnetic induction sensor. It was towed in a pulka by foot or by snowmobile (only at station PS144_023_01_ICE02) and was measuring the total thickness including snow. If snow was present on the floe, the MAGNA probe was used to measure snow depths along the GEM track in intervals of a few meters. The survey track was mostly chosen in representative straight lines, sometimes passing other sites where thickness distribution information was desirable. During the first two stations (PS144_007_01_ICE01, PS144_023_01_ICE02) melt ponds, open or with thin ice cover, were present that were avoided. For calibration purpose a wooden ladder was used to carry out measurements at stepwise increasing distances to the conductive water. The ice thickness at the calibration site was determined at five bore holes. More bore hole measurements were carried out at the sites of the GNSS stations.

Preliminary results

After every ice station the collected GEM-2 data were calibrated, thicknesses were computed, drift corrected and transformed to equidistant steps. The drift correction is based on the positional data gathered by the GNNS stations and was used to translate and rotate all data points to their position on the floe at the reference time (see Tab. 6.3). From the five frequencies available (1.5 kHz – 93 kHz), all preliminary ice thickness were based on the 5.325 kHz inphase measurements. This frequency was selected to closely match the frequency of the EM-Bird measurements. Further, at higher frequencies on thin ice the assumptions for the calibration brake down as shielding effects come into play. The resulting thickness data from station PS144_067_01_ICE05 is shown on the map in Figure 6.19. Figure 6.15 shows GEM measured ice thickness estimates alongside the thickness data gathered by the EM-Bird during station PS144_085_01_ICE07. Further, these data are used to generate thickness distributions for each ice station as presented in Figure 6.16.

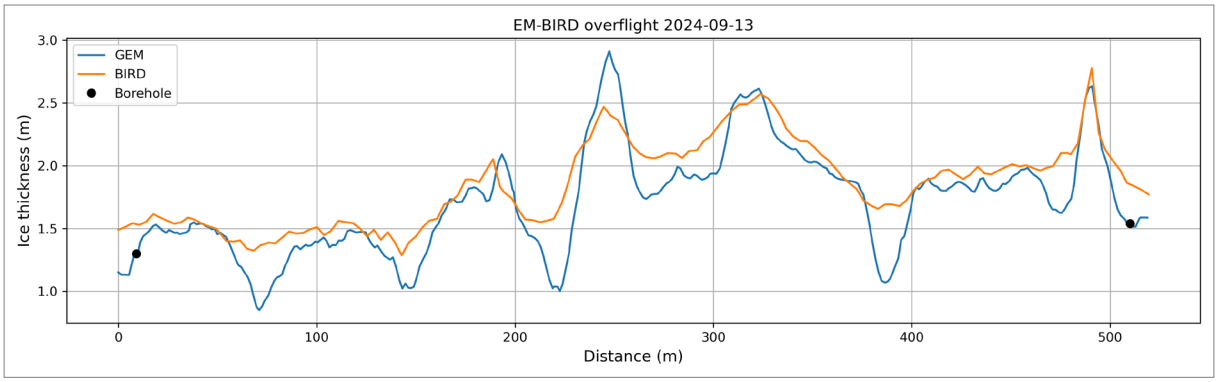

Fig. 6.15: EM-Bird overflight along GEM track during ice station PS144_085_01_ICE07, including additional in situ borehole measurements

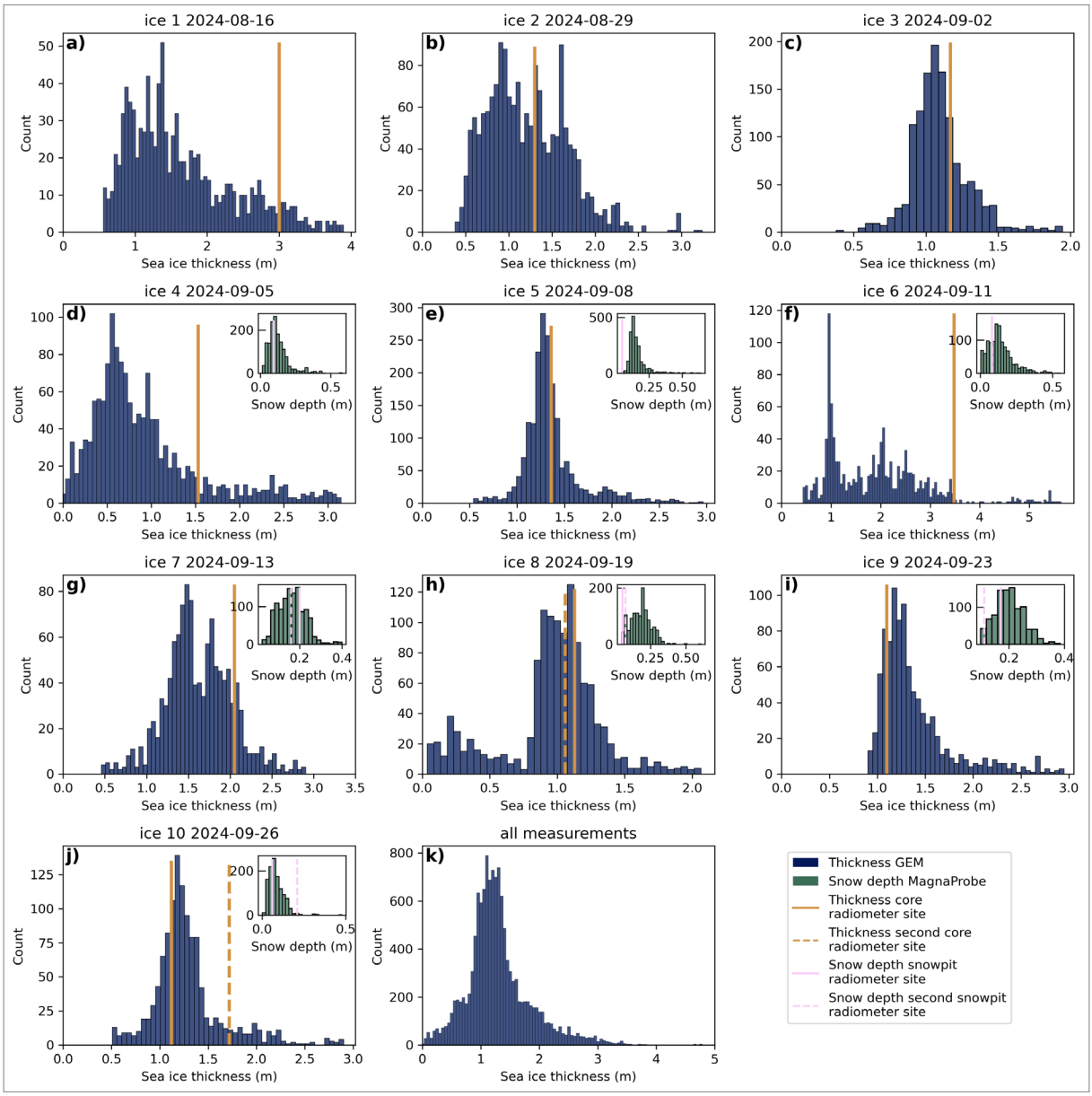

Fig. 6.16: Sea ice and snow thickness distributions from the GEM and MagnaProbe measurements during the ice stations. The ice thickness is derived from measurements at 5.325 kHz and quality controlled by excluding measurements that differed by more than 1 m from the median sea ice thickness. Vertical lines indicate the thickness of snow and ice at the radiometer site (for further information please see the end of this section and Section 6.5).

Drone lidar and photogrammetry measurements

Work at sea

In addition to the drone work done for navigational purposes as described in Section 6.2, drone surveys were also conducted during all ice stations to obtain orthoimages and Digital Elevation Models (DEMs) of the research areas. During PS144 we used two drone models: a DJI Mavic 3 equipped with an RGB Hasselblad L2D-20c camera model and a DJI Matrice 350 RTK equipped with a DJI L2 laser scanner payload. This payload is a combination of an RGB camera and a laser scanner.

Prior and during PS144 we established work flows in a python environment to program automated grid surveys which incorporated ice drift estimates in the mission planning to obtain optimal image overlap for photogrammetric reconstructions of the ice surface. This was necessary as all commercial mission planning software stops working at 85°N latitude and depending on the magnitude of ice drift the latter cannot be ignored in the mission planning. Only for flights on short notice we needed to fall back on manual control of the drone. The live mission planning tool for drifting sea ice conditions established during PS144 is now ready to use for upcoming expeditions.

During the ice stations, the drones have been operated from the vessels helicopter deck and directly from the ice. We did GPS assisted manual flights as well as automatic grid surveys. However, take-off and landing were done manually due to the moving (drifting) vessel/ice floe. After the flight, the L2 raw data was processed in the DJI Terra software and the point clouds were exported in a standard *.las format for further processing. The images acquired by the DJI Mavic 3 were exported in *.DNG raw and *.JPG format. All images were drift corrected using the GNSS data acquired contemporaneously by the GNSS reference stations. Ground Control Points (GCPs) were selected from the drifting GNSS stations at the reference times indicated in Table 6.3. Depending on the images contrast during the flight drift corrected DEMs and orthoimages of different quality were generated for all ice stations.

Preliminary results

Automated grid surveys

By employing Structure from Motion (SfM) photogrammetry on the DJI Mavic 3 images we were able to generate orthomosaics and DEMs of all ice stations listed in Tables 3 and 4 (for further information on the general method see also Neckel et al., 2023). Depending on local conditions (e.g. visibility, snow cover, ice drift) during the drone flights different level of quality could be reached. Results could be significantly improved by GCPs measured with drifting DGPS receivers and an initial drift correction of the images prior to the SfM pipeline. Furthermore, we could show that automated grid missions are superior over manual flights covering larger areas with constant footprint overlap being a prerequisite for proper image alignment during SfM processing. Figure 6.17 shows the proposed drift correction scheme established during PS144. While Figure 6.17a shows the original flight planning for ice station PS144_134_01_ICE10 including an image overlap of 80% along track and 60% across track Figure 6.17b shows the same grid employing a temporally integrated drift correction of -0.05 and -0.13 m s^{-1} in x and y direction respectively as measured prior to the drone survey. Finally, Figure 6.17c shows the actual positions of the drone after a drift correction with the *in situ* measured GNSS station data.

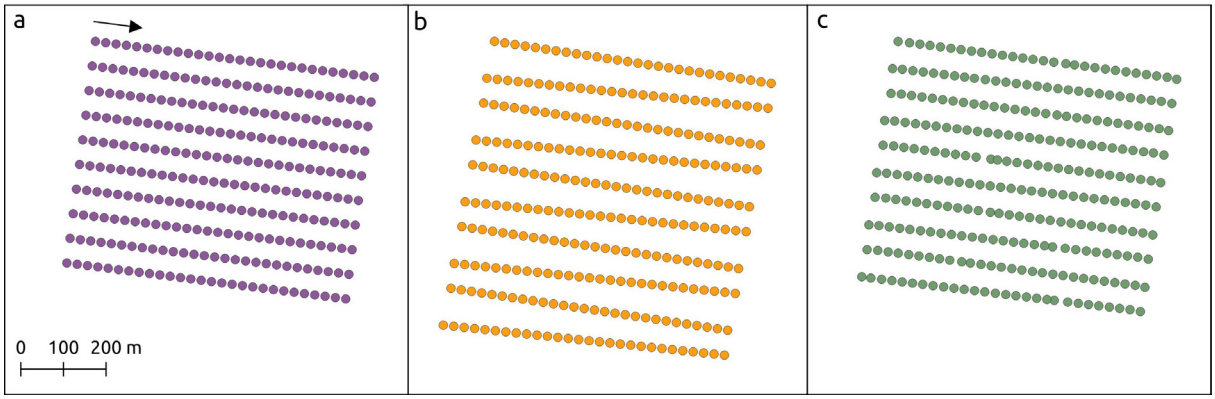

Fig. 6.17: Proof of concept of correcting grid flights over drifting sea ice. Grid flight of drone survey as conducted during ice station PS144_134_01_ICE10. The originally planned survey grid with an image overlap of 80% along track and 60% across track is shown in (a) with the black arrow indicating the flight direction of the drone. The drift corrected grid as uploaded to the drone is shown in (b) employing a drift estimate of -0.05 and -0.13 m s^{-1} in x and y direction respectively. The final drift corrected actual flight pattern is shown in (c) employing GNSS station data from the ice floe.

Drone retrieval of melt pond bathymetry

Figure 6.18 shows results of ice station PS144_007_01_ICE01 being the only ice station of PS144 with open melt ponds. While Figure 6.18a shows an orthoimage of a melt pond the corresponding DEM is shown in Figure 6.18b. The drone data are spatially adjusted using data of four GNSS stations of which three are located in the vicinity of the melt pond. Figure 6.18c shows transect data measured by the Surface Pond Level Information Sensing Hardware (SPLISH) which is a ruler with a flat base to minimise measuring outliers. Figure 6.18c also shows the corresponding data samples from the photogrammetric DEM. This is in line with results published by Fuchs et al., 2024 highlighting the possibility to derive melt pond bathymetry and hence pond volume from photogrammetric datasets.

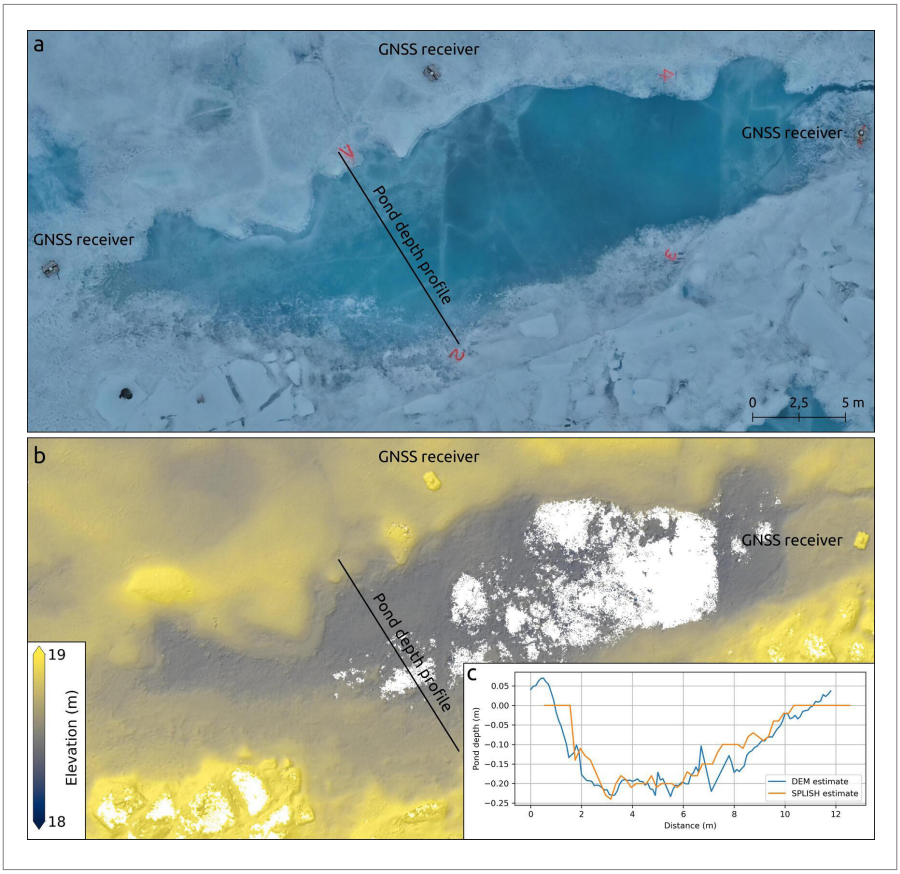

Fig. 6.18: Orthomosaic (a) and DEM (b) of a melt pond covered by a drone survey conducted during ice station PS144_007_01_ICE01. In situ transect data along the black line is shown in (c) including the corresponding data samples from the photogrammetric DEM.

Drone lidar and photogrammetry measurements

As an example, we show results of drone data from ice station PS144_67_01_ICE05 (Fig. 6.19), but a drift corrected orthomosaic is available for all ice stations which can be very useful for all groups that were working on the ice. In Figure 6.19a we show co-located data of ice thickness estimates from GEM and EM-Bird measurements with a COSMO SkyMed image in the background. Figure 6.19b shows a large scale orthomosaic of the ice floe acquired from an automated grid survey as described above. Here also some borehole measurements are shown in order to validate ice thickness estimates from other sources. Figure 6.19c shows surface elevations from the photogrammetric drone survey. During this ice station we had favorable weather conditions (e.g. no clouds, good visibility) yielding to accurate results when GCP data are included in the post processing of the drone data. This also becomes evident when comparing the data with preliminary lidar data from the L2 sensor on board the Matrice 350 RTK drone (Fig. 6.19d).

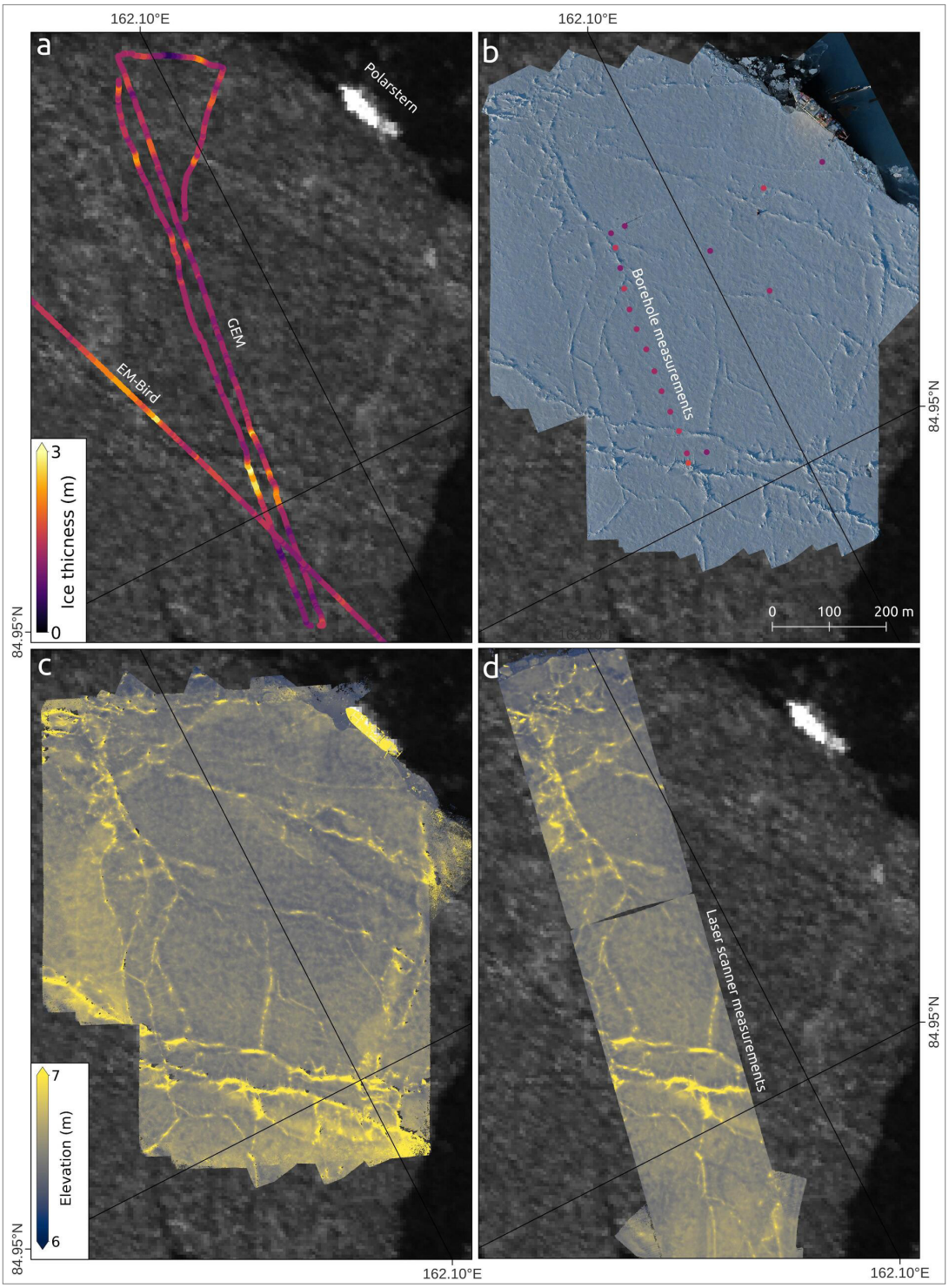

Fig. 6.19: Data example of ice station PS144_067_01_ICE05, referenced to station time 2024-09-08T15:00:00. A COSMO-SkyMed (Constellation of Small Satellites for Mediterranean basin Observation) radar image is shown in the background. Polarstern is clearly visible by strong backscatter. Ice thickness estimates from GEM and EM-Bird surveys (a) are shown next to a drone orthoimage with in situ ice thickness measurements from boreholes (b). Surface elevations above WGS-84 ellipsoid are shown from photogrammetric (c) and lidar (d) drone surveys.

Ice and (snow) measurements in the radiometer footprint

Work at sea

In the beginning of each ice station, we determined the footprint of the radiometers that were installed on board (see Section 6.5) with the help of the known position within the visual images recorded from the A-Deck to be able to conduct measurements within the footprint. The calculated elliptical footprint sizes assuming instrument heights of 20 m are about 2.2 m times 3.6 m (HATPRO, minor and major axes) and 0.75 m times 1.26 m (MiRAC-P, minor and major axes), however, the actually observed area on the ice was larger.

We then measured within the footprint of the radiometers:

- Vertical profiles of sea ice temperature, salinity and density at a vertical resolution of 5 cm for the upper 20 cm to achieve a higher vertical resolution for the upper part, which dominates the influence on the microwave signal, while the rest was sampled in 10 cm steps
- Snow temperature, density, salinity and stratigraphy (traditional snow pit),
- SnowImager measurements of the surface (instrument from the SLF Davos, https://www.snowimager.ch/). The SnowImager takes photos at 850 and 940 nm and can thus either be used to measure surface reflectance at these wavelengths by placing it on top of the surface (Macfarlane et al., 2023), which we did along short transects of about 5 to 7 meters; or to image a snow profile in the snow pit, which can be used to derive density and specific surface area profiles (Matzl et al., 2006)
- cm-scale surface roughness (Structure from Motion photogrammetry)

Snow and ice permittivity at 50 MHz measured with a Stevens HydraProbe

Taking snow and surface scattering layer samples for further processing after the cruise to determine the microstructure with X-ray micro-computed tomography (microCT) at the SLF Davos

Snow permittivity measurements with the Denoth capacitance probe (Denoth 1989; instrument from the SLF Davos, https://snow-sen.com/) from which information about snowpack wetness and density can be derived

Usually, the measurements in the footprint were performed by defining a T-shaped transect for the SnowImager (measuring surface reflectance by taking photos from above), with side lengths of 5 to 7 meters, thus larger than the actual radiometer footprints. Surface temperature and snow depth were determined along the transect. At one to three sites within the transect around fifty photos of the surface were taken with an Olympus E-M5 digital camera from different angles to be analyzed with photogrammetry software. Coded targets were placed within the photos, so that the images contain information about distances. From this, the surface topography and roughness at the centimeter scale can be retrieved, which is an important parameter for the microwave emission and scattering.

Starting with ice station PS144_050_01_ICE04, we also encountered snow within the radiometer footprint and did one or two snow pit measurements, including snow stratigraphy, temperature and density profiles (with a density cutter with a volume of 100 cm^3) and images of the snow profile with the SnowImager. The Stevens HydraProbe Soil Sensor was inserted directly in the snow to measure the dielectric permittivity at 50 MHz, a quantity related to the wetness of the snow. Each dielectric permittivity measured was repeated once. The snow permittivity was also measured with the Denoth probe, measuring the capacitance of the snow

at its surface. At most ice stations snow or surface scattering layer samples were taken with a 8 cm corer to be later used for microstructure analysis by microCT measurements at the SLF in Davos, Switzerland.

Ice cores in the footprint (usually right below the snow pit) were obtained with a 9 cm Kovacs corer. Temperature, salinity and density were all measured for one core. After temperature measurements, the cores were cut and weighted on the ice to obtain the density and then taken to the ship for salinity measurements (Greisinger G1410 salinometer).

For in total 30 ice core sections at different ice stations, we measured the dielectric permittivity of the ice at 50 MHz using the Stevens HydraProbe Soil Sensor that was deployed by drilling holes into the cut surface of the ice core.

After coring, we took videos of the under-ice surface with a GoPro camera in a waterproof housing that was mounted on an extension pole.

Preliminary (expected) results

Measurements of the snow and ice surface (and its variability) were performed during the ice stations within the footprint of the MWRs, and help to relate the (micro)physical properties like ice temperature profiles or snow density to the microwave signal. Figure 6.16 shows the measured ice thicknesses and snow depths in relation to the overall distributions on the floe derived from GEM and MagnaProbe measurements, respectively. While the radiometer site was mostly representative of the floe in terms of these quantities, especially during ice station 4 (4 September 2024) and 6 (10 September 2024) the ice was considerably thicker at our site than the mode derived from the GEM measurements.

Table 6.6 gives on overview of the bulk properties of the sea ice in terms of salinity, density and temperature as well as a short description of the (snow) surface. In most cases, salinities and densities were rather low compared to typical values for first-year ice. Comparisons to the ice core measurements of other groups will help to quantify the spatial variability on the floes. Also, the under-ice videos help to qualitatively assess the spatial variability, e.g., there were large gradients in thicknesses and ice keels on 29 August 2024 and 10 September 2024 and rather level under-ice surfaces on 12 August 2024.

Figure 6.20 shows an example of the SnowImager measurements: The surface hoar encountered on 13 September 2024 is visible in the surface reflectance measurements (left). The interface between surface scattering layer and different snow layers are visible on the snow profile image (right). The stratification agrees with our observations of three different snow layers in our snow pit.

Such datasets of physical properties and co-located microwave brightness temperatures help to evaluate and advance models of microwave emissions of snow and sea ice. As an example we show simulated brightness temperatures from the microwave radiative transfer model *SMRT* (Picard et al., 2018) using the observed sea ice and snow properties as input for the model in Figure 6.21. Correlation lengths describing the microstructure of the snow were estimated based on the snow type but can be improved with the results from the microCT in the future. Similarly, the surface roughness was set to zero but the photogrammetry results will enable refining these settings. Despite these limitations, the model is able to capture the frequency dependence of the brightness temperatures well compared to the measured brightness temperatures (see Section 6.5), which is a promising preliminary result.

Tab. 6.6: Overview of physical ice properties derived from the sea ice cores and a short description of the surface at the radiometer site and the taken microCT samples. Bulk values are calculated as weighted average from the measured vertical profiles.

Ice station	Bulk ice density wkgm^{-3})	Bulk ice temperature (°C)	Bulk ice salinity (psu)	Snow/Surface and microCT sample description
PS144_007_01_ICE01	822	-1.1	1.5	none (surface scattering layer; SSL), temperature of both CT samples when taken: -0.2 °C
PS144_023_01_ICE02	686	-0.2	0.0	none (SSL), CT sample temperature: -0.4 °C (sample 1), -0.4 °C (sample 2)
PS144_042_01_ICE03	809	-0.6	1.2	none (SSL), no CT sample
PS144_050_01_ICE04	863	-1.0	1.6	around 9.5 cm snow with three thin ice layers and surface hoar at coring site with CT sample temperature: -1.8°C (center sample 1); liquid melt pond below snow at end of transect with sample temperature: -3.2°C/-0.9°C (surface/interface sample 2)
PS144_067_01_ICE05	808	-1.5	1.9	2 cm snow with loose icy SSL beneath at coring site with CT sample temperature: -7.6°C/-3.5°C (surface/interface sample 2); around 4.5 cm of snow 180 cm away from transect with CT sample temperature: -7.6°C/-4.3°C (surface/interface sample 1)
PS144_080_01_ICE06	907	-1.4	2.4	Variable snow depth at site mostly below 1 cm (higher in surrounding area); CT sample temperature at coring site with no snow: -2.6°C/-1.9°C (surface/interface sample 2); 8 cm of snow with CT sample temperature -2.5°C/-2.2°C (surface/interface sample 1) at snow pit 1, 1.5 m away from transect start; light snowfall (needles)
PS144_085_01_ICE07	857	-0.9	1.5	Snow depths between 5 and 14 cm, surface hoar, three thin ice crusts within the snow separating snow layers (snow pit 1, mostly faceted snow); around 9 cm snow at snow pit 1 with CT sample, temperature: -6.7°C/-5.1°C (surface/interface sample 1), around 13 cm snow at snow pit 2 with CT sample, temperature: -6.6°C/-5°C (surface/interface sample 2), diamond dust at start of station

Ice station	Bulk ice density wkgm^{-3})	Bulk ice temperature (°C)	Bulk ice salinity (psu)	Snow/Surface and microCT sample description
PS144_109_01_ICE08	825/836	**-2.2/-1.7**	2.0/1.9	Snow depths between 3 and 7.5 cm, Snow pit 1 around 5 cm mostly new snow/snow plates (PPpl), with CT sample temperature: -10.2°C/-6.7°C (surface/interface sample 1); snow pit 2 7.5 cm snow
PS144_123_02_ICE09	872	-1.9	1.7	Snow depths between 4 and 9 cm, snow pit 1 around 8 cm faceted with stellar dendrites on top; snow pit 2 with CT sample, 7.5 cm snow, stellar dendrites on top, some depth hoar at SSL interface, CT sample temperatures: -13.2°C/-5.8°C (surface/interface sample 1)
PS144_134_01_ICE10	783/876	-2.2/-2.7	4.1/2.2	Snow depths between 3 and 10 cm, 6 cm of snow and some saline SSL beneath at snow pit 1 with CT sample (surface/interface temperatures sample 1: -8.9°C/-6°C), dendrites on top, faceted,

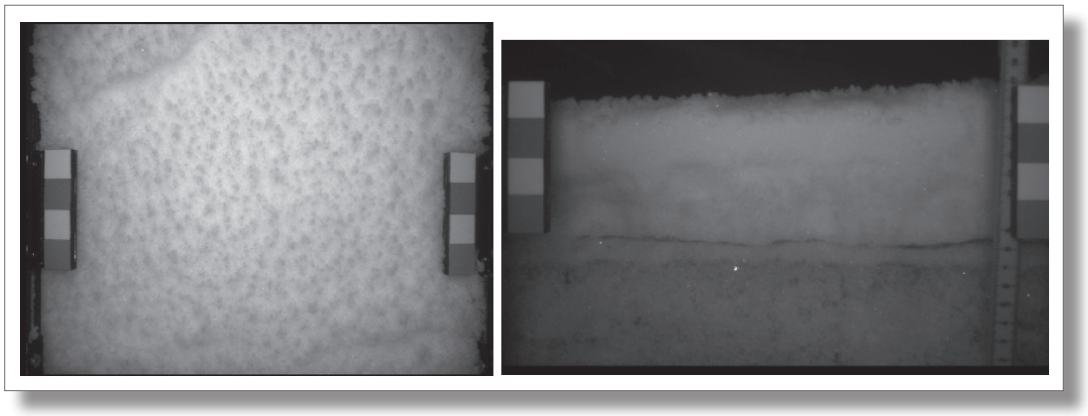

Fig. 6.20: Images taken with the SnowImager (uncalibrated) during ice station 7 on 13 September 2024. Left: Reflectance measurements of the surface hoar at 850 nm. Right: Snow profile imaged at 940 nm

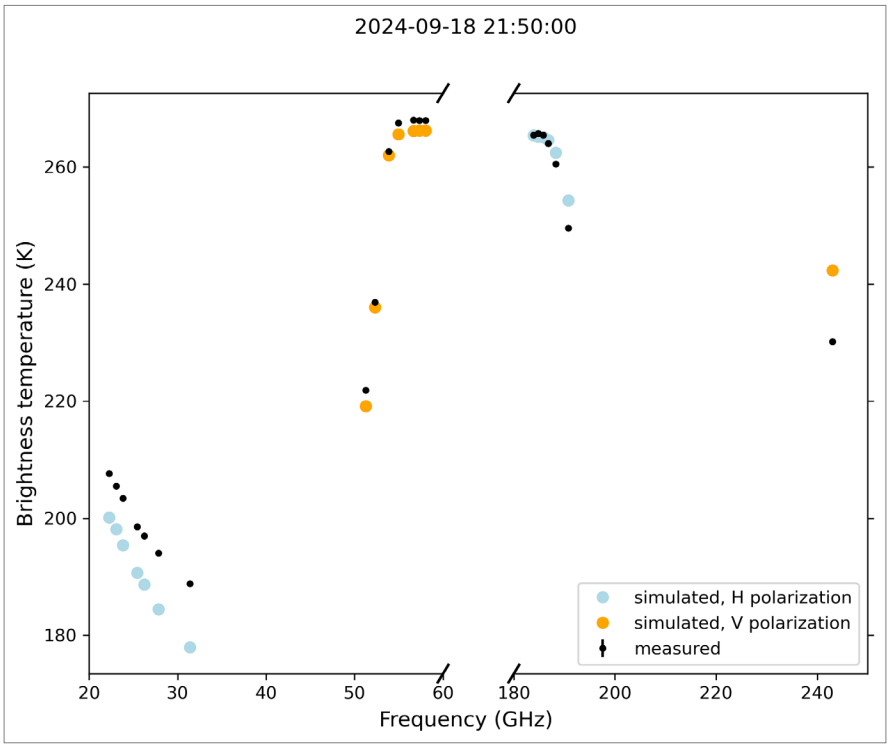

Fig. 6.21 :Measured and simulated microwave brightness temperatures from the radiometer site at the North Pole ice station (18 September 2024). The model results are obtained from the SMRT model using snow and sea ice information collected in situ.

6.5 Atmospheric and surface microwave emissivity measurements

Work at sea

Atmospheric measurements

A set of active and passive remote sensing instruments was operated on board: a G-band differential absorption radar (GRaWAC; G-Band Radar for Water Vapor and Arctic Clouds; PS144_0_Underway-13), a W-band cloud radar (MiRAC-A; Microwave Radiometer for Arctic Clouds - Active; PS144_0_Underway-12), two MWRs covering the 22 to 340 GHz frequency range (HATPRO and MiRAC-P; PS144_0_Underway-14 and PS144_0_Underway-16), and total sky cameras in the visual (VIS) and infrared (IR) spectral range (PS144_0_Underway-20). Additional atmospheric measurements include a laser disdrometer for precipitation measurements (PS144_0_Underway-19), an ultrasonic anemometer for wind measurements (PS144_0_Underway-18) as well as sun photometer measurements including microtops sun photometers to collect data for AERONET (remote sensing aerosol network; sensor label microtops_16826). Auxiliary information about roll and pitch were collected by two additional inertial measurement units (a Raspberry Pi IMU, PS144_0_Underway-21, and a *witmotion* inclinometer, Mini-IMU, PS144_0_Underway-17) and a 20 Hz record of the ship's Hydrins sensor. Radiosondes were launched daily at 00 UTC in addition to the launches at 06 and 12 UTC by DWD. More frequent launches were performed during special weather events.

A Ramses spectral radiometer (type Trios Ramses VIS ACC, Sensor ID SAMIP_5068, PS144_0_Underway-9) recorded spectral solar irradiance in 10 min intervals during the entire expedition. The first spectrum was recorded on 11 August 2024 12:36 UTC and the last spectrum on 4 October 2024 09:00 UTC. When the SUIT was deployed, the Ramses recorded in burst mode, recording up to 3000 spectra a day, while on other days a lower frequency of 144 spectra is available.

In collaboration with the VAMPIRE team, the GAIA project, that was involved in the previous cruise PS143/2, could continue the measurement of several aerosol chemical and physical properties, cloud physical properties, radiation and meteorological data also during the PS144 cruise (PS144_0_Underway-23), broadly extending GAIA's dataset and allowing data comparison exercises and integrated approaches with the complementary VAMPIRE data. GAIA's dataset of the physical-chemical quantities are needed as input to the modelling tools newly implemented in GAIA, with the aim of gaining information on georeferenced climatic impact of different aerosol sources and types on a large latitude range. A complete list of the measured properties and details on the methodologies may be found in PS143/2 booklet and cruise report.

Surface microwave emission measurements

The microwave radiometers HATPRO and MiRAC-P were also used for continuous surface emission measurements. These observations were complemented by surface cameras (VIS, PS144_0_Underway-22, and IR, PS144_0_Underway-15), which operated at a temporal resolution of 1 s and 2 s, respectively. Both cameras covered the field of view of the MWRs. Only the outer surface scan angles were not covered by the IR camera.

Instrument setup: Installation, settings, calibration and data availability

Installation

The instruments were located on the upper A-deck (microwave radiometers, cameras) and the Peildeck (radars, disdrometer, ultrasonic anemometer), as can be seen in Figures 6.22 and 6.23. The Peildeck is 1.62 m above the A-Deck. The Mini-IMU was installed in the observation alley on the A-Deck. The microwave radiometers were installed at the railing on port site of the upper A-deck with unobstructed surface and sky view from 35° to 180° perpendicular to the ship's heading. The radiometers' receivers were as close together as possible to ensure overlapping footprints. During the entire cruise, the radiometers were flipped by 90° to scan atmosphere and surface by rotating the internal mirror. Right next to the radiometers, a sky camera (MOBOTIX) was installed on the railing. The sky camera records visual (fish eye sensor Mx-O-SMA-S-6D016-X) and infrared images (IR sensor Mx-O-SMA-TS-R079) every minute. On the other side, a FLIR A315 infrared camera and a GoPro HERO11 visual camera were installed at an incidence angle of 53°. The infrared camera recorded images every second and the visual camera every 2 seconds. The two radars were installed on the port site of the Peildeck. GRaWAC was located in front of MiRAC-A. Both instruments were aligned to sample the same atmospheric volume. The RaspberryPi IMU was mounted on the housing of MiRAC-A. GRaWAC records its roll and pitch angles with an internal sensor. The instruments were positioned with transmitter towards port side for MiRAC-A and towards starboard side for GRaWAC. Next to the radars on the railing of the upper to the lower Peildeck, an OTT Parsivel² laser disdrometer and an ultrasonic anemometer (uSonic-3 Scientific Cage MP) were installed on poles. To limit vibrations we reduced the height of the poles to sensorhead heights of about 1.95 m (Parsivel) and 1.75 m (ultrasonic) but the ship motion could still have caused slight vibrations of these two instruments. The laser beam of the disdrometer pointed perpendicular to the ship's heading. The ultrasonic was aligned with its internal north arrow towards the

front of the ship. Both instruments were close to the crow's nest and potentially affected by precipitation shadowing effects. The time of all instruments except GoPro were synchronized with the ship's time server.

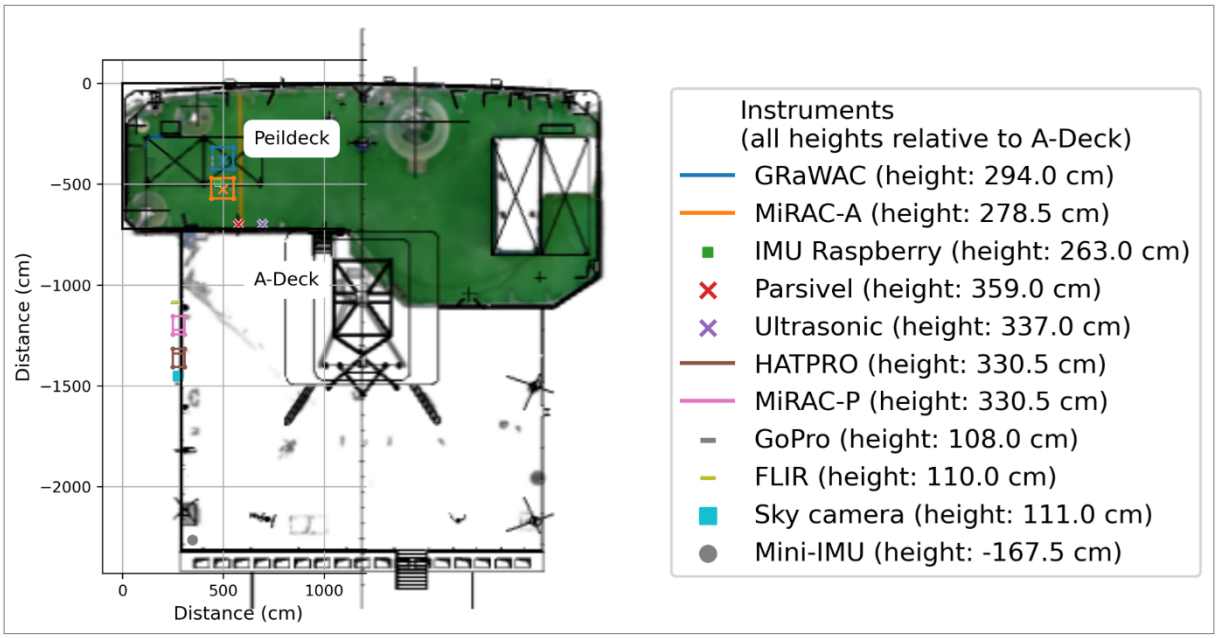

Fig. 6.22: Instrument locations on the A-deck and Peildeck

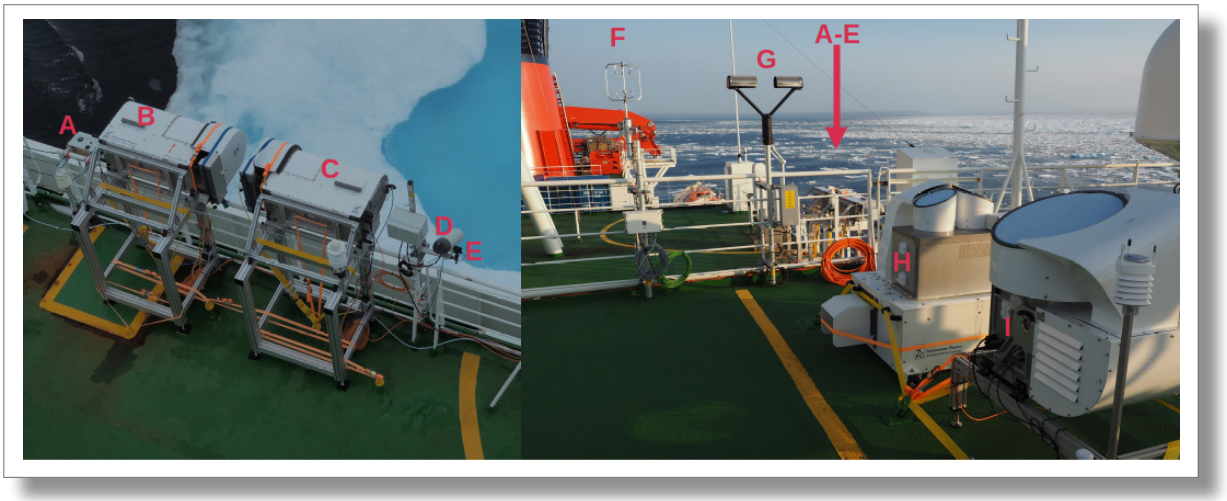

Fig. 6.23: Installed instruments from the VAMPIRE project: Sky camera (A), microwave radiometer HATPRO (B), microwave radiometer MiRAC-P (C), infrared surface camera (FLIR, D), visual surface camera (E), ultrasonic anemometer (F), laser disdrometer (G) and cloud radars MiRAC-A (H) and GRaWAC (I)

Settings: microwave radiometer scan definitions and radar chirp settings

The microwave radiometers alternated between atmospheric and surface scans by adjusting the internal mirror. Both radiometers repeated a series of scans every 30 minutes with an integration time of 1 s (0°: nadir; 180°: zenith):

- zenith: 180° (360 s)
- surface: 127° (15 s), 53° (155 s for HATPRO and 175 s for MiRAC-P), 127° (15 s)
- surface scan: 35°, 45°, 55°, 65°, 115°, 125°, 135°, 145° (15 s each)
- boundary layer scan: 180°, 120°, 109.2°, 104.4°, 101.4°, 98.4°, 96.6°, 95.4°, 94.8°, 94.2° (10 s each)

The scans were started at 0 or 30 minutes past each hour in the following order: surface scan, zenith, surface, zenith, surface, boundary layer scan, and zenith. The final zenith scan was shortened to 270 s. Both instruments performed gain calibrations for 10 s at the beginning of each zenith scan. The surface observations started on our transit to the ice on 11 August 2024 at 19:00 (19:30) UTC for HATPRO (MiRAC-P) over open ocean.

Due to the internal instrument control, especially of HATPRO, scans took longer than specified, so that HATPRO and MiRAC-P did not measure at the same viewing angle simultaneously in the beginning. However, we managed to fix the measurement settings and from 14 August 2024, 22:30 UTC, the time of the individual scans was as desired and both instruments were synchronized. Surface observations ended on 5 October 2024 at 09:30 UTC, again over open ocean.

As the radiometers were flipped by 90°, the measured polarization is changed accordingly, and we measure mixed polarizations under angles other than 0 or 90°.

Tab. 6.7: Chirp settings for the two radars, first two were used for most of the period 10 August 2024 to 29 August 2024, while the latter two were used from 29 August 2024 to the end of measurements.

Instrument, chirp number	Min. height	Max. height	Resolution	Chirp repetition	Doppler vel. max
MiRAC-A, 1	100	400	3.2	4096	8.7
	400	1200	7.5	3072	8.2
	1200	3000	9.7	2048	4.0
	3000	12000	23.8	1536	3.1
GRaWAC, 5	100	400	16.0	6144	4.8
	400	1200	17.8	4096	4.3
	1200	3000	23.6	3072	2.4
	3000	12000	28.6	2048	1.6
MiRAC-A, 5	150	1000	4.2	3072	8.3
	1000	4000	9.4	4096	3.9
	4000	10000	16.3	2048	1.9
GRaWAC, 6	150	1000	13.3	3584	4.3
	1000	4000	23.5	6144	3.4
	4000	10000	25.0	2560	1.6

Table 6.7 shows the chirp settings for the two radars. First, chirp settings 1 for MiRAC-A and 5 for GRaWAC were used. However, due to software problems with GRaWAC, we had to change its chirp settings on 29 August 2024 so that measurements could keep running. To facilitate a comparison of the two radars' data, we also changed MiRAC-A's chirp settings on 29 August 2024. Since then, apart from missing data (see paragraph *Data availability* below) and short trials with other settings, these chirp settings have run continuously until the end of the measuring period.

Calibration of cloud radars and microwave radiometers

We conducted calibrations with liquid nitrogen of the radars and microwave radiometers at both the start and midpoint of the cruise. GRaWAC was calibrated on 9 August 2024 and on 11 September 2024. MiRAC-A was calibrated on 9 August 2024 and 12 September 2024. Only the calibration on 12 September 2024 was successful, because we covered the transmitter with an absorber. Several unsuccessful attempts to calibrate MiRAC-A were performed before 12 September 2024. MiRAC-P was calibrated on 8 August 2024 and on 11 September 2024. HATPRO was calibrated on 9 August 2024 and 11 September 2024. We measured the brightness temperatures of liquid nitrogen target after the calibration to confirm the success of the calibration.

Data availability

All instruments operated nearly continuously while *Polarstern* was within the sea ice. The daily sample count, relative to nominal sampling frequency, was close to 100% on most days (Fig. 6.24). Below are periods of reduced data quality or availability:

- MiRAC-A: Radar reflectivity artifacts (10 August 2024–12 September 2024) due to liquid nitrogen calibration without absorber above transmitter. Partly off on 27 August 2024 due to falling ice. Possible timestamp drift (10 August–16 September 2024) from GPS. Inoperative (31 August–3 September 2024) due to software issues. Data gap on 6 September 2024 (binary files only). Several changes of chirp settings, changed to the final setting on 29 August 2024.
- GRaWAC: Intermittent recordings (10–26 August 2024) due to software issues. Partly off on 27 August 2024 due to falling ice. Possible GPS-related timestamp drift (10 August–16 September 2024). Several changes of chirp settings, changed to the final setting on 29 August 2024.
- HATPRO: Every second scan missing (10–13 August 2024). Scan adjustments (10-14 August 2024). Accumulation of liquid/ice on radomes (10–20 August 2024) due to reduced blower speed and heater failure. Surface scans only on parts of 27 August 2024 due to falling ice. Possible timestamp drift (10 August–16 September 2024). Only zenith scan (5 to 9 October 2024).
- MiRAC-P: Scan adjustments (10–14 August 2024). Surface scans only on parts of 27 August 2024 due to falling ice. Possible timestamp drift (10 August–16 September 2024). High TB noise at 340 GHz (1.3 K) compared to other channels (0.2–0.3 K) during the entire cruise. Only zenith scan (5 to 9 October 2024).
- FLIR: Inaccurate time (13–26 August 2024).
- Radiosonde: Six sondes missing (16–20 August 2024) due to issues with the ship's GPS antenna. No humidity recorded at 00 UTC on 23 August 2024.

At two periods during the cruise we increased the launch frequency of radiosondes. From 26 August 2024, 18:00 UTC, to 27 August 2024, 12:00 UTC, we launched a radiosonde every three hours to monitor a warm air intrusion. Additionally, we deployed extra radiosondes at 18:00 UTC as we neared the ice edge on our return, allowing us to more precisely capture the transition from the closed ice pack through the marginal ice zone to the open ocean.

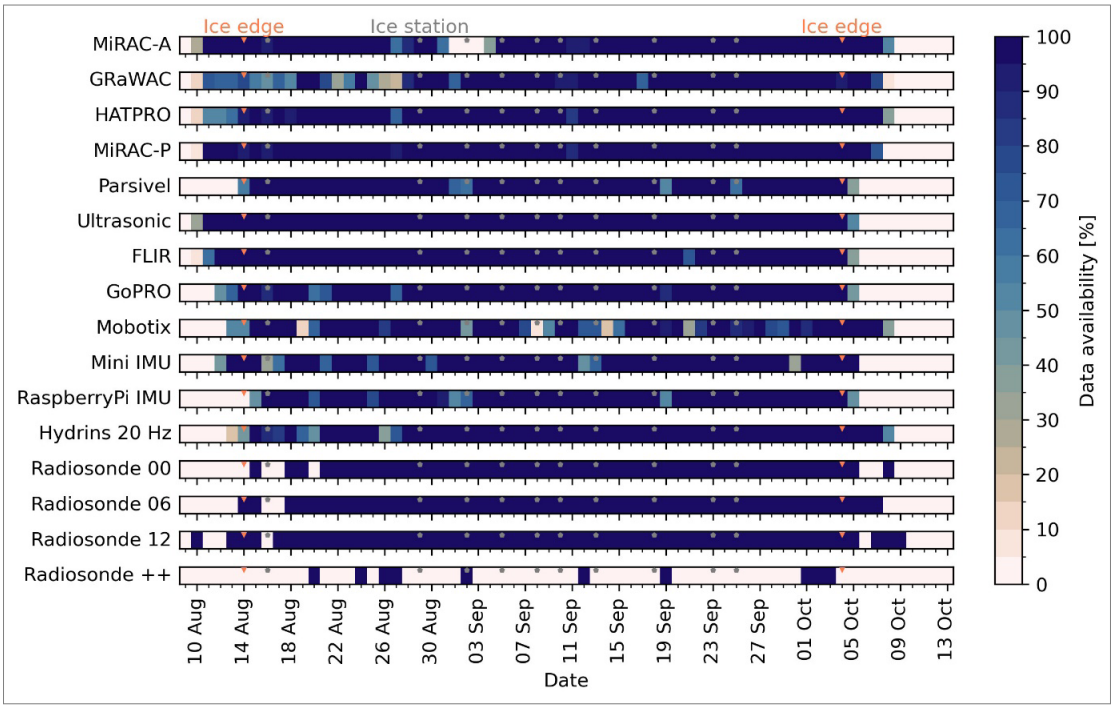

Fig. 6.24: Daily data availability from 9 August to 13 October 2024. Symbols indicate the ice edge and ice stations.

Preliminary results

Atmospheric measurements: Clouds

The two radars GRaWAC and MiRAC-A measure cloud particles in the G- and W-band that enable measuring different hydrometeor sizes. Through the combination of both radars sampling the same volume, we can detect cloud regions with smaller droplet sizes, an identifying factor of supercooled liquid droplets. The dual-frequency measurements of GRaWAC near the water absorption line at 183 GHz also allows for vertical profiling of water vapor.

Figure 6.25 shows a case study of a mixed-phase cloud with LWP about 250 g/m² based on HATPRO, showing radar reflectivities at 94 and 167 GHz, dual-frequency ratio of 94 and 167 GHz, the signal of the dual absorption radar in the G-band, and Doppler velocity. The radar reflectivities show a precipitating cloud, also visible in the Doppler velocity, where negative values indicate a downward movement of hydrometeors. A large gradient occurs in the dual-frequency ratio at a height of 2500 m which might result from a phase change from frozen in the lower part of the cloud to liquid on top, where the liquid attenuation in the G-band is larger, thus leading to a more pronounced difference in reflectivities between the frequencies. This is even more pronounced in the differential absorption radar (DAR) signal where very little liquid attenuation occurs below 2500 m but the attenuation strongly increases in higher altitudes.

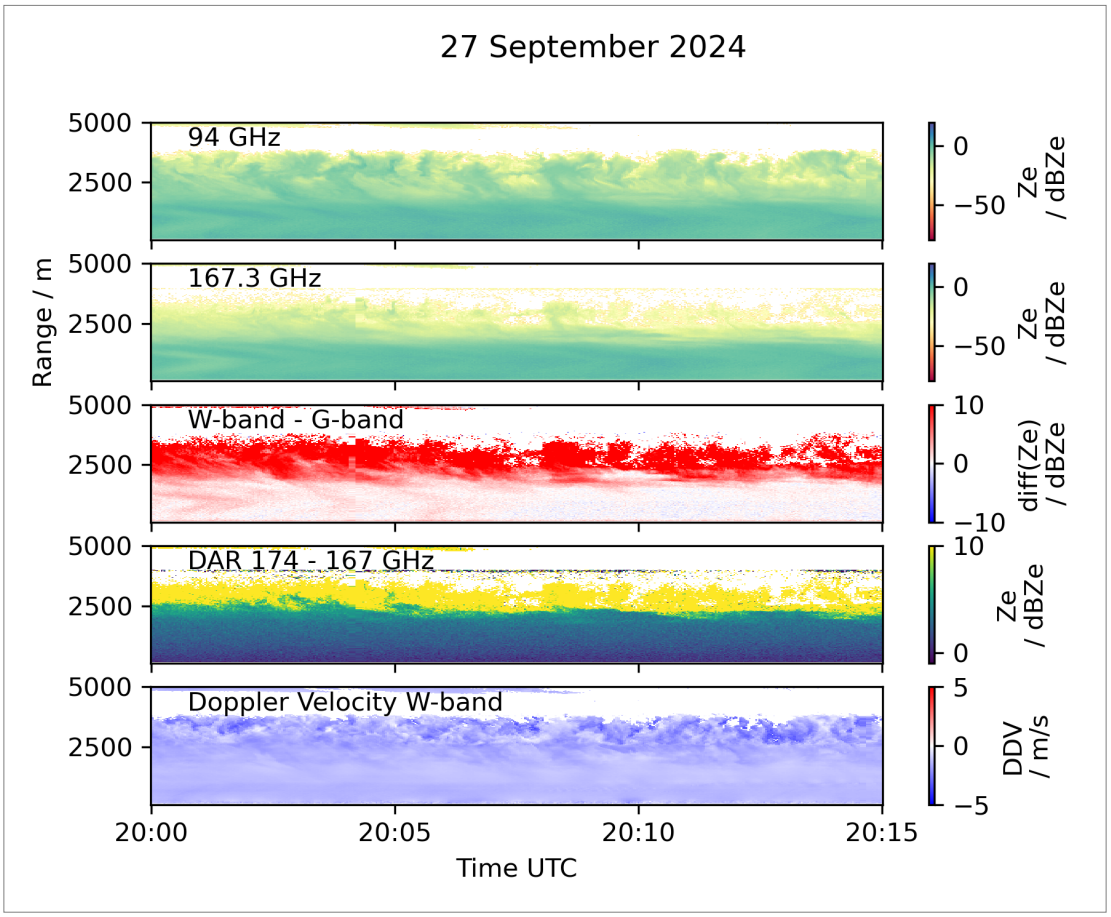

Fig. 6.25: Radar reflectivity at 94 and 167.3 GHz (W-band and G-band), their differences, the differential absorption radar (DAR) signal and the W-band Doppler velocity for a case study on 27 September 2024

Atmospheric measurements: Water vapor and temperature profile

The microwave radiometer observations from HATPRO and MiRAC-P provide information on the vertical profiles of water vapor and temperature as well as integrated water vapor. Figure 6.26 presents the HATPRO water vapor and temperature time series in comparison to radiosondes. The observations capture the transition from warm and humid Arctic summer to autumn freeze-up in early September. The driest conditions were observed in the Central Arctic in September with IWV as low as 4.5 kg/m². August features several events with elevated IWV, which are well captured by the continuous HATPRO data. Throughout September, the temperatures remained mostly below freezing level. The preliminary retrieval agrees well with radiosonde data with expected deficiencies in small-scale vertical temperature and humidity gradients. Improved retrieval results will be available from the synergy between HATPRO and MiRAC-P and from the addition of boundary layer scans. These observations provide reference data for satellite microwave retrievals of IWV for the central Arctic sea-ice region.

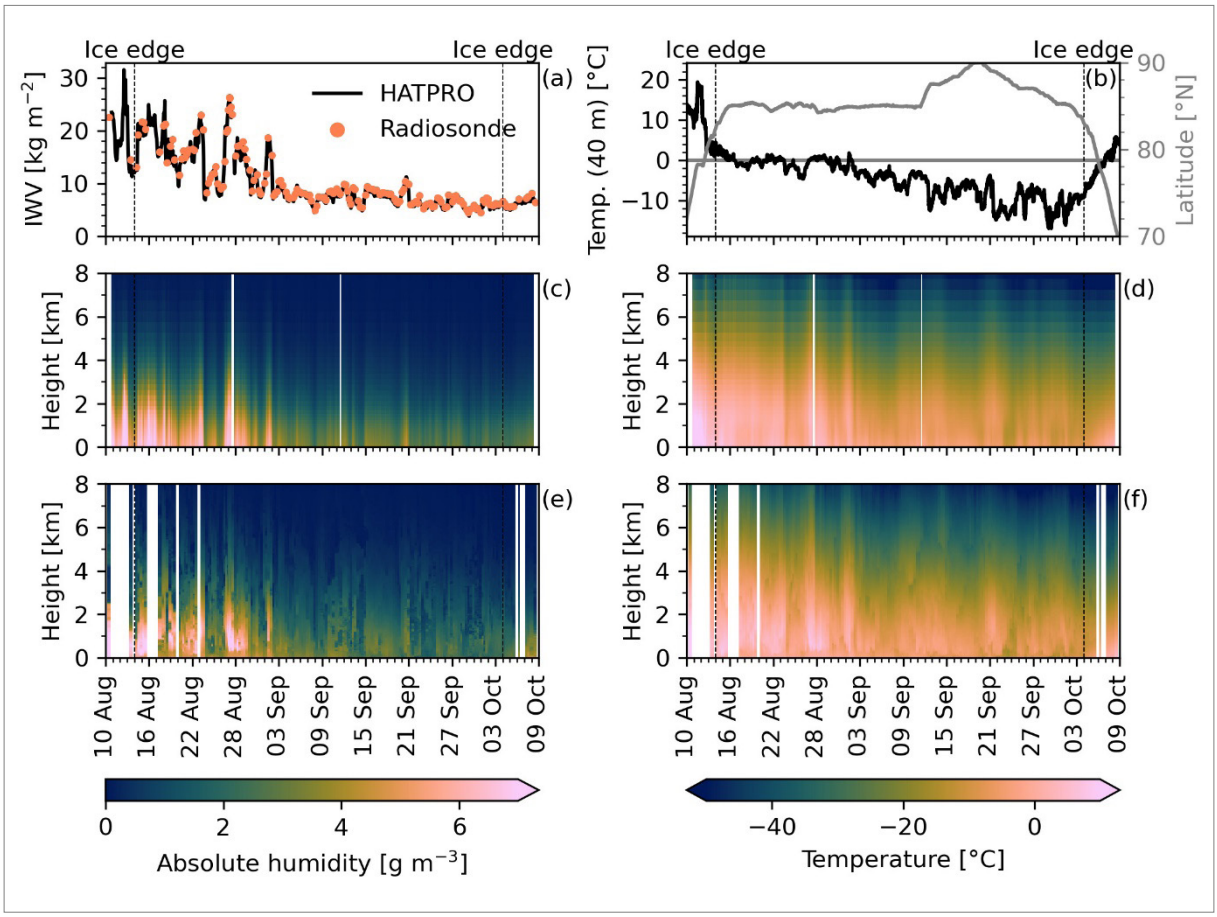

Fig. 6.26: Water vapor and temperature from HATPRO and radiosondes. (a) integrated water vapor (IWV), (b) temperature measured at the ship and ship latitude, (c) absolute humidity from HATPRO, (d) temperature from HATPRO, (e) absolute humidity from radiosondes, and (f) temperature from radiosonde

Surface microwave emission measurements

The ice surface measurements aim to increase the knowledge on microwave emissivity of the sea ice and its spatio-temporal variability at different frequencies at satellite footprint scales when *Polarstern* is moving through the ice. The time of the year of the expedition is of great value here, as we encountered many different surface classes during the cruise, covering a large part of the life cycle of sea ice. That is, we observed open water, young sea ice at different stages including grease ice, nilas, nilas with frost flowers, grey ice, pancake ice, as well as first-year and multi-year ice. While the sea ice surface was bare ice (surface scattering layer) with open melt ponds in the beginning of the cruise, with the start of September it started to snow and the ice was snow-covered.

Accordingly, the surface temperatures that we measured with the infrared camera also cover a large range of about 40 Kelvin. When comparing the IR measurements with the measured surface temperatures during the ten ice stations, we found a constant bias in the IR measurements of 3.58 K, which needs to be taken into account (in addition to IR surface emissivities) to derive actual surface temperatures from the IR brightness temperatures.

Figure 6.27 shows the histograms of the surface microwave observations at the different frequencies at 53° off-nadir. Open ocean and ice-covered surfaces are clearly distinguishable at 22 to 31 GHz (Fig. 6.27a) with the mode at lower brightness temperature indicating open ocean and the one at higher brightness temperature ice-covered surfaces. In contrast, the frequencies in the 58 GHz oxygen absorption complex are dominated by the atmosphere between radiometer and surface (Fig. 6.27c)) and show a clear surface signal only at the lower two frequencies (Fig. 6.27b). By including the downwelling brightness temperatures that were measured right before and after each surface observation and the measured surface temperatures from the IR camera in future analyses, we will be able to derive the 'pure' surface emissions to reveal more about the microwave signal at different frequencies for different surface types.

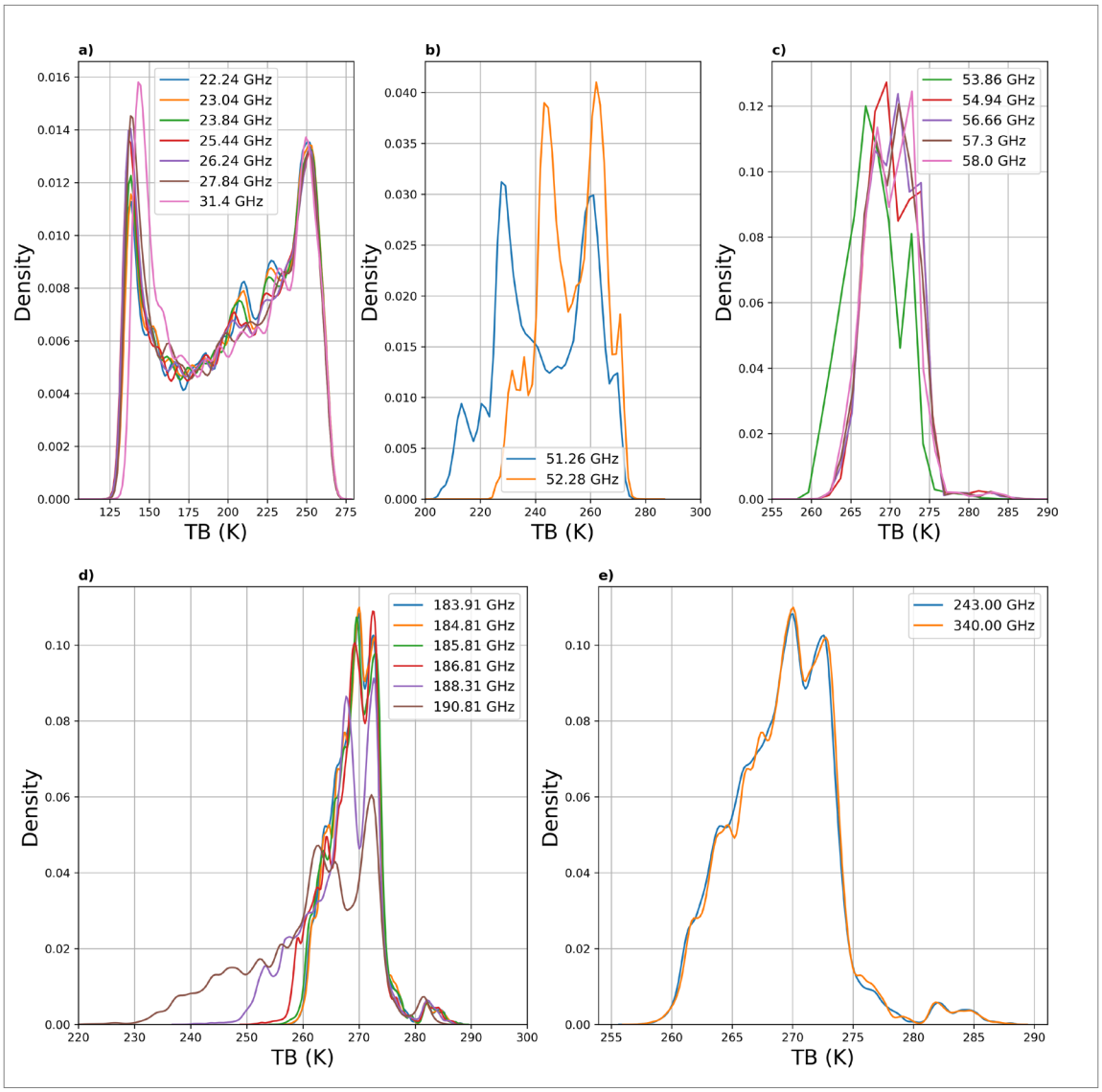

Fig. 6.27: Microwave brightness temperature measured by HATPRO (first row) and MiRAC-P (second row) of the surface at 53° off-nadir around the water vapor absorption line at 22 to 31 GHz, a),; in the 58 GHz oxygen absorption complex, b) and c); around the water vapor absorption line at 183 GHz, c); and at the high frequencies 243 and 340 GHz, d), vertical polarization. The number of observations is 802396 (916307) corresponding to around 223 (255) hours for HATPRO (MiRAC-P).

Data management

Environmental data will be archived, published, and disseminated according to international standards by the World Data Center PANGAEA Data Publisher for Earth & Environmental Science (www.pangaea.de) within two years of the end of the cruise. By default, the CC-BY license will be applied.

Any other data will be submitted to an appropriate long-term archive that provides unique and stable identifiers for the datasets and allows open online access to the data.

This expedition was supported by the Helmholtz Research Programme “Changing Earth – Sustaining our Future” Topic 2, Subtopic 1.

The VAMPIRE project is supported by the Deutsche Forschungsgemeinschaft (DFG, German Research Foundation) through the Transregional Collaborative Research Centre TRR-172 “ArctiC Amplification: Climate Relevant Atmospheric and SurfaCe Processes, and Feedback Mechanisms (AC)3” (grant 268020496)

In all publications based on this expedition, the **Grant No. AWI_PS144_05** will be quoted and the following publication will be cited:

Alfred-Wegener-Institut Helmholtz-Zentrum für Polar- und Meeresforschung (2017) Polar Research and Supply Vessel POLARSTERN Operated by the Alfred-Wegener-Institute. Journal of large-scale research facilities, 3, A119. http://dx.doi.org/10.17815/jlsrf-3-163.

References

Belter HJ, Krumpen T, von Albedyll L, Alekseeva TA, Birnbaum G, Frolov SV, Hendricks S, Herber A, Polyakov I, Raphael I, Ricker R, Serovetnikov, SS, Webster M, Haas C (2021) Interannual variability in Transpolar Drift summer sea ice thickness and potential impact of Atlantification. The Cryosphere 15:2575–2591. https://doi.org/10.5194/tc-15-2575-2021

Codiga, D., 2021. UTide Unified Tidal Analysis and Prediction Functions [WWW Document]. URL. https://www.mathworks.com/matlabcentral/leexchange/46523-utide-unied-tidal-analysis-and-prediction-functions. (Accessed 9 October 2024).

Denoth A (1989) Snow dielectric measurements. Adv. Space Res. 9:233–243.

Fuchs N, von Albedyll L, Birnbaum G, Linhardt F, Oppelt N, Haas C (2024) Sea ice melt pond bathymetry reconstructed from aerial photographs using photogrammetry: a new method applied to MOSAiC data. The Cryosphere 18:2991–3015. https://doi.org/10.5194/tc-18-2991-2024

Hutchings JK, Delamere J, Heil P (2018) The Ice Watch Manual, Draft 2018/06/30 for ASSIST v4.1. Draft Technical Report, University of Alaska Fairbanks, USA. http://icewatch.gina.alaska.edu/

Macfarlane AR, Dadic R, Smith MM, Light B, Nicolaus M, Henna-Reetta H, Webster M, Linhardt F, Hämmerle S, Schneebeli M (2023) Evolution of the microstructure and reflectance of the surface scattering layer on melting, level Arctic sea ice. Elementa: Science of the Anthropocene 11(1): 00103. https://doi.org/10.1525/elementa.2022.00103

Matzl M, Schneebeli M (2006) Measuring specific surface area of snow by near-infrared photography. Journal of Glaciology. 52(179):558–564. https://doi.org/10.3189/172756506781828412

Neckel N, Zeising O, Steinhage D, Helm V, Humbert A (2020) Seasonal Observations at 79°N Glacier (Greenland) From Remote Sensing and *in situ* Measurements. Front. Earth Sci. 8:142. https://doi.org/10.3389/feart.2020.00142

Neckel N, Fuchs N, Birnbaum G, Hutter N, Jutila A, Buth L, Von Albedyll L, Ricker R, Haas C (2023) Helicopter-borne RGB orthomosaics and photogrammetric digital elevation models from the MOSAiC Expedition. Sci Data 10:426. https://doi.org/10.1038/s41597-023-02318-5.

Nicolaus N, Perovich D, Spreen G et al. (2022) Overview of the MOSAiC expedition: Snow and sea ice. Elementa: Science of the Anthropocene 10(1):000046. https://doi.org/10.1525/elementa.2021.000046

Picard G, Sandells M, Löwe H (2018) SMRT: an active–passive microwave radiative transfer model for snow with multiple microstructure and scattering formulations (v1.0). Geosci. Model Dev. 11: 2763–2788. https://doi.org/10.5194/gmd-11-2763-2018

Spreen G, Kaleschke L, Heygster G (2008) Sea ice remote sensing using AMSR-E 89 GHz channels J. Geophys. Res.,. 113:C02S03. https://doi.org/10.1029/2005JC003384

Tadono T, Ishida H, Oda F, Naito S, Minakawa K, & Iwamoto H (2014) Precise Global DEM Generation by ALOS PRISM, ISPRS Ann. Photogramm. Remote Sens. Spatial Inf. Sci. II-4:71–76. https://doi.org/10.5194/isprsannals-II-4-71-2014

Takaku J, Tadono T, Doutsu M, Ohgushi F, Kai H (2020) Updates of 'AW3D30' alos global digital surface model with other open access datasets. Int. Arch. Photogramm. Remote Sens. Spatial Inf. Sci., XLIII-B4-2020 183–189. https://doi.org/10.5194/isprs-archives-XLIII-B4-2020-183-2020

Tétreault P, Kouba J, Héroux P, Legree P (2005) CSRS-PPP: an internet services for GPS user access to the Canadian spatial reference frame. Geomatica 59(1):17–28. https://doi.org/10.5623/geomat-2005-0004

Webster MA, Holland M, Wright NC, Hendricks S, Hutter N, Itkin P, Light B, Linhardt F, Perovich DK, Raphael IA, Smith MM, Von Albedyll L, Zhang J (2022) Spatiotemporal evolution of melt ponds on Arctic sea ice: MOSAiC observations and model results. Elementa: Science of the Anthropocene 10 (1): 000072. https://doi.org/10.1525/elementa.2021.000072.

WMO (1989) WMO sea ice nomenclature. World Meteorological Organization, Geneva, Switzerland, WMO/OMM/BMO 259-TP-145, suppl. 5.

Tab. 6.3: List of all ice stations of PS144.

Next to the respective GPS reference times we list the associated geographic positions, contemporary acquired SAR data and some additional remarks. The column labelled 'Ice Station' refers to the corresponding ship-registered ice station event (without leading zeros). The addition of 'ICE01' to 'ICE10' is chapter specific and links the event labels to Figure 6.13.

Ice Station	Date	GPS Reference Time	Latitude	Longitude	SAR data	Ice age (~60 km radius)	Comments
PS144_007_01_ICE01	2024-08-16	2024-08-16 17:00:00	85.05805	42.93493	TDX1_SAR__MGD_RE___SC_S_SRA_20240816T075225_20240816T075244	2 years	No snow, open melt ponds
PS144_010_01_DirtyIce	2024-08-19	2024-08-19 13:00:00	85.25657	83.59989	TDX1_SAR__MGD_RE___SC_S_SRA_20240819T052545_20240819T052614	2 years	
PS144_023_01_ICE02	2024-08-29	2024-08-29 22:00:00	84.50036	115.72034	CSG_SSAR2_GEC_B_0101_STR_024_HH_RD_F_20240829101620_20240829101627_1_F_85N_Z61_N00	1 year	no snow, frozen melt ponds
PS144_042_01_ICE03	2024-09-02 - 2024-09-03	2024-09-02 23:00:00	84.83094	128.87743	TDX1_SAR__MGD_RE___SC_S_SRA_20240903T010728_20240903T010750	1 year	little snow (<5cm)
PS144_050_01_ICE04	2024-09-04 - 2024-09-05	2024-09-05 09:09:21	85.02579	139.94363	CSG_SSAR2_GEC_B_0101_STR_022_HH_RD_F_20240905090917_20240905090924_1_F_85N_Z61_N00	1 year	snow
PS144_067_01_ICE05	2024-09-08	2024-09-08 15:00:00	84.94667	162.09426	CSG_SSAR1_GEC_B_0101_STR_022_HH_RD_F_20240908073814_20240908073821_1_F_85N_Z61_N00	1 year	snow
PS144_080_01_ICE06	2024-09-10 - 2024-09-11	2024-09-11 01:00:00	84.93331	179.41320		1 year	snow
PS144_085_01_ICE07	2024-09-12 - 2024-09-13	2024-09-13 09:00:00	87.50035	178.72568	CSG_SSAR2_GEC_B_0101_STR_022_HH_RA_F_20240912160638_20240912160645_1_F_88N_Z61_N00	2 years	snow, low contrast
PS144_109_01_ICE08	2024-09-18 - 2024-09-19	2024-09-19 09:20:15	89.95154	-142.69616	CSG_SSAR1_GEC_B_0101_STR_026_HH_RD_F_20240919092011_20240919092018	2 years	North pole, snow
PS144_123_02_ICE09	2024-09-23	2024-09-23 10:00:00	88.07016	59.95280	CSG_SSAR2_GEC_B_0101_STR_027_HH_RD_F_20240923125924_20240923125931_1_F_88N_Z61_N00	4 years	Foggy, snow
PS144_134_01_ICE10	2024-09-25 - 2024-09-26	2024-09-26 06:00:00	87.04715	57.07384	CSG_SSAR2_GEC_B_0101_STR_027_HH_RD_F_20240925133611_20240925133618_1_F_87N_Z61_N00	4 years	snow

Tab. 6.4: Detailed list of all devices employed during the ice stations listed in Table 6.3. Labels refer to the event labels listed in AWI's O2A database.

	Device	Label	Start (UTC)	Stop (UTC)	Comments
PS144_007_01_ ICE01	GEM-512	PS144_007_ GEM	2024-08-16 15:57:43	2024-08-16 16:37:36	Ice station survey
	Magnaprobe (Katrin)	PS144_7_ Magna-Katrin	2024-08-16 13:45:11	2024-08-16 14:50:18	By chem team, no snow
	Mavic flight 1	PS144_007_ MAVIC1	2024-08-16 11:40:37	2024:08:16 11:54:47	Pre-station flight (1st grid flight test)
	Mavic flight 2	PS144_007_ MAVIC2	2024-08-16 18:16:29	2024-08-16 18:54:50	Ice station flight (manual)
	DJI Matrice 350 RTK	PS144_007_ M350	2024-8-16 14:10:00	2024-8-16 14:25:00	Testflight: Nadir and Overview Images
	GPS1	PS144_007_ GPS1	2024-08-16 14:33:15	2024-08-16 19:12:14	DGPS measurement at ice station
	GPS2	PS144_007_ GPS2	2024-08-16 15:17:44	2024-08-16 19:02:40	DGPS measurement at ice station
	GPS5	PS144_007_ GPS5	2024-08-16 14:16:50	2024-08-16 19:09:43	DGPS measurement at ice station
	GPS6	PS144_007_ GPS6	2024-08-16 14:25:45	2024-08-16 19:09:40	DGPS measurement at ice station
	Ice core (radiometer footprint)	PS144_007_ ps144_ physics_coring	2024-08-16 17:00:00	2024-08-16 18:30:00	1 core
	Snow and surface (radiometer footprint)	PS144_007_ ps144_snow_ sip	2024-08-16 13:40:00	2024-08-16 15:50:00	no snow, 1 CT sample (bare ice/SSL), 42 SnowImager photos, 1 surface roughness site
	SPLISH	PS144_007_ SPLISH	2024-08-16 17:00:00	2024-08-16 17:45:00	Depth profiles of two melt ponds
PS144_010_01_ DirtyIce	GPS1	PS144_010_ GPS1	2024-08-19 12:36:20	2024-08-19 14:15:50	DGPS measurement on vessel
	Mavic	PS144_010_ MAVIC	2024-08-19 13:14:41	2024-08-19 13:16:07	Short manual flight on short notice

	Device	Label	Start (UTC)	Stop (UTC)	Comments
PS144_023_01_ ICE02	GEM-512	PS144_023_ GEM	2024-08-29 18:58:50	2024-08-29 19:32:47	Ice station survey, GEM towed by snowmobile
	Magnaprobe (Katrin)	PS144_23_ Magna-Katrin	2024-08-29 17:47:59	2024-08-29 19:20:09	By chem team, no snow
	Mavic	PS144_023_ MAVIC	2024-08-29 21:08:59	2024-08-29 22:03:11	Ice station flight (manual)
	DJI Matrice 350 RTK	PS144_023_ M350	2024-08-29 13:20:00	2024-08-29 13:40:00	Automatic Survey Processed in Terra:”20240829-RGB Survey 2. Eisstation”
	GPS1	PS144_023_ GPS1	2024-08-29 14:28:45	2024-08-30 09:49:13	DGPS measurement at ice station
	GPS2	PS144_023_ GPS2	2024-08-29 15:45:13	2024-08-30 09:39:28	DGPS measurement at ice station
	GPS3	PS144_023_ GPS3	2024-08-29 15:19:44	2024-08-30 09:32:41	DGPS measurement at ice station
	GPS4	PS144_023_ GPS4	2024-08-29 15:00:12	2024-08-30 09:55:22	DGPS measurement at ice station
	GPS5	PS144_023_ GPS5	2024-08-29 16:13:15	2024-08-30 09:43:59	DGPS measurement at ice station
	GPS6	PS144_023_ GPS6	2024-08-29 15:33:44	2024-08-30 09:36:15	DGPS measurement at ice station
	Ice core (radiometer footprint)	PS144_023_ ps144_ physics_coring	2024-08-29 19:45:00	2024-08-29 21:30:00	1 core
	Snow and surface (radiometer footprint)	PS144_023_ ps144_snow_ sip	2024-08-29 17:20:00	2024-08-30 09:20:00	no snow, 2 CT samples (bare ice/(saline) SSL), 48 SnowImager photos, 2 surface roughness sites

	Device	Label	Start (UTC)	Stop (UTC)	Comments
PS144_042_01_ ICE03	GEM-512	PS144_042_ GEM	2024-09-02 22:38:52	2024-09-03 00:16:31	Ice station survey
	Mavic	PS144_042_ MAVIC	2024-09-02 23:01:30	2024-09-02 23:32:04	Ice station grid flight
	DJI Matrice 350 RTK	PS144_042_ M350_Lidar	2024-09-02 22:10:00	2024-09-02 22:30:00	Lidartest Processed in Terra:"20240903-Eisstation-Lidar"
	DJI Matrice 350 RTK	PS144_042_ M350_Cam	2024-09-02 22:10:00	2024-09-02 22:30:00	Automatic Survey Processed in Terra:"20240903-Eisstation-RGB"
	GPS1	PS144_042_ GPS1	2024-09-02 21:28:15	2024-09-03 00:26:46	DGPS measurement at ice station
	GPS2	PS144_042_ GPS2	2024-09-02 21:53:20	2024-09-03 00:22:28	DGPS measurement at ice station
	GPS5	PS144_042_ GPS5	2024-09-02 21:09:20	2024-09-03 00:19:33	DGPS measurement at ice station
	Ice core (radiometer footprint)	PS144_042_ ps144_ physics_coring	2024-09-02 22:00:00	2024-09-02 23:30:20	1 core
	Snow and surface (radiometer footprint)	PS144_042_ ps144_snow_ sip	2024-09-02 21:30:00	2024-09-02 23:20:00	no snow, no CT sample, 5 SnowImager measurements (no transect, 2 sites), 1 surface roughness site
PS144_ICE_ RIDGE	Mavic	PS144_ICE_ RIDGE_MAVIC	2024-09-03 18:48:14	2024-09-03 18:52:48	Short stop at a large ice ridge, short manual flight from vessel

	Device	Label	Start (UTC)	Stop (UTC)	Comments
PS144_050_01_ ICE04	GEM-512	PS144_050_ GEM	2024-09-05 11:48:57	2024-09-05 13:11:24	Ice station survey
	Mavic	PS144_050_ MAVIC	2024-09-05 08:03:23	2024-09-05 08:10:15	Ice station grid flight
	DJI Matrice 350 RTK	PS144_050_ M350	2024-09-05 07:10	2024-09-05 07:30	2 flight lines Processed in Terra:”20240905-Lidar-ICE4”
	Magnaprobe (Steffi)	PS144_050_ MAGNA	2024-09-05 11:48:40	2024-09-05 13:04:47	Ice station survey, co-located with GEM
	Magnaprobe (Katrin)	PS144_50_ Magna-Katrin	2024-09-05 00:40:06	2024-09-05 01:42:57	By chem team
	GPS1	PS144_050_ GPS1	2024-09-04 22:54:51	2024-09-05 16:34:40	DGPS measurement at ice station
	GPS2	PS144_050_ GPS2	2024-09-04 22:32:44	2024-09-05 16:58:52	DGPS measurement at ice station
	GPS3	PS144_050_ GPS3	2024-09-04 23:38:44	2024-09-05 16:51:16	DGPS measurement at ice station
	GPS4	PS144_050_ GPS4	2024-09-04 23:12:13	2024-09-05 16:40:31	DGPS measurement at ice station
	GPS5	PS144_050_ GPS5	2024-09-04 23:23:45	2024-09-05 16:45:12	DGPS measurement at ice station
	GPS6	PS144_050_ GPS6	2024-09-04 22:46:20	2024-09-05 16:55:04	DGPS measurement at ice station
	Ice core (radiometer footprint)	PS144_050_ ps144_ physics_coring	2024-09-05 09:30:00	2024-09-05 11:00:00	1 core
	Snow and surface (radiometer footprint)	PS144_050_ ps144_snow_ sip	2024-09-05 07:00:00	2024-09-05 11:00:00	1 snow pit, 2 CT samples, 7 SnowImager photos (battery problems), 1 surface roughness site, 11 Denoth measurements

	Device	Label	Start (UTC)	Stop (UTC)	Comments
PS144_067_01_ ICE05	GEM-512	PS144_067_ GEM	2024-09-08 13:21:25	2024-09-08 15:17:29	Ice station survey
	Mavic	PS144_067_ MAVIC	2024-09-08 19:14:59	2024-09-08 19:49:24	Ice station grid flight
	DJI Matrice 350 RTK	PS144_067_ M350_1	2024-09-08 17:00	2024-09-08 17:25	2 flight lines Processed in Terra: ”20240908-Lidar-ICE5” “20240908-Lidar-ICE5-2”
	DJI Matrice 350 RTK	PS144_067_ M350_2	2024-09-08 18:00	2024-09-08 18:20	2 flight lines Processed in Terra: ”20240908-Lidar-ICE5-3” “20240908-Lidar-ICE5-4”
	Magnaprobe (Steffi)	PS144_067_ MAGNA	2024-09-08 13:13:19	2024-09-08 15:22:13	Ice station survey, co-located with GEM
	Magnaprobe (Katrin)	PS144_67_ Magna-Katrin	2024-09-08 08:34:13	2024-09-08 10:07:17	By chem team
	GPS1	PS144_067_ GPS1	2024-09-08 09:10:45	2024-09-08 20:05:40	DGPS measurement at ice station
	GPS2	PS144_067_ GPS2	2024-09-08 08:46:35	2024-09-08 19:50:55	DGPS measurement at ice station
	GPS3	PS144_067_ GPS3	2024-09-08 09:41:25	2024-09-08 20:26:35	DGPS measurement at ice station
	GPS4	PS144_067_ GPS4	2024-09-08 08:59:15	2024-09-08 19:59:05	DGPS measurement at ice station
	GPS5	PS144_067_ GPS5	2024-09-08 09:22:15	2024-09-08 20:22:30	DGPS measurement at ice station
	GPS6	PS144_067_ GPS6	2024-09-08 09:31:45	2024-09-08 20:09:35	DGPS measurement at ice station
	Ice core (radiometer footprint)	PS144_067_ ps144_ physics_coring	2024-09-08 09:30:00	2024-09-08 11:40:00	1 core
	Snow and surface (radiometer footprint)	PS144_067_ ps144_snow_ sip	2024-09-08 08:40:00	2024-09-08 10:40:00	1 snow pit, 2 CT samples, 19 SnowImager photos, 2 surface roughness sites, no Denoth measurements

	Device	Label	Start (UTC)	Stop (UTC)	Comments
PS144_080_01_ ICE06	GEM-512	PS144_080_ GEM	2024-09-11 02:00:35	2024-09-11 02:49:54	Ice station survey
	Mavic	PS144_080_ MAVIC	2024-09-11 00:55:55	2024-09-11 01:06:49	Ice station grid flight
	DJI Matrice 350 RTK	PS144_080_ M350	2024-09-10 22:50	2024-09-10 23:15	2 flight lines Processed in Terra: “20240910-Lidar-ICE6” ”20240910-Lidar-ICE6-2”
	Magnaprobe (Steffi)	PS144_080_ MAGNA	2024-09-11 01:46:03	2024-09-11 02:51:56	Ice station survey, co-located with GEM
	GPS1	PS144_080_ GPS1	2024-09-10 22:54:45	2024-09-11 03:11:50	DGPS measurement at ice station
	GPS2	PS144_080_ GPS2	2024-09-10 22:43:05	2024-09-11 03:20:35	DGPS measurement at ice station
	GPS3	PS144_080_ GPS3	2024-09-10 22:24:35	2024-09-11 03:25:15	DGPS measurement at ice station
	GPS4	PS144_080_ GPS4	2024-09-10 22:16:45	2024-09-11 03:28:30	DGPS measurement at ice station
	Ice core (radiometer footprint)	PS144_080_ ps144_ physics_coring	2024-09-10 23:45:00	2024-09-11 01:30:00	1 core
	Snow and surface (radiometer footprint)	PS144_080_ ps144_snow_ sip	2024-09-10 22:40:00	2024-09-10 23:40:00	2 snow pits, 2 CT samples, 22 SnowImager photos, 2 surface roughness sites, 2 Denoth measurements

	Device	Label	Start (UTC)	Stop (UTC)	Comments
PS144_085_01_ ICE07	GEM-512	PS144_085_ GEM	2024-09-13 10:20:52	2024-09-13 11:14:48	Ice station survey
	Mavic	PS144_085_ MAVIC	2024-09-13 08:47:26	2024-09-13 09:28:23	Ice station grid flight, very low contrast
	DJI Matrice 350 RTK	PS144_085_ M350_Cam	2024-09-13 19:25:00	2024-09-13 19:50	Nadir and Overview Images
	DJI Matrice 350 RTK	PS144_085_ M350_Lidar	2024-09-13 08:00:00	2024-09-13 08:25	2 flight lines Processed in Terra: “20240913-Lidar-ICE7” ”20240913-Lidar-ICE7-2”
	Magnaprobe (Steffi)	PS144_085_ MAGNA	2024-09-13 10:18:21	2024-09-13 11:16:24	Ice station survey, co-located with GEM
	Magnaprobe (Katrin)	PS144_85_ Magna-Katrin	2024-09-12 22:48:06	2024-09-12 23:35:08	By chem team
	GPS1	PS144_085_ GPS1	2024-09-12 20:44:10	2024-09-13 18:37:05	DGPS measurement at ice station
	GPS2	PS144_085_ GPS2	2024-09-12 20:24:30	2024-09-13 19:13:10	DGPS measurement at ice station
	GPS3	PS144_085_ GPS3	2024-09-12 21:11:45	2024-09-13 19:02:25	DGPS measurement at ice station
	GPS4	PS144_085_ GPS4	2024-09-12 21:21:15	2024-09-13 19:22:40	DGPS measurement at ice station
	GPS5	PS144_085_ GPS5	2024-09-12 20:55:15	2024-09-13 18:42:20	DGPS measurement at ice station
	GPS6	PS144_085_ GPS6	2024-09-12 21:04:30	2024-09-13 18:50:35	DGPS measurement at ice station
	Ice core (radiometer footprint)	PS144_085_ ps144_ physics_coring	2024-09-13 12:30:00	2024-09-13 14:30:00	1 core
	Snow and surface (radiometer footprint)	PS144_085_ ps144_snow_ sip	2024-09-13 10:45:00	2024-09-13 12:00:00	2 snow pits, 2 CT samples, 22 SnowImager photos, 2 surface roughness sites, 1 Denoth measurement

	Device	Label	Start (UTC)	Stop (UTC)	Comments
PS144_109_01_ ICE08	GEM-512	PS144_109_ GEM	2024-09-19 10:26:54	2024-09-19 11:22:25	Ice station survey
	Mavic	PS144_109_ MAVIC	2024-09-18 23:13:52	2024:09:18 23:22:23	Ice station manual flight
	Magnaprobe (Steffi)	PS144_109_ MAGNA	2024-09-19 10:26:04	2024-09-19 11:26:36	Ice station survey, co-located with GEM
	Magnaprobe (Katrin)	PS144_109_ Magna-Katrin	2024-09-19 00:14:04	2024-09-19 02:31:12	By chem team
	GPS2	PS144_109_ GPS2	2024-09-18 22:36:05	2024-09-19 21:17:55	DGPS measurement at ice station
	GPS3	PS144_109_ GPS3	2024-09-18 22:50:05	2024-09-19 20:53:45	DGPS measurement at ice station
	GPS4	PS144_109_ GPS4	2024-09-18 23:00:15	2024-09-19 20:57:35	DGPS measurement at ice station
	GPS5	PS144_109_ GPS5	2024-09-18 22:20:25	2024-09-19 21:01:40	DGPS measurement at ice station
	GPS6	PS144_109_ GPS6	2024-09-18 22:10:00	2024-09-19 21:07:30	DGPS measurement at ice station, data gaps
	Ice core (radiometer footprint)	PS144_109_ ps144_ physics_coring	2024-09-18 23:15:00	2024-09-19 15:40:00	2 cores
	Snow and surface (radiometer footprint)	PS144_109_ ps144_snow_ sip	2024-09-18 22:15:00	2024-09-19 15:40:00	2 snow pits, 1 CT sample, 30 SnowImager photos, 3 surface roughness sites, no Denoth measurements

	Device	Label	Start (UTC)	Stop (UTC)	Comments
PS144_123_02_ ICE09	GEM-512	PS144_123_ GEM	2024-09-23 08:21:32	2024-09-23 09:07:03	Ice station survey
	Mavic	PS144_123_ MAVIC	2024-09-23 09:18:43	2024-09-23 10:01:38	Ice station grid flight, very low contrast
	DJI Matrice 350 RTK	PS144_123_ M350	2024-09-23 08:50	2024-09-23 09:10	2 flight lines Processed in Terra: “20240923-Lidar-ICE9” ”20240923-Lidar-ICE9-2”
	Magnaprobe (Katrin)	PS144_123_ Magna-Katrin	2024-09-23 07:50:29	2024-09-23 09:11:34	By chem team, co-located with gem
	GPS2	PS144_123_ GPS2	2024-09-23 07:07:45	2024-09-23 11:49:30	DGPS measurement at ice station
	GPS3	PS144_123_ GPS3	2024-09-23 07:25:45	2024-09-23 11:46:25	DGPS measurement at ice station
	GPS4	PS144_123_ GPS4	2024-09-23 07:10:45	2024-09-23 11:39:25	DGPS measurement at ice station, used as rover
	GPS5	PS144_123_ GPS5	2024-09-23 07:17:15	2024-09-23 11:42:15	DGPS measurement at ice station
	Ice core (radiometer footprint)	PS144_123_ ps144_ physics_coring	2024-09-23 06:45:00	2024-09-23 09:30:00	1 core
	Snow and surface (radiometer footprint)	PS144_123_ ps144_snow_ sip	2024-09-23 06:45:00	2024-09-23 08:45:00	2 snow pits, 1 CT sample, 21 SnowImager photos, 3 surface roughness sites, no Denoth measurements

	Device	Label	Start (UTC)	Stop (UTC)	Comments
PS144_134_01_ ICE10	GEM-512	PS144_134_ GEM	2024-09-26 01:29:24	2024-09-26 02:18:43	Ice station survey
	Mavic	PS144_134_ MAVIC	2024-09-26 04:49:53	2024:09:26 05:08:44	Ice station grid flight
	DJI Matrice 350 RTK	PS144_134_ M350_Lidar	2024-09-26 18:05	2024-09-16 18:30	4 flight lines Processed in Terra: “20240916-Lidar-ICE10.1” ”20240916-Lidar-ICE10.2” “20240916-Lidar-ICE10.3” “20240916-Lidar-ICE10.4”
	Matrice-Cam	PS144_134_ M350_Cam	2024-09-25 08:00	2024-09-25 08:50	2 flights: Ice detection with live view
	Magnaprobe (Steffi)	PS144_134_ MAGNA	2024-09-26 01:24:39	2024-09-26 02:18:18	Ice station survey, co-located with GEM
	Magnaprobe (Katrin)	PS144_134_ Magna-Katrin	2024-09-25 23:48:23	2024-09-26 19:58:08	By chem team, co-located with GEM
	GPS2	PS144_134_ GPS2	2024-09-26 03:09:15	2024-09-26 19:50:20	DGPS measurement at ice station
	GPS3	PS144_134_ GPS3	2024-09-24 21:58:30	2024-09-26 20:02:30	DGPS measurement at ice station, started recording on vessel
	GPS4	PS144_134_ GPS4	2024-09-26 03:16:15	2024-09-26 19:01:30	DGPS measurement at ice station
	GPS5	PS144_134_ GPS5	2024-09-25 06:53:50	2024-09-26 20:07:25	DGPS measurement at ice station, started recording on vessel
	GPS6	PS144_134_ GPS6	2024-09-26 03:24:00	2024-09-26 19:12:30	DGPS measurement at ice station
	Ice core (radiometer footprint)	PS144_134_ ps144_ physics_coring	2024-09-26 02:00:00	2024-09-26 04:00:00	2 cores
	Snow and surface (radiometer footprint)	PS144_134_ ps144_snow_ sip	2024-09-26 00:40:00	2024-09-26 14:58:48	2 snow pits, 1 CT sample, 35 SnowImager photos, 2 surface roughness sites, no Denoth measurements

7. PELAGIC AND SEA-ICE BIOLOGY – PSB

Hauke Flores[1], Magnus Lucassen[1], Serdar Sakinan[2], Kim Vane[1], Youngju Lee[3], Jannis Hümmling[1], Kamila Faizieva[4], Nils Koschnick[1], Sandra Murawski[1], Martina Vortkamp[1], Insa Kaphegyi[5], Jan Zimmermann[5], Michiel van Dorssen[6]; not on board: Doreen Kohlbach[1], Katja Metfies[1], Barbara Niehoff[1], Fokje Schaafsma[2], Jutta Wollenburg[1], Eun Jin Yang[3], Christoph Stransky[7], Sarah Maes[8], Pauline Snoeijs-Leijonmalm[9]

[1]DE.AWI
[2]NL.WMR
[3]KR.KOPRI
[4]AT.Uni-Wien
[5]DE.UHH
[6]NL.vDMet
[7]DE.TI
[8]BE.EV-ILVO
[9]SW.SU

Grant-No. AWI_ AWI_ PS144_06

Objectives

In light of rapid environmental changes in the Arctic Ocean, notably unprecedented ice melt and alterations in oceanic circulation patterns, there is a pressing need to understand the ecosystem dynamics in this remote region. The Central Arctic Ocean Fisheries Agreement (**CAOFA**) emphases the necessity to advance scientific knowledge before considering ecologically sustainable fisheries development. Our expedition ArcWatch-2 is part of the **ArcWatch** campaign in the Central Arctic Ocean (CAO) between 2023 and 2027, as part of the *Programme-Oriented-Research (POF) IV* programme of the Helmholtz association. In order to understand impacts of the climate crisis and predict the future development of the coupled physical-chemical-biological system in the Arctic Ocean, ArcWatch in conjunction with MOSAiC 2019-2020, the approximately 20 Synoptic Arctic Survey (SAS) expeditions 2020-2022, and various observing frameworks by national and international networks (e.g., FRAM, the Nansen Legacy, SUDARCO, Arctic PASSION), aim for systematic interdisciplinary long-term observations in the Arctic Ocean. This is accomplished by sampling of a predefined set of physical, chemical and biological core parameters, applying unified standards and protocols across temporal and spatial scales as part of time series observation in the Arctic Ocean. This approach provides us with adequate information to estimate consequences of the climate crisis on Arctic ecosystems, including the remote CAO.

Besides research related to POF IV, work of parts of the team Pelagic- and Sea-Ice Biology (PSB) is performed under the auspices of the EU-tender *SciCAO* which aims to broaden the knowledge basis on the distribution of fish and their prey in the CAO as part of the Joint Programme for Scientific Research and Monitoring (JPSRM) of the CAOFA. JPSRM-relevant sampling is coordinated with the project Korean Polar Research Institute (KOPRI) programme *Korea- Arctic Ocean Warming and Response of Ecosystem* (K-AWARE) on expedition ARA15B with *Araon* in the Pacific Arctic.

The overarching objective of team PSB is to elucidate the biogeochemical and ecological processes governing primary productivity, biodiversity, trophic interactions and the biological carbon pump within the CAO. Through a systematic interdisciplinary approach integrating physical oceanography, sea-ice physics, marine biology and biogeochemistry we aim to provide crucial insights into the functioning of the unique 3.3 million km^2 ecosystem around the North Pole that until recently was permanently ice-covered. The results of ArcWatch-2 will

produce crucial information for the development of effective conservation and management strategies in the CAO. Our expedition aims to achieve the following specific goals:

1. **Collect core parameters of ArcWatch and POF IV for long-term observations:** We will comprehensively assess the biological landscape of the CAO ecosystem, ranging from microbial communities to fish populations, while elucidating trophic linkages and the biological carbon pump. This investigation will encompass sampling of particulate organic matter (POM), ice algae, phytoplankton, zooplankton, protist DNA and cryogenic gypsum across the water column and sea ice habitats. Phytoplankton analysis will be complemented by high-resolution taxonomic analysis from KOPRI.
2. **Investigate the distribution and abundance of fish and their prey in the CAO (SciCAO):** Through a hydroacoustic survey and sampling of fish, zooplankton and metazoan eDNA, we will document the spatial distribution and abundance of fish species within the CAO, along with their associated prey communities. Transcriptomic studies in conjunction with ecophysiological proxies of collected fish in comparison to existing field and laboratory samples will be used to assess the status and adaptational potential of the specimens from CAO. This study will provide essential baseline data for the JPSRM.
3. **Contribute to the record on foraminifera in the changing CAO in relation to paleo-oceanographic sediment records:** By examining foraminifera populations in zooplankton samples collected from the CAO, we aim to compare present changes in relation to past environmental conditions.

Work at sea

The biological and biogeochemical parameters sampled during ArcWatch-2 complement each other for the purpose of obtaining a system understanding of biodiversity and ecosystem functions. They were organised in three closely interconnected work packages (WP).

WP1 ArcWatch core parameters and other POF IV-related sampling

Using **water samples collected with the CTD rosette**, we sampled POM for various parameters (e.g., carbon, nitrogen, pigments, trophic biomarkers, eDNA for analyses of eukaryotic protist biodiversity, and of metazoan communities; Table 7.1) from different depths, including the subsurface, the chl *a* max, the surface backscatter maximum (SBM, Flores et al., 2023), 50-100 m, the Atlantic Water, and the Arctic Deep Water. The sampled water was filtered on board on appropriate filters, and the filters were stored frozen until analysis in the home laboratories. In addition, eucaryote protist DNA was sampled with an **AutoFIM**, which collected underway-water samples from a seawater intake at about 11 m depth near the ship's bow. Particle distribution in the water column was recorded with an Underwater Vision Profiler (**UVP**). The mesozooplankton community was sampled with a **Multinet** (Hydrobios, 0.25 m^2 opening, 150 µm mesh) at 5 standard depths (1,500-1,000, 1,000-500, 500-200, 200-50, 50-0 m). The Multinet was run in real-time mode using the Deck Command Unit to communicate with the Multinet in order to open the nets manually at depth according to the integrated pressure sensor. Flowmeter readings were recorded for estimations of sampled water volume. Macrozooplankton was sampled with a Rectangular Midwater Trawl (**RMT**). The RMT consisted of a rectangular frame with an effective mouth opening of 8 m^2 (RMT-8) and a 5-mm mesh krill net. A 300 µm zooplankton net with an effective mouth opening of 1 m^2 (RMT-1) initially mounted above the RMT-8 was removed after the first haul due to handling difficulties. The RMT was equipped with a pressure sensor to record the depth of the net during trawling. A Hydrobios impeller flowmeter was used to estimate the volume of water sampled in m^3. At two ice stations, macrozooplankton was also sampled from 1,000 m to the surface

with a 2-m diameter ring net (**MIK net**, 3.14 m^2 opening, 1 mm mesh), but low catch numbers indicated limited functionality of this net. Taxonomic samples from the zooplankton nets were preserved on a 4% formaldehyde-seawater solution, and will later be analysed at AWI with a ZooScan. For trophic biomarker and pollutant analysis bulk stable isotope analysis (BSIA), fatty acid composition and isotopic fractionation (FA-CSIA, Kohlbach et al., 2016), amino acid carbon isotopes (AA-CSIA, Vane et al., 2023), pollutants, macrozooplankton was collected from catches of the RMT net and preserved frozen at -80°C.

On the **sea-ice stations** conducted during ArcWatch-2, we sampled the same general parameters as in the water column by sampling sea-ice cores (Tab. 7.2). For each ice core, we measured the core length, the ice thickness using a thickness gauge, snowdepth and freeboard. One temperature/salinity (TS), one nutrients, and one cryogenic mineral core were each cut in 10 cm sections. In TS cores, temperature was measured immediately after retrieval of the core at the center of each 10-cm section. Salinity and nutrients were measured after melting at room temperature in darkness on board. From cores sampled for cryogenic minerals, 10-cm sections were processed immediately after the ice station, according to the SOP for cryogenic minerals. A core for Raman analysis and an archive ice core were transported frozen at -20°C back to AWI. For ecological parameters, 6 to 12 “ECO” cores were collected for analysis of pooled samples. The ECO cores were sectioned in 4 sections: bottom 10 cm, bottom center piece, top center piece and top 10 cm. The corresponding sections of all ECO cores were pooled together in polyethylene barrels. On the ship, we added 500 ml filtered seawater (0.2 µm pore size) per 10 cm ice core to each ECO core section barrel, and let the ice cores melt in darkness at 4°C. To accelerate melting, the barrels with center pieces were melted at room temperature. Under-ice water and, after melting (24-48 hours after each ice station), ice core water was filtered for the different parameters. For the same parameters as the ice cores and CTD water samples, we collected under-ice water from the ice-water interface (IWI) and, where present, meltponds using a simple peristaltic pump, and from the SBM using a Niskin bottle with a messenger. To document the procedure, an updated SOP for sea ice samples was created based on the SOPs of the Nansen Legacy, MOSAiC and SAS2021 Oden expeditions.

In addition, we sampled polar cod *Boreogadus saida* and other under-ice fauna with a Surface and Under-Ice Trawl (**SUIT**). The SUIT was equipped with two separate nets besides each other: a 300 µm mesh zooplankton net with a mouth opening of 0.4 x 2 m, and a 7mm half-mesh shrimp net with a mouth opening of 1.6 x 2 m. A sensor array consisting of a CTD (Sea & Sun) with integrated fluorerscence probe and altimeter, a Nortek Aquadopp ADCP, two RAMSES hyperspectral probes (TriOS) to estimate ice algae biomass, and a GoPro camera enabled the recording of environmental data profiles. Sampling profiles were defined as the period between the time that the towing cable was deployed to the desired length (100-150 m), and the time when we started hauling the SUIT back to the ship. Current speed data from the ADCP was used to estimate the distance and area sampled by multiplying average current velocity with the duration of each profile and the width of the SUIT.

To calibrate ice-algae biomass estimates from hyperspectral profiles of the SUIT sensors, we conducted L-arm measurements on the ice with a hyperspectral Ramses sensor during the sea-ice stations (Castellani et al., 2020). At seven ice stations, we performed measurements of under-ice light spectra (300-900 nm) with an l-arm. At each l-arm deployment, we conducted 3 spectral measurements, and collected three ice cores corresponding to each exact light spectrum measurement point. The ice cores were each melted completely according to the SOP for the ECO cores. At the AWI, filters will be analyzed for chlorophyll *a* content using HPLC. In combination, under-ice spectral measurements and their corresponding chlorophyll *a* concentration will be used to generate a model which allows to infer chlorophyll *a* content in sea ice from under-ice spectral profiles obtained from the spectral sensors mounted on the SUIT.

WP2 SciCAO sampling

The EU-project *SciCAO* aims to contribute to baseline knowledge on the distribution of fish in the CAO and the ecosystem supporting it. *SciCAO* sampling was therefore complementary to the ArcWatch core parameter sampling, and results will be obtained in combined analysis of both sets of parameters.

The distribution of fish and its zooplankton prey in the water column was measured continuously throughout the expedition with the **EK80** echosounder of *Polarstern*. The EK80 provides continuous profiles of hydroacoustic backscatter at 38, 70, 120 and 200. These four frequencies were calibrated and operated in broadband mode throughout the expedition with following pulse settings:

Pulse type: LFM up
Pulse Duration: 2.048 ms
Power (W) : Maximum for each channel
Spectra (Start – End frequencies) : Maximum bandwidth
Ramping: Fast

The effective target detection ranges of these 4 frequencies are different, particularly with respect to fish. For example, while 38 kHz provides good signal quality down to 600 m for a wide size range of most fish targets and large macrozooplankton. This effective range (signal to noise ratio or SNR) decreases with increased frequency, therefore recording ranges were adjusted individually per each channel such that:

For 38 and 70 kHz: 800 m
For 120 kHz: 400 m
For 200 kHz: 250 m

Data was recorded directly to the mass data management system (MDM) through the network, initially as 200 MB then 2 GB packages. 200 MB limit results in a separate file for each minute of data. It was suspected that creation of such high number of files can result in software crash time to time, therefore larger file size found to be more convenient. The EK80 survey was conducted according to the SOP established for JPSRM sampling during the *European Fish Inventory of the Central Arctic Ocean* (EFICA) project (2019-2023; Snoeijs-Leijonmalm et al., 2021). The EK80 was calibrated using an underwater robot positioning a calibration sphere according to a method established during MOSAiC (Snoeijs-Leijonmalm et al., 2022b).

In order to estimate abundance and biomass of fish and zooplankton from acoustic backscatter data, it is necessary to know the species composition and size distribution of animals in the water column. While the size range of zooplankton is covered by the net sampling of the ArcWatch core parameters, the pelagic fish community on Transect III was sampled with a **pelagic fish trawl**, wherever ice conditions allowed. The pelagic trawl targeted the Atlantic Water layer near the North Pole and in the Eastern Amundsen Basin (100-600 m depth, where most fish are expected to occur (Fig. 2; Snoeijs-Leijonmalm et al., 2022b), as well as hitherto not sampled areas in the Makarov Basin west of the Lomonosov Ridge. Pelagic fish were also sampled with **longlines** from sea-ice stations, following EFICA SOPs (Snoeijs-Leijinmalm et al., 2021). To this end, baited longlines were deployed through a hole in the ice, and at least 200 m away from the ship and any other installations with deep-hanging wires at the earliest possible moment prior to the commencement of an ice stations, and recovered at the latest possible time. The presence of fish in the water column was further investigated by means of metazoan **eDNA** sampled near the surface, in the Atlantic Water layer, and below the AW. On an opportunistic basis, we deployed **baited traps** to sample ice amphipods and polar cod (Snoeijs-Leijonmalm et al., 2022). Additionally, a conventional fyke net was deployed directly under the ice at three ice stations. The fyke consisted of a stainless-steel half-circle

opening (about 1,4 x 1,0 m) equipped with two floating bodies and 7 consecutive plastic rings of decreasing size, resulting in a length of about eight meters including the cod end. For use under the ice the fyke was modified by balancing the floating bodies with a respective counterweight of each ring. The opening was weighted down so that it could first sink under the ice where the fyke could extent in the current, and was finally hauled up and fixed under the ice. Both, traps and fykes were baited with fermented fish byproducts and additionally (on the final station) with smashed amphipods caught BY the SUIT and RMT, respectively.

Fish caught were dissected on board in order to obtain samples for diet, otolith analysis, trophic biomarkers, fecundity, physiological condition, transcriptomic analyses, and population genomics. These samples were preserved according to their EFICA SOPs (Snoeijs-Leijonmalm et al., 2021), and will be analysed in the home laboratories of the SciCAO partners. eDNA sequences will be analysed from the COI, 12S, 16S and 18S amplicons, and metazoan species composition will be obtained from international reference databases (e.g. MIDORI). Polar cod will be targeted with a new specific primer from the mitochondrial D-loop region, allowing for analysis of spatial patterns in relative abundance (Kawakami et al., 2023). For the estimation of the field metabolic rate (FMR) during the life history of the caught fish based on otolith calcium carbonate $\delta^{13}C$ values (Trueman et al., 2023), we will also sample the $\delta^{13}C$ of dissolved organic carbon (DIC) in the water surface and column, and the under-ice habitat.

WP3 Other project-based sampling

We collected **protist DNA** samples from sea-ice and pelagic samples to characterize the eukaryotic microbial community composition to address the dynamics of the cryo-pelagic coupling in biodiversity in autumn with special emphasis on the re-freezing. These data will be used in combination with data collected within the framework of FRAM and MOSAiC to infer on linkages between sea-ice coverage and eukaryotic microbial biodiversity. This information is part of the INSPRIES PhD project of Jannis Hümmling and the EU-Project **OBAMA_Next** to develop species distribution models that will eventually suggest scenarios for eukaryotic microbial biodiversity, dynamics and distribution in a seasonally ice-free Arctic Ocean.

We studied the influences of changes in sea ice melting and oceanic circulation patterns on the **phytoplankton community** distributions. To understand the ecosystem response in the pan-Arctic region, sampling conducted during the ArcWatch-2 expedition in the Atlantic Arctic Ocean will be compared with those obtained through the **K-AWARE** expedition in the Pacific Arctic Ocean. Ice algae were collected from sea-ice cores and will be analyzed using microscope in a laboratory after the cruise. Phytoplankton will be analyzed at KOPRI using IFCB. To calibrate the results of IFCB, samples for microscopic analysis, photosynthetic pigment concentration, and picophytoplankton abundance were collected for analysis in the laboratory using microscopy, HPLC, and flow cytometer, respectively.

To elucidate **trophic relationships** and dependencies within the lower trophic food web of the CAO under current environmental conditions, samples of ice algae (ice corer), phytoplankton (CTD), zooplankton (different nets; WP1) and fish (pelagic trawl, SUIT; WP2) were collected for analysis of biomolecules that can be used for indicating the trophic transfer of carbon from under-ice and pelagic primary producers to higher trophic levels. This included the relative composition of fatty acids and highly branched isoprenoids, and isotopic ratios of bulk organic material, fatty acids and amino acids. The main objective was to quantify the dependency of the food web on ice algae *vs.* specific phytoplankton groups, and trace the transfer of these carbon sources to zooplankton and fish. To simultaneously identify the pollution burden of the lower trophic food web, major contaminants (POPs, PFAS) will be identified and quantified in the same species. Collected samples will contribute to the Helmholtz Young Investigator project ***Double-Trouble*** aiming at understanding the trophic structure of the CAO food web

under cumulative stress from warming and (increasing) anthropogenic pollution. The samples will complement samples of the same parameters collected during a CAO expedition in July/ August 2024 led by the Norwegian Polar Institute.

Planktonic foraminifera were sampled at depth intervals of 1,500-800, 800-100, 100-50, 50-25, and 25-0 meters. Samples from the planktonic foraminifera were stored in 97% ethanol with 2 grams of rose Bengal stain per liter for later analyses at AWI.

Preliminary results

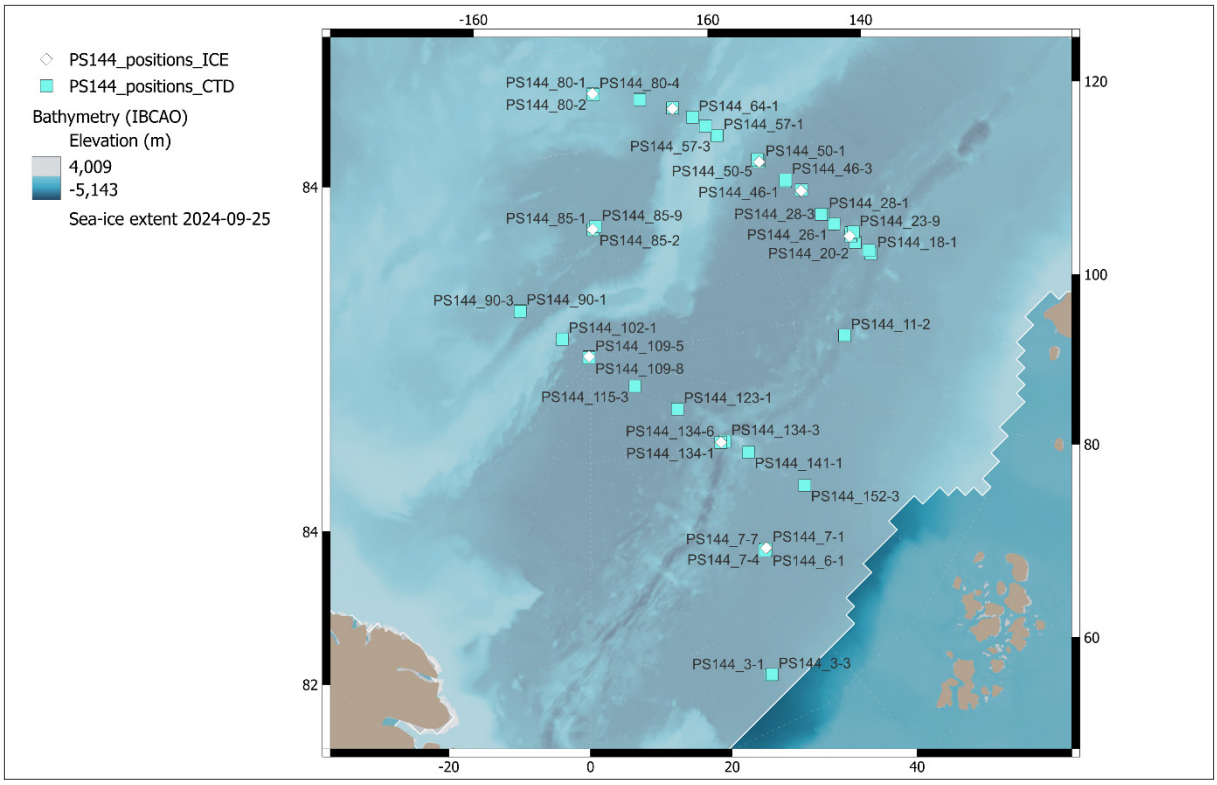

Fig. 7.1: Distribution of CTD stations and ice stations sampled by team PSB during PS144

WP1

Biogeochemical and ecological parameters were sampled from 46 CTDs at 26 sampling sites during PS144 (Fig. 7.1, Tab. 7.1). The spatial resolution of CTD casts was somewhat denser on Transect III (24 casts) than on Transect II (13 casts), with 9 casts sampled during transit. We collected water samples for the following parameters: pigments, C/N content and stable isotoppes (POC), nutrients, eDNA, protist DNA, and cryogenic minerals. The depth distribution of the sampling of each parameter is shown in Table 7.1. Altogether, we collected 1,142 samples for the WP1 parameters, including metazoan eDNA (WP2), protist DNA and size-fractionated chlorophyll *a*, and cryogenic minerals (WP3).

Tab. 7.1: Summary of biogeochemical and ecological parameters sampled with the CTD during PS144. The numbers indicate the number of sampling sites (stations) at which a parameter was sampled at the respective depth. AA Biom = amino acid biomarkers, Cryog min = cryogenic minerals, Frac Chl *a* = size-fractionated chlorophyll *a* concentration, IWI = ice-water interface, Lip Biom = lipid biomarkers, Metaz eDNA = metazoan eDNA, MP = meltponds, POC = particulate organic matter for C/N content and stable isotope measurements, Prot DNA = DNA samples for protists, SBM = surface backscatter maximum.

Depth feature	Pig-ments	Metaz eDNA	POC	Prot DNA	Frac Chl a	AA Biom	Lip Biom	Cryog min	Total
CTD_surface	22	18	22	22	22			15	26
CTD_Chlmax	22	22	22	22	22	18	18	14	24
Below chl max				20	20				18
CTD_SBM	22	22	21	1	1			17	25
CTD_CDOM_max	1			1	1				1
CTD_50m	22			21	21			1	22
CTD_100m	22			22	22				23
CTD_AW		22	20			18	17	15	26
Below AW		20	20					2	25
CTD_bottom		14						13	18
Unaccounted	1						1		2
Total	23	22	22	22	22	18	18	20	26

The **Underwater Vision Profiler (UVP)** was deployed a total of 50 times. However, due to low battery voltage in two instances and one malfunction, 47 valid casts were recorded. These casts covered a total water column of 130.117 meters, and 52,479 images were captured (Fig. 7.2). The majority of images were taken in transect III (20,402 images, corresponding to 0.33 images per meter), followed by transect II (16,197 images, or 0.37 images per meter) and transect I (4,209 images, yielding 0.56 images per meter).

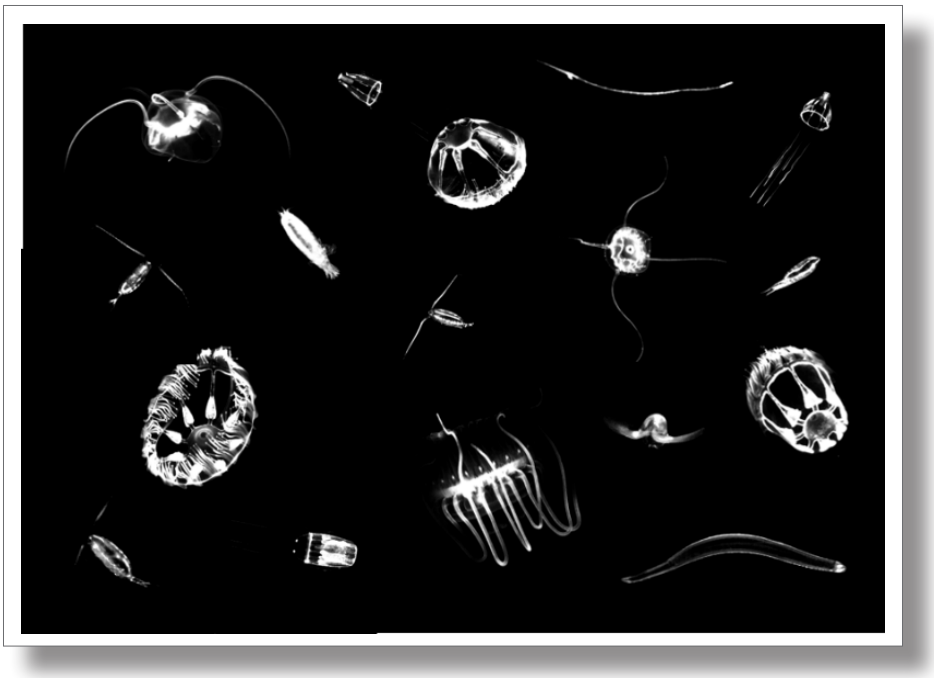

Fig. 7.2: Example of zooplankton images from the UVP

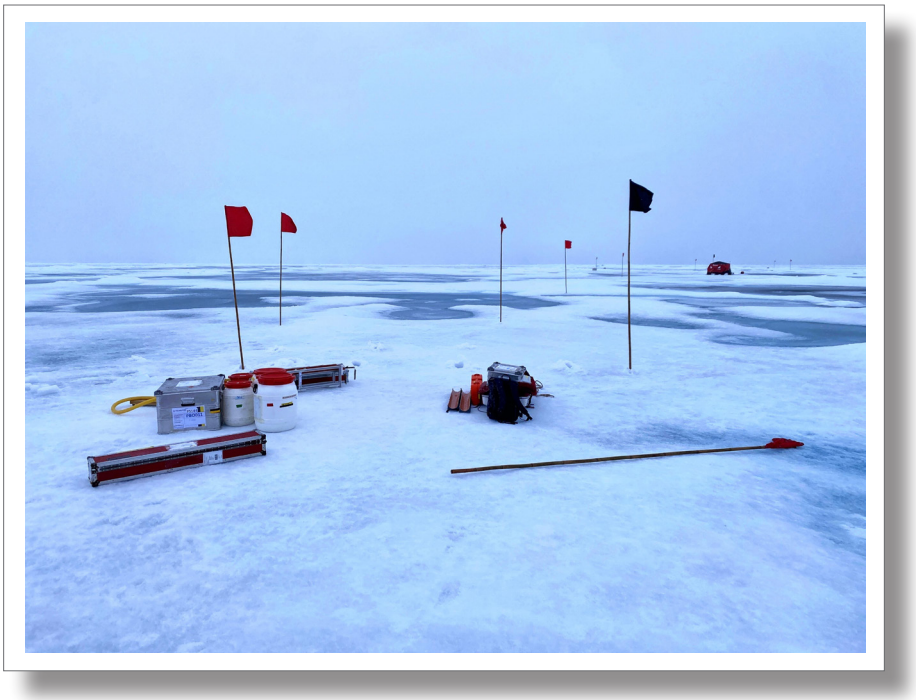

Fig. 7.3: Example of a coring site (station 23)

Biogeochemical and ecological parameters of **sea ice** were sampled at nine ice stations (Fig. 7.1, Tab. 7.2). At each ice station, we selected a coring site at least 100 m from the ship, if visibility was suffient to allow safe working (Fig. 7.3). We collected ice cores for the following

parameters: Temperature and salinity (TS), nutrients, cryogenic minerals, Raman analysis, the same biogeochemical and ecological parameters as in the CTD water sampling, and an archive core (Fig. 7.4).

Fig. 7.4: Example of an ice core for ecological parameters (station 85). All ice cores were photographed for documentation.

Tab. 7.2: Summary of biological/biogeochemical parameters samples collected during PS144 at ice stations.

AA Biom = amino acid biomarkers, Cryog min = cryogenic minerals, Frac Chl *a* = size-fractionated chlorophyll *a* concentration, IWI = ice-water interface, Lip Biom = lipid biomarkers, Metaz eDNA = metazoan eDNA, MP = meltponds, POC = particulate organic matter for C/N content and stable isotope measurements, Prot DNA = DNA samples for protists, SBM = surface backscatter maximum.

Device	Depth feature	Pig-ments	Metaz eDNA	POC	Prot DNA	Frac Chl *a*	NUT	AA Biom	Lip Biom	Cryog min	Total
Ice corer	sea ice	9	8	9	9	9	9	9	9	8	9
Under-ice pump	IWI	9	7	9	9	9	4	1	1	8	9
	MP	1		1				1			1
	SBM	8	7	8			1				8
Total		9	9	9	9	9	9	9	9	9	9

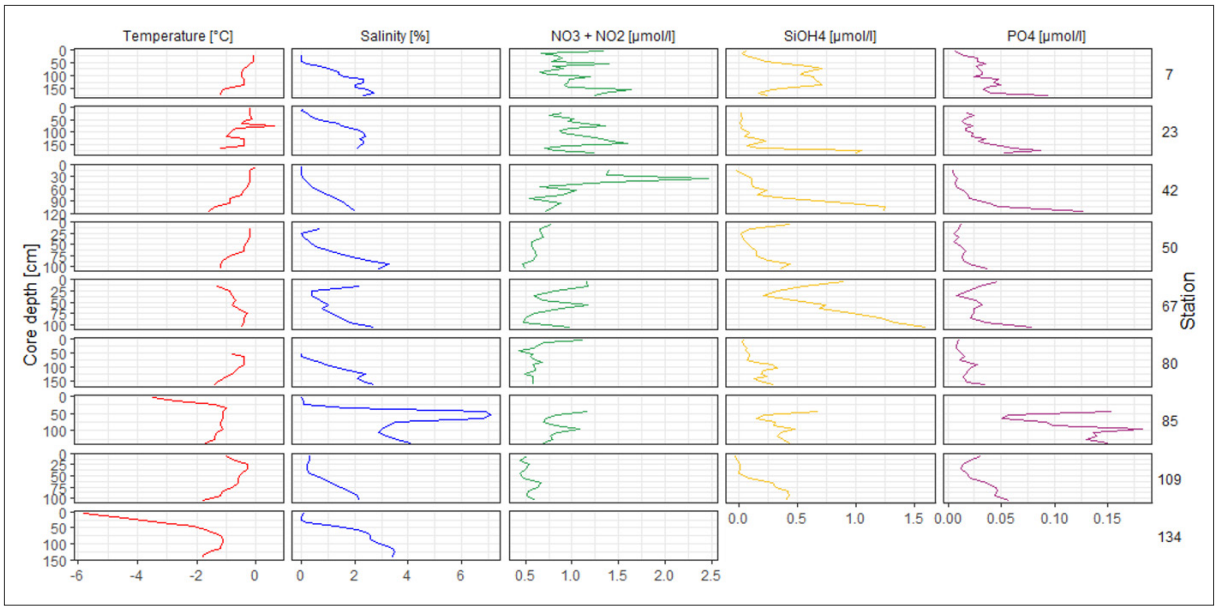

Fig. 7.5: Profiles of temperature, salinity, nitrate + nitrite, silicate and phosphate in ice cores collected during PS144

Altogether, we collected 160 ice cores from nine ice stations. The majority of the cores was taken on Transect III (Station 23-80). The ice was a mixture of first-year ice (FYI; four stations) and second-year ice (SYI; four stations), with one station at the end of Transect III being multi-year ice (MYI; station 80). The ice average ice thickness was 119 cm (range: 51-194), and the average core length was 124 cm (range: 47-204 cm). Further details are shown in Table 7.3. The temperature- and salinity profiles at the nine sea-ice stations showed a great variety of profile shapes. In the temperature profiles, a seasonal transition from warm surface temperatures at stations 7 to 67 to cold surface temperatures with internal temperature maxima at stations 80-34 was apparent Figure 7.5. The depth profiles of Nitrate + Nitrite concentrations were highly variable, with no distinct patterns. The highest values were found at station 42, where Nitrate + Nitrite showed a distinct subsurface maximum. Silicate and phosphate values co-varied, with low values near the surface and high values at the ice-water interface at most stations (Fig. 7.5).

Tab. 7.3: Summary statistics of sea-ice sampling sites and ice cores collected during PS144. For further information please see the end of the chapter.

Multinet: We sampled mesozooplankton at 10 stations, and foraminifera at 8 stations, yielding 50 and 40 samples, respectively (Tab. 7.4). The mesozooplankton samples will be analysed at AWI with a ZooScan for biomass estimates and diversity.

Tab. 7.4: Summary statistics of Multinet deployments on PS144.
Numbers give numbers of stations sampled in each sampling area. Each multinet deployment yielded five zooplankton samples.

Type of multinet	Transit 1	Transect III	Transit 2	Transect II	Total
Mesozooplankton	1	6	1	2	10
Foraminifera	1	4	1	2	8
Total	**2**	**10**	**2**	**4**	**18**

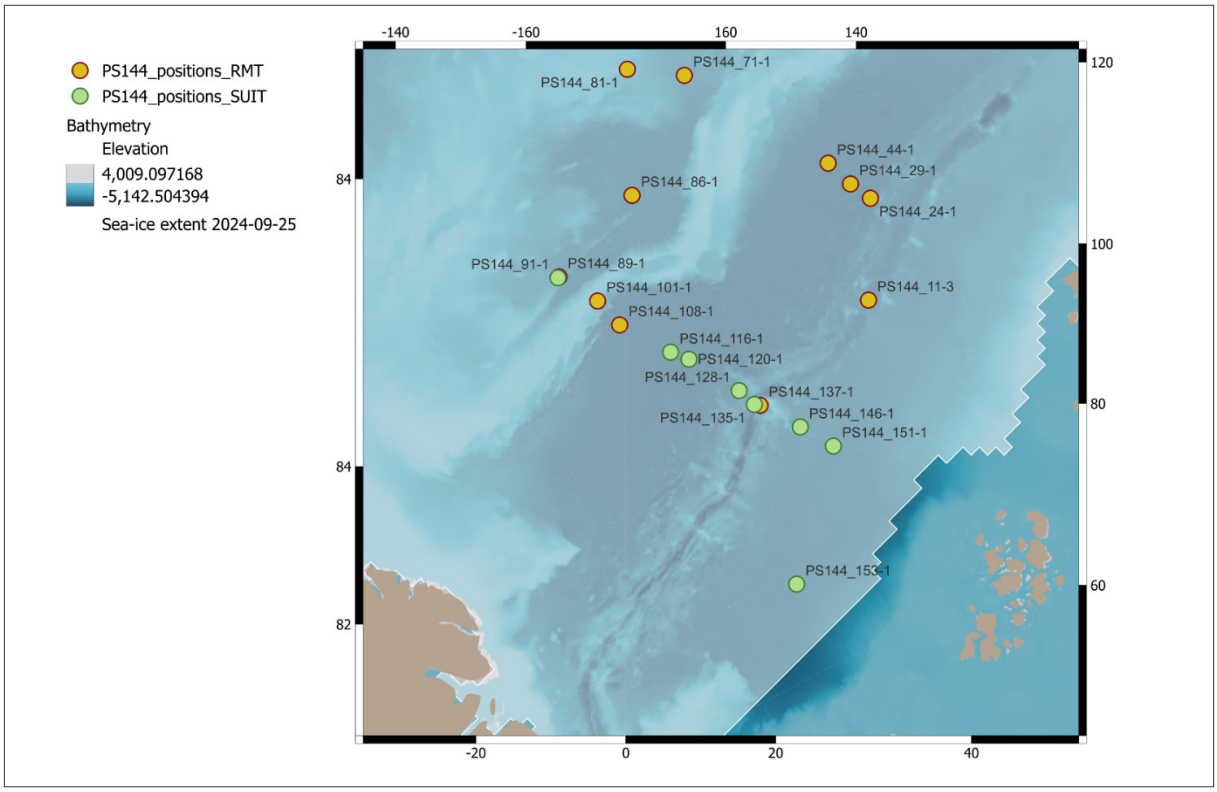

Fig. 7.6: Distribution of RMT and SUIT deployments during PS144.

RMT: The target depth of the RMT deployments was the Deep Scattering Layer (DSL) as identified by the EK80, which was situated between 300 and 450 m. We sampled altogether eleven stations with the RMT. Five stations were sampled on Transect III, three stations on Transect II, and two stations on transits between these transects (Fig. 7.6; Tab. 7.5). The maximum sampling depth ranged between 320 m (station 86) and 700 m (station 137). On three stations (86, 89, 137), the towing wire was caught by sea ice, leading to prolongued trawls and/or greater sampling depth than intended (Tab. 7.5).

In terms of total abundance of macrozooplankton, station 108 at the North Pole reached the highest values (0.22 ind. m^{-3}). The lowest abundance was recorded at station 81 in the Makarov Basin (0.04 ind. m^{-3}; Fig. 7.7). We found at least 30 taxa of macrozooplankton in the RMT samples. At most stations, the taxonomic composition was dominated by chaetognaths, predominantly *Sagitta maxima* and *Pseudosagitta gazellae*. The second most abundant taxon where amphipods, mostly *Themisto* spp. In the Makarov Basin, the ratio between *T. abyssorum* and *T. libellula* was considerably lower than in the Eurasian Basin (Fig. 7.7). Conversely,

euphausiids (*Thysanoessa* spp.) were more abundant in the Eurasian Basin than in the Makarov Basin. Ctenophores (*Beroe* spp. and *Mertensia* spp.), and the shrimp *Hymenodora glacialis* were sampled at all stations. Three myctophids *Benthosema glaciale* were caught at station 24 and station 89.

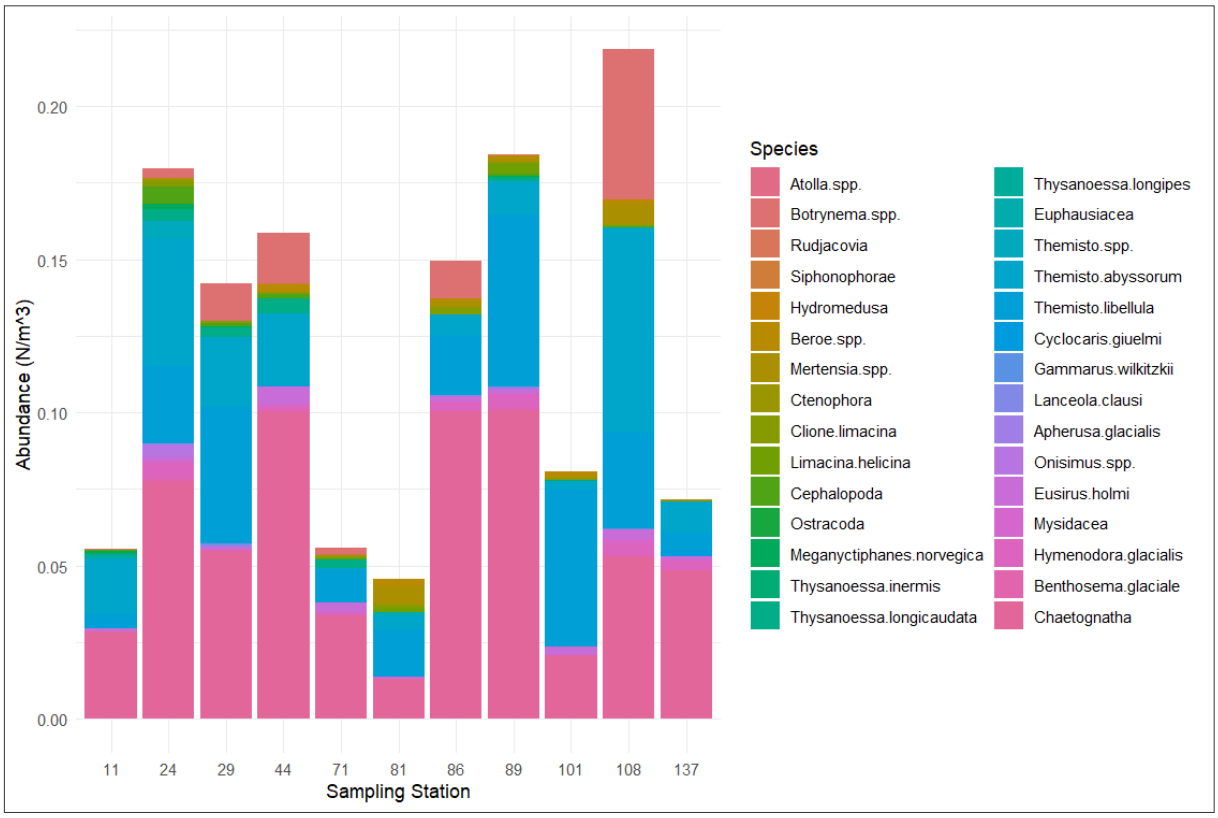

Fig. 7.7: Taxonomic composition of RMT catches during PS144. Abundances relative to sampling effort are expressed in numbers per m^3 of filtered water.

Tab. 7.5: RMT deployments on PS144

Event Label	Section	Date	Latitude [°N]	Longitude [°E]	Target depth [m]	Max depth [m]	Trawl duration [h]	Remarks
PS144_11-3	Transit 1	2024-08-20	85.17	95.52	450	450	0.5	
PS144_24-1	Transect III	2024-08-30	84.55	117.13	450	430	0.5	
PS144_29-1	Transect III	2024-08-31	84.75	121.86	420	447	0.5	
PS144_44-1	Transect III	2024-09-03	84.88	128.40	450	430	0.5	
PS144_71-1	Transect III	2024-09-09	84.94	166.74	350	380	0.5	
PS144_81-1	Transect III	2024-09-11	84.96	179.66	300	324	0.5	
PS144_86-1	Transit 2	2024-09-14	87.45	177.25	300	320	1.3	wire on ice
PS144_89-1	Transect II	2024-09-16	88.38	-124.91	350	465	1.1	wire on ice
PS144_101-1	Transect II	2024-09-17	89.28	-128.68	320	325	0.5	
PS144_108-1	Transect II	2024-09-18	89.87	-77.70	380	395	0.7	
PS144_137-1	Transect II	2024-09-27	86.88	58.66	350	700	1.4	wire on ice

SUIT. The SUIT was deployed on Transect II and Transit 3 only. Deployment sites were chosen with the help of satellite pictures and the ice radar. When drift correction was accurate, satellite pictures considerably improved our ability to identify suitable sampling sites. We sampled eight stations with the SUIT (Fig. 7.6; Tab. 7.6). On three stations, the sampling could not be concluded because the SUIT was damaged by heavy ice (station 91), *Polarstern* got stuck in ice (station 135), or the SUIT was lost (station 151; Tab. 7.6). The towing speed during sampling ranged between 0.3 m s^{-1} at station 91 and 1.1 m s^{-1} (0.6 and 2.2 knots) at station 135. The distance sampled ranged between 204 m at station 151 and 1,937 m at station 146. Approximate mean ice draft ranged between 0.6 m at station 151 and 2.2 m at station 135 (Tab. 7.6). Mean under-ice chlorophyll concentrations ranged between 0.3 µg L^{-1} at station 91 and 0.9 µg L^{-1} at station 121. Details on under-ice water temperature and salinity are shown in Table 7.6.

The catch of the zooplankton net was preserved quantitatively on 4% formaldehyde-seawater solution, and will be analyzed at the AWI. Animals from the shrimp net were enumerated by taxon and sampled frozen for analyses of trophic biomarkers, pollutants and genetics. In terms of total abundance of under-ice fauna from the shrimp net, station 116 near the North Pole reached the highest values (850 ind. ha^{-1}). The lowest abundance (< 50 ind. ha^{-1}) was recorded at station 153 at the end of Transect II (Fig. 7.8). We found at least 14 taxa of under-ice fauna in the shrimp net samples. The taxonomic composition was dominated by amphipods, predominantly *Themisto libellula, Apherusa glacialis* and *Eusirus holmi* (Fig. 7.8). Interestingly, we found one undidentified benthic polyhaete at station 128. Altogether 14 Polar cod were caught at stations 91 and 128-151.

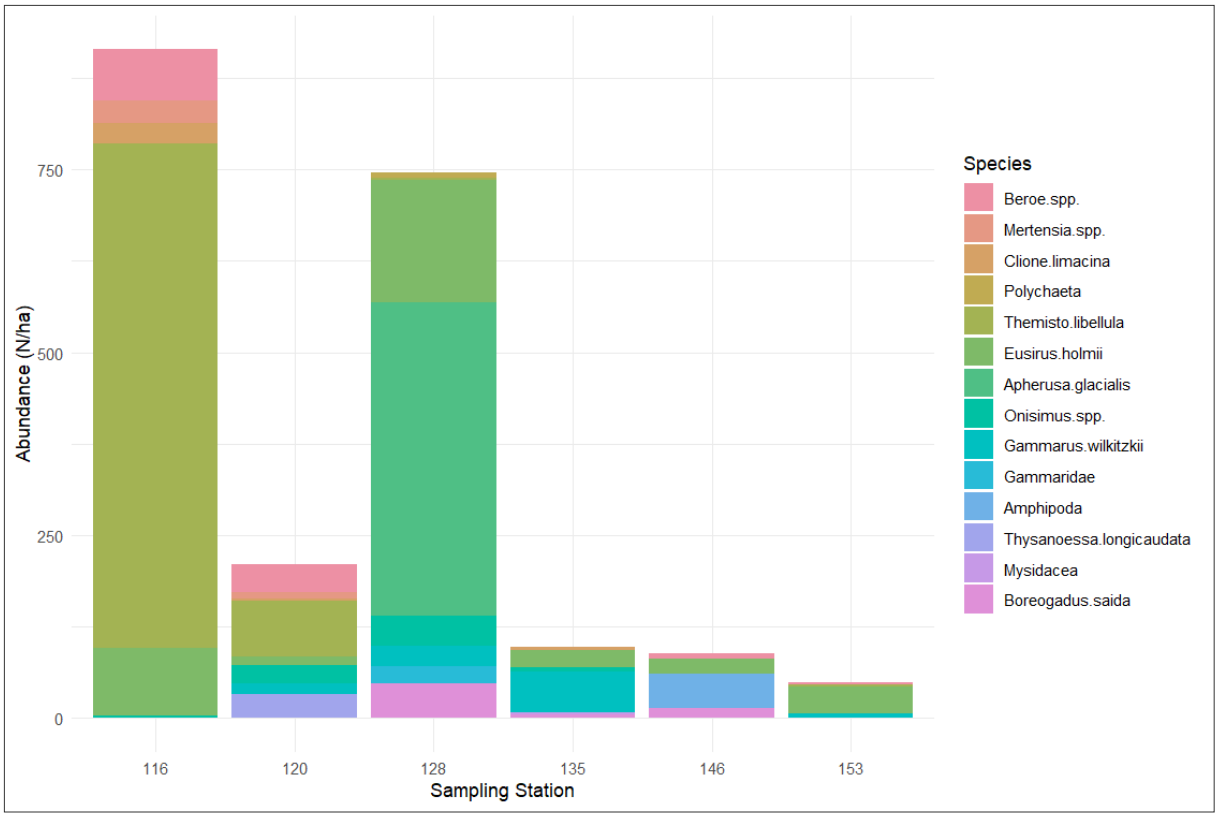

*Fig. 7.8: Taxonomic composition of SUIT catches during PS144. Abundances relative to sampling effort are expressed in numbers per ha (1ha = 100*100 m). Data only shown for stations with trawl distances > 300 m.*

Tab. 7.6: SUIT deployments on PS144, Transect II

Event Label	Date	Latitude [°N]	Longitude [°E]	Distance [m]	Draft [m] (mean ± SD)	Temp. [°C] (mean ± SD)	Salinity (mean ± SD)	Remarks
PS144_91-1	2024-09-16	88.37	-123.98	263	1.9 ± 0.5	-1.67 ± 0.002	30.5 ± 0.1	SUIT damaged
PS144_116-1	2024-09-21	88.95	57.42	1322	0.7 ± 0.1	-1.71 ± 0.002	31.2 ± 0.1	
PS144_121-1	2024-09-22	88.56	60.47	1858	0.7 ± 0.2	-1.71 ± 0.001	30.9 ± 0.3	
PS144_128-1	2024-09-24	87.39	59.38	1711	1.3 ± 0.7	-1.80 ± 0.001	32.5 ± 0.9	
PS144_135-1	2024-09-25	86.99	57.81	903	2.2 ± 1.8	-1.80 ± 0.002	32.4 ± 0.2	SUIT stuck in ice
PS144_146-1	2024-09-29	85.98	59.34	1937	1.7 ± 0.9	-1.81 ± 0.002	32.8 ± 0.3	
PS144_151-1	2024-09-30	85.22	59.46	204	0.6 ± 0.3	-1.81 ± 0.003	26.9 ± 0.4	SUIT lost
PS144_153-1	2024-10-03	83.82	33.25	1530	N/A	N/A	N/A	

WP2

EK80: The Simrad EK80 echosounder was calibrated at the beginning of the survey and operated continuously throughout the expedition. The ping rate was adjusted to cover a maximum range of 800 m, although the full water column depth often exceeded this range. This limit was set because horizontal resolution depends on the ping rate (number of pings per unit time). The ping rate is primarily constrained by the observation range, as each new pulse can only be transmitted after the previous pulse has travelled to the maximum range and returned. For instance, if the observation range is set to 1,500 m, a delay of at least two seconds is needed before the next pulse can be sent. For this expedition, the maximum observation range was set at 800 m, and the ping interval was adjusted between 1.5 and 1.8 seconds to maximize horizontal resolution. However, when false bottom echoes occurred, the ping rate was modified to keep these disturbances outside the observation range.

For this expedition, a decision was made to use broadband, frequency-modulated (FM) signals instead of narrowband, continuous wave (CW) signals. This choice significantly improved range resolution, enabling fine-scale detection and characterization of individual fish. The enhancement is primarily due to the pulse compression technique: a relatively longer pulse is transmitted to increase energy in the water, and frequency modulation allows the returned echoes to be processed into much finer resolution using a matched filter. Although longer pulse durations in this technique improve the signal-to-noise ratio (SNR), they can also create issues when strong and weak targets are close together, as the stronger target's sidelobes may interfere with processing the weaker target. Trials carried out at the beginning of the expedition, testing pulse durations of 1 ms, 2 ms, and 4 ms, showed that 2 ms was optimal and was thus maintained as the standard setting.

In general, these echosounder settings provided adequate resolution to be able to track and follow individual fish. E.g., at least 7 detections from an individual fish at 350 m at a speed of 4 knots (Fig.7.9). The total amount of data collected throughout 50 days (from Svalbard back to Svalbard) was about 20 TB.

Calibration: The calibration was performed while *Polarstern* was anchored in Adventfjorden in Longyearbyen in Svalbard on the night of 11 August 2024 and the early morning of the next day. A small underwater drone was used to deploy and operate the calibration sphere (38.1 mm Tungsten Carbide) from the moon pool of the *Polarstern*. While all 4 frequencies (38,70,120 and 200 kHz) were calibrated in narrow band mode, only 38 khz and 70 kHz were was calibrated in FM mode. While the low visibility in the water and relatively stronger current complicated the work, especially locating the calibration sphere under the transducer and moving the sphere around within the acoustic beam, the calibration was successful with adequate coverage of the beam and qood quality hits and the center of the beam especially necessary for adjusting the gain. A portable CTD was deployed at the same location for the necessary environmental values. While drone calibration proved to be a successful method, the water visibility turned out to an important factor to take into account in future trials.

While initial quality checks verified the validity of the calibration trials, a conclusive analysis was not completed during the expedition. However, a calibration report will be in early 2025.

Tab. 7.7: Summary statistics of EK80 recordings.

Section	Total File size [TB]	Number of Files	Start	End
Transit 1	2.57	13440	8/13/2024 12:00	8/21/2024 15:00
Medivac	2.19	11355	8/21/2024 15:00	8/28/2024 6:00
Transect III	4.63	24143	8/28/2024 6:00	9/12/2024 19:00
Transit 2	1.12	5826	9/12/2024 19:00	9/16/2024 10:41
Transect II	4.89	8876	9/16/2024 10:41	10/1/2024 15:00
Transit 3	0.87	455	10/1/2024 15:00	10/3/2024 12:00

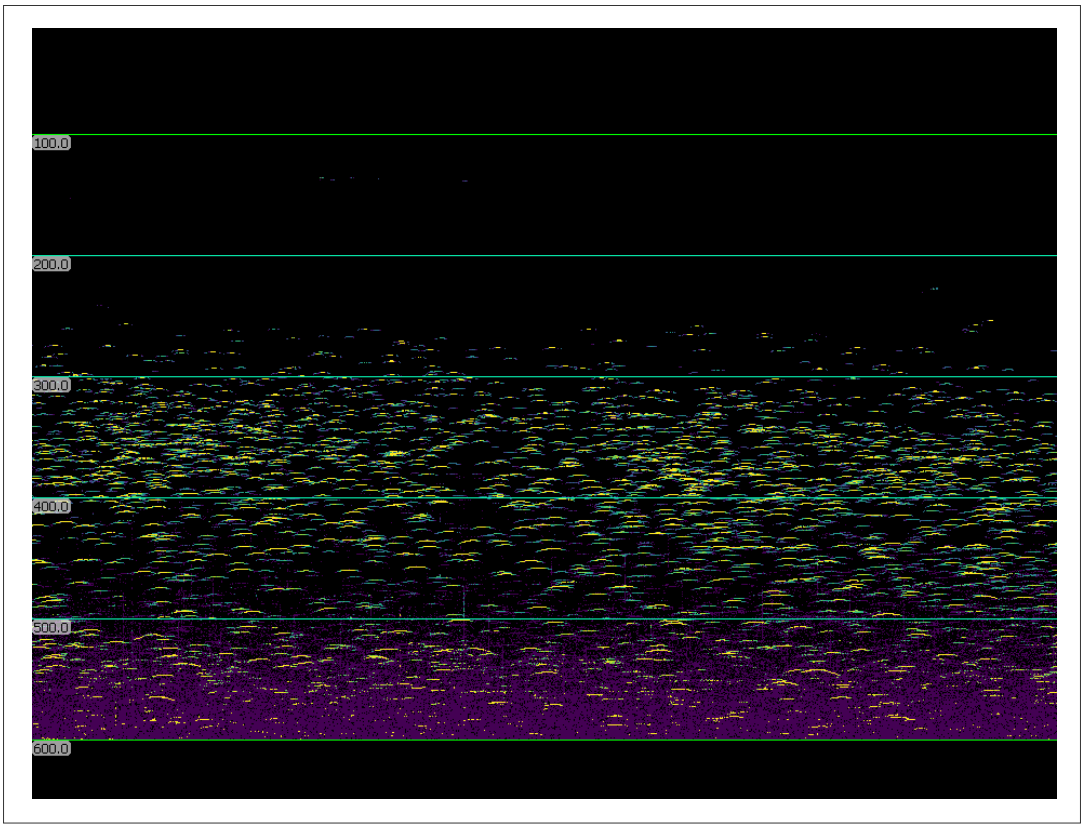

Fig. 7.9: Sample echogram from one of the pelagic trawl stations (PS144_062). Yellow horizontal lines are indicative of individual targets, most likely Benthosema glaciale.

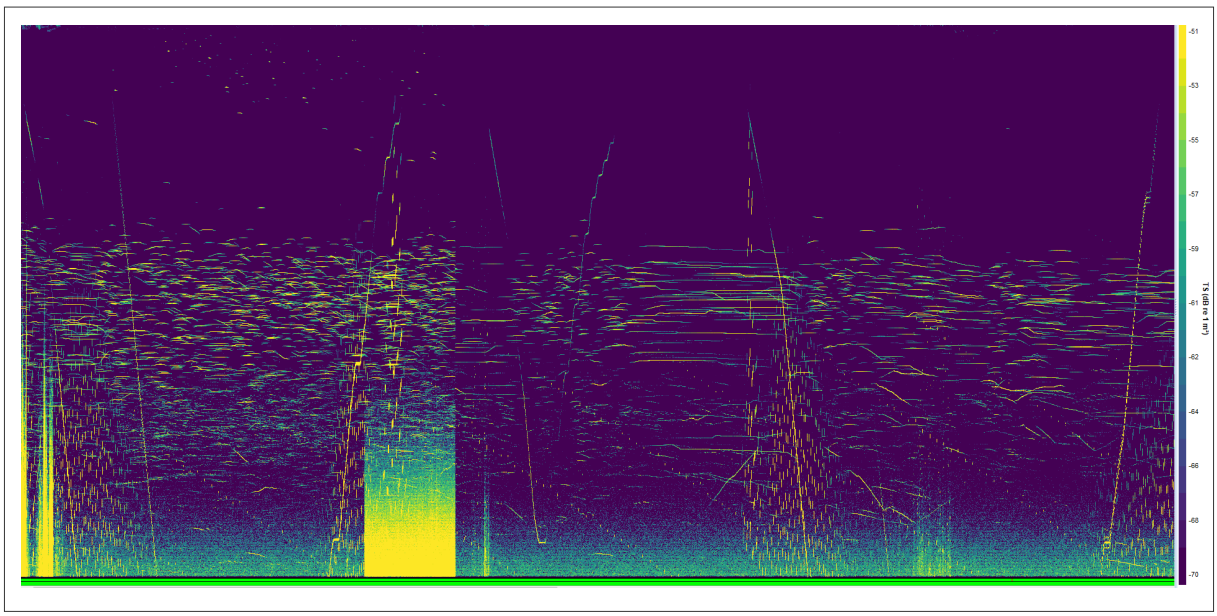

Fig. 7.10: Sample echogram as an example to illustrate data quality during the CTD station showing a section from surface to 800m. The data was resampled to compress 12 hours section into the same frame. The horizontal marks in the center of the echogram (from ca 300m to 600m) are due to swimbladered fish. The diagonal lines on the echogram show the backscatter from the rosette and the cable. Vertical dashed lines interference from the LADCP running during the CTD deployment. The section towards middle part of the echogram with strong yellow gradient from bottom upwards indicates ship related noise, most likely due to bow thruster.

While EK80 did not suffer from major noise problems at the stations and in the sections where ship steamed in ice-free waters, at the times when ship was breaking ice, data quality and representativeness dropped very sharply (Fig. 7.10). In addition to ice-breaking noise, few noise problems were encountered during the stations such as, interference from the LADCP and altimeter sensors from the CTD, bow thruster activity during the stations, and in few occasions the multibeam system. Most of these latter noise sources are in form of spikes and can be dealt with during the post processing. For instance, since the data collected in broadband mode, the ADCP and Multibeam signature can be identified by a spectral analysis and filtered from the data. Some preliminary test with Echoview postprocessing software on board resulted in promising level of cleaning.

Acoustic measurements vs catch: While the number of fish individuals caught by the pelagic net was small, it was considered representative with respect to potential number of fish detected by the EK80 system. Fig. 7.11 illustrates the portion sampled by pelagic trawl relative to the coverage of the acoustic beam.

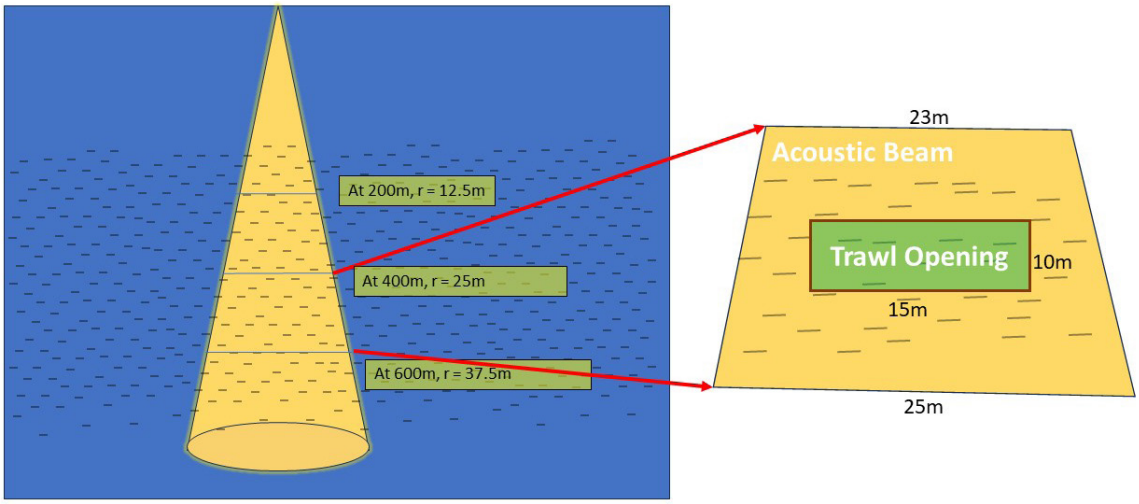

Fig. 7.11: Volume sampled by pelagic trawl relative to the coverage of the acoustic beam.

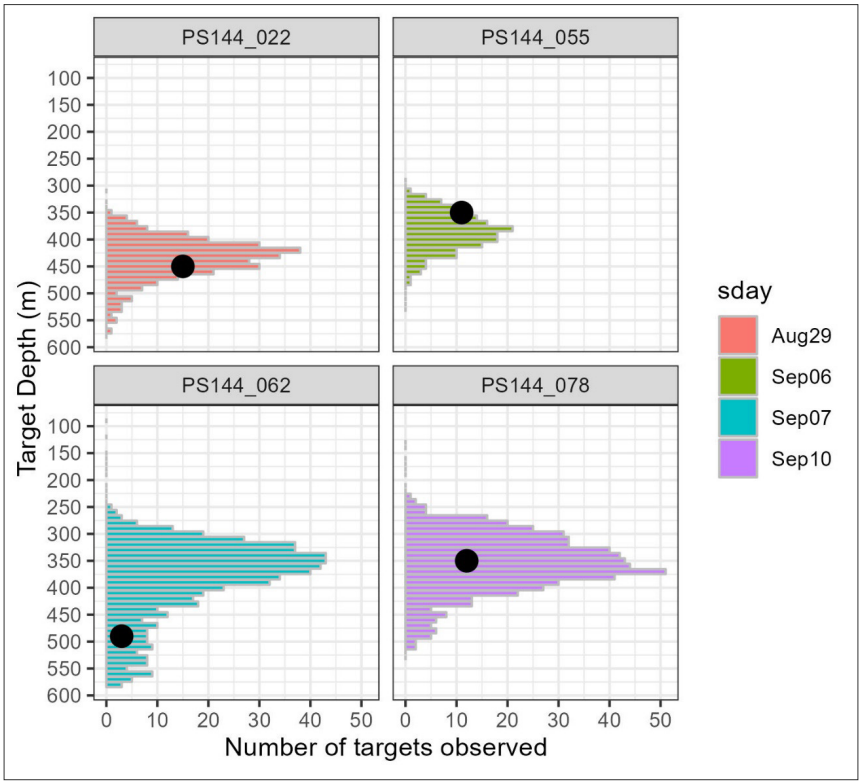

Fig. 7.12: Number of fish that could have been captured during the trawl sampling vs actual catch.

Figure 7.12 provides an approximate illustration of the potential number of fish that could have been captured, assuming a 100% catch efficiency under conditions of such low densities. This estimation indicates that the catch was within the same order of magnitude of echosounder observations. Since the main purpose of the catch was to identify the species/size composition

of the echosounder observations (in addition to biological sampling purpose), the small discrepancies are not considered as an issue as the main source of quantitative estimation will be based on the acoustic detections. In addition to that, the catchability is a complex parameter depending on many factors and not necessarily in linear fashion. For example, the herding effect of the net is one important factor in guiding the fish from the mouth of the net towards the center and eventually to the codend. As the front part of the net has larger mesh size exceeding fish size, the herding is especially critical at this stage. It is known that school forming fish consistently exhibit such behavior as a form of predator avoidance. However, in scattered fish in very small densities, such as *Benthosema glaciale* in the Arctic Ocean, it is not well known. Target tracking substantially improves the reliability of the detected targets and accuracy o the estimations. However, such a software module was not available onboard during the expedition. Current estimations of acoustic targets may have resulted in slight over-estimation due to noise which will later be eliminated via target detection.

The consistent DSL as known to occupy the depths from 300 m to 600m from the previous expeditions has been observed continuously during this expedition as well. While the 38 kHz echosounder provided a clear picture of this layer, unfortunately the SNR of the other frequencies including the 70 kHz was not sufficient to cover this range. Therefore 38 kHz is the only source of information for characterizing the fish distribution. The primary characteristic of this layer was the presence of distinct individual targets with an average TS around -53 dB (SD = 1.5). This distribution agrees well with the catches from this depth. During the initial part of the expedition (first half of the expedition), the center of mass was located between the 400-500 m (E.g. PS144_015 and PS144_022). After the first week of September, this layer started to move upwards gradually, reaching almost to 200 m at around North Pole. Near the North Pole we also found the only dense aggregation of potentially larger fish, as observed during MOSAiC leg 1 and leg 5 (station 109; Fig. 7.13). Unfortunately, the sea-ice conditions in this region did not allow to deploy the pelagic trawl. The identity of these strong targets can therefore only be estimated based on our eDNA analysis.

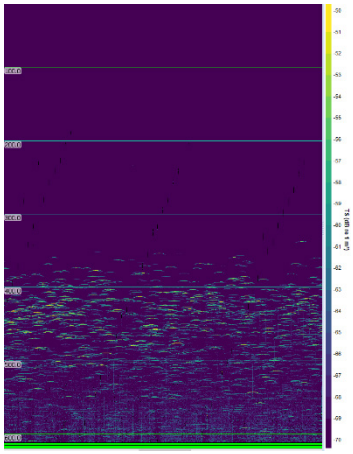

PS144_015 PSN_PS Pelagic Trawl

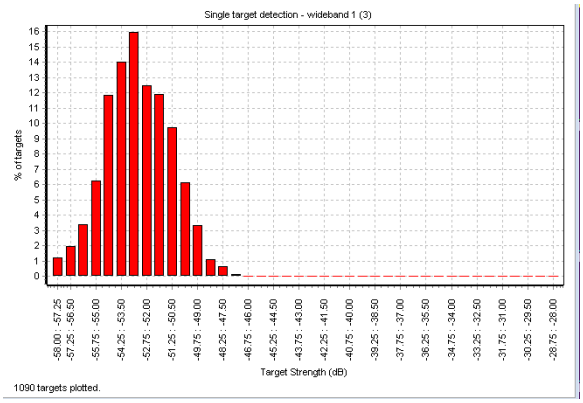

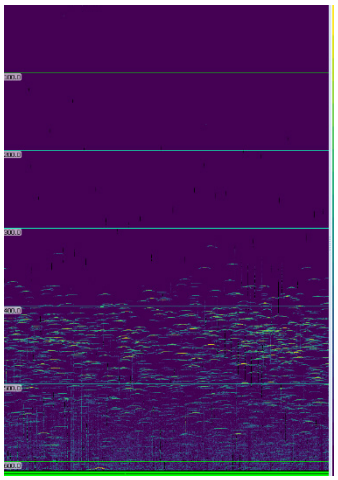

PS144_022 PSN_PS Pelagic Trawl

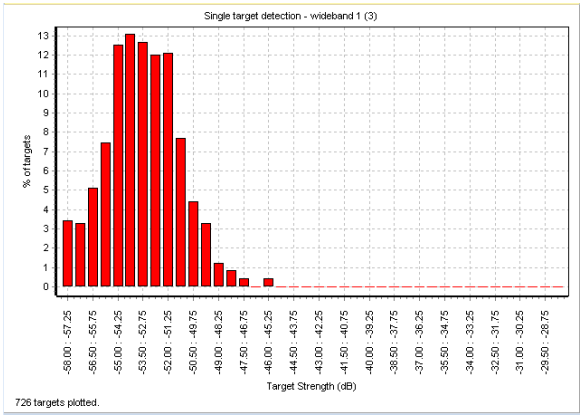

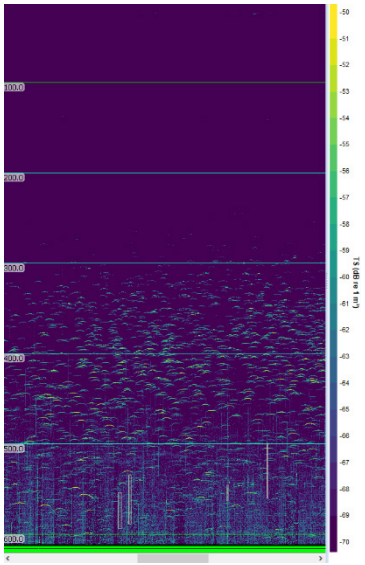

PS144_055 PSN_PS Pelagic Trawl

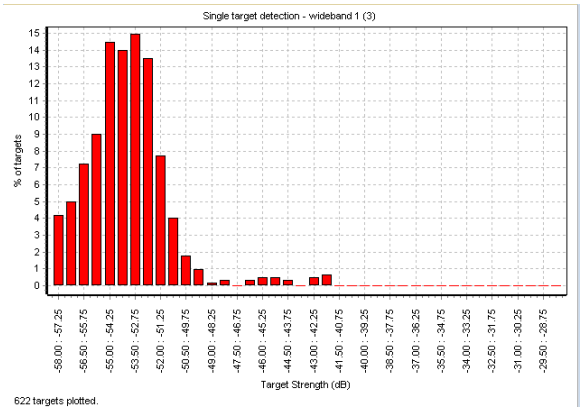

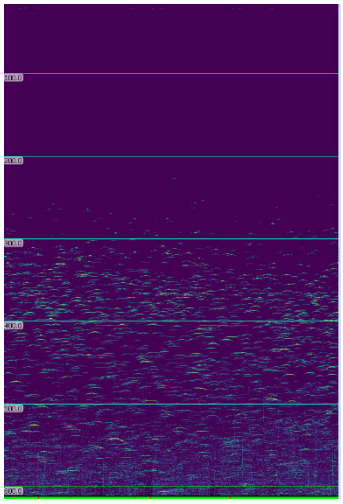

PS144_062 PSN_PS Pelagic Trawl

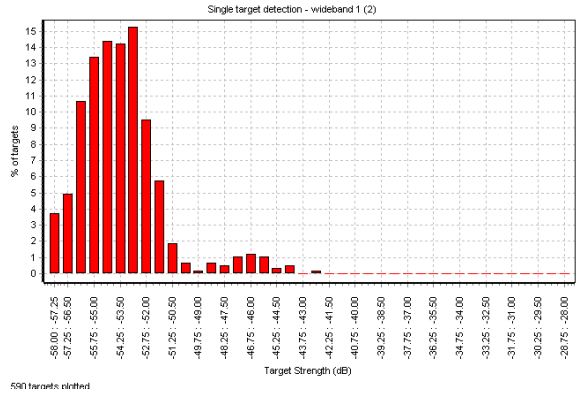

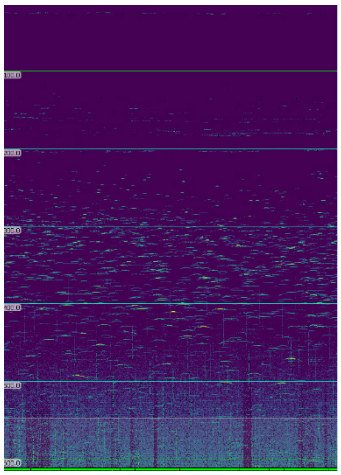

PS144_078 PSN_PS Pelagic Trawl

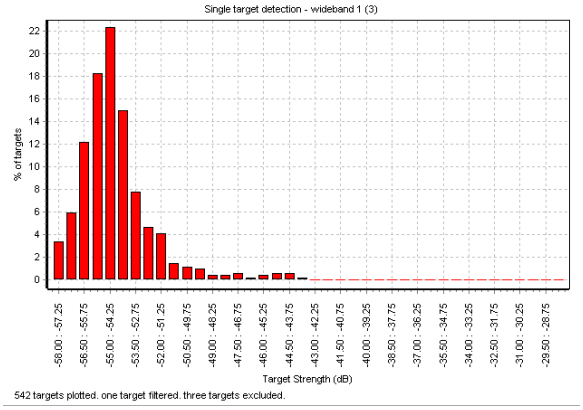

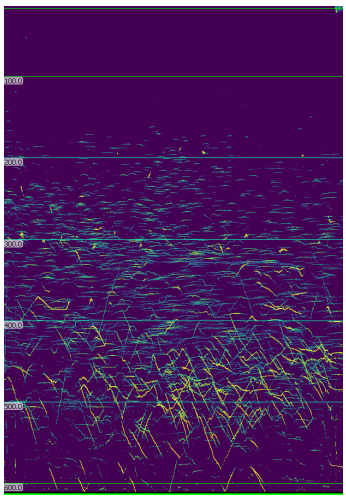

PS144_0109 – North Pole

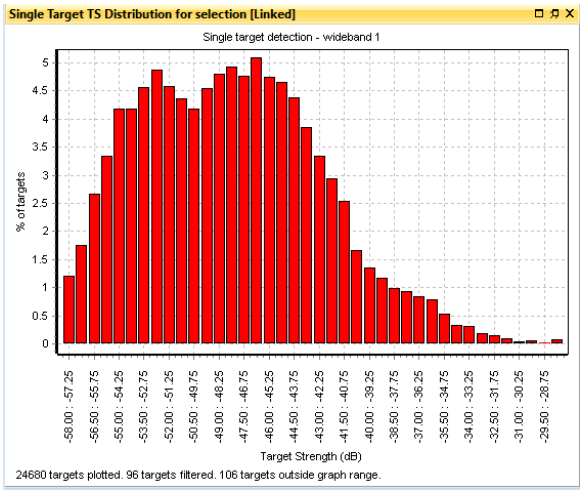

Fig. 7.13: Examples of echograms (left) and target strength distribution (right) during deployments of the pelagic trawl, and at station 109 near the North Pole.

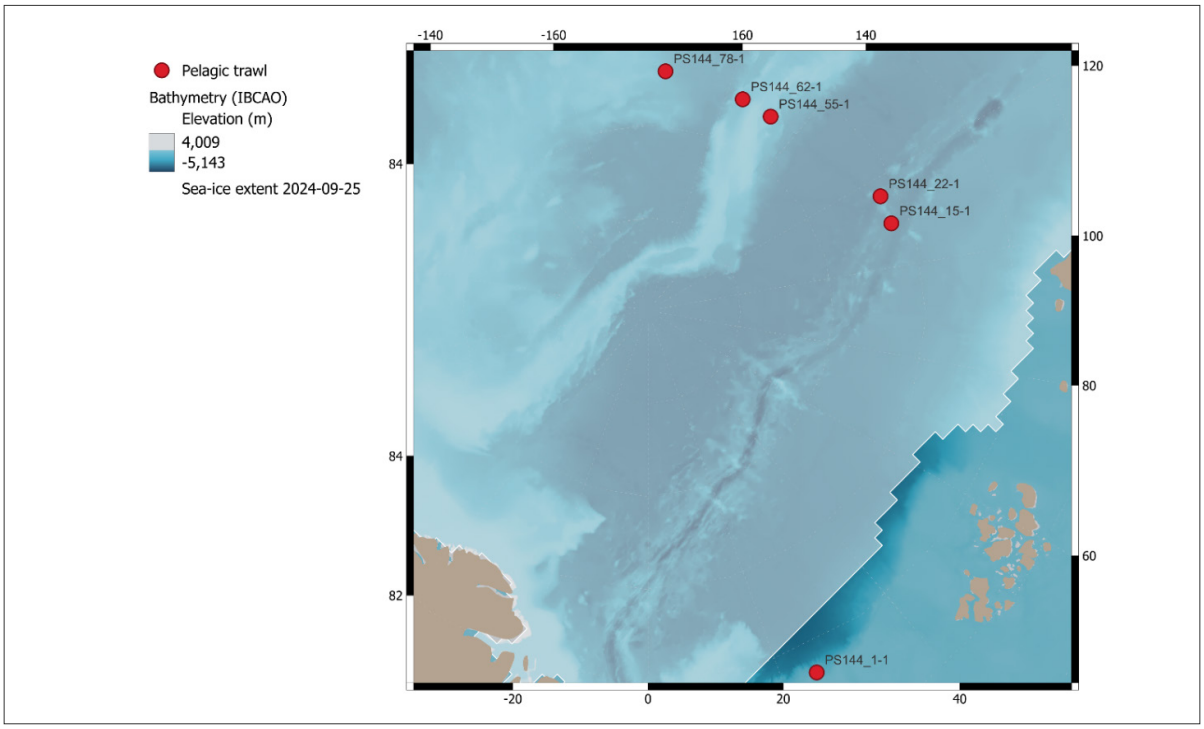

Fig. 7.14: Distribution of pelagic trawl deployments during PS144

Pelagic trawl: Pelagic trawls were performed at one test station (station 1) on the Svalbard shelf break, and five stations on Transect III (Fig. 7.14). The target depth was determined based on 38 kHz backscatter profiles from the EK80. In most cases, this was the center of the DSL (300-500) m. At station 1, the DSL was absent, and we targeted a backscatter maximum at 50 m depth. At station 62, we detected several signals with target strengths indicating larger fish between 500 and 600 m (Fig. 7.13), and the fishing depth was therefore adjusted to 550 m (Tab. 7.8).

Altogether, the pelagic trawl caught 72 finfish, not counting larvae (Tab. 7.8). At station 1, the catch (19 fish) was composed of larval and juvenile fish, including horse mackerel *Trachurus trachurus*, Greenland halibut *Reinhardtius hippoglossoides*, snailfish *Liparis* sp., twohorn sculpin *Icelus bicornis*, and Gadidae (Fig. 7.15). We also caught 109 larval flatfish (Pleuronectiformes), and 16 squid larvae. On Transect III, the only fish species caught were the lanternfish *Benthosema glaciale* (44 fish) and, occasionally polar cod *Boreogadus saida* (9 fish) which was probably caught near the surface (Fig. 7.15). The invertebrate catch was dominated by the amphipod *Themisto libellula* and shrimp (mainly *Hymenodora glacialis*). At station 62 where we fished below the DSL, we caught a large number of shrimp (588) and 7 larval and 1 juvenile squid (probably *Gonatus fabricii*) over 10 cm in size (Fig. 7.16). These results suggest that the DSL in the research area was predominantly inhabited by one species *Benthosema glaciale*, at low density but with a relatively even distribution.

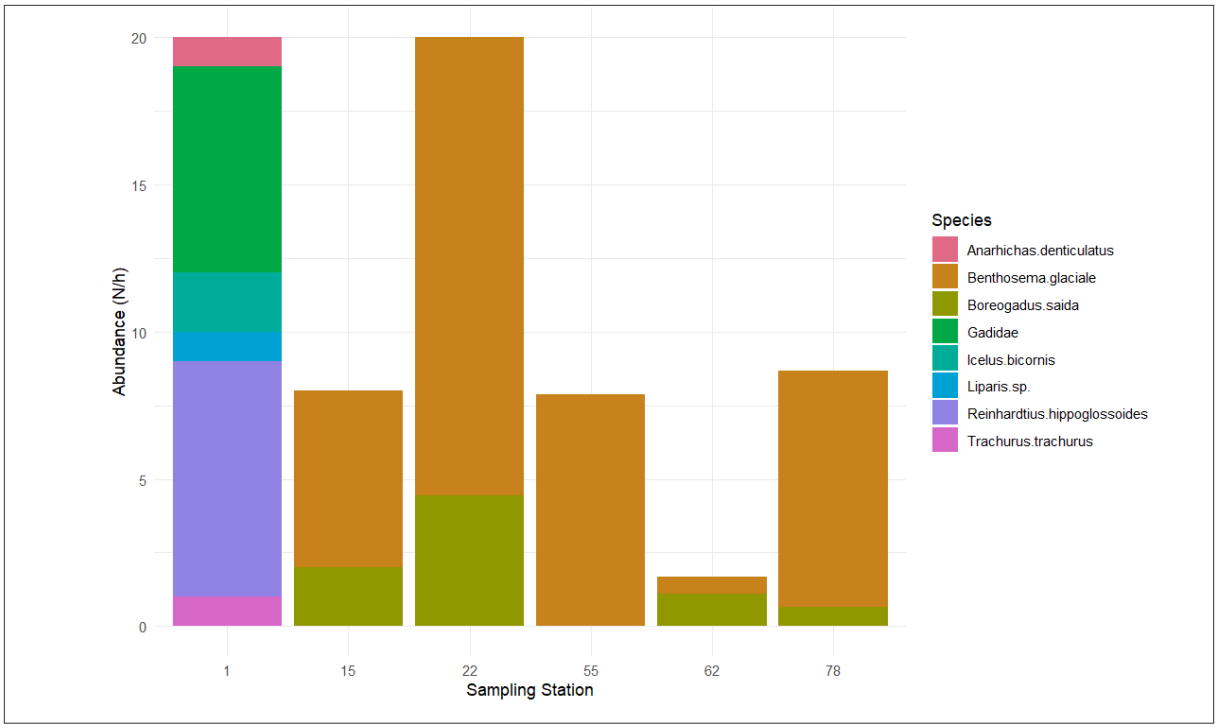

Fig. 7.15: Taxonomic composition of finfish caught with the pelagic trawl during PS144. Abundances relative to sampling effort are expressed in numbers per hour trawled (N/h).

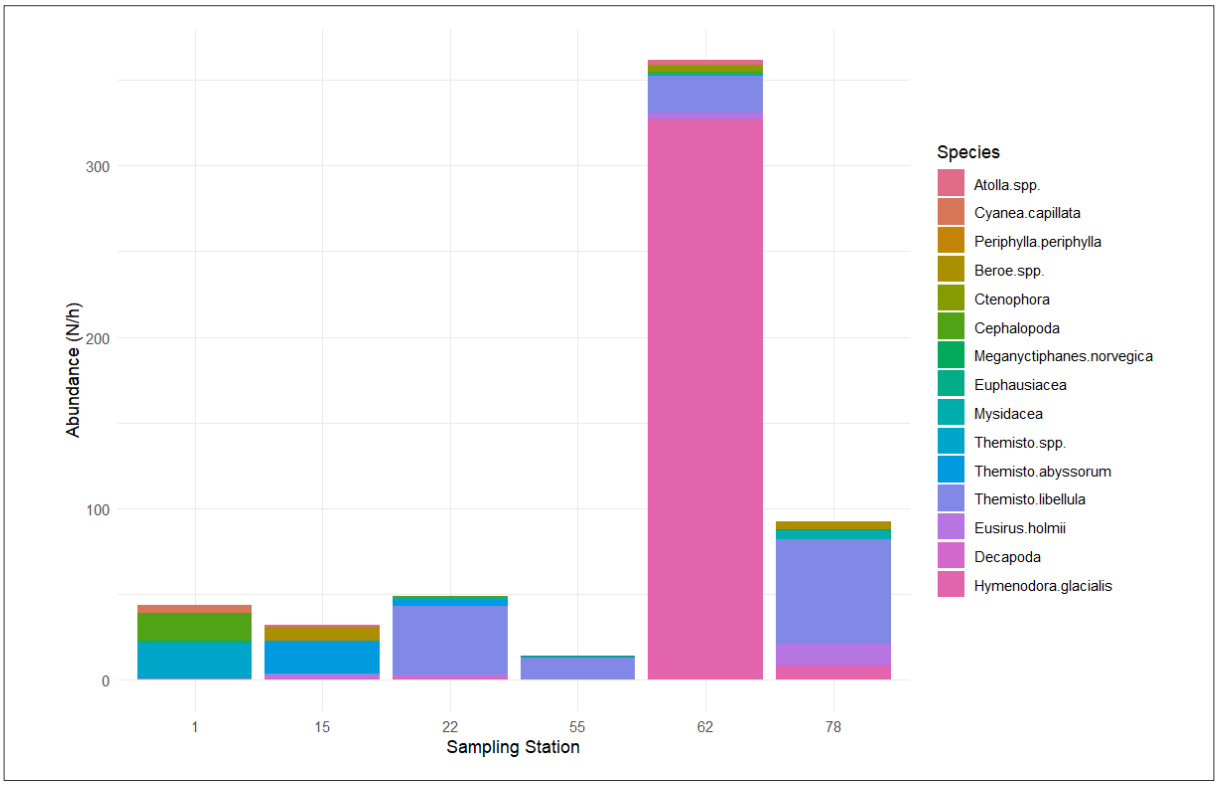

Fig. 7.16: Taxonomic composition of invertebrates caught with the pelagic trawl during PS144. Abundances relative to sampling effort are expressed in numbers per hour trawled (N/h).

Tab. 7.8: Overview of pelagic trawls conducted during PS144

Event	Date	Latitude [°N]	Longitude [°E]	Target depth [m]	Time trawled [h]	No of fish caught
PS144_1-1	2024-08-13	81.411	25.038	50	1	19
PS144_15-1	2024-08-21	84.426	109.687	450	1	8
PS144_22-1	2024-08-29	84.414	116.132	450	0.9	18
PS144_55-1	2024-09-06	85.056	147.638	350	1.4	11
PS144_62-1	2024-09-07	85.014	155.818	550	1.8	3
PS144_78-1	2024-09-10	84.835	175.810	350	1.5	13
Total						72

Longlines and traps: At all “super” ice stations in transect 3 and transect 2, fishing from the ice flow were conducted. All fishing devices were deployed at the earliest after opening the ice stations and were recovered as the latest cast on ice. Longlines were used to catch possible large predatory fish within the Atlantic water layer (Fig. 7.17, 7.18). Therefore, a combination of headlines and three different longlines with 170, 130 and 230 hooks, respectively, were used to reach a maximum line length between 506 and 614 metres (Tab. 7.9). Due to varying and partly strong currents at depth underneath the ice the realized maximum depth of the longline could not exactly be determined. The deployment time varied between stations with a minimum of 14 and a maximum of 36.5 hours. Despite some reasonable backscatter signals in the EK80 at several stations, no fish was caught at any station. Three separate longlines were used over time and the squid bait was frozen on the line afterwards and reused for 2 or 3 deployments. Only at ice station 4 (PS144_050_01_ICE04), severe problems occurred during recovery of the longline because of heavy load on the line or the hooks getting caught on ice ridges underneath the ice. Finally, more than 50 % of the deepest hooks were without bait, twisted or lost. Due to the long distance to the ship and other devices on the ice flow it seems unlikely that the longline got stuck by these devices and some biological activity seems likely. It remains unclear whether other large predators (e.g. seals) were responsible for this anomaly.

Fig. 7.17: Deployment of longlines through an ice hole. The main line was coiled in a bucket and the hooks attached by a monofile line and a swivel to it were sorted in systematic order around the bucket. Pieces of squid were used as bait. Photo: Magnus Lucassen).

Fig. 7.18: Recovery of longlines using an electrical line hauler (Northlift LH 300). Photo: Magnus Lucassen

To catch polar cod, a fyke net was modified to be deployed directly under the ice at three ice stations (Fig. 7.19, Fig. 7.20). Deployment times were similar to those of the longlines. Directly at the first try (ice station 4), one polar cod was caught, being in perfect condition. As we aimed to transport a number of living animals to Bremerhaven, the fish was initially kept alive in a recirculating aquarium system at 0°C. As no further intact fish were caught at a later stage of the cruise this specimen was finally sacrificed, and tissue samples were taken for ecological and transcriptomic studies.

Fig. 7.19: Deployment of the fyke net under ice. Photo: Magnus Lucassen

Several under-ice traps were deployed six times in conjunction with the longlines to sample ice amphipods and polar cod (Snoeijs-Leijonmalm et al., 2022). Despite adequate deployment times, no fish could be caught by this device. Even no ice amphipod found its way into the trap.

The used bait (fermented fish by-products) was utilized successfully for fish and amphipods throughout several expeditions to the Southern Ocean, but even bait from the the natural habitat (smashed shrimp from the RMT) did not attract more fish. Altogether, the low success of all ice fishing devices aligns to the overall low biological activity as observed by EK80, PSN, SUIT, RMT and multinet.

Fig. 7.20: The fyke net under ice. Photo: Hauke Flores

Tab. 7.9: Overview of fish sampling efforts at ice stations during PS144.
Fk = fyke; FR = fishing rod; LL = longline

Station	Date	Latitude	Longitude	LL	No of hooks	LL length [m]	Head rope [m]	Time (h)	Fk	No of traps	FR
10	2024-08-19	85.26	83.60	-					-	-	+
23	2024-08-29	84.50	115.72	+	170	306	200	17	-	2	
50	2024-09-04 - 2024-09-05	85.03	139.94	+	170	306	290	17	+	2	
67	2024-09-08	84.95	162.09	+	130	234	330	14	-	4	
85	2024-09-12 - 2024-09-13	87.50	178.73	+	130	234	340	19	-	2	
109	2024-09-18 - 2024-09-19	89.95	-142.70	+	230	414	200	24.5	+	2	
123	2024-09-23	88.07	59.95	-				-	-		+
134	2024-09-25 - 2024-09-26	87.05	57.07	+	230	414	200	36.5	+	2	

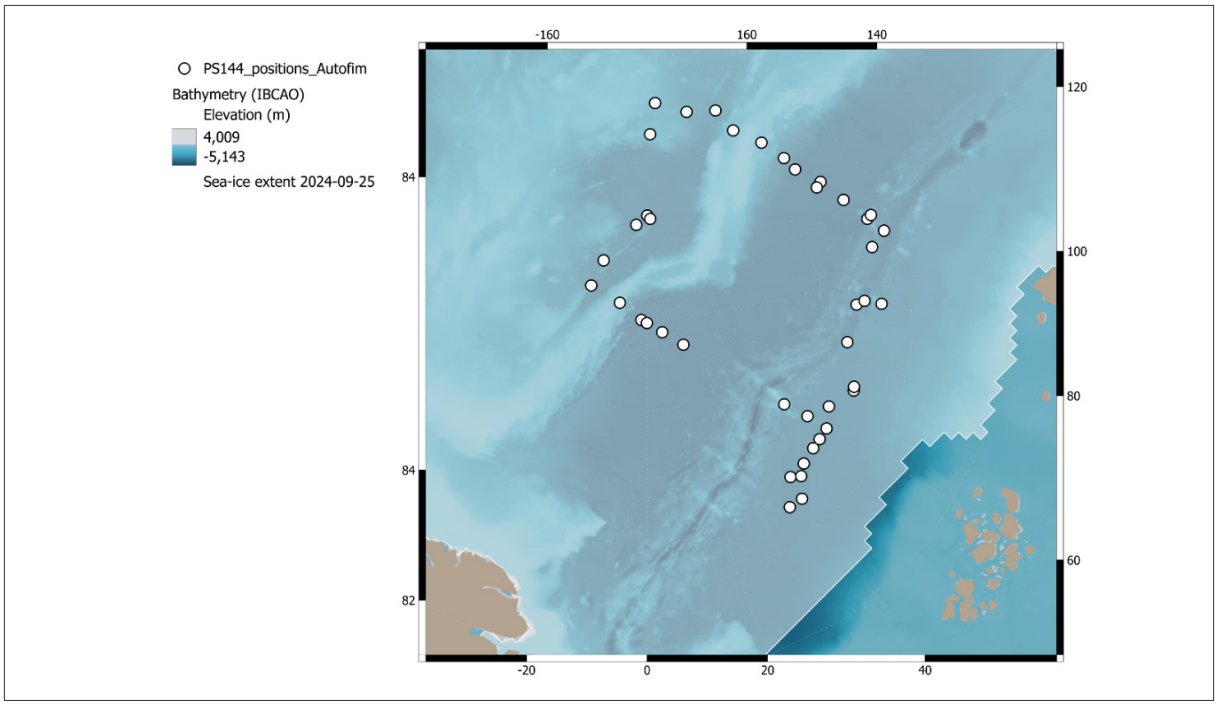

Fig. 7.21: Distribution of AutoFim samples during PS144

WP3

Protist DNA: During this expedition we aimed to improve the understanding of the eukaryotic microbial community composition to address the dynamics of the cryo-pelagic coupling in biodiversity in autumn with special emphasis on the re-freezing. For this, 2,000 ml of seawater for both Chlorophyl *a* and eukaryotic DNA analysis were taken within the upper 100 meters of the water column during 22 CTD stations (Tab. 7.1). Per CTD, samples from five water depths (100 meter, 50 meter, Surface, Chlorophyl maximum and Below chlorophyl maximum) were collected using plastic bottles. In addition, ice cores and under ice water were taken at nine ice stations using ice corers and under ice hand pumps (Tab. 7.2). Altogether, size-fractionated chlorophyll *a* and protist DNA samples were taken at 22 CTD stations and nine ice stations (Tab. 7.1, Tab. 7.2).

To create a more coherent picture, underway samples were collected using the automated and remote-controlled filtration system for marine microbes (AutoFim) (Metfies et al., 2016) adaptations and evaluations which are documented in a number of different publications, and the results of the recently completed field testing which are introduced in this paper. The observation strategy is organized at four different levels. At level 1, samples are collected at high spatiotemporal resolution using the remotely controlled automated filtration system AUTOFIM. Resulting samples can either be preserved for later laboratory analyses, or directly subjected to molecular surveillance of key species aboard the ship via an automated biosensor system or quantitative polymerase chain reaction (level 2 (Fig. 7.21, 7.22). From 15 August 2024 to 12 October 2024 this system took, except for some days of maintenance duration, daily water samples from ten meters depth below the ship (Tab. 7.10). Per run the AutoFim system collected samples at up to six filters, which were fixed with P-buffer and after being removed from the system stored at -80°C until further analysis at the AWI. Until 12 October 2024, we collected 52 AutoFim samples (Tab. 7.10).

After being collected, the 2,000 ml of either seawater or under ice water were run through a size fractionated filtration using 47 mm PC membrane filter and a vacuum pump. For Chlorophyll the water was first filtered through a 3 µm filter, collected and afterwards filtered through a 0.4 µm filter. For the eukaryotic DNA the procedure was similar to the one for Chlorophyll, but at the beginning the water was filtered through a 10 µm filter, before being filtered through 3 µm and 0.4 µm filters. All filtrations were conducted under dark conditions with limited light intrusion to prevent particles from being degraded. After filtration all filters were stored at -80°C until further analysis at the AWI.

For Chlorophyll and DNA only ice from the bottom 10 cm of the ice core was used. When the core sections had melted, 1,000-2,000 ml of water were collected for Chlorophyll analysis and filtered as described above. The same amount of water was used for DNA analysis but filtered on a Sterivex filter using a peristaltic pump. All samples were stored at -80°C until further analysis at the AWI.

Fig. 7.22: The AutoFim.
Photo: Jannis Hümmling

Tab. 7.10: Overview of AutoFim samples taken during PS144
Transit = Transit phase, Medivac = Medivac phase, station, T I = Transect I, T II = Transect II, T III = Transect III

Transect	Number of samples
Transit 1 & 2	9
Medivac	6
Transect III	15
Transect II	13
Transect I	3
Home Transit	6
Total	52

Phytoplankton diversity: To investigate phytoplankton diversity, water samples for microscopy, Imaging Flow Cytobot (IFCB), and flow cytometric analysis were collected from 2 to 5 depths (surface, chlorophyll a maximum, subsurface backscattering maximum depth, 50 m, 100 m) in the upper 100 m at 22 stations, using a 12-L PVC Niskin water sampler attached to a CTD rosette system (Tab. 7.11). Subsamples for ice algae were taken from the ice cores and seawater samples from under-ice water and subsurface backscattering maximum depth at 9 ice stations. To fill gaps in the geographic distribution of phytoplankton between stations, discrete water samples were also collected while underway, using the ship's seawater supply at a nominal depth of 7 m along the cruise track.

Seawater samples for IFCB analysis were collected in polypropylene bottles, fixed with glutaraldehyde (final concentration: 0.5%) for 1 hour, and stored at -20 ºC until analysis. Phytoplankton species abundance will be determined using the IFCB, which collects images of particles containing chlorophyll fluorescence in the laboratory at KOPRI (Olson and Sosik, 2007). All digital micrographs will be automatically classified using a supervised machine learning strategy (Laney and Sosik, 2014). For microscopic analysis, seawater samples from Niskin bottles were collected in polypropylene bottles, preserved with glutaraldehyde (final concentration 0.5%), and stored at -20 oC until analysis. Sample volumes of 20 - 100 mL will be filtered through Gelman GN-6 Metricel filters (0.45 µm pore size, 25 mm diameter) to prepare microscopic slides in a water-soluble embedding medium (HPMA, 2-hydroxypropyl

methacrylate) at KOPRI. The HPMA slides will be used for identification and estimation of cell concentration and biovolume. Seawater samples for picophytoplankton were fixed for 15 min with glutaraldehyde (final concentration: 0.1%) and stored at -80 ºC until analysis. Samples will be analyzed on a Accuri C6 flow cytometer (Becton Dickinson) equipped with an air-cooled argon laser (488 nm, 15 mW) to enumerate picophytoplankton abundance at KOPRI. Picophytoplankton groups will be identified and enumerated using the characteristics of 90°-angle light scatter, orange fluorescence from phycoerythrin, and red fluorescence from chlorophyll (Marie et al.,, 1997). Raw data from the flow cytometer will be processed using the FlowJo programme (Tree Star, www.flowjo.com).

Tab. 7.11: Numbers of stations sampled for phytoplankton and picophytoplankton abundance in the Transect II (T II), Transect III (T III), and transit section during the PS144 expedition

		CTD	FSW	ICE	Total
Transit 1	IFCB	3	16	1	20
Transit 1	Microscope	1	7	1	9
Transit 1	FCM		13		13
Transect III	IFCB	11		5	16
Transect III	Microscope	11		5	16
Transect III	FCM	11			11
Transit 2	IFCB	1		1	2
Transit 2	Microscope	1		1	2
Transit 2	FCM	1			1
Transect II	IFCB	7		2	9
Transect II	Microscope	7		2	9
Transect II	FCM	7			7
Total IFCB		22	16	9	47
Total Microscope		20	7	9	36
Total FCM		19	13		32

Foraminifera: Fossil foraminiferal assemblages are widely used for palaeoenvironmental reconstructions. However, for the correct interpretation of fossil data, it is crucial to improve our understanding of the correlation between environmental variability in the ocean and the distribution of living planktonic foraminifera. The objective of this expedition is to sample different depth intervals within the water column to examine the abundance and distribution of planktonic foraminifera at the various water masses. Eight multinet casts with a mesh size of 55 µm were conducted to collect planktonic foraminifera (Tab. 7.4). J. Wollenburg will analyse the net samples. Expected results will provide an insight into regional understanding and calibration of climate proxy indicators used in marine geology.

Data management

Environmental data will be archived, published and disseminated according to international standards by the World Data Center PANGAEA Data Publisher for Earth & Environmental Science (https://www.pangaea.de) within two years after the end of the expedition at the latest. By default, the CC-BY license will be applied.

Molecular data (DNA and RNA data) will be archived, published and disseminated within one of the repositories of the International Nucleotide Sequence Data Collaboration (INSDC, www.insdc.org) comprising of EMBL-EBI/ENA, GenBank and DDBJ).

Any other data will be submitted to an appropriate long-term archive that provides unique and stable identifiers for the datasets and allows open online access to the data.

This expedition was supported by the Helmholtz Research Programme “Changing Earth – Sustaining our Future” Topic 6, Subtopic 6.1. and 6.3.

In all publications based on this expedition, the **Grant No. AWI_PS144_06** will be quoted and the following publication will be cited:

Alfred-Wegener-Institut Helmholtz-Zentrum für Polar- und Meeresforschung (2017) Polar Research and Supply Vessel POLARSTERN Operated by the Alfred-Wegener-Institute. Journal of large-scale research facilities, 3, A119. http://dx.doi.org/10.17815/jlsrf-3-163.

References

Castellani G, Schaafsma FL, Arndt S, Lange BA, Peeken I, Ehrlich J, David C, Ricker R, Krumpen T, Hendricks S, Schwegmann S, Massicotte P, Flores H (2020) Large-Scale Variability of Physical and Biological Sea-Ice Properties in Polar Oceans. Frontiers in Marine Science 7:ARTN 536 https://doi.org/10.3389/fmars.2020.00536

Kawakami T, Yamazaki A, Jiang H-C, Ueno H, Kasai A (2023) Frontiers in Marine Science: https://doi.org/10.3389/fmars.2023.1193083

Kohlbach D, Graeve M, Lange BA, David C, Peeken I, Flores H (2016) The importance of ice algae-produced carbon in the central Arctic Ocean ecosystem: Food web relationships revealed by lipid and stable isotope analyses. Limnol Oceanogr 61:2027–2044 https://doi.org/10.1002/lno.10351

Laney S R, Sosik H M, 2014. Phytoplankton assemblage structure in and around a massive under-ice bloom in the Chukchi Sea. Deep-Sea Res. II, 105:30–41

Marie D, Partensky F. Jacquet S, Vaulot D (1997) Enumeration and cell-cycle analysis of natural populations of marine picoplankton by flow cytometry using the nucleic-acid stain SYBR Green I. Appl Environ Microb, 14:113-118

Metfies K, Schroeder F, Hessel J, Wollschläger J, Micheller S, Wolf C, Kilias E, Sprong P, Neuhaus S, Frickenhaus S & Petersen W (2016) High-resolution monitoring of marine protists based on an observation strategy integrating automated on-board filtration and molecular analyses. Ocean Science *12*(6):1237–1247. https://doi.org/10.5194/os-12-1237-2016

Olson R J, Sosik H M (2007) A submersible imaging-in-flow instrument to analyze nano- and microplankton: Imaging FlowCytobot. Limnol. Oceanogr. Methods 5:195–203.

Snoeijs-Leijonmalm P, Flores H, Niehoff B, Sakinan S, Svenson A, Castellani G, Hildebrandt N (2021) Ecosystem mapping in the Central Arctic Ocean (CAO) during the MOSAiC Expedition. Final Report. European Commission. 90 pp.

Snoeijs-Leijonmalm P and the SAS-Oden 2021 Scientific Party (2022a) Expedition Report SWEDARCTIC Synoptic Arctic Survey 2021 with icebreaker *Oden*. Swedish Polar Research Secretariat. 300 pp.

Snoeijs-Leijonmalm P, Flores H, Sakinan S, Hildebrandt N, Svenson A, Castellani G, Vane K, Mark FC, Heuzé C, Tippenhauer S, Niehoff B, Hjelm J, Sundberg JH, Schaafsma FL, Engelmann R (2022b) Unexpected fish and squid in the central Arctic deep scattering layer. Sci Adv 8:eabj7536 https://doi.org/10.1126/sciadv.abj7536

Trueman CN, Artetxe-Arrate I, Kerr LA, Meijers AJS, Rooker JR, Sivankutty R, Arrizabalaga H, Belmonte A, Deguara S, Goñi N, Rodriguez-Marin E, Dettman DL, Santos MN, Karakulak FS, Tinti F, Tsukahara Y, Fraile I (2023) Thermal sensitivity of field metabolic rate predicts differential futures for bluefin tuna juveniles across the Atlantic Ocean. Nat Commun 14:7379 https://doi.org/10.1038/s41467-023-41930-2

Vane K, Cobain MRD, Trueman CN, Vonnahme TR, Rokitta S, Polunin NVC, Flores H (2023) Tracing basal resource use across sea-ice, pelagic, and benthic habitats in the early Arctic spring food web with essential amino acid carbon isotopes. Limnol Oceanogr n/a https://doi.org/10.1002/lno.12315

Tab. 7.3: Summary statistics of sea-ice sampling sites and ice cores collected during PS144. Min = minimum value; Max = maximum value; N = Number of cores sampled; SBM = surface backscatter maximum; Stn = sampling site identifier (code after "PS144_" in event label)

Transect	Stn	Ice class	SBM [m]	N	Snow depth [cm]			Ice thickness [cm]			Freeboard [cm]			Core length [cm]		
					Mean	Min	Max	Mean	Min	Max	Mean	Min	Max	Mean	Min	Max
T'sit 1	7	SYI	NA	9	1.3	1	3	130.1	110	153	25.6	-2	110	148.3	90	177
T'sect III	23	SYI	26	17	1.5	1	5	120.4	111	155	13.9	-8	25	150.9	117	188
	42	FYI	25	14	1.5	1	2	130.8	108	150	16.0	2	32	132.7	109	161
	50	FYI	25	17	6.3	3	12	93.9	83	102	11.6	5	19	95.9	82	112
	67	FYI	25	23	5.4	0	12	90.7	51	114	8.8	-6	21	86.6	47	107
	80	MYI	23	20	5.6	0	11	141.2	116	194	16.4	7	27	144.5	119	204
T'sit 2	85	SYI	27	20	13.9	10	19	114.8	92	135	9.4	5	16	121.5	88	162
T'sect II	109	FYI	21	20	24.0	11	32	123.3	114	137	18.5	13	32	115.2	108	124
	134	SYI	28	20	3.8	3	5	136.6	123	148	15.2	6	25	139.0	123	153
Total				160	7.8	0	32	119.4	51	194	14.3	-8	110	124.1	47	204

8. AUTONOMOUS BUOY MEASUREMENTS

Mario Hoppmann[1], Benjamin Rabe[1], [1]DE.AWI
Jacob Allerholt[1], Jialiang Zhu[2] [2]CH.OUC
not on board: Marcel Nicolaus[1], Tao Li[2], [3]FR.SHOM
Olivier Desprez de Gesincourt[3], Sébastien Pere[3], [4]EDU.DARTMOUTH
Don Perovich[4], Jeff O'Brien[5], [5]EDU.WHOI
Sylvia Cole[5], John Toole[5], Ignatius Rigor[6], [6]EDU.UNI-Washington
Matthieu Labaste[7], Nathalie Sennechael[7] [7]FR.LOCEAN

Grant-No. AWI_PS144_03 and AWI_PS144_05

Objectives

The Arctic Ocean is a region of crucial importance for the ongoing global change, manifesting as the significant sea-ice retreat (Intergovernmental Panel on Climate Change, 2022), the unprecedented rise in near-surface air temperature (nearly four times the global rate, Rantanen et al., 2022), and the more recently observed Atlantification in the Eurasian Basin (Polyakov et al., 2017). The Arctic Ocean is also closely linked to the adjacent oceans and seas, and hence has a profound impact on regional and even global ocean circulation patterns and atmospheric temperatures at lower latitudes (Wu et al., 2013).

With emerging new technologies, autonomous observations have gained more importance in the Arctic Ocean in the past two decades, and they yield great potential to fill many of the current knowledge gaps. Especially the development of advanced ice-tethered (profiling) systems that are able to measure and send data while drifting with the sea ice, have helped immensely to close significant gaps in seasonal and regional observing. Most prominent examples of these kinds of instruments include the Woods Hole Oceanographic Institution Ice-tethered Profiler (WHOI-ITP; Toole et al., 2011), the Naval Postgraduate School Autonomous Ocean Flux Buoys (AOFB; Stanton et al., 2012), the Ice-Atmosphere-Ocean Observation System (IAOOS; Athanase et al., 2019), the Drift-Towing Ocean Profiler (DTOP), along with several different kinds of sea-ice mass balance buoys (Richter-Menge et al., 2006; Jackson et al., 2013; Planck et al., 2019), CTD-chain buoys (Hoppmann et al., 2022), and Snow Buoys (Nicolaus et al., 2021). Building on the success of using autonomous instrumentation during the Multidisciplinary drifting Observatory for the Study of Arctic Climate (MOSAiC) experiment (Rabe et al., 2024) and the PS138 expedition in 2023, during PS144 we aim to continuously observe a multitude of variables in the coupled atmosphere-ice-ocean system along the Transpolar Drift. We utilize many of the same platforms deployed during previous expeditions, and expect this dataset to provide an excellent opportunity to compare these new results with prior observations. Our buoy deployments are supported by the International Arctic Buoy Programme at the University of Washington (IABP, 2023), the overarching body coordinating the basin-wide deployments of autonomous ice-tethered instruments throughout the Arctic Ocean region.

Work at sea

PS138 Buoy recoveries

Sixteen buoys originally deployed during PS138 in August 2023 were recovered during PS144 in August 2024 (Fig. 8.1, Tab. 8.1).

Tab. 8.1: For further information please see the end of this chapter.

In addition to the hardware and sensors that were refurbished on the ship for immediate redeployment, or that are going to be refurbished at home, several buoys also recorded additional data that had not been sent via Iridium. A total of 11 recovered SBE37 microcats and one Wetlabs ECO Triplet fluorometer collected additional internal 2-minute data that had not been transmitted (Tab. 8.2). Figure 8.2 shows an exemplary time series of 2-minute pressure, temperature, and salinity obtained from the internal memory of the six individual SBE37 microcats as part of CTD buoy 2023O20 until their recovery in August 2024.

The SBE37 instruments on CTD buoy 2023O16 unexpectedly did not have any internally recorded data. The same issue was reported from CTD buoy 2023O23 by our Icelandic colleague A. Macrander, who helped to recover the buoy close to Iceland via fish trawler *Jökull ÞH299* on 19 August 2024. The problem is currently under investigation together with the manufacturer (Pacific Gyre, USA).

Tab. 8.2: Overview of recovered CTD buoys and corresponding SBE37 microcats.

Buoy shortname	Original name	SBE37 serial	nominal depth [m]	prelim. data check
2023O16	AWI-SVP5S-0003	21100	10 m	no data
		21103	20 m	no data
		21113	50 m	no data
		21114	75 m	no data
		21084	100 m	no data
2023O19	AWI-SVP5S-0009	22542	10 m	ok
		22543	20 m	ok
		22544	50 m	ok
		22545	75 m	ok
		22546	100 m	Instrument time off by 1h. Instrument stopped a few weeks earlier.
2023O20	AWI-SVP6S-0001	Triplet 6504	4 m	tbd
		22547	5 m	ok
		22548	10 m	ok
		22549	20 m	ok
		22552	50 m	ok
		22553	75 m	ok
		22554	100 m	ok

Fig. 8.1: Initial photos of buoys recovered during PS144. Buoys recovered from original PS138 ice station a-b) ICE5N1, c) ICE5-N3, d – l) ICE5, m-n) ICE5-N2, o-q) ICE4.

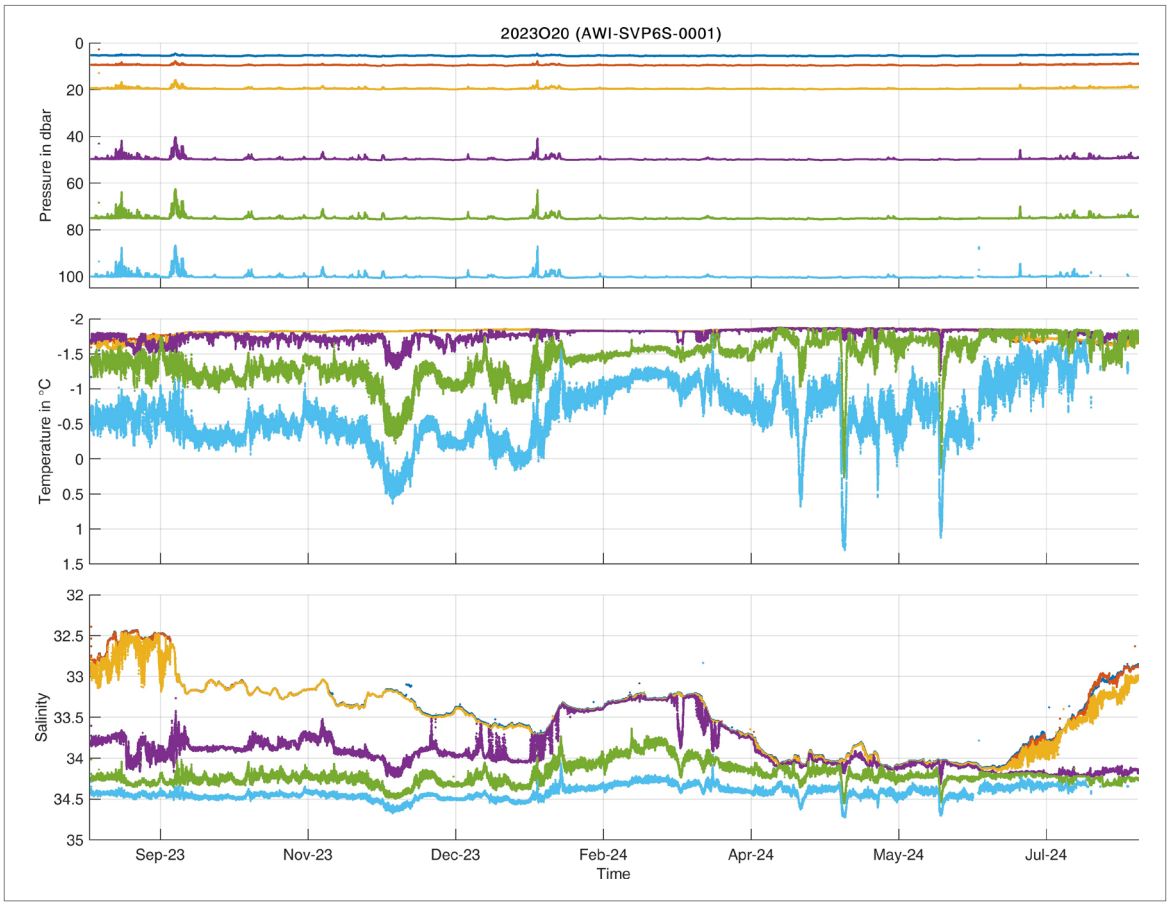

Fig. 8.2: Preliminary time-series of 2-minute pressure, temperature, and salinity obtained by recovered CTD buoy 2023O20, deployed during PS138 in August 2023

Buoy deployments

During PS144, we deployed the following buoys:

Snow Buoy

The Snow Buoy (MetOcean, Canada) measures snow depth and basic meteorological parameters (Fig. 8.3c). It consists of a hull containing the batteries and electronics, along with a 1.5 m tall mast that is equipped with a barometer, air temperature sensor, GPS- and Iridium antennas, and four ultrasonic pingers. During deployment, the hull is placed inside the ice. The four pingers mounted on the mast regularly measure the distance to the surface, providing the temporal evolution of snow depth around the buoy. Data is transmitted hourly via the Iridium satellite network, and also contributes to the Global Telecommunication System (GTS).

SIMBA - Snow and Ice Mass Balance Array

The SIMBA (SAMS Enterprise, Scotland) is a thermistor-chain ice mass balance buoy that measures the small-scale temperature gradient through the atmosphere-snow-ice-ocean boundary (Fig. 8.3f). The buoy consists of a yellow case that houses the battery, main electronics and auxiliary sensors, and a thermistor chain. A typical thermistor chain is 4.80 m long, with 240 thermistors at 0.02 m spacing. Additionally, the chain is equipped with 240 resistors that are able to actively heat the environment, which enables a better discrimination of the

interfaces between the different media. These interfaces can be determined from temperature and heating profiles using manual or automated methods. Auxiliary sensors include GPS, barometric pressure, air temperature and tilt. The data is transmitted via Iridium. Most SIMBAs are configured to measure and transmit four temperature and one heating profile per day.

Ocean Profilers (WHOI-ITP, IAOOS, DTOP)

We deployed three types of ocean profilers: the Woods Hole Ice-Tethered Profiler (Fig. 8.3a), the LOCEAN IAOOS (Fig. 8.3d) platform, and the OUC Drift-Towing Ocean Profiler (Fig. 8.3h). The WHOI-ITPs and IAOOS are composed of a surface unit mounted in/on a large floatation, and an ocean profiler that climbs/descends along an 800 m inductive modem tether. The profilers are equipped with SeaBird CTDs as a standard, and optional optical sensors for oxygen and turbidity. The WHOI-ITP profiler uses a motor to move up and down the tether, whereas the IAOOS uses buoyancy to control profiler depth. The latter system also measures basic meteorological parameters, and includes a SIMBA mounted on the surface float. Profiles are conducted 1-2 times per day. The OUC DTOP consists of a surface unit with basic meterological sensors, and a buoyancy-driven profiler that is attached to the underside of the surface unit via a regular 125-200 m cable. Several shallow profiles are obtained daily. Data of all platforms is sent out via Iridium.

CTD buoy

The CTD (chain) buoy (Pacific Gyre, USA) consists of an oval surface buoy containing the batteries and electronics, and a 100 m inductive tether with several instruments that measure physical (and optical) properties of the ocean. Most of the CTD buoys are equipped with 5 x SBE37IMP microcats mounted on the tether at 10, 20, 50, 75 and 100 m. They record seawater temperature, conductivity/salinity and pressure internally at 2-minute intervals. The surface buoy polls the individual sensors for a measurement every 10 minutes, which is then transmitted via Iridium along with the GPS position. The position data is provided to the GTS as well.

SIMB - Seasonal Ice Mass balance Buoy

The Seasonal Ice Mass balance Buoy (SIMB, Cryosphere Innovations, USA) is a floatable, tube-shaped buoy that detects surface and bottom ice/snow accumulation and ablation using ultrasonic pingers above and below the ice. It is also equipped with a thermistor chain mounted at the side of the hull. Data is transmitted at hourly intervals via the Iridium satellite network.

Sidekick camera buoy

The Sidekick camera buoy (Pacific Gyre, USA) consists of a peli case with two integrated webcams facing in opposite directions. They record images at variable intervals, and transmit these via the Iridium network. This buoy was contributed by the International Arctic Buoy Programme.

DAMP - Drifting Arctic Meteorological Platform

The Drifting Arctic Meteorological Platform (DAMP) is a floatable weather station that incorporates a suite of meteorological sensors. Of the two DAMPs deployed during PS144, one was equipped with a wind sensor. These buoys were contributed by the International Arctic Buoy Programme.

GPS buoys with meteorological sensors

We deployed different types of GPS drifters that were partly also equipped with barometric pressure and surface temperature sensors. These included 11 SVP-B buoys (MetOcean,

Canada) with barometric pressure sensors, and one Universal Tracker (Pacific Gyre, USA). Data of all these buoys are reported to the GTS. The MetOcean buoys were provided by SHOM/MeteoFrance.

Buoy deployments during regular ice stations

As part of the regular ice station work programme, 32 buoys were deployed on each ice floe at a location referred to as “buoy site”. The locations of these sites were determined during the floe exploration phase, and were commonly situated around ~300 m from the ship’s anchoring spot. The site was also chosen not to consist of ice thicker than ~1.7 m, to facilitate the deployment of the instrumentation through holes in the ice. The number and types of instruments varied greatly among ice stations, and was mostly determined by region to maximise the number of instruments deployed upstream in the Transpolar Drift. The instruments measuring different parameters in the atmosphere, ice and ocean were co-deployed to allow analysis of the coupled system. Table 8.3 presents a summary of all buoys deployed during regular ice stations.

Tab. 8.3: For further information please see the end of this chapter.

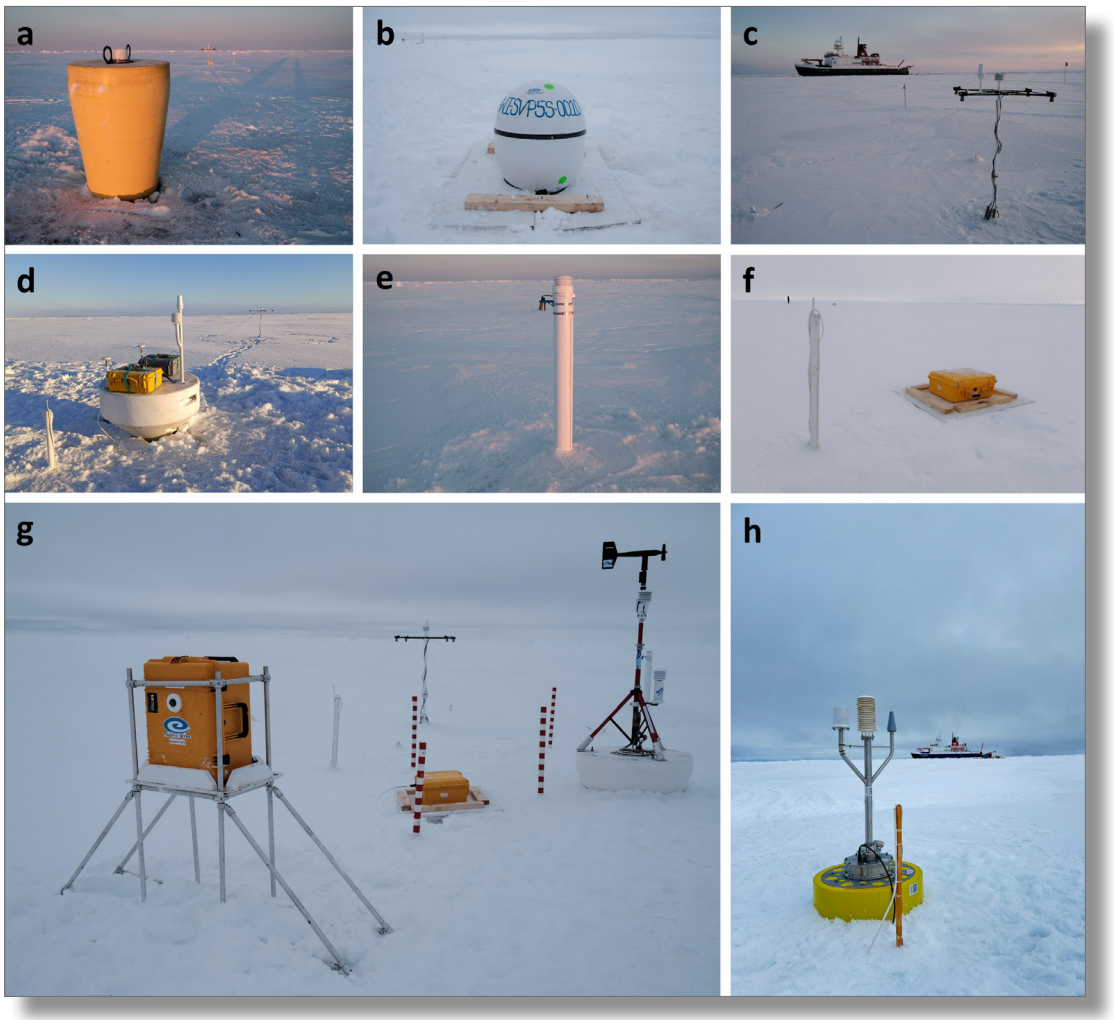

Fig. 8.3: Exemplary buoys deployed during regular ice stations: a) WHOI-ITP 2023W9 (ITP106); b) Pacific Gyre CTD Buoy 2024O21; c) MetOcean Snow Buoy 2024S131; d) LOCEAN IAOOS 2024W11 and SIMBA 2024T120; e) Cryosphere Innovations SIMB 2024I15; f) SIMBA 2024T120; g) Pacific Gyre SideKick 2024K2, APL-UW DAMP 2024A7, SIMBA 2024T117; h) DTOP 2024V8.

Along-track buoy deployments

Eleven GPS drifters equipped with surface temperature and barometric pressure sensors were deployed along the cruise track on a regular basis (Tab. 8.4, Fig. 8.4, 8.5) as a complement to the instruments installed during the ice stations. The main aim of these deployments was to achieve a better coverage of barometric pressure measurements in the notoriously undersampled Arctic Ocean for the improvement of weather forecasts, also at lower latitudes. These buoys were deployed in different areas along the cruise track, at a distance of 30-50 nmi from other GTS buoys to achieve maximum coverage. They were deployed mostly by mummy chair from the ship.

Tab. 8.4: For further information please see the end of this chapter.

Fig. 8.4: Overview of all GPS buoys deployed during PS144. a-k) MetOcean SVP-Bs 2024P299 – 2024P309 deployed during transit according to Table 8.4. f) Pacific Gyre Universal Tracker marking the FloatBoats (see next paragraph).

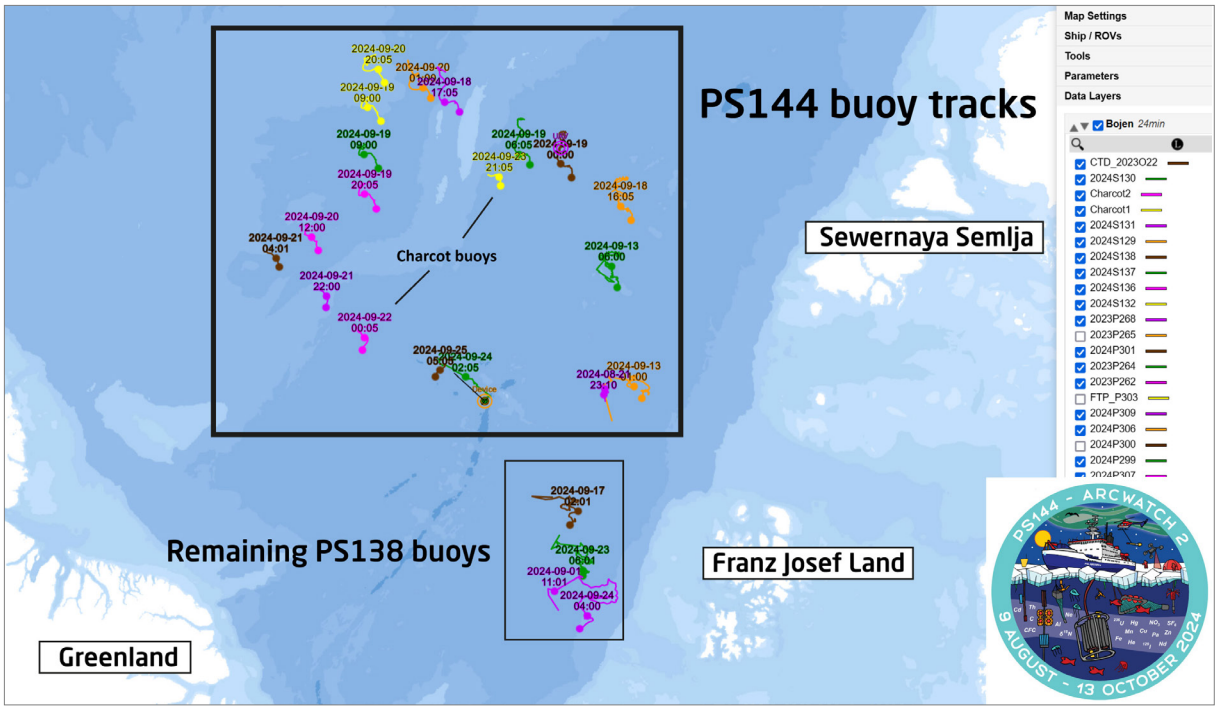

Fig. 8.5: Screenshot of Polarstern mapviewer, showing buoy deployment locations and exemplary trajectories until 26 September 2024

Float Your Boat Outreach activity

As part of the FloatYourBoat Outreach activity led by the International Arctic Buoy Programme, we deployed a large number of wooden boats (*cf.* Fig. 8.6) along with our buoys at the North Pole station ICE7. These numbered boats were painted by school classes and students, and are traceable, when found, via floatboat.org. These were complemented by a smaller number of boats painted by cruise participants. As long as the ice floe remains intact, the boats can be tracked via Pacific Gyre Universal Tracker 2024P311 on meereisportal.de. The buoy was placed right next to the boats.

Here's a short summary of the Float your Boat concept (Forcucci et al., 2022):

"*Following the legacy of the early Arctic explorers, Float Your Boat (FYB) is a unique and fun outreach programme that provides a novel opportunity for students and the public to learn about the Arctic Ocean. Participants decorate toy wooden boats with words and art, and the boats are deployed on Arctic Ocean ice floes by icebreakers. Personal connections to the Arctic develop with the anticipation and excitement of the boats being reported on distant shores years later by beachcombers. The brand "www.floatboat.org" is burned into the wood so that anyone finding a boat can visit the website and report the discovery. […] Students tracked their drift across the ocean in real time through IABP meteorological buoys, deployed at the same time as the boats, using the IABP webpage https://iabp.apl.uw.edu/Float_Your_Boat.html and the project's Facebook page https://www.facebook.com/floatboat.org.*"

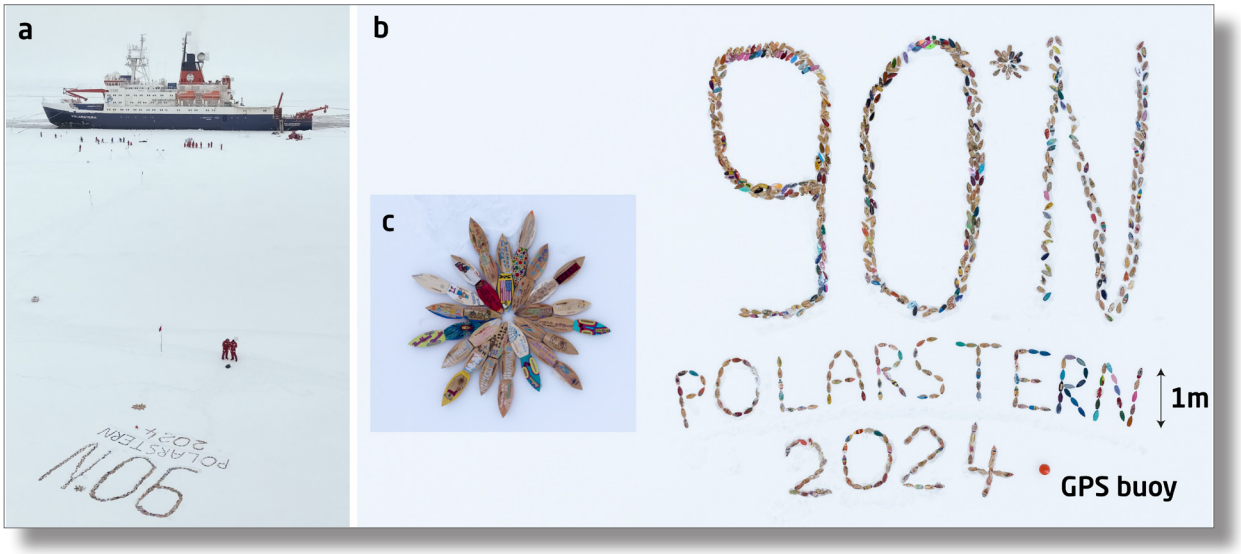

Fig. 8.6: Photo collage of our FloatYourBoat deployment at the North Pole

Data management

All buoy data are transmitted via the Iridium satellite network, and decoded and stored on dedicated servers of the respective buoy manufacturer. Most of the data are provided, displayed and updated daily on the data portal section of meereisportal.de. The provided information includes deployment sheets, buoy metadata, maps, and the measured parameters themselves. Additionally, selected buoy data is fed into the database of the International Arctic Buoy Programme (IABP) and the WMO's Global Telecommunications System (GTS), from where they are immediately available for public use.

The data will be archived, published, and disseminated according to international standards and FAIR principles by the World Data Center PANGAEA Data Publisher for Earth & Environmental Science (https://www.pangaea.de) one year after a buoy ceased operation. By default, the CC-BY license will be applied.

Any other data will be submitted to an appropriate long-term archive that provides unique and stable identifiers for the datasets and allows open online access to the data.

We acknowledge financial support by the USIABP and Ignatius Rigor for covering a large part of the buoys' Iridium costs.

This expedition was supported by the Helmholtz Research Programme "Changing Earth – Sustaining our Future" Topic 2, Subtopics 1 and 4

In all publications based on this expedition, the Grant Nos**. AWI_PS144_03, AWI_PS144_05 or AWI_PS144_00** will be quoted.

References

Athanase M, Sennéchael N, Garric G, Koenig Z, Boles E, Provost C (2019) New Hydrographic Measurements of the Upper Arctic Western Eurasian Basin in 2017 Reveal Fresher Mixed Layer and Shallower Warm Layer Than 2005–2012 Climatology. J Geophys Res Oceans 124(2):1091–1114. https://doi.org/10.1029/2018JC014701

Forcucci D, Rigor I, Ermold W, Stern H (2022) Float your boat: Launching students into the Arctic Ocean. Oceanography 35(3–4):228–229, https://doi.org/10.5670/oceanog.2022.102

Hoppmann M, Kuznetsov I, Fang Y-C, Rabe B (2022) Mesoscale observations of temperature and salinity in the Arctic Transpolar Drift: a high-resolution dataset from the MOSAiC Distributed Network. Earth Syst Sci Data 14(11):4901–4921. https://doi.org/10.5194/essd-14-4901-2022

IABP (2023) https://iabp.apl.uw.edu/, last accessed 30 June, 2023

Intergovernmental Panel On Climate Change (IPCC) (2022) The Ocean and Cryosphere in a Changing Climate: Special Report of the Intergovernmental Panel on Climate Change. 1st ed. Cambridge University Press. https://doi.org/10.1017/9781009157964

Jackson K, Wilkinson J, Maksym T, Meldrum D, Beckers J, Haas C, Mackenzie D (2013) A Novell and Low-Cost Sea Ice Mass Balance Buoy. Journal of Atmospheric and Oceanic Technology 30(11): 2676–2688. https://doi.org/10.1175/JTECH-D-13-00058.1

Nicolaus M, Hoppmann M, Arndt S, Hendricks S, Katlein C, Nicolaus A, Rossmann L, Schiller M, Schwegmann S (2021) Snow Depth and Air Temperature Seasonality on Sea Ice Derived From Snow Buoy Measurements. Front Mar Sci 8:655446. https://doi.org/10.3389/fmars.2021.65544

Planck CJ, Whitlock J, Polashenski C, Perovich D (2019) The evolution of the seasonal ice mass balance buoy. Cold Regions Science and Technology 165:102792. https://doi.org/10.1016/j.coldregions.2019.102792

Polyakov IV, Pnyushkov AV, Alkire MB, Ashik IM, Baumann TM, Carmack EC, Goszczko I, Guthrie J, Ivanov VV, Kanzow T, et al. (2017) Greater role for Atlantic inflows on sea-ice loss in the Eurasian Basin of the Arctic Ocean. Science 356(6335):285–291. https://doi.org/10.1126/science.aai8204

Rabe B, Cox CJ, Fang Y-C, Goessling H, Granskog MA, Hoppmann M, Hutchings JK, Krumpen T, Kuznetsov I, Lei R Li T, Maslowski W, Nicolaus M, Perovich D, Persson O, Regnery J, Rigor I, Shupe MD, Sokolov V, Spreen G, Stanton T, Watkins DM, Blockley E, Buenger HJ, Cole S, Fong A, Haapala J, Heuzé C, Hoppe CJM, Janout M, Jutila A, Katlein C, Krishfield R, Lin L, Ludwig V, Morgenstern A, O'Brien J, Zurita AQ, Rackow T, Riemann-Campe K, Rohde J, Shaw W, Smolyanitsky V,Solomon A, Sperling A, Tao R, Toole J, Tsamados M, Zhu J, Zuo G (2024) The MOSAiC Distributed Network: Observing the coupled Arctic system with multidisciplinary, coordinated platforms. Elem Sci Anth 12: 00103. https://doi.org/10.1525/elementa.2023.00103

Rantanen M, Karpechko AYu, Lipponen A, Nordling K, Hyvärinen O, Ruosteenoja K, Vihma T, Laaksonen A (2022) The Arctic has warmed nearly four times faster than the globe since 1979. Commun Earth Environ 3(1):168. https://doi.org/10.1038/s43247-022-00498-3

Richter-Menge JA, Perovich DK, Elder BC, Claffey K, Rigor I, Ortmeyer M (2006) Ice mass- balance buoys: a tool for measuring and attributing changes in the thickness of the Arctic sea-ice cover. Ann Glaciol 44:205–210. https://doi.org/10.3189/172756406781811727

Stanton TP, Shaw WJ, Hutchings JK (2012) Observational study of relationships between incoming radiation, open water fraction, and ocean-to-ice heat flux in the Transpolar Drift: 2002-2010: OCEAN/ ICE FLUXES IN THE ARCTIC. J Geophys Res 117:(C7). https://doi.org/10.1029/2011JC007871

Toole J, Krishfield R, Timmermans M-L, Proshutinsky A (2011) The Ice-Tethered Profiler: Argo of the Arctic. Oceanog 24(3):126–135. https://doi.org/10.5670/oceanog.2011.64

Wu B, Handorf D, Dethloff K, Rinke A, Hu A (2013) Winter Weather Patterns over Northern Eurasia and Arctic Sea Ice Loss. Monthly Weather Review 141(11):3786–3800. https://doi.org/10.1175/MWR-D-13-00046.1

Tab. 8.1: Overview of recovered buoys that were originally deployed during PS138 in August 2023. This table does not include CTD buoy 2023O23 recovered close to Iceland by fish trawler *Jökull ÞH299*.

Shortname	Buoy type	IMEI	Original name	PS138 station	Deployment time	Recovery time	Event label	Comment
2023O20	CTD buoy	300534060151880	AWI-SVP6S-0001	ICE5	2023-08-28 13:00:00	2024-08-17 05:00:00	PS144_8_ BuoyRecovery_001	recovered in good condition
2023I11	SIMB	300434066254600	DARTMOUTH 2023 #3		2023-08-29 12:00:00	2024-08-17 05:00:00	PS144_8_ BuoyRecovery_002	no recovery for scientific reasons
2023W6	WHOI-ITP*	300025060518220	ITP140		2023-08-28 16:40:00	2024-08-17 05:00:00	PS144_8_ BuoyRecovery_003	surface unit recovered
2023S127	Snow Buoy	300234060729780			2023-08-28 13:20:00	2024-08-17 05:00:00	PS144_8_ BuoyRecovery_004	recovered with tilted frame, refurbished
2023T106	SIMBA	300534063056460	AWI 11-02 long chain		2023-08-28 13:45:00	2024-08-17 05:00:00	PS144_8_ BuoyRecovery_005	box flooded
2023R25	Radiation station	300025060615750	BOS089		2023-08-30 16:00:00	2024-08-17 05:00:00	PS144_8_ BuoyRecovery_006	recovered in good condition
SnowTATOS1	SnowTATOS	300434068070720			2023-08-29 12:00:00	2024-08-17 05:00:00	PS144_8_ BuoyRecovery_007	disfunctional, recovered
2023K1	Sidekick	300534062721510	APL-SK-0003		2023-08-29 12:00:00	2024-08-17 05:00:00	PS144_8_ BuoyRecovery_008	recovered in good condition
2023O16	CTD buoy	300234068164710	AWI-SVP5S-0003	ICE5-N1	2023-08-29 15:10:00	2024-08-15 20:00:00	PS144_4_ BuoyRecovery_001	recovered in good condition
2023T109	SIMBA	300534061784850	PRIC 12-01		2023-08-29 15:30:00	2024-08-15 20:00:00	PS144_4_ BuoyRecovery_002	recovered in good condition
2023S124	Snow Buoy	300234060726880			2023-08-30 08:00:00	2024-08-15 20:00:00	PS144_4_ BuoyRecovery_003	broken, no recovery possible
2023O22	CTD buoy	300534064364470	AWI-SVP5S-0011	ICE5-N2	2023-08-30 17:40:00	2024-08-25 09:00:00	PS144_Heli_ BuoyRecovery_001	recovery not possible, ice thickness ~2.2m
2023S125	Snow Buoy	300234060727760			2023-08-30 17:50:00	2024-08-25 09:00:00	PS144_Heli_ BuoyRecovery_002	recovered wth broken mast
2023T103	SIMBA	300234065171790	FMI 05 10		2023-08-30 18:05:00	2024-08-25 09:00:00	PS144_Heli_ BuoyRecovery_003	not found, GPS position 3nm away
2023O19	CTD buoy	300534060057710	AWI-SVP5S-0009	ICE5-N3	2023-08-31 22:00:00	2024-08-16 00:00:00	PS144_5_ BuoyRecovery_001	recovered in good condition
2023T105	SIMBA	300534063054440	AWI 11-01		2023-08-31 22:00:00	2024-08-16 00:00:00	PS144_5_ BuoyRecovery_002	recovered in good condition
2023S122	Snow Buoy	300234060330560			2023-08-31 22:00:00	2024-08-16 00:00:00	PS144_5_ BuoyRecovery_003	recovered with tilted frame, refurbished

Tab. 8.3: Overview of buoys deployed during PS144 ice stations. The asterisk marks buoys that were refurbished from the PS138 recoveries (see above paragraph). This table does not include 2 SIMBAs and 2 Snow Buoys deployed by our colleagues in the same area and period from the tourist vessel Le Commandant Charcot in July/September 2024

Buoy type	Short name	Original name	IMEI	WMO ID	Deployment time	Depl. Lat [Deg]	Depl. Lon [Deg]	Event label	Additional Information
LOCEAN IAOOS	2024W12		300025010345860		2024-08-30 03:10:00	84.4184	115.6712	PS144_23_Buoy_001	
SAMS ice mass balance buoy	2024T122	LOCEAN 07-05	300234066298810		2024-08-30 03:10:00	84.4184	115.6712	PS144_23_Buoy_002	ice thickness 1.65m, FB 0.12m, scattering layer 0.02m; thermistor 22 at surface
MetOcean Snow Buoy	2024S129		300234062922670	5802062	2024-08-30 08:50:00	84.4245	115.6047	PS144_23_Buoy_003	snow depth 0 cm
WHOI Ice-Tethered Profiler	2024W8	ITP96	300025010920080		2024-09-05 06:00:00	85.0137	139.7935	PS144_50_Buoy_001	ice thickness 1.6m
Cryosphere Innov. Seasonal IMB	2024I14	2024Dartmouth#1	301434060104880		2024-09-05 07:00:00	85.0137	139.7935	PS144_50_Buoy_002	ice thickness 1.3m, snow depth: 0.17m, FB: 0.11m; 15m from DAMP
APL weather station	2024A8	DAMP010			2024-09-05 06:00:00	85.0137	139.7935	PS144_50_Buoy_003	ice thickness ~1.6m; 20m from ITP96
SAMS ice mass balance buoy	2024T108	AWI 11-04	300534063050420		2024-09-05 07:30:00	85.0186	139.8414	PS144_50_Buoy_004	ice thickness 0.92m, snow depth 0.08m, FB 0.06m; thermistor 25 at surface
Drift-Towing Ocean Profiler	2024V6	DTOP202301	300534065822480		2024-09-05 08:40:00	85.0159	139.8414	PS144_50_Buoy_005	
MetOcean Snow Buoy	2024S130		300534066618760	7801686	2024-09-05 06:30:00	84.0149	139.8414	PS144_50_Buoy_006	SH1: 0.12m, SH2: 0.12m, SH3: 0.13m, SH4: 0.1m; 15m from DAMP
WHOI Ice-Tethered Profiler	2024W9	ITP106	300025010922080		2024-09-08 12:55:00	84.9450	161.9910	PS144_67_Buoy_001	
Cryosphere Innov. Seasonal IMB	2024I15	2024Dartmouth#2	301434060041150		2024-09-08 12:55:00	84.9449	161.9878	PS144_67_Buoy_002	ice thickness 1.34m, snow depth 0.08m, FB 0.16m; 10 from Snow Buoy, 10 m from SIMBA

Buoy type	Short name	Original name	IMEI	WMO ID	Deployment time	Depl. Lat [Deg]	Depl. Lon [Deg]	Event label	Additional Information
SAMS ice mass balance buoy	2024T116	AWI 11-07	300534063051450		2024-09-08 12:45:00	84.9447	161.9848	PS144_67_Buoy_003	ice thickness 1.27m, snow depth 0.1m, FB 0.1m; thermistor 34 at surface, frozen snow
Drift-Towing Ocean Profiler	2024V7	DTOP202305	300534065829130		2024-09-08 12:45:00	84.9425	161.9656	PS144_67_Buoy_004	
MetOcean Snow Buoy	2024S131		300534066610750	6801864	2024-09-08 12:55:00	84.9450	161.9910	PS144_67_Buoy_005	snow depth 0.08; snow frozen
APL weather station	2024A7	DAMP008	300534060426630		2024-09-11 06:00:00	84.9592	179.5390	PS144_80_Buoy_001	
WHOI Ice-Tethered Profiler	2024W10	ITP133	300125060315490		2024-09-11 06:00:00	84.9592	179.5390	PS144_80_Buoy_002	
Cryosphere Innov. Seasonal IMB	2024I16	2024Dartmouth#3	30143060109890		2024-09-11 06:00:00	84.9592	179.5390	PS144_80_Buoy_003	ice thickness 1.33m, snow depth/surface layer 0.1m, FB 0.16m
SAMS ice mass balance buoy	2024T117	AWI 11-08	300534063052380		2024-09-11 06:00:00	84.9592	179.5390	PS144_80_Buoy_004	ice thickness 1.37m, snow depth 0.06m, FB 0.12m
MetOcean Snow Buoy	2024S132		300534066611760	7801684	2024-09-11 06:00:00	84.9592	179.5390	PS144_80_Buoy_005	SH1: 0.05m, SH2: 0 m, SH3: 0m, SH4: 0.07m
Drift-Towing Ocean Profiler	2024V8	DTOP202302	300534065826500		2024-09-11 03:40:00	84.9459	179.3859	PS144_80_Buoy_006	
Pacific Gyre CTD Buoy	2024O21	AWI-SVP5S-0010	300534064364400	6801886	2024-09-11 06:00:00	84.9592	179.5390	PS144_80_Buoy_007	
Pacific Gyre Sidekick camera buoy	2024K2*	Sidekick_003	300534062721510		2024-09-11 06:00:00	84.9592	179.5390	PS144_80_Buoy_008	
LOCEAN IAOOS	2024W11		300025010343290		2024-09-13 01:45:00	87.5120	178.8962	PS144_85_Buoy_001	
SAMS ice mass balance buoy	2024T120	LOCEAN 07-06	300234066291810		2024-09-13 01:45:00	87.5120	178.8962	PS144_85_Buoy_002	ice thickness 1.32m, snow depth 0.07m, FB 0.08m; thermistor 25 at surface; 1m from IAOOS

Buoy type	Short name	Original name	IMEI	WMO ID	Deployment time	Depl. Lat [Deg]	Depl. Lon [Deg]	Event label	Additional Information
MetOcean Snow Buoy	2024S136*		300234060729780	2802066	2024-09-13 01:20:00	87.5120	178.9074	PS144_85_Buoy_003	SH1: 0.16m, SH2: 0.16m, SH3: 0.14m, SH4: 0.14m; 15 m from IAOOS
LOCEAN IAOOS	2024W13		300025010637460		2024-09-19 04:05:00	89.9494	-150.2867	PS144_109_Buoy_001	
SAMS ice mass balance buoy	2024T121	LOCEAN 07-03	300234066292850		2024-09-19 04:05:00	89.9494	-150.2867	PS144_109_Buoy_002	ice thickness 1.23m, snow depth 0.14m, FB 0.09m; thermistor 25 at surface; 1m from IAOOS
Pacific Gyre Universal Tracker	2024P311	AWI-UT-0006	300534064263630	1801779	2024-09-19 16:45:00	89.9650	-130.8405	PS144_109_Buoy_003	deployed at FloatBoats site
MetOcean Snow Buoy	2024S138*	2023S123	300234060543140	7801685	2024-09-23 08:30:00	88.0716	59.8645	PS144_123_Buoy_001	SH1: 0.18m, SH2: 0.24m, SH3: 0.19m, SH4: 0.18m
SAMS ice mass balance buoy	2024T118	AWI 11-09	300534063051410		2024-09-23 08:50:00	88.0716	59.8751	PS144_123_Buoy_002	ice thickness 1.15m, snow depth 0.16m, FB 0.09m; thermistor 31 at surface; 10m from Snow Buoy
MetOcean Snow Buoy	2024S137*	2023S122	300234060330560	6801865	2024-09-25 07:30:00	86.9913	58.4583	PS144_134_Buoy_001	SH1: 0.06 m, SH2: 0.04 m, SH3: 0.04 m, SH4: 0.06 m; refurbished buoy with slightly tilted frame
SAMS ice mass balance buoy	2024T101	AWI 09-10	300534061349520		2024-09-25 07:50:00	86.9930	58.4328	PS144_134_Buoy_002	ice thickness 1.45m, snow depth 0.05m, FB 0.19m; thermistor 32 at surface; 10m from Snow Buoy

Tab. 8.4: Overview of MetOcean SVP-Bs deployed during transit. These buoys were provided by EUMETNET/SHOM to increase the barometric pressure coverage in the Arctic Ocean.

Shortname	IMEI	WMO id	Deployment time (UTC)	Depl. Lat [Deg]	Depl. Lon [Deg]	Event label	Additional information
2024P299	300534065281030	6301583	2024-08-20 14:45:00	85.1266	94.8740	PS144_12-2	small MYI floe, 70m diameter; ice thickness >2m
2024P300	300534065282020	6301584	2024-08-21 03:35:00	84.7750	103.8398	PS144_14-1	MYI floe; 150 x 100m; ice thickness >2m
2024P301	300534065282030	6301585	2024-09-01 02:25:00	84.9013	129.0614	PS144_33-1	MYI floe 150 x 150m; ice thickness >2m
2024P302	300534065822750	6301586	2024-09-06 23:07:00	85.0371	150.4949	PS144_57-4	250 x 150m
2024P303	300534065283030	6301587	2024-09-07 15:54:00	85.0371	155.6366	PS144_63-1	250 x 150m; ice thickness 1.40m, snow depth 0.02m, FB 0.23m
2024P306	300534065286030	6401600	2024-09-09 21:12:00	84.9444	169.2364	PS144_73-5	500 x 500m; ice thickness 1m
2024P304	300534065285030	6301589	2024-09-11 19:40:00	85.7677	178.9300	PS144_83-1	500 x 500m; ice thickness ~1.5m
2024P305	300534065825770	6401599	2024-09-12 06:10:00	86.7227	179.8155	PS144_84-1	
2024P307	300534065287020	6401601	2024-09-15 07:58:00	88.0224	-148.8019	PS144_88-2	min 1500 x 1500m
2024P308	300534065287030	6401602	2024-09-16 10:25:00	87.8196	-125.0207	PS144_Heli_ Buoy_001	50 x 50 m, ice thickness ~1.5m
2024P309	300534065829800	6401604	2024-09-17 09:46:00	89.0615	-125.4820	PS144_98-1	huge MYI floe, ice thickness >2m

APPENDIX

A.1 TEILNEHMENDE INSTITUTE / PARTICIPATING INSTITUTES

A.2 FAHRTTEILNEHMER:INNEN / CRUISE PARTICIPANTS

A.3 SCHIFFSBESATZUNG / SHIP‘S CREW

A.4 STATIONSLISTE/STATION LIST PS144

A.5 ICE STATION MAPS

A.1 TEILNEHMENDE INSTITUTE / PARTICIPATING INSTITUTES

Affiliation	Address
On board	
AT.UIBK.AC	University of Innsbruck Innrain 52 6020 Innsbruck Austria
AT.Uni-Wien	University of Vienna Department of Palaeontology Josef-Holaubek-Platz 2 (UZA II) 1090 Vienna Austria
CH.ETH	Eidgenössische Technische Hochschule Zürich Universitätstrasse 16 CHN E31.1 8092 Zürich Switzerland
CN.OUC	Ocean University of China 238 Songling Road Qingdao Shandong 266100 China
DE. CAU	Kiel University Christian-Albrechts-Univertität zu Kiel Fakultät Mathematik und Naturwissenschaft Leibniz-Labor für Altersbestimmung und Isotopenforschung Max-Eyth-Straße 11-13 24118 Kiel
DE.AWI	Alfred-Wegener-Institut Helmholtz-Zentrum für Polar- und Meeresforschung Postfach 120161 27515 Bremerhaven Germany

Affiliation	Address
On board	
DE.DRF	DRF Luftrettung gAG Laval Avenue E312 77836 Rheinmünster Germany
DE.DRIFT-NOISE	Drift Noise GmbH Polar Services Stavendamm 17 28195 Bremen
DE.DWD	Deutscher Wetterdienst Seewetteramt Bernhard Nocht Str. 76 20359 Hamburg Germany
DE.GEOMAR	GEOMAR Helmholtz-Zentrum für Ozeanforschung Wischhofstraße 1-3 24148 Kiel Germany
DE.NHC	Northern HeliCopter GmbH Gorch-Fock-Str., 103 26721 Emden Germany
DE.TUBS	Technische Universität Braunschweig Langer Kamp 19C 38106 Braunschweig
DE.UHH	Universität Hamburg Fakultät für Mathematik, Informatik und Naturwissenschaften Fachbereich Biologie Institut für marine Ökosystem- und Fische-reiwissenschaften Große Elbstraße 133 22767 Hamburg
DE.UHB.UIP	Institut für Umweltphysik Universität Bremen Otto-Hahn Allee 1 D-28359 Bremen Germany

Affiliation	Address
On board	
DE.UNI-BREMEN	Universität Bremen Leobener Straße, NW2a 28359 Bremen Germany
DE.UNI-KOELN	University of Cologne Institute of Geophysics and Meteorology Pohligstr. 3 50969 Köln Germany
DE.UOL	Carl von Ossietzky Universität Oldenburg Carl-von-Ossietzky-Str. 9-11 26129 Oldenburg Germany
EDU.DARTMOUTH	Thayer School of Engineering Dartmouth College Hanover, NH 03755 USA
FR.MIO	Aix Marseille Université Institute Méditerranéen d'Océanologie 163 Avenue de Luminy 13288 Marseille France
KR.KOPRI	Korea Polar Research Institute 26, Sondomirae-ro Yeonsu-gu Incheon 21990 Republic of Korea
NL.vDMet	Van Dorssen Metaalbewerking Scheepsreparaties Stoomport 7i 1792 CT Oudeschild (Texel) The Netherlands
NL.WMR	Stichting Wageningen Marine Research Haringkade 1 1976 CP IJmuiden The Netherlands
SI.NTU	Nanyang Technological University, Asian School of the Environment, Singapore, Singapore.

Affiliation	Address
On board	
SW.UGOT	University of Gothenburg Department of Earth Sciences Box 460 405 30 Göteborg Sweden
TW.NAMR	National Academy of Marine Research 11F. No. 25, Chenggong 2nd Rd. Qianzhen Dist. Kaohsiung 806614 Taiwan
UK.ED	The University of Edinburgh School of Geosciences, College of Science and Engineering EH9 3JW United Kingdom
UK.UNI-SOUTHAMPTON-SOES	University of Southampton School of Ocean and Earth Science Water Front Campus, National Oceanography Centre SO14 3ZH Southampton United Kingdom
US.ATM	Texas A&M University Department of Marine and Coastal Environmental Science Texas A&M University at Galveston, Department of Oceanography Galveston, TX 77553 USA

Affiliation	Address
Not on board	
BE.EV-ILVO	Eigen Vermogen van het Instituut voor Landbouw-. Visserij- en Voedingsonderzoek, van Gansberghelaan 92, 9820 Merelbeke, Belgium
DE.BSH	Bundesamt für Seeschifffahrt und Hydrographie Bundesbehörde im Geschäftsbereich des Bundesministeriums für Digitales und Verkehr Bernhard-Nocht-Str. 78 20359 Hamburg Germany
DE.EUMETNET	EUMETNET SNC L'Institut Royal Météorologique Avenue Circulaire 3 1180 Bruxelles, Belgique
DE.FMI	Finnish Meteorological Institute Erik Palménin aukio 1 00101 Helsinki Finland
DE.PRIC	Key Laboratory for Polar Science of the MNR Polar Research Institute of China Pudong New District Shanghai China
DE.TI	Johann Heinrich von Thünen-Institut, Bundesforschungsinstitut für ländliche Räume, Wald und Fischerei Bundesallee 50, 38116 Braunschweig Germany
EDU.UNI-Washington	University of Washington Applied Physics Laboratory 1013 NE 40th Street Seattle, WA 98105-6698

Affiliation	Address
Not on board	
EDU.WHOI	Woods Hole Oceanographic institution 266 Woods Hole Road MS #2 Woods Hole MA 02543 United States
FR.LOCEAN	Laboratoire d'Océanographie et du Climat: Expérimentations et approches numériques. Unité Mixte de Recherche 7159 CNRS / IRD / Université Pierre et Marie Curie/MNHN. Institut Pierre Simon Laplace. Boîte 100 - 4, place Jussieu 75252 PARIS Cedex 05. France
FR.UBO	Université de Bretagne Occidentale Institut Universitaire Européen de la Mer 3 rue des Archives 29238 Brest cedex 3 France
GOV.FLORIDA	University of South Florida College of Marine Science 140 7th Avenue South St.Petersburg, FL 33701 USA
SI.NTU	Nanyang Technological University Asian School of the Environment 50 Nanyang Avenue, Singapore 639798
SI.NUS	National University of Singapore Department of Geography 1 Arts Link, Kent Ridge, Singapore 117568
SW.SU	Stockholms Universitet Universitetsvagen 10 10691 Stockholm Sweden

Affiliation	Address
Not on board	
TW.SUNYAT-SEN	National Sun Yat-sen University Department of Oceanography No. 70 Lienhai Rd. Gushan Dist. Kaohsiung 804201 Taiwan
UK.UEA	University of East Anglia School of Environmental Sciences Norwich Research Park Norwich, Norfolk NR4 7TJ United Kingdom

A.2 FAHRTTEILNEHMER:INNEN / CRUISE PARTICIPANTS

Name/ Last name	Vorname/ First name	Institut/ Institute	Beruf/ Profession	Fachrichtung/ Discipline
Allerholt	Jacob	DE.AWI	Technician	Oceanography
Amon	Rainer	US.TA&M	Scientist	Oceanography
Bahlmann	Jonathan	DE.DRIFT-NOISE	Scientist	Geophysics
Bettinelli	Alexandra	DE.AWI	PhD student	Biology
Brauer	Jens	DE.NHC	Pilot	Helicopter Service
Buehler	Linnea	DE.UNI-KOELN	PhD student	Meteorology
Faizieva	Kamila	A.UW	PhD student	other geo sciences
Flores	Hauke	DE.AWI	Scientist	Biology
Fu	Ke-Hsien	TW.NARM	Scientist	Oceanography
Gäng	Frederik	DE.UOL	PhD student	other geo sciences
Geibert	Walter	DE.AWI	Scientist	other geo sciences
Gischler	Michael	DE.NHC	Pilot	Helicopter Service
Gorniak	Rebecca	DE.AWI	Student (Master)	Biology
Heuzé	Céline	SW.UGOT	Scientist	Oceanography
Hoppmann	Mario	DE.AWI	Scientist	Oceanography
Huhn	Olliver	DE.UNI-BREMEN	Scientist	Oceanography
Hümmling	Jannis	DE.AWI	PhD student	Biology
Kaphegyi	Insa	DE.UHH	Student (Bachelor)	Biology
Kaphegyi	Kari	A.UI	Student (Master)	Biology
Kolar	Jonathan	DE.UNI-BREMEN	Student (Master)	Physics
Kordes	Thomas	DE.AWI	Engineer	Engineering Sciences
Koschnick	Nils	DE.AWI	Engineer	Biology
Krisch	Stephan	DE.GEOMAR, DE.TUBS	Scientist	Oceanography
Lee	Youngju	KOR.KOPRI	Scientist	Biology
Lucassen	Magnus	DE.AWI	Scientist	Biology
McOscar	Dwayne	DE.NHC	Technician	Helicopter Service
Mech	Mario	DE.UNI-KOELN	Scientist	Meteorology
Murawski	Sandra	DE.AWI	Technician	Biology
Neckel	Niklas	DE.AWI	Scientist	Glaciology
Neumann	Zoe	DE.CAU	Student (Bachelor)	Geology

Name/ Last name	Vorname/ First name	Institut/ Institute	Beruf/ Profession	Fachrichtung/ Discipline
Palmer	Freya	UK.UEDINGBURGH	Scientist	Oceanography
Pin	Aude	DE.GEOMAR	Student (Master)	Oceanography
Rabe	Benjamin	DE.AWI	Scientist	Oceanography
Risse	Nils	DE.UNI-KOELN	PhD student	Meteorology
Rode	Joerg	DE.NHC	Engineer	Engineering Sciences
Rodrigues	Andreia	FR.MIOM	Scientist	Biology
Rohleder	Christian	DE.DWD	Technician	Logistics
Ruan	Yaqing	DE.GEOMAR	PhD student	Oceanography
Rueckert	Janna	DE.UIP	Scientist	Physics
Sakinan	Serdar	NL.WMR	Scientist	Biology
Scheiwiller	Marcel	CH.ETH	PhD student	Oceanography
Stimac	Ingrid	DE.AWI	Technician	Chemistry
Suresh	Simran	DE.AWI	PhD student	Oceanography
Suter	Patrick	DE.DWD	Scientist	Meteorology
Tippenhauer	Sandra	DE.AWI	Scientist	Oceanography
Torres Valdes	Sinhue	DE.AWI	Scientist	Oceanography
Trace-Kleeberg	Sunke	UK.USOTON	PhD student	Oceanography
van Dorssen	Michiel	NL.vDMet	Technician	Biology
Vane	Kim	DE.AWI	Scientist	Biology
Voelkner	Christian	DE.AWI	Engineer	Biology
Vortkamp	Martina	DE.AWI	Technician	Biology
Wong	Carmen	SW.UGOT	PhD student	other geo sciences
Zhu	Jialiang	CN.OUC	PhD student	Oceanography
Zimmermann	Jan	DE.UHH	Student (Bachelor)	Biology

A.3 SCHIFFSBESATZUNG / SHIP‘S CREW

No	Name / Last Name	Vorname / First name	Position / Rank
1	Schwarze	Stefan	Master
2	Grundmann	Uwe	C/M
3	Ziemann	Olaf	C/E
4	Eckenfels	Hannes	2/M Cargo
5	Weiß	Daniel	2/M
6	Peine	Lutz	2/M
7	Dr. Guba	Klaus	Doc
8	Frank	Gerhard	E/E Com.
9	Rusch	Torben	2/E
10	Krinfeld	Oleksandr	2/E
11	Jassmann	Marvin	2/E
12	Pommerencke	Bernd	E/E SET
13	Frank	Gerhard	E/E Brücke
14	Zivanov	Stefan	E/E Labor
15	Winter	Andreas	E/E Sys
15	Krüger	Lars	E/E Winde
17	Meier	Jan	Bosun
18	Keller	Jürgen	Carpenter
19	Loew	Caspar	MPR
20	Stubenrauch	Paula	MPR
21	Töben	Carlotta	MPR
22	Buchholz	Karl Erik	MPR
23	Probst	Lorenz	MPR
24	Buchholz	Joscha	MPR
25	Möller	Falko	MPR
26	Schade	Tom	MPR
27	Decker	Jens	MPR
28	Mahlmann	Oliver	MPR

No	Name / Last Name	Vorname / First name	Position / Rank
29	Bäcker	Andreas	MPR
30	Siegel	Kilian	MPR
31	Niebuhr	Tim	MPR
32	Plehn	Marco	Fitter/E
33	Schneider	Denise	Trainee
34	Skrzipale	Mitja	Cook
35	Fehrenbach	Martina	2./Cook
36	Loibl	Patrick	2./Cook
37	Witusch	Petra	C/Stew.
38	Ilk	Romy	Stew./Nurse
39	Stocker	Eileen	2./Stew.
40	Golla	Gerald	2./Stew.
41	Holl	Claudia	2./Stew.
42	Shi	Wubo	2./Stew.
43	Chen	Jirong	2./Stew.
44	Chen	Quanlun	2./Stew.

A.4 STATIONSLISTE / STATION LIST PS144

Station list of expedition PS144 from Tromsø – Bremerhaven;
the list details the action log for all stations along the cruise track.

See https://www.pangaea.de/expeditions/events/PS144 to display the station (event) list for expedition PS144.
This version contains Uniform Resource Identifiers for all sensors listed under https://sensor.awi.de. See https://www.awi.de/en/about-us/service/computing-centre/data-flow-framework.html for further information about AWI's data flow framework from sensor observations to

Event label	Optional label	Date/Time	Latitude [Deg]	Longitude [Deg]	Depth [m]	Gear	Action	Comment
PS144-track		2024-08-09T00:00:00	69.67800	18.98980		CT	Station start	Tromsø - Bremerhaven
PS144-track		2024-10-13T00:00:00	53.56750	8.55480		CT	Station end	Tromsø - Bremerhaven
PS144_0_Underway-1		2024-08-09T11:00:40	69.74732	19.14243	12	SWEAS	Station start	
PS144_0_Underway-1		2024-10-13T09:01:45	53.55755	8.55965	2.9	SWEAS	Station end	
PS144_0_Underway-2		2024-08-09T14:20:05	70.21617	20.37113		MAG	Station start	
PS144_0_Underway-2		2024-10-12T15:02:39	55.94647	6.12314	36.3	MAG	Station end	
PS144_0_Underway-3		2024-08-09T14:21:39	70.22266	20.37610	448.5	GRAV	Station start	
PS144_0_Underway-3		2024-10-12T15:02:07	55.94757	6.12224	36.4	GRAV	Station end	
PS144_0_Underway-4		2024-08-09T14:59:01	70.37018	20.36172	72.5	ADCP	Station start	
PS144_0_Underway-4		2024-10-12T14:59:06	55.95396	6.11868	36	ADCP	Station end	
PS144_0_Underway-5	Thermosalinograph Keel 1	2024-08-09T15:10:33	70.41141	20.30693	143.6	TSG	Station start	
PS144_0_Underway-5	Thermosalinograph Keel 1	2024-10-12T15:06:13	55.93912	6.12866	36.2	TSG	Station end	
PS144_0_Underway-6	Thermosalinograph Keel 2	2024-08-09T15:11:29	70.41475	20.30245	149.2	TSG	Station start	
PS144_0_Underway-6	Thermosalinograph Keel 2	2024-10-12T15:06:23	55.93877	6.12892	36.1	TSG	Station end	
PS144_0_Underway-7		2024-08-09T15:12:35	70.41869	20.29737	131.3	FBOX	Station start	
PS144_0_Underway-7		2024-10-12T15:05:01	55.94163	6.12683	36.5	FBOX	Station end	

** Comments are limited to 130 characters. See https://www.pangaea.de/expeditions/events/PS144 to show full comments in conjunction with the station (event) list for expedition PS144*

Event label	Optional label	Date/Time	Latitude [Deg]	Longitude [Deg]	Depth [m]	Gear	Action	Comment
PS144_0_Underway-8		2024-08-12T18:00:00	79.89468	9.52125	465.6	CAME	Station start	
PS144_0_Underway-8		2024-10-07T08:10:00	75.01656	16.57111	191.1	CAME	Station end	
PS144_0_Underway-9		2024-08-10T12:00:00	74.10015	16.27072	413.4	RAMSES_ ACC-VIS	Station start	
PS144_0_Underway-9		2024-10-04T09:12:22	82.69469	30.70305	3695	RAMSES_ ACC-VIS	Station end	
PS144_0_Underway-10		2024-08-13T08:25:00	81.40576	22.28684	553.6	HVAIR	Station start	
PS144_0_Underway-10		2024-10-11T11:30:00	59.82597	4.00468	268.4	HVAIR	Station end	
PS144_0_Underway-12		2024-08-09T08:00:00	69.74732	19.14244	11.9	MiRAC-A	Station start	
PS144_0_Underway-12		2024-10-08T12:30:00	70.62633	12.64654	2622.5	MiRAC-A	Station end	
PS144_0_Underway-13		2024-08-09T08:00:00	69.74732	19.14244	11.9	GRaWAC	Station start	
PS144_0_Underway-13		2024-10-08T12:45:00	70.60045	12.61466	2641.8	GRaWAC	Station end	
PS144_0_Underway-14	PROfiler FOGHAT	2024-08-09T08:00:00	69.74732	19.14244	11.9	HATPRO	Station start	
PS144_0_Underway-14	PROfiler FOGHAT	2024-10-08T09:00:00	71.13171	13.28045	2217.4	HATPRO	Station end	
PS144_0_Underway-15		2024-08-09T08:00:00	69.74732	19.14244	11.9	IR_CAM	Station start	
PS144_0_Underway-15		2024-10-05T08:45:00	80.90493	30.37061	118.1	IR_CAM	Station end	
PS144_0_Underway-16		2024-08-09T08:00:00	69.74732	19.14244	11.9	MiRAC-P	Station start	
PS144_0_Underway-16		2024-10-08T12:08:45	70.66463	12.69369	2597.1	MiRAC-P	Station end	
PS144_0_Underway-17		2024-08-12T15:14:00	79.43359	8.69688	150.5	IMU	Station start	
PS144_0_Underway-17		2024-10-06T08:50:00	77.58985	28.08642	154.2	IMU	Station end	
PS144_0_Underway-18		2024-08-09T08:00:00	69.74732	19.14244	11.9	3D-UA	Station start	
PS144_0_Underway-18		2024-10-05T13:00:00	80.27083	29.97236	177.2	3D-UA	Station end	
PS144_0_Underway-19		2024-08-09T08:00:00	69.74732	19.14244	11.9	DISDRO	Station start	
PS144_0_Underway-19		2024-10-05T08:45:00	80.90493	30.37061	118.1	DISDRO	Station end	
PS144_0_Underway-20		2024-08-09T08:00:00	69.74732	19.14244	11.9	TSI	Station start	
PS144_0_Underway-20		2024-10-08T09:00:00	71.13171	13.28045	2217.4	TSI	Station end	
PS144_0_Underway-21		2024-08-09T08:00:00	69.74732	19.14244	11.9	IMU	Station start	
PS144_0_Underway-21		2024-10-04T06:25:00	82.70572	30.82700	3692.3	IMU	Station end	
PS144_0_Underway-22		2024-08-09T08:00:00	69.74732	19.14244	11.9	GOPRO	Station start	

Event label	Optional label	Date/Time	Latitude [Deg]	Longitude [Deg]	Depth [m]	Gear	Action	Comment
PS144_0_Underway-22		2024-10-05T10:55:00	80.58420	30.16572	372.8	GOPRO	Station end	
PS144_0_Underway-23		2024-08-09T08:00:00	69.74732	19.14244	11.9	GAIA	Station start	
PS144_0_Underway-23		2024-10-13T09:01:05	53.55755	8.55965	2.9	GAIA	Station end	
PS144_1-1		2024-08-13T12:39:25	81.37652	25.22545	464.5	FTRW-P	Station start	
PS144_1-1		2024-08-13T16:44:21	81.44240	24.64845	475	FTRW-P	Station end	
PS144_1-2		2024-08-13T16:09:17	81.43987	24.68524	477	XCTD	Station start	
PS144_1-2		2024-08-13T16:13:56	81.44022	24.67848	475	XCTD	Station end	
PS144_0_Underway-11		2024-08-13T16:45:00	81.44245	24.64781	475	ICERAD	Station start	
PS144_0_Underway-11		2024-10-04T12:55:00	82.44662	30.88218	3506.8	ICERAD	Station end	
PS144_0_Underway-27		2024-08-13T16:50:00	81.46400	24.65200		ICEOBS	max depth	
PS144_2-1		2024-08-13T20:19:22	81.97684	25.55911	3578.8	XCTD	Station start	
PS144_2-1		2024-08-13T20:28:16	81.98528	25.57616	3591.3	XCTD	Station end	
PS144_2-2	Arvor-I_24DE006	2024-08-13T20:31:11	81.98736	25.58048	3592.5	ARVORFL	Station start	
PS144_2-2	Arvor-I_24DE006	2024-08-13T20:38:44	81.99571	25.59039	3598.2	ARVORFL	Station end	
PS144_3-1	Piglet	2024-08-14T08:21:39	83.03926	29.80615	3853.9	CTD-RO	max depth	
PS144_3-2	LilliFe	2024-08-14T10:23:17	83.03964	29.89821	3854	CTD-TM	max depth	
PS144_3-3	Piglet	2024-08-14T12:07:13	83.04497	29.97973	3850.9	CTD-RO	max depth	
PS144_0_Underway-26		2024-08-15T04:20:00	84.20066	34.23996	3403.9	TAP	max depth	
PS144_0_Underway-25		2024-08-15T13:15:00	84.66704	37.67127	3945.8	AUTOFIM	Station start	
PS144_0_Underway-25		2024-10-12T15:01:32	55.94875	6.12119	35.9	AUTOFIM	Station end	
PS144_4-1		2024-08-15T19:33:38	84.91692	40.88325	3935.2	MUMMY	Station start	Buoy recovery on ice
PS144_4-1		2024-08-15T21:01:42	84.91923	40.86869	3935.2	MUMMY	Station end	Buoy recovery on ice
PS144_4_ BuoyRecovery_001	2023O16	2024-08-15T20:00:00	84.91692	40.88325		BUOY	max depth	recovery
PS144_4_ BuoyRecovery_002	2023T109	2024-08-15T20:00:00	84.91692	40.88325		BUOY	max depth	recovery
PS144_4_ BuoyRecovery_003	2023S124	2024-08-15T20:00:00	84.91692	40.88325		BUOY	max depth	recovery
PS144_5_ BuoyRecovery_003	2023S122	2024-08-16T00:00:00	85.01450	39.94960		BUOY	max depth	recovery

Event label	Optional label	Date/Time	Latitude [Deg]	Longitude [Deg]	Depth [m]	Gear	Action	Comment
PS144_5_ BuoyRecovery_001	2023O19	2024-08-16T00:00:00	85.01450	39.94960		BUOY	max depth	recovery
PS144_5_ BuoyRecovery_002	2023T105	2024-08-16T00:00:00	85.01450	39.94960		BUOY	max depth	recovery
PS144_5-1		2024-08-16T00:16:33	85.01357	39.95045	3934.9	MUMMY	Station start	Buoy recovery on ice
PS144_5-1		2024-08-16T01:12:56	85.01450	39.94960	3934.8	MUMMY	Station end	Buoy recovery on ice
PS144_6-1	Piglet	2024-08-16T07:16:30	85.03735	42.70188	3929	CTD-RO	max depth	
PS144_7_Brine		2024-08-16T11:21:00	85.05805	42.93493		SNOW	max depth	Brine
PS144_7-1		2024-08-16T11:21:02	85.06361	42.97749	3927.5	ICE	Station start	bad view
PS144_7-1		2024-08-16T20:50:27	85.05422	42.69272	3929.2	ICE	Station end	bad view
PS144_007_MAVIC1	Mavic3	2024-08-16T11:40:37	85.05800	42.93500		UAV	max depth	Pre-station flight (1st grid flight test)
PS144_07_UICE_ Pump		2024-08-16T13:12:17	85.06361	42.97749		UICE_ Pump	max depth	Under-ice water and surface backscatter maximum
PS144_07_SI_ corer_9cm		2024-08-16T13:12:22	85.06361	42.97749		MARKII	max depth	Bio coring event
PS144_007_ps144_ snow_sip		2024-08-16T13:40:00	85.06361	42.97749		MULT	max depth	no snow. 1 CT sample (bare ice/SSL). 42 SnowImager photos. 1 surface roughness site
PS144_7_Magna-Katrin		2024-08-16T13:45:00	85.05805	42.93493		MAGNA	max depth	Snow thickness measurements
PS144_7_SnowCup		2024-08-16T13:45:00	85.05805	42.93493		SNOW	max depth	Snow Samples and Melt Pond Water
PS144_7-2	LilliFe	2024-08-16T14:00:49	85.06296	42.98625	3927.4	CTD-TM	max depth	
PS144_007_M350	DJI Matrice 350 RTK	2024-08-16T14:10:00	85.06361	42.97749		UAV	max depth	Testflight: Nadir and Overview Images
PS144_007_GPS5	GPS_Station5	2024-08-16T14:16:50	85.06361	42.97749		GPS	max depth	DGPS measurement at ice station
PS144_7_RDI300	ADCP_ WH300_9271	2024-08-16T14:20:00	85.06030	42.98970		ADCP	max depth	deployment. MSS site
PS144_007_GPS6	GPS_Station6	2024-08-16T14:25:45	85.06361	42.97749		GPS	max depth	DGPS measurement at ice station

Event label	Optional label	Date/Time	Latitude [Deg]	Longitude [Deg]	Depth [m]	Gear	Action	Comment
PS144_007_GPS1	GPS_Station1	2024-08-16T14:33:15	85.06361	42.97749		GPS	max depth	DGPS measurement at ice station
PS144_7_MSS_1	MSS_90D_075	2024-08-16T14:57:00	85.06030	42.98970		MSS	max depth	series of 9 profiles; casts 1-5 with cage
PS144_007_GPS2	GPS_Station2	2024-08-16T15:17:44	85.06361	42.97749		GPS	max depth	DGPS measurement at ice station
PS144_7_miniMooring	PS144_mini_ mooring	2024-08-16T15:34:00	84.42310	115.60810		MOOR	max depth	MSS site
PS144_7_Nortek1000	Nortek_ S1000_52160	2024-08-16T15:34:00	85.06030	42.98970		ADCP	max depth	MSS site
PS144_007_GEM	gem2-512	2024-08-16T15:57:43	85.05800	42.93500		GEM-2	max depth	Ice station survey
PS144_7-3		2024-08-16T16:47:52	85.05936	42.94150	3927.7	MSN	Station start	
PS144_7-3		2024-08-16T18:53:33	85.05575	42.83191	3928.6	MSN	Station end	
PS144_007_ps144_ physics_coring		2024-08-16T17:00:00	85.06361	42.97749		CORE	max depth	1 core
PS144_007_SPLISH		2024-08-16T17:00:00	85.06361	42.97749		RULER	max depth	Depth profiles of two melt ponds
PS144_007_MAVIC2	Mavic3	2024-08-16T18:16:29	85.05800	42.93500		UAV	max depth	Ice station flight (manual)
PS144_7-4	Piglet	2024-08-16T20:51:00	85.05422	42.69205	3929.3	CTD-RO	max depth	
PS144_7-5		2024-08-16T22:52:44	85.05387	42.55472	3929.9	MSN	Station start	
PS144_7-5		2024-08-17T01:30:29	85.05304	42.42406	3931.1	MSN	Station end	
PS144_7-6		2024-08-17T01:27:50	85.05310	42.42595	3930.3	MIK-N	Station start	
PS144_7-6		2024-08-17T02:38:35	85.05099	42.37434	3930.1	MIK-N	Station end	
PS144_7-7	Piglet	2024-08-17T03:08:13	85.04990	42.34985	3930.2	CTD-RO	max depth	
PS144_8_ BuoyRecovery_004	2023S127	2024-08-17T05:00:00	85.03454	42.34097		BUOY	max depth	recovery
PS144_8_ BuoyRecovery_007	SnowTATOS1 buoy	2024-08-17T05:00:00	85.03454	42.34097		BUOY	max depth	
PS144_8_ BuoyRecovery_003	2023W6	2024-08-17T05:00:00	85.03454	42.34097		BUOY	max depth	recovery
PS144_8_ BuoyRecovery_005	2023T106	2024-08-17T05:00:00	85.03454	42.34097		BUOY	max depth	recovery

Event label	Optional label	Date/Time	Latitude [Deg]	Longitude [Deg]	Depth [m]	Gear	Action	Comment
PS144_8_ BuoyRecovery_006	2023R25	2024-08-17T05:00:00	85.03454	42.34097		BUOY	max depth	recovery
PS144_8_ BuoyRecovery_001	2023O20	2024-08-17T05:00:00	85.03454	42.34097		BUOY	max depth	recovery
PS144_8_ BuoyRecovery_008	2023K1	2024-08-17T05:00:00	85.03454	42.34097		BUOY	max depth	recovery
PS144_8_ BuoyRecovery_002	2023I11	2024-08-17T05:00:00	85.03454	42.34097		BUOY	max depth	recovery
PS144_8-1		2024-08-17T05:00:03	85.03454	42.34097	3930.1	MUMMY	Station start	Buoy recovery on ice
PS144_8-1		2024-08-17T07:20:14	85.03156	42.20226	3930.9	MUMMY	Station end	Buoy recovery on ice
PS144_9-1	LilliFe	2024-08-18T07:00:19	85.25644	59.73417	3841.1	CTD-TM	max depth	
PS144_010_GPS1	GPS_Station1	2024-08-19T12:36:20	85.25492	83.61135		GPS	max depth	DGPS measurement on vessel
PS144_10_ CleanCoring_1		2024-08-19T13:07:00	85.25555	83.60737		MARKII	max depth	dirty ice sampling
PS144_10-1		2024-08-19T13:07:12	85.25555	83.60737	3715.2	MUMMY	Station start	
PS144_10-1		2024-08-19T14:15:40	85.24535	83.62747	3749.9	MUMMY	Station end	
PS144_010_MAVIC	Mavic3	2024-08-19T13:14:41	85.25700	83.60000		UAV	max depth	Short manual flight on short notice
PS144_11-1	LilliFe	2024-08-20T02:57:12	85.11812	95.48716	4579.4	CTD-TM	max depth	
PS144_11-2	Piglet	2024-08-20T06:43:08	85.11730	95.37861	4582.4	CTD-RO	max depth	
PS144_11-3		2024-08-20T11:55:07	85.16768	95.51687	4427.4	RMT	Station start	
PS144_11-3		2024-08-20T14:22:01	85.12690	94.90527	4543.6	RMT	Station end	
PS144_12-1	2024P299	2024-08-20T14:38:46	85.12644	94.88411	3512.5	ISVP	Station start	
PS144_12-1	2024P299	2024-08-20T14:51:22	85.12611	94.86537	2511.6	ISVP	Station end	
PS144_12-2		2024-08-20T14:46:28	85.12623	94.87204	3436.6	MUMMY	Station start	drone flight
PS144_12-2		2024-08-20T15:00:06	85.12586	94.85450	4527	MUMMY	Station end	drone flight
PS144_13-1		2024-08-20T17:54:12	85.06689	97.13148	3955.5	XCTD	Station start	1st attempt failed; station aborted
PS144_13-1		2024-08-20T18:03:31	85.06668	97.11902	4474.7	XCTD	Station end	1st attempt failed; station aborted
PS144_13-2		2024-08-20T19:28:26	85.02055	98.30448	4331.5	XCTD	Station start	

Event label	Optional label	Date/Time	Latitude [Deg]	Longitude [Deg]	Depth [m]	Gear	Action	Comment
PS144_13-2		2024-08-20T19:40:36	85.02176	98.32344		XCTD	Station end	
PS144_13-3		2024-08-20T21:02:33	84.95169	99.75142	4173.8	XCTD	Station start	
PS144_13-3		2024-08-20T21:15:59	84.94969	99.81656	4186	XCTD	Station end	
PS144_13-4		2024-08-20T22:42:14	84.92225	101.09958	4028.7	XCTD	Station start	
PS144_13-4		2024-08-20T22:53:40	84.92231	101.07951	4028.7	XCTD	Station end	
PS144_13-5		2024-08-21T00:27:49	84.85901	102.33639	4063.9	XCTD	Station start	
PS144_13-5		2024-08-21T00:41:48	84.85721	102.34340	4062.7	XCTD	Station end	
PS144_13-6		2024-08-21T02:13:08	84.81314	103.54303	4015.7	XCTD	Station start	
PS144_13-6		2024-08-21T02:29:19	84.81083	103.52906	4018.5	XCTD	Station end	
PS144_14-1	2024P300	2024-08-21T03:07:14	84.77749	103.87920	3958.8	ISVP	Station start	
PS144_14-1	2024P300	2024-08-21T03:47:28	84.77493	103.83621	4007.2	ISVP	Station end	
PS144_13-7		2024-08-21T05:31:13	84.70260	104.77522	3611.4	XCTD	Station start	
PS144_13-7		2024-08-21T05:46:56	84.70377	104.76616	3871.1	XCTD	Station end	
PS144_13-8		2024-08-21T07:39:00	84.62913	105.82395	3960.5	XCTD	Station start	
PS144_13-8		2024-08-21T07:50:38	84.63004	105.83478	3962.3	XCTD	Station end	
PS144_13-9		2024-08-21T09:45:34	84.57606	107.22341	3996.9	XCTD	Station start	1st try faild; 2nd attempt to the water
PS144_13-9		2024-08-21T10:03:55	84.57600	107.24632	3997.1	XCTD	Station end	1st try faild; 2nd attempt to the water
PS144_13-10		2024-08-21T11:21:14	84.55043	108.45430	4001.7	XCTD	Station start	
PS144_13-10		2024-08-21T11:32:48	84.55021	108.47770	3785.6	XCTD	Station end	
PS144_15-1		2024-08-21T14:56:30	84.42613	109.68730	3935.4	FTRW-P	Station start	
PS144_15-1		2024-08-21T17:00:34	84.36016	109.68192	4025.3	FTRW-P	Station end	
PS144_16-1	Arvor-I_24DE007	2024-08-21T17:22:36	84.39097	109.57478	4025.2	ARVORFL	Station start	
PS144_16-1	Arvor-I_24DE007	2024-08-21T17:26:17	84.39136	109.56813	4023.8	ARVORFL	Station end	
PS144_0_Underway-24		2024-08-23T11:45:00	85.07881	71.91304	3815.3	MBES	Station start	
PS144_0_Underway-24		2024-09-26T23:05:00	87.03438	55.65299	4226.4	MBES	Station end	
PS144_Heli_BuoyRecovery_001	2023O22	2024-08-25T09:00:00				BUOY	max depth	recovery

Event label	Optional label	Date/Time	Latitude [Deg]	Longitude [Deg]	Depth [m]	Gear	Action	Comment
PS144_Heli_ BuoyRecovery_003	2023T103	2024-08-25T09:00:00				BUOY	max depth	recovery
PS144_Heli_ BuoyRecovery_002	2023S125	2024-08-25T09:00:00				BUOY	max depth	recovery
PS144_Heli_EM-Bird_001		2024-08-25T11:09:26	85.25689	55.39796		EMB	max depth	Good triangle survey. fog came in at the western side of the survey
PS144_RASSS-1		2024-08-25T23:20:00	85.21600	67.60500		SNOW	max depth	Snow Sample
PS144_17-1		2024-08-28T04:28:37	84.21988	109.69522	4076.7	XCTD	Station start	
PS144_17-1		2024-08-28T04:59:41	84.22449	109.68337	4053.2	XCTD	Station end	
PS144_18-1	Piglet	2024-08-28T07:05:04	84.27083	110.68969	3984.6	CTD-RO	max depth	
PS144_18-2	LilliFe	2024-08-28T09:21:34	84.28521	111.01072	4048.8	CTD-TM	max depth	
PS144_18-3	Piglet	2024-08-28T12:57:01	84.27255	111.44257	4044	CTD-RO	max depth	
PS144_18-4		2024-08-28T14:46:42	84.26717	111.46982	4044.5	MSN	Station start	
PS144_18-4		2024-08-28T16:54:44	84.27678	111.44939	4043.2	MSN	Station end	
PS144_19-1		2024-08-28T19:32:27	84.37503	112.25372	3215.3	XCTD	Station start	
PS144_19-1		2024-08-28T19:41:24	84.37767	112.27677	3277	XCTD	Station end	
PS144_20-1	LilliFe	2024-08-28T21:51:07	84.46318	113.74960	2518.4	CTD-TM	max depth	
PS144_20-2	Piglet	2024-08-28T23:47:20	84.45445	113.93032	2677.3	CTD-RO	max depth	
PS144_21-1		2024-08-29T02:46:13	84.51462	114.83852	4021.3	XCTD	Station start	
PS144_21-1		2024-08-29T03:08:41	84.51511	114.81520	4011.1	XCTD	Station end	
PS144_22-1		2024-08-29T05:15:00	84.42933	115.68631	3775.3	FTRW-P	Station start	
PS144_22-1		2024-08-29T09:38:00	84.38668	116.73000	4053.8	FTRW-P	Station end	
PS144_23_Brine		2024-08-29T12:32:00	84.50036	115.72034		SNOW	max depth	Brine
PS144_23-1		2024-08-29T12:32:42	84.51170	115.39221	4141.7	ICE	max depth	
PS144_023_M350	DJI Matrice 350 RTK	2024-08-29T13:20:00	84.51170	115.39221		UAV	max depth	Automatic Survey Processed in Terra:20240829-RGB Survey 2. Eisstation
PS144_23_ CleanCoring_1		2024-08-29T14:00:00	84.51170	115.39221		MARKII	max depth	10 Cores; IceStation #2

Event label	Optional label	Date/Time	Latitude [Deg]	Longitude [Deg]	Depth [m]	Gear	Action	Comment
PS144_23_UICE_ Pump		2024-08-29T14:19:03	84.51170	115.39221		UICE_ Pump	max depth	Under-ice water and surface backscatter maximum
PS144_23_SI_ corer_9cm		2024-08-29T14:19:34	84.51170	115.39221		MARKII	max depth	Bio coring event
PS144_023_GPS1	GPS_Station1	2024-08-29T14:28:45	84.51170	115.39221		GPS	max depth	DGPS measurement at ice station
PS144_23-2	Piglet	2024-08-29T14:46:38	84.48922	115.33426	4111.8	CTD-RO	max depth	
PS144_23_Lline_1		2024-08-29T15:00:00	84.51170	115.39221		LLDEP	max depth	Longline deployment for project SciCAO
PS144_023_GPS4	GPS_Station4	2024-08-29T15:00:12	84.51170	115.39221		GPS	max depth	DGPS measurement at ice station
PS144_023_GPS3	GPS_Station3	2024-08-29T15:19:44	84.51170	115.39221		GPS	max depth	DGPS measurement at ice station
PS144_23_RDI300	ADCP_ WH300_9271	2024-08-29T15:21:00	84.42310	115.60810		ADCP	max depth	deployment. MSS site
PS144_023_GPS6	GPS_Station6	2024-08-29T15:33:44	84.51170	115.39221		GPS	max depth	DGPS measurement at ice station
PS144_023_GPS2	GPS_Station2	2024-08-29T15:45:13	84.51170	115.39221		GPS	max depth	DGPS measurement at ice station
PS144_23_ CleanCoring_2		2024-08-29T16:03:00	84.51170	115.39221		PUMP	max depth	Under ice water; IceStation #2
PS144_023_GPS5	GPS_Station5	2024-08-29T16:13:15	84.51170	115.39221		GPS	max depth	DGPS measurement at ice station
PS144_23_MSS_1	MSS_90D_075	2024-08-29T16:19:00	84.48950	115.25780		MSS	max depth	series of 16 profiles; protective cage unmounted
PS144_23_ FISHTRAP_PS		2024-08-29T17:00:13	84.51170	115.39221		TRAPF	max depth	Under-ice trap deployment for project SciCAO
PS144_23_Nortek1000	Nortek_ S1000_52160	2024-08-29T17:10:00	84.42310	115.60810		ADCP	max depth	floe edge
PS144_023_ps144_ snow_sip		2024-08-29T17:20:00	84.51170	115.39221		MULT	max depth	no snow. 2 CT samples (bare ice/(saline) SSL). 48 SnowImager photos. 2 surface roughness sites

Event label	Optional label	Date/Time	Latitude [Deg]	Longitude [Deg]	Depth [m]	Gear	Action	Comment
PS144_23_SnowCup		2024-08-29T17:47:00	84.50036	115.72034		SNOW	max depth	Snow Samples
PS144_23_Magna-Katrin		2024-08-29T17:47:00	84.50036	115.72034		MAGNA	max depth	Snow thickness measurements
PS144_23_RDI600	ADCP_19316	2024-08-29T18:17:00	84.42310	115.60810		ADCP	max depth	deployment. floe edge
PS144_23_miniMooring	PS144_mini_mooring	2024-08-29T18:17:00	84.42310	115.60810		MOOR	max depth	floe edge
PS144_023_GEM	gem2-512	2024-08-29T18:58:50	84.50000	115.72000		GEM-2	max depth	Ice station survey. GEM towed by snowmobile
PS144_23-3	LilliFe	2024-08-29T19:35:10	84.50803	115.35968	4136.6	CTD-TM	max depth	
PS144_023_ps144_physics_coring		2024-08-29T19:45:00	84.51170	115.39221		CORE	max depth	1 core
PS144_023_MAVIC	Mavic3	2024-08-29T21:08:59	84.50000	115.72000		UAV	max depth	Ice station flight (manual)
PS144_23-4		2024-08-29T21:37:19	84.50276	115.65750	4211	MSN	Station start	
PS144_23-4		2024-08-30T00:07:44	84.46345	115.87634	4151.3	MSN	Station end	
PS144_23-5	Piglet	2024-08-30T02:05:38	84.42787	115.78723	3790.8	CTD-RO	max depth	
PS144_23_Buoy_002	2024T122	2024-08-30T03:10:00	84.41840	115.67120		BUOY	max depth	deployment. SAMS ice mass balance buoy
PS144_23_Buoy_001	2024W12	2024-08-30T03:10:00	84.41840	115.67120		BUOY	max depth	deployment. LOCEAN IAOOS
PS144_23-6		2024-08-30T04:02:31	84.40981	115.56856	3281	MSN	Station start	
PS144_23-6		2024-08-30T06:16:53	84.41469	115.42462	3825	MSN	Station end	
PS144_23-7		2024-08-30T06:20:39	84.41503	115.42432	3826.4	MIK-N	Station start	
PS144_23-7		2024-08-30T07:21:50	84.41963	115.45873	3823.8	MIK-N	Station end	
PS144_23-8	LilliFe	2024-08-30T08:39:28	84.42174	115.57519	3338.1	CTD-TM	max depth	
PS144_23_MSS_2	MSS_90D_075	2024-08-30T08:50:00	84.42310	115.60810		MSS	max depth	series of 2 profiles; protective cage unmounted
PS144_23_Buoy_003	2024S129	2024-08-30T08:50:00	84.42450	115.60470		BUOY	max depth	deployment. MetOcean Snow Buoy
PS144_23-9	Piglet	2024-08-30T10:46:46	84.40745	115.82157	3248.9	CTD-RO	max depth	
PS144_24-1		2024-08-30T15:00:20	84.55054	117.13092	3840.8	RMT	Station start	
PS144_24-1		2024-08-30T18:00:00	84.62580	116.78007	3460.9	RMT	Station end	
PS144_25-1		2024-08-30T18:51:47	84.61537	117.43770	3004.2	XCTD	Station start	

Event label	Optional label	Date/Time	Latitude [Deg]	Longitude [Deg]	Depth [m]	Gear	Action	Comment
PS144_25-1		2024-08-30T19:01:37	84.61619	117.45249	2994.2	XCTD	Station end	
PS144_26-1	Piglet	2024-08-30T22:43:43	84.65984	119.22773	4393	CTD-RO	max depth	
PS144_27-1		2024-08-31T02:14:42	84.71798	120.38270	4394.7	XCTD	Station start	
PS144_27-1		2024-08-31T02:23:00	84.71900	120.37770	4394.3	XCTD	Station end	
PS144_28-1	Piglet	2024-08-31T05:43:10	84.77104	121.90207	4388.9	CTD-RO	max depth	
PS144_28-2	LilliFe	2024-08-31T09:12:44	84.79472	122.01312	4385	CTD-TM	max depth	
PS144_28-3	Piglet	2024-08-31T11:49:41	84.78183	122.13211	4384.3	CTD-RO	max depth	
PS144_29-1		2024-08-31T13:06:11	84.75512	121.86148	4386.8	RMT	Station start	
PS144_29-1		2024-08-31T15:01:23	84.78338	121.97483	4384.8	RMT	Station end	
PS144_30-1		2024-08-31T16:59:58	84.81338	123.81874	4381.9	XCTD	Station start	
PS144_30-1		2024-08-31T17:12:20	84.81816	123.80591	4382.2	XCTD	Station end	
PS144_31-1	Piglet	2024-08-31T20:53:46	84.84785	125.73679	4373.3	CTD-RO	max depth	
PS144_32-1		2024-09-01T00:13:12	84.85344	127.48923	4362.4	XCTD	Station start	
PS144_32-1		2024-09-01T00:27:25	84.84973	127.52741	4362	XCTD	Station end	
PS144_33-1	2024P301	2024-09-01T02:07:14	84.90354	129.03494	4351.7	ISVP	Station start	
PS144_33-1	2024P301	2024-09-01T02:37:35	84.90052	129.06144	4351.9	ISVP	Station end	
PS144_34-1	CAO1-01	2024-09-01T03:30:00	84.90810	129.30304	4347.4	MOOR	Station start	recovery
PS144_34-1	CAO1-01	2024-09-01T19:11:56	84.90909	130.01889	4343.8	MOOR	Station end	recovery
PS144_RASSS-2		2024-09-01T20:18:00	84.91700	130.14000		SNOW	max depth	Snow Sample
PS144_35-1	Piglet	2024-09-01T20:53:52	84.92077	130.22428	4342.8	CTD-RO	max depth	
PS144_36-1		2024-09-01T22:54:52	84.92003	130.51559	4341.4	MSN	Station start	
PS144_36-1		2024-09-02T01:09:20	84.89671	130.63972	4340	MSN	Station end	
PS144_37-1	Piglet	2024-09-02T03:44:22	84.87002	129.65644	4347.1	CTD-RO	max depth	
PS144_38-1	CAO2-01	2024-09-02T06:31:54	84.88326	129.69263	4346	MOOR	Station start	recovery
PS144_38-1	CAO2-01	2024-09-02T10:30:28	84.87851	129.79169	4344.6	MOOR	Station end	recovery
PS144_39-1	LilliFe	2024-09-02T12:36:02	84.86369	128.95798	4351	CTD-TM	max depth	
PS144_40-1		2024-09-02T13:36:24	84.84865	128.91198	4350.7	MSN	Station start	
PS144_40-1		2024-09-02T15:36:19	84.82689	128.72174	4352.2	MSN	Station end	
PS144_41-1	Piglet	2024-09-02T17:18:02	84.82567	128.53484	4353.4	CTD-RO	max depth	

Event label	Optional label	Date/Time	Latitude [Deg]	Longitude [Deg]	Depth [m]	Gear	Action	Comment
PS144_42-1		2024-09-02T20:40:26	84.84029	128.60996	4353.2	ICE	Station start	
PS144_42-1		2024-09-03T01:02:00	84.80642	128.90875	4349.6	ICE	Station end	
PS144_42-2		2024-09-02T21:02:37	84.84059	128.64760	4352.6	FR	max depth	
PS144_042_GPS5	GPS_Station5	2024-09-02T21:09:20	84.84029	128.60996		GPS	max depth	DGPS measurement at ice station
PS144_42_SI_ corer_9cm		2024-09-02T21:17:03	84.84029	128.60996		MARKII	max depth	Bio coring event
PS144_42_UICE_ Pump		2024-09-02T21:17:10	84.84029	128.60996		UICE_ Pump	max depth	Under-ice water and surface backscatter maximum
PS144_42_ CleanCoring_1		2024-09-02T21:20:00	84.84029	128.60996		MARKII	max depth	11 Cores; IceStation #3
PS144_42_SI_ corer_9cm_Larm		2024-09-02T21:22:01	84.84029	128.60996		MARKII	max depth	Bio coring event
PS144_42_Larm		2024-09-02T21:22:44	84.84029	128.60996		LIOP	max depth	Hyperspectral under-ice light measurement
PS144_042_GPS1	GPS_Station1	2024-09-02T21:28:15	84.84029	128.60996		GPS	max depth	DGPS measurement at ice station
PS144_042_ps144_ snow_sip		2024-09-02T21:30:00	84.84029	128.60996		MULT	max depth	no snow. no CT sample. 5 SnowImager measurements (no transect. 2 sites). 1 surface roughness site
PS144_042_GPS2	GPS_Station2	2024-09-02T21:53:20	84.84029	128.60996		GPS	max depth	DGPS measurement at ice station
PS144_042_ps144_ physics_coring		2024-09-02T22:00:00	84.84029	128.60996		CORE	max depth	1 core
PS144_042_M350_ Cam	DJI Matrice 350 RTK	2024-09-02T22:10:00	84.84029	128.60996		UAV	max depth	Automatic Survey Processed in Terra:20240903-Eisstation-RGB
PS144_042_M350_ Lidar	DJI Matrice 350 RTK	2024-09-02T22:10:00	84.84029	128.60996		UAV	max depth	Lidartest Processed in Terra:20240903-Eisstation-Lidar
PS144_42_FRod1	PS144_42-2?	2024-09-02T22:30:26	84.84059	128.64760		FR	max depth	Line fishing for project SciCAO
PS144_042_GEM	gem2-512	2024-09-02T22:38:52	84.83100	128.87700		GEM-2	max depth	Ice station survey

Event label	Optional label	Date/Time	Latitude [Deg]	Longitude [Deg]	Depth [m]	Gear	Action	Comment
PS144_42_ CleanCoring_2		2024-09-02T22:44:00	84.84029	128.60996		PUMP	max depth	Under ice water; IceStation #3
PS144_042_MAVIC	Mavic3	2024-09-02T23:01:30	84.83100	128.87700		UAV	max depth	Ice station grid flight
PS144_43-1	CAO1-02	2024-09-03T06:36:14	84.89332	129.13136	4350.9	MOOR	Station start	deployment
PS144_43-1	CAO1-02	2024-09-03T10:14:29	84.90543	129.25841	4348.5	MOOR	Station end	deployment
PS144_44-1		2024-09-03T11:45:38	84.88371	128.39266	4356.5	RMT	Station start	
PS144_44-1		2024-09-03T13:40:17	84.88831	128.84165	4354.2	RMT	Station end	
PS144_45-1		2024-09-03T15:57:47	84.92849	130.57632	4341.4	XCTD	Station start	
PS144_45-1		2024-09-03T16:08:10	84.93615	130.63241	4340.8	XCTD	Station end	
PS144_ICE_RIDGE_ MAVIC	Mavic3	2024-09-03T18:48:14	85.00400	130.88500		UAV	max depth	Short stop at a large ice ridge. short manual flight from vessel
PS144_46-1	Piglet	2024-09-03T21:14:52	84.95529	132.42460	4321.3	CTD-RO	max depth	
PS144_50_Lline_1		2024-09-03T23:10:43	85.03270	139.44607		LLDEP	max depth	Longline deployment for project SciCAO
PS144_46-2	LilliFe	2024-09-03T23:20:15	84.94707	132.54261	4319.6	CTD-TM	max depth	
PS144_50_Fyke		2024-09-03T23:30:21	85.03270	139.44607		NET	max depth	Under-ice fyke deployment for project SciCAO
PS144_50_ FISHTRAP_PS		2024-09-03T23:30:22	85.03270	139.44607		TRAPF	max depth	Under-ice trap deployment for project SciCAO
PS144_46-3	Piglet	2024-09-04T02:51:05	84.91299	132.48722	4320.8	CTD-RO	max depth	
PS144_RASSS-3		2024-09-04T04:12:00	84.90400	132.40600		SNOW	max depth	Snow Sample
PS144_47-1		2024-09-04T06:50:13	84.96394	134.21714	4298.5	XCTD	Station start	
PS144_47-1		2024-09-04T06:58:27	84.96320	134.22665	4298.5	XCTD	Station end	
PS144_48-1	Piglet	2024-09-04T13:17:40	84.98395	135.95947	4254	CTD-RO	max depth	
PS144_49-1		2024-09-04T17:44:56	85.01911	137.63333	3945.6	XCTD	Station start	
PS144_49-1		2024-09-04T17:56:23	85.03265	137.64205	4115	XCTD	Station end	
PS144_50_Brine		2024-09-04T20:30:00	85.02579	139.94363		SNOW	max depth	Brine
PS144_50-1		2024-09-04T20:30:28	85.03270	139.44607	3933	ICE	Station start	
PS144_50-1		2024-09-05T19:01:01	85.04015	140.08536	3842	ICE	Station end	

Event label	Optional label	Date/Time	Latitude [Deg]	Longitude [Deg]	Depth [m]	Gear	Action	Comment
PS144_50_ CleanCoring_1		2024-09-04T21:33:00	85.03270	139.44607		MARKII	max depth	12 Cores; IceStation #4
PS144_050_GPS2	GPS_Station2	2024-09-04T22:32:44	85.03270	139.44607		GPS	max depth	DGPS measurement at ice station
PS144_050_GPS6	GPS_Station6	2024-09-04T22:46:20	85.03270	139.44607		GPS	max depth	DGPS measurement at ice station
PS144_050_GPS1	GPS_Station1	2024-09-04T22:54:51	85.03270	139.44607		GPS	max depth	DGPS measurement at ice station
PS144_050_GPS4	GPS_Station4	2024-09-04T23:12:13	85.03270	139.44607		GPS	max depth	DGPS measurement at ice station
PS144_050_GPS5	GPS_Station5	2024-09-04T23:23:45	85.03270	139.44607		GPS	max depth	DGPS measurement at ice station
PS144_050_GPS3	GPS_Station3	2024-09-04T23:38:44	85.03270	139.44607		GPS	max depth	DGPS measurement at ice station
PS144_50-2	Piglet	2024-09-05T00:07:03	85.02611	139.67749	3956.5	CTD-RO	max depth	
PS144_50_Magna-Katrin		2024-09-05T00:40:00	85.02579	139.94363		MAGNA	max depth	Snow thickness measurements
PS144_50_SnowCup		2024-09-05T00:40:00	85.02579	139.94363		SNOW	max depth	Snow Samples
PS144_50_Nortek1000	Nortek_ S1000_52160	2024-09-05T01:43:00	85.02500	140.13610		ADCP	max depth	floe edge
PS144_50_miniMooring	PS144_mini_ mooring	2024-09-05T01:43:00	85.02500	140.13610		MOOR	max depth	floe edge
PS144_50_ÂµMooring	PS144_micro_ mooring	2024-09-05T01:43:00	85.02500	140.13610		MOOR	max depth	floe edge
PS144_50-3	LilliFe	2024-09-05T03:12:57	85.01501	139.76587	3960.6	CTD-TM	max depth	
PS144_50-4		2024-09-05T04:55:45	85.01417	139.76564	3960.8	MSN	Station start	
PS144_50-4		2024-09-05T06:48:13	85.01877	139.79515	3959.3	MSN	Station end	
PS144_50_Buoy_003	2024A8	2024-09-05T06:00:00	85.01370	139.79350		BUOY	max depth	deployment. APL weather station
PS144_50_Buoy_001	2024W8	2024-09-05T06:00:00	85.01370	139.79350		BUOY	max depth	deployment. WHOI Ice-Tethered Profiler

Event label	Optional label	Date/Time	Latitude [Deg]	Longitude [Deg]	Depth [m]	Gear	Action	Comment
PS144_50_Buoy_006	2024S130	2024-09-05T06:30:00	84.01490	139.84140		BUOY	max depth	deployment. MetOcean Snow Buoy
PS144_50_UICE_ Pump		2024-09-05T06:36:16	85.03270	139.44607		UICE_ Pump	max depth	Under-ice water and surface backscatter maximum
PS144_50_SI_ corer_9cm		2024-09-05T06:36:16	85.03270	139.44607		MARKII	max depth	Bio coring event
PS144_050_ps144_ snow_sip		2024-09-05T07:00:00	85.03270	139.44607		MULT	max depth	1 snow pit. 2 CT samples. 7 SnowImager photos (battery problems). 1 surface roughness site. 11 Denoth measurements
PS144_50_Buoy_002	2024I14	2024-09-05T07:00:00	85.01370	139.79350		BUOY	max depth	deployment. Cryosphere Innov. Seasonal IMB
PS144_050_M350	DJI Matrice 350 RTK	2024-09-05T07:10:00	85.03270	139.44607		UAV	max depth	2 flight lines Processed in Terra:20240905-Lidar-ICE4
PS144_50_Buoy_004	2024T108	2024-09-05T07:30:00	85.01860	139.84140		BUOY	max depth	deployment. SAMS ice mass balance buoy
PS144_050_MAVIC	Mavic3	2024-09-05T08:03:23	85.02600	139.94400		UAV	max depth	Ice station grid flight
PS144_50-5	Piglet	2024-09-05T08:16:07	85.02409	139.86382	3957.4	CTD-RO	max depth	
PS144_50_Buoy_005	2024V6	2024-09-05T08:40:00	85.01590	139.84140		BUOY	max depth	deployment. Drift-Towing Ocean Profiler
PS144_050_ps144_ physics_coring		2024-09-05T09:30:00	85.03270	139.44607		CORE	max depth	1 core
PS144_50-6		2024-09-05T10:08:39	85.02808	139.99543	3897.5	MSN	Station start	
PS144_50-6		2024-09-05T12:07:40	85.02590	140.10532	3465.9	MSN	Station end	
PS144_50_RDI300	ADCP_ WH300_9271	2024-09-05T11:16:00	85.02500	140.13610		ADCP	max depth	deployment. MSS site
PS144_050_MAGNA		2024-09-05T11:48:40	85.03270	139.44607		MAGNA	max depth	Ice station survey. co-located with GEM
PS144_050_GEM	gem2-512	2024-09-05T11:48:57	85.02600	139.94400		GEM-2	max depth	Ice station survey
PS144_50_MSS_1	MSS_90D_075	2024-09-05T12:21:00	85.02500	140.13610		MSS	max depth	series of 10 profiles; protective cage unmounted
PS144_50-7	LilliFe	2024-09-05T13:24:54	85.02330	140.12920	3418.3	CTD-TM	max depth	

Event label	Optional label	Date/Time	Latitude [Deg]	Longitude [Deg]	Depth [m]	Gear	Action	Comment
PS144_50-8		2024-09-05T14:37:19	85.02225	140.11240	3439.4	MIK-N	Station start	Station aborted. device not ready
PS144_50-8		2024-09-05T14:53:43	85.02237	140.10558	3420.5	MIK-N	Station end	Station aborted. device not ready
PS144_50-9	Piglet	2024-09-05T15:42:35	85.02358	140.08377	3493.9	CTD-RO	max depth	
PS144_51-1		2024-09-05T20:07:59	85.05370	140.80165		XCTD	Station start	
PS144_51-1		2024-09-05T20:38:30	85.05082	141.11823	3600.8	XCTD	Station end	
PS144_52-1	Piglet	2024-09-05T23:43:47	85.06451	142.92737	3399.7	CTD-RO	max depth	
PS144_53-1		2024-09-06T03:07:38	85.07425	144.74663	2733.3	XCTD	Station start	
PS144_53-1		2024-09-06T03:48:33	85.07523	144.72865	2729.1	XCTD	Station end	
PS144_54-1	Piglet	2024-09-06T07:06:50	85.08744	146.34548	2166.8	CTD-RO	max depth	
PS144_55-1		2024-09-06T12:01:04	85.05629	147.63819	1717.2	FTRW-P	Station start	
PS144_55-1		2024-09-06T14:30:58	84.98227	147.10439	1381.1	FTRW-P	Station end	
PS144_56-1		2024-09-06T16:07:21	85.07057	148.45501	1807.9	XCTD	Station start	
PS144_56-1		2024-09-06T16:22:31	85.07059	148.53016	1802.9	XCTD	Station end	
PS144_57-1	Piglet	2024-09-06T19:29:39	85.08041	150.47914	955.1	CTD-RO	max depth	
PS144_57-2	LilliFe	2024-09-06T20:33:31	85.08143	150.51470	954	CTD-TM	max depth	
PS144_57-3	Piglet	2024-09-06T22:03:44	85.08404	150.50204	948.9	CTD-RO	max depth	
PS144_57-4	2024P302	2024-09-06T22:50:12	85.08558	150.48643	946.7	ISVP	Station start	
PS144_57-4	2024P302	2024-09-06T23:10:57	85.08655	150.48937	945.2	ISVP	Station end	
PS144_58-1		2024-09-07T00:40:49	85.04322	151.89333	845.7	XCTD	Station start	
PS144_58-1		2024-09-07T00:45:40	85.04416	151.88489	845.1	XCTD	Station end	
PS144_58-2	Ice fishing	2024-09-07T01:33:07	85.03827	151.69528	858.5	ICE	Station start	
PS144_58-2	Ice fishing	2024-09-07T01:56:39	85.03915	151.70118	855.2	ICE	Station end	
PS144_59-1	Piglet	2024-09-07T04:32:36	85.02737	153.74914	1544.3	CTD-RO	max depth	
PS144_60-1		2024-09-07T07:10:40	85.00612	155.41679	2518.3	XCTD	Station start	
PS144_60-1		2024-09-07T07:21:32	85.00599	155.41030	2517.8	XCTD	Station end	
PS144_Heli_EM-Bird_002		2024-09-07T07:53:59	85.00958	155.42890		EMB	max depth	Foggy conditions towards the end
PS144_61-1	Arvor-I_24DE008	2024-09-07T09:19:24	84.98859	156.67631	2531.7	ARVORFL	Station start	

Event label	Optional label	Date/Time	Latitude [Deg]	Longitude [Deg]	Depth [m]	Gear	Action	Comment
PS144_61-1	Arvor-I_24DE008	2024-09-07T09:22:24	84.99042	156.67300	2532.2	ARVORFL	Station end	
PS144_62-1		2024-09-07T11:08:30	84.97007	155.84710	2522.9	FTRW-P	Station start	
PS144_62-1		2024-09-07T14:40:56	85.11178	155.01720	2469.3	FTRW-P	Station end	
PS144_63-1	2024P303	2024-09-07T15:41:21	85.03899	155.63132	2536.8	ISVP	Station start	
PS144_63-1	2024P303	2024-09-07T16:00:03	85.03695	155.63330	2536.5	ISVP	Station end	
PS144_64-1	Piglet	2024-09-07T18:39:18	84.96954	157.12258	2511.4	CTD-RO	max depth	
PS144_65-1	LilliFe	2024-09-07T22:16:34	84.98064	159.07450	3443	CTD-TM	max depth	
PS144_65-2	Piglet	2024-09-08T00:23:37	84.98367	159.04378	3428.3	CTD-RO	max depth	
PS144_66-1		2024-09-08T03:07:27	84.97029	160.49236	3562.6	XCTD	Station start	
PS144_66-1		2024-09-08T03:20:14	84.97248	160.59037	3565.1	XCTD	Station end	
PS144_67-1		2024-09-08T05:24:00	84.96026	161.87108	3560.5	ICE	Station start	
PS144_67-1		2024-09-08T23:17:32	84.93765	162.20318	3558.9	ICE	Station end	
PS144_67_UICE_ Pump		2024-09-08T07:35:51	84.96026	161.87108		UICE_ Pump	max depth	Under-ice water and surface backscatter maximum
PS144_67-2	Piglet	2024-09-08T07:54:46	84.94324	161.90125	3560.2	CTD-RO	max depth	
PS144_67_SI_ corer_9cm		2024-09-08T07:55:22	84.96026	161.87108		MARKII	max depth	Bio coring event
PS144_67_Lline_1		2024-09-08T08:00:48	84.96026	161.87108		LLDEP	max depth	Longline deployment for project SciCAO
PS144_67_Magna-Katrin		2024-09-08T08:34:00	84.94667	162.09426		MAGNA	max depth	Snow thickness measurements
PS144_67_SnowCup		2024-09-08T08:34:00	84.94667	162.09426		SNOW	max depth	Snow Samples
PS144_067_ps144_ snow_sip		2024-09-08T08:40:00	84.96026	161.87108		MULT	max depth	1 snow pit. 2 CT samples. 19 SnowImager photos. 2 surface roughness sites. no Denoth measurements
PS144_067_GPS2	GPS_Station2	2024-09-08T08:46:35	84.96026	161.87108		GPS	max depth	DGPS measurement at ice station
PS144_067_GPS4	GPS_Station4	2024-09-08T08:59:15	84.96026	161.87108		GPS	max depth	DGPS measurement at ice station

Event label	Optional label	Date/Time	Latitude [Deg]	Longitude [Deg]	Depth [m]	Gear	Action	Comment
PS144_67_ FISHTRAP_PS		2024-09-08T09:00:42	84.96026	161.87108		TRAPF	max depth	Under-ice trap deployment for project SciCAO
PS144_067_GPS1	GPS_Station1	2024-09-08T09:10:45	84.96026	161.87108		GPS	max depth	DGPS measurement at ice station
PS144_067_GPS5	GPS_Station5	2024-09-08T09:22:15	84.96026	161.87108		GPS	max depth	DGPS measurement at ice station
PS144_067_ps144_ physics_coring		2024-09-08T09:30:00	84.96026	161.87108		CORE	max depth	1 core
PS144_067_GPS6	GPS_Station6	2024-09-08T09:31:45	84.96026	161.87108		GPS	max depth	DGPS measurement at ice station
PS144_067_GPS3	GPS_Station3	2024-09-08T09:41:25	84.96026	161.87108		GPS	max depth	DGPS measurement at ice station
PS144_67-3	LilliFe	2024-09-08T09:42:17	84.93920	161.88927	3560.4	CTD-TM	max depth	
PS144_67_RDI300	ADCP_ WH300_9271	2024-09-08T11:02:00	84.93960	162.18450		ADCP	max depth	deployment. MSS site
PS144_Heli_EM-Bird_003		2024-09-08T11:47:29	84.93682	161.84550		EMB	max depth	Ice station over flight (station 67. ice station 5)
PS144_67_Buoy_004	2024V7	2024-09-08T12:45:00	84.94250	161.96560		BUOY	max depth	deployment. Drift-Towing Ocean Profiler
PS144_67_Buoy_003	2024T116	2024-09-08T12:45:00	84.94470	161.98480		BUOY	max depth	deployment. SAMS ice mass balance buoy
PS144_67-4	Piglet	2024-09-08T12:54:51	84.94485	161.95292	3560.8	CTD-RO	max depth	
PS144_67_Buoy_002	2024I15	2024-09-08T12:55:00	84.94490	161.98780		BUOY	max depth	deployment. Cryosphere Innov. Seasonal IMB
PS144_67_Buoy_005	2024S131	2024-09-08T12:55:00	84.94500	161.99100		BUOY	max depth	deployment. MetOcean Snow Buoy
PS144_67_Buoy_001	2024W9	2024-09-08T12:55:00	84.94500	161.99100		BUOY	max depth	deployment. WHOI Ice-Tethered Profiler
PS144_067_MAGNA		2024-09-08T13:13:19	84.96026	161.87108		MAGNA	max depth	Ice station survey. co-located with GEM
PS144_067_GEM	gem2-512	2024-09-08T13:21:25	84.94700	162.09400		GEM-2	max depth	Ice station survey
PS144_67-5		2024-09-08T14:29:49	84.94581	162.03825	3562.6	MSN	Station start	

Event label	Optional label	Date/Time	Latitude [Deg]	Longitude [Deg]	Depth [m]	Gear	Action	Comment
PS144_67-5		2024-09-08T16:31:54	84.94075	162.14634	3560.3	MSN	Station end	
PS144_67_Nortek1000	Nortek_ S1000_52160	2024-09-08T14:56:00	84.93960	162.18450		ADCP	max depth	MSS site
PS144_67-6		2024-09-08T16:32:38	84.94071	162.14683	3560.2	MSN	Station start	
PS144_67-6		2024-09-08T18:23:02	84.93474	162.18614	3558.9	MSN	Station end	
PS144_067_M350_1	DJI Matrice 350 RTK	2024-09-08T17:00:00	84.96026	161.87108		UAV	max depth	2 flight lines Processed in Terra:20240908-Lidar-ICE5.20240908-Lidar-ICE5-2
PS144_67_MSS_1	MSS_90D_075	2024-09-08T17:09:00	84.93960	162.18450		MSS	max depth	series of 8 profiles; protective cage unmounted
PS144_67_Larm		2024-09-08T17:45:32	84.96026	161.87108		LIOP	max depth	Hyperspectral under-ice light measurement
PS144_067_M350_2	DJI Matrice 350 RTK	2024-09-08T18:00:00	84.96026	161.87108		UAV	max depth	2 flight lines Processed in Terra:20240908-Lidar-ICE5-3.20240908-Lidar-ICE5-4
PS144_067_MAVIC	Mavic3	2024-09-08T19:14:59	84.94700	162.09400		UAV	max depth	Ice station grid flight
PS144_67-7	Piglet	2024-09-08T19:48:52	84.93225	162.18804	3558.8	CTD-RO	max depth	
PS144_67_SI_ corer_9cm_Larm		2024-09-08T20:20:47	84.96026	161.87108		MARKII	max depth	Bio coring event
PS144_67-8	LilliFe	2024-09-08T22:51:08	84.93648	162.19742	3558.8	CTD-TM	max depth	
PS144_68-1		2024-09-09T02:06:38	84.95231	163.96303	3599.8	XCTD	Station start	
PS144_68-1		2024-09-09T02:24:24	84.96194	164.00223	3605.2	XCTD	Station end	
PS144_69-1	Piglet	2024-09-09T05:24:22	84.95276	165.78476	3501.2	CTD-RO	max depth	
PS144_70-1	Ice fishing	2024-09-09T07:43:49	84.94883	165.78662	3499.3	ICE	Station start	
PS144_70-1	Ice fishing	2024-09-09T08:06:13	84.94850	165.78440	3499.2	ICE	Station end	
PS144_Heli_EM-Bird_004		2024-09-09T09:46:26	84.94877	166.49910		EMB	max depth	Survey was ended due to fog (error 113 at ~10:11)
PS144_71-1		2024-09-09T10:08:31	84.94398	166.74012	3480.6	RMT	Station start	
PS144_71-1		2024-09-09T11:40:26	84.97756	166.41739	3505.5	RMT	Station end	
PS144_72-1		2024-09-09T13:09:27	84.94894	167.38061	3465.2	XCTD	Station start	
PS144_72-1		2024-09-09T13:23:30	84.95363	167.34813	3466	XCTD	Station end	

Event label	Optional label	Date/Time	Latitude [Deg]	Longitude [Deg]	Depth [m]	Gear	Action	Comment
PS144_73-1	Piglet	2024-09-09T15:45:50	84.93921	169.27767	3423.1	CTD-RO	max depth	
PS144_73-2	LilliFe	2024-09-09T16:42:16	84.94316	169.26439	3424	CTD-TM	max depth	
PS144_73-3		2024-09-09T17:42:12	84.94636	169.25910	3424.3	XCTD	Station start	
PS144_73-3		2024-09-09T17:52:58	84.94678	169.25958	3424.4	XCTD	Station end	
PS144_73-4	Piglet	2024-09-09T19:16:30	84.94863	169.26676	3424.6	CTD-RO	max depth	
PS144_73-5	2024P306	2024-09-09T20:49:00	84.94771	169.25569	3424.5	ISVP	Station start	
PS144_73-5	2024P306	2024-09-09T21:18:33	84.94398	169.24203	3424.2	ISVP	Station end	
PS144_80_UICE_ Pump		2024-09-09T22:03:17	84.92259	179.57723		UICE_ Pump	max depth	Under-ice water and surface backscatter maximum
PS144_74-1		2024-09-09T23:00:06	84.92513	170.99531	3368.9	XCTD	Station start	
PS144_74-1		2024-09-09T23:14:16	84.93128	171.01052	3365.2	XCTD	Station end	
PS144_80_Larm		2024-09-10T00:00:36	84.92259	179.57723		LIOP	max depth	Hyperspectral under-ice light measurement
PS144_75-1	Piglet	2024-09-10T01:57:22	84.93269	172.70362	3188.3	CTD-RO	max depth	
PS144_76-1		2024-09-10T05:18:20	84.92876	174.38665	2931.5	XCTD	Station start	
PS144_76-1		2024-09-10T05:36:01	84.92673	174.43644	2932.9	XCTD	Station end	
PS144_77-1	Piglet	2024-09-10T08:31:01	84.91914	176.27111	2627.5	CTD-RO	max depth	
PS144_78-1		2024-09-10T11:14:15	84.84616	175.67431	2870.8	FTRW-P	Station start	
PS144_78-1		2024-09-10T14:02:42	84.75890	176.66584	2774.9	FTRW-P	Station end	
PS144_79-1		2024-09-10T17:10:35	84.91134	177.90554	2448	XCTD	Station start	
PS144_79-1		2024-09-10T17:19:30	84.91822	177.93236	2407.4	XCTD	Station end	
PS144_79-2		2024-09-10T17:32:13	84.93383	177.93886	2347.6	XCTD	Station start	
PS144_79-2		2024-09-10T17:50:47	84.93944	177.88254	2329.9	XCTD	Station end	
PS144_80-1		2024-09-10T20:05:00	84.92259	179.57723	1980.1	ICE	Station start	
PS144_80-1		2024-09-11T06:56:22	84.96012	179.57340	2187	ICE	Station end	
PS144_80_ CleanCoring_1		2024-09-10T21:00:00	84.92259	179.57723		MARKII	max depth	2 Cores; IceStation #6
PS144_80_ CleanCoring_2		2024-09-10T21:14:00	84.92259	179.57723		PUMP	max depth	Under ice water; IceStation #6
PS144_80-2	Piglet	2024-09-10T21:22:42	84.92065	179.55521	1974.1	CTD-RO	max depth	

Event label	Optional label	Date/Time	Latitude [Deg]	Longitude [Deg]	Depth [m]	Gear	Action	Comment
PS144_80_SI_ corer_9cm		2024-09-10T22:03:37	84.92259	179.57723		MARKII	max depth	Bio coring event
PS144_080_GPS4	GPS_Station4	2024-09-10T22:16:45	84.92259	179.57723		GPS	max depth	DGPS measurement at ice station
PS144_080_GPS3	GPS_Station3	2024-09-10T22:24:35	84.92259	179.57723		GPS	max depth	DGPS measurement at ice station
PS144_080_ps144_ snow_sip		2024-09-10T22:40:00	84.92259	179.57723		MULT	max depth	2 snow pits. 2 CT samples. 22 SnowImager photos. 2 surface roughness sites. 2 Denoth measurements
PS144_080_GPS2	GPS_Station2	2024-09-10T22:43:05	84.92259	179.57723		GPS	max depth	DGPS measurement at ice station
PS144_080_M350	DJI Matrice 350 RTK	2024-09-10T22:50:00	84.92259	179.57723		UAV	max depth	2 flight lines Processed in Terra:20240910-Lidar-ICE6.20240910-Lidar-ICE6-2
PS144_080_GPS1	GPS_Station1	2024-09-10T22:54:45	84.92259	179.57723		GPS	max depth	DGPS measurement at ice station
PS144_80-3	LilliFe	2024-09-10T23:31:05	84.92324	179.46900	1981.6	CTD-TM	max depth	
PS144_080_ps144_ physics_coring		2024-09-10T23:45:00	84.92259	179.57723		CORE	max depth	1 core
PS144_80_SI_ corer_9cm_Larm		2024-09-11T00:00:01	84.92259	179.57723		MARKII	max depth	Bio coring event
PS144_080_MAVIC	Mavic3	2024-09-11T00:55:55	84.93300	179.41300		UAV	max depth	Ice station grid flight
PS144_080_MAGNA		2024-09-11T01:46:03	84.92259	179.57723		MAGNA	max depth	Ice station survey. co-located with GEM
PS144_080_GEM	gem2-512	2024-09-11T02:00:35	84.93300	179.41300		GEM-2	max depth	Ice station survey
PS144_80-4	Piglet	2024-09-11T02:25:13	84.94191	179.41484	2117.9	CTD-RO	max depth	
PS144_80-5		2024-09-11T03:31:53	84.94961	179.44075	2157.2	MSN	Station start	
PS144_80-5		2024-09-11T05:33:43	84.95831	179.52688	2191.2	MSN	Station end	
PS144_80_Buoy_006	2024V8	2024-09-11T03:40:00	84.94590	179.38590		BUOY	max depth	deployment. Drift-Towing Ocean Profiler
PS144_80_Buoy_007	2024O21	2024-09-11T06:00:00	84.95920	179.53900		BUOY	max depth	deployment. Pacific Gyre CTD Buoy

Event label	Optional label	Date/Time	Latitude [Deg]	Longitude [Deg]	Depth [m]	Gear	Action	Comment
PS144_80_Buoy_004	2024T117	2024-09-11T06:00:00	84.95920	179.53900		BUOY	max depth	deployment. SAMS ice mass balance buoy
PS144_80_Buoy_005	2024S132	2024-09-11T06:00:00	84.95920	179.53900		BUOY	max depth	deployment. MetOcean Snow Buoy
PS144_80_Buoy_001	2024A7	2024-09-11T06:00:00	84.95920	179.53900		BUOY	max depth	deployment. APL weather station
PS144_80_Buoy_003	2024I16	2024-09-11T06:00:00	84.95920	179.53900		BUOY	max depth	deployment. Cryosphere Innov. Seasonal IMB
PS144_80_Buoy_008	2024K2	2024-09-11T06:00:00	84.95920	179.53900		BUOY	max depth	deployment. Pacific Gyre Sidekick camera buoy
PS144_80_Buoy_002	2024W10	2024-09-11T06:00:00	84.95920	179.53900		BUOY	max depth	deployment. WHOI Ice-Tethered Profiler
PS144_81-1		2024-09-11T07:54:47	84.95809	179.66591	2144.7	RMT	Station start	
PS144_81-1		2024-09-11T09:49:05	84.88749	179.51337	1897.9	RMT	Station end	
PS144_82-1		2024-09-11T14:30:05	85.32705	178.15696	2757.4	XCTD	Station start	
PS144_82-1		2024-09-11T14:39:44	85.33034	178.15511	2774	XCTD	Station end	
PS144_82-2		2024-09-11T19:18:12	85.76798	178.94325	2356.8	XCTD	Station start	
PS144_82-2		2024-09-11T19:30:46	85.76811	178.93580	2355.3	XCTD	Station end	
PS144_83-1	2024P304	2024-09-11T19:32:47	85.76816	178.93444	2355.1	ISVP	Station start	
PS144_83-1	2024P304	2024-09-11T19:45:49	85.76849	178.92501	2354.2	ISVP	Station end	
PS144_82-3		2024-09-12T00:22:13	86.21478	-179.94144	3715.3	XCTD	Station start	
PS144_82-3		2024-09-12T00:28:38	86.21737	-179.95660	3948.8	XCTD	Station end	
PS144_82-4		2024-09-12T04:39:55	86.63023	179.54958	3978.1	XCTD	Station start	
PS144_82-4		2024-09-12T04:54:12	86.63855	179.54309	3978	XCTD	Station end	
PS144_84-1	2024P305	2024-09-12T06:01:30	86.72250	179.83920	3983.3	ISVP	Station start	
PS144_84-1	2024P305	2024-09-12T06:20:37	86.72315	179.82094	3983.6	ISVP	Station end	
PS144_82-5		2024-09-12T11:28:02	87.08044	179.23652	3993.7	XCTD	Station start	
PS144_82-5		2024-09-12T11:34:10	87.07923	179.15839	3993.5	XCTD	Station end	
PS144_Heli_EM-Bird_005		2024-09-12T14:31:45	87.25851	179.49370		EMB	max depth	
PS144_85_ FISHTRAP_PS		2024-09-12T18:41:22	87.51503	179.09715		TRAPF	max depth	Under-ice trap deployment for project SciCAO

Event label	Optional label	Date/Time	Latitude [Deg]	Longitude [Deg]	Depth [m]	Gear	Action	Comment
PS144_85-1		2024-09-12T19:07:15	87.51503	179.09715	3995.3	ICE	Station start	
PS144_85-1		2024-09-13T19:57:16	87.47120	178.03548	3994.7	ICE	Station end	
PS144_85_CleanCoring_1		2024-09-12T20:04:00	87.51503	179.09715		MARKII	max depth	3 Cores; IceStation #7
PS144_085_GPS2	GPS_Station2	2024-09-12T20:24:30	87.51503	179.09715		GPS	max depth	DGPS measurement at ice station
PS144_85_CleanCoring_2		2024-09-12T20:25:00	87.51503	179.09715		PUMP	max depth	Under ice water; IceStation #7
PS144_85_RDI300	ADCP_WH300_9271	2024-09-12T20:43:00	87.51310	179.03650		ADCP	max depth	deployment. MSS site
PS144_085_GPS1	GPS_Station1	2024-09-12T20:44:10	87.51503	179.09715		GPS	max depth	DGPS measurement at ice station
PS144_085_GPS5	GPS_Station5	2024-09-12T20:55:15	87.51503	179.09715		GPS	max depth	DGPS measurement at ice station
PS144_085_GPS6	GPS_Station6	2024-09-12T21:04:30	87.51503	179.09715		GPS	max depth	DGPS measurement at ice station
PS144_085_GPS3	GPS_Station3	2024-09-12T21:11:45	87.51503	179.09715		GPS	max depth	DGPS measurement at ice station
PS144_85_MSS_1	MSS_90D_075	2024-09-12T21:14:00	87.51310	179.03650		MSS	max depth	series of 10 profiles; protective cage unmounted
PS144_085_GPS4	GPS_Station4	2024-09-12T21:21:15	87.51503	179.09715		GPS	max depth	DGPS measurement at ice station
PS144_85_Lline_1		2024-09-12T21:30:39	87.51503	179.09715		LLDEP	max depth	Longline deployment for project SciCAO
PS144_85_SnowCup		2024-09-12T22:48:00	87.50035	178.72568		SNOW	max depth	Snow Samples and Frost flowers
PS144_85_Magna-Katrin		2024-09-12T22:48:00	87.50035	178.72568		MAGNA	max depth	Snow thickness measurements
PS144_85_Buoy_003	2024S136*	2024-09-13T01:20:00	87.51200	178.90740		BUOY	max depth	deployment. MetOcean Snow Buoy
PS144_85_Buoy_001	2024W11	2024-09-13T01:45:00	87.51200	178.89620		BUOY	max depth	deployment. LOCEAN IAOOS
PS144_85_Buoy_002	2024T120	2024-09-13T01:45:00	87.51200	178.89620		BUOY	max depth	deployment. SAMS ice mass balance buoy

Event label	Optional label	Date/Time	Latitude [Deg]	Longitude [Deg]	Depth [m]	Gear	Action	Comment
PS144_85-2	Piglet	2024-09-13T04:34:17	87.51895	178.84942	3995.9	CTD-RO	max depth	
PS144_085_M350_Lidar	DJI Matrice 350 RTK	2024-09-13T08:00:00	87.51503	179.09715		UAV	max depth	2 flight linesProcessed in Terra:20240913-Lidar-ICE7.20240913-Lidar-ICE7-2
PS144_85_MSS_2	MSS_90D_075	2024-09-13T08:29:00	87.50290	178.75150		MSS	max depth	series of 21 profiles; protective cage unmounted
PS144_85_UICE_Pump		2024-09-13T08:30:30	87.51503	179.09715		UICE_Pump	max depth	Under-ice water and surface backscatter maximum
PS144_85_Larm		2024-09-13T08:30:48	87.51503	179.09715		LIOP	max depth	Hyperspectral under-ice light measurement
PS144_85_SI_corer_9cm		2024-09-13T08:30:49	87.51503	179.09715		MARKII	max depth	Bio coring event
PS144_085_MAVIC	Mavic3	2024-09-13T08:47:26	87.50000	178.72600		UAV	max depth	Ice station grid flight. very low contrast
PS144_85_SI_corer_9cm_Larm		2024-09-13T09:14:27	87.51503	179.09715		MARKII	max depth	Bio coring event
PS144_85-3	LilliFe	2024-09-13T09:47:10	87.50124	178.69980	3996	CTD-TM	max depth	
PS144_085_MAGNA		2024-09-13T10:18:21	87.51503	179.09715		MAGNA	max depth	Ice station survey. co-located with GEM
PS144_085_GEM	gem2-512	2024-09-13T10:20:52	87.50000	178.72600		GEM-2	max depth	Ice station survey
PS144_085_ps144_snow_sip		2024-09-13T10:45:00	87.51503	179.09715		MULT	max depth	2 snow pits. 2 CT samples. 22 SnowImager photos. 2 surface roughness sites. 1 Denoth measurement
PS144_85-4		2024-09-13T11:53:16	87.49568	178.53941	3995.5	MSN	Station start	
PS144_85-4		2024-09-13T13:53:31	87.49114	178.38854	3994.5	MSN	Station end	
PS144_085_ps144_physics_coring		2024-09-13T12:30:00	87.51503	179.09715		CORE	max depth	1 core
PS144_85-5		2024-09-13T13:52:11	87.49120	178.39011	3994.5	XCTD	Station start	
PS144_85-5		2024-09-13T14:02:44	87.49074	178.37819	3994.4	XCTD	Station end	
PS144_Heli_EM-Bird_006		2024-09-13T15:21:19	87.49057	178.64360		EMB	max depth	Ice station over flight (station 85. ice station 7)
PS144_85-6	Piglet	2024-09-13T15:36:45	87.48615	178.27847	3993.9	CTD-RO	max depth	

Event label	Optional label	Date/Time	Latitude [Deg]	Longitude [Deg]	Depth [m]	Gear	Action	Comment
PS144_85-7		2024-09-13T17:31:12	87.47957	178.17258	3994.5	MSN	Station start	
PS144_85-7		2024-09-13T19:26:25	87.47284	178.06466	3994.7	MSN	Station end	
PS144_085_M350_Cam	DJI Matrice 350 RTK	2024-09-13T19:25:00	87.51503	179.09715		UAV	max depth	Nadir and Overview Images
PS144_85-8	LilliFe	2024-09-13T20:49:18	87.46847	177.98724	3994.5	CTD-TM	max depth	
PS144_85-9	Piglet	2024-09-13T23:02:28	87.46175	177.86877	3994.1	CTD-RO	max depth	
PS144_86-1		2024-09-14T00:11:18	87.45228	177.25483	3992.5	RMT	Station start	
PS144_86-1		2024-09-14T01:51:23	87.46866	176.99322	3995.4	RMT	Station end	
PS144_Heli_EM-Bird_007		2024-09-14T08:32:08	87.60901	-174.88260		EMB	max depth	First flight of the day
PS144_87-1		2024-09-14T14:45:31	87.69246	-170.63243	3984.3	XCTD	Station start	
PS144_87-1		2024-09-14T14:55:01	87.69422	-170.46531	3558.6	XCTD	Station end	
PS144_Heli_EM-Bird_008		2024-09-14T17:03:24	87.75826	-168.25090		EMB	max depth	Second flight of the day (error 113 occured again. data receiving delay)
PS144_87-2		2024-09-15T00:24:37	87.85609	-159.93466	3697	XCTD	Station start	
PS144_87-2		2024-09-15T00:36:31	87.86019	-160.01481	3700.4	XCTD	Station end	
PS144_87-3		2024-09-15T07:35:05	88.02145	-148.85991	2735.5	XCTD	Station start	
PS144_87-3		2024-09-15T07:52:59	88.02196	-148.82873	2736.5	XCTD	Station end	
PS144_88-1	2024P307	2024-09-15T07:55:30	88.02203	-148.82431	2736.7	ISVP	Station start	
PS144_88-1	2024P307	2024-09-15T08:04:13	88.02230	-148.80947	2737.2	ISVP	Station end	
PS144_87-4		2024-09-15T17:05:39	88.19526	-137.75794		XCTD	Station start	
PS144_87-4		2024-09-15T17:25:12	88.19625	-137.72287		XCTD	Station end	
PS144_89-1		2024-09-16T01:01:57	88.38328	-124.91491	3578	RMT	Station start	
PS144_89-1		2024-09-16T02:34:04	88.36421	-124.68953	3571.8	RMT	Station end	
PS144_90-1	Piglet	2024-09-16T04:19:14	88.36630	-124.53091	3559.5	CTD-RO	max depth	
PS144_90-2	LilliFe	2024-09-16T07:17:18	88.36966	-124.25745	3542.9	CTD-TM	max depth	
PS144_Heli_EM-Bird_009		2024-09-16T07:25:14	88.36370	-124.22240		EMB	max depth	Error 113 occured again. bird needed restart
PS144_90-3	Piglet	2024-09-16T09:42:45	88.37240	-124.09701	3528.8	CTD-RO	max depth	

Event label	Optional label	Date/Time	Latitude [Deg]	Longitude [Deg]	Depth [m]	Gear	Action	Comment
PS144_Heli_XCTD-01	XCTD_MK150_1	2024-09-16T10:12:00	87.81910	-124.97210		XCTD	max depth	
PS144_Heli_XCTD-02	XCTD_MK150_1	2024-09-16T10:43:00	87.95590	-123.00470		XCTD	max depth	
PS144_Heli_XCTD-03	XCTD_MK150_1	2024-09-16T11:13:00	88.09360	-124.92712		XCTD	max depth	
PS144_Heli_XCTD-04	XCTD_MK150_1	2024-09-16T11:43:00	88.22950	-123.03210		XCTD	max depth	
PS144_91-1		2024-09-16T13:12:31	88.37363	-123.99033	3516.1	SUIT	Station start	
PS144_91-1		2024-09-16T14:34:15	88.38036	-123.62799	3477.8	SUIT	Station end	
PS144_92-1		2024-09-16T17:39:06	88.46905	-124.57966	3205.5	XCTD	Station start	
PS144_92-1		2024-09-16T17:54:41	88.46841	-124.75463	3236	XCTD	Station end	
PS144_93-1		2024-09-16T19:30:46	88.56709	-126.19888		XCTD	Station start	
PS144_93-1		2024-09-16T19:41:54	88.56763	-126.17623	3993.3	XCTD	Station end	
PS144_94-1	Piglet	2024-09-16T22:56:34	88.68342	-123.88873	3996	CTD-RO	max depth	
PS144_95-1		2024-09-17T02:01:43	88.76900	-126.18429	3997	XCTD	Station start	
PS144_95-1		2024-09-17T02:16:04	88.76935	-126.16950	3996.6	XCTD	Station end	
PS144_96-1		2024-09-17T04:14:46	88.87867	-125.63640	2978.8	XCTD	Station start	
PS144_96-1		2024-09-17T04:31:23	88.88051	-125.23443	3204.6	XCTD	Station end	
PS144_97-1	Piglet	2024-09-17T08:02:48	89.01108	-125.73580	1657.9	CTD-RO	max depth	
PS144_98-1	2024P309	2024-09-17T09:40:49	89.06055	-125.52321	1244.6	ISVP	Station start	
PS144_98-1	2024P309	2024-09-17T09:51:17	89.06061	-125.51751	1244.2	ISVP	Station end	
PS144_Heli_Buoy_001	2024P308	2024-09-17T09:46:00	89.06150	-125.48200		BUOY	max depth	deployment. MetOcean SVP-B
PS144_99-1		2024-09-17T11:07:17	89.12969	-126.88979	1362.1	XCTD	Station start	
PS144_99-1		2024-09-17T11:23:25	89.12781	-126.89268	1351.4	XCTD	Station end	
PS144_100-1		2024-09-17T14:15:17	89.25163	-126.01096	1659.5	XCTD	Station start	
PS144_100-1		2024-09-17T14:28:02	89.25811	-126.29355	1666.7	XCTD	Station end	
PS144_101-1		2024-09-17T14:39:29	89.27181	-127.40572	1678.3	RMT	Station start	
PS144_101-1		2024-09-17T16:42:20	89.25828	-123.51705	1626.3	RMT	Station end	
PS144_102-1	Piglet	2024-09-17T18:55:49	89.33560	-125.42402	1675.6	CTD-RO	max depth	
PS144_102-2	LilliFe	2024-09-17T20:35:30	89.33479	-125.38236	1663.8	CTD-TM	max depth	
PS144_102-3	Piglet	2024-09-17T22:58:45	89.33498	-125.39298	1671	CTD-RO	max depth	
PS144_103-1		2024-09-18T02:16:08	89.45279	-124.62322	3555.1	XCTD	Station start	

Event label	Optional label	Date/Time	Latitude [Deg]	Longitude [Deg]	Depth [m]	Gear	Action	Comment
PS144_103-1		2024-09-18T02:30:02	89.45311	-124.61572	3513.7	XCTD	Station end	
PS144_104-1		2024-09-18T03:59:54	89.56978	-126.23816	3943.5	XCTD	Station start	
PS144_104-1		2024-09-18T04:25:06	89.57581	-126.63682	4235.2	XCTD	Station end	
PS144_105-1	Piglet	2024-09-18T07:34:38	89.66187	-126.48511	4249.9	CTD-RO	max depth	
PS144_106-1		2024-09-18T11:06:49	89.77917	-115.79117	4243.4	XCTD	Station start	
PS144_106-1		2024-09-18T11:21:43	89.78089	-116.77830	4245.3	XCTD	Station end	
PS144_107-1		2024-09-18T13:06:15	89.88996	-118.33202	4254.8	XCTD	Station start	
PS144_107-1		2024-09-18T13:21:22	89.89227	-119.05343	4237.3	XCTD	Station end	
PS144_108-1		2024-09-18T14:59:59	89.87299	-78.59905	4249.7	RMT	Station start	
PS144_108-1		2024-09-18T17:15:25	89.96215	-74.01842	4267.5	RMT	Station end	
PS144_109-1		2024-09-18T19:30:30	89.94484	-150.66699	4263.8	ICE	Station start	
PS144_109-1		2024-09-19T23:46:42	89.94336	80.37481	4281.8	ICE	Station end	
PS144_109_ CleanCoring_1		2024-09-18T21:15:00	89.94484	-150.66699		MARKII	max depth	4 Cores; IceStation #8
PS144_109_Fyke		2024-09-18T21:30:40	89.94484	-150.66699		NET	max depth	Under-ice fyke deployment for project SciCAO
PS144_109_ CleanCoring_2		2024-09-18T21:38:00	89.94484	-150.66699		PUMP	max depth	Under ice water; IceStation #8
PS144_109_SI_ corer_9cm		2024-09-18T22:09:03	89.94484	-150.66699		MARKII	max depth	Bio coring event
PS144_109_UICE_ Pump		2024-09-18T22:09:05	89.94484	-150.66699		UICE_ Pump	max depth	Under-ice water and surface backscatter maximum
PS144_109_GPS6	GPS_Station6	2024-09-18T22:10:00	89.94484	-150.66699		GPS	max depth	DGPS measurement at ice station. data gaps
PS144_109_ps144_ snow_sip		2024-09-18T22:15:00	89.94484	-150.66699		MULT	max depth	2 snow pits. 1 CT sample. 30 SnowImager photos. 3 surface roughness sites. no Denoth measurements
PS144_109_GPS5	GPS_Station5	2024-09-18T22:20:25	89.94484	-150.66699		GPS	max depth	DGPS measurement at ice station

Event label	Optional label	Date/Time	Latitude [Deg]	Longitude [Deg]	Depth [m]	Gear	Action	Comment
PS144_109_RDI300	ADCP_ WH300_9271	2024-09-18T22:30:00	89.94610	-153.49560		ADCP	max depth	deployment. MSS site
PS144_109_Lline		2024-09-18T22:30:22	89.94484	-150.66699		LLDEP	max depth	Longline deployment for project SciCAO
PS144_109_ Nortek1000	Nortek_ S1000_52160	2024-09-18T22:35:00	89.94610	-153.49560		ADCP	max depth	MSS site
PS144_109_GPS2	GPS_Station2	2024-09-18T22:36:05	89.94484	-150.66699		GPS	max depth	DGPS measurement at ice station
PS144_109_GPS3	GPS_Station3	2024-09-18T22:50:05	89.94484	-150.66699		GPS	max depth	DGPS measurement at ice station
PS144_109_GPS4	GPS_Station4	2024-09-18T23:00:15	89.94484	-150.66699		GPS	max depth	DGPS measurement at ice station
PS144_109-2	Piglet	2024-09-18T23:03:39	89.94475	-151.12200	4263.8	CTD-RO	max depth	
PS144_109_MAVIC	Mavic3	2024-09-18T23:13:52	89.95200	-142.69600		UAV	max depth	Ice station manual flight
PS144_109_ps144_ physics_coring		2024-09-18T23:15:00	89.94484	-150.66699		CORE	max depth	2 cores
PS144_109_ FISHTRAP_PS		2024-09-18T23:30:46	89.94484	-150.66699		TRAPF	max depth	Under-ice trap deployment for project SciCAO
PS144_109_MSS_1	MSS_90D_075	2024-09-18T23:49:00	89.94610	-153.49560		MSS	max depth	series of 8 profiles; protective cage unmounted
PS144_109_Magna-Katrin		2024-09-19T00:14:00	89.95154	-142.69616		MAGNA	max depth	Snow thickness measurements
PS144_109_SnowCup		2024-09-19T00:54:00	89.95154	-142.69616		SNOW	max depth	Snow Samples and Water from Lead
PS144_109-3	LilliFe	2024-09-19T01:08:40	89.94741	-150.49154	4264.5	CTD-TM	max depth	
PS144_109-4		2024-09-19T02:55:56	89.94936	-148.49951	4264.2	MSN	Station start	
PS144_109-4		2024-09-19T05:02:05	89.95019	-145.31559	4264.1	MSN	Station end	
PS144_109_Buoy_002	2024T121	2024-09-19T04:05:00	89.94940	-150.28670		BUOY	max depth	deployment. SAMS ice mass balance buoy
PS144_109_Buoy_001	2024W13	2024-09-19T04:05:00	89.94940	-150.28670		BUOY	max depth	deployment. LOCEAN IAOOS
PS144_109-5	Piglet	2024-09-19T06:53:24	89.95003	-142.84301	4264	CTD-RO	max depth	
PS144_109-6		2024-09-19T09:03:47	89.95050	-140.93792	4263.8	MSN	Station start	

Event label	Optional label	Date/Time	Latitude [Deg]	Longitude [Deg]	Depth [m]	Gear	Action	Comment
PS144_109-6		2024-09-19T11:06:59	89.95325	-139.54333	4264.1	MSN	Station end	
PS144_109_MAGNA		2024-09-19T10:26:04	89.94484	-150.66699		MAGNA	max depth	Ice station survey. co-located with GEM
PS144_109_GEM	gem2-512	2024-09-19T10:26:54	89.95200	-142.69600		GEM-2	max depth	Ice station survey
PS144_109-7	LilliFe	2024-09-19T12:34:09	89.95624	-137.88453	4264.5	CTD-TM	max depth	
PS144_109_MSS_2	MSS_90D_075	2024-09-19T12:45:00	89.95770	-140.42090		MSS	max depth	series of 5 profiles; protective cage unmounted
PS144_109_Larm		2024-09-19T15:04:10	89.94484	-150.66699		LIOP	max depth	Hyperspectral under-ice light measurement
PS144_109_SI_ corer_9cm_Larm		2024-09-19T15:13:32	89.94484	-150.66699		MARKII	max depth	Bio coring event
PS144_109_Buoy_003	2024P311	2024-09-19T16:45:00	89.96500	-130.84050		BUOY	max depth	deployment. Pacific Gyre Universal Tracker
PS144_109-8	Piglet	2024-09-19T16:54:03	89.96386	-128.03777	4266.4	CTD-RO	max depth	
PS144_110-1		2024-09-20T01:02:17	89.84439	63.35177	4301.7	XCTD	Station start	
PS144_110-1		2024-09-20T01:15:33	89.84260	64.60119	4025.1	XCTD	Station end	
PS144_111-1	Piglet	2024-09-20T05:08:03	89.67484	59.72660	4323.9	CTD-RO	max depth	
PS144_112-1		2024-09-20T13:12:03	89.52865	63.18288	4344.7	XCTD	Station start	
PS144_112-1		2024-09-20T13:33:37	89.52674	63.17002	4344.7	XCTD	Station end	
PS144_113-1	Piglet	2024-09-20T18:06:30	89.35049	59.68328	4367.5	CTD-RO	max depth	
PS144_114-1		2024-09-20T22:23:36	89.20755	60.43051	4378.7	XCTD	Station start	Station canceled
PS144_114-1		2024-09-20T22:27:53	89.20725	60.37945	4358.6	XCTD	Station end	Station canceled
PS144_115-1	Piglet	2024-09-21T04:22:46	89.02542	59.45064	4395.1	CTD-RO	max depth	cancelled due to ice situation
PS144_115-2	LilliFe	2024-09-21T07:55:52	89.01330	59.00991	4395.7	CTD-TM	max depth	
PS144_115-3	Piglet	2024-09-21T11:05:46	88.99927	58.86845	4396.3	CTD-RO	max depth	
PS144_Heli_EM-Bird_010		2024-09-21T14:36:05	88.95821	56.79076		EMB	max depth	Data receiving delay. bird needed a restart
PS144_116-1		2024-09-21T15:32:47	88.94844	57.43845	4398.6	SUIT	Station start	
PS144_116-1		2024-09-21T17:59:43	88.94305	59.40437	4397.8	SUIT	Station end	
PS144_117-1		2024-09-21T23:25:46	88.88076	59.41921	4404.2	XCTD	Station start	

Event label	Optional label	Date/Time	Latitude [Deg]	Longitude [Deg]	Depth [m]	Gear	Action	Comment
PS144_117-1		2024-09-21T23:33:53	88.87474	59.50435	4404.8	XCTD	Station end	
PS144_118-1	Piglet	2024-09-22T05:00:19	88.69984	60.65111	4410.2	CTD-RO	max depth	
PS144_119-1		2024-09-22T09:39:53	88.55924	59.98119	3280.2	XCTD	Station start	
PS144_119-1		2024-09-22T09:54:33	88.55910	60.00502	4414.3	XCTD	Station end	
PS144_120-1		2024-09-22T12:23:52	88.56193	60.45652	4414.3	SUIT	Station start	
PS144_120-1		2024-09-22T13:54:12	88.54853	61.63431	4414.9	SUIT	Station end	
PS144_121-1	Piglet	2024-09-22T19:10:46	88.39684	60.16096	4415.2	CTD-RO	max depth	
PS144_122-1		2024-09-22T23:48:37	88.23951	61.31530		XCTD	Station start	
PS144_122-1		2024-09-23T00:31:13	88.23524	61.59273	4417.9	XCTD	Station end	
PS144_123-1	Piglet	2024-09-23T04:20:59	88.07883	60.18641	4416.1	CTD-RO	max depth	
PS144_123-2		2024-09-23T05:45:13	88.07211	59.71527	4416.3	ICE	Station start	
PS144_123-2		2024-09-23T14:44:47	88.05867	59.93024	4417.6	ICE	Station end	
PS144_123_ps144_ physics_coring		2024-09-23T06:45:00	88.07211	59.71527		CORE	max depth	1 core
PS144_123_ps144_ snow_sip		2024-09-23T06:45:00	88.07211	59.71527		MULT	max depth	2 snow pits. 1 CT sample. 21 SnowImager photos. 3 surface roughness sites. no Denoth measurements
PS144_123_SnowCup		2024-09-23T06:56:00	88.07016	59.95280		SNOW	max depth	Snow Samples
PS144_123_GPS2	GPS_Station2	2024-09-23T07:07:45	88.07211	59.71527		GPS	max depth	DGPS measurement at ice station
PS144_123_GPS4	GPS_Station4	2024-09-23T07:10:45	88.07211	59.71527		GPS	max depth	DGPS measurement at ice station. used as rover
PS144_123_GPS5	GPS_Station5	2024-09-23T07:17:15	88.07211	59.71527		GPS	max depth	DGPS measurement at ice station
PS144_123_GPS3	GPS_Station3	2024-09-23T07:25:45	88.07211	59.71527		GPS	max depth	DGPS measurement at ice station
PS144_123_Magna-Katrin		2024-09-23T07:50:00	88.07016	59.95280		MAGNA	max depth	Snow thickness measurements
PS144_123-3	LilliFe	2024-09-23T08:00:29	88.07151	59.82801	4416.4	CTD-TM	max depth	
PS144_123_GEM	gem2-512	2024-09-23T08:21:32	88.07000	59.95300		GEM-2	max depth	Ice station survey

Event label	Optional label	Date/Time	Latitude [Deg]	Longitude [Deg]	Depth [m]	Gear	Action	Comment
PS144_123_Buoy_001	2024S138*	2024-09-23T08:30:00	88.07160	59.86450		BUOY	max depth	deployment. MetOcean Snow Buoy
PS144_123_Buoy_002	2024T118	2024-09-23T08:50:00	88.07160	59.87510		BUOY	max depth	deployment. SAMS ice mass balance buoy
PS144_123_M350	DJI Matrice 350 RTK	2024-09-23T08:50:00	88.07211	59.71527		UAV	max depth	2 flight linesProcessed in Terra:20240923-Lidar-ICE9.20240923-Lidar-ICE9-2
PS144_123_MAVIC	Mavic3	2024-09-23T09:18:43	88.07000	59.95300		UAV	max depth	Ice station grid flight. very low contrast
PS144_123-4	Piglet	2024-09-23T11:51:00	88.06448	59.96127	4417.1	CTD-RO	max depth	
PS144_124-1		2024-09-23T16:17:33	87.93035	60.04979		XCTD	Station start	
PS144_124-1		2024-09-23T16:31:51	87.93018	60.04357	4418	XCTD	Station end	
PS144_125-1	Piglet	2024-09-23T21:13:11	87.75673	60.05925	4281.6	CTD-RO	max depth	
PS144_126-1		2024-09-24T01:54:34	87.60177	60.03781		XCTD	Station start	
PS144_126-1		2024-09-24T02:22:23	87.59918	59.99836	4403.7	XCTD	Station end	
PS144_127-1	Piglet	2024-09-24T04:36:32	87.42812	60.28169	3596.3	CTD-RO	max depth	
PS144_134_Lline_1		2024-09-24T06:30:14	86.98215	58.66148		LLDEP	max depth	Longline deployment for project SciCAO
PS144_134_ FISHTRAP_PS		2024-09-24T07:30:19	86.98215	58.66148		TRAPF	max depth	Under-ice trap deployment for project SciCAO
PS144_128-1		2024-09-24T08:57:07	87.38847	59.37304	4024.9	SUIT	Station start	
PS144_128-1		2024-09-24T10:14:10	87.39901	60.04149	3837.8	SUIT	Station end	
PS144_134_Fyke		2024-09-24T09:00:01	86.98215	58.66148		NET	max depth	Under-ice fyke deployment for project SciCAO
PS144_129-1		2024-09-24T11:21:31	87.33762	59.64177	3509	XCTD	Station start	
PS144_129-1		2024-09-24T11:36:45	87.33349	59.68017	3502.5	XCTD	Station end	
PS144_130-1	LilliFe	2024-09-24T16:25:02	87.33243	59.19872	3698	CTD-TM	max depth	
PS144_131-1		2024-09-24T18:24:54	87.22523	59.72478	3872.9	XCTD	Station start	
PS144_131-1		2024-09-24T18:34:36	87.22998	59.71382	3824.8	XCTD	Station end	
PS144_132-1		2024-09-24T21:40:26	87.10298	60.44897	3508.4	XCTD	Station start	
PS144_132-1		2024-09-24T21:52:17	87.10596	60.46787	3367	XCTD	Station end	

Event label	Optional label	Date/Time	Latitude [Deg]	Longitude [Deg]	Depth [m]	Gear	Action	Comment
PS144_134_GPS3	GPS_Station3	2024-09-24T21:58:30	87.03683	57.55971		GPS	max depth	DGPS measurement at ice station. started recording on vessel
PS144_133-1		2024-09-25T00:22:54	86.97136	61.03308	4117.2	XCTD	Station start	
PS144_133-1		2024-09-25T00:46:08	86.96990	61.08610	2771.3	XCTD	Station end	
PS144_134-1		2024-09-25T04:45:19	86.98120	58.69814	4639.8	ICE	Station start	
PS144_134-1		2024-09-26T20:53:07	87.03520	55.84290	4743.9	ICE	Station end	
PS144_134_ CleanCoring_1		2024-09-25T05:38:00	86.98120	58.69814		MARKII	max depth	3 Cores; IceStation #10
PS144_134_ Nortek1000	Nortek_ S1000_52160	2024-09-25T06:04:00	86.98820	58.50470		ADCP	max depth	MSS site
PS144_134_ÂµMooring	PS144_micro_ mooring	2024-09-25T06:04:00	86.98820	58.50470		MOOR	max depth	MSS site
PS144_134_RDI300	ADCP_ WH300_9271	2024-09-25T06:13:00	86.98820	58.50470		ADCP	max depth	deployment. MSS site
PS144_134_ CleanCoring_2		2024-09-25T06:31:00	86.98120	58.69814		PUMP	max depth	Under ice water; IceStation #10
PS144_134_MSS_1	MSS_90D_075	2024-09-25T06:35:00	86.98820	58.50470		MSS	max depth	series of 4 profiles; protective cage unmounted; sensor SH1 changed
PS144_134_GPS5	GPS_Station5	2024-09-25T06:53:50	87.03683	57.55971		GPS	max depth	DGPS measurement at ice station. started recording on vessel
PS144_134_Buoy_001	2024S137*	2024-09-25T07:30:00	86.99130	58.45830		BUOY	max depth	deployment. MetOcean Snow Buoy
PS144_134_Buoy_002	2024T101	2024-09-25T07:50:00	86.99300	58.43280		BUOY	max depth	deployment. SAMS ice mass balance buoy
PS144_134_M350_ Cam	DJI Matrice 350 RTK	2024-09-25T08:00:00	87.03683	57.55971		UAV	max depth	2 flights:Ice detection with live view
PS144_135-1		2024-09-25T09:53:51	86.98643	57.81348		SUIT	Station start	
PS144_135-1		2024-09-25T11:06:39	87.00029	57.98227	4743.3	SUIT	Station end	
PS144_134-2		2024-09-25T12:09:46	86.98277	58.65421	4736.3	XCTD	Station start	

Event label	Optional label	Date/Time	Latitude [Deg]	Longitude [Deg]	Depth [m]	Gear	Action	Comment
PS144_134-2		2024-09-25T12:24:37	86.98315	58.64158	4749	XCTD	Station end	
PS144_134-3	Piglet	2024-09-25T14:49:12	86.98822	58.47151	4895.7	CTD-RO	max depth	
PS144_134-4	LilliFe	2024-09-25T19:15:15	87.00452	58.11425	4760.9	CTD-TM	max depth	
PS144_134_Magna-Katrin		2024-09-25T23:48:00	87.04715	57.07384		MAGNA	max depth	Snow thickness measurements
PS144_134_SnowCup		2024-09-25T23:53:00	87.04715	57.07384		SNOW	max depth	Snow Samples
PS144_134_MSS_2	MSS_90D_075	2024-09-25T23:59:00	87.03780	57.49800		MSS	max depth	series of 13 profiles; protective cage unmounted
PS144_134_UICE_Pump		2024-09-26T00:10:17	87.03683	57.55971		UICE_Pump	max depth	Under-ice water and surface backscatter maximum
PS144_134_SI_corer_9cm		2024-09-26T00:10:25	87.03683	57.55971		MARKII	max depth	Bio coring event
PS144_134-5		2024-09-26T00:25:05	87.03750	57.52206	4239.6	MSN	Station start	
PS144_134-5		2024-09-26T02:19:52	87.03911	57.39666	4294.3	MSN	Station end	
PS144_134_ps144_snow_sip		2024-09-26T00:40:00	87.03683	57.55971		MULT	max depth	2 snow pits. 1 CT sample. 35 SnowImager photos. 2 surface roughness sites. no Denoth measurements
PS144_134_MAGNA		2024-09-26T01:24:39	87.03683	57.55971		MAGNA	max depth	Ice station survey. co-located with GEM
PS144_134_GEM	gem2-512	2024-09-26T01:29:24	87.04700	57.07400		GEM-2	max depth	Ice station survey
PS144_134_ps144_physics_coring		2024-09-26T02:00:00	87.03683	57.55971		CORE	max depth	2 cores
PS144_134_Larm		2024-09-26T03:00:28	87.03683	57.55971		LIOP	max depth	Hyperspectral under-ice light measurement
PS144_134-6	Piglet	2024-09-26T03:07:23	87.04034	57.33018	4243.2	CTD-RO	max depth	
PS144_134_GPS2	GPS_Station2	2024-09-26T03:09:15	87.03683	57.55971		GPS	max depth	DGPS measurement at ice station
PS144_134_GPS4	GPS_Station4	2024-09-26T03:16:15	87.03683	57.55971		GPS	max depth	DGPS measurement at ice station
PS144_134_GPS6	GPS_Station6	2024-09-26T03:24:00	87.03683	57.55971		GPS	max depth	DGPS measurement at ice station

Event label	Optional label	Date/Time	Latitude [Deg]	Longitude [Deg]	Depth [m]	Gear	Action	Comment
PS144_134_SI_ corer_9cm_Larm		2024-09-26T03:36:02	87.03683	57.55971		MARKII	max depth	Bio coring event
PS144_134-7		2024-09-26T03:48:03	87.04163	57.27354	4222.8	MSN	Station start	
PS144_134-7		2024-09-26T05:50:45	87.04602	57.12389	4248.3	MSN	Station end	
PS144_134_MAVIC	Mavic3	2024-09-26T04:49:53	87.04700	57.07400		UAV	max depth	Ice station grid flight
PS144_134-8		2024-09-26T10:49:58	86.99014	58.58943		XCTD	Station start	
PS144_134-8		2024-09-26T11:00:18	86.98983	58.58000	4835.9	XCTD	Station end	
PS144_134-9	Piglet	2024-09-26T13:34:25	86.98393	58.36996	4680.7	CTD-RO	max depth	
PS144_134_M350_ Lidar	DJI Matrice 350 RTK	2024-09-26T18:05:00	87.03683	57.55971		UAV	max depth	4 flight linesProcessed in Terra:20240916-Lidar-ICE10.1.20240916-Lidar-ICE10.2.20240916-Lidar-ICE10.3.20240916-Lidar-ICE10.4
PS144_134_MSS_3	MSS_90D_075	2024-09-26T18:06:00	87.03640	56.07980		MSS	max depth	series of 3 profiles; protective cage unmounted
PS144_134_MSS_4	mss_90L_097	2024-09-26T19:45:00	87.03620	55.97630		MSS	max depth	series of 2 profiles; protective cage unmounted; MSS with self-recording module
PS144_134-10	LilliFe	2024-09-26T22:42:39	87.03460	55.68315	4391.1	CTD-TM	max depth	
PS144_136-1		2024-09-27T05:59:42	86.91721	58.64340	4457.5	XCTD	Station start	
PS144_136-1		2024-09-27T06:24:26	86.91575	58.58373	4383.8	XCTD	Station end	
PS144_137-1		2024-09-27T07:55:36	86.89577	58.52403	3223.2	RMT	Station start	
PS144_137-1		2024-09-27T10:03:37	86.93769	58.03514	4169.5	RMT	Station end	
PS144_138-1	Piglet	2024-09-27T15:13:30	86.74462	58.94479	2941.9	CTD-RO	max depth	
PS144_139-1		2024-09-27T18:01:04	86.69755	58.64753	2905.4	XCTD	Station start	
PS144_139-1		2024-09-27T18:16:40	86.68939	58.52386	2819.4	XCTD	Station end	
PS144_140-1		2024-09-27T21:02:06	86.58904	58.39057	3126.3	XCTD	Station start	
PS144_140-1		2024-09-27T21:17:10	86.58904	58.36524	3123.4	XCTD	Station end	
PS144_141-1	Piglet	2024-09-28T03:12:39	86.48372	59.92672	2121.8	CTD-RO	max depth	
PS144_141-2	LilliFe	2024-09-28T05:42:47	86.48836	59.65070	2118.2	CTD-TM	max depth	

Event label	Optional label	Date/Time	Latitude [Deg]	Longitude [Deg]	Depth [m]	Gear	Action	Comment
PS144_Heli_EM-Bird_011		2024-09-28T07:22:24	86.49400	59.63479		EMB	max depth	
PS144_141-3	Piglet	2024-09-28T07:23:07	86.49203	59.49537	2093.9	CTD-RO	max depth	
PS144_142-1		2024-09-28T11:07:11	86.37722	59.99866	2389.9	XCTD	Station start	
PS144_142-1		2024-09-28T11:19:45	86.37518	60.04222	2534.6	XCTD	Station end	
PS144_143-1		2024-09-28T13:35:55	86.25648	59.76581	2673.5	XCTD	Station start	
PS144_143-1		2024-09-28T13:55:54	86.26056	59.70689	2881.2	XCTD	Station end	
PS144_144-1		2024-09-28T17:54:05	86.16679	60.13504	3908.5	XCTD	Station start	
PS144_144-1		2024-09-28T18:17:18	86.16761	60.11541	3908.8	XCTD	Station end	
PS144_144-2	Piglet	2024-09-28T19:49:14	86.16955	60.02306	3909.1	CTD-RO	max depth	
PS144_144-3	LilliFe	2024-09-28T23:09:35	86.16989	59.87894	3910.2	CTD-TM	max depth	
PS144_144-4	Piglet	2024-09-29T01:22:47	86.16778	59.78439	3910.5	CTD-RO	max depth	
PS144_145-1		2024-09-29T05:21:54	86.00730	59.53908	3916.4	XCTD	Station start	
PS144_145-1		2024-09-29T05:38:44	86.00670	59.53201	3916.4	XCTD	Station end	
PS144_146-1		2024-09-29T06:59:52	85.97805	59.34602	4189.1	SUIT	Station start	
PS144_146-1		2024-09-29T08:34:25	85.94112	59.08521	3916.2	SUIT	Station end	
PS144_147-1	Piglet	2024-09-29T12:48:17	85.82678	59.81182	3927.1	CTD-RO	max depth	
PS144_148-1		2024-09-29T17:22:53	85.68015	60.05447	3932.6	XCTD	Station start	
PS144_148-1		2024-09-29T17:40:21	85.67921	60.03048	3932.6	XCTD	Station end	
PS144_149-1	Piglet	2024-09-29T22:04:38	85.51671	59.95916	3935.6	CTD-RO	max depth	
PS144_149-2	LilliFe	2024-09-30T00:30:43	85.51400	59.87408	3935.9	CTD-TM	max depth	
PS144_150-1		2024-09-30T03:00:19	85.39854	59.83627	3930.9	XCTD	Station start	
PS144_150-1		2024-09-30T03:17:50	85.39832	59.82824	3930.5	XCTD	Station end	
PS144_151-1		2024-09-30T06:28:07	85.22121	59.46478	3924.7	SUIT	Station start	
PS144_151-1		2024-09-30T14:24:39	85.22180	59.22497	3927.4	SUIT	Station end	
PS144_152-1	Piglet	2024-09-30T17:35:24	85.24646	59.71853	3925.5	CTD-RO	max depth	
PS144_152-2	LilliFe	2024-09-30T20:39:55	85.24288	59.59382	3925.7	CTD-TM	max depth	
PS144_152-3	Piglet	2024-09-30T22:46:06	85.24050	59.50794	3927.2	CTD-RO	max depth	
PS144_153-1		2024-10-03T11:00:52	83.82497	33.25794	4029.4	SUIT	Station start	
PS144_153-1		2024-10-03T13:16:03	83.80756	33.05480	4028.2	SUIT	Station end	

Event label	Optional label	Date/Time	Latitude [Deg]	Longitude [Deg]	Depth [m]	Gear	Action	Comment
PS144_154-1	LilliFe	2024-10-03T14:13:48	83.79867	32.94595	4026.7	CTD-TM	max depth	
PS144_155-1		2024-10-04T02:14:56	82.92915	30.91129	3824.5	XCTD	Station start	
PS144_155-1		2024-10-04T02:32:22	82.92061	31.00157	3811.7	XCTD	Station end	
PS144_155-2		2024-10-04T03:24:36	82.82919	30.86140	3760.9	XCTD	Station start	
PS144_155-2		2024-10-04T03:37:49	82.81574	30.82511	3763	XCTD	Station end	
PS144_156-1		2024-10-04T04:37:52	82.70323	30.81347	3691.7	XCTD	Station start	
PS144_156-1		2024-10-04T04:55:45	82.70367	30.82379	3691.1	XCTD	Station end	
PS144_156-2	Piglet	2024-10-04T06:23:38	82.70576	30.82649	3692	CTD-RO	max depth	
PS144_156-3	LilliFe	2024-10-04T09:19:26	82.69408	30.69226	3694.8	CTD-TM	max depth	
PS144_156-4	Arvor-I_24DE009	2024-10-04T11:14:05	82.62351	30.84020	3647.2	ARVORFL	Station start	
PS144_156-4	Arvor-I_24DE009	2024-10-04T11:19:56	82.61678	30.87956	3642.1	ARVORFL	Station end	
PS144_155-3		2024-10-04T11:28:16	82.59988	30.86992	3633.8	XCTD	Station start	
PS144_155-3		2024-10-04T11:46:26	82.57793	30.84830	3626.6	XCTD	Station end	
PS144_155-4		2024-10-04T12:27:39	82.48172	30.79480	3542.7	XCTD	Station start	
PS144_155-4		2024-10-04T12:39:07	82.48154	30.87997	3534.3	XCTD	Station end	
PS144_155-5		2024-10-04T13:21:42	82.38592	30.84997	3465.7	XCTD	Station start	
PS144_155-5		2024-10-04T13:36:46	82.38343	30.97173	3444.4	XCTD	Station end	
PS144_155-6		2024-10-04T14:18:55	82.28334	30.83830	3378.7	XCTD	Station start	
PS144_155-6		2024-10-04T14:33:21	82.28871	30.94174	3374.8	XCTD	Station end	
PS144_155-7		2024-10-04T15:18:38	82.17834	30.86194	3318.9	XCTD	Station start	
PS144_155-7		2024-10-04T15:33:37	82.16101	30.86405	3313.2	XCTD	Station end	
PS144_155-8		2024-10-04T16:11:03	82.07052	30.87043	2050.3	XCTD	Station start	
PS144_155-8		2024-10-04T16:17:29	82.06321	30.86978	3252	XCTD	Station end	
PS144_155-9		2024-10-04T16:56:59	81.96591	30.88570	3192.8	XCTD	Station start	
PS144_155-9		2024-10-04T17:09:26	81.95371	30.88669	3191.8	XCTD	Station end	
PS144_157-1		2024-10-04T18:00:17	81.85400	30.88919	3166.3	XCTD	Station start	
PS144_157-1		2024-10-04T18:12:09	81.85395	30.88977	3165.7	XCTD	Station end	
PS144_157-2	Piglet	2024-10-04T19:30:25	81.85331	30.89273	3165.6	CTD-RO	max depth	
PS144_157-3	LilliFe	2024-10-04T22:08:11	81.85370	30.89969	3162	CTD-TM	max depth	

Event label	Optional label	Date/Time	Latitude [Deg]	Longitude [Deg]	Depth [m]	Gear	Action	Comment
PS144_155-10		2024-10-04T23:52:47	81.73523	30.85580	3076.9	XCTD	Station start	
PS144_155-10		2024-10-05T00:05:36	81.72170	30.88014	3063.8	XCTD	Station end	
PS144_155-11		2024-10-05T00:39:27	81.63718	30.82621	2353.1	XCTD	Station start	
PS144_155-11		2024-10-05T01:08:00	81.62344	30.93164	2846.8	XCTD	Station end	
PS144_158-1	Piglet	2024-10-05T02:26:23	81.52943	30.79449	828.4	CTD-RO	max depth	
PS144_158-2	LilliFe	2024-10-05T03:52:11	81.52988	30.79338	829.9	CTD-TM	max depth	
PS144_159-1	Piglet	2024-10-05T14:35:11	80.08463	29.90661	305.2	CTD-RO	max depth	

* *Comments are limited to 130 characters. See https://www.pangaea.de/expeditions/events/PS144 to show full comments in conjunction with the station (event) list for expedition PS144*

Abbreviation	Method/Device
3D-UA	3D ultrasonic anemometer
ADCP	Acoustic Doppler Current Profiler
ARVORFL	ARVOR I Profiling Float (NKE Instrumentation)
AUTOFIM	Automated Filtration for Marine Microbes
BUOY	Buoy
CAME	Camera
CORE	Core
CT	Underway cruise track measurements
CTD-RO	CTD/Rosette
CTD-TM	CTD/Rosette, trace metal clean
DISDRO	Disdrometer
EMB	Electro-magnetic Bird (EM-Bird)
FBOX	FerryBox
FR	Fishing rod
FTRW-P	Pelagic fish trawl
GAIA	GAIA Atmosphere Observatory
GEM-2	Ground-based Electromagnetic Induction Sounding Device
GOPRO	Digital Camera, GoPro
GPS	Global positioning system
GRAV	Gravimetry
GRaWAC	G-band Radar for Arctic Water vapour And Clouds
HATPRO	Humidity And Temperature PROfiler, Radiometer Physics GmbH
HVAIR	High volume air sampler
ICE	Ice station
ICEOBS	Ice observation
ICERAD	Ice radar
IMU	Inertial measurement unit
IR_CAM	Infrared camera
ISVP	Surface velocity profiler
LIOP	Light/Optics
LLDEP	Longline deployment
MAG	Magnetometer
MAGNA	Magnaprobe
MARKII	Mark II motorized coring device, Kovacs Enterprise Inc
MBES	Multibeam echosounder
MIK-N	Midwater Ring Net
MOOR	Mooring
MSN	Multiple opening/closing net

Abbreviation	Method/Device
MSS	Micro structure probe
MULT	Multiple investigations
MUMMY	Mummychair
MiRAC-A	Microwave Radar and radiometer for Arctic Clouds - Active
MiRAC-P	Microwave Radar and radiometer for Arctic Clouds - Passive
NET	Net
PUMP	Water pump
RAMSES_ACC-VIS	Hyperspectral UV-VIS Radiometer, TriOS, RAMSES-ACC-VIS
RMT	Rectangular midwater trawl
RULER	Ruler stick
SNOW	Snow/ice sample
SUIT	Surface and under ice trawl
SWEAS	Ship Weather Station
TAP	Tap
TRAPF	Trap, fish
TSG	Thermosalinograph
TSI	Total sky imager, visual and infrared
UAV	Unmanned aerial vehicle
UICE_Pump	Under ice pump
XCTD	Expendable CTD

A.5 ICE STATION MAPS

This chapter shows maps of the ice stations, when the ice was accessed by gangway. Maps are available for ICE1 to ICE4 and ICE6 to ICE10. No map was created for ICE5, as an aerial photograph could not be obtained due to adverse weather conditions. The geographic position of each station along the cruise track is shown in Figure 1.1 and the main characteristics and statistics of each ice station are summarized in Table 6.3. Event labels are given in the figure captions. The distances (see scale) are estimated from known distances between markers and installations and contain uncertainties within a few meters. In addition, distortions in the images from the stitching processes may occur. Approximate locations of different ice station activity are shown as yellow labels: Profiling for turbulent microstructure (MSS), coring for biological analysis (Bio Coring), coring for trace-metal clean analysis (Clean Coring), various activity related to sampling and measurements related to sea ice / snow / surface radiation analysis (Radiation), deployment of autonomous ice-tethered instrument systems (Buoys), fishing by long lines and other devices (Long Lines). If activities are missing that does not mean they were not performed, as these maps represent only a preliminary look at the layout of each ice station. Any labels outside / at the edge of the aerial photos represent activity outside or at the edge of the photographed domain. If available, locally measured ice thickness is given by black labels.

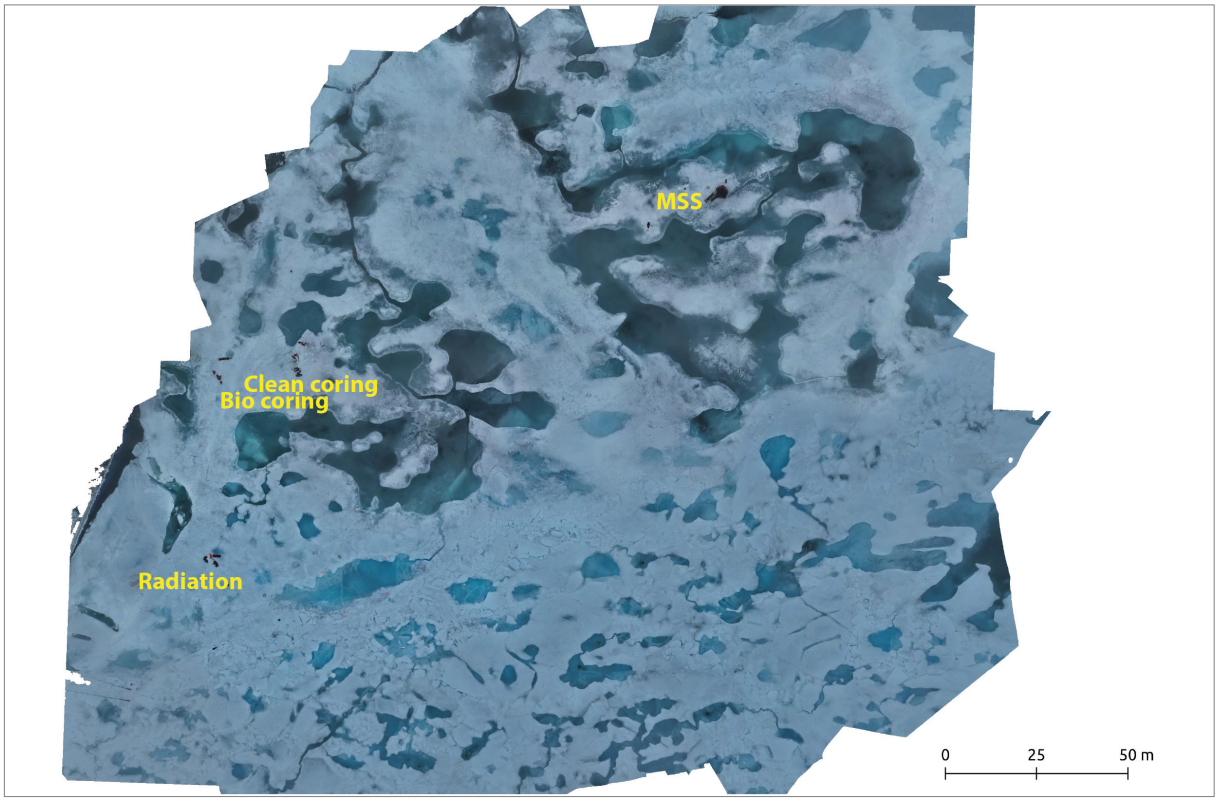

Fig. A.5.1: Preliminary map of ice station ICE1 (PS144_7_1).

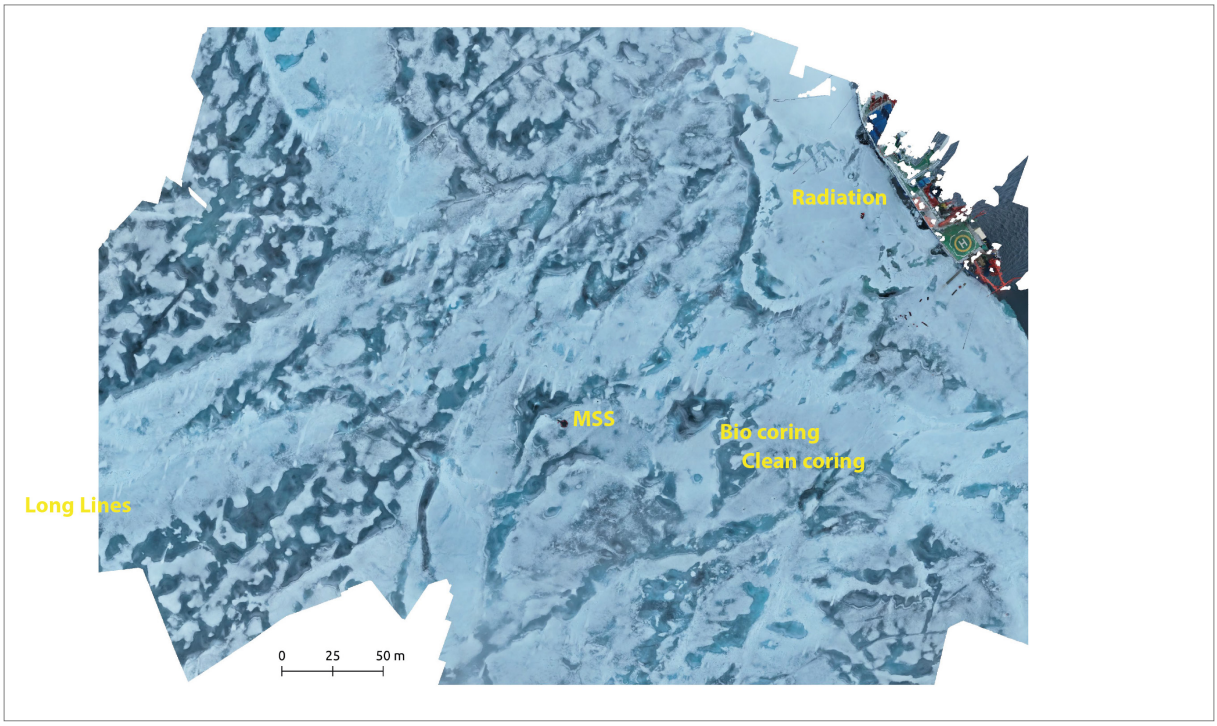

Fig. A.5.2: Preliminary map of ice station ICE2 (PS144_23-1).

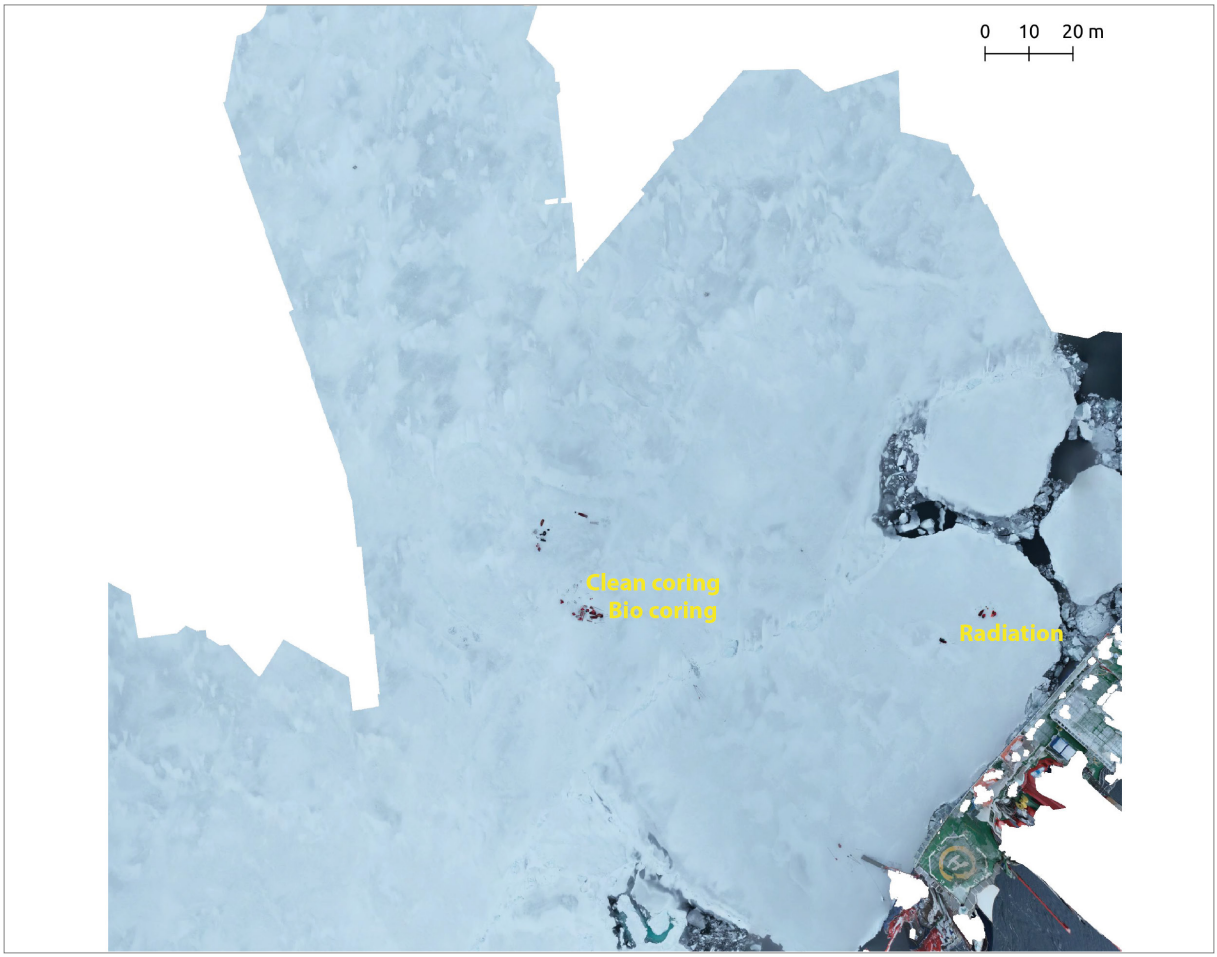

Fig. A.5.3: Preliminary map of ice station ICE3 (PS144_42-1).

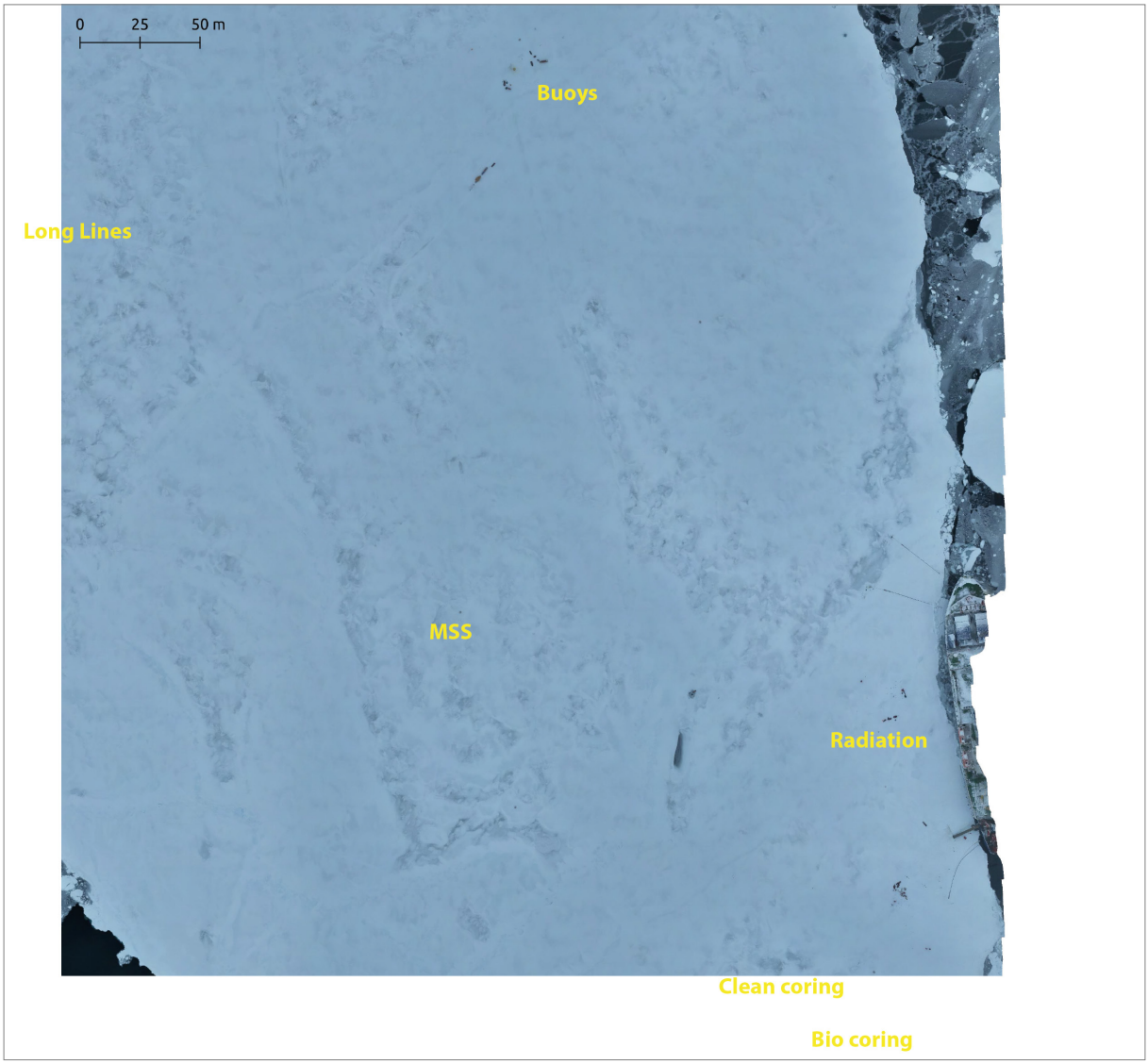

Fig. A.5.4: Preliminary map of ice station ICE4 (PS144_50-1).

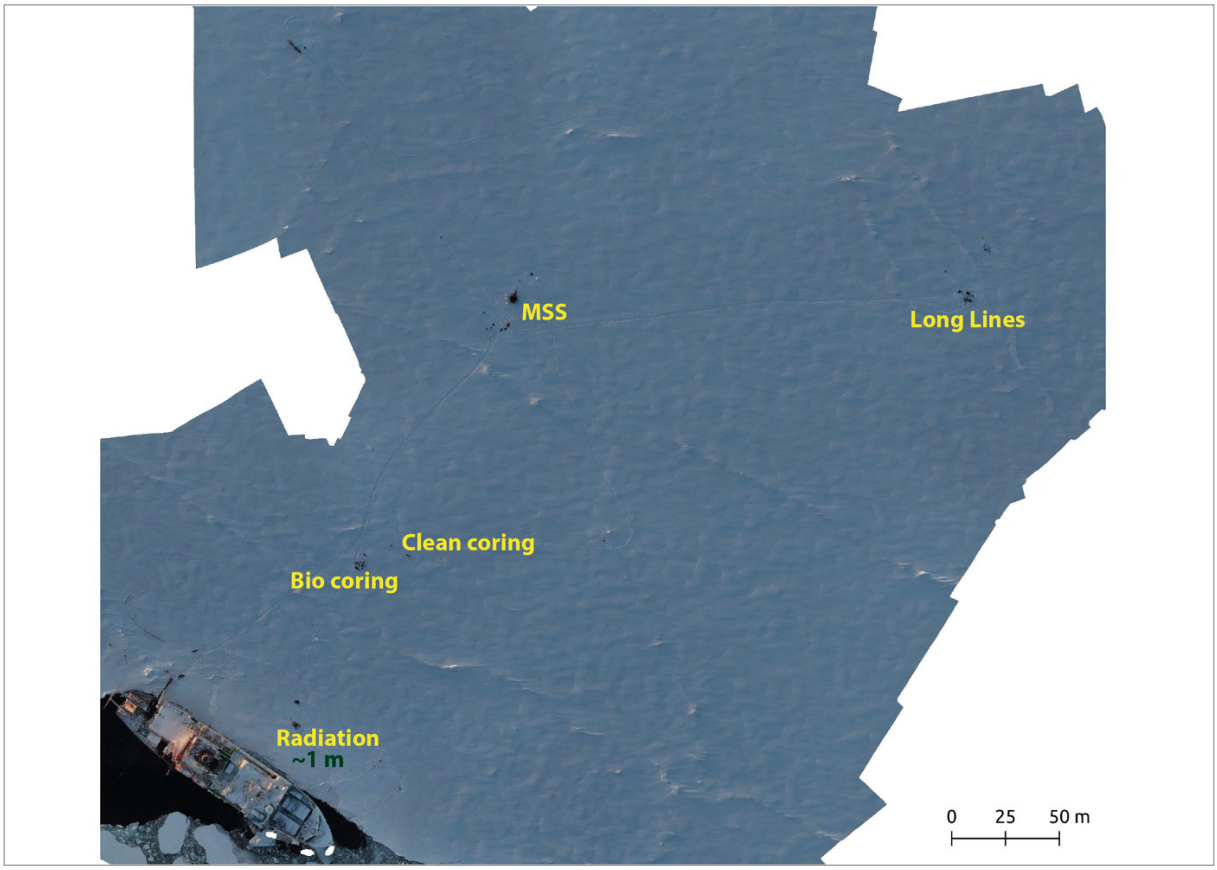

Fig. A.5.5: Preliminary map of ice station ICE6 (PS144_80-1).

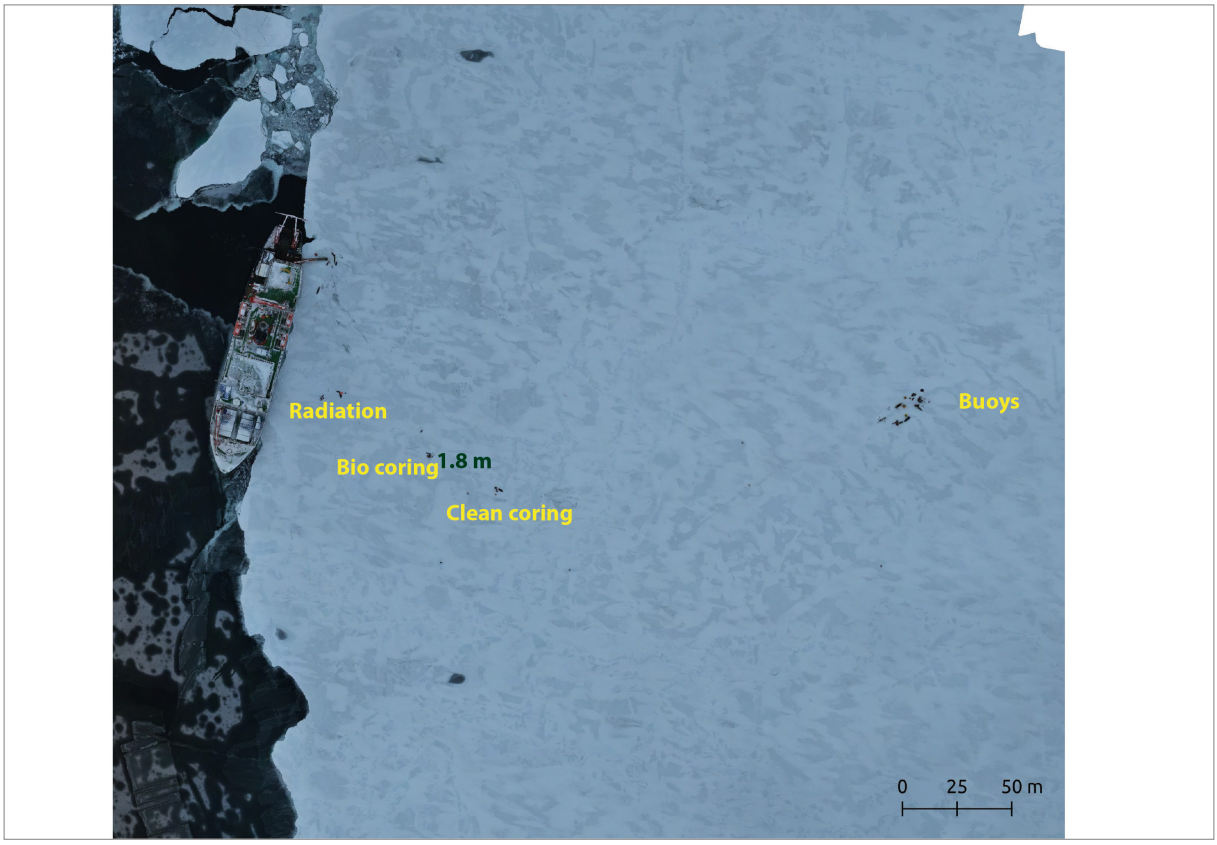

Fig. A.5.6: Preliminary map of ice station ICE7 (PS144_85-1).

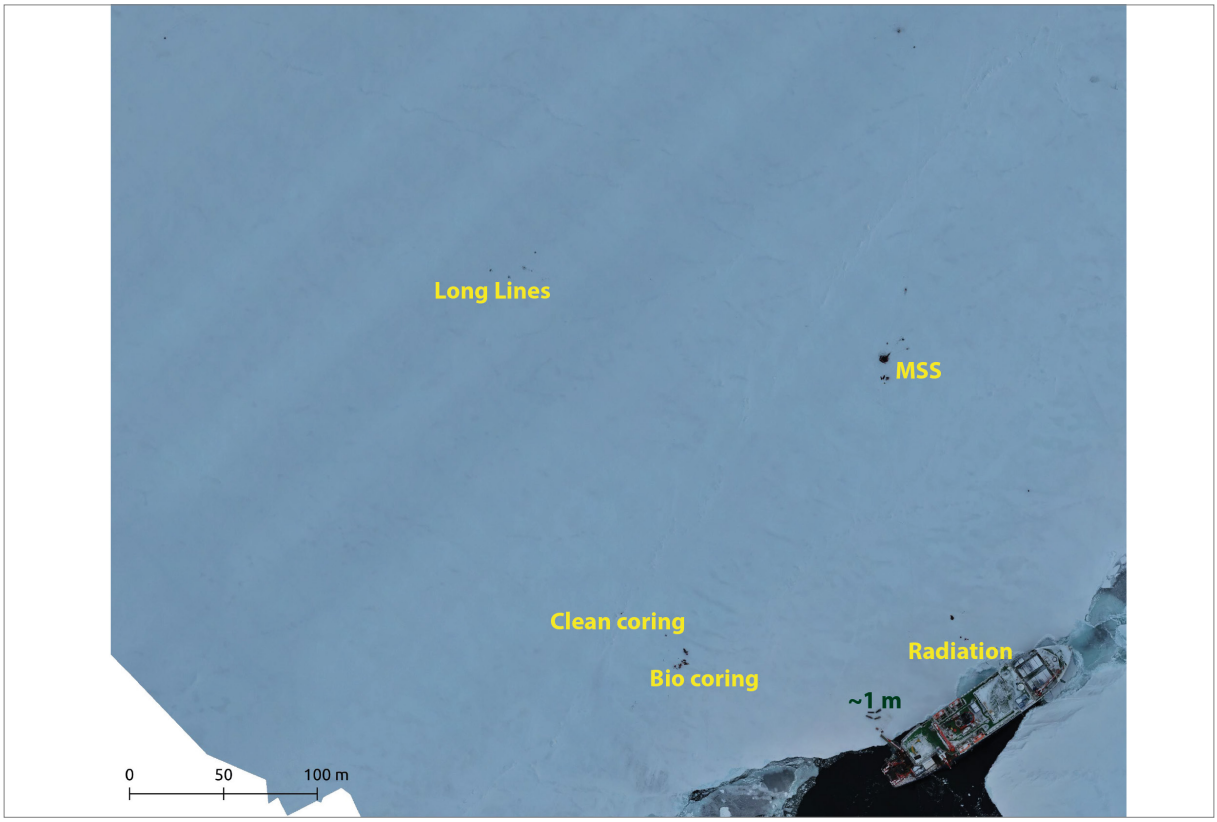

Fig. A.5.7: Preliminary map of ice station ICE8 (PS144_109-1).

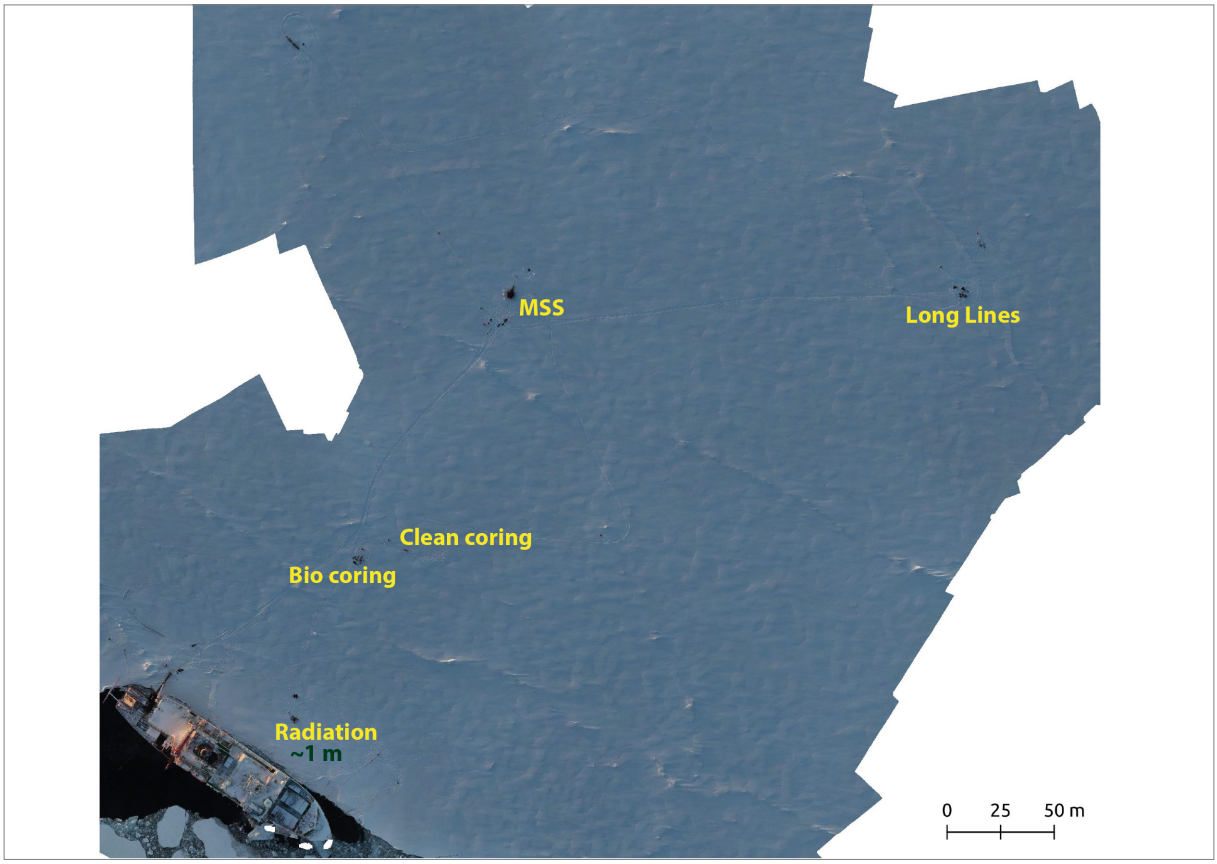

Fig. A.5.8: Preliminary map of ice station ICE9 (PS144_123-1).

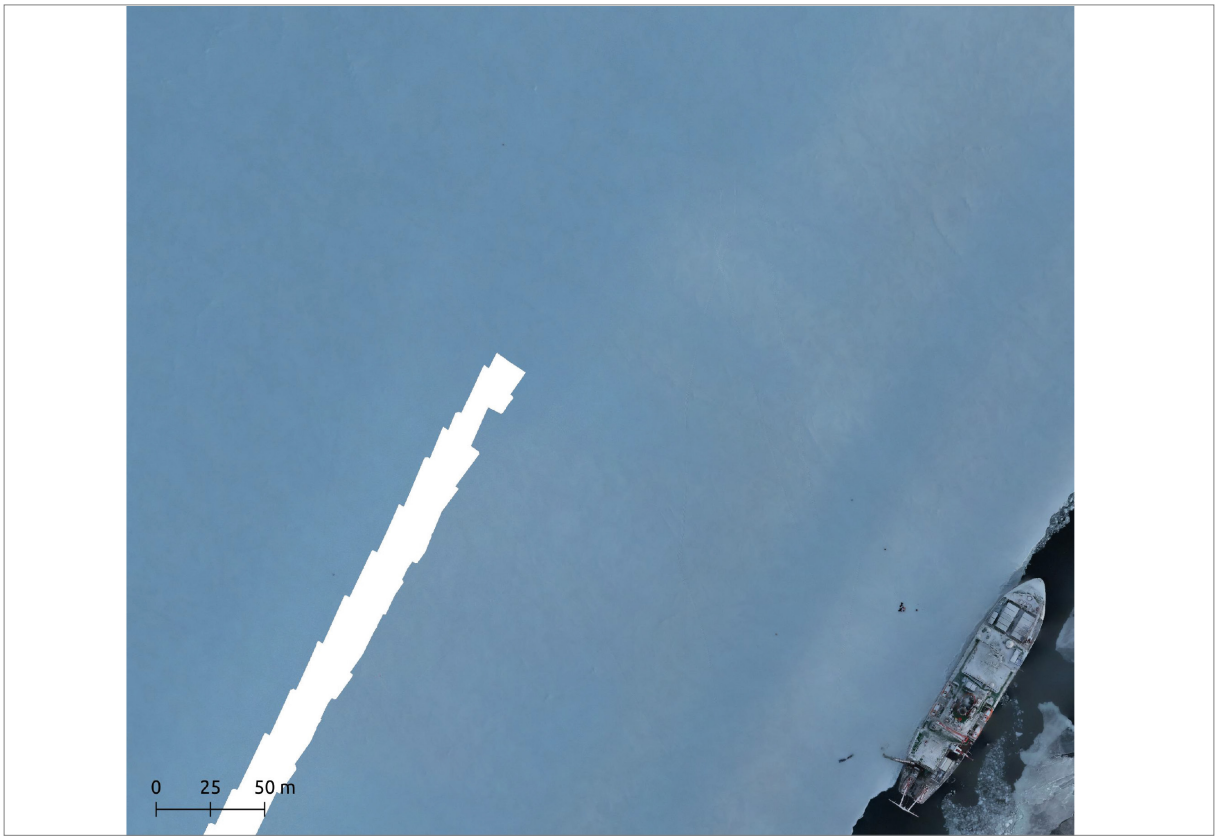

Fig. A.5.9: Preliminary map of ice station ICE10 (PS144_134-1).

Die **Berichte zur Polar- und Meeresforschung** (ISSN 1866-3192) werden beginnend mit dem Band 569 (2008) als Open-Access-Publikation herausgegeben. Ein Verzeichnis aller Bände einschließlich der Druckausgaben (ISSN 1618-3193, Band 377-568, von 2000 bis 2008) sowie der früheren **Berichte zur Polarforschung** (ISSN 0176-5027, Band 1–376, von 1981 bis 2000) befindet sich im electronic Publication Information Center **(ePIC)** des Alfred-Wegener-Instituts, Helmholtz-Zentrum für Polar- und Meeresforschung (AWI); see https://epic.awi.de. Durch Auswahl “Reports on Polar- and Marine Research“ (via “browse”/”type”) wird eine Liste der Publikationen, sortiert nach Bandnummer, innerhalb der absteigenden chronologischen Reihenfolge der Jahrgänge mit Verweis auf das jeweilige pdf-Symbol zum Herunterladen angezeigt.

The **Reports on Polar and Marine Research** (ISSN 1866-3192) are available as open access publications since 2008. A table of all volumes including the printed issues (ISSN 1618-3193, Vol. 377-568, from 2000 until 2008), as well as the earlier **Reports on Polar Research** (ISSN 0176-5027, Vol. 1–376, from 1981 until 2000) is provided by the electronic Publication Information Center **(ePIC)** of the Alfred Wegener Institute, Helmholtz Centre for Polar and Marine Research (AWI); see URL https://epic.awi.de. To generate a list of all Reports, use the URL http://epic.awi.de and select “browse”/”type” to browse ”Reports on Polar and Marine Research”. A chronological list in declining order will be presented, and pdf-icons displayed for downloading.

Zuletzt erschienene Ausgaben:

Recently published issues:

794 (2025) The Expedition PS144 of the Research Vessel POLARSTERN to the Arctic Ocean in 2024, edited by Benjamin Rabe and Walter Geibert with contributions of the participants

793 (2025) The Expedition PS141 of the Research Vessel POLARSTERN to the Davis Sea and Mawson Sea in 2024, edited by Sebastian Krastel with contributions of the participants

792 (2025) Climate Signals from Neumayer, coastal Dronning Maud Land, Antarctica: A 33-Year statistical Analysis of Snow Accumulation in a Stake Farm, by Valerie Reppert

791 (2025) TIDAL–HX01: Trialing Innovative Data Acquisition from a Platform of Opportunity – the HX Vessel MS FRIDTJOF NANSEN, edited by Andreas Herber, Laura Köhler, Verena Meraldi, Katja Metfies, Melf Paulsen, Daniel Pröfrock, Tobias Steinhoff and Hongyan Xi with contributions of the participants

790 (2024) The Expedition PS140 of the Research Vessel POLARSTERN to the Cooperation Sea and Davis Sea in 2023 / 2024, edited by Marcus Gutjahr and Oliver Esper with contributions of the participants

789 (2024) The Expedition PS142 of the Research Vessel POLARSTERN to the Atlantic Ocean in 2024, edited by Simon Dreutter with contributions of the participants

788 (2024) The Expedition PS138 of the Research Vessel POLARSTERN to the Arctic Ocean in 2024 edited by Antje Boetius and Christina Bienhold with contributions of the participants

786 (2024) The MOSES Sternfahrt Expeditions of the Research Vessels ALBIS, LITTORINA, LUDWIG PRANDTL and MYA II to the Elbe River, Elbe Estuary and German Bight in 2023 edited by Ingeborg Bussmann, Martin Krauss, Holger Brix, Norbert Kamjunke, Björn Raupers and Tina Sanders with contributions of the participants

785 (2024) The Expeditions PS139 / 1 and PS139 / 2 of the Research Vessel POLARSTERN to the Atlantic Ocean in 2023, edited by Simon Dreutter and Claudia Hanfland with contributions of the participants

ALFRED-WEGENER-INSTITUT
HELMHOLTZ-ZENTRUM FÜR POLAR-
UND MEERESFORSCHUNG

BREMERHAVEN

Am Handelshafen 12
27570 Bremerhaven
Telefon 0471 4831-0
Telefax 0471 4831-1149
www.awi.de

HELMHOLTZ